

**Detrital zircon U-Pb geochronology and Hf isotope geochemistry of the
Laberge Group: synorogenic siliciclastic record of early Mesozoic
crustal thickening and tectonic evolution of the Whitehorse
trough in the northern Canadian Cordillera**

By Leigh van Drecht

A Thesis submitted to the School of Graduate studies
in partial fulfillment of the requirements for the degree of

Master of Science, Department of Earth Sciences
Memorial University of Newfoundland

June, 2019

St. John's Newfoundland and Labrador

Abstract

The Laberge Group consists of synorogenic, marginal-marine to deep-marine strata that were deposited in the Whitehorse trough of central Yukon during the collision of the northern Intermontane terranes along the western Laurentian margin. New detrital zircon U-Pb-Hf data from Laberge Group rock units constrain the Early to Middle Jurassic depositional ages and provenance of Whitehorse trough strata and determine their relationship to the unroofing history of adjacent basement successions. The Whitehorse trough initiated in the Sinemurian as a long, narrow basin that subsequently grew to the west, east, and south by Aalenian time and was sourced by Paleozoic Yukon-Tanana and Stikinia basement rocks and their synorogenic Late Triassic-Early Jurassic plutonic suites. Late Triassic-Middle Jurassic detrital zircon grains from the northern apex of the Whitehorse trough record an excursion to subchondritic $\epsilon_{\text{Hf}(t)}$ values that coincides with the burial of Intermontane terranes and may record crustal thickening proximal to northern regions of the basin.

Acknowledgments

Fieldwork and analytical support for this project were provided by the Yukon Geological Survey and NSERC Discovery Grants to Dr. Luke Beranek. I am indebted to Maurice Colpron, Esther Bordet, and Matt Hutchison who provided support, mentorship and helpful discussions throughout this study and to Daphnee Tuzlak, Sarah Ellis, Pia Blake, and Alexina Boileau for their assistance in the field. Helicopter support was provided by Heli Dynamics and TRK. Thank you to Markus Wälle and Rebecca Lam of the CREAT microanalysis facility (MAF) for their assistance. Their expertise was extremely helpful during the collection of my data. Thank you to John Hanchar who provided helpful comments to improve this thesis.

Lastly, I would like to thank my supervisor Dr. Luke Beranek, the Beranek Research Group, my office mates, my family, and my friends in St. John's who have made Newfoundland a warm and happy home.

Table of Contents

Abstract	ii
Acknowledgments.....	iii
Table of Contents	iv
List of tables.....	viii
List of figures	ix
List of Abbreviations and Symbols.....	xi
List of appendices	xiii
Chapter 1: Introduction	15
1.1 Geological background	18
1.1.1 Orocline model	18
1.1.2 Crustal thickening, exhumation, and pluton emplacement.....	21
1.1.4 Mesozoic stratigraphic framework	24
1.1.4.1 Stikinia and Quesnellia.....	24
1.1.4.2 Laberge Group.....	25
1.2 Objectives	27
1.3 Methods	28
1.3.1 Field work and sample collection.....	29
1.3.2 Analytical methods	29
1.3.3 Maximum depositional age.....	31
1.3.4 Sediment provenance.....	32
1.3.5 Crustal evolution.....	32
1.4 Co-authorship statement	33

1.5 Presentation.....	34
References.....	34
Chapter 1 Figures	48
Chapter 2: Detrital zircon U-Pb geochronology and Hf isotope geochemistry of the Laberge Group, central Yukon: synorogenic siliciclastic record of early Mesozoic crustal thickening and tectonic evolution of the Whitehorse trough in the northern Canadian Cordillera	52
2.1 Abstract.....	52
2.2 Introduction.....	53
2.3 Geological background	56
2.3.1 Yukon-Tanana	56
2.3.2 Slide Mountain.....	59
2.3.3 Cache Creek.....	60
2.3.4 Stikinia and Quesnellia.....	60
2.3.5 Tectonic evolution	62
2.4 Whitehorse trough geology	64
2.4.1 Laberge Group stratigraphy	64
2.4.2 Jurassic regional burial and exhumation.....	66
2.4.3 Late Triassic-Middle Jurassic plutonism.....	67
2.5 Methods	68
2.6 Results.....	72
2.6.1 Tanglefoot formation	72
2.6.2 Richthofen formation.....	74

2.7 Discussion.....	78
2.7.1 Timing of Laberge Group deposition	78
2.7.1.1 Tanglefoot formation.....	79
2.7.1.2 Richthofen formation.....	80
2.7.1.3 Spatial trends of basal Laberge Group strata.....	82
2.7.2 Sediment provenance.....	83
2.7.2.1 Inheritance	83
2.7.2.2 Paleozoic populations	84
2.7.2.3 Mesozoic populations	86
2.7.2.4 Sediment pathways and provenance evolution.....	88
2.7.3 Early Mesozoic tectonic evolution	90
2.7.4 Subsidence	93
2.8 Conclusions.....	96
References.....	99
Chapter 2 Tables	117
Chapter 2 Figures	119
Chapter 3: Summary and future research.....	130
3.1 Summary	130
3.2 Future research.....	133
3.2.1 Provenance and tectonic history of the southern Whitehorse trough	133
3.2.2 Paleocurrent measurements in the Laberge Group	134
3.2.3 Multi-mineral approach to provenance and thermochronology of the Whitehorse trough.....	134

References.....	135
Appendix A: Stratigraphic logs.....	137
Appendix B: Hand sample and thin section photographs	138
Appendix C: Grain maps.....	144
Appendix D: Laser ablation split stream analytical data	168
Appendix E: Isoplot diagrams.....	292
Appendix F: Yukon Exploration and Geology publications.....	138

List of tables

Chapter 2

Table 2.1 Summary of $\varepsilon_{\text{Nd(t)}}$ and $\varepsilon_{\text{Hf(t)}}$ values and locations of potential Yukon-Tanana, Stikinia and Quesnellia source regions for Whitehorse trough strata.

Table 2.2 Summary of Laberge Group sample locations and maximum depositional ages calculated in this study.

List of figures

Chapter 1

Figure 1.1 Paleozoic-early Mesozoic terranes and Jurassic sedimentary basins of the North American Cordillera after Colpron and Nelson (2011).

Figure 1.2 Regional geology of central Yukon and Laberge Group detrital zircon sample locations modified from Colpron et al. (2015).

Figure 1.3 (A) Map of the Insular and Intermontane terranes, North American parautochthon, and Late Triassic-Middle Jurassic plutonic suites near the Whitehorse trough after Colpron (2018). (B) $\varepsilon_{\text{Hf(t)}}$ vs. U-Pb age plot of the Late Triassic to Middle Jurassic plutonic suites after Sack et al. (2019).

Figure 1.4 Upper Paleozoic-Mesozoic stratigraphy of the Stikinia, Quesnellia, and Whitehorse trough compiled by Colpron et al. (2015).

Chapter 2

Figure 2.1 Paleozoic-early Mesozoic terranes and Jurassic sedimentary basins of the North American Cordillera after Colpron and Nelson (2011).

Figure 2.2 Regional geology of central Yukon and Laberge Group detrital zircon sample locations modified from Colpron et al. (2015).

Figure 2.2 Upper Paleozoic-Mesozoic stratigraphy of Stikinia, Quesnellia, and Whitehorse trough complied by Colpron et al. (2015).

Figure 2.4 (A) Map of the Insular and Intermontane terranes, North American parautochthon, and Late Triassic-Middle Jurassic plutonic suites near the Whitehorse trough after Colpron (2018). (B) $\varepsilon_{\text{Hf(t)}}$ vs. U-Pb age plot of the Late Triassic to Middle Jurassic plutonic suites after Sack et al., 2019.

Figure 2.5 Measured stratigraphic sections of the Tanglefoot formation along the Robert Campbell Highway.

Figure 2.6 Detrital zircon $\varepsilon_{\text{Hf(t)}}$ vs. U-Pb age plot of the Tanglefoot formation.

Figure 2.7 Detrital zircon $\varepsilon_{\text{Hf(t)}}$ vs. U-Pb age plot of the Richthofen formation.

Figure 2.8 Maximum depositional ages of Laberge Group strata plotted from west to east and north to south.

Figure 2.9 Sinemurian to Aalenian basin evolution of the Whitehorse trough based on maximum depositional ages of basal Laberge Group strata.

Figure 2.10 Normalized age probability plots for the Tanglefoot formation, Richthofen formation, and Laberge Group.

Figure 2.11 $\epsilon_{\text{Hf(t)}}$ vs. U-Pb age plot of cores and rims from Laberge Group detrital zircon grains.

List of Abbreviations and Symbols

Ar: argon

ca.: circa

CHUR: chondritic uniform reservoir

CL: cathodoluminescence

DM: depleted mantle

$\epsilon_{\text{Hf}(t)}$: age-corrected epsilon hafnium

$\epsilon_{\text{Nd}(t)}$: age-corrected epsilon neodymium

e.g.: exempli gratia; for example

Ga: billion years

He: helium

Hf: hafnium

Hz: hertz

ICP-MS: inductively coupled plasma mass spectrometer

ID-TIMS: isotope dilution thermal ionization mass spectrometry

J/cm²: joules per square centimeter

K: potassium

Kbar: kilobar

km: kilometer

km/m.y.: kilometer per million year

LASS: laser ablation split stream

L/min: litre per minute

Lu: lutetium

Lu-Hf: lutetium-hafnium

m: meter

MC-ICP-MS: multi-collector inductively coupled plasma mass spectrometer

m.y.: million years

Ma: million years ago

n: number

Nd: neodymium

NSERC: Natural Science and Engineering Research Council of Canada

O: oxygen

OIB: ocean-island basalt

Pb: lead

SD: standard deviation

SEM: scanning electron microscope

Sm-Nd: samarium-neodymium

U: uranium

U-Pb: uranium-lead

μm: micron

̄x: mean

σ: sigma

<: less than

>: greater than

List of appendices

Appendix A: Stratigraphic logs

Appendix B: Hand sample and thin section photographs

B.1 Hand samples

B.2 Thin sections

Appendix C: Grain maps

C.1 16-LVD-001B, Robert Campbell Highway

C.2 16-LVD-001C, Robert Campbell Highway

C.3 16-LVD-004, Robert Campbell Highway

C.4 16-LVD-009, Mount Laurier

C.5 16-LVD-021, Richthofen Island

C.6 16-LVD-022, Eastern shoreline of Lake Laberge

C.7 16-LVD-023, Eastern shoreline of Lake Laberge

C.9 17-LVD-018, Conglomerate Mountain

C.10 17-LVD-027, Takhini Subdivision

C.11 17-LVD-030, Mount Byng

C.12 17-LVD-034, Mount Slim

C.13 17-LVD-038, King Lake

C.14 16-LVD-007, Klondike Highway

Appendix D: Laser ablation split stream analytical data

Table D.1 U-Pb isotope ratios and isotopic ages

Table D.2 Lu-Hf isotope ratios

D.3 U-Pb and Hf standards

Appendix E: Isoplot

E.1 Concordia plots

E.2 TuffZirc plots

E.3 Weighted mean plots

E.4 Unmix plots

Appendix F: Yukon exploration & geology fieldwork publications

F.1 van Drecht et al. (2017)

F.2 van Drecht and Beranek (2018)

Chapter 1: Introduction

The composition of siliciclastic sediments is controlled by many factors, including climate, topography, plate tectonic setting, and scale of the depositional system (e.g., Dickinson and Suczek, 1979; Dickinson and Valloni, 1980; Ingersoll, 1993; Johnsson, 1993; Link et al., 2005). Locally-derived provenance signatures are predicted for convergent margin basin deposits as a result of synsedimentary magmatism, regional uplift, and erosion (e.g., Dickinson, 1974; Dickinson and Suczek, 1979; Dickinson et al., 1983; Cawood et al., 2009, 2012). Detrital zircon U-Pb provenance techniques have proven to be especially useful for stratigraphic investigations that attempt to constrain the maximum depositional age, source, and paleogeography of synorogenic rock units, including those along long-lived accretionary margins that are reworked by regional deformation, metamorphism, and magmatism (e.g., Willner et al., 2008; Wu et al., 2010; Anfinson et al., 2012). The characterization of siliciclastic sediment through detrital zircon Hf isotope analysis in addition to U-Pb geochronology is useful to improve the identification of source regions and provide insight into the crustal evolution of these source regions (e.g., Hawkesworth and Kemp, 2006; Kemp et al., 2006; Flowerdew et al., 2007; Iizuka et al., 2010; Beranek et al., 2013; Pecha et al., 2016; Liu et al., 2017). Detrital zircon Hf isotope data have also become useful for monitoring periods of crustal thickening and continental arc development along accretionary margins that are defined by excursions towards subchondritic values, informally known as “pull-downs” (e.g., Gehrels and Pecha, 2014; DeCelles and Graham, 2015).

The northern Cordillera is comprised of parautochthonous North American margin strata in the east and the accreted Intermontane, Insular, and Alaskan terranes in central and

western parts of the mountain belt (Fig. 1.1; e.g., Monger and Price, 2002; Nelson et al., 2013). The early Mesozoic accretionary history of the northern Canadian Cordillera is marked by the collision and accretion of the peri-Laurentian Intermontane arc terranes (Yukon-Tanana, Stikinia, and Quesnellia) and in part recorded by synorogenic strata of the Early-Middle Jurassic Whitehorse trough (Figs. 1.1 and 1.2; e.g., Mihalynuk et al., 1994; Dickie and Hein, 1995; Nelson et al., 2013; Colpron et al., 2015). Late Triassic-Early Jurassic collision and accretion along the western Laurentian margin resulted in crustal thickening and burial of Intermontane terrane basement rocks to 5-9 kbar (~18-33 km) followed by rapid exhumation along the eastern, western, and northern flanks of the Whitehorse trough at a rate of ~4 km/m.y. (e.g., Hart et al., 1995; Johnston and Erdmer, 1995; Villeneuve et al., 2003; Berman et al., 2007; Knight et al., 2013; Colpron et al., 2015; Clark, 2017; Kellett et al., 2018). Subsequent erosion of the northern Intermontane terranes and tectonic subsidence in the Whitehorse trough resulted in the deposition of the Laberge Group, a 3000 m-thick succession of marginal-marine and deep-marine strata that extends from the Carmacks region in the central Yukon to the Dease Lake region of northern British Columbia (Fig. 1.2; e.g., Tempelman-Kluit, 1979; Dickie and Hein, 1994; Lowey, 2004, 2008; Colpron et al., 2015). Laberge Group strata unconformably overlie various shallow-water, arc-marginal rock units of the Lewes River Group (Mesozoic Stikinia) and indicate a rapid change in depositional environment (Cairnes, 1910; Tempelman-Kluit, 1984; Dickie and Hein, 1995; Lowey 2004, 2008; Colpron et al., 2007). Proximal or marginal-marine strata of the Tanglefoot formation at the base of the Laberge Group are restricted to the northern apex of the Whitehorse trough, whereas distal or deep-marine strata assigned to the Richthofen formation are restricted to central regions, suggesting a south-directed deepening of the basin (Fig. 1.2; e.g., Dickie and

Hein, 1995; Tempelman-Kluit, 1984; Lowey, 2004, 2009). Published detrital zircon U-Pb data further suggest that the Laberge Group strata were locally sourced from Late Triassic-Early Jurassic arc- to collision-related plutons and pre-Mesozoic basement domains of the peri-Laurentian Yukon-Tanana, Stikinia, and Quesnellia terranes (Colpron et al., 2015). Laberge Group strata in central Yukon yield Hettangian-Pliensbachian and Pliensbachian-Toarcian maximum depositional ages along the central axis and western edge of the basin, respectively, and suggest an east to west younging trend and westerly growth of the Whitehorse trough (Colpron et al., 2015).

Despite recent advances in understanding Whitehorse trough stratigraphy (e.g., Hart et al., 1995; Shirmohammad et al., 2011; Colpron et al., 2015), the precise timing of the Laberge Group deposition and relative sediment contributions of Yukon-Tanana, Quesnellia, and Stikinia basement assemblages and their Late Triassic-Middle Jurassic plutonic suites during regional exhumation remains uncertain. In this thesis, I report the physical stratigraphy and detrital zircon U-Pb-Hf composition of 12 Laberge Group rock samples to investigate the stratigraphic response to Jurassic unroofing and test the relationships between the timing of terrane accretion, exhumation, and Whitehorse trough sedimentation. The ICP-MS (inductively coupled plasma mass spectrometer) and MC-ICP-MS (multi-collector inductively coupled plasma mass spectrometer) laser ablation split stream (LASS) method, which features simultaneous collection of U-Pb and Hf (or Nd) isotopes, was used to discriminate Yukon-Tanana, Stikinia, and Quesnellia sediment sources in the central Yukon and characterize isotopic trends associated with Jurassic tectonism and crustal thickening in the Canadian Cordillera. New maximum depositional ages for the basal Laberge Group and select locations

higher in stratigraphy are proposed to constrain the timing of basin development and provenance evolution of the Whitehorse trough.

1.1 Geological background

The Yukon-Tanana, Stikinia, and Quesnellia arc terranes and the Slide Mountain and Cache Creek oceanic terranes underlie the core of the northern Cordillera. The Whitehorse trough is positioned at the center of an inverted ‘V’-shaped geometry configured by the Intermontane terranes during their accretion to the western Laurentian margin (Fig. 1.1; Nelson and Mihalynuk, 1993; Mihalynuk et al., 1994). Proposed tectonic models to account for this geometry include strike-slip duplication of the Intermontane terranes (Wernicke and Klepacki, 1988) and counterclockwise or oroclinal bending of Stikinia, Yukon-Tanana, and Slide Mountain that resulted in the entrapment of the Cache Creek terrane (e.g., Nelson and Mihalynuk, 1993; Mihalynuk et al., 1994). Oroclinal bending is generally considered as the most viable model to explain this geometry, however, these ideas remain controversial (e.g., Nelson et al., 2013; Colpron et al., 2015).

1.1.1 Orocline model

The Intermontane terranes evolved in the peri-Laurentian realm and interacted with the western Laurentian margin from the Devonian to Jurassic periods (e.g., Nelson et al., 2013). Stikinia and Quesnellia make up the majority of the Intermontane terranes and are comprised of Mississippian to Permian arc-related basement rocks (e.g., Takhini and Boswell assemblages), Triassic plutonic and volcanic rocks, and Jurassic volcanic and sedimentary rocks (e.g., Monger et al., 1991; Hart, 1997; Colpron et al., 2006; Nelson et al., 2006, 2013;

Sack et al., 2019). The Yukon-Tanana terrane consists of variably deformed and metamorphosed mid- to late Paleozoic arc successions (Finlayson, Klinkit, Klondike assemblages) that were built upon and intrude a pre-Late Devonian continental margin succession (Snowcap assemblage) of northwest Laurentian affinity (e.g., Mortensen, 1992; Colpron et al., 2006; Piercy and Colpron, 2009). Basement rocks of the Yukon-Tanana terrane were separated from the Laurentian margin following Late Devonian-Early Mississippian back-arc extension that resulted from slab rollback of the downgoing plate (e.g., Mortensen, 1992; Nelson et al., 2006). Continued extension in the back-arc region led to the opening of the Slide Mountain Ocean and westward transport of Yukon-Tanana and related peri-Laurentian terranes, analogous to the modern Japanese arc-Sea of Japan system (e.g., Murphy et al., 2006; Colpron et al., 2006, 2007). Outboard of the Laurentian margin, Carboniferous to Permian magmatic arcs that comprise the Finlayson, Klinkit, Klondike assemblages were built upon Yukon-Tanana basement rocks (e.g., Piercy et al., 2006; Colpron et al., 2007; Nelson et al., 2013). The Stikinia and Quesnellia arc terranes also evolved in the peri-Laurentian realm outboard of the Laurentian margin following the opening of the Slide Mountain Ocean (e.g., Colpron et al., 2007; Nelson et al., 2013). Quesnellia basement rocks (Lay Range succession and Harper Ranch Group) are consistent in stratigraphy, age, and geochemistry to the Late Mississippian to early Permian Klinkit assemblage of the Yukon-Tanana (e.g., Simard et al., 2003; Colpron et al., 2007) and are inferred to link the development of Quesnellia/Stikinia to Yukon-Tanana (e.g., Colpron et al., 2007; Nelson et al., 2013).

Westward subduction that led to the closure of the Slide Mountain Ocean is linked to a

mid- to late Permian polarity reversal beneath the Yukon-Tanana, Stikinia, and Quesnellia terranes (Tempelman-Kluit 1979; Mihalynuk et al., 1994; Piercy et al., 2006; Nelson et al., 2013). Yukon-Tanana, Stikinia, and Quesnellia were subsequently transported cratonwards and within proximity to the western Laurentian margin by the late Permian (Beranek et al., 2010; Beranek and Mortensen, 2011). Following the final closure of the Slide Mountain Ocean, the polarity of subduction again reversed and eastward subduction was renewed beneath the western edge of North America from the mid-Triassic to Early Jurassic (Beranek and Mortensen, 2011; Nelson et al., 2013). A primitive Permian-Triassic intraoceanic arc (Kutcho arc) carried towards the margin on the downgoing plate collided with the northern Cordilleran margin by the Late Triassic (e.g., Mihalynuk et al., 1994; Schiarizza 2011, 2012). Mihalynuk et al. (1994) suggested that the configuration of Yukon-Tanana, Stikinia, Quesnellia and the impinging Kutcho arc are analogous to the modern Aleutian and Kurile arcs and Emperor Seamount chain in the North Pacific Ocean. The collision of the Kutcho arc and/or seafloor spreading behind Stikinia are inferred as the potential driving forces for oroclinal bending, where Stikinia and Quesnellia acted as the outer and inner limbs, respectively, and Yukon-Tanana as the hinge (Mihalynuk et al., 1994). Counterclockwise rotation isolated the Cache Creek Ocean between Stikinia and Quesnellia in the Early Jurassic (Mihalynuk et al., 1994). A modern analogue for the initiation of oroclinal bending is observed in the southwest Pacific Ocean with the collision of the Carolina Rise with the Mariana arc, which has produced an oroclinal bend where the Yap and Mariana trenches act as the limbs (McCabe and Uyeda, 1983; Mihalynuk et al., 1994). This arc-arc collision and seafloor spreading in the Philippine Sea resulted in a greater than 50° clockwise rotation of Guam, however, an oceanic assemblage is not entrapped in the Carolina Rise region (McCabe

and Uyeda, 1983; Mihalynuk et al., 1994). Continued rotation of Stikinia caused the subduction of Cache Creek oceanic crust to transition from a single eastward subduction zone to a bivergent system with westward subduction beneath the Stikinia terrane and eastward subduction beneath the Quesnellia terrane (Mihalynuk et al., 1994). A modern analogue to this bivergent tectonic configuration occurs between the Eurasian and Philippine plates where oceanic assemblages of the Molucca sea are subducting eastward beneath the Halmahera arc and westward beneath the Sangihe arc (Morris et al., 1983; Mihalynuk et al., 1994). The Early-Middle Jurassic Whitehorse trough was deposited on top of the northern Intermontane terranes and is interpreted to have developed in a forearc position at the center of the orocinal bend (e.g., Tempelman-Kluit, 1979; Mihalynuk et al., 1994; Colpron et al., 2015). Dickie and Hein (1995) suggested that initial subsidence in the basin was irregular and rapid and is likely attributed to a combination of movement along basin-bounding faults and relative sea level rise. The Cache Creek Ocean closed by the Middle Jurassic and its oceanic assemblages were emplaced onto northeastern Stikinia, marking the final accretion of the Intermontane terranes against the continental margin (e.g., Mihalynuk et al., 1994; Nelson et al., 2013).

1.1.2 Crustal thickening, exhumation, and pluton emplacement

The Early Jurassic imbrication of the northern Intermontane terranes resulted in rapid crustal thickening and exhumation in Yukon and northern British Columbia (e.g., Johnston and Erdmer, 1995; Johnston et al., 1996; Villeneuve et al., 2003; Berman et al., 2007; Knight et al., 2013). Thermobarometric data and metamorphic petrology indicate that Yukon-Tanana rocks located along the western flank and north of the Whitehorse trough were buried at 5-9 kbar (~18-33 km) and subsequently exhumed to upper crustal levels by the Sinemurian-

Pliensbachian (195-186 Ma) (e.g., Johnston and Erdmer, 1995; Johnston et al., 1996; Villeneuve et al., 2003; Berman et al., 2007; Knight et al., 2013). Eclogite clasts collected from a distinct latest Pliensbachian-earliest Toarcian conglomerate unit of the Laberge Group in northern British Columbia suggest rapid Early Jurassic exhumation rates of ~4 km/m.y. and are interpreted to be sourced from the suture between Yukon-Tanana and Stikinia (Kellett et al., 2018). Regional exhumation was likely driven by buoyant extrusion during slab rollback, upper-plate retreat, transtension, slab breakoff, or syn- to post-collisional extension at the boundary of Yukon-Tanana and Stikinia (Kellett et al., 2018). Subsidence in the Whitehorse trough is coeval with the rapid exhumation of the Intermontane terranes, however, there are no estimates on the rates of subsidence within the basin (e.g., Dickie and Hein, 1995; Lowey, 2008; Colpron et al., 2015).

Intermontane terrane burial and subsequent exhumation were accompanied by Late Triassic-Middle Jurassic plutonism (Fig. 1.3a; e.g., Johnston et al., 1995, 1996; Tafti, 2005; Colpron et al., 2016; Yukon Geological Survey, 2017). The Late Triassic Stikine suite (ca. 216-206 Ma) is oldest plutonic suite and consists of granodiorite, diorite, and gabbro units that crop out in restricted areas southwest of Whitehorse and northwest of Carmacks (Fig. 1.3a; e.g., Hart and Radloff, 1990, Colpron et al., 2016). Stikine plutonic suite rocks located southwest of Whitehorse (Fish Lake and Friday Creek) yield superchondritic zircon $\varepsilon_{\text{Hf(t)}}$ values that range from +9.7 to +11.5 (Fig. 1.3b; Sack et al., 2019). The Late Triassic-Early Jurassic Minto plutonic suite (ca. 204-194 Ma) crops out near the northern apex of the Whitehorse trough to the northwest and east of Carmacks and is comprised of granodiorite, quartz monzonite, granite, and minor syenite plutons that are best represented by the Tatchun

pluton ($\epsilon_{\text{Hf(t)}}$: -9.5 to +9.5), Granite Mountain pluton ($\epsilon_{\text{Hf(t)}}$: -12.7 to +10.1), Minto pluton ($\epsilon_{\text{Hf(t)}}$: +0.8 to +10.9) and Thirtymile pluton ($\epsilon_{\text{Hf(t)}}$: -1.0 to +3.8) (Fig. 1.3b; e.g., Tafti and Mortensen, 2003; Colpron et al., 2016; Sack et al., 2019). The Early Jurassic Long Lake suite (ca. 192-178 Ma) is characterized by granodiorite and granite units of the Aishihik pluton, Big Creek, Sawtooth, and Englishman plutons, and Logtung quartz diorite that predominately crop out northwest and along the western edge of the Whitehorse trough (Colpron et al., 2016; Joyce et al., 2016). The Aishihik ($\epsilon_{\text{Hf(t)}}$: -27.3 to +12.1) and Big Creek plutons ($\epsilon_{\text{Hf(t)}}$: -3.6 to +1.7) crop out northwest and along western side of the Whitehorse trough and yield dominantly subchondritic to chondritic zircon $\epsilon_{\text{Hf(t)}}$ values, whereas the Sawtooth pluton ($\epsilon_{\text{Hf(t)}}$: -6.2 to +11.6), Englishman pluton ($\epsilon_{\text{Hf(t)}}$: +1.6 to +3.7) and Logtung quartz diorite ($\epsilon_{\text{Hf(t)}}$: -2.9 to +1.4) crop out in smaller regions along the southeastern edge of the Whitehorse trough and yield chondritic to superchondritic zircon $\epsilon_{\text{Hf(t)}}$ values (Fig. 1.3b; Colpron et al., 2016; Sack et al., 2019). The Middle Jurassic Bryde (ca. 172-168 Ma) and Middle to Late Jurassic McGregor (ca. 163-160 Ma) suite granitoids are the youngest plutonic rocks adjacent to the Whitehorse trough. The Bryde suite includes alkali syenite, diorite, and monzodiorite that crops out in the Atlin Lake ($\epsilon_{\text{Hf(t)}}$: +4.7 to +7.0), Marsh Lake ($\epsilon_{\text{Hf(t)}}$: +0.9 to +3.8), and Teslin Crossing ($\epsilon_{\text{Hf(t)}}$: +6.5 to +8.4) regions near Whitehorse and to the north of Carmacks, whereas the McGregor suite ($\epsilon_{\text{Hf(t)}}$: +0.9 to +11.1) is apparently restricted to the McGregor pluton locality north of Carmacks (Fig. 1.3a; Colpron et al., 2016; Sack et al., 2019).

1.1.4 Mesozoic stratigraphic framework

1.1.4.1 Stikinia and Quesnellia

Mesozoic Quesnellia is comprised of augite-phyric basalt, andesite, volcaniclastic rocks and minor carbonate rocks assigned to the Upper Triassic Semenof formation, whereas Mesozoic Stikinia in central Yukon consists of shallow-water, arc-marginal, and arc-related rocks of the Joe Mountain formation and Lewes River Group (Fig. 1.4; e.g., Tempelman-Kluit, 1984; Dickie and Hein, 1995; Hart, 1997; Simard and Devine, 2003). The Middle Triassic Joe Mountain formation consists of pillow basalt, massive basalt, siliciclastic and calcareous strata, and microdiorite and gabbro intrusions with pervasive low temperature chlorite and epidote alteration (Hart, 1997). Joe Mountain formation rocks primarily crop out in the Joe Mountain and Mount Byng regions east of Whitehorse and yield island arc tholeiite and mid-ocean ridge geochemical signatures (Figs. 1.2 and 1.4; Hart, 1997; Bordet, 2016).

The Upper Triassic Lewes River Group overlies the Joe Mountain formation and is comprised of a 3000 m-thick assemblage of basalt and andesite, flow breccia, mafic tuff, conglomerate, greywacke, limestone, and shale assigned to the Povoas and Aksala formations (Fig. 1.4; Tempelman-Kluit, 1984; Dickie and Hein, 1995; Hart, 1997). The Carnian Povoas formation represents the main volcanic unit of the Lewes River Group and is characterized by high-K basalt, andesite, and volcanic breccia with island arc to calc-alkaline geochemical signatures (Fig. 1.4; Tempelman-Kluit, 1984, 2009; Hart, 1997). Rocks assigned to the Povoas formation crop out in central, northern, and eastern regions of the Whitehorse trough. The Upper Triassic Aksala formation represents a volcanic lull following Carnian magmatism and consists of the Casca (Carnian-Norian), Hancock (Norian-Rhaetian) and Mandanna (Rhaetian)

members (Fig. 1.4; Tempelman-Kluit, 2009; Hart, 1997). The basal Casca member consists of lithic sandstone, argillite, and conglomerate overlain by reefal limestone of the Hancock member (e.g., Tempelman-Kluit, 1984; Hart, 1997; Bordet, 2016, 2017). Maroon lithic sandstone, mudstone, and conglomeratic units of the Mandanna member, which overlies and interfingers with the Hancock member, are discontinuous across central Yukon (Tempelman-Kluit, 1984; Dickie and Hein, 1995; Hart, 1997).

1.1.4.2 Laberge Group

The Whitehorse trough is an extensive Early to Middle Jurassic sedimentary basin that extends >600 km from the Carmacks region of central Yukon to the Dease Lake region of northern British Columbia (Fig. 1.1). Lower to Middle Jurassic Laberge Group strata define the Whitehorse trough and comprise ~3000 m of immature siliciclastic strata that unconformably overlie different units of the Lewes River Group (Fig. 1.4; e.g., Wheeler, 1961; Tempelman-Kluit, 1984; Dickie and Hein, 1995; Lowey, 2008). Field mapping and seismic surveys indicate that southwest-verging open folds and thrust faults deform the Whitehorse trough (Colpron et al., 2007; White et al., 2012). In central Yukon, the Sinemurian-Bajocian Tanglefoot and Richthofen formations constitute the Laberge Group (Tempelman-Kluit, 1984; Dickie and Hein, 1995; Lowey, 2004). The Tanglefoot formation consists of sandstone, mudstone, and conglomerate units with abundant coal, terrestrial plant material, and vertebrate fossils that are indicative of marginal marine to tidal environments, whereas the Richthofen formation contains graded siltstone to sandstone and mudstone couplets and conglomerate units ammonites, belemnites, planktonic fossils, and trace fossils (*Helminthopsis*, *Phycosiphon*, *Planolites*) characteristic of deep marine environments (e.g.,

Wheeler, 1961; Tempelman-Kluit, 1984; Long 1986; Hart, 1997; Gordey et al., 1998; Lowey, 2004; Colpron et al., 2015; Hutchison, 2017; van Drecht et al., 2017). Tanglefoot formation strata are restricted to the northern apex of the Whitehorse trough and Richthofen formation strata are confined to central regions of the Whitehorse trough, suggesting a south-directed deepening of the basin (Tempelman-Kluit, 1984; Dickie and Hein, 1995; Lowey, 2004, 2008; Hutchison, 2017). Epiclastic and felsic tuff and flow units assigned to the Nordenskiöld dacite occur in both formations (Tempelman-Kluit, 1984) and record Early Jurassic eruptive events at 188.1 ± 0.4 Ma, 187.2 ± 0.4 Ma, and 186.5 ± 0.3 Ma (Colpron and Friedman, 2008).

Clast- to matrix-supported, polymictic, cobble to boulder (volcanic, plutonic, sedimentary) conglomerate units occur in the Tanglefoot and Richthofen formations and likely represent debris flow, sheet flood, and bar deposits of a submarine fan delta system (e.g., Dickie and Hein, 1988, 1995; Hart et al., 1995; Lowey, 2004, 2008; van Drecht et al., 2017). Paleoflow indicators (channel scours, nested flute casts, grooves, and imbricated clasts) are indicative of fanlobe migration and predominately show east to northeast- and southwest-directed sediment transport along the western and eastern edges of the Whitehorse trough, respectively. Sediment pathways for the conglomerate units are typically transverse with respect to the north-to-south, longitudinal axis of the Whitehorse trough (e.g., Wheeler, 1961; Dickie and Hein, 1988, 1995; Hart et al., 1995; Lowey, 2004). In northern British Columbia, Inklin Formation strata yield paleoflow indicators that suggest Sinemurian axial paleoflow was replaced by Pliensbachian transverse paleoflow (Johannson et al., 1997). Conglomerate clast types include augite-phyric basalt, andesite, tuff, granite, granodiorite, diorite, sandstone, volcanogenic sandstone, and limestone (Hart et al., 1995). Basal conglomerate units are predominated by volcanic and sedimentary clasts, whereas younger strata contain a larger

proportion of plutonic clasts that imply unroofing of the adjacent arc (Dickie and Hein, 1995; Hart et al., 1995; Johannson et al., 1997; Shirmohammad et al., 2011). U-Pb dates of plutonic clasts and detrital zircon grains are dominated by Late Triassic-Early Jurassic and minor Paleozoic populations from local Intermontane basement and plutonic sources, implying that Whitehorse trough subsidence was synchronous with the rapid exhumation of the Intermontane terranes (Hart et al., 1995; Gordey et al., 1998; Colpron et al., 2015). Sinemurian to Toarcian maximum depositional ages of basal Laberge Group rocks based on detrital zircon U-Pb geochronology broadly imply a southwest-younging of strata across the Whitehorse trough (Colpron et al., 2015). Upper Jurassic to Lower Cretaceous fluvio-deltaic rocks of the Tantalus Formation mark the end of deposition in the Whitehorse trough (Fig. 1.4; e.g., Tempelman-Kluit, 1984; Hart and Radloff, 1990; Dickie and Hein, 1995; Colpron et al., 2015).

1.2 Objectives

The Whitehorse trough developed in a convergent tectonic regime on top of the Intermontane terranes during the Early to Middle Jurassic. This study utilizes stratigraphic relationships, detrital zircon U-Pb geochronology, and Hf isotope geochemistry of Laberge Group strata to investigate the relationship(s) between the timing of Intermontane terrane accretion, regional exhumation, and Whitehorse trough sedimentation in central Yukon. The four primary objectives of this study are as follows:

- 1) Constrain plausible source regions, sediment pathways, and Sinemurian-Aalenian provenance evolution of the Whitehorse trough through targeted detrital zircon U-Pb-Hf isotope studies of Laberge Group strata. Furthermore, test if exhumed rocks that

yield unique subchondritic $\epsilon_{\text{Hf(t)}}$ values located west of the trough acted as dominant source regions using the distribution of subchondritic detrital zircon grains in Laberge Group units;

- 2) Determine the timing of basal strata and test the westerly growth model of the Whitehorse trough (Colpron et al., 2015) by calculating the maximum depositional ages of Laberge Group strata with detrital zircon U-Pb geochronology;
- 3) Document periods of crustal thickening (excursions towards subchondritic values or “pull-downs”) and continental arc development along the Cordilleran margin using detrital zircon U-Pb geochronology and Hf isotope geochemistry of Laberge Group strata;
- 4) Constrain the basin filling history to identify potential early Mesozoic subsidence mechanisms within the Whitehorse trough that provided accommodation space during and after northern Intermontane collision and exhumation.

1.3 Methods

Zircon incorporates several isotope systems (e.g., U-Pb, Lu-Hf, O, and He) that are useful for solving a variety of geological problems (e.g. Wilde et al., 2001; Hanchar and Watson, 2003; Kemp et al., 2007; Fedo et al., 2003; Gehrels, 2014). Zircon is particularly useful in sediment provenance studies due to its resistance to chemical and mechanical breakdown and ability to survive multiple sedimentary cycles (e.g., Kemp et al., 2006; Link et al., 2005; Flowerdew et al., 2007; Gehrels, 2014; Pecha et al., 2016).

1.3.1 Field work and sample collection

Detrital zircon samples for this study were collected over two field seasons at locations throughout the Whitehorse trough in central Yukon (Fig. 1.2). In 2016, Laberge Group studies were focused along the Robert Campbell Highway near Carmacks and field sites along the eastern shoreline of Lake Laberge and flanks of Mount Laurier (van Drecht et al., 2017). In 2017, Laberge Group strata were studied at the Conglomerate Mountain, Fish Lake, Takhini subdivision, Mount Byng, and Mount Slim localities (van Drecht and Beranek, 2018). A total of 23 Laberge Group rock samples were used for petrographic studies, 12 of which were analyzed for detrital zircon U-Pb geochronology and Hf isotope geochemistry.

1.3.2 Analytical methods

Standard rock crushing, sieving, and heavy liquid (bromoform and methylene iodide) density separation were done at Memorial University of Newfoundland. Approximately 130 zircon grains from each sample were mounted in epoxy, ground, polished, and imaged with cathodoluminescence (CL) using a JEOL JSM 7100F Field Emission Scanning Electron Microscope (SEM). Zircon CL grain maps guided the selection of laser spot locations to avoid complex zoning, inherited cores, fractures, or regions of Pb-loss.

U-Pb and Hf isotope ratios were acquired using the ICP-MS and MC-ICP-MS laser ablation split stream (LASS) method at Memorial University of Newfoundland following the methods of Goudie et al. (2014) and Fisher et al. (2014). Analyses were completed in four sessions (3 to 4 days per session) over an eleven-month period. A GeoLas 193 nm excimer laser used a 40 μm diameter beam with a frequency of 10 Hz and fluence of 5 J/cm². Background levels were measured for 30 s followed by 60 s of ablation and 30 s of washout

after each analysis. The ablated material was carried out of the laser cell in flow of He gas of 1 L/min and split downstream to simultaneously measure U-Pb isotopes with a ThermoFinnigan Element XR single-collector ICP-MS and Hf isotopes with a ThermoFinnigan Neptune multi-collector ICP-MS (e.g., Goudie et al., 2014, Fisher et al., 2014) with N₂ added to each mass spectrometer to increase sensitivity. Standard-sample bracketing used 91500 (U-Pb) and Plešovice (Lu-Hf) as primary reference materials to correct for instrument drift, downhole fractionation, and mass bias. R33, 02123, Temora, and QGNG were used as secondary standards. 91500 yielded a weighted ²⁰⁶Pb/²³⁸U age of 1062.2 ± 1.3 Ma (*n* = 248, 2SD), in agreement with the published ID-TIMS age of 1062.4 ± 0.4 Ma (Wiedenbeck et al., 1995). Plešovice yielded a weighted ¹⁷⁶Hf/¹⁷⁷Hf = 0.282481 ± 0.000019 (*n* = 249, 2SD), within uncertainty of the published value of 0.282482 ± 0.000013 (Sláma et al., 2008).

Isotope ratios were reduced using the Iolite 3.4 extension for IgorPro (Paton et al., 2011) and VizualAge data reduction scheme (Petrus and Kamber, 2012). A ‘best age’ was then assigned to each grain using the ²⁰⁶Pb/²³⁸U date if less than 1100 Ma and the ²⁰⁷Pb/²⁰⁶Pb date if greater than 1100 Ma. Analyses were excluded based on the following criteria:

- (1) >10% uncertainty in ²⁰⁶Pb/²³⁸U date (2 σ).
- (2) >10% uncertainty in ²⁰⁷Pb/²⁰⁶Pb date (2 σ), unless the ²⁰⁶Pb/²³⁸U date is <500 Ma.
- (3) >10% discordance or >5% reverse discordance, unless ²⁰⁶Pb/²³⁸U date is <500 Ma.

Concordance is not reported for ²⁰⁶Pb/²³⁸U ages <500 Ma because of the large uncertainty in ²⁰⁷Pb/²⁰⁶Pb (e.g., Gehrels and Pecha, 2014).

U-Pb results are presented in normalized probability density diagrams generated with the Normalized Probability Plot Excel macro developed at the Arizona Laserchron Center,

University of Arizona (www.geo.arizona.edu/alc). Probability age peaks were calculated using the AgePick Excel macro developed at Arizona LaserChron Center (www.geo.arizona.edu/alc). Hf isotope data is presented as an age-corrected $\epsilon_{\text{Hf(t)}}$ value versus the LA-ICP-MS U-Pb crystallization age of individual zircon grains and include the chondritic uniform reservoir (CHUR) values of Bouvier et al. (2008), depleted mantle (DM) values of Vervoort and Blichert-Toft (1999), and crustal evolution trends using present day $^{176}\text{Lu}/^{177}\text{Hf} = 0.0115$ (Vervoort and Patchett, 1996; Vervoort et al., 1999).

1.3.3 Maximum depositional age

The youngest detrital zircon crystals were used to estimate the maximum depositional age of Laberge Group strata because synsedimentary magmatism typically accompanies convergent margin activity (Dickinson and Gehrels, 2009; Cawood et al., 2012). Maximum depositional ages in this study were calculated using a population of young grains rather than the youngest detrital zircon due to the inherent lack of reproducibility (Dickinson and Gehrels, 2009). The following methods were used:

- 1) The weighted mean for a cluster of three or more grains that overlap at 2σ (Dickinson and Gehrels, 2009). Maximum depositional ages calculated with this method generally yield the youngest depositional ages and represent the young shoulder of the youngest peak.
- 2) Unmix routine in Isoplot. This method identifies and separates age-components within a grouping of dates that overlap (Ludwig, 2008). I used $\epsilon_{\text{Hf(t)}}$ values to assess if an identified age-component represents a separate detrital zircon population. The

Unmix routine generally yields maximum depositional ages comparable to the weighted mean of a cluster of three or more grains.

- 3) Youngest age peak calculated using the AgePick Excel macro. This macro calculates the maximum in age probability of a population that includes 3 or more analyses.
- 4) TuffZirc routine in Isoplot (Ludwig, 2008). This algorithm returns the median age of the largest cluster of ages and typically represents the age of the youngest peak.

1.3.4 Sediment provenance

U-Pb ages and Hf isotope compositions were compared to established reference frames surrounding the Whitehorse trough to determine the provenance of Laberge Group strata (e.g., Tempelman-Kluit, 1984; Hart, 1990; Sack et al., 2019). Although many potential source rocks in the northern Cordillera lack whole-rock or zircon Hf isotope constraints, several Yukon-Tanana, Stikinia, and Quesnellia rock assemblages have been characterized by whole-rock lithogeochemical and Nd isotope studies (e.g., Piercey et al., 2006) and allow comparisons to Laberge Group detrital zircon Hf isotope results. Potential source regions were therefore determined by converting published $\varepsilon_{\text{Nd(t)}}$ values to $\varepsilon_{\text{Hf(t)}}$ values using the correlation equation $\varepsilon_{\text{Hf(t)}} = 1.36 \varepsilon_{\text{Nd(t)}} + 3$ (Vervoort and Blichert-Toft, 1999).

1.3.5 Crustal evolution

Lu and Hf isotopes fractionate during magma generation and record the crustal evolution of the silicate Earth (Kinny and Maas, 2003). Fractionation occurs because Hf is incompatible and preferentially goes into the melt, which results in the generation of enriched

crust ($\text{Lu/Hf} < \text{CHUR}$) and depleted mantle ($\text{Lu/Hf} > \text{CHUR}$) relative to the chondritic uniform reservoir (CHUR) (Kinny and Maas, 2003). Deviation from CHUR at the time of crystallization is expressed as epsilon Hf ($\epsilon_{\text{Hf(t)}}$), where values of 0 are expected for chondritic compositions of the unfractionated mantle, negative values reflect the enriched crust, and positive values reflect the subcontinental mantle lithosphere and depleted mantle (Kinny and Maas, 2003). Zircon Hf isotope compositions are therefore controlled by the proportion of depleted mantle and evolved crustal material incorporated in the melt during crystallization (Kinny and Maas, 2003). Detrital zircon Hf isotope signatures can be used to monitor juvenile magmatic contributions and periods of crustal reworking that are apparently defined by excursions towards subchondritic isotope values or “pull-downs” (e.g., Gehrels and Pecha, 2014; DeCelles and Graham, 2015). For example, Pecha et al. (2016) used detrital zircon U-Pb-Hf studies to resolve the timing of crustal thinning (mostly superchondritic Hf isotope values) and crustal thickening (mostly subchondritic Hf isotope values) episodes within the Paleozoic Yukon-Tanana arc of southeastern Alaska.

1.4 Co-authorship statement

The design and identification of this research project are credited to Dr. Luke Beranek and Maurice Colpron (Yukon Geological Survey). The author concluded all primary research activities including stratigraphic log measurement, sample collection, sample preparation, and data reduction. Heavy liquid mineral separation was conducted by the author under the supervision of Dr. John Hanchar. The author did the LASS analyses and U-Pb-Hf data reduction with assistance from Dr. Rebecca Lam and Dr. Markus Wölle. The primary editor of this manuscript is Dr. Luke Beranek, with secondary editing by Dr. John Hanchar. Dr. Matt

Hutchison (Yukon Geological Survey) contributed as a coauthor on a current research publication for this project (van Drecht et al., 2017).

1.5 Presentation

This thesis is written in manuscript format and consists of three chapters and supplementary appendices. The first chapter is an introduction and overview chapter that discusses the regional geology of the study area, previous work, methods, and objectives of this study. Chapter 2 presents the primary observations and findings of this study. This chapter is written as a manuscript and intended for publication in *Lithosphere* or an equivalent international peer-reviewed scientific journal. The final chapter provides a summary and discusses future work that will contribute to the findings of this study. Repetition occurs between chapters and is a result of the manuscript format of this thesis. Supplementary appendices include measured stratigraphic logs, photomicrographs, cathodoluminescence images of detrital zircon grains and laser spot locations, U-Pb and Hf isotope ratio datasets, Isoplot diagrams, and current research articles published in Yukon Geology and Exploration 2017 and 2018.

References

Anfinson, O.A., Leier, A.L., Gaschnig, R., Embry, A.F., and Dewing, K., 2012, U-Pb and Hf isotopic data from Franklinian Basin strata: insights into the nature of Crockerland and the timing of accretion, Canadian Arctic Islands: Canadian Journal of Earth Sciences, v. 49, p 1316-1328, doi:10.1139/e2012-067.

Beranek, L.P., Mortensen, J.K., Orchard, M.J., and Ullrich, T., 2010, Provenance of North American Triassic strata from west-central and southeastern Yukon: correlations with coeval strata in the Western Canada Sedimentary Basin and Canadian Arctic Islands: Canadian Journal of Earth Sciences, v. 47, p. 53-73, doi: 10.1139/E09-065.

Beranek, L.P., and Mortensen, J.K., 2011, The timing and provenance record of the Late Permian Klondike orogeny in northwestern Canada and arc-continent collision along western North America: Tectonics, v. 30, 23 p, doi:10.1029/2010TC002849.

Beranek, L.P., van Staal, C.S., McClelland, W.C., Israel, S., and Mihalynuk, M., 2013, Detrital zircon Hf isotopic composition indicate a northern Caledonian connection for the Alexander terrane: Lithosphere, v. 5, p. 163-168, doi:10.1130/L255.1

Berman, R.G., Ryan, J.J., Gordey, S.P., and Villeneuve, M., 2007, Permian to Cretaceous polymetamorphic evolution of the Stewart River region, Yukon-Tanana terrane, Yukon, Canada: P-T evolution linked with in situ SHRIMP monazite geochronology: Journal of Metamorphic Geology, v. 25, p. 803-827, doi:10.1111/j.1525-1314.2007.00729.x.

Bordet, E., 2016, Preliminary results on the Middle Triassic-Middle Jurassic stratigraphy and structure of the Teslin Mountain area, southern Yukon, *in* MacFarlane, K.E., and Nordling, M.G., eds., Yukon Exploration and Geology, 2015: Yukon Geological Survey, p.43-61.

Bordet, E., 2017, Updates on the Middle Triassic-Middle Jurassic stratigraphy and structure of the Teslin Mountain and east Lake Laberge areas, south-central Yukon, *in* MacFarlane, K.E., and Weston, L.H., eds., Yukon Exploration and Geology 2016: Yukon Geological Survey, p.1-24.

Bouvier, A., Vervoort, J.D., and Patchett, P.J., 2008, The Lu-Hf and Sm-Nd composition of CHUR: Constraints from unequilibrated chondrites and implications for the bulk composition of terrestrial planets: Earth and Planetary Science Letter, v. 273, p. 48-57, doi:10.1016/j.epsl.2008.06.010.

Cairnes, D.D., 1910, Preliminary memoir on the Lewes and Nordenskiöld rivers coal district, Yukon Territory: Geological Survey of Canada, Memoir 5, 70 p.

Cawood, P.A., Kröner, A., and Collins, W.J., 2009, Accretionary orogens through Earth history: Geological Society, London, Special Publication 318, p. 1-36, doi:10.1144/SP318.1.

Cawood, P.A., Hawkesworth, C.J., and Dhuime, B., 2012, Detrital zircon record and tectonic setting: Geology, v. 40, p. 875-878, doi:10.1130/G32945.1.

Clark, A.D., 2017, Tectonometamorphic history of mid-crustal rocks at Aishihik Lake, southwest Yukon: Simon Fraser University (MSc thesis), Burnaby, Canada, 153 p.

Colpron, M., Nelson, J.L., and Murphy, D.C., 2006, A tectonostratigraphic framework for the pericratonic terranes of the northern Cordillera, *in* Colpron, M. and Nelson, J.L., eds., Paleozoic Evolution and Metallogeny of Pericratonic Terranes at the Ancient Pacific Margin of North America, Canadian and Alaskan Cordillera: Geological Association of Canada, Special Paper 45, p. 1-23.

Colpron, M., Nelson, J.L., and Murphy, D.C., 2007, Northern Cordilleran terranes and their interactions through time: Geological Society of American Today, v.17, no. 4/5, doi:10.1130/GSAT01704-5A.1.

Colpron, M., and Friedman, R.M., 2008, U-Pb zircon ages for the Nordenskiöld formation (Laberge Group) and Cretaceous intrusive rock, Whitehorse trough, Yukon, *in* Emond, D.S., Blackburn, L.R., Hill, R.P., and Weston, L.H., eds., Yukon Exploration and Geology 2007: Yukon Geological Survey, p. 139-151.

Colpron, M., Crowley, J.L., Gehrels, G., Long, D.G.F., Murphy, D.C., Beranek, L., and Bickerton, L., 2015, Birth of the northern Cordilleran orogeny, as recorded by detrital zircons in Jurassic synorogenic strata and regional exhumation in Yukon: Lithosphere, v. 7, p. 541-562, doi:10.1130/L451.1

Colpron, M., Israel, S., Murphy, D., Pigage, L., and Moynihan, D., 2016, Yukon Bedrock Geology Map: Yukon Geological Survey, Open File 2016-1, 1:10 000 scale map and legend.

Colpron, M., Sack, P., Crowley, J., Allan, M., 2017, Late Triassic to Middle Jurassic magmatism in the Intermontane terranes of Yukon: Cordilleran Tectonics Workshop, Vancouver, BC, Abstracts, p. 30.

DeCelles, P.G., and Graham, S.A., 2015, Cyclical processes in the North American Cordilleran orogenic system: *Geology*, v. 43, p. 499-502, doi:10.1130/G36482.1.

Dickie, J.R., and Hein, R.J., 1988, Facies and depositional setting of Laberge conglomerates (Jurassic), Whitehorse trough, *in* Yukon Geology, v. 2: Exploration and Geological Services Division, Yukon, Indian and Northern Affairs Canada, p. 26-32.

Dickie, J.R., and Hein, F.J., 1995, Conglomeratic fan deltas and submarine fans of the Jurassic Laberge Group, Whitehorse trough, Yukon Territory, Canada: fore-arc sedimentation and unroofing of a volcanic island-arc complex: *Sedimentary Geology*, v. 98, p. 263–292, doi:10.1016/0037-0738(95)00036-8.

Dickinson, W.R., 1974, Plate tectonics and sedimentation, *in* Dickinson, W.R., ed., Tectonics and Sedimentation: Society of Economic Paleontology and Mineralogists Special Publication 22, p. 1-27.

Dickinson, W.R., and Suczek, C.A., 1979, Plate Tectonic and Sandstone Compositions: The American Association of Petroleum Geologists, v. 36, no. 12, p. 2164-2182.

Dickinson, W.R., and Valloni, R., 1980, Plate settings and provenance of sands in modern ocean basins: *Geology*, v. 8, p.82-86.

Dickinson, W.R., Beard, L.S., Brakenridge, G.R., Erjavec, J.L., Ferguson, R.C., Inman, K.F., Kneppe, R.A., Lindberg, F.A., and Ryberg, P.T., 1983, Provenance of North American

Phanerozoic sandstones in relation to tectonic setting: Geological Society of America Bulletin, v. 94, p. 222-235.

Dickinson, W.R., and Gehrels, G.E., 2009, Use of U-Pb ages of detrital zircons to infer maximum depositional ages of strata: A test against a Colorado Plateau Mesozoic database: Earth and Planetary Science Letters, v. 288, p. 115-125, doi:10.1016/j.epsl.2009.09.013.

Fedo, C.M., Sircombe, K.N., Rainbird, R.H., 2003, Detrital Zircon Analysis of the Sedimentary Record: Reviews in Mineralogy and Geochemistry, v. 53, 1, p. 277-301.

Fisher C.M., Vervoort, J.D., and DuFrane, S.A., 2014, Accurate Hf isotopic determinations of complex zircons using the “laser ablation split stream” method: Geochemistry, Geophysics, Geosystems, v. 15, p. 121-139, doi:10.1002/2013GC004962.

Flowerdew, M.J., Millar, I.L., Curtis, M.L., Vaughan, A.P.M., Horstwood, M.S.A., Whitehouse, M.J., and Fanning, C.M., 2007, Combined U-Pb geochronology and Hf isotope geochemistry of detrital zircons from early Paleozoic sedimentary rocks, Ellsworth-Whitmore Mountains block, Antarctica: Geological Society of American Bulletin, v. 119, p. 275-288, doi:10.1130/B25891.1.

Gehrels, G., 2014, Detrital Zircon U-Pb Geochronology Applied to Tectonics: Annual Review of Earth and Planetary Sciences, v. 42, p. 127-149, doi:10.1146/annurev-earth-050212-124012.

Gehrels, G., and Pecha, M., 2014, Detrital zircon U-Pb geochronology and Hf isotope geochemistry of Paleozoic and Triassic passive margin strata of western North America: Geosphere, v. 10, p. 49-65, doi:10.1130/GES00889.1.

Goudie, D.J., Fisher, C.M., Hanchar, J.M., and Crowley, J.L., 2014, Simultaneous in situ determination of U-Pb and Sm-Nd isotopes in monazite by laser ablation ICP-MS: Geochemistry, Geophysics, Geosystems, v. 15, p. 2575-2600, doi:10.1002/2014GC005431.

Hanchar, J.M. and Watson, E.B., 2003, Zircon Saturation Thermometry: Reviews in Mineralogy and Geochemistry, v. 53, p. 89-112, doi:10/2113/0530089.

Hart, C.J.R., 1997, A Transect across Northern Stikinia: Geology of the Northern Whitehorse Map Area, Southern Yukon Territory (105D/13–16): Exploration and Geological Services Division, Yukon Region, Indian and Northern Affairs Canada, Bulletin 8, 112 p.

Hart, C.J.R., and Radloff, J.K., 1990, Geology of Whitehorse, Alligator Lake, Fenwick Creek, Carcross and Part of Robinson Map Areas (105D/11, 6, 3, 2 & 7): Yukon Geological Survey Open-File 1990-4(G), scale 1:50,000.

Hart, C.J.R., Dickie, J.R., Ghosh, D.K., and Armstrong, R.L., 1995, Provenance constraints for Whitehorse trough conglomerate: U-Pb zircon dates and initial Sr ratios of granitic clasts in Jurassic Laberge Group, Yukon Territory, *in* Miller, D.M., and Busby, C., eds., Jurassic Magmatism and Tectonics of the North American Cordillera: Geological Society of America Special Paper 299, p. 47–63.

Hawkesworth, C.J., and Kemp, A.I.S., 2006, Using hafnium and oxygen isotopes in zircons to unravel the record of crustal evolution: Chemical Geology, v. 226, p. 144-162.

Hutchison, M.P., 2017, Whitehorse trough: Past, present and future petroleum research – with a focus on reservoir characterization of the northern Laberge Group: Yukon Geological Survey, Open File 2017-2, 48 p.

Iizuka, T., Komiya, T., Rino, S., Maruyama, S., Hirata, T., 2010, Detrital zircon evidence for Hf isotopic evolution of granitoid crust and continental growth: *Geochimica et Cosmochimica Acta*, v. 74, p. 2450-2472.

Ingersoll, R.V., Kretchmer, A.G., and Valles, P.K., 1993, The effect of sampling scale on actualistic sandstone petrofacies: *Sedimentology*, v. 40, p. 937-953.

Johannson, G.G., Smith, P.L., and Gordey, S.P., 1997, Early Jurassic evolution of the northern

Stikinian arc: evidence from the Laberge Group, northwestern British Columbia:
Canadian Journal of Earth Science, v. 34, p. 1030-1057.

Johnsson, M.J., 1993, The system controlling the composition of clastic sediments, *in*
Johnsson, M.J., and Basu, A., eds., Processes Controlling the Composition of Clastic
Sediments: Geological Society of America Special Paper, 284, p. 1-19.

Johnston, S.T., and Erdmer, P, 1995, Hot-side-up aureole in southwest Yukon and limits on
terrane assembly of the northern Canadian Cordillera: Geology, v. 23, no. 5, p 419-422.

Johnston, S.T., Mortensen, J.K., and Erdmer, P., 1996, Igneous and metaigneous age
constraints for the Aishihik metamorphic suite, southwest Yukon: Canadian Journal of
Earth Sciences, v. 33, p. 1543–1555.

Joyce, N.L., Colpron, M., Allan, M.M., Sack, P.J., Crowley, J.L., and Chapman, J.B., 2016,
New U-Pb zircon dates from the Aishihik batholith, southern Yukon, *in* K.E.
MacFarlane and M.G. Nordling eds., Yukon Exploration and Geology 2015: Yukon
Geological Survey, P.131-149.

Kellett, D.A., Weller, O.M., Zagorevski, A., Regis, D., 2018, A petrochronological approach
for the detrital record: Tracking mm-sized eclogite clasts in the northern Canadian
Cordillera: Earth and Planetary Science Letters, v. 494, p. 23-31,
doi:10.1016/j.epsl.2018.04.036.

Kemp, A.I.S., Hawkesworth, C.J., Paterson, B.A., and Kinny, P.D., 2006, Episodic growth of
the Gondwana supercontinent from hafnium and oxygen isotopes in zircon: Nature, v.
439, p. 580-583.

Kemp, A.I.S., Hawkesworth, C.J., Foster, G.L., Paterson, B.A., Woodhead, J.D., Hergt, J.M.,
Gray, C.M., and Whitehouse, M.J., 2007, Magmatic and Crustal Differentiation History
of Granitic Rocks from Hf-O Isotopes in Zircon: Science, v. 315, p 980-983,
doi:10.1126/science.1136154.

Kinny, P.D. and Mass, R., 2003, Lu-Hf and Sm-Nd isotope systems in zircon: Reviews in Mineralogy and Geochemistry, v. 12, p. 328-34, doi:10.21223/0530327.

Knight, E., Schneider, D.A., and Ryan, J., 2013, Thermochronology of the Yukon-Tanana Terrane, West-Central Yukon: Evidence for Jurassic Extension and Exhumation in the Northern Canadian Cordillera: The Journal of Geology, v. 121, p. 371-400, doi:10.1086/670721.

Link, P.K., Fanning, C.M., and Beranek, L., 2005, Reliability and longitudinal change of detrital-zircon age spectra in the Snake River system, Idaho and Wyoming: An example of reproducing the bump barcode: Sedimentary Geology, v. 182, p. 101-142, doi:10.1016/j.sedgeo.2005.07.012.

Liu, X-C., Wu, Y-B., Fisher, C.M., Hanchar, J.M., Beranek, L., Gao, S., and Wang, H., 2017, Tracing crustal evolution by U-Th-Pb, Sm-Nd, and Lu-Hf isotopes in detrital monazite and zircon from modern rivers: Geology, v. 45, p. 103-106, doi: 10.1130/G38720.1.

Long, D.G.F., 1986, Coal in Yukon, *in* Morin, J.A., ed., Mineral Deposits of the Northern Cordillera: Canadian Institute of Mining and Metallurgy Special Volume 37, p. 311-318.

Lowey, G.W., 2004, Preliminary lithostratigraphy of the Laberge Group (Jurassic), south-central Yukon: Implications concerning the petroleum potential of the Whitehorse trough, *in* Emond, D.S., and Lewis, L.L., eds., Yukon Exploration and Geology 2003: Yukon Geological Survey, p. 129–142.

Lowey, G.W., 2008, Summary of the stratigraphy, sedimentology and hydrocarbon potential of the Laberge Group (Lower–Middle Jurassic), Whitehorse trough, Yukon, *in* Emond, D.S., Blackburn, L.R., Hill, R.P., and Weston, L.H., eds., Yukon Exploration and Geology 2007: Yukon Geological Survey, p. 179–197.

Lowey, G.W., Long, D.G.F., Fowler, M.G., Sweet, A.R., and Orchard, M.J., 2009, Petroleum source rock potential of Whitehorse trough: A frontier basin in south-central Yukon:

Bulletin of Canadian Petroleum Geology, v. 57, p. 350–386,
doi:10.2113/gscpgbull.57.3.350.

Ludwig, K.R., 2008, User's Manual for Isoplot 3.70 – A Geochronological Toolkit for Microsoft Excel: Berkeley Geochronology Center Special Publication 4, 76 p.

McCabe, R., and Uyeda, S., 1983, Hypothetical Model for the Bending of the Mariana Arc *in* Hayes, D. eds., The Tectonic and Geologic Evolution of Southeast Asian Seas and Islands: Part 2: Geophysical Monograph Series, v. 27, p. 281-292.

Mihalynuk, M.G., Nelson, J., and Diakow, L.J., 1994, Cache Creek terrane entrapment: Oroclinal paradox within the Canadian Cordillera: Tectonics, v. 13, p. 575–595, doi:10.1029 /93TC03492.

Morris, J.D., Jezek, P.A., Hart, S.R., and Gill, J.B., 1983, The Halmahera Island, Molucca Sea Collision Zone, Indonesia: A Geochemical Survey *in* Hayes, D. eds., The Tectonic and Geologic Evolution of Southeast Asian Seas and Islands: Part 2: Geophysical Monograph Series, v. 27, p. 373-387.

Mortensen, J.K., 1992, Pre–mid-Mesozoic tectonic evolution of the Yukon-Tanana terrane, Yukon and Alaska: Tectonics, v. 11, p. 836–853, doi:10.1029/91TC01169.

Murphy, D.C., Mortensen, J.K., Piercy, S.J., Orchard, M.J., and Gehrels, G.E., 2006, Mid-Paleozoic to early Mesozoic tectonostratigraphy evolution of Yukon-Tanana and Slide Mountain terranes and affiliated overlap assemblages, Finlayson Lake massive sulphide district, southeastern Yukon, *in* Colpron, M. and Nelson, J.L., eds., Paleozoic Evolution and Metallogeny of Pericratonic Terranes at the Ancient Pacific Margin of North America, Canadian and Alaskan Cordillera: Geological Association of Canada, Special Paper 45, p. 75-105.

Nelson, J.L., and Mihalynuk, M., 1993, Cache Creek ocean: Closure or enclosure?: Geology, v. 21, p. 173-176, doi:10.1130/0091-7613(1993)021<0173:CCOCOE>2.3CO;2.

Nelson, J.L., Colpron, M., Piercey, S.J., Dusel-Bacon, C., Murphy, D.C., and Root, C.F., 2006, Paleozoic tectonic and metallogenic evolution of the pericratonic terranes in Yukon, northern British Columbia and eastern Alaska, *in* Colpron, M. and Nelson, J.L., eds., Paleozoic Evolution and Metallogeny of Pericratonic Terranes at the Ancient Pacific Margin of North America, Canadian and Alaskan Cordillera: Geological Association of Canada, Special Paper 45, p. 323-360.

Nelson, J.L., Colpron, M., and Israel, S., 2013, The Cordillera of British Columbia, Yukon, and Alaska: Tectonics and metallogeny, *in* Colpron, M., Bissig, T., Rusk, B.G., and Thompson, J.F.H., eds., Tectonics, Metallogeny and Discovery: The North American Cordillera and Similar Accretionary Settings: Society of Economic Geologists Special Publication 17, p. 53–103.

Paton, C., Hellstrom, J., Paul, B., Woodhead, J., and Hergt, J., 2011, Iolite: Freeware for the visualisation and processing of mass spectrometric data: Journal of Analytical Atomic Spectrometry, v. 26, p. 2508-2518, doi:10.1039/C1JA10172B.

Pecha, M.E., Gehrels, G.E., McClelland, W.C., Giesler, D., White, C., and Yokelson, I., 2016, Detrital zircon U-Pb geochronology and Hf isotope geochemistry of the Yukon-Tanana terrane, Coast Mountain, southeast Alaska: Geosphere, v. 12, no. 5, doi:10.1130/GES01303.1.

Petrus, J., and Kamber, B.S., 2012, VizualAge: A Novel Approach to Laser Ablation ICP-MS U-Pb Geochronology Data Reduction: Geostandards and Geoanalytical Research, v. 36, 24 p., doi:10.1111/j.1751-908X.2012.00158.x.

Piercey, S.J., Nelson, J.L., Colpron, M., Dusel-Bacon, C., Simard, R-L. and Roots, C.F., 2006, Paleozoic magmatism and crustal recycling along the ancient Pacific margin of North American, northern Canadian Cordillera, *in* Colpron, M. and Nelson, J.L., eds., Paleozoic Evolution and Metallogeny of Pericratonic Terranes at the Ancient Pacific Margin of North America, Canadian and Alaskan Cordillera: Geological Association of Canada, Special Paper 45, p. 281-322.

Sack, P.J., Colpron, M., Crowley, J.L., Ryan, J.J., Allan, M.M., Beranek, L.P., Joyce, N., and Mortensen, J.K., 2019, Atlas of Late Triassic-Jurassic plutons in Yukon: Yukon Geological Survey Open File, in press.

Schiarizza, P., 2011, Geology of the Kutcho assemblage between Kutcho Creek and the Tucho River, northern British Columbia (NTS 104I/01), *in* Geological Fieldwork 2010: British Columbia Ministry of Energy, Mines and Petroleum Resources paper 2011-1, p. 99-118.

Schiarizza, P., 2012, Geology of the Kutcho Assemblage between the Kehlechoa and Tucho Rivers, northern British Columbia (NTS 104I/01, 02), *in* Geological Fieldwork 2011: British Columbia Ministry of Energy, Mines and Petroleum Resources paper 2012-1, p. 75-98.

Shirmohammad, F., Smith, P.L., Anderson, R.G., and McNicoll, V.J., 2011, The Jurassic succession at Lisadale Lake (Tulsequah map area, British Columbia, Canada) and its bearing on the tectonic evolution of the Stikine terrane: *Volumnia Jurassica*, v. 9, p. 43-60.

Simard, R.-L., Dostal, J., and Roots, C.F., 2003, Development of late Paleozoic volcanic arcs in the Canadian Cordillera: An example from the Klinkit Group, northern British Columbia and southern Yukon: *Canadian Journal of Earth Sciences*, v. 40, p. 907–924, doi:10.1139/e03-025.

Sláma, J., Kosler, J., Condon, D., Crowley, J.L., Gerdes, A., Hanchar, J.M., Horstwood, S.A., Morris, G.A., Nasdala, L., Norberg, N., Schaltegger, U., Schoene, B., Tubrett, M., and Whitehouse, M.J., 2008, Plešovice zircon – A new natural reference material for U-Pb and Hf isotopic microanalysis: *Chemical Geology*, v. 249, p. 1-35, doi:10.1016/j.chemgeo.2007.11.005.

Tafti, R., 2005, Nature and Origin of the Early Jurassic Copper (-Gold) Deposits at Minto and Williams Creek, Carmacks Copper Belt, Western Yukon: Examples of Deformed

Porphyry Deposits [M.Sc. thesis]: Vancouver, British Columbia, Canada, University of British Columbia, 213 p.

Tafti, R., and Mortensen, J.K., 2004, Early Jurassic porphyry (?) copper (-gold) deposits at Minto and Williams Creek, Carmacks Copper Belt, western Yukon, *in* Emond, D.S., and Lewis, L.L., eds., Yukon Exploration and Geology 2003: Yukon Geological Survey, p. 289-303.

Tempelman-Kluit, D.J., 1979, Transported cataclasite, ophiolite and granodiorite in Yukon: Evidence of arc-continent collision: Geological Survey of Canada, Paper 79-14, 27 p.

Tempelman-Kluit, D.J., 1984, Geology, Laberge (105E) and Carmacks (105I), Yukon Territory: Geological Survey of Canada, Open File 1101, scale 1:250 000.

Tempelman-Kluit, D.J., 2009, Geology of Carmacks and Laberge map areas, central Yukon: Incomplete draft manuscript on stratigraphy, structure and its early interpretation (ca. 1986): Geological Survey of Canada, open File 5982, 399 p.

van Drecht, L.H., Beranek, L.P., and Hutchison, H., 2017, Jurassic stratigraphy and tectonic evolution of the Whitehorse trough, central Yukon: Project outline and preliminary field results, *in* MacFarlane, K.E., and Weston, L.H., eds., Yukon Exploration and Geology 2016: Yukon Geological Survey, p. 207-223.

van Drecht, L.H., and Beranek, L.P., 2018, New investigations of basal Laberge Group stratigraphy Whitehorse trough, central Yukon, *in* MacFarlane, K.E., eds., Yukon Exploration and Geology 2017: Yukon Geological Survey, p. 151-163.

Vervoort, J.D., and Blichert-Toft, J., 1999, Evolution of the depleted mantle: Hf isotope evidence from juvenile rocks through time: *Geochemica et Cosmochimica Acta*, v. 63, p. 533-556, doi:10.1016/S0016-7037(98)00274-9.

Vervoort, J.D., and Patchett, P.J., 1996, Behaviour of hafnium and neodymium isotopes in the crust: Constraints from Precambrian crustally derived granites: *Geochemica et Cosmochimica Acta*, v. 60, p. 3717-3733, doi:10.1016/0016-7037(96)00201-3.

Villeneuve, M.E., Ryan J.J., Gordey, S.P., and Piercy, S.J., 2003, Detailed thermal and provenance history of the Stewart River area (Yukon-Tanana terrane, western Yukon) through application of SHRIMP, $^{40}\text{Ar}/^{39}\text{Ar}$, and TIMS, *in* Geological Association of Canada-Mineral Association of Canada annual meeting. Vancouver, BC, Geological Association of Canada, Abstract 344.

Wernicke, B., and Klepaki, D.W., 1988, Escape hypothesis for the Stikine block: *Geology*, v. 16, p.461-464, doi:10.1130/0091-7613(1988)016<0461:EHFTSB>2.3.CO;2.

Wheeler, J.O., 1961, Whitehorse map-area, Yukon Territory: Geological Survey of Canada, Memoir 312, 156 p.

White, D., Colpron, M., and Buffett, G., 2012, Seismic and geological constraints on the structure of the northern Whitehorse trough, Yukon, Canada: *Bulletin of Canadian Petroleum Geology*, v. 60, p.239-255.

Wiedenbeck, M., Allé, P., Corfu, F., Griffin, W.L., Meier, M., Oberli, F., Quadt, A.V., Roddick, J.C., and Spiegel, W., 1995, Three natural zircon standards for U-Th-Pb, Lu-Hf, trace element and REE analyses: *Geostandards Newsletter*, v. 19, p. 1-23.

Wilde, S.A., Valley, J.W., Peck, W.H., and Graham, C.M., 2001, Evidence from detrital zircons for the existence of continental crust and oceans on the Earth 4.4 Gyr ago: *Nature*, v. 409, p. 175-178.

Willner, A.P., Gerdes, A., and Massonne, H.-J., 2008, History of crustal growth and recycling at the Pacific convergent margin of South America at latitudes 29°-36°S revealed by a U-Pb and Lu-Hf isotope study of detrital zircon from late Paleozoic accretionary systems: *Chemical Geology*, v. 253, p. 114-129, doi:10.106/j.chemgeo.2008.04.016.

Wu, F-Y., Ji, W-Q., Liu, C-Z., Chung, S-L., 2010, Detrital zircon U-Pb and Hf isotopic data from the Xigaze fore-arc basin: Constraints on Transhimalayan magmatic evolution in southern Tibet: Chemical Geology, v. 271, p. 13-25,
doi:10.1016/j.chemgeo.2009.12.007.

Yukon Geological Survey, 2017. Yukon Digital Bedrock geology:
www.geology.gov.yk.ca/update_yukon_bedrock_geology_map.html, accessed: February 2, 2017.

Chapter 1 Figures

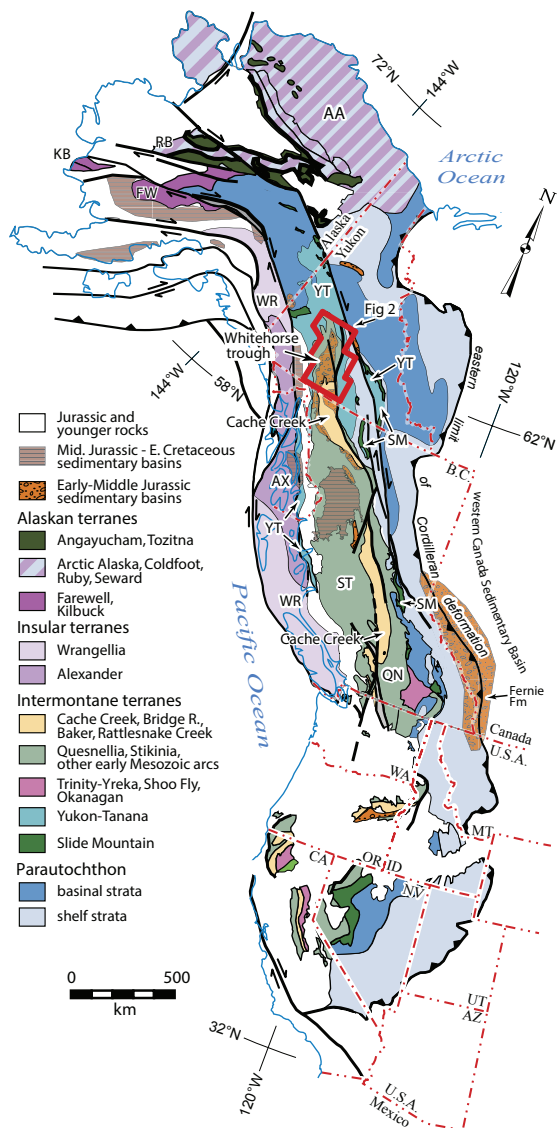


Figure 1.1. Terrane and Jurassic sedimentary basin map of the North American Cordillera after Colpron and Nelson (2011). The red outline shows the location of Figure 1.2.

Abbreviations: AA-Arctic Alaska terrane; AX-Alexander terrane; AZ-Arizona, B.C.-British Columbia; CA-California; FW-Farewell terrane; ID-Idaho; KB-Kilbuck terrane; Mt-Montana; NV-Nevada; Or-Oregon; QN-Quesnellia; RB-Ruby terrane; SM-Slide Mountain terrane; ST-Stikinia terrane; UT-Utah; WA-Washington; WR-Wrangellia terrane; YT-Yukon-Tanana; U.S.A-United States of America.

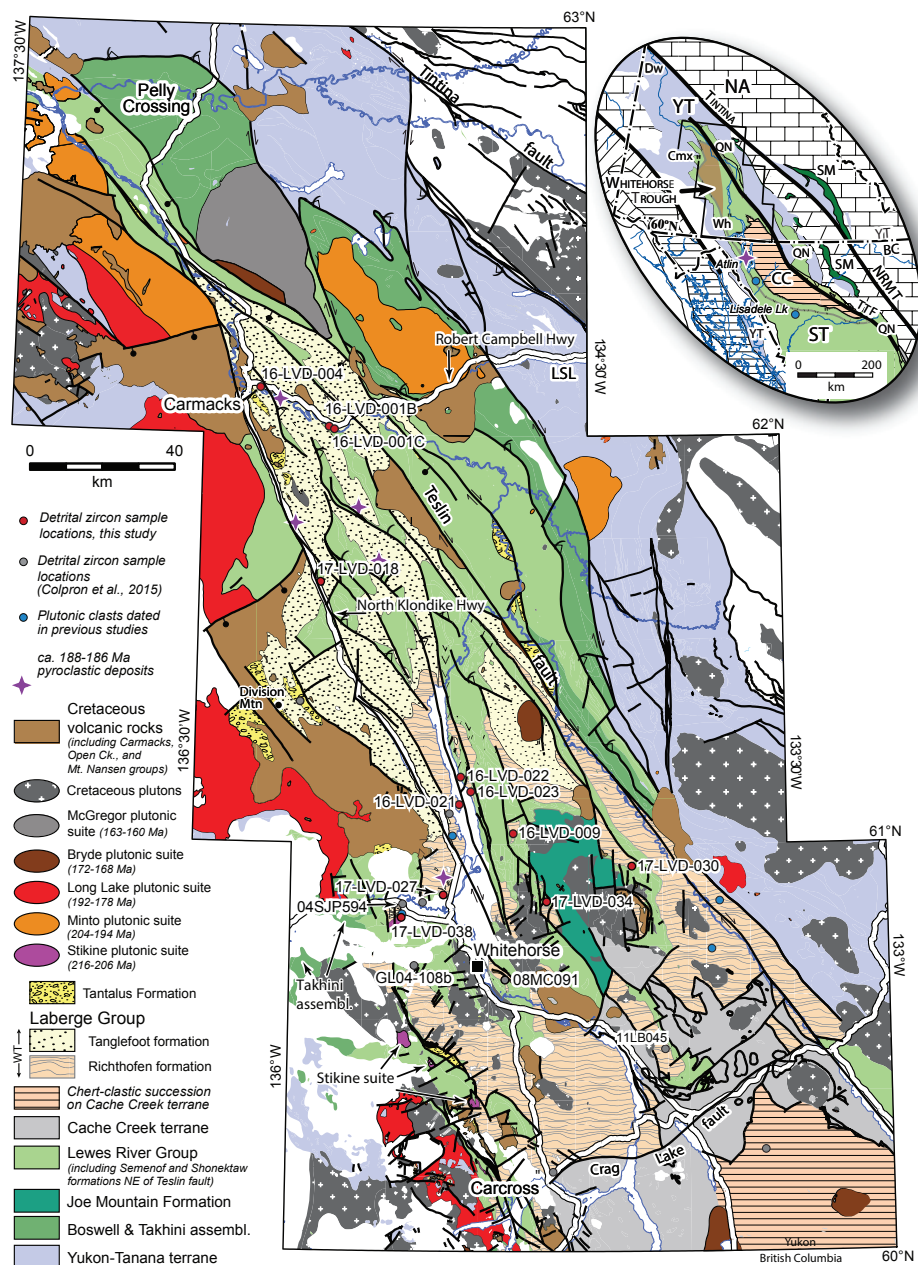


Figure 1.2. Regional geology of the Whitehorse trough area modified from Colpron et al. (2015). Detrital zircon sampling locations for this study are denoted by red dots. Grey dots denote detrital zircon sample locations of Colpron et al. (2015) and blue dots denote previously dated plutonic clasts by Hart et al. (1995) and Gordey et al. (1998). Purple stars denote locations of pyroclastic deposits dated by Colpron and Friedman (2008) and Hart et al. (1997). The inset shows Intermontane terranes and their present geometry. Abbreviations: CC-Cache Creek terrane; CMx-Carmacks; Dw-Dawson; LSL-Little Salmon Lake; NA-rocks of ancestral North America; NRMT-Northern Rocky Mountain Trench Fault; QN-Quesnellia; SM-Slide Mountain terrane; ST-Stikinia; TTF-Teslin-Thibert fault; Wh-Whitehorse; YT-Yukon-Tanana terrane.

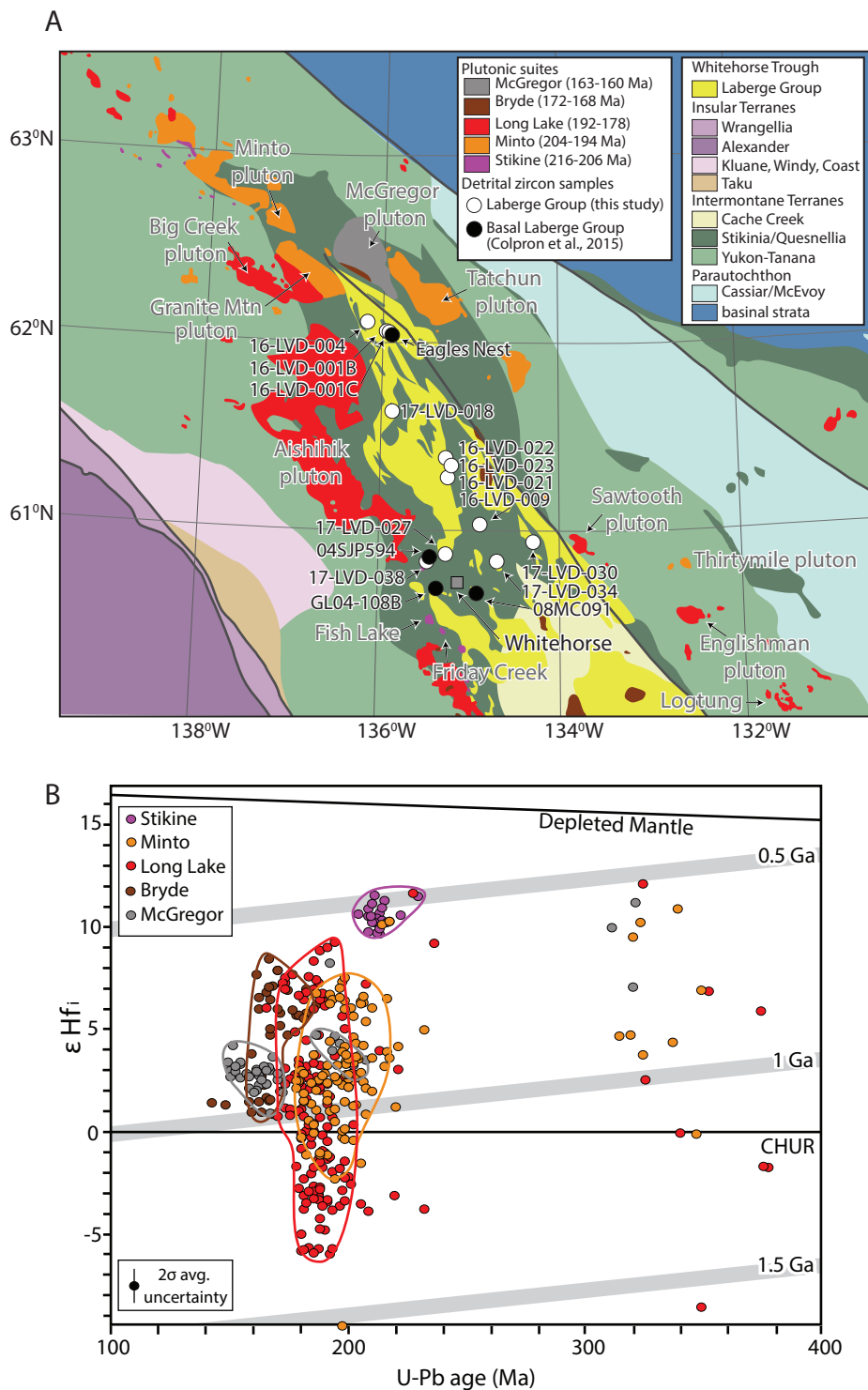


Figure 1.3. (A) Map of the Insular and Intermontane terranes, North American parautochthon, Whitehorse trough, and Late Triassic-Middle Jurassic plutonic suites after Colpron (2018). Detrital zircon sample locations from this study are denoted by white dots and basal detrital zircon samples of Colpron et al. (2015) are denoted by black dots. (B) $\epsilon\text{Hf}_{(t)}$ vs. U-Pb age plot of the Late Triassic to Middle Jurassic plutonic suites. DM-depleted mantle (Vervoort and Blichert-Toft, 1999); CHUR-Chondritic uniform reservoir (Bouvier et al., 2008); Grey crustal evolution lines correspond to $^{176}\text{Lu}/^{177}\text{Hf}=0.0115$ (Vervoort and Patchett, 1996; Vervoort et al., 1999).

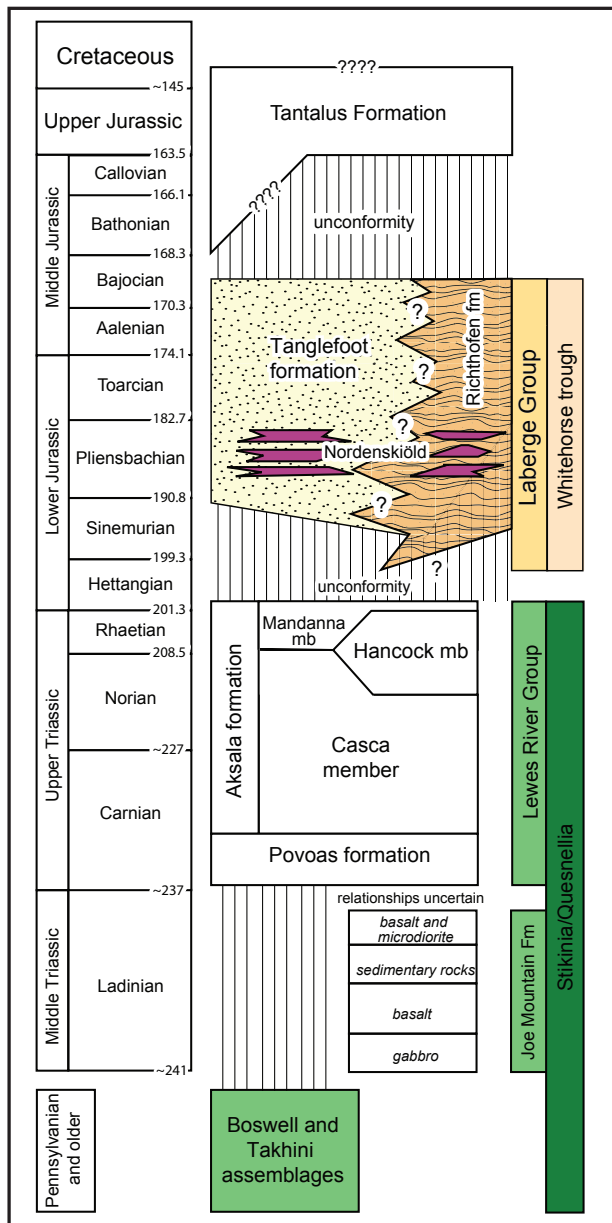


Figure 1.4. Upper Paleozoic-Mesozoic stratigraphy of Stikinia, Quesnellia, and Whitehorse trough complied by Colpron et al. (2015).

Chapter 2: Detrital zircon U-Pb geochronology and Hf isotope geochemistry of the Laberge Group, central Yukon: synorogenic siliciclastic record of early Mesozoic crustal thickening and tectonic evolution of the Whitehorse trough in the northern Canadian Cordillera

2.1 Abstract

Lower to Middle Jurassic syn-collisional strata of the Laberge Group record the basin filling history of the Whitehorse trough in central Yukon, Canada, and constrain the timing of early Mesozoic ocean closure, collision, and subsequent exhumation of the northern Intermontane terranes along western North America. New detrital zircon U-Pb-Hf results acquired by the laser ablation split-stream technique define Early Jurassic maximum depositional ages for basal Laberge Group strata and indicate that the Whitehorse trough initiated by the Sinemurian as a long, narrow collisional basin that subsequently extended to the west, east, and south by Aalenian time. The initial shape and subsidence history of the basin imply a pull-apart history for the Whitehorse trough that resulted from sinistral strike-slip faulting during the south-directed closure of the northern Cache Creek Ocean and time-transgressive collision between Yukon-Tanana-Stikinia and Quesnellia.

Late Triassic-Early Jurassic (216-178 Ma) and Paleozoic (390-252 Ma) detrital zircon grains correspond to local derivation from collision-related plutons and basement domains of the Yukon-Tanana, Stikinia, and Quesnellia terranes, respectively. Sediment was transported in south-, east- and west-directed sediment pathways and a Sinemurian-Pliensbachian shift from longitudinal, south-directed transport to transverse, east-directed transport is recorded in

the northern apex of the trough. Detrital zircon Hf isotope results show a Late Triassic-Middle Jurassic excursion to subchondritic signatures that coincide with the burial and regional metamorphism of Intermontane terranes and may record the timing of crustal thickening near the northern apex and along the western edge of the basin. Crustal thickening may have begun as early as the Rhaetian and persisted until the Toarcian-Aalenian. Laberge Group deposition was coincident with the establishment of the Canadian Rockies foreland basin system and likely indicates hinterland-retroarc linkages along the northern Cordilleran margin.

2.2 Introduction

The composition of siliciclastic sediments is generally related to plate tectonic setting and scale of the depositional system (e.g., Dickinson and Suczek, 1979; Dickinson and Valloni, 1980; Dickinson et al., 1983; Ingersoll et al., 1993; Link et al., 2005). Locally-derived provenance signatures are predicted for most convergent margin basin deposits that develop in response to crustal thickening, regional uplift, and erosion (e.g., Dickinson, 1974; Cawood et al., 2009, 2012). Detrital zircon U-Pb provenance studies have shown to be especially useful for stratigraphic investigations that attempt to constrain the maximum depositional age, source, and paleogeography of synorogenic rock units, including those along long-lived accretionary margins that are reworked by regional deformation, metamorphism and magmatism (e.g., Willner et al., 2008; Wu et al., 2010; Anfinson et al., 2012). The addition of Hf isotope geochemistry of detrital zircon grains to U-Pb geochronology has provided sediment provenance studies to more fully characterize regional crustal evolution and improve the identification of source regions in modern and ancient mountain belts (e.g., Hawkesworth and Kemp, 2006; Kemp et al., 2006; Flowerdew et al., 2007; Iizuka et al., 2010; Beranek et

al., 2013; Pecha et al., 2016; Liu et al., 2017). Additionally, detrital zircon Hf isotope compositions provide an opportunity to monitor periods of crustal thickening in accretionary mountain belts that are apparently defined by excursions towards subchondritic values during orogenesis, also referred to as “pull-downs” (e.g., Gehrels and Pecha, 2014; DeCelles and Graham, 2015).

The North American Cordillera is an accretionary orogen that consists of parautochthonous North American margin strata in the east and the accreted Intermontane, Insular, and Alaskan terranes in central and western parts of the mountain belt (Fig. 2.1; e.g., Monger and Price, 2002; Nelson et al., 2013). The early Mesozoic accretionary history of the northern Cordillera is marked by the imbrication of the Intermontane terranes and subsequent deposition of synorogenic strata within the Whitehorse trough (Fig. 2.1). The Early to Middle Jurassic basin in central Yukon and northern British Columbia may have initiated in a forearc position adjacent to early Mesozoic arcs, but transitioned into a collision-related depocenter after the closure of the northern Cache Creek Ocean (Fig. 2.1; e.g., Mihalynuk et al., 1994; Dickie and Hein, 1995; English and Johnston, 1995; Nelson et al., 2013; Colpron et al., 2015). Late Triassic-Early Jurassic collision and accretion resulted in crustal thickening and burial of Yukon-Tanana and Stikinia to 5-9 kbar (~18-33 km), followed by exhumation along the eastern, western, and northern flanks of the Whitehorse trough at a rate of ~4 km/m.y. (Johnston and Erdmer, 1995; Johnston et al., 1996; Villeneuve et al., 2003; Berman et al., 2007; Knight et al., 2013; Clark, 2017; Kellett et al., 2018). Erosion and tectonic subsidence in central Yukon resulted in the deposition of the Laberge Group, a ~3000 m-thick succession of marginal-marine and deep-marine strata (e.g., Tempelman-Kluit, 1979; Dickie and Hein, 1994; Mihalynuk et al., 1995; Lowey, 2004; 2008) that were locally sourced from Late

Triassic-Early Jurassic arc- to collision-related plutons and enclosing basement domains of the peri-Laurentian Yukon-Tanana and oceanic Stikinia and Quesnellia terranes (Colpron et al., 2015). The available biostratigraphic and zircon U-Pb data broadly suggest that basal Laberge Group strata in central Yukon young from the east to west between the Sinemurian and Toarcian and imply westerly growth of the Whitehorse trough (Colpron et al., 2015). Laberge Group sedimentation was coeval with initial deposition of the Fernie Formation and foreland basin subsidence in British Columbia and Alberta (Fig. 2.1; Cant and Stockmal, 1989; Price 1994; Pană et al., 2018), which suggests that the Whitehorse trough is genetically linked to the early rise of the Cordilleran orogen (Colpron et al., 2015).

Despite advances in understanding Whitehorse trough stratigraphy (e.g., Hart et al., 1995; Shirmohammad et al., 2011; Colpron et al., 2015), the precise timing of Laberge Group deposition and relative sediment contributions of Yukon-Tanana, Quesnellia, and Stikinia basement assemblages and their Late Triassic-Middle Jurassic plutonic suites during regional exhumation remains uncertain. In this paper, we report the detrital zircon U-Pb and Hf data for 12 Laberge Group rock samples in order to investigate the stratigraphic response of Jurassic unroofing and test the relationships between the timing of terrane accretion, exhumation, and Whitehorse trough sedimentation. The laser ablation split-stream (LASS) technique, which allows for the simultaneous collection of U-Pb and Hf isotopes, was used to discriminate sediment source regions in central Yukon and characterize isotopic trends associated with Jurassic tectonism and crustal thickening in the northern Canadian Cordillera. New maximum depositional ages for the basal Laberge Group and select locations higher in stratigraphy are proposed to constrain the timing of basin development, provenance evolution of the Whitehorse trough, and their significance to orogen development.

2.3 Geological background

The Whitehorse trough is positioned at the center of an inverted ‘V’-shaped configuration characterized by the Intermontane terranes (Yukon-Tanana, Slide Mountain, Stikinia, Quesnellia, and Cache Creek) in the northern Canadian Cordillera (Fig. 2.1; Nelson and Mihalynuk, 1993; Mihalynuk et al., 1994). The evolution of this geometry remains controversial; proposed models include strike-slip duplication of the Intermontane terranes (Wernicke and Klepachki, 1988), and counterclockwise or oroclinal bending of Stikinia and Yukon-Tanana that resulted in the entrapment of oceanic rock units of the Cache Creek terrane (e.g., Nelson and Mihalynuk, 1993; Mihalynuk et al., 1994). Oroclinal bending is considered by most workers as the most viable model to explain this configuration (e.g., Nelson et al., 2013; Colpron et al., 2015). The following section summarizes the tectonic history of the Intermontane terranes and focuses on available whole rock and zircon U-Pb, Nd, and Hf isotopic and geochemical data to provide a framework for potential source regions.

2.3.1 Yukon-Tanana

The Yukon-Tanana terrane consists of variably deformed and metamorphosed mid- to late Paleozoic arc successions (Finlayson, Klinkit, Klondike assemblages) that were built upon and intrude a pre-Late Devonian continental margin basement (Snowcap assemblage) (e.g., Mortensen, 1992; Colpron et al., 2006, 2007). The Middle to Late Devonian Ecstall cycle (390-365 Ma) is the oldest recognized magmatic episode in Yukon-Tanana and documents the establishment of a west-facing continental arc along the western Laurentian margin (e.g., Nelson et al., 2006; Piercy et al., 2006). Arc-related magmatic rocks in the Ecstall belt of

northwestern British Columbia include a Middle Devonian (385 Ma) tonalitic augen gneiss that yields a $\varepsilon_{\text{Nd(t)}}$ value of -4.1 (Table 2.1; Gareau and Woodsworth, 2000). Following the establishment of the Middle to Late Devonian continental arc, slab rollback of the subducting plate resulted in mafic to felsic igneous rocks of the Finlayson cycle (365-357 Ma) that yield arc, arc-rift, and back-arc signatures and are spatially associated with extension-related volcanogenic massive sulphide mineralization (Piercey et al., 2006, Nelson et al., 2006). In the Finlayson Lake region in southeastern Yukon, Finlayson cycle rocks yield $\varepsilon_{\text{Nd(t)}}$ values that range from -9.5 to +8.5 (Table 2.1; Piercey, 2001; Piercey et al., 2002, 2003, 2004). Sustained extension in the backarc region resulted in the separation of the frontal part of the magmatic arc from the continental margin and Late Devonian to Early Mississippian opening of the Slide Mountain Ocean (e.g., Murphy et al., 2006; Colpron et al., 2007). Early Mississippian arc-backarc magmatic activity is assigned to the Wolverine cycle and represents the main period of rifting that separated Yukon-Tanana from the western Laurentian margin (Colpron et al., 2006; Piercey et al., 2006). Wolverine cycle units in the Finlayson Lake, Little Kalzas Lake, and Teslin regions include felsic rocks of the Simpson Range plutonic suite ($\varepsilon_{\text{Nd(t)}}$: -12.9 to -7.4), mafic ($\varepsilon_{\text{Nd(t)}}$: +6.9) to felsic ($\varepsilon_{\text{Nd(t)}}$: -8.2 to -7.1) rocks of the Wolverine Lake group, felsic rocks of the Nisutlin assemblage ($\varepsilon_{\text{Nd(t)}}$: -6.2 to -2.5), and intermediate-felsic rocks of the Little Kalzas formation ($\varepsilon_{\text{Nd(t)}}$: -7.9 to -1.3) (Table 2.1; Creaser et al., 1997; Stevens et al., 1995; Piercey, 2001; Piercey et al., 2003).

By the Late Mississippian, Yukon-Tanana had developed into a pericratonic arc that was separated from the Laurentian margin by the intervening Slide Mountain Ocean, analogous to the modern Japanese arc-Sea of Japan system (e.g., Creaser et al., 1997; Nelson

et al., 2013). This period is designated the Little Salmon cycle (342-314 Ma) and characterized by Late Mississippian arc to intra-arc rift magmatism focused in the southern region of Yukon-Tanana (Colpron et al., 2006, 2007; Piercey et al., 2006). Rocks assigned to the Little Salmon cycle crop out in the Glenyon area of central Yukon and include mafic to felsic rocks of the Tatlmain batholith (340 Ma) and ocean island basalt (OIB)-type rocks of the Little Salmon formation ($\varepsilon_{\text{Nd(t)}}$: +7.3) (Table 2.1; Colpron et al., 2006, Nelson et al., 2006; Piercey et al., 2006; Simard et al., 2007).

The Middle Mississippian to early Permian development of Yukon-Tanana is recorded by Klinkit assemblage volcanic, volcanioclastic, and carbonate rocks, including mafic arc magmatism assigned to the Klinkit cycle (314-269 Ma; Colpron et al., 2006; Piercey et al., 2006). Tholeiitic and calc-alkaline arc rocks of the Klinkit assemblage yield $\varepsilon_{\text{Nd(t)}}$ values of +6.7 to +7.4 in the Wolf Lake-Jennings River region of southern Yukon and $\varepsilon_{\text{Nd(t)}}$ values of +5.4 to +9.3 in the Finlayson Lake region (Table 2.1; Creaser et al., 1999; Simard et al., 2003; Piercey et al., 2006). The superchondritic nature of Klinkit cycle magmatism suggests that depleted asthenosphere was the principal contributor to Pennsylvanian-Early Permian magmatism (Simard et al., 2003; Piercey et al., 2006).

A mid- to late Permian transition to west-dipping subduction along the eastern edge of Yukon-Tanana resulted in the establishment of the Klondike arc (Klondike cycle, 269-253 Ma) and subsequent consumption of the Slide Mountain Ocean (Nelson et al., 2006). Calc-alkaline rocks of the Klondike cycle are predominately represented by augen granitoids (Sulphur Creek orthogneiss), the Klondike schist, and volcanic and volcanioclastic rocks that crop out in the Stewart River, Wolf Lake-Jennings River and Fortymile River localities of

western and southern Yukon (e.g., Mortensen, 1990; Colpron et al., 2006; Piercy et al., 2006). Subchondritic signatures for the augen granitoids ($\epsilon_{\text{Nd(t)}}$: -15.3 to -2.0) and Klondike schist units ($\epsilon_{\text{Nd(t)}}$: -9.9 to -1.5) indicate significant crustal contributions to Klondike magmatism (Metcalfe, 1981; Ruks et al., 2006). Yukon-Tanana was transported cratonward during the closure of the Slide Mountain Ocean and collided with the western Laurentian margin during the late Permian Klondike orogeny (Beranek and Mortensen, 2011).

2.3.2 Slide Mountain

The Slide Mountain terrane is a Late Devonian to mid-Permian oceanic assemblage that is generally in faulted contact with western Laurentian margin rocks to the east and Intermontane arc terranes to the west (e.g., Ferri, 1997; Colpron et al., 2005; Colpron et al., 2006; Murphy et al., 2006; Piercy et al., 2012). Slide Mountain assemblage rocks consist of chert, argillite, basalt, serpentinite, and gabbro units that likely developed in an ocean basin thousands of kilometers wide (Struik and Orchard, 1985; Ferri, 1997). Slide Mountain terrane rocks in Yukon dominantly crop out in the Finlayson Lake region where they have been displaced ~430 km to the southeast by the dextral Tintina fault (Murphy and Mortensen, 2003; Murphy et al., 2006). In southeastern Yukon, mafic and ultramafic rocks of the Campbell Range formation yield $\epsilon_{\text{Nd(t)}}$ values of -4 to +8.9 and mafic rocks of the Anvil assemblage yield $\epsilon_{\text{Nd(t)}}$ values of +4.1 to +6.4 (Table 2.1; Creaser et al., 1997; Piercy et al., 2012). Mississippian to Permian mafic rocks of the Fennell Formation in south-central British Columbia have $\epsilon_{\text{Nd(t)}}$ values of +7.7 to +10.2 (Table 2.1; Smith and Lambert, 1995; Patchett and Gehrels, 1997).

2.3.3 Cache Creek

The Cache Creek terrane includes Pennsylvanian to Early Jurassic ultramafic rocks, mafic volcanic rocks, ribbon chert, and limestone with exotic Tethyan corals and verbeekinid fusulinaceans (Ross and Ross, 1983; Cordey et al., 1987; Stanley, 1994). Late Permian-Early Triassic Kutcho assemblage rocks of the Cache Creek terrane additionally include mafic to felsic volcanic rocks (English and Johnston, 2005; Schiarizza, 2011, 2012). The Cache Creek terrane was emplaced on top of Stikinia following the closure of the Cache Creek Ocean through bilateral subduction beneath Stikinia and Quesnellia (Mihalynuk et al., 2004, Nelson et al., 2013). In central British Columbia, Cache Creek terrane rocks yield $\varepsilon_{\text{Nd(t)}}$ values of +4.3 to +8.3 and Kutcho assemblage rocks yield $\varepsilon_{\text{Nd(t)}}$ values of +7.5 to +9.1 (Table 2.1; Smith and Lambert, 1995; Childe and Thompson, 1997; Patchett and Gehrels, 1997). Greywacke units in southern Yukon that are correlative with the Laberge Group yield unimodal Late Triassic to Early Jurassic detrital zircon age distributions with a ca. 208 Ma age peak (Colpron et al., 2015).

2.3.4 Stikinia and Quesnellia

Stikinia and Quesnellia are comprised of Mississippian to Permian arc-related basement rocks, Triassic plutonic and volcanic rocks, and Jurassic volcanic and sedimentary rocks (e.g., Monger et al., 1991; Hart, 1997; Colpron et al., 2006; Nelson et al., 2006, 2013; Sack et al., 2019). The isotopic compositions of Stikinia and Quesnellia rocks are remarkably similar, however, the terranes are separated by the Cache Creek terrane (e.g., Dostal et al., 1999, 2009; Mihalynuk et al., 2004). Quesnellia basement rocks (Lay Range succession and

Harper Ranch Group) are consistent in stratigraphy, age, and geochemistry to the Late Mississippian to early Permian Klinkit assemblage (e.g., Simard et al., 2003; Colpron et al., 2007) and are inferred to link the development of Quesnellia with Yukon-Tanana (e.g., Simard et al., 2003; Colpron et al., 2007; Nelson et al., 2013).

Basement rocks of Stikinia and Quesnellia in central Yukon include volcanic, siliciclastic, and carbonate rocks of the Mississippian Takhini assemblage and Upper Devonian to Lower Mississippian Boswell assemblage (e.g., Tempelman-Kluit, 1984; Colpron et al., 2006). The Takhini assemblage crops out west of Whitehorse, whereas the Boswell assemblage crops out along the eastern edge and north of the Whitehorse trough (Fig. 2.2; Hart, 1997; Simard and Devine, 2003; Colpron et al., 2016). The Boswell assemblage is overlain by the Upper Triassic Semenof formation, which consists of augite-phyric basalt, andesite, volcaniclastic rocks and minor carbonate rocks (Tempelman-Kluit, 1984, Simard and Devine, 2003). Correlative Upper Triassic volcanic and sedimentary rocks of the Quesnel Takla Group in north-central British Columbia yield $\varepsilon_{\text{Nd(t)}}$ values of +6.0 to +8.0 (Table 1; Dostal et al., 2009).

The Middle Triassic volcanic Joe Mountain formation, Upper Triassic volcanic Povoas formation, and Upper Triassic siliciclastic strata of the Aksala formation overlie Paleozoic basement rocks and represent Mesozoic Stikinia in central Yukon (Fig. 2.3). The Middle Triassic Joe Mountain formation consists of pillow basalt, massive basalt, siliciclastic and calcareous strata, and microdiorite and gabbro intrusions with pervasive low temperature chlorite and epidote alteration (Hart, 1997). Rocks of the Joe Mountain formation primarily crop out in the Joe Mountain and Mount Byng region east of Whitehorse (Fig. 2.2) and yield

island arc tholeiite and mid-ocean ridge geochemical affinities (Hart, 1997; Bordet, 2016). The Carnian Povoas formation overlies the Joe Mountain formation and consists of high-K basalt, andesite, and volcanic breccia with island arc to calc-alkaline geochemical signatures (Fig. 2.3; Hart, 1997). Rocks assigned to the Povoas formation crop out in central, northern, and eastern regions of the Whitehorse trough. In north-central British Columbia, the correlative Upper Triassic Takla Group of Stikinia yields tholeiitic to calc-alkaline signatures and $\epsilon_{\text{Nd(t)}}$ values of +6.2 to +7.7 (Table 2.1; Dostal et al., 1999).

The Upper Triassic Aksala formation was deposited during a volcanic lull and consists of shallow-water, arc-marginal rocks of the Casca (Carnian-Norian), Hancock (Norian-Rhaetian) and Mandanna (Rhaetian) members (Fig. 2.3; Tempelman-Kluit, 1984; Hart 1997). The basal Casca member consists of lithic sandstone, argillite, and conglomerate units that are overlain by reefal limestone of the Hancock member (e.g., Tempelman-Kluit, 1984; Hart, 1997; Bordet, 2016, 2017). Maroon lithic sandstone, mudstone, and conglomeratic units of the Mandanna member, which overlies and interfingers with the Hancock member, are discontinuous across central Yukon (Tempelman-Kluit, 1984; Dickie and Hein, 1995; Hart, 1997).

2.3.5 Tectonic evolution

Westward subduction that led to the closure of the Slide Mountain Ocean is linked to a mid- to late Permian polarity reversal beneath the Yukon-Tanana, Stikinia, and Quesnellia terranes (Tempelman-Kluit 1979; Mihalynuk et al., 1994; Nelson et al., 2013). The Intermontane arc terranes were subsequently transported cratonwards and within proximity to the western Laurentian margin by the late Permian (Beranek et al., 2010; Beranek and

Mortensen, 2011). Following the final closure of the Slide Mountain Ocean, the polarity of subduction reversed and eastward subduction initiated beneath the western edge of North America by the Middle to Late Triassic (Beranek and Mortensen, 2011; Nelson et al, 2013). A Permian-Triassic intraoceanic arc (Kutcho arc) carried towards the margin on the downgoing plate collided with the northern Cordilleran margin by the latest Triassic (e.g., Mihalynuk et al., 1994; Schiarizza 2011, 2012). Mihalynuk et al. (1994) suggested that the configuration of Yukon-Tanana, Stikinia, Quesnella, and the impinging Kutcho arc are analogous to the modern Aleutian and Kurile arcs and Emperor Seamount chain in the North Pacific Ocean. The collision of the Kutcho arc and/or seafloor spreading behind Stikinia are inferred as the potential driving forces for oroclinal bending, where Stikinia and Quesnella acted as the outer and inner limbs, respectively, and Yukon-Tanana as the hinge (Mihalynuk et al., 1994). Counterclockwise rotation isolated the Cache Creek Ocean between Stikinia and Quesnella in the Early Jurassic (Mihalynuk et al., 1994). A modern analogue for the initiation of oroclinal bending is observed in the southwest Pacific Ocean with the collision of the Carolina Rise and Mariana arc, which has produced an oroclinal bend where the Yap and Mariana trenches act as the limbs (McCabe and Uyeda, 1983; Mihalynuk et al., 1994). This arc-arc collision and seafloor spreading in the Philippine Sea resulted in a greater than 50° clockwise rotation of Guam, however, an oceanic assemblage is not entrapped in the Carolina Rise region (McCabe and Uyeda, 1983; Mihalynuk et al., 1994). Continued rotation of Stikinia caused the subduction of Cache Creek oceanic crust to transition from a single eastward subduction zone to a bivergent system with westward subduction beneath the Stikinia terrane and eastward subduction beneath the Quesnella terrane (Mihalynuk et al., 1994). A modern analogue to this bivergent tectonic configuration occurs between the Eurasian and Philippine plates where

oceanic assemblages of the Molucca Sea are subducting eastward beneath the Halmahera arc and westward beneath the Sangihe arc (Morris et al., 1983; Mihalynuk et al., 1994). The Whitehorse trough was deposited on top of the northern Intermontane terranes and developed near the hinge of the south-facing orocline (e.g., Tempelman-Kluit, 1979; Mihalynuk et al., 1994; Colpron et al., 2015). Dickie and Hein (1995) suggested that initial subsidence in the basin was irregular and rapid and is likely attributed to a combination of movement along basin-bounding faults and relative sea level rise. The southward-closing Cache Creek Ocean was consumed by Middle Jurassic time and its oceanic assemblages were emplaced onto Stikinia along regional thrust faults, marking the final accretion of the Intermontane terranes against the continental margin (e.g., Mihalynuk et al., 1994, 2004; Nelson et al., 2013).

2.4 Whitehorse trough geology

2.4.1 Laberge Group stratigraphy

The Whitehorse trough is an extensive sedimentary basin that extends >600 km from the Carmacks region of central Yukon to the Dease Lake region of northern British Columbia (Fig. 2.1). Lower to Middle Jurassic Laberge Group strata define the Whitehorse trough and comprise ~3000 m of immature siliciclastic strata that unconformably overlie different units of the Lewes River Group (Fig. 2.2; e.g., Wheeler, 1961; Tempelman-Kluit, 1984; Dickie and Hein, 1995; Lowey, 2008). In central Yukon, the Tanglefoot and Richthofen formations constitute the Laberge Group (Tempelman-Kluit, 1984; Dickie and Hein, 1995; Lowey, 2004). The Tanglefoot formation consists of sandstone, mudstone, and conglomerate units with abundant coal, terrestrial plant material, and vertebrate fossils that are indicative of marginal

marine to tidal environments, whereas the Richthofen formation contains graded siltstone to sandstone and mudstone couplets and conglomerate units with ammonites, belemnites, planktonic fossils, and trace fossils (*Helminthopsis*, *Phycosiphon*, *Planolites*) characteristic of deep marine environments (e.g., Wheeler, 1961; Tempelman-Kluit, 1984; Long 1986; Hart, 1997; Gordey et al., 1998; Lowey, 2004; Colpron et al., 2015; van Drecht et al., 2017).

Tanglefoot and Richthofen formation strata are restricted to the northern and central regions of the Whitehorse trough, respectively, suggesting a south-directed deepening of the basin (Tempelman-Kluit, 1984; Dickie and Hein, 1995; Lowey, 2004, 2008; Hutchison, 2017). Epiclastic and felsic tuff and flow units assigned to the Nordenskiöld dacite occur in both formations (Tempelman-Kluit, 1984) and record Pliensbachian eruptive events at 188.1 ± 0.4 Ma, 187.2 ± 0.4 Ma, and 186.5 ± 0.3 Ma (Colpron and Friedman, 2008).

Clast- to matrix-supported, polymictic, cobble to boulder (volcanic, plutonic, sedimentary) conglomerate units occur in the Tanglefoot and Richthofen formations and likely represent debris flow, sheet flood, and bar deposits of a fan delta system (e.g., Dickie and Hein, 1988, 1995; Hart et al., 1995; Lowey, 2004; van Drecht et al., 2017). Paleoflow indicators are indicative of fanlobe migration and predominately show east- to northeast- and southwest-directed sediment transport along the western and eastern edges of the Whitehorse trough, respectively. Sediment pathways for the conglomerate units are typically transverse to the north-to-south, longitudinal axis of the Whitehorse trough (e.g., Wheeler, 1961; Dickie and Hein, 1988, 1995; Hart et al., 1995; Lowey, 2004). In northern British Columbia, Inklin Formation strata yield paleoflow indicators that suggest Sinemurian axial paleoflow was replaced by Pliensbachian transverse paleoflow (Johannson et al., 1997). Conglomerate clast types include augite-phyric basalt, andesite, tuff, granite, granodiorite, diorite, sandstone,

volcanogenic sandstone, and limestone (Hart et al., 1995). Basal conglomerate units are dominated by volcanic and sedimentary clasts, whereas younger strata contain a larger proportion of plutonic clasts that imply unroofing of the adjacent arc (Dickie and Hein, 1995; Hart et al., 1995; Johannson et al., 1997; Shirmohammad et al., 2011). U-Pb dates of plutonic clasts and detrital zircon grains from the Laberge Group are dominated by Late Triassic-Early Jurassic and minor Paleozoic populations that indicate local Intermontane terrane basement and collision-related pluton sources (Hart et al., 1995; Gordey et al., 1998; Colpron et al., 2015). Proposed Sinemurian to Toarcian maximum depositional ages for basal Laberge Group strata imply westerly younging of the Whitehorse trough during Intermontane collision and exhumation (e.g., Colpron et al., 2015). Post-collisional fluvial-deltaic rocks of the Middle Jurassic to Lower Cretaceous Tantalus Formation mark the end of Whitehorse trough deposition (Fig. 2.2; Tempelman-Kluit, 1984; Hart and Radloff, 1990).

2.4.2 Jurassic regional burial and exhumation

The petrology, thermobarometry, and mica cooling histories of Yukon-Tanana rocks indicate burial to 5-9 kbar (~18-33 km) during Hettangian-Sinemurian (~200-190 Ma) amphibolite-facies metamorphism followed by ~15-20 km exhumation to upper crustal levels by the Sinemurian-Pliensbachian (~195-186 Ma; e.g., Johnston and Erdmer, 1995; Johnston et al., 1996; Villeneuve et al., 2003; Berman et al., 2007; Knight et al., 2013; Clark, 2017). Eclogite clasts collected from a distinct latest Pliensbachian-earliest Toarcian conglomerate unit of the Laberge Group in northern British Columbia further suggest Early Jurassic exhumation rates of ~4 km/m.y. and are interpreted to be sourced from the suture between Yukon-Tanana and Stikinia (Kellett et al., 2018). Regional exhumation was likely driven by

buoyant extrusion during slab rollback, upper-plate retreat, transtension, slab breakoff, or syn-to post-collisional extension at the boundary of Yukon-Tanana and Stikinia (Kellett et al., 2018). Whitehorse trough subsidence was broadly coeval with the rapid exhumation of the Intermontane terranes (Colpron et al., 2015), however, there are no published estimates for subsidence rates within the basin (e.g., Dickie and Hein, 1995; Lowey, 2008).

2.4.3 Late Triassic-Middle Jurassic plutonism

Late Triassic to Middle Jurassic plutonism accompanied the collision and rapid exhumation of Yukon-Tanana, Stikinia, and Quesnellia in the northern Cordillera (e.g., Johnston et al., 1995, 1996; Tafti, 2005; Colpron et al., 2016). In central Yukon, the Late Triassic Stikine plutonic suite (ca. 216-206 Ma) consists of granodiorite, diorite, and gabbro units that crop out in restricted areas southwest of Whitehorse and northwest of Carmacks (Figs. 2.2 and 2.4a; e.g., Hart and Radloff, 1990, Colpron et al., 2016). Stikine plutonic suite rocks in the Friday Creek and Fish Lake localities yield superchondritic zircon $\epsilon_{\text{Hf(t)}}$ values that range from +9.7 to +11.5 (Fig. 2.4b; Sack et al., 2019). The Late Triassic to Early Jurassic Minto plutonic suite (ca. 204-194 Ma) crops out near the northern apex of the Whitehorse trough to the northwest and east of Carmacks (Figs. 2.2 and 2.4a). The Minto suite is comprised of granodiorite, quartz monzonite, granite, and minor syenite bodies that are best represented by the Tatchun pluton ($\epsilon_{\text{Hf(t)}}$: -9.5 to +9.5), Granite Mountain pluton ($\epsilon_{\text{Hf(t)}}$: -12.7 to +10.1), Minto pluton ($\epsilon_{\text{Hf(t)}}$: +0.8 to +10.9) and Thirtymile pluton ($\epsilon_{\text{Hf(t)}}$: -1.0 to +3.8) (Fig. 2.4b; e.g., Tafti and Mortensen, 2003; Colpron et al., 2016; Sack et al., 2019). The Early Jurassic Long Lake suite (ca. 192-178 Ma) is characterized by granodiorite and granite units of the Aishihik pluton, Big Creek, Sawtooth, and Englishman plutons, and Logtung quartz

diorite (Colpron et al., 2016; Joyce et al., 2016). The Aishihik ($\epsilon_{\text{Hf(t)}}$: -27.3 to +12.1) and Big Creek plutons ($\epsilon_{\text{Hf(t)}}$: -3.6 to +1.7) crop out northwest and along western side of the Whitehorse trough and yield dominantly subchondritic to chondritic zircon $\epsilon_{\text{Hf(t)}}$ values, whereas the Sawtooth pluton ($\epsilon_{\text{Hf(t)}}$: -6.2 to +11.6), Englishman pluton ($\epsilon_{\text{Hf(t)}}$: +1.6 to +3.7) and Logtung quartz diorite ($\epsilon_{\text{Hf(t)}}$: -2.9 to +1.4) crop out in smaller regions along the southeastern edge of the Whitehorse trough and yield chondritic to superchondritic zircon $\epsilon_{\text{Hf(t)}}$ values (Fig. 2.2 and 2.4a, b; Colpron et al., 2016; Sack et al., 2019). Middle Jurassic Bryde (ca. 172-168 Ma) and Middle to Late Jurassic McGregor (ca. 163-160 Ma) suite granitoids are the youngest plutonic rocks adjacent to the Whitehorse trough. The Bryde suite crops out in the Atlin Lake, Marsh Lake, and Teslin Crossing regions near Whitehorse and to the north of Carmacks (Figs. 2.2 and 2.4a; Colpron et al., 2016). Alkali syenite from Marsh Lake yields dominantly chondritic ($\epsilon_{\text{Hf(t)}}$: +0.9 to +3.8) values, whereas diorite and monzodiorite from the Atlin Lake ($\epsilon_{\text{Hf(t)}}$: +4.7 to +7.0) and Teslin Crossing ($\epsilon_{\text{Hf(t)}}$: +6.5 to +8.4) regions yield dominantly superchondritic values (Fig. 2.4b; Sack et al., 2019). The McGregor suite is apparently restricted to the McGregor pluton locality north of Carmacks and yields chondritic to superchondritic zircon $\epsilon_{\text{Hf(t)}}$ values that range from +0.9 to +11.1 (Fig. 2.4b; Colpron et al., 2016; Sack et al., 2019).

2.5 Methods

Four samples of the Tanglefoot formation (16-LVD-001B, 16-LVD-001C, 16-LVD-004 and 17-LVD-018) and eight samples of the Richthofen formation (16-LVD-009, 16-LVD-021, 16-LVD-022, 16-LVD-023, 17-LVD-027, 17-LVD-030, 17-LVD-034, 17-LVD-038)

were collected for detrital zircon U-Pb geochronology and Hf isotope geochemistry (Fig. 2.2). Standard rock crushing, sieving, and heavy liquid (bromoform and methylene iodide) density separations were done at Memorial University of Newfoundland. Approximately 130 zircon grains from each sample were mounted in epoxy, ground, polished, and imaged using cathodoluminescence (CL) with a JEOL JSM 7100F Field Emission Scanning Electron Microscope (SEM). Zircon CL grain maps guided the selection of analytical spot locations to avoid complex zoning and fractures.

Detrital zircon U-Pb-Hf data were collected at Memorial University of Newfoundland using the laser ablation split-stream (LASS) approach outlined by Fisher et al. (2014) and Goudie et al. (2014). Analyses were completed in four sessions (3 to 4 days per session) over an eleven-month period

A GeoLas 193 nm excimer laser used a 40 μm diameter beam with a frequency of 10 Hz and fluence of 5 J/cm². Background levels were measured for 30 s followed by 60 s of ablation and 30 s of washout after each analysis. The ablated material was carried out of the laser cell in flow of He gas of 1 L/min and split downstream to simultaneously measure U-Pb isotopes with a ThermoFinnigan Element XR single-collector inductively coupled plasma mass spectrometer (ICP-MS) and Hf isotopes with a ThermoFinnigan Neptune multi-collector ICP-MS (e.g., Goudie et al., 2014, Fisher et al., 2014) with N₂ added to each mass spectrometer to increase sensitivity. Standard-sample bracketing used 91500 (U-Pb) and Plešovice (Lu-Hf) as primary reference materials to correct for instrument drift and downhole fractionation, and mass bias. R33, 02123, Temora, and QGNG were used as secondary standards. 91500 yielded a weighted $^{206}\text{Pb}/^{238}\text{U}$ age of 1062.2 ± 1.3 Ma ($n = 248$, 2SD), in

agreement with the published ID-TIMS age of 1062.4 ± 0.4 Ma (Wiedenbeck et al., 1995).

Plešovice yielded a weighted $^{176}\text{Hf}/^{177}\text{Hf} = 0.282481 \pm 0.000019$ ($n = 249$, 2SD), within

uncertainty of the published value of 0.282482 ± 0.000013 (Sláma et al., 2008).

Isotope ratios were reduced using the Iolite 3.4 extension for IgorPro (Paton et al., 2011) and VizualAge data reduction scheme (Petrus and Kamber, 2012). A ‘best age’ was then assigned to each grain using the $^{206}\text{Pb}/^{238}\text{U}$ date if less than 1100 Ma and the $^{207}\text{Pb}/^{206}\text{Pb}$ date if greater than 1100 Ma. Analyses were excluded based on the following criteria:

(1) >10% uncertainty in $^{206}\text{Pb}/^{238}\text{U}$ date (2σ).

(2) >10% uncertainty in $^{207}\text{Pb}/^{206}\text{Pb}$ date (2σ), unless the $^{206}\text{Pb}/^{238}\text{U}$ date is <500 Ma.

(3) >10% discordance or >5% reverse discordance, unless $^{206}\text{Pb}/^{238}\text{U}$ date is <500 Ma.

Concordance is not reported for $^{206}\text{Pb}/^{238}\text{U}$ ages <500 Ma because of the large uncertainty in $^{207}\text{Pb}/^{206}\text{Pb}$ (e.g., Gehrels and Pecha, 2014).

U-Pb results are presented in normalized probability density diagrams generated with the Normalized Probability Plot Excel macro developed at the Arizona Laserchron Center, University of Arizona (www.geo.arizona.edu/alc). Probability age peaks were calculated using the AgePick Excel macro developed at Arizona LaserChron Center (www.geo.arizona.edu/alc). Hf isotope data are presented in age-corrected $\varepsilon_{\text{Hf}(t)}$ values versus U-Pb crystallization age plots and include the chondritic uniform reservoir (CHUR) values of Bouvier et al. (2008), depleted mantle (DM) values of Vervoort and Blichert-Toft (1999), and crustal evolution trends using present day $^{176}\text{Lu}/^{177}\text{Hf} = 0.0115$ (Vervoort and Patchett, 1996; Vervoort et al., 1999).

The youngest detrital zircon crystals were used to estimate the maximum depositional age of Laberge Group strata because synsedimentary magmatism typically accompanies convergent margin activity (Dickinson and Gehrels, 2009; Cawood et al., 2012). Maximum depositional ages in this study were calculated using a population of young grains rather than the youngest detrital zircon due to the inherent lack of reproducibility (Dickinson and Gehrels, 2009). The following methods were used:

- 1) The weighted mean for a cluster of three or more grains that overlap at 2σ (Dickinson and Gehrels, 2009). Maximum depositional ages calculated with this method generally yield the youngest depositional ages and represent the young shoulder of the youngest peak.
- 2) Unmix routine in Isoplot. This method identifies and separates age-components within a grouping of dates that overlap (Ludwig, 2008). We used $\varepsilon_{\text{Hf(t)}}$ values to assess if an identified age-component represents a separate detrital zircon population. The Unmix routine generally yields maximum depositional ages comparable to the weighted mean of a cluster of three or more grains.
- 3) Youngest age peak calculated using the AgePick Excel macro. This macro calculates the maximum in age probability of a population that includes 3 or more analyses.
- 4) TuffZirc routine in Isoplot (Ludwig, 2008). This algorithm returns the median age of the largest cluster of ages and typically represents the age of the youngest peak.

2.6 Results

2.6.1 Tanglefoot formation

Buff-green, cross-bedded feldspathic lithic arenite (sample 16-LVD-001C; $n = 102/120$) is the oldest rock unit sampled along the Robert Campbell Highway (Figs. 2.2 and 2.5) and occurs stratigraphically beneath a Pliensbachian crystal-lithic tuff dated at 187.1 ± 0.2 Ma (Colpron and Friedman, 2008; van Drecht et al., 2017). This sandstone unit is composed of lithic fragments (45%; volcanic and carbonate rock clasts), quartz (35%), and sericite altered feldspar (20%). Clear to pink detrital zircon crystals are elongate, spherical to fragmentated, and range in size from 60 to 200 μm . Sector and/or growth zoning typical of magmatic zircon grains are evident in CL images. The sample yields a bimodal population of Early Triassic to Early Jurassic (98%) detrital zircon grains that range from 252 ± 6 to 191 ± 5 Ma with probability age peaks ca. 201 and 228 Ma (Fig. 2.6). Early Triassic to Early Jurassic zircon grains yield $\varepsilon_{\text{Hf}(t)}$ values that range from -4.6 to +12.1 (Fig. 2.6). Detrital zircon grains that range from 213 ± 7 to 191 ± 5 Ma and 242 ± 6 to 217 ± 5 Ma (80%) have $\varepsilon_{\text{Hf}(t)}$ values that cluster between -0.2 and +5 and +10 and +12, respectively. A single Pennsylvanian zircon (308 ± 3 Ma) yielded an $\varepsilon_{\text{Hf}(t)}$ value of +2.4.

A buff-coloured, medium- to very coarse-grained, feldspathic lithic arenite that forms a lens within a cobble to boulder conglomerate (sample 16-LVD-001B; $n = 104/120$) is located 15 m above sample 16-LVD-001C, but below the 187.1 ± 0.2 Ma crystal lithic tuff (Figs. 2.2 and 2.5; van Drecht et al., 2017). This sandstone is composed of lithic fragments (40%; volcanic rocks clasts), sericite altered feldspar (30%), quartz (30%), and clay. Clear to pink to

brown detrital zircon crystals are elongate to spherical and range in size from 50 to 300 μm . Most grains display oscillatory zoning in CL. This sample is characterized by a unimodal Late Triassic to Early Jurassic population (98%) that ranges from 219 ± 8 to 185 ± 7 Ma with a probability age peak ca. 195 Ma (Fig. 6). This Late Triassic to Early Jurassic population has $\varepsilon_{\text{Hf(t)}}$ values that range from -4.7 to +9.4 with a dominant cluster between -4.7 and -2.6 and a smaller, broad cluster between -0.2 and +4.7 (Fig. 6). Two Mississippian grains of 342 ± 7 and 353 ± 11 Ma have $\varepsilon_{\text{Hf(t)}}$ values of -3.8 and +4.1 respectively.

Buff-coloured lithic arenite that lies stratigraphically above the 187.1 ± 0.2 Ma crystal lithic tuff (sample 16-LVD-004; $n = 98/109$) is the youngest sample analyzed along the Robert Campbell Highway (Figs. 2.2 and 2.5; van Drecht et al., 2017). This sandstone unit is composed of quartz (55%), sericite altered feldspar (30%), and lithic fragments (15%; volcanic rock clasts). Clear to pink to yellow-brown detrital zircon crystals are elongate to spherical and range in size from 80 to 250 μm . Zircon grains typically display growth zoning with few sector-zoned grains observed in CL. This sample is characterized by a dominant Late Triassic to Early Jurassic zircon population that ranges from 212 ± 9 to 176 ± 3 Ma (92%) with a probability age peak ca. 185 Ma (Fig. 2.6). Most $\varepsilon_{\text{Hf(t)}}$ values range from -4.3 to +4.8 and one 212 ± 9 Ma zircon yields a $\varepsilon_{\text{Hf(t)}}$ value of +8.8 (Fig. 2.6). An early to mid-Paleozoic (8%) population has a probability age peak ca. 338 Ma and yields $\varepsilon_{\text{Hf(t)}}$ values between -8.7 and -5.7. Two Middle Mississippian zircon grains have $\varepsilon_{\text{Hf(t)}}$ values of +4 and +8.7.

Maroon, medium- to coarse-grained, feldspathic lithic arenite mapped as the Triassic Mandanna formation crops out beneath massive conglomerate at Conglomerate Mountain (sample 17-LVD-018; $n = 111/120$), ~40 km south of Carmacks (Fig. 2.2; van Drecht and

Beranek, 2018). This sample contains lithic fragments (35%; sandstone and volcanic rock clasts), sericite altered feldspar (59%), and minor quartz (6%). Clear to pink-brown detrital zircon crystals are elongate to spherical and range in size from 70 to 200 μm . CL images display sector to growth zoning. The sample has a bimodal distribution of Late Triassic to Early Jurassic (48%) and Late Devonian to Early Triassic (52%) zircon grains (Fig. 2.6). The youngest grouping ranges from 221 ± 4 to 180 ± 4 Ma and yields probability age peaks ca. 185 and 205 Ma (Fig. 2.6). These zircon grains have $\epsilon_{\text{Hf(t)}}$ values that range from +0.9 to +11.5 with an average of +7 (Fig. 2.6). Late Devonian to Early Triassic zircon grains range from 373 ± 7 to 248 ± 4 Ma and have a probability age peak ca. 313 Ma (Fig. 2.6). This population has $\epsilon_{\text{Hf(t)}}$ values that range from +5.7 to +12.7 and cluster around +10.

2.6.2 Richthofen formation

Crystal lithic tuff (sample 17-LVD-038; $n = 27/28$) that nonconformably overlies 216.35 ± 0.23 Ma gabbro of the Povoas formation (Fig. 2.2; Colpron, 2011) crops out near King Lake, ~20 km northwest of Whitehorse (van Drecht and Beranek, 2018). Clear to pink detrital zircon crystals from this tuff are typically elongate, display oscillatory zoning in CL, and range in size from 100 to 300 μm . This sample is dominantly composed of Late Triassic to Middle Jurassic (96%) detrital zircon grains that range from 203 ± 3 to 172 ± 2 Ma with probability age peaks ca. 173 and 190 Ma (Fig. 2.7). Late Triassic to Middle Jurassic detrital zircon grains have $\epsilon_{\text{Hf(t)}}$ values that range from -4.1 to +5 and cluster around -3 (Fig. 2.7).

Dark-blue, bioclastic lithic wacke of the Richthofen formation (sample 17-LVD-027; $n = 51/65$) overlies Lewes River Group limestone in the Takhini subdivision area, ~20 km

northwest of Whitehorse (Fig. 2.2; van Drecht and Beranek, 2018). This wacke unit is primarily comprised of lithic fragments (96%; carbonate and volcanic lithics) with minor quartz (4%). Lower to Middle Jurassic *Pinna* sp. (bivalve) and undetermined coarse-ribbed pectinoid bivalve and ammonite fossils were collected from this locality (R. Blodgett, 2018, pers. comm.). Clear to pink detrital zircon crystals are elongate to spherical, display growth zoning in CL, and range in size from 70 to 160 μm . This sample yields Late Triassic to Early Jurassic (96%) detrital zircon grains that range from 216 ± 3 to 181 ± 3 Ma with a probability age peak ca. 198 Ma. $\varepsilon_{\text{Hf(t)}}$ values for this sample range from +4.9 to +12.1 (Fig. 2.7). Two Pennsylvanian grains at 315 ± 9 and 359 ± 6 Ma are also present, with the latter having an $\varepsilon_{\text{Hf(t)}}$ value of -8.5 (Fig. 2.7).

Green, very poorly sorted, feldspathic lithic arenite (sample 16-LVD-021; $n = 93/110$) forms the matrix of cobble to boulder conglomerate units on Richthofen Island in Lake Laberge (Fig. 2.2; van Drecht et al., 2017). This sandstone sample is composed of lithic fragments (56%; volcanic, carbonate, sandstone rock clasts), sericite altered feldspar (40%), and minor quartz (4%). Clear to pink detrital zircon crystals are typically elongate and range in size from 70 to 220 μm . Zoning ranges from sector to growth zoning in CL. Late Triassic to Early Jurassic (97%) zircon grains range from 232 ± 3 to 186 ± 3 Ma with a probability age peak ca. 210 Ma (Fig. 2.7). Late Triassic to Early Jurassic zircon have $\varepsilon_{\text{Hf(t)}}$ values that range from +3.1 to +13.9 with a main cluster between +4.4 and +7.8 (Fig. 2.7). Three Paleozoic zircon grains at 340 ± 7 , 343 ± 10 , and 464 ± 8 Ma yield $\varepsilon_{\text{Hf(t)}}$ values at +11.8, +12.8 and +8.2, respectively.

Lithic feldspathic arenite collected along the eastern shoreline of Lake Laberge (sample 16-LVD-022; $n = 97/110$; van Drecht et al., 2017) contains feldspar (70%), lithic fragments (28%; volcanic, carbonate, and mudstone rock clasts) and minor quartz (2%). Clear to pink-brown detrital zircon crystals are typically elongate and range in size from 60 to 280 μm . Growth zoning is commonly observed in CL. The sample is mostly composed of Late Triassic to Early Jurassic (98%) detrital zircon grains that range from 217 ± 5 to 194 ± 3 Ma with a probability age peak ca. 205 Ma (Fig. 2.7). Late Triassic to Early Jurassic zircon grains have $\varepsilon_{\text{Hf(t)}}$ values that cluster between +2.8 and +5.3 and one zircon with a $\varepsilon_{\text{Hf(t)}}$ value of -0.2 (Fig. 2.7). Two Middle Mississippian zircon grains at 333 ± 5 and 339 ± 6 Ma yield $\varepsilon_{\text{Hf(t)}}$ values of +6.3 and +5.4, respectively (Fig. 2.7).

Bioclastic lithic wacke (sample 16-LVD-023; $n = 21/55$) with mud rip-up clasts was collected along the eastern shoreline of Lake Laberge (Fig. 2.2; van Drecht et al., 2017). This sample is composed of lithic fragments (68%; mudstone, carbonate, and volcanic rock clasts), sericite altered feldspar (31%), and minor quartz (1%). Clear to pink detrital zircon crystals are elongate to spherical, display oscillatory zoning in CL, and range in size from 80 to 150 μm . Permian to Early Jurassic zircon grains (72%) range from 270 ± 8 to 185 ± 2 Ma with probability age peaks ca. 185, 195, and 202 Ma (Fig. 2.7). Three Middle Devonian to Early Mississippian (14%) zircon grains yield 356 ± 4 ($\varepsilon_{\text{Hf(t)}}: -5.8$), 363 ± 6 ($\varepsilon_{\text{Hf(t)}}: +1.2$), and 390 ± 10 Ma ages (Fig. 2.7). Three Precambrian (14%) zircon grains are also present at 1474 ± 51 , 2563 ± 26 ($\varepsilon_{\text{Hf(t)}}: +0.9$), and 2829 ± 23 Ma.

Parallel laminated, fine- to medium-grained, feldspathic lithic arenite (sample 16-LVD-009; $n = 73/100$) overlies Lewes River Group limestone along the eastern flank of

Mount Laurier, ~40 km northeast of Whitehorse (Fig. 2.2; van Drecht et al., 2017). The feldspathic lithic arenite contains lithic fragments (50%; volcanic and carbonate rock clasts), sericite altered feldspar (45%), and minor quartz (5%). Abundant amphibole defines lamination. Clear to pink to yellow-brown detrital zircon crystals are elongate to spherical and range in size from 60 to 180 μm . Zoning is typically igneous growth zoning in CL. Late Triassic to Early Jurassic (58%) zircon range from 225 ± 5 to 190 ± 7 Ma and yield a probability age peak ca. 205 Ma (Fig. 2.7). $\varepsilon_{\text{Hf(t)}}$ values for this population occur from +3 to +6.3 (Fig. 2.6). Mississippian to Permian zircon grains (42%) show a broader range from 356 ± 8 to 269 ± 4 Ma with a probability age peak ca. 329 Ma and $\varepsilon_{\text{Hf(t)}}$ values of +2.3 to +10.7 (Fig. 2.7).

Dark grey to buff, fine- to medium-grained, feldspathic lithic arenite (sample 17-LVD-034; $n = 82/92$) that overlies Lewes River Group limestone was collected at Mount Slim, ~30 km northeast of Whitehorse (Fig. 2.2; van Drecht and Beranek, 2018). This sample is composed of lithic fragments (58%; volcanic and carbonate rock clasts), sericite altered feldspar (36%), and minor quartz (5%). Clear to pink detrital zircon crystals are elongate to spherical, typically igneous growth zoning in CL, and range in size from 100 to 300 μm . Middle Triassic to Early Jurassic zircon grains (40%) occur from 244 ± 6 to 178 ± 8 to Ma with probability age peaks ca. 185, 201, and 225 Ma (Fig. 2.7). Mississippian to Permian (59%) zircon grains range from 350 ± 4 to 262 ± 5 Ma with probability age peaks ca. 310 and 330 Ma (Fig. 2.7). Middle Triassic to Early Jurassic zircon grains yield $\varepsilon_{\text{Hf(t)}}$ values of -3.2 to +10.6 and Paleozoic zircon grains have values that range from -2.7 to +10.9. One Paleoproterozoic zircon at 2263 ± 74 Ma yields a $\varepsilon_{\text{Hf(t)}}$ value of -10.8.

Dark grey-blue, medium-grained, lithic wacke (sample 17-LVD-030; $n = 91/105$) that overlies pebble to cobble limestone conglomerate was collected southeast of the Mount Byng, ~50 km northeast of Whitehorse (van Drecht and Beranek, 2018). This sample contains lithic fragments (92%; carbonate, volcanic, and mudstone rock clasts), sericite altered feldspar (6%), minor quartz (2%). Clear to pink detrital zircon crystals are mostly elongate, display igneous growth zoning in CL, and are 80 to 300 μm in size. Middle Triassic to Early Jurassic (67%) detrital zircon grains make up the dominant population and range from 250 ± 5 to 175 ± 2 Ma (Fig. 2.7). Silurian to Permian detrital zircon grains (33%) make up a broad population that range from 419 ± 6 to 257 ± 4 Ma (Fig. 2.7). This sample has probability age peaks ca. 193, 251, 254, 289, 301, 316, 328 and 392 Ma (Fig. 2.7). Late Triassic to Early Jurassic zircon grains have $\varepsilon_{\text{Hf}(t)}$ values between +1.7 and +12 with two clusters around +4 and +10. Silurian to Permian zircon grains have $\varepsilon_{\text{Hf}(t)}$ values between -7.6 and +11.8 (Fig. 2.7).

2.7 Discussion

2.7.1 Timing of Laberge Group deposition

The timing of Jurassic synorogenic deposition in central Yukon is broadly constrained by zircon U-Pb geochronology, biostratigraphy, and their stratigraphic position between the Late Triassic Lewes River Group and Middle Jurassic to Early Cretaceous Tantalus Formation (e.g., Bostock, 1936; Tempelman-Kluit, 1984; Pálfy and Hart, 1995; Johannson et al., 1997; Clapham et al., 2002; Lowey, 2004; Hart et al., 2005; Shirmohammad et al., 2011; Colpron et al., 2015). Syndepositional magmatism is typical along convergent margins and allows for the reasonable estimation of depositional ages through detrital zircon maximum depositional age

calculations (Dickinson and Gehrels, 2009; Cawood et al., 2012). The weighted mean of the three or more youngest grains that overlap at 2σ and the Unmix routine in Isoplot represent the youngest detrital zircon grains; these likely provide the best approximation of maximum depositional ages for syndepositional Laberge Group strata. Previous studies (Shirmohammad et al., 2001; Colpron et al., 2015) have furthermore indicated that the youngest zircon grains in Laberge Group strata are consistent with biostratigraphic ages. Youngest age peak calculations (TuffZirc and AgePick) provide the most conservative estimate for maximum depositional age; these methods likely yield a maximum depositional age that is older than the true depositional age (Dickinson and Gehrels, 2009; Cawood et al., 2012).

2.7.1.1 Tanglefoot formation

Three samples of Tanglefoot formation sandstone were collected along the Robert Campbell Highway in the northern apex of the Whitehorse trough (Figs. 2.2 and 2.5; van Drecht et al., 2017). Unmix, TuffZirc, and AgePick calculations for 16-LVD-001C feldspathic lithic arenite, the stratigraphically oldest sample analyzed from the Tanglefoot formation, indicate Hettangian maximum depositional ages (200 Ma to 199.59 ± 2.6 Ma; Table 2.2). The weighted mean of six young grains from 16-LVD-001C, however, suggest a Sinemurian (193.5 ± 2.6 Ma) maximum depositional age (Table 2.2). 16-LVD-001B a feldspathic lithic arenite, collected 15 m above the previous sample, yields Sinemurian (ca. 195 Ma) to Pliensbachian (187.2 ± 0.72 Ma to 186.5 ± 0.59 Ma) maximum depositional ages using the TuffZirc-AgePick and weighted mean-Unmix routines, respectively. AgePick and TuffZirc calculations for 16-LVD-004 lithic arenite, the youngest sample collected along the Robert Campbell highway, indicate Pliensbachian maximum depositional ages (185 Ma to 183.2

+0.6/-1.5), whereas weighted mean and Unmix methods yielded Toarcian maximum depositional age (181.4 ± 0.61 Ma to 177.4 ± 1.8 Ma). These new depositional age estimates are consistent with the Pliensbachian (187.1 ± 0.2 Ma) crystal lithic tuff (Colpron and Friedman, 2008) that crops out beneath the Pliensbachian-Toarcian lithic arenite (16-LVD-004) and above the Sinemurian-Pliensbachian feldspathic lithic arenite (16-LVD-001B).

Maroon feldspathic lithic arenite that crops out at Conglomerate Mountain along the North Klondike Highway uniformly yields Pliensbachian (186.1 ± 1.4 to 184.2 ± 8.4 Ma) maximum depositional ages. Previous bedrock mapping studies assigned this unit to the Triassic Mandanna formation (Colpron et al., 2002), but our new U-Pb data confirm that these Conglomerate Mountain strata should be included in the Laberge Group.

2.7.1.2 Richthofen formation

Crystal lithic tuff collected along the western edge of the Whitehorse trough at King Lake (17-LVD-038) yields weighted mean, Unmix, TuffZirc, and AgePick ages that straddle the Toarcian-Aalenian boundary ($174.1 +1.45/-2.05$ Ma to 173 Ma). This basal unit is in depositional contact with 216 Ma gabbro of the Stikine suite (Colpron, 2011) and suggests that the Laberge-Lewes River Group unconformity at this locality spans >42 m.y.

Bioclastic lithic wacke that crops out in the Takhini subdivision area (17-LVD-027) yields TuffZirc-AgePick ages that indicate a Sinemurian (ca. 198 Ma to $193.8 +1.4/-2.4$) maximum depositional age, whereas the weighted mean of three young grains and the Unmix age indicate a younger Toarcian (182.3 ± 2.4 to 182.3 ± 2.5) maximum depositional age. Sinemurian-Toarcian maximum depositional ages are consistent with the Lower to Middle Jurassic age indicated by fossil specimens.

The Unmix, AgePick, and TuffZirc ages of feldspathic lithic arenite (16-LVD-021) collected from Richthofen Island indicate a Norian-Rhaetian (ca. 210 to 204.56 ± 0.77) maximum depositional age and the weighted mean of five young grains yields a Sinemurian (195.3 ± 3.5 Ma) maximum depositional age. Lithic feldspathic arenite (16-LVD-022) collected on the eastern shoreline of Lake Laberge yields a Rhaetian ($205.8 +0.6/-0.8$ to ca. 205) maximum depositional age with the AgePick-TuffZirc routines and a Hettangian-Sinemurian (199.52 ± 0.96 to 196.2 ± 2.8) maximum depositional age with the weighted mean-Unmix methods. South of sample 16-LVD-022, bioclastic lithic wacke (16-LVD-023) on the eastern shoreline of Lake Laberge yields Unmix-TuffZirc ages that suggest a Rhaetian-Sinemurian ($202 +3.2/-5$ to 196.29 ± 1.1) maximum depositional age. However, the weighted mean of four young grains and the AgePick routine indicates a younger Pliensbachian (185.5 ± 1.8 to ca. 185) maximum depositional age.

Feldspathic lithic arenite (16-LVD-009) collected along the eastern flank of Mount Laurier yields AgePick-TuffZirc ages that suggest a Rhaetian (ca. 205 to $204.5 +2.4/-2.1$) maximum depositional age and weighted mean-Unmix ages that indicate a Sinemurian (195.8 ± 1.6 Ma to 197.44 ± 1 Ma) maximum depositional age (Table 2.2). Northeast of Mount Laurier, the TuffZirc age of feldspathic lithic arenite (17-LVD-034) that crops out at Mount Slim indicates a Rhaetian-Hettangian ($201.75 +1.95/-1.55$) maximum depositional age. The Unmix age, AgePick, and weighted mean ages for the Mount Slim sample imply a younger Sinemurian to Pliensbachian (191.54 ± 0.94 Ma to 184.4 ± 5.6 Ma) maximum depositional age (Table 2.2).

Lithic wacke (16-LVD-030) collected at Mount Byng along the eastern edge of the Whitehorse trough yields TuffZirc-AgePick (ca. 193 to $192.7 +2.1/-1.2$) ages that indicate a Sinemurian maximum depositional age, whereas a younger Toarcian (185 ± 1.3 to 183.5 ± 0.97) maximum depositional age is suggested by the weighed mean of ten young grains and the Unmix routine.

2.7.1.3 Spatial trends of basal Laberge Group strata

Basal Laberge Group sandstone units located along the central axis of the Whitehorse trough (16-LVD-001C and 16-LVD-009) yield Rhaetian to Sinemurian maximum depositional ages, whereas basal samples near the western edge of the Whitehorse trough (17-LVD-038 and 17-LVD-027) yield younger Sinemurian to Aalenian maximum depositional ages (Figs. 2.2 and 2.8; Table 2). These calculations indicate that Laberge Group deposition began by the Sinemurian, confirming previous hypotheses that collision-related sedimentation in central Yukon was ongoing by the late Pliensbachian (Colpron et al., 2015). The spatial trends in maximum depositional age are also consistent with the westerly-younging of basal strata hypothesized by Colpron et al. (2015) (samples 04SJP594, GL04-108B, Eagles Nest Bluff, and 08MC091 in Fig. 2.8). New results from this study furthermore indicate that basal samples located in the eastern (17-LVD-030) and south-central (17-LVD-034) regions of the Whitehorse trough have Sinemurian-Pliensbachian and Rhaetian-Toarcian maximum depositional ages, respectively, which imply contemporaneous easterly- and southerly-younging trends (Figs. 2.2 and 2.8; Table 2.2). The west-, east-, and south-directed younging of basal strata suggest that initial Sinemurian subsidence within the Whitehorse trough was concentrated in a narrow depocenter that extended ~120 km from Eagles Nest Bluff in the

north to Mount Laurier in the south (Fig. 2.9). Following initial subsidence, basal strata expanded to the west, east, and south during the Pliensbachian to Aalenian (Fig. 2.9).

2.7.2 Sediment provenance

Previous studies have demonstrated that the Laberge Group strata contain Devonian-Permian and Late Triassic-Early Jurassic detrital zircon grains sourced from adjacent Intermontane terranes (Hart et al., 1995; Johannson et al., 1997; Gordey et al., 1998; Shirmohammad et al., 2011; Colpron et al., 2015). Laberge Group samples analyzed during this study yield similar detrital zircon age populations (Fig. 2.10); however, new LASS U-Pb-Hf results further resolve Whitehorse trough source regions and paleogeography. Although many potential source rocks in the northern Cordillera lack whole-rock Hf or zircon Hf isotope constraints, several Yukon-Tanana, Stikinia, and Quesnellia rock assemblages have been characterized by whole-rock Nd isotope geochemistry (e.g., Piercey et al., 2006) and allow comparisons to Laberge Group detrital zircon Hf isotope results. Potential source regions were therefore determined by converting published $\varepsilon_{\text{Nd(t)}}$ values to $\varepsilon_{\text{Hf(t)}}$ values using the correlation equation $\varepsilon_{\text{Hf(t)}} = 1.36 \varepsilon_{\text{Nd(t)}} + 3$ (Vervoort and Blichert-Toft, 1999).

2.7.2.1 Inheritance

Inherited Late Devonian to Middle Pennsylvanian zircon grains in the Late Triassic-Early Jurassic Tatchun pluton (Minto suite), Early Jurassic Minto pluton (Minto suite) and Early Jurassic Aishihik pluton (Long Lake suite) yield a wide range of $\varepsilon_{\text{Hf(t)}}$ values from -8.6 to +12.1 and indicate provenance from Yukon-Tanana and/or Paleozoic Stikinia/Quesnellia country rocks (Fig 2.11; Sack et al., 2019). Some of the coarsest Laberge Group detrital zircon

crystals ($n = 15$) similarly yield Mississippian-Pennsylvanian and Norian-Rhaetian cores with $\epsilon_{\text{Hf(t)}}$ values that cluster between +1.6 to +12.1 and Late Triassic-Early Jurassic rims that cluster between +0.9 to +6.9 (Fig. 2.11). These results imply that Paleozoic detrital zircon populations at least partially represent inherited zircon grains from adjacent Late Triassic-Early Jurassic plutonic suites. Four detrital zircon grains also yield Mesoarchean to Mesoproterozoic ages and likely reflect inheritance from plutons that intrude the pre-Late Devonian continental margin basement assemblage of Yukon-Tanana or recycling of inherited grains from these Yukon-Tanana sources (Snowcap assemblage; Piercy and Colpron, 2009).

2.7.2.2 Paleozoic populations

Four Laberge Group samples (17-LVD-018, 16-LVD-009, 17-LVD-030, 17-LVD-034) yield Late Devonian to Permian chondritic to superchondritic ($\epsilon_{\text{Hf(t)}}: +1$ to +12.7) detrital zircon populations that are consistent with Yukon-Tanana and Slide Mountain terrane rocks in central Yukon (Figs. 2.6 and 2.7). Potential source rocks include the Wolverine Lake group ($\epsilon_{\text{Hf(t)}}: +12.4$), Little Salmon formation ($\epsilon_{\text{Hf(t)}}: +12.9$), Tatlmain suite, Klinkit Group ($\epsilon_{\text{Hf(t)}}: +12.1$ to +13.1), Klondike assemblage, Anvil assemblage ($\epsilon_{\text{Hf(t)}}: +8.6$ to +11.7), and Campbell Range formation ($\epsilon_{\text{Hf(t)}}: -2$ to +15.1) (Table 1; Fig. 2.7; e.g. Creaser et al., 1997; Piercy et al., 2001, 2003, 2012; Simard et al., 2003, 2007) that crop out north and east of the Whitehorse trough and northeast of the Tintina fault. Dextral restoration (~430 km) of the late Mesozoic-Cenozoic Tintina fault places some of these sources to the north of the Whitehorse trough (Gabrielse et al., 2006).

Superchondritic detrital zircon grains are consistent with Cache Creek terrane ($\epsilon_{\text{Hf(t)}}: +8.8$ to +14.3) and Kutcho assemblage ($\epsilon_{\text{Hf(t)}}: +13.2$ to +15.5) of southern Yukon and northern

British Columbia (Table 2.2; Figs. 2.6 and 2.7; Smith and Lambert, 1995; Childe and Thompson, 1997; Patchett and Gehrels, 1997). However, the Laberge Group sandstone and conglomerate samples in this study lack chert clasts that are characteristic of the Cache Creek terrane (e.g., Cordey et al., 1991), which suggests that such oceanic assemblages were not a significant source.

Takhini and Boswell assemblage rocks of Stikinia and Quesnellia, respectively, represent alternative sources for Mississippian to Permian detrital zircon grains in the Laberge Group strata. The Takhini assemblage is restricted to a small region west of Whitehorse, whereas the Boswell assemblage crops out to the north and along the eastern flank of the Whitehorse trough (Fig. 2.2). East- to northeast- and southwest-directed paleoflow indicators (Hart et al., 1995; Johannson et al., 1997) suggest sediment was sourced from regions that surround the Whitehorse trough and therefore indicate both assemblages represent potential source regions. The distribution of chondritic to superchondritic Yukon-Tanana source rocks north and east of the Whitehorse trough, however, suggests that the Boswell assemblage is the most probable source.

Subchondritic detrital zircon grains ($\epsilon_{\text{Hf(t)}}$: -1.1 to -8.7) in Laberge Group strata are consistent being sourced from Yukon-Tanana rocks (Kudz Ze Kayah formation, Grass Lakes suite, Simpson Range suite, Nisutlin assemblage, and Little Kalzas formation) (Table 1; Figs. 2.6 and 2.7). However, subchondritic detrital zircon grains comprise a minor population ($n = 9$) and suggest that evolved Paleozoic source rocks only contributed a minor sediment supply to the Whitehorse trough (Table 2.1; Figs. 2.6 and 2.7).

2.7.2.3 Mesozoic populations

Middle Triassic to Middle Jurassic (242 – 172 Ma) detrital zircon grains yield subchondritic to superchondritic Hf isotope compositions that are consistent with Stikinia/Quesnellia rocks and the Late Triassic-Middle Jurassic plutonic suites adjacent to the Whitehorse trough (Figs. 2.4, 2.6, and 2.7). Detrital zircon populations form tight clusters in U-Pb-Hf space, some of which are unique to individual samples, suggesting derivation from unique point sources. A minor population of Middle Triassic detrital zircon grains occur in Hettangian-Sinemurian feldspathic lithic arenite (16-LVD-001C, Tanglefoot formation) and are consistent with Joe Mountain formation source rocks (Fig. 2.6). Although whole rock Hf isotope data are not available for these Middle Triassic strata, detrital chlorite and epidote grains recognized in Laberge Group rocks are consistent with the pervasive chlorite and epidote alteration found in the Joe Mountain formation (Hart, 1997). In central Yukon, the Joe Mountain formation crops out east of Lake Laberge in the Mount Byng region. However, Laberge Group strata proximal to the Joe Mountain formation (16-LVD-009, 17-LVD-030, and 17-LVD-034) do not yield superchondritic detrital zircon grains. The distribution of superchondritic Middle Triassic detrital grains in Laberge Group strata suggests an alternative superchondritic Middle Triassic source similar to that Joe Mountain formation existed near the northern apex of the Whitehorse trough.

Late Triassic superchondritic ($\epsilon_{\text{Hf(t)}}$: +8.2 to +13.9) detrital zircon grains are consistent with the isotopic signatures of the Stikine plutonic suite (216-206 Ma; $\epsilon_{\text{Hf(t)}}$: +9.7 to +11.5), Povoas formation (Stikinia), and Semenof formation (Quesnellia) rocks. Stikine plutonic suite rocks crop out southwest and north of the Whitehorse trough and Upper Triassic rocks of

Stikinia and Quesnellia crop out throughout central Yukon (Fig. 2.4). Furthermore, Hart et al. (1995) documented augite and augite-feldspar-phyric basaltic andesite clasts in Richthofen formation conglomerate units that are consistent with Povoas formation provenance. Stikine plutonic suite rocks are spatially associated with Povoas formation rocks to the west and north of the Whitehorse trough, however, Hart et al. (1995) concluded that Stikine plutonic suite rocks were more extensive during the Early Jurassic based on the volume of Late Triassic plutonic clasts in conglomerate units. Therefore, the sediment transport pathways for Late Triassic superchondritic detrital zircon grains are northeast-, east- and south-directed however, the uncertain distribution of Stikine plutonic suite rocks in the Early Jurassic suggests alternative sediment pathways are possible.

Late Triassic to Middle Jurassic detrital zircon grains that yield chondritic-superchondritic compositions ($\epsilon_{\text{Hf(t)}}$: 0 to +7.5) occur throughout Laberge Group strata and are consistent with the Tatchun ($\epsilon_{\text{Hf(t)}}$: -9.5 to +9.5), Granite Mountain ($\epsilon_{\text{Hf(t)}}$: -12.7 to +10.1), Minto ($\epsilon_{\text{Hf(t)}}$: +0.8 to +10.9) and Thirtymile ($\epsilon_{\text{Hf(t)}}$: -1.0 to +3.8) plutons of the Minto plutonic suite (204-194 Ma) and the Aishihik ($\epsilon_{\text{Hf(t)}}$: -27.3 to +12.1), Big Creek ($\epsilon_{\text{Hf(t)}}$: -3.6 to +1.7), Sawtooth ($\epsilon_{\text{Hf(t)}}$: -6.2 to +11.6), Logtung ($\epsilon_{\text{Hf(t)}}$: -2.9 to +1.4), and Englishman ($\epsilon_{\text{Hf(t)}}$: +1.6 to +3.7) plutons of the Long Lake plutonic suite (192-178 Ma) (Figs. 2.4, 2.6 and 2.7). Source rocks crop out east, west, and north of the Whitehorse trough, therefore the sediment transport pathways for Late Triassic to Middle Jurassic chondritic-superchondritic detrital zircon grains are west-, east-, and south-directed (Fig. 2.4).

Late Triassic to Middle Jurassic subchondritic ($\epsilon_{\text{Hf(t)}}$: -4.7 and -0.5) detrital zircon grains occur in feldspathic lithic arenite (16-LVD-001B, Tanglefoot formation) and lithic

arenite (16-LVD-004, Tanglefoot formation) strata and crystal lithic tuff (17-LVD-038, Richthofen formation) located in the northern apex and along the western edge of the Whitehorse trough. Detrital zircon grains are consistent with subchondritic signatures recorded by the Granite Mountain, Big Creek, and Aishihik plutons (Minto and Long Lake suites) that crop out near the northern apex and western edge of the Whitehorse trough (Figs. 2.4, 2.6, and 2.7). Therefore, it is likely that the subchondritic detrital zircon grains were transported by east-directed drainage systems.

2.7.2.4 Sediment pathways and provenance evolution

Laberge Group detrital zircon populations are consistent with proximal source regions that surround the Whitehorse trough, which is characteristic of convergent margin basin deposits that develop in response to crustal thickening, regional uplift, and erosion (e.g., Dickinson, 1974; Cawood et al., 2009, 2012). Paleozoic detrital zircon grains are consistent with Yukon-Tanana and Paleozoic Quesnellia (Boswell formation) sources located north and east of the Whitehorse trough and with inherited zircon grains from the Tatchun, Minto, and Aishihik plutons (Fig. 2.4) located north and west of the Whitehorse trough. Therefore, Paleozoic detrital zircon grains argue for south-, east-, and west-directed sediment pathways within the Whitehorse trough. Late Triassic to Middle Jurassic detrital zircon grains were sourced from Upper Triassic Stikinia/Quesnellia rocks and the Stikine, Minto, and Long Lake plutonic suites (Figs. 2.4, 2.6 and 2.7). Detrital zircon grains that yield chondritic-superchondritic isotopic compositions are consistent with plutons located east, west, and north of the Whitehorse trough, whereas subchondritic detrital zircon grains are consistent with

Minto and Long Lake suite plutonic rocks located along the western edge of the Whitehorse trough.

Tanglefoot formation strata collected along the Robert Campbell Highway demonstrate upsection changes in both sedimentary lithofacies and provenance (Figs. 2.5 and 2.6; van Drecht et al., 2017). Cross-bedded, Hettangian-Sinemurian (16-LVD-001C) feldspathic lithic sandstone units at the base of the succession yield superchondritic detrital zircon grains derived from the Joe Mountain, Povoas, and Semenof formations and Stikine plutonic suite, and chondritic detrital zircon grains sourced from the Minto and Long Lake plutonic suites (Table 2.2; Figs. 2.4, 2.5, and 2.6). These source regions are coincident to the north of the study area, generally indicating south-directed, longitudinal sediment transport along the northern apex of the Whitehorse trough. Massive, Sinemurian-Pliensbachian conglomeratic strata (16-LVD-001B) overlies the basal feldspathic lithic arenite units and document the influx of subchondritic to chondritic detrital zircon grains sourced from the Granite Mountain, Big Creek, and Aishihik plutons along the northwestern and western edge of the Whitehorse trough (Figs. 2.4, 2.5, 2.6). Pliensbachian-Toarcian lithic arenite units, the youngest recognized along the Robert Campbell Highway, also yield chondritic-subchondritic detrital zircon grains and imply that Minto and Long Lake plutonic suite rocks were sustained as source regions through east-directed, transverse drainage systems (Figs. 2.5 and 2.6). In northern British Columbia, Johannson et al. (1997) documented an analogous shift in the Inklin Formation from axial paleoflow in the Sinemurian to predominately transverse paleoflow in the Pliensbachian. However, the influx of detrital zircon grains with subchondritic Hf isotope compositions in the Tanglefoot formation is not observed in correlative Sinemurian-Pliensbachian strata of the Richthofen formation. Therefore, north-to-

south sediment transport was sustained in distal regions of the trough or transverse sediment pathways in distal regions sourced chondritic-superchondritic rocks. Subchondritic detrital zircon grains ($\epsilon_{\text{Hf}(t)}$: -4.4 to -2.7) in the Richthofen formation are restricted to a Toarcian-Aalenian crystal lithic tuff unit at King Lake (17-LVD-038) and indicate an eruptive event that was genetically related to the emplacement of the Aishihik pluton (Fig. 2.7; Table 2.2).

Mesozoic subchondritic detrital zircon grain populations are absent from Pliensbachian feldspathic lithic arenite units at Conglomerate Mountain (17-LVD-018) despite their proximity to the Granite Mountain, Big Creek, and Aishihik plutons (Figs. 2.2 and 2.5). Furthermore, Pliensbachian feldspathic lithic arenite units yield a superchondritic ($\epsilon_{\text{Hf}(t)}$: +9 to +12.7) Paleozoic population with a 313 Ma age peak (Fig. 2.5) that indicates strata at Conglomerate Mountain had distinctive sediment derivation with respect to other Lower Jurassic strata along the Robert Campbell Highway.

Paleozoic detrital zircon grains in distal Richthofen formation strata occur in feldspathic lithic arenite and lithic wacke (16-LVD-009, 17-LVD-030, and 17-LVD-034) strata that are in central and eastern regions of the Whitehorse trough and suggest west-directed sediment pathways. However, Colpron et al. (2015) documented significant Paleozoic populations (>30%) in two Richthofen formation samples (GL04-108B and 04SJP594) located on the western edge of the Whitehorse trough (Fig. 2.2), which indicates that sediment derived east of the Whitehorse trough was transported further west or Paleozoic source regions located west of the Whitehorse trough also contributed to the sediment supply.

2.7.3 Early Mesozoic tectonic evolution

Zircon Hf isotope compositions are controlled by the proportion of depleted mantle,

lithospheric mantle, and crustal material incorporated in the melt during crystallization (Kinny and Maas, 2003). Melts derived from the mantle or the melting of juvenile rocks typically yield positive $\epsilon_{\text{Hf(t)}}$ values, whereas the increasing assimilation of continental crustal material results in progressively more negative $\epsilon_{\text{Hf(t)}}$ values (Kinny and Maas, 2003). Detrital zircon Hf isotope signatures can therefore be used to monitor juvenile magmatic contributions and periods of crustal reworking that are apparently defined by excursions towards subchondritic isotope values or “pull-downs” (e.g., Gehrels and Pecha, 2014; DeCelles and Graham, 2015). For example, Pecha et al. (2016) used detrital zircon Hf isotope geochemistry to resolve periods of magmatism related to crustal thickening in the Yukon-Tanana terrane of southeastern Alaska.

Laberge Group detrital zircon grains record a Late Triassic-Middle Jurassic pull-down from superchondritic $\epsilon_{\text{Hf(t)}}$ values of +12.3 to subchondritic $\epsilon_{\text{Hf(t)}}$ values -4.7. Late Triassic-Middle Jurassic detrital zircon grains are sourced from the Stikine, Long Lake, and Minto plutonic suites and are coeval with the Early Jurassic burial (ca. 200-186 Ma) of Yukon-Tanana rocks in the Stewart River and Aishihik Lake regions to moderate-deep crustal levels (Figs. 2.6 and 2.7; Johnston and Erdmer, 1995; Berman et al., 2007; Clark, 2017). The $\epsilon_{\text{Hf(t)}}$ pull-down and subchondritic magmatism is therefore attributed to collision-related crustal thickening of the Intermontane terranes after closure of the northern Cache Creek Ocean. Subchondritic values may alternatively reflect contamination from evolved Yukon-Tanana basement rocks (Snowcap assemblage; Piercy and Colpron, 2009) that were intruded by Late Triassic-Early Jurassic plutons, however, the published evidence is most consistent with early Mesozoic magmatism being coincident with crustal thickening processes (e.g., Colpron et al.,

2015).

Subchondritic detrital zircon grains are restricted to Laberge Group strata located in the northern apex and along western edge of the Whitehorse trough (16-LVD-001B, 16-LVD-004, and 17-LVD-038). Late Triassic to Early Jurassic Minto plutonic suite (ca. 204-194 Ma) rocks north of the Whitehorse trough yield chondritic to superchondritic values, whereas the Early Jurassic Long Lake plutonic suite (ca. 192-178 Ma) rocks along the western edge of the trough (Big Creek and Aishihik plutons) yield subchondritic to chondritic values (Fig. 2.4; Sack et al., 2019). Metamorphic mineral assemblages in Yukon-Tanana amphibolite-facies basement rocks formed at pressures of 7-9 kbar and the early phases of collision-related intrusive activity likely took place at 5-7 kbar in the Aishihik and Stewart River regions (Johnston et al., 1996; Berman et al., 2007; Clark, 2017). Subchondritic detrital zircon grains restricted to the northern apex and western edge of the Whitehorse trough therefore approximate the locations of rapidly buried source regions.

Late Triassic-Early Jurassic crustal thickening was overall contemporaneous with the time-transgressive, southward closure of the Cache Creek Ocean and collision-related deformation and metamorphism of Intermontane terrane rocks in central Yukon (e.g., Johnston et al., 1995, 1996; Mihalynuk et al., 2004; Berman et al., 2007; Nelson et al., 2013; Colpron et al., 2016). If correct, the subchondritic detrital zircon grains indicate that collision may have initiated as early as the Rhaetian and continued southwards until the Toarcian-Aalenian (Figs. 2.6 and 2.7). Burial of the Intermontane terranes was followed by the rapid Early Jurassic exhumation of Yukon-Tanana basement rocks, including ~15-20 km of exhumation along the Willow Creek fault (e.g., Johnston et al., 1996; Villeneuve et al., 2003; Knight et al., 2013). Hettangian-Sinemurian (16-LVD-001C) and Sinemurian-Pliensbachian (16-LVD-001B) strata

contain detrital zircon grains from the 216-206 Ma Stikine suite and 184 Ma Aishihik batholith, respectively, and furthermore indicate rapid exhumation and erosion following pluton emplacement. Eclogite clasts collected from latest Pliensbachian-earliest Toarcian strata in northern British Columbia yield exhumation rates (~4 km/m.y.) and are compatible with regional uplift being driven by syn- to post-collisional extension at the boundary of Yukon-Tanana and Stikinia (Kellett et al., 2018).

2.7.4 Subsidence

The counterclockwise rotation of Stikinia followed the late Permian closure of the Slide Mountain Ocean, late Permian-Early Triassic collision of Yukon-Tanana and related terranes along the western Laurentian margin, and the establishment of a Middle to Late Triassic continental arc system from Yukon to southern California (e.g., Mihalynuk et al., 1994; Beranek and Mortensen, 2011). This rotation led to the isolation and entrapment of the Cache Creek Ocean between the adjacent Stikinia and Quesnellia terranes (Mihalynuk et al., 1994). The Whitehorse trough likely developed as an Early Jurassic collisional depocenter near the hinge of the orocinal bend after the bilateral closure of the Cache Creek terrane beneath Stikinia and Quesnellia (Mihalynuk, 1994; English and Johnston, 1995; Nelson et al., 2013; Colpron et al., 2015). Collision-related sedimentation began as a result of the rapid exhumation and erosion of Intermontane terrane rocks located in north and west of the basin (e.g., Johnston et al., 1995, 1996; Villeneuve et al., 2003; Knight et al., 2013; Colpron et al., 2015). Dickie and Hein (1995) suggested that rapid subsidence in the basin was accommodated by basin-bounding faults and relative sea level rise, although these mechanisms have not been rigorously tested. New maximum depositional ages of basal strata

indicate the Whitehorse trough initiated by the Sinemurian as a narrow depocenter that extended ~120 km from Eagles Nest Bluff in the north to Mount Laurier in the south (Fig. 2.9). This elongate shape is consistent with the initial depocenter being generated as a flexural basin or a pull-apart basin during and after the south-directed closure of the Cache Creek Ocean (see Colpron et al., 2015). In central Yukon, Lower to Middle Jurassic strata unconformably overlie different units of the Lewes River Group and suggest variable topography within Mesozoic Stikinia prior to Laberge Group sedimentation (e.g., Wheeler, 1961; Tempelman-Kluit, 1984; Dickie and Hein, 1995; Lowey, 2008). If early Laberge Group sedimentation was controlled by topographic high stands created by large reefs (as suggested by massive limestone), then older basal strata should overlie regional low standing strata (limestone conglomerate). However, Sinemurian to Toarcian basal samples (17-LVD-030 and 17-LVD-027) overlie limestone conglomerate, whereas older Rhaetian to Toarcian basal strata (16-LVD-009, 17-LVD-034, 08MC091) overlie massive limestone. Therefore, Laberge Group deposition was not likely governed exclusively by topographic highs. Following initial deposition, Colpron et al. (2015) suggested the Whitehorse trough developed into a collisional, wedge-top basin by the Pliensbachian. Wedge-top basin development is coeval with the Pliensbachian-Aalenian expansion of basal strata to the west, east, and south.

The tectonothermal history of Yukon-Tanana rocks in the Stewart River and McQuesten regions of central Yukon have been attributed to transtensional exhumation (e.g., Johnston et al., 1996; Knight et al., 2003; Villeneuve et al., 2003; Berman et al., 2007). Devonian-Mississippian plutonic and volcanic rocks of the Reid Lakes complex and pre-Late Devonian to late Permian Yukon-Tanana rocks in the McQuesten region of central Yukon are juxtaposed by the NW-SE trending Willow Creek fault, an extensional structure within the

northern Teslin fault system that accommodated ~15-20 km of Early Jurassic exhumation (Knight et al., 2003). Early Jurassic transtensional exhumation recorded by these Yukon-Tanana rocks is coeval with Early Jurassic Laberge Group sedimentation and therefore suggest a pull-apart basin origin for the Whitehorse trough during oblique convergence and collision. Coeval Yukon-Tanana exhumation and Whitehorse trough subsidence are conceivably explained by compression and transtension in a strike-slip tectonic regime as broadly predicted by south-directed closing of the northern Cache Creek Ocean. The younging of basal strata suggests that the Whitehorse trough expanded to the west, east, and south during the Pliensbachian to Aalenian following initial Sinemurian subsidence (Fig. 2.9).

Early Jurassic basins that were located to the north and west of the Whitehorse trough are characterized by the Faro Peak and Macauley Ridge formations, respectively, and yield detrital zircon populations and maximum depositional ages that are consistent with Laberge Group strata (Colpron et al., 2015). Colpron et al. (2015) suggested these two basins were either isolated in the Early Jurassic and had common source regions, or that the Whitehorse trough was once more extensive (Colpron et al., 2015). In the sinistral strike-slip regime interpreted here for the Whitehorse trough, the Faro Peak and Macauley Ridge formations are probably isolated transtensional basins that developed near splays in the Teslin fault system. Furthermore, Early Jurassic exhumation in the McQuesten region of central Yukon occurred between these two isolated basins and Whitehorse trough, suggesting that an Early Jurassic regionally extensive basin was unlikely.

Late Triassic-Early Jurassic crustal thickening events recorded by Intermontane basement rocks and Laberge Group detrital zircon grains are attributed to the collision and accretion of Stikinia along the western Laurentian margin following the closure of the

northern Cache Creek Ocean (e.g., Johnston and Erdmer, 1995; Johnston et al., 1996; Villeneuve et al., 2003; Berman et al., 2007; Colpron et al., 2015; Clark, 2017). Collision of the Intermontane terranes occurred adjacent to foreland basin subsidence in British Columbia and Alberta and is coeval with the initial deposition of the Early Jurassic Fernie Formation (Fig. 2.1; Cant and Stockmal, 1989; Price 1994; Pană, et al., 2018). These synchronous events argue for Rhaetian to Toarcian-Aalenian crustal thickening have resulted in lithospheric flexure in the foreland region and subsequent Early Jurassic establishment the Canadian Rockies foreland basin system (Pană et al., 2018).

2.8 Conclusions

The Whitehorse trough developed atop the northern Intermontane terranes of central Yukon and northern British Columbia by the Sinemurian and was related to post-collisional exhumation of basement assemblages and collision-related plutons. Maximum depositional ages of basal Laberge Group strata indicate that the Whitehorse trough developed as pull-apart depocenter in a transtensional tectonic regime during the south-directed closure of the northern Cache Creek Ocean. The basin expanded to the west, east, and south in the Pliensbachian-Aalenian following initial Early Jurassic subsidence, however, it was not likely connected to other isolated basins positioned north of the Whitehorse trough.

Laberge Group strata yield Late Triassic-Early Jurassic and subsidiary Paleozoic detrital zircon grains that were derived from 216 to 178 Ma arc- to collision-related plutons and basement domains of the Yukon-Tanana, Stikinia, and Quesnellia terranes. Hf isotopes in zircon reveal that superchondritic-chondritic Paleozoic and early Mesozoic detrital zircon grains were transported by south-, east-, and west-directed sediment transport systems,

whereas subchondritic early Mesozoic detrital zircon grains were transported by predominately east-directed sediment systems. An influx of subchondritic detrital zircon grains derived from the Granite Mountain, Big Creek, and Aishihik (Minto and Long Lake suites) plutons record a Sinemurian-Pliensbachian shift from longitudinal, south-directed transport to transverse, east-directed sediment pathways in the northern apex of the trough.

Closure of the northern Cache Creek Ocean and crustal thickening during the collision of Yukon-Tanana and Stikinia is recorded by a Late Triassic-Middle Jurassic excursion to subchondritic signatures. Crustal thickening is interpreted to have commenced as early as the Rhaetian and continued until the Toarcian-Aalenian. The prevalence of subchondritic detrital zircon grains in the northern apex of the trough and distribution of subchondritic $\epsilon_{\text{Hf(t)}}$ isotope signatures recorded by the Stikine, Minto and Long Lake plutonic suite (Sack et al., 2019) source rocks indicate crustal thickening was concentrated along the western edge and north of the Whitehorse trough. Collision of the Intermontane terranes and syn-collisional deposition in the Whitehorse trough is coeval with foreland basin subsidence in British Columbia and Alberta and supports the early Jurassic development of the Canadian Rockies foreland system (e.g., Colpron et al., 2015; Pană et al., 21018).

Results in this study demonstrate that the U-Pb age and Hf isotope composition of detrital zircon grains from syn-collisional strata record the crustal and tectonic evolution of the source rocks and basin, respectively, and approximate the position of subchondritic, chondritic and superchondritic source regions relative to the basin. This integrated methodology is useful to characterize syn-collisional strata in accretionary tectonic regimes where the original shape

and thickness of the basin may not be preserved and source rocks have been reworked by regional deformation, metamorphism and magmatism.

References

- Anfinson, O.A., Leier, A.L., Gaschnig, R., Embry, A.F., and Dewing, K., 2012, U-Pb and Hf isotopic data from Franklinian Basin strata: insights into the nature of Crockerland and the timing of accretion, Canadian Arctic Islands: Canadian Journal of Earth Sciences, v. 49, p 1316-1328, doi:10.1139/e2012-067.
- Beranek, L.P., Mortensen, J.K., Orchard, M.J., and Ullrich, T., 2010, Provenance of North American Triassic strata from west-central and southeastern Yukon: correlations with coeval strata in the Western Canada Sedimentary Basin and Canadian Arctic Islands: Canadian Journal of Earth Sciences, v. 47, p. 53-73, doi: 10.1139/E09-065.
- Beranek, L.P., and Mortensen, J.K., 2011, The timing and provenance record of the Late Permian Klondike orogeny in northwestern Canada and arc-continent collision along western North America: Tectonics, v. 30, 23 p, doi:10.1029/2010TC002849.
- Beranek, L.P., van Staal, C.S., McClelland, W.C., Israel, S., and Mihalynuk, M., 2013, Detrital zircon Hf isotopic composition indicate a northern Caledonian connection for the Alexander terrane: Lithosphere, v. 5, p. 163-168, doi:10.1130/L255.1
- Berman, R.G., Ryan, J.J., Gordey, S.P., and Villeneuve, M., 2007, Permian to Cretaceous polymetamorphic evolution of the Stewart River region, Yukon-Tanana terrane, Yukon, Canada: P-T evolution linked with *in situ* SHRIMP monazite geochronology: Journal of Metamorphic Geology, v. 25, p. 803-827, doi:10.1111/j.1525-1314.2007.00729.x.
- Bostock, H.S., 1936, Carmacks District, Yukon: Geological Survey of Canada Memoir 189, 67 p.
- Bostock, H.S., and Lees, E.J., 1938, Laberge map-area, Yukon: Geological Survey of Canada, Memoir 217, 32 p.
- Bordet, E., 2016, Preliminary results on the Middle Triassic-Middle Jurassic stratigraphy and structure of the Teslin Mountain area, southern Yukon, *in* MacFarlane, K.E., and

Nordling, M.G., eds., Yukon Exploration and Geology, 2015: Yukon Geological Survey, p.43-61.

Bordet, E., 2017, Updates on the Middle Triassic-Middle Jurassic stratigraphy and structure of the Teslin Mountain and east Lake Laberge areas, south-central Yukon, *in* MacFarlane, K.E., and Weston, L.H., eds., Yukon Exploration and Geology 2016: Yukon Geological Survey, p.1-24.

Bouvier, A., Vervoort, J.D., and Patchett, P.J., 2008, The Lu-Hf and Sm-Nd composition of CHUR: Constraints from unequilibrated chondrites and implications for the bulk composition of terrestrial planets: Earth and Planetary Science Letter, v. 273, p. 48-57, doi:10.1016/j.epsl.2008.06.010.

Cant, D.J., and Stockmal, G.S., 1989, The Alberta foreland basin: relationship between stratigraphy and Cordilleran terrane-accretion events: Canadian Journal of Earth Sciences, v. 26, p. 1964-1975, doi:10.1139/e89-166.

Cawood, P.A., Kröner, A., and Collins, W.J., 2009, Accretionary orogens through Earth history: Geological Society, London, Special Publication 318, p. 1-36, doi:10.1144/SP318.1.

Cawood, P.A., Hawkesworth, C.J., and Dhuime, B., 2012, Detrital zircon record and tectonic setting: Geology, v. 40, p. 875-878, doi:10.1130/G32945.1.

Childe, F.C., and Thompson, J.F.H., 1997, Geological setting, U-Pb geochronology, and radiogenic isotopic characteristics of the Permo-Triassic Kutcho Assemblage, north-central British Columbia: Canadian Journal of Earth Sciences, v. 34, p. 1310-1324, doi:10.1139/e17-104.

Clapham, M.E., Smith, P.L., and Tipper, H.W., 2002, Lower to Middle Jurassic stratigraphy, ammonoid fauna and sedimentary history of the Laberge Group in the Fish Lake syncline, northern Whitehorse Trough, Yukon, Canada, *in* Emond, D.S., Weston, L.H., and Lewis, L.L., eds., Yukon Exploration and Geology 2001: Exploration and

Geological Services Division, Yukon Region, Indian and Northern Affairs Canada, p. 73-85.

Clark, A.D., 2017, Tectonometamorphic history of mid-crustal rocks at Aishihik Lake, southwest Yukon: Simon Fraser University (MSc thesis), Burnaby, Canada, 153 p.

Cockfield, W.E., and Bell, A.H., 1926, Whitehorse District, Yukon: Geological Survey of Canada, Memoir 150, 63 p.

Coney, P.J., Jones, D.L., and Monger, J.W.H., 1980, Cordilleran suspect terranes: Nature, v. 288, p. 329-333.

Colpron, M., Murphy, D.C., Nelson, J.L., Roots, C.F., Gladwin, K., Gordey, S.P., Abbott, G. and Lipovsky, P.S., 2002, Preliminary geological map of Glenlyon (105L/1-7,11-14) and northeast Carmacks (115L/9,16) areas, Yukon Territory (1:125 000 scale): Exploration and Geological Services Division, Yukon Region, Indian and Northern Affairs Canada, Open File 2002-9.

Colpron, M., Nelson, J.L., and Murphy, D.C., 2006, A tectonostratigraphic framework for the pericratonic terranes of the northern Cordillera, *in* Colpron, M. and Nelson, J.L., eds., Paleozoic Evolution and Metallogeny of Pericratonic Terranes at the Ancient Pacific Margin of North America, Canadian and Alaskan Cordillera: Geological Association of Canada, Special Paper 45, p. 1-23.

Colpron, M., Nelson, J.L., and Murphy, D.C., 2007, Northern Cordilleran terranes and their interactions through time: Geological Society of American Today, v.17, no. 4/5, doi:10.1130/GSAT01704-5A.1.

Colpron, M., and Friedman, R.M., 2008, U-Pb zircon ages for the Nordenskiöld formation (Laberge Group) and Cretaceous intrusive rock, Whitehorse trough, Yukon, *in* Emond, D.S., Blackburn, L.R., Hill, R.P., and Weston, L.H., eds., Yukon Exploration and Geology 2007: Yukon Geological Survey, p. 139-151.

Colpron, M., 2011, Geological compilation of Whitehorse trough – Whitehorse (105D), Lake Laberge (105E), and part of Carmacks (115I), Glenyon (105L), Aishihik Lake (115H), Quiet Lake (105F) and Teslin (105C): Yukon Geological Survey Geoscience Map 2011-1, scale 1:250 000.

Colpron, M., and Nelson, J.L., 2011, A Digital Atlas of Terranes for the Northern Cordilleran: BC Geofile 2011-11.

Colpron, M., Crowley, J.L., Gehrels, G., Long, D.G.F., Murphy, D.C., Beranek, L., and Bickerton, L., 2015, Birth of the northern Cordilleran orogeny, as recorded by detrital zircons in Jurassic synorogenic strata and regional exhumation in Yukon: *Lithosphere*, v. 7, p. 541-562, doi:10.1130/L451.1

Colpron, M., Israel, S., Murphy, D., Pigage, L., and Moynihan, D., 2016, Yukon Bedrock Geology Map: Yukon Geological Survey, Open File 2016-1, 1:10 000 scale map and legend.

Cordey, F., Gordey, S.P., and Orchard, M.J., 1991, New biostratigraphic data for the northern Cache Creek terrane, Teslin map area, southern Yukon, *in* Current Research, Part E: Geological Survey of Canada Paper 91-1E, p. 67-76.

Creaser, R.A., Erdmer, P., Stevens, R.A., and Grant, S.L., 1997, Tectonic affinity of Nisutlin and Anvil assemblage strata from the Teslin tectonic zone, northern Canadian Cordillera: Constraints from neodymium isotope and geochemical evidence: *Tectonics*, v. 16, p.107-121.

Creaser, R.A., Goodwin-Bell, J-A.S., and Erdmer, P., 1999, Geochemical and Nd isotopic constraints for the origin of eclogite protoliths, northern Cordillera; implications for the Paleozoic tectonic evolution of the Yukon-Tanana terrane: *Canadian Journal of Earth Sciences*, v. 36, p.1697-1709

DeCelles, P.G., and Giles, K.A., 1996, Foreland basin systems: *Basin Research*, v. 8, p. 105-123.

- DeCelles, P.G., and Graham, S.A., 2015, Cyclical processes in the North American Cordilleran orogenic system: *Geology*, v. 43, p. 499-502, doi:10.1130/G36482.1.
- Dickie, J.R., and Hein, F.J., 1995, Conglomeratic fan deltas and submarine fans of the Jurassic Laberge Group, Whitehorse trough, Yukon Territory, Canada: fore-arc sedimentation and unroofing of a volcanic island-arc complex: *Sedimentary Geology*, v. 98, p. 263–292, doi:10.1016/0037-0738(95)00036-8.
- Dickinson, W.R., 1974, Plate tectonics and sedimentation, *in* Dickinson, W.R., ed., Tectonics and Sedimentation: Society of Economic Paleontology and Mineralogists Special Publication 22, p. 1-27.
- Dickinson, W.R., and Suczek, C.A., 1979, Plate Tectonic and Sandstone Compositions: The American Association of Petroleum Geologists, v. 36, no. 12, p. 2164-2182.
- Dickinson, W.R., and Valloni, R., 1980, Plate settings and provenance of sands in modern ocean basins: *Geology*, v. 8, p.82-86.
- Dickinson, W.R., Beard, L.S., Brakenridge, G.R., Erjavec, J.L., Ferguson, R.C., Inman, K.F., Kneppe, R.A., Lindberg, F.A., and Ryberg, P.T., 1983, Provenance of North American Phanerozoic sandstones in relation to tectonic setting: *Geological Society of America Bulletin*, v. 94, p. 222-235.
- Dickinson, W.R., and Gehrels, G.E., 2009, Use of U-Pb ages of detrital zircons to infer maximum depositional ages of strata: A test against a Colorado Plateau Mesozoic database: *Earth and Planetary Science Letters*, v. 288, p. 115-125, doi:10.1016/j.epsl.2009.09.013.
- Dostal, J., Keppie, D.J., and Ferri, F., 1999, Extrusion of high-pressure Cache Creek rocks into the Triassic Stikinia-Quesnellia arc of the Canadian Cordillera: implications for terrane analysis of ancient orogens and palaeogeography, *in* Murphy, J.B., Keppie, J.D., and Hynes, A.J., eds., Ancient Orogenes and Modern Analogues: Geological Society, London, Special Publications, v. 327, p. 71-87, doi:10.1144/SP327.5.

Dostal, J., Gale, V., and Church, B.N., 1999, Upper Triassic Takla Group volcanic rocks, Stikine Terrane, north-central British Columbia: geochemistry, petrogenesis, and tectonic implications: Canadian Journal of Earth Sciences, v. 36, p. 1483-1494.

English, J.M., and Johnston, S.T., 2005, Collisional orogenesis in the northern Canadian Cordillera: Implications for Cordilleran crustal structure, ophiolite emplacement, continental growth, and the terrane hypothesis: Earth and Planetary Science Letters, v. 232, p. 333-344, doi:10.1016/j.epsl.2005.01.025.

Ferri, F., 1997, Nina Creek Group and Lay Range assemblage, north-central British Columbia: remnants of late Paleozoic oceanic and arc terranes: Canadian Journal of Earth Sciences, v. 34, p. 854-874.

Fisher C.M., Vervoort, J.D., and DuFrane, S.A., 2014, Accurate Hf isotopic determinations of complex zircons using the “laser ablation split stream” method: Geochemistry, Geophysics, Geosystems, v. 15, p. 121-139, doi:10.1002/2013GC004962.

Flowerdew, M.J., Millar, I.L., Curtis, M.L., Vaughan, A.P.M., Horstwood, M.S.A., Whitehouse, M.J., and Fanning, C.M., 2007, Combined U-Pb geochronology and Hf isotope geochemistry of detrital zircons from early Paleozoic sedimentary rocks, Ellsworth-Whitmore Mountains block, Antarctica: Geological Society of American Bulletin, v. 119, p. 275-288, doi:10.1130/B25891.1.

Gabrielse, H., Murphy, D.C., and Mortensen, J.K., 2006, Cretaceous and Cenozoic dextral orogeny-parallel displacements, magmatism, and paleogeography, north-central Canadian Cordillera, *in* Haggart, J.W., Enkin, R.J. and Monger, J.W.H., eds., Paleogeography of the North American Cordillera: Evidence For and Against Large-Scale Displacements: Geological Association of Canada Special Paper 46, p. 255-276.

Gareau, S.A., and Woodsworth, G.J., 2000, Yukon-Tanana terrane in the Scotia-Quaal belt, Coast Plutonic Complex, central-western British Columbia, *in* Stowell, H.H. and McClelland, W.C., eds., Tectonics of the Coast Mountains in SE Alaska and Coastal

British Columbia: Geological Society of America Special Paper 343, p. 23-43.

Gehrels, G., and Pecha, M., 2014, Detrital zircon U-Pb geochronology and Hf isotope geochemistry of Paleozoic and Triassic passive margin strata of western North America: *Geosphere*, v. 10, p. 49-65, doi:10.1130/GES00889.1.

Grant, S.L., 1997, Geochemical, radiogenic tracer isotopic, and U-Pb geochronological studies of Yukon-Tanana terranes rocks from the Money Klippe, southeastern Yukon, Canada [M.Sc. thesis]: University of Alberta, 177 p.

Gordey, S.P., McNicoll, V.J., and Mortensen, J.K., 1998, New U-Pb ages from the Teslin area, southern Yukon, and their bearing on terrane evolution in the northern Cordillera, *in* Current Research 1998-F: Geological Survey of Canada, p.129-148.

Goudie, D.J., Fisher, C.M., Hanchar, J.M., and Crowley, J.L., 2014, Simultaneous in situ determination of U-Pb and Sm-Nd isotopes in monazite by laser ablation ICP-MS: *Geochemistry, Geophysics, Geosystems*, v. 15, p. 2575-2600, doi:10.1002/2014GC005431.

Hart, C.J.R., 1997, A Transect across Northern Stikinia: Geology of the Northern Whitehorse Map Area, Southern Yukon Territory (105D/13–16): Exploration and Geological Services Division, Yukon Region, Indian and Northern Affairs Canada, Bulletin 8, 112 p.

Hart, C.J.R., and Radloff, J.K., 1990, Geology of Whitehorse, Alligator Lake, Fenwick Creek, Carcross and Part of Robinson Map Areas (105D/11, 6, 3, 2 & 7): Yukon Geological Survey Open-File 1990-4(G), scale 1:50,000.

Hart, C.J.R., Dickie, J.R., Ghosh, D.K., and Armstrong, R.L., 1995, Provenance constraints for Whitehorse trough conglomerate: U-Pb zircon dates and initial Sr ratios of granitic clasts in Jurassic Laberge Group, Yukon Territory, *in* Miller, D.M., and Busby, C., eds., Jurassic Magmatism and Tectonics of the North American Cordillera: Geological Society of America Special Paper 299, p. 47–63.

Hawkesworth, C.J., and Kemp, A.I.S., 2006, Using hafnium and oxygen isotopes in zircons to unravel the record of crustal evolution: *Chemical Geology*, v. 226, p. 144-162.

Hutchison, M.P., 2017, Whitehorse trough: Past, present and future petroleum research – with a focus on reservoir characterization of the northern Laberge Group: Yukon Geological Survey, Open File 2017-2, 48 p.

Iizuka, T., Komiya, T., Rino, S., Maruyama, S., Hirata, T., 2010, Detrital zircon evidence for Hf isotopic evolution of granitoid crust and continental growth: *Geochimica et Cosmochimica Acta*, v. 74, p. 2450-2472.

Ingersoll, R.V., and Busby, C.J., 1995, Tectonics of sedimentary basins, *in* Busby, C.J., and Ingersoll, R.V., eds., *Tectonics of sedimentary basins*: Blackwell Science, p. 3–43.

Ingersoll, R.V., Kretchmer, A.G., and Valles, P.K., 1993, The effect of sampling scale on actualistic sandstone petrofacies: *Sedimentology*, v. 40, p. 937-953.

Johannson, G.G., Smith, P.L., and Gordey, S.P., 1997, Early Jurassic evolution of the northern Stikine arc: evidence from the Laberge Group, northwestern British Columbia: *Canadian Journal of Earth Science*, v. 34, p. 1030-1057.

Johnston, S.T., and Erdmer, P., 1995, Hot-side-up aureole in southwest Yukon and limits on terrane assembly of the northern Canadian Cordillera: *Geology*, v. 23, no. 5, p 419-422.

Johnston, S.T., Mortensen, J.K., and Erdmer, P., 1996, Igneous and metaigneous age constraints for the Aishihik metamorphic suite, southwest Yukon: *Canadian Journal of Earth Sciences*, v. 33, p. 1543–1555.

Joyce, N.L., Colpron, M., Allan, M.M., Sack, P.J., Crowley, J.L., and Chapman, J.B., 2016, New U-Pb zircon dates from the Aishihik batholith, southern Yukon, *in* K.E. MacFarlane and M.G. Nordling eds., *Yukon Exploration and Geology 2015: Yukon Geological Survey*, P.131-149.

Kellett, D.A., Weller, O.M., Zagorevski, A., Regis, D., 2018, A petrochronological approach

for the detrital record: Tracking mm-sized eclogite clasts in the northern Canadian Cordillera: *Earth and Planetary Science Letters*, v. 494, p. 23-31,
doi:10.1016/j.epsl.2018.04.036.

Kemp, A.I.S., Hawkesworth, C.J., Paterson, B.A., and Kinny, P.D., 2006, Episodic growth of the Gondwana supercontinent from hafnium and oxygen isotopes in zircon: *Nature*, v. 439, p. 580-583.

Kinny, P.D., and Maas, R., 2003, Lu-Hf and Sm-Nd isotope systems in zircon. *Reviews in Mineralogy and Geochemistry*, v. 12, p. 328-34, doi:10.2113/0530327.

Knight, E., Schneider, D.A., and Ryan, J., 2013, Thermochronology of the Yukon-Tanana Terrane, West-Central Yukon: Evidence for Jurassic Extension and Exhumation in the Northern Canadian Cordillera: *The Journal of Geology*, v. 121, p. 371-400,
doi:10.1086/670721.

Link, P.K., Fanning, C.M., and Beranek, L., 2005, Reliability and longitudinal change of detrital-zircon age spectra in the Snake River system, Idaho and Wyoming: An example of reproducing the bump barcode: *Sedimentary Geology*, v. 182, p. 101-142,
doi:10.1016/j.sedgeo.2005.07.012.

Liu, X-C., Wu, Y-B., Fisher, C.M., Hanchar, J.M., Beranek, L., Gao, S., and Wang, H., 2016, Tracing crustal evolution by U-Th-Pb, Sm-Nd, and Lu-Hf isotopes in detrital monazite and zircon from modern rivers: *Geology*, v. 45, p. 103-106, doi: 10.1130/G38720.1.

Logan, J.M., and Mihalynuk, M.G., 2014, Tectonic controls on early Mesozoic paired alkaline porphyry deposit belts ($\text{Cu-Au} \pm \text{Ag-Pt-Pd-Mo}$) within the Canadian Cordillera: *Economic Geology and the Bulletin of the Society of Economic Geologists*, v. 109, p. 827–858, doi:10.2113 /econgeo.109.4.827.

Long, D.G.F., 1986, Coal in Yukon, *in* Morin, J.A., ed., *Mineral Deposits of the Northern Cordillera*: Canadian Institute of Mining and Metallurgy Special Volume 37, p. 311-318.

Lowey, G.W., 2004, Preliminary lithostratigraphy of the Laberge Group (Jurassic), south-central Yukon: Implications concerning the petroleum potential of the Whitehorse trough, *in* Emond, D.S., and Lewis, L.L., eds., Yukon Exploration and Geology 2003: Yukon Geological Survey, p. 129–142.

Lowey, G.W., 2008, Summary of the stratigraphy, sedimentology and hydrocarbon potential of the Laberge Group (Lower–Middle Jurassic), Whitehorse trough, Yukon, *in* Emond, D.S., Blackburn, L.R., Hill, R.P., and Weston, L.H., eds., Yukon Exploration and Geology 2007: Yukon Geological Survey, p. 179–197.

Lowey, G.W., Long, D.G.F., Fowler, M.G., Sweet, A.R., and Orchard, M.J., 2009, Petroleum source rock potential of Whitehorse trough: A frontier basin in south-central Yukon: Bulletin of Canadian Petroleum Geology, v. 57, p. 350–386, doi:10.2113/gscpgbull.57.3.350.

Ludwig, K.R., 2008, User’s Manual for Isoplot 3.70 – A Geochronological Toolkit for Microsoft Excel: Berkeley Geochronology Center Special Publication 4, 76 p.

McCabe, R., and Uyeda, S., 1983, Hypothetical Model for the Bending of the Mariana Arc *in* Hayes, D. eds., The Tectonic and Geologic Evolution of Southeast Asian Seas and Islands: Part 2: Geophysical Monograph Series, v. 27, p. 281-292.

Metcalfe, P., 1981, Petrogenesis of the Klondike formation, Yukon Territory [MS.c. thesis], University of Manitoba, Winnipeg, M.B., 305 p.

Mihalynuk, M.G., Nelson, J., and Diakow, L.J., 1994, Cache Creek terrane entrapment: Oroclinal paradox within the Canadian Cordillera: Tectonics, v. 13, p. 575–595, doi:10.1029 /93TC03492.

Monger, J.W.H., and Irving, E., 1980. Northward displacement of north-central British Columbia: Nature, v. 285, p. 289-294.

- Monger, J.W.H., Wheeler, J.O., Tipper, H.W., Gabrielse, H., Harms, T., Struik, L.C., Campbell, R.B., Dodds, C.J., Gehrels, G.E., and O'Brien, J., 1991, Part B. Cordilleran terranes, Upper Devonian to Middle Jurassic assemblages (Chapter 8), *in* Gabrielse, H., and Yorath, C.J., eds., Geology of the Cordilleran Orogen in Canada: Geological Survey of Canada, Geology of Canada 4, p. 281–327.
- Monger, J., and Price, R., 2002, The Canadian Cordillera: Geology and Tectonic Evolution: Canadian Society of Exploration Geophysicists Recorder, v. 27, p. 17-36.
- Morris, J.D., Jezek, P.A., Hart, S.R., and Gill, J.B., 1983, The Halmahera Island, Molucca Sea Collision Zone, Indonesia: A Geochemical Survey *in* Hayes, D. eds., The Tectonic and Geologic Evolution of Southeast Asian Seas and Islands: Part 2: Geophysical Monograph Series, v. 27, p. 373-387.
- Mortensen, J.K., 1992, Pre–mid-Mesozoic tectonic evolution of the Yukon-Tanana terrane, Yukon and Alaska: Tectonics, v. 11, p. 836–853, doi:10.1029/91TC01169.
- Murphy, D.C., and Mortensen, J.K., 2003, Late Paleozoic and Mesozoic features constrain displacement on Tintina Fault and limit large-scale orogen-parallel displacement in the Northern Cordillera (abstract): Geological Association of Canada, Program of Abstracts, v. 28, Abstract 151.
- Murphy, D.C., Mortensen, J.K., Piercy, S.J., Orchard, M.J., and Gehrels, G.E., 2006, Mid-Paleozoic to early Mesozoic tectonostratigraphy evolution of Yukon-Tanana and Slide Mountain terranes and affiliated overlap assemblages, Finlayson Lake massive sulphide district, southeastern Yukon, *in* Colpron, M. and Nelson, J.L., eds., Paleozoic Evolution and Metallogeny of Pericratonic Terranes at the Ancient Pacific Margin of North America, Canadian and Alaskan Cordillera: Geological Association of Canada, Special Paper 45, p. 75-105.

Nelson, J.L., and Bradford, J.A., 1993, Geology of the Midway – Cassiar area, northern British Columbia: B.C. Ministry of Energy, Mines and Petroleum Resources, Bulletin 83, 94 p.

Nelson, J.L., and Mihalynuk, M., 1993, Cache Creek ocean: Closure or enclosure?: Geology, v. 21, p. 173-176, doi:10.1130/0091-7613(1993)021<0173:CCOCOE>2.3CO;2.

Nelson, J.L., and Friedman, R.M., 2004, Superimposed Quesnel (late Paleozoic–Jurassic) and Yukon-Tanana (Devonian–Mississippian) arc assemblages, Cassiar Mountains, northern British Columbia: Field, U-Pb and igneous petrochemical evidence: Canadian Journal of Earth Sciences, v. 41, p. 1201–1235, doi:10.1139/e04-028.

Nelson, J.L., Colpron, M., Piercy, S.J., Dusel-Bacon, C., Murphy, D.C., and Root, C.F., 2006, Paleozoic tectonic and metallogenic evolution of the pericratonic terranes in Yukon, northern British Columbia and eastern Alaska, *in* Colpron, M. and Nelson, J.L., eds., Paleozoic Evolution and Metallogeny of Pericratonic Terranes at the Ancient Pacific Margin of North America, Canadian and Alaskan Cordillera: Geological Association of Canada, Special Paper 45, p. 323-360.

Nelson, J.L., and Gehrels, G.E., 2007, Detrital zircon geochronology and provenance of the southeastern Yukon-Tanana terrane: Canadian Journal of Earth Sciences, v. 44, p. 297-316, doi:10.1139/E06-105.

Nelson, J.L., Colpron, M., and Israel, S., 2013, The Cordillera of British Columbia, Yukon, and Alaska: Tectonics and metallogeny, *in* Colpron, M., Bissig, T., Rusk, B.G., and Thompson, J.F.H., eds., Tectonics, Metallogeny and Discovery: The North American Cordillera and Similar Accretionary Settings: Society of Economic Geologists Special Publication 17, p. 53–103.

Pálfy, J., and Hart, C.J.R., 1995, Biostratigraphy of the Lower and Middle Jurassic Laberge Group, Whitehorse map area (105D), southern Yukon, *in* Yukon Exploration and

Geology 1994, Exploration and Geological Services Division, Yukon, Indian and Northern Affairs Canada, p. 73-86.

Pană, D.I., Poulton, T.P., and DuFrane, S.A., 2018, U-Pb detrital zircon dating supports Early Jurassic initiation of the Cordilleran foreland basin in southwestern Canada: Geological Society of American Bulletin, doi:10.1130/B31862.1.

Paton, C., Hellstrom, J., Paul, B., Woodhead, J., and Hergt, J., 2011, Iolite: Freeware for the visualisation and processing of mass spectrometric data: Journal of Analytical Atomic Spectrometry, v. 26, p. 2508-2518, doi:10.1039/C1JA10172B.

Pecha, M.E., Gehrels, G.E., McClelland, W.C., Giesler, D., White, C., and Yokelson, I., 2016, Detrital zircon U-Pb geochronology and Hf isotope geochemistry of the Yukon-Tanana terrane, Coast Mountain, southeast Alaska: Geosphere, v. 12, no. 5, doi:10.1130/GES01303.1.

Petrus, J., and Kamber, B.S., 2012, VizualAge: A Novel Approach to Laser Ablation ICP-MS U-Pb Geochronology Data Reduction: Geostandards and Geoanalytical Research, v. 36, 24 p., doi:10.1111/j.1751-908X.2012.00158.x.

Piercey, S.J., 2001, Petrology and tectonic setting of mafic and felsic volcanic and intrusive rocks in the Finlayson Lake volcanic-hosted massive sulphide (VHMS) district, Yukon, Canada: A record of mid-Paleozoic arc and back-arc magmatism and metallogeny [Ph.D. thesis], University of British Columbia, Vancouver, B.C., 305 p.

Piercey, S.J., Murphy, D.C., Mortensen, J.K., Paradis, S. and Creaser, R.A., 2002, Geochemistry and tectonic significance of alkalic mafic magmatism in the Yukon-Tanana terrane, Finlayson Lake region, Yukon: Canadian Journal of Earth Sciences, v. 39, p. 1729-1744.

Piercey, S.J., Mortensen, J.K. and Creaser, R.A., 2003, Neodymium isotope geochemistry of felsic volcanic and intrusive rocks from the Yukon-Tanana terrane in the Finlayson Lake region, Yukon, Canada: Canadian Journal of Earth Sciences, v. 40, p. 77-97.

Piercey, S.J., Murphy, D.C., Mortensen, J.K. and Creaser, R.A., 2004, The mid-Paleozoic initiation of the northern Cordilleran marginal back-arc basin: Geological, geochemical and neodymium isotopic evidence from the oldest mafic magmatic rocks in Yukon-Tanana terrane, Finlayson Lake district, southeast Yukon, Canada: Geological Society of America Bulletin, v. 32, p. 1087-1106.

Piercey, S.J., Nelson, J.L., Colpron, M., Dusel-Bacon, C., Simard, R-L. and Roots, C.F., 2006, Paleozoic magmatism and crustal recycling along the ancient Pacific margin of North American, northern Canadian Cordillera, *in* Colpron, M. and Nelson, J.L., eds., Paleozoic Evolution and Metallogeny of Pericratonic Terranes at the Ancient Pacific Margin of North America, Canadian and Alaskan Cordillera: Geological Association of Canada, Special Paper 45, p. 281-322.

Piercey, S.J., and Colpron, M., 2009, Composition and provenance of the Snowcap assemblage, basement to the Yukon-Tanana terrane, northern Cordillera: Implications for Cordilleran crustal growth: *Geosphere*, v. 5, no. 5, p. 439-464, doi:10.1130/GS00505.1.

Piercey, SJ., Murphy, D.C., and Creaser, R.A., 2012, Lithosphere-asthenosphere mixing in a transform-dominated late Paleozoic backarc basin: Implications for northern Cordilleran crustal growth and assembly: *Geosphere*, v. 8, no. 3, p. 716-739, doi:10.1130/GES00757.1.

Price, R.A., 1994, Cordilleran tectonics and the evolution of the western Canada sedimentary basin, *in* Mossop, G., and Shestyn, I., eds., Geologic Atlas of the Western Canada Sedimentary Basin: Calgary: Alberta Research Council and Canadian Society of Petroleum Geologist, p. 13-24.

Reading, H.G., 1982, Sedimentary basins and global tectonics: Proceedings of Geologists' Association, v. 93, p. 321-350.

Ruks, T.W., Piercy, S.J., Ryan, J.J., Villeneuve, M.E., and Creaser, R.A., 2006, Mid- to late Paleozoic K-feldspar augen granitoids of the Yukon-Tanana terrane, Yukon, Canada: Implications for crustal growth and tectonic evolution of the northern Cordillera: Geological Society of America Bulletin, v. 118, no. 9/10, doi:10.1130/B25854.1

Sack, P.J., Colpron, M., Crowley, J.L., Ryan, J.J., Allan, M.M., Beranek, L.P., Joyce, N., and Mortensen, J.K., 2019, Atlas of Late Triassic-Jurassic plutons in Yukon: Yukon Geological Survey Open File, in press.

Schiarizza, P., 2011, Geology of the Kutcho assemblage between Kutcho Creek and the Tucho River, northern British Columbia (NTS 104I/01), *in* Geological Fieldwork 2010: British Columbia Ministry of Energy, Mines and Petroleum Resources paper 2011-1, p. 99-118.

Schiarizza, P., 2012, Geology of the Kutcho Assemblage between the Kehlechoa and Tucho Rivers, northern British Columbia (NTS 104I/01, 02), *in* Geological Fieldwork 2011: British Columbia Ministry of Energy, Mines and Petroleum Resources paper 2012-1, p. 75-98.

Shirmohammad, F., Smith, P.L., Anderson, R.G., and McNicoll, V.J., 2011, The Jurassic succession at Lisadale Lake (Tulsequah map area, British Columbia, Canada) and its bearing on the tectonic evolution of the Stikine terrane: *Volumnia Jurassica*, v. 9, p. 43-60.

Simard, R.-L., and Devine, F., 2003, Preliminary geology of the southern Semenof Hills, central Yukon (105E/1,7,8), *in* Emond, D.S., and Lewis, L.L., eds., Yukon Exploration and Geology 2002: Yukon Geological Survey, p. 213–222.

Simard, R.-L., Dostal, J., and Roots, C.F., 2003b, Development of late Paleozoic volcanic arcs in the Canadian Cordillera: An example from the Klinkit Group, northern British Columbia and southern Yukon: *Canadian Journal of Earth Sciences*, v. 40, p. 907–924, doi:10.1139/e03-025.

Sláma, J., Kosler, J., Condon, D., Crowley, J.L., Gerdes, A., Hanchar, J.M., Horstwood, S.A., Morris, G.A., Nasdala, L., Norberg, N., Schaltegger, U., Schoene, B., Tubrett, M., and Whitehouse, M.J., 2008, Plešovice zircon – A new natural reference material for U-Pb and Hf isotopic microanalysis: Chemical Geology, v. 249, p. 1-35, doi:10.1016/j.chemgeo.2007.11.005.

Snyder, D.B., Roberts, B.J., and Gordey, S.P., 2003, Contrasting seismic characteristics of three major faults in northwestern Canada: Canadian Journal of Earth Sciences, v. 42, p. 1223-1237, doi:10.1139/E05-027.

Steven, R.A., Erdmer, P., Creaser, R.A., and Grant, S.L., 1995, Mississippian assembly of the Nisutlin assemblage: evidence from primary contact relationships and Mississippian magmatism in the Teslin tectonic zone, part of the Yukon-Tanana terrane of south-central Yukon: Canadian Journal of Earth Sciences, v. 33, p. 103-116.

Struik, L.C., and Orchard, M.J., 1985, Late Paleozoic conodonts from ribbon chert delineate imbricate thrusts within the Antler Formation of the Slide Mountain terrane, central British Columbia: Geology, v. 13, p. 794-798.

Tafti, R., 2005, Nature and Origin of the Early Jurassic Copper (-Gold) Deposits at Minto and Williams Creek, Carmacks Copper Belt, Western Yukon: Examples of Deformed Porphyry Deposits [M.Sc. thesis]: Vancouver, British Columbia, Canada, University of British Columbia, 213 p.

Tafti, R., and Mortensen, J.K., 2004, Early Jurassic porphyry (?) copper (-gold) deposits at Minto and Williams Creek, Carmacks Copper Belt, western Yukon, in Emond, D.S., and Lewis, L.L., eds., Yukon Exploration and Geology 2003: Yukon Geological Survey, p. 289-303.

Tempelman-Kluit, D.J., 1979, Transported cataclasite, ophiolite and granodiorite in Yukon: Evidence of arc-continent collision: Geological Survey of Canada, Paper 79-14, 27 p.

Tempelman-Kluit, D.J., 1984, Geology, Laberge (105E) and Carmacks (105I, Yukon Territory: Geological Survey of Canada, Open File 1101, scale 1:250 000.

Tozer, E., 1958, Stratigraphy of the Lewes River Group (Triassic), central Laberge area, Yukon Territory: Geological Survey of Canada, Bulletin 43, 28 p.

van Drecht, L.H., Beranek, L.P., and Hutchison, H., 2017, Jurassic stratigraphy and tectonic evolution of the Whitehorse trough, central Yukon: Project outline and preliminary field results, *in* MacFarlane, K.E., and Weston, L.H., eds., Yukon Exploration and Geology 2016: Yukon Geological Survey, p. 207-223.

van Drecht, L.H., and Beranek, L.P., 2018, New investigations of basal Laberge Group stratigraphy Whitehorse trough, central Yukon, *in* MacFarlane, K.E., eds., Yukon Exploration and Geology 2017: Yukon Geological Survey, p. 151-163.

Vervoort, J.D., and Blichert-Toft, J., 1999, Evolution of the depleted mantle: Hf isotope evidence from juvenile rocks through time: *Geochemica et Cosmochimica Acta*, v. 63, p. 533-556, doi:10.1016/S0016-7037(98)00274-9.

Vervoort, J.D., and Patchett, P.J., 1996, Behaviour of hafnium and neodymium isotopes in the crust: Constraints from Precambrian crustally derived granites: *Geochemica et Cosmochimica Acta*, v. 60, p. 3717-3733, doi:10.1016/0016-7037(96)00201-3.

Vervoort, J.D., Patchett, P.J., Blichert-Toft, J., and Albarède, F., 1999, Relationships between Lu-Hf and Sm-Nd isotopic systems in the global sedimentary system: *Earth and Planetary Science Letters*, v. 168, p. 79-99, doi:10.1016/S0012-821X(99)00047-3.

Vervoort, J.D., and Blichert-Toft, J., 1999, Evolution of the depleted mantle: Hf isotope evidence from juvenile rocks through time: *Geochimica et Cosmochimica Acta*, v. 63, no. 3/4, p 533-556.

Villeneuve, M.E., Ryan J.J., Gordey, S.P., and Piercy, S.J., 2003, Detailed thermal and provenance history of the Stewart River area (Yukon-Tanana terrane, western Yukon)

through application of SHRIMP, $^{40}\text{Ar}/^{39}\text{Ar}$, and TIMS, *in* Geological Association of Canada-Mineral Association of Canada annual meeting. Vancouver, BC, Geological Association of Canada, Abstract 344.

Wernicke, B., and Klepacki, D.W., 1988, Escape hypothesis for the Stikine block: *Geology*, v. 16, p.461-464, doi:10.1130/0091-7613(1988)016<0461:EHFTSB>2.3.CO;2.

Wheeler, J.O., 1961, Whitehorse map-area, Yukon Territory: Geological Survey of Canada, Memoir 312, 156 p.

White, D., Colpron, M., and Buffett, G., 2012, Seismic and geological constraints on the structure of the northern Whitehorse trough, Yukon, Canada: *Bulletin of Canadian Petroleum Geology*, v. 60, p.239-255.

Wiedenbeck, M., Allé, P., Corfu, F., Griffin, W.L., Meier, M., Oberli, F., Quadt, A.V., Roddick, J.C., and Spiegel, W., 1995, Three natural zircon standards for U-Th-Pb, Lu-Hf, trace element and REE analyses: *Geostandards Newsletter*, v. 19, p. 1-23.

Willner, A.P., Gerdes, A., and Massonne, H.-J., 2008, History of crustal growth and recycling at the Pacific convergent margin of South America at latitudes 29°-36°S revealed by a U=Pb and Lu-Hf isotope study of detrital zircon from late Paleozoic accretionary systems: *Chemical Geology*, v. 253, p. 114-129, doi:10.106/j.chemgeo.2008.04.016.

Wu, F-Y., Ji, W-Q., Liu, C-Z., Chung, S-L., 2010, Detrital zircon U-Pb and Hf isotopic data from the Xigaze fore-arc basin: Constraints on Transhimalayan magmatic evolution in southern Tibet: *Chemical Geology*, v. 271, p. 13-25, doi:10.1016/j.chemgeo.2009.12.007.

Yarnell, J.M., Stanley., G., and Hart, C.J., 1999, New paleontological investigations of Upper Triassic shallow-water reef carbonates (Lewes River Group) in the Whitehorse area, Yukon, *in* Roots, C.F., and Emond, D.S., eds., Yukon Exploration and Geology 1998: Exploration and Geological Services Division, Yukon, Indian and Northern Affairs Canada, p. 179-184.

Chapter 2 Tables

Terrane	Cycle	Age (Ma)	Location	Formation/Group/Suite	Geochemical Signature	$\epsilon_{\text{Nd(t)}}$	$\epsilon_{\text{Hf(t)}} = 1.36$ $\epsilon_{\text{Nd}} + 3.0^*$	Reference
Yukon-Tanana	Ecstall	390-365	Ecstall belt, B.C.	Big Falls	calc-alkalic arc	-4	-2.4	Gareau and Woodsworth, 2000
	Finalyson	365-357	Finlayson Lake	Cleaver Lake, Waters Creek and Fire Lake formations	IAT, I-IAT, MORB, NEB, BON	-4.8 to +0.1	-3.5 to +3.1	Piercey et al., 2003
				Kudz Ze Kayah	within-plate (A-type)	-9.5 to -7.8	-9.9 to -7.6	Piercey et al., 2003
				Wind Lake	OIB-like; NED; T-NEB; BABB	-2.8 to +1.1	-0.8 to +4.5	Piercey et al., 2002
				Fire Lake	E-MORB	-1.6 to +8.5	+0.8 to +14.6	Piercey, 2001; Piercey et al., 2004
				Grass Lakes suite	within-plate (A-type); plutonic equivalent to Kudz Ze Kayah	-7.8 to -9.5	-7.6 to -9.9	Piercey et al., 2003
	Wolverine	357-342	Finlayson Lake	Simpson Range suite	calc-alkalic	-12.9 to -7.4	-14.5 to -7.1	Piercey et al., 2003
				Wolverine Lake Group	within-plate (A-type)	-8.2 to -7.1	-8.2 to -6.7	Piercey et al., 2003
			Teslin	Nisutlin assemblage	N-MORB	+6.9	+12.4	Piercey, 2001
			Little Kalzas Lake	Little Kalzas formation	calc-alkalic	-6.2 to -2.5	-5.4 to -0.4	Stevens et al., 1995
Little Salmon	342-314	Little Salmon Lake	Little Salmon formation	OIB	calc-alkalic	-7.9 to -1.3	-7.7 to +1.2	Simard et al., 2007
Klinkit	314-269	Wolf Lake/Jennings River	Klinkit Group	OIB	calc-alkalic; OIB	+6.7 to +7.4	+12.1 to +13.1	Simard, 2003
Klondike	269-253	Stewart River	Augen granitoids	calc-alkalic	calc-alkalic	-15.3 to -2.0	-17.8 to -0.3	Ruks et al., 2006
		Klondike region	Klondike Schist	calc-alkalic	calc-alkalic	-9.9 to -1.5	-10.5 to -1.0	Metcalfe, 1981; Ruks et al., 2006
Slide Mountain	Mississippian to Permian	Teslin	Anvil assemblage	calc-alkalic (continental margin, rift-like?)	calc-alkalic (continental margin, rift-like?)	+4.1 to +6.4	+8.6 to +11.7	Creaser et al., 1997
		Finlayson Lake	Campbell Range Formation	OIB, E-MORB, N-MORB, BABB	OIB, E-MORB, N-MORB, BABB	-4 to +8.9	-2 to +15.1	Piercey et al., 2012
		south-central B.C.	Fenell Formation	N-MORB; back-arc	N-MORB; back-arc	+7.7 to +10.2	+13.5 to +16.9	Smith and Lambert, 1995; Patchett and Gehrels, 1997
Cache Creek	Carboniferous	south-central B.C.	Cache Creek terrane	tholeiitic, OIB	tholeiitic, OIB	+4.3 to +8.3	+8.8 to +14.3	Smith and Lambert, 1995; Patchett and Gehrels, 1997
	Late Permian to Early Triassic	north-central B.C.	Kutcho assemblage	tholeiitic	tholeiitic	+7.5 to +9.1	+13.2 to +15.5	Childe and Thompson, 1997
Quesnellia	Upper Triassic	north-central, B.C.	Quesnel Takla Group	IAT	IAT	+6.0 to +8.0	+11.3 to +13.9	Dostal, 2009
		north-central, B.C.	Nicola Group; pyroclastic	intermediate	intermediate	+3.6 to +7.6	+7.9 to +13.3	Patchett and Gehrels., 1997
Stikinia	Mississippian		Takhini Assemblage					Hart, 1997
	Middle Triassic	Joe Mountain	Joe Mountain Formation	IAT, MORB	IAT, MORB			Hart, 1997
	Upper Triassic	north-central, B.C.	Stikine Takla Group	IAT	IAT	+6.2 to +7.7	+11.5 to +13.6	Dostal, 1999
	Upper Triassic	central Yukon	Povoas Formation	calc-alkalic basalt, IAT	calc-alkalic basalt, IAT			Hart, 1997

*Vervoort and Blichert-Toft, 1999

Table 2.1 Summary of $\epsilon_{\text{Nd(t)}}$ and $\epsilon_{\text{Hf(t)}}$ values and locations of potential Yukon-Tanana, Stikinia and Quesnellia source regions for Whitehorse trough strata.

Sample name	Formation	Location	UTM				Maximum depositional ages				
			Zone	Easting	Northing	Datum	Weighted mean 2σ*	Unmix age	Youngest peak		Age
									TuffZirc	AgePick*	
16-LVD-001B	Tanglefoot	Robert Campbell Highway	08V	455577E	6877512N	NAD 83	186.54 ± 0.59	187.2 ± 0.73	195.35 +1.85/-0.85	195	Sinemurian to Pliensbachian
16-LVD-001C	Tanglefoot	Robert Campbell Highway	08V	455577E	6877512N	NAD 83	193.5 ± 2.6	199.59 ± 0.88	199.9 +3.4/-3.4	200	Hettangian to Sinemurian
16-LVD-004	Tanglefoot	Robert Campbell Highway	08V	436493E	6888370N	NAD 83	177.4 ± 1.8	181.42 ± 0.61	183.2 +0.6/-1.5	185	Pliensbachian to Toarcian
17-LVD-018	Tanglefoot	Conglomerate Mountain	08V	453930E	6833117N	NAD 83	184.2 ± 8.4	186.13 ± 1.4	186.10 +5.6/-5.9	185	Pliensbachian
16-LVD-009	Richthofen	Mount Laurier	08V	507457E	6765804N	NAD 83	195.8 ± 1.6	197.44 ± 1	204.5 +2.4/-2.1	205	Rhaetian to Sinemurian
16-LVD-021	Richthofen	Richthofen Island	08V	491272E	6775151N	NAD 83	195.3 ± 3.5	204.56 ± 0.77	209.5 +0.8/-1	210	Norian to Sinemurian
16-LVD-022	Richthofen	Lake Laberge	08V	493602E	6778206N	NAD 83	196.2 ± 2.8	199.52 ± 0.96	205.8 +0.6/-0.8	205	Rhaetian to Sinemurian
16-LVD-023	Richthofen	Lake Laberge	08V	495522E	6774110N	NAD 83	185.5 ± 1.8	196.29 ± 1.1	202 +3.2/-5	185	Rhaetian to Pliensbachian
17-LVD-027	Richthofen	Takhini subdivision	08V	488086E	6748844N	NAD 83	182.3 ± 2.4	182.3 ± 2.5	193.8 +1.4/-2.4	198	Sinemurian to Toarcian
17-LVD-030	Richthofen	Mount Byng	08V	539547E	6757952N	NAD 83	185 ± 1.3	183.5 ± 0.97	192.7 +2.1/-1.2	193*	Sinemurian to Toarcian
17-LVD-034	Richthofen	Mount Slim	08V	514475E	6751661N	NAD 83	184.4 ± 5.6	191.54 ± 0.94	201.75 +1.95/-1.55	185	Rhaetian to Toarcian
17-LVD-038	Richthofen	King Lake	08V	474374E	6742564N	NAD 83	173.5 ± 2.8	173.54 ± 1.5	174.15 +1.45/-2.05	173	Toarcian to Aalenian

* based on three or more grains

Table 2.2. Summary of Laberge Group sample locations and maximum depositional ages calculated in this study.

Chapter 2 Figures

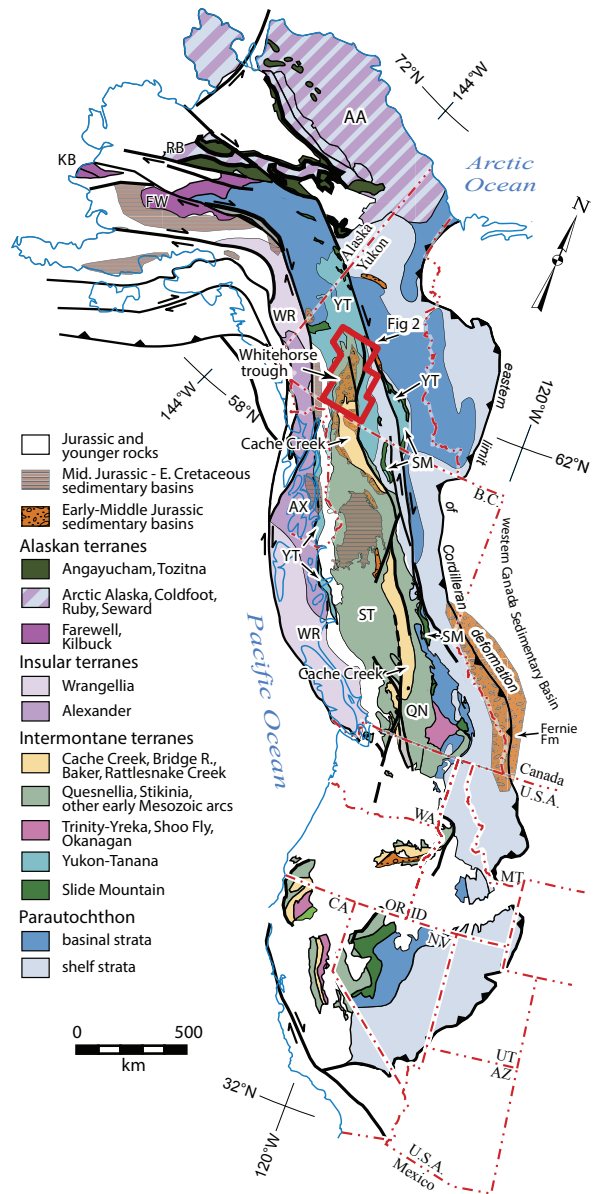


Figure 2.1. Terrane and Jurassic sedimentary basin map of the North American Cordillera after Colpron and Nelson (2011). The red outline shows the location of Figure 2.2.

Abbreviations: AA-Arctic Alaska terrane; AX-Alexander terrane; AZ-Arizona, B.C.-British Columbia; CA-California; FW-Farewell terrane; ID-Idaho; KB-Kilbuck terrane; Mt-Montana; NV-Nevada; Or-Oregon; QN-Quesnellia; RB-Ruby terrane; SM-Slide Mountain terrane; ST-Stikinia terrane; UT-Utah; WA-Washington; WR-Wrangellia terrane; YT-Yukon-Tanana; U.S.A-United States of America.

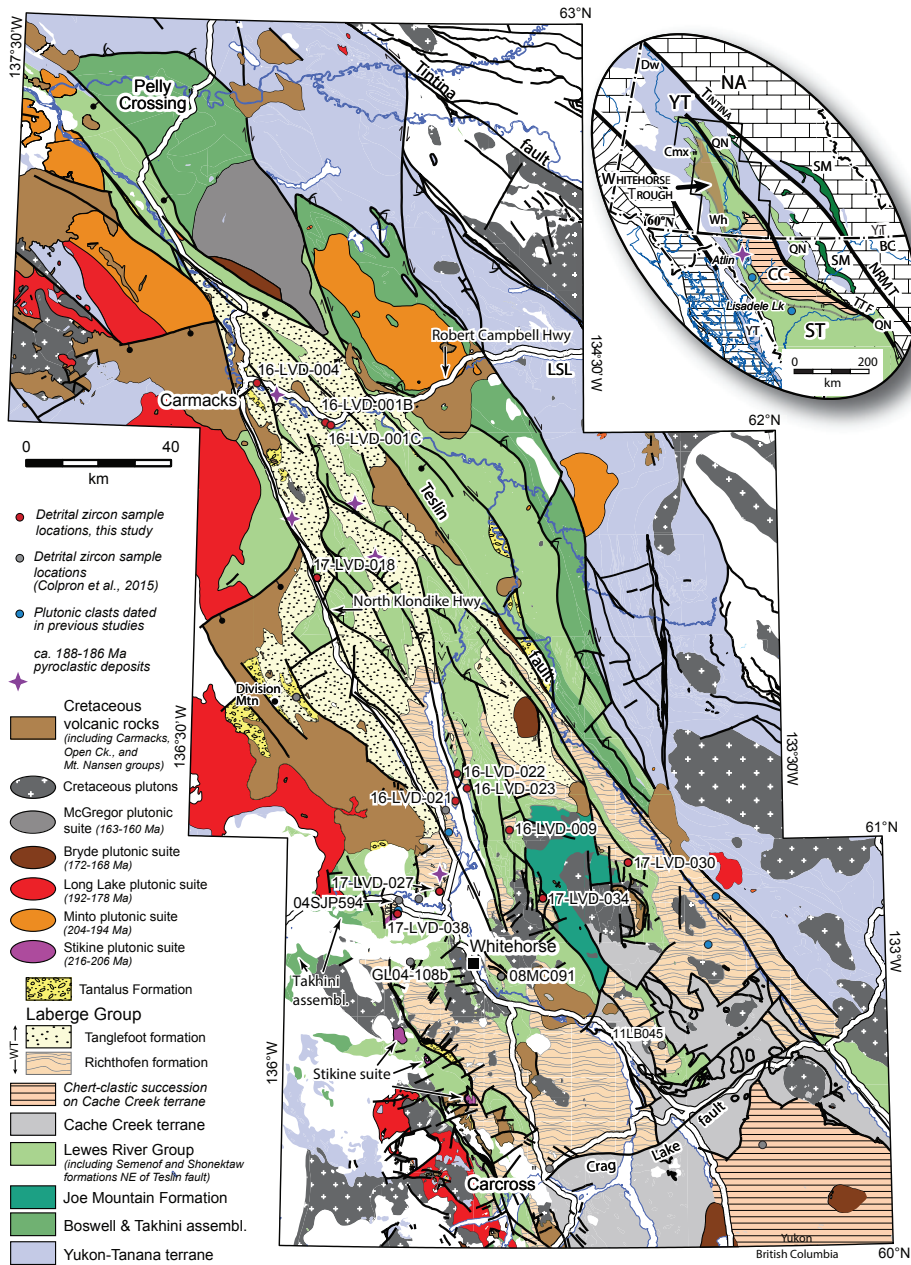


Figure 2.2. Regional geology of the Whitehorse trough area modified from Colpron et al. (2015). Detrital zircon sampling locations for this study are denoted by red dots. Grey dots denote detrital zircon sample locations of Colpron et al. (2015) and blue dots denote previously dated plutonic clasts by Hart et al. (1995) and Gordey et al. (1998). Purple stars denote locations of pyroclastic deposits dated by Colpron and Friedman (2008) and Hart et al. (1997). The inset shows Intermontane terranes and their present geometry. Abbreviations: CC-Cache Creek terrane; CMx-Carmacks; Dw-Dawson; LSL-Little Salmon Lake; NA-rocks of ancestral North America; NRMT-Northern Rocky Mountain Trench Fault; QN-Quesnellia; SM-Slide Mountain terrane; ST-Stikinia; TTF-Teslin-Thibert fault; Wh-Whitehorse; YT-Yukon-Tanana terrane.

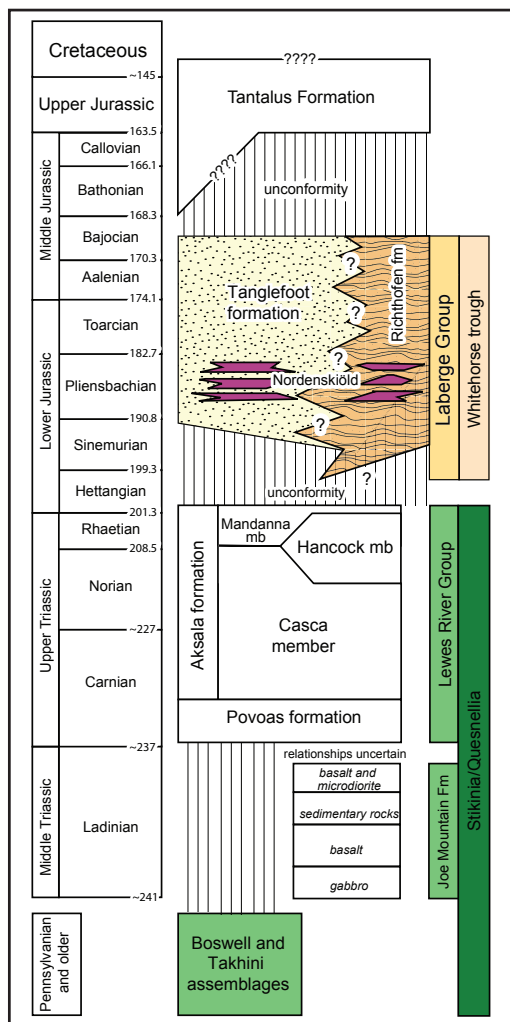


Figure 2.3. Upper Paleozoic-Mesozoic stratigraphy of Stikinia, Quesnellia, and Whitehorse trough complied by Colpron et al. (2015).

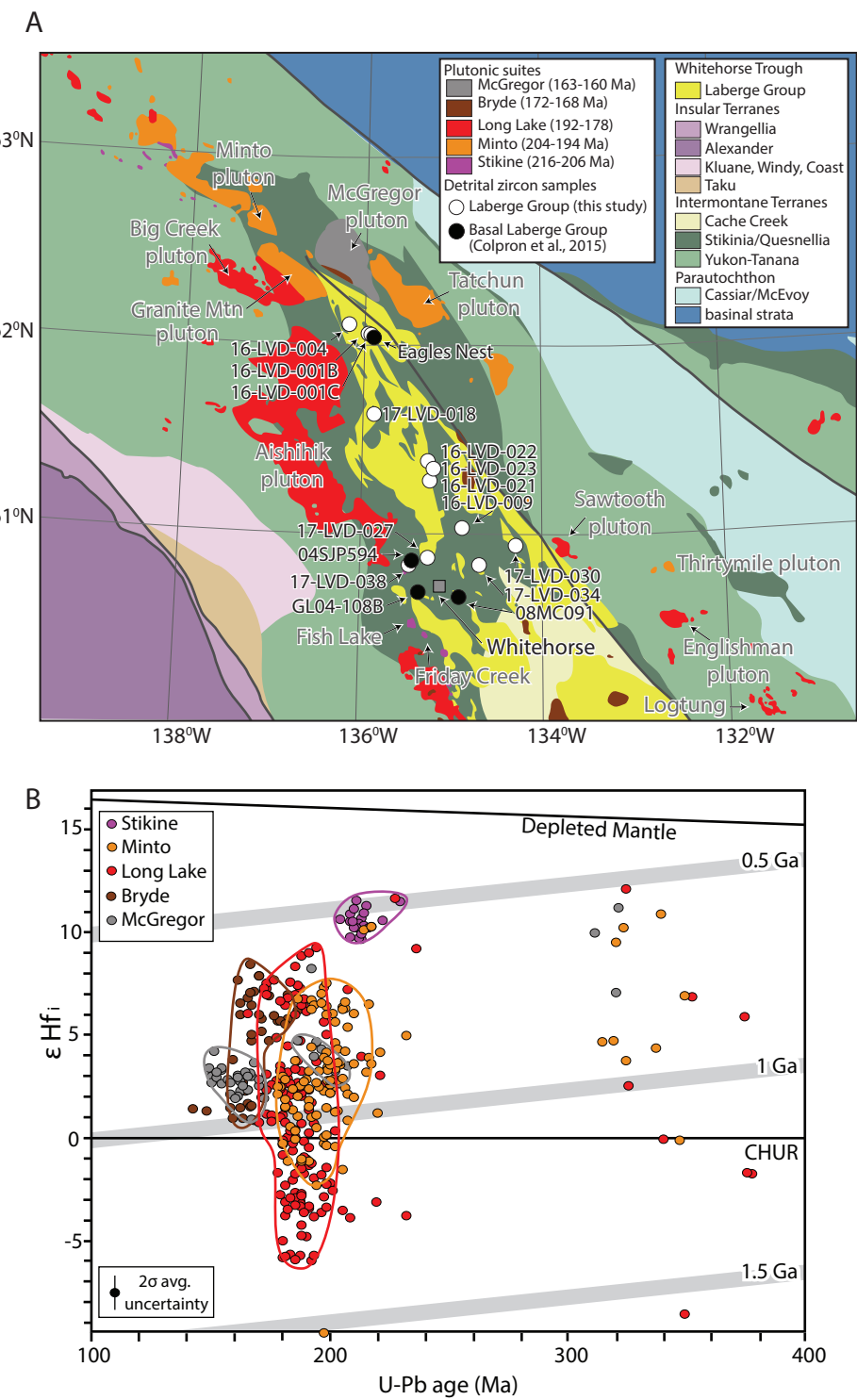


Figure 2.4. (A) Map of the Insular and Intermontane terranes, North American parautochthon, Whitehorse trough, and Late Triassic-Middle Jurassic plutonic suites after Colpron (2018). Detrital zircon sample locations from this study are denoted by white dots and basal detrital zircon samples of Colpron et al. (2015) are denoted by black dots. (B) $\epsilon_{\text{Hf}}^{\text{(t)}}$ vs. U-Pb age plot of the Late Triassic to Middle Jurassic plutonic suites. DM-depleted mantle (Vervoort and Blichert-Toft, 1999); CHUR-Chondritic uniform reservoir (Bouvier et al., 2008); Grey crustal evolution lines correspond to $^{176}\text{Lu}/^{177}\text{Hf}=0.0115$ (Vervoort and Patchett, 1996; Vervoort et al., 1999).

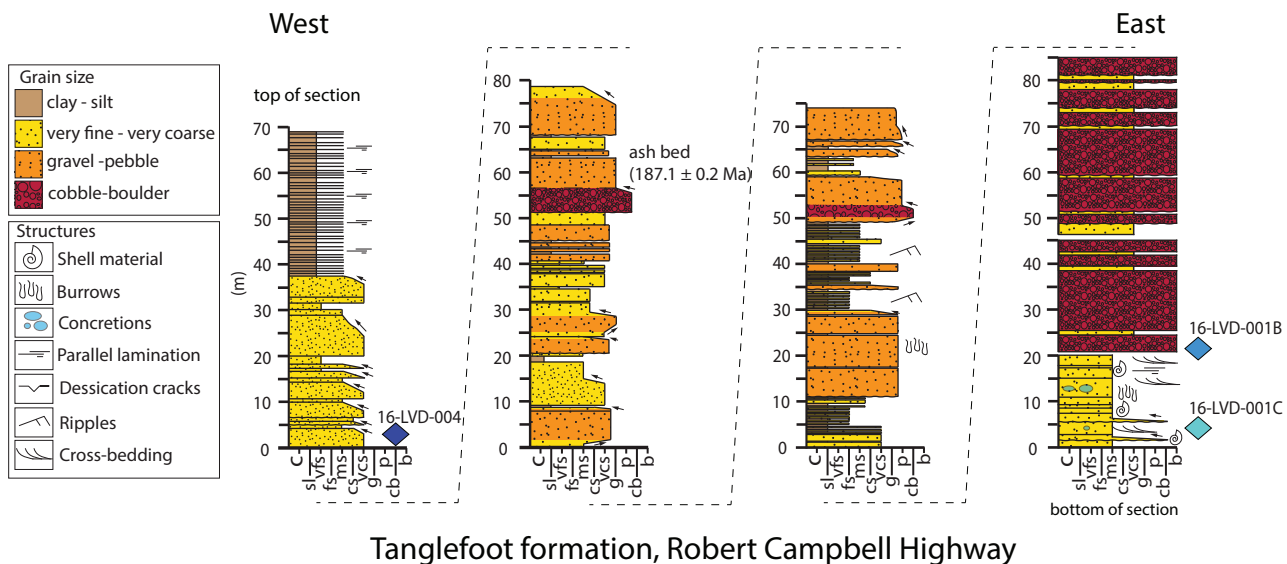


Figure 2.5. Measured stratigraphic sections of the Tanglefoot formation, Robert Campbell Highway, central Yukon. Stratigraphic sections young from east to west. Coordinates for the base of each section: 16-LVD-001C: zone 08V 455577E 687751N NAD 83, 16-LVD-001B: zone 08V 453930E 6833117N, 16-LVD-004: zone 08V 436493E 6888370N NAD 8. Pliensbachian ash bed date was reported by Colpron and Friedman (2008). Arrows indicate fining or coarsening upward trends. Grain size abbreviations: c-clay, sl-silt, vfs-very fine grained, fs-fine-grained, ms-medium-grained, cs-coarse-grained, vcs-very coarse-grained, g-granule, p-pebble, cb-cobble, and b-boulder.

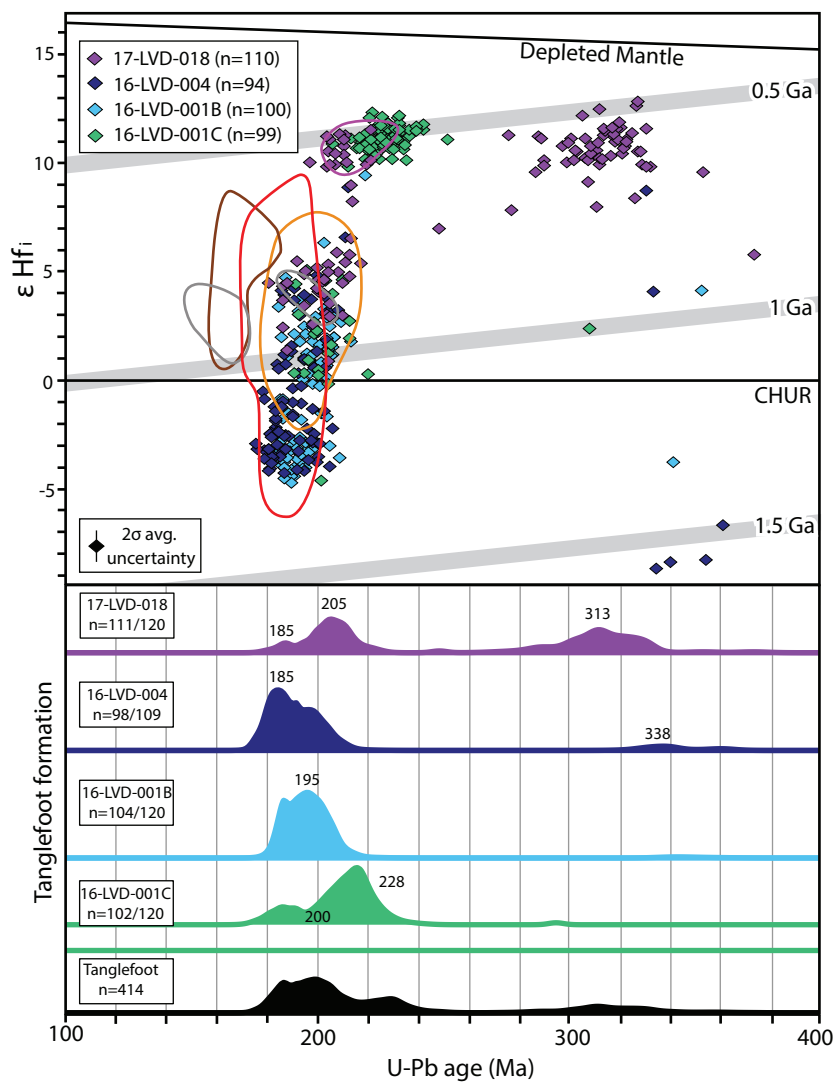


Figure 2.6. U-Pb and Hf isotope data for Tanglefoot formation samples. Fields define Late Triassic-Middle Jurassic plutonic suites shown in Figure 2.4. See Figure 2.4 caption for abbreviations.

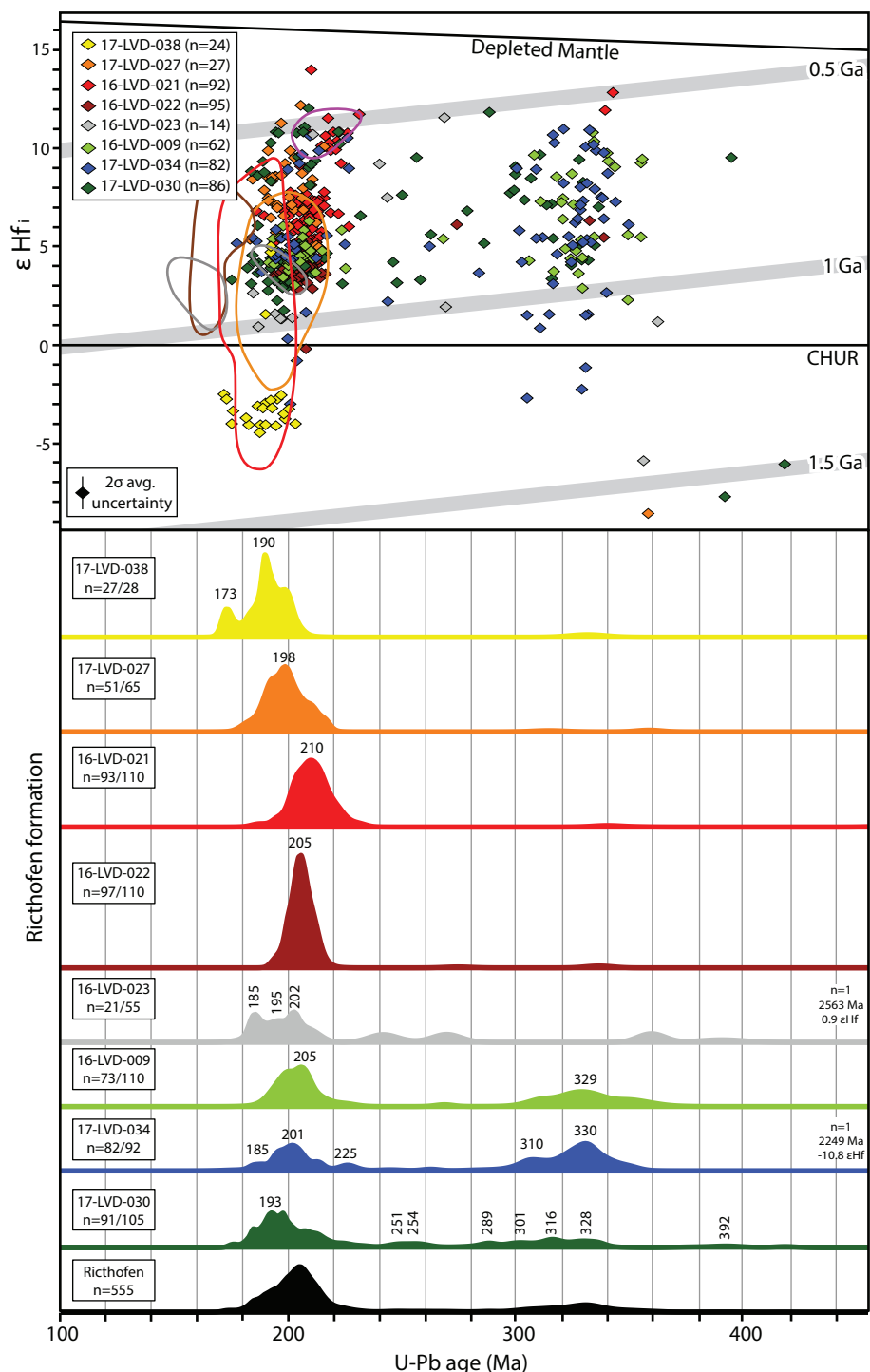


Figure 2.7. U-Pb and Hf isotope data for Richthofen formation samples. DM-depleted mantle (Vervoort and Blichert-Toft, 1999); Fields define Late Triassic-Middle Jurassic plutonic suites shown in Figure 2.4. See Figure 2.4 caption for abbreviations.

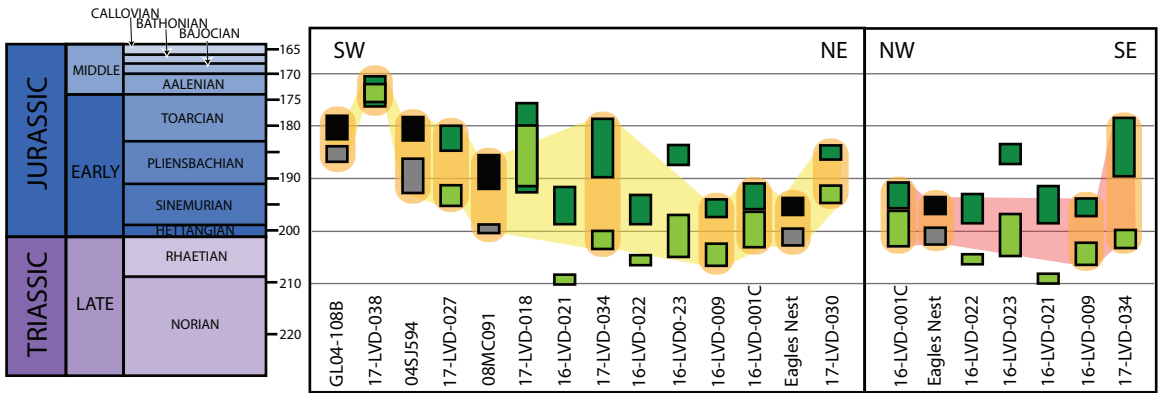


Figure 2.8. Maximum depositional age calculations for Laberge Group strata. Samples from this study are green and Colpron et al. (2015) samples are in black/grey. Light green and grey boxes represent TuffZirc ages; Dark green and black boxes represent weighted mean age; Orange fields denote basal Laberge Group strata; The trend of maximum depositional ages from west to east is shown by the yellow field; The trend of maximum depositional ages from northwest to southeast is shown by the red field. See Figure 2.2 for sample locations.

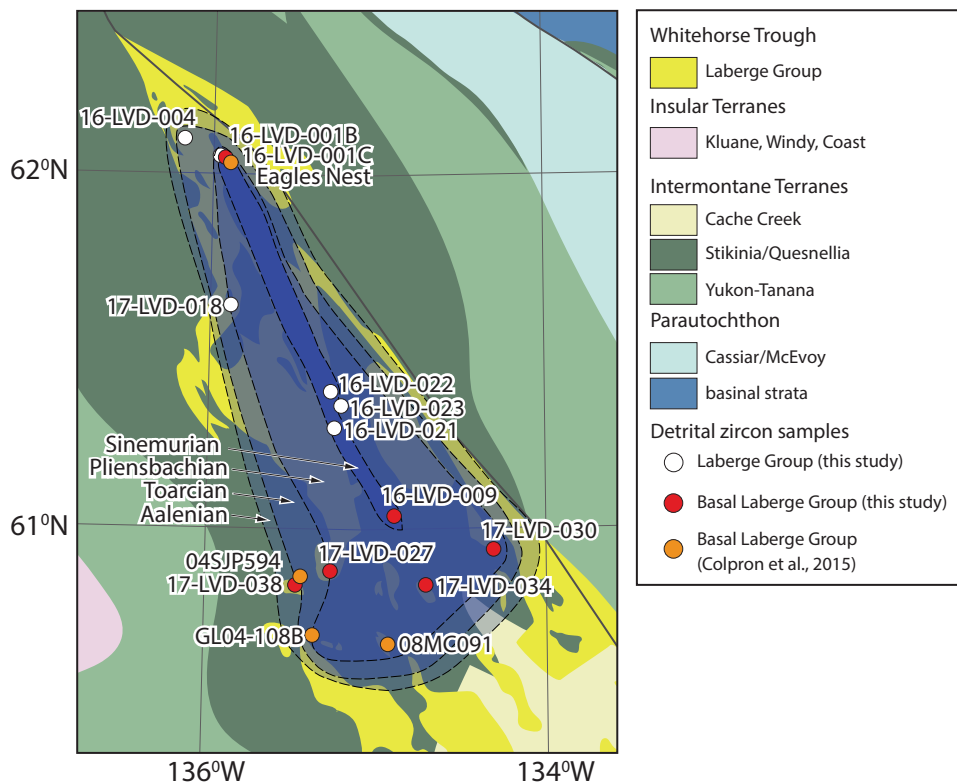


Figure 2.9. Sinemurian to Aalenian basin evolution of the Whitehorse trough based on maximum depositional ages of basal Laberge Group strata using the weighted mean of 3 or more young zircon grains. Laberge Group strata are denoted by white (non-basal strata; this study), red (basal strata; this study) and orange (basal strata; Colpron et al. (2015) dots. Blue fields represent the distribution of samples that yield Sinemurian, Pliensbachian, Toarcian, and Aalenian maximum depositional ages.

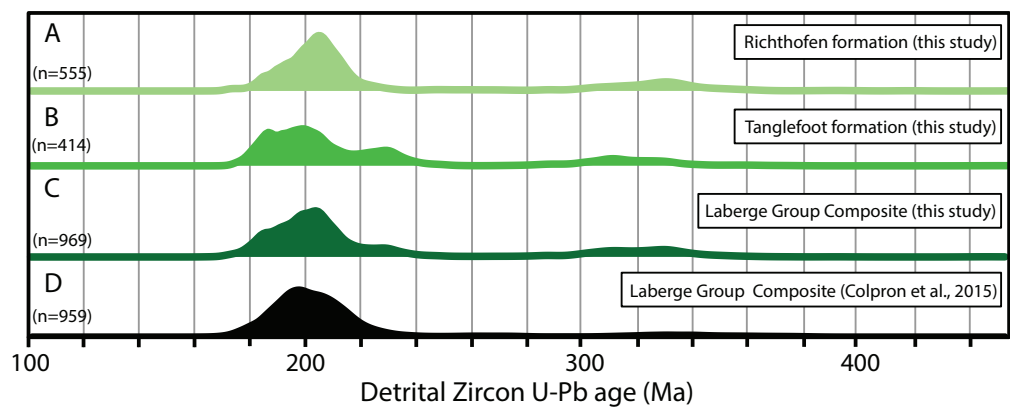


Figure 2.10. Composite normalized probability plots of the (A) Richthofen formation, (B) Tanglefoot formation, (C) composite Laberge Group of this study; and (D) composite Laberge group of Colpron et al. (2015).

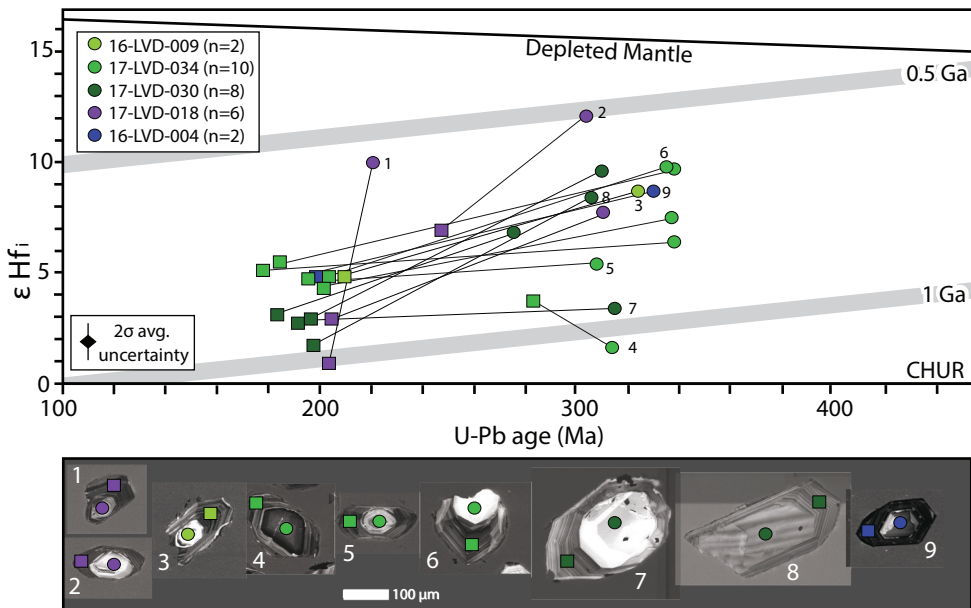


Figure 2.11. (A) U-Pb and Hf isotope data of Laberge Group detrital zircon cores and rims. Line connecting data points show the core to rim relationship of a single grain. See Figure 2.4 caption for abbreviations. (B) CL images of detrital zircon crystals. Numbers 1-9 denote the data points in A that correspond to each grain.

Chapter 3: Summary and future research

3.1 Summary

Lower to Middle Jurassic syn-collisional strata of the Laberge Group record the basin filling history of the Whitehorse trough and therefore the early Mesozoic accretionary history of the northern Canadian Cordillera. The Whitehorse trough overlaps several of the northern Intermontane terranes and is interpreted as a collisional basin that formed during the entrapment and closure of the northern Cache Creek Ocean. Yukon-Tanana terrane rocks located along the western flank and north of the Whitehorse trough were buried at 5-9 kbar (~18-33 km) during imbrication and subsequently exhumed 15-20 km to upper crustal levels by the Sinemurian-Pliensbachian (195-186 Ma). Rapid exhumation and significant erosion in central Yukon led to the deposition of the ~3000 m-thick Laberge Group, which is comprised of proximal marginal-marine strata in the northern apex of the Whitehorse trough and distal deep-marine strata in central regions. The oldest maximum depositional ages of basal Laberge Group strata are Sinemurian and correspond to rock units located along the center axis of the basin in Yukon. These data are consistent with the Whitehorse trough originating as a long, narrow depocenter that extended from the present-day Eagles Nest region in the north to the Mount Laurier area in the south. The initial shape is consistent with a pull-apart origin for the Whitehorse trough that resulted from regional transtension and strike-slip faulting during the closure of the northern Cache Creek Ocean and collision of Stikinia. A transcurrent regime is compatible with the terrane-bounding Teslin fault system of central Yukon and tectonic evolution of the Intermontane terranes and Whitehorse trough (Colpron et al., 2015). Samples located west of the Whitehorse trough yield younger maximum depositional ages and are

consistent with the westerly growth suggested by Colpron et al. (2015); however, progressively younger maximum depositional ages are also recorded south and east and indicate easterly and southerly growth of the basin following initial Early Jurassic subsidence.

Laberge Group strata are characterized by Late Triassic-Early Jurassic and subsidiary Paleozoic detrital zircon populations that indicate local derivation from the 216-178 Ma arc- to collision-related plutons and basement domains of the Yukon-Tanana, Stikinia, and Quesnellia terranes (Colpron et al., 2015). Proximal source regions are consistent with locally-derived provenance signatures that are predicted for convergent margin basin deposits and develop in response to crustal thickening, regional uplift, and erosion (e.g., Dickinson, 1974; Cawood et al., 2009, 2012). Paleozoic detrital zircon grains are consistent with Yukon-Tanana and Paleozoic Quesnellia (Boswell formation) rocks located north and east of the Whitehorse trough and yield inherited cores consistent with the Tatchun, Minto, and Aishihik pluton sources. Paleozoic detrital zircon grains therefore suggest south-directed, longitudinal sediment transport and east-directed, transverse drainage systems into the Whitehorse trough. Mesozoic superchondritic to chondritic Hf isotope signatures are consistent with derivation from Stikinia/Quesnellia (Joe Mountain, Povoas and/Semenof formations) and the Stikine, Minto and Long Lake plutonic suites. These source regions are coincident north and west of the Whitehorse trough, although smaller occurrences of Stikine, Minto, and Long Lake suite rocks crop out in central and eastern regions and generally suggest south-directed, longitudinal sediment transport. The Tanglefoot formation records a Sinemurian-Pliensbachian influx of subchondritic detrital zircon grains consistent with evolved signatures recorded by the Granite Mountain, Big Creek, and Aishihik plutons (Minto and Long Lake suites) that crop out northwest and west of the Whitehorse trough. These source regions suggest a shift to southeast

and east, transverse sediment pathways that are also recorded in the Inklin Formation of northern British Columbia.

Detrital zircon $\varepsilon_{\text{Hf(t)}}$ values record a Late Triassic-Middle Jurassic excursion to subchondritic signatures or a “pull-down” that is likely attributed to the collision of Stikinia and the closure of the northern Cache Creek Ocean, which resulted in Early Jurassic burial metamorphism and crustal thickening of the Intermontane terranes (e.g., Johnston and Erdmer, 1995; Villeneuve et al., 2003; Berman et al., 2007; Clark, 2017). Colpron et al. (2015) suggested that convergence between the northern Intermontane terranes and western Laurentian margin began by the Sinemurian-Pliensbachian, however, the subchondritic detrital zircon Hf isotope compositions in feldspathic lithic arenite (16-LVD-001B), lithic arenite (16-LVD-004) and crystal lithic tuff (17-LVD-038) units indicate crustal thickening likely began as early as the Rhaetian and continued until the Toarcian-Aalenian. The spatial distribution of subchondritic $\varepsilon_{\text{Hf(t)}}$ isotopic signatures in Laberge Group strata suggest that the greatest amounts of crustal thickening primarily occurred along the western edge and north of the Whitehorse trough. This trend is consistent with the distribution of subchondritic $\varepsilon_{\text{Hf(t)}}$ isotope signatures recorded by the Stikine, Minto, and Long Lake plutonic suites that surround the Whitehorse trough (Sack et al., 2019). Collision of the Intermontane terranes and syn-collisional deposition in the Whitehorse trough is coincident with the establishment of the Canadian Rockies foreland basin system and likely indicates hinterland-retroarc linkages along the northern Cordilleran margin (e.g., Colpron et al., 2015; Pană et al., 21018).

This study demonstrates that combined detrital zircon U-Pb age and Hf isotope results, especially using the LASS technique, from syn-collisional strata accurately records the crustal

and tectonic evolution of source rocks and basins, respectively. Furthermore, the distribution of superchondritic, chondritic, and subchondritic detrital zircon grains in Laberge Group strata approximate the position of evolved, chondritic, and juvenile source regions relative to the basin. This approach may be useful in other modern and ancient mountain belts where the original shape and thickness of the basin may not be preserved and source rocks have been reworked by regional deformation, metamorphism, and magmatism.

3.2 Future research

3.2.1 Provenance and tectonic history of the southern Whitehorse trough

This study determined that synorogenic Laberge Group rocks were sourced from the basement assemblages of the Yukon-Tanana, Stikinia, and Quesnellia terranes and associated Stikine, Minto, and Long Lake plutonic suites. Detrital zircon Hf isotope compositions also likely record crustal thickening events that occurred during the convergence of the Intermontane terranes against the western Laurentian margin. This study focused on the source-to-sink history and tectonic evolution of the northern region of the Whitehorse trough in central Yukon, however, the basin extends south to the Dease Lake region of northern British Columbia. Future work could therefore focus on the Hf isotope composition of plutons in southern regions of the Intermontane terranes and U-Pb-Hf detrital zircon studies of Jurassic synorogenic strata in the Dease Lake region. This approach would: 1) document the crustal evolution of the ‘distal limbs’ of the proposed orocline in British Columbia, 2) allow for a comparison to the ‘hinge’ region of the oroclinal bend tectonic model proposed for the Intermontane terranes; and 3) determine if the provenance trends and tectonic evolution are consistent between the northern and southern Whitehorse trough.

3.2.2 Paleocurrent measurements in the Laberge Group

This study suggested that there was a shift from longitudinal to transverse sediment pathways based on the distribution of probable source regions and provenance evolution of Laberge Group strata. This shift is also documented in the Inklin Formation of northern British Columbia (Johannson et al., 1997). A future study that targets detailed measurement of paleocurrents at multiple stratigraphic levels of the Laberge Group in central Yukon will build upon this hypothesis and yield a more robust sediment accumulation history for the Whitehorse trough.

3.2.3 Multi-mineral approach to provenance and thermochronology of the Whitehorse trough

Zircon is considered ideal for provenance investigations because of its robust behaviour in sedimentary cycles, but other minerals like monazite, apatite, and mica have been utilized in other studies globally (e.g., Hietpas et al., 2010; Liu et al., 2017). These detrital minerals would provide further insight into the provenance and thermochronological evolution of Laberge Group strata and source regions. Although monazite is more susceptible to chemical and mechanical weathering processes, it can record metamorphic events that may not be recorded by zircon (e.g., Hietpas et al., 2010, 2011). A study that compares the U-Pb ages of detrital monazite in Laberge Group strata may yield a more complete history of metamorphic events not recorded by zircon. Zircon (ZFT) or apatite fission track (AFT) analyses can also be used to constrain thermal histories and can be compared to known exhumation rates of bedrock sources that surround the Whitehorse trough. $^{40}\text{Ar}/^{39}\text{Ar}$ cooling ages of Laberge Group detrital micas may also be used to identify bedrock source regions with known thermal histories and better constrain source-to-sink pathways.

References

- Berman, R.G., Ryan, J.J., Gordey, S.P., and Villeneuve, M., 2007, Permian to Cretaceous polymetamorphic evolution of the Stewart River region, Yukon-Tanana terrane, Yukon, Canada: P-T evolution linked with *in situ* SHRIMP monazite geochronology: *Journal of Metamorphic Geology*, v. 25, p. 803-827, doi:10.1111/j.1525-1314.2007.00729.x.
- Cawood, P.A., Kröner, A., and Collins, W.J., 2009, Accretionary orogens through Earth history: Geological Society, London, Special Publication 318, p. 1-36, doi:10.1144/SP318.1.
- Cawood, P.A., Hawkesworth, C.J., and Dhuime, B., 2012, Detrital zircon record and tectonic setting: *Geology*, v. 40, p. 875-878, doi:10.1130/G32945.1.
- Clark, A.D., 2017, Tectonometamorphic history of mid-crustal rocks at Aishihik Lake, southwest Yukon: Simon Fraser University (MSc thesis), Burnaby, Canada, 153 p.
- Colpron, M., Crowley, J.L., Gehrels, G., Long, D.G.F., Murphy, D.C., Beranek, L., and Bickerton, L., 2015, Birth of the northern Cordilleran orogeny, as recorded by detrital zircons in Jurassic synorogenic strata and regional exhumation in Yukon: *Lithosphere*, v. 7, p. 541-562, doi:10.1130/L451.1
- Dickinson, W.R., 1974, Plate tectonics and sedimentation, *in* Dickinson, W.R., ed., *Tectonics and Sedimentation*: Society of Economic Paleontology and Mineralogists Special Publication 22, p. 1-27.
- Hietpas, J., Samson, S., Moecher, D., and Schmitt, A.K., 2010, Recovering tectonic events from the sediment record: monazite plays in high fidelity: *Geology*, v. 38, no. 2, p. 167-170, doi:10.1130/G30265.1.
- Hietpas, J., Samson, S., and Moecher, D., 2011, A direct comparison of the ages of detrital monazite versus detrital zircon in Appalachian foreland basin sandstones: Searching for

the record of Phanerozoic orogenic events: Earth and Planetary Science Letters, v. 310, p. 488-497, doi:10.1016/j.epsl.2011.08.033.

Johannson, G.G., Smith, P.L., and Gordey, S.P., 1997, Early Jurassic evolution of the northern Stikinian arc: evidence from the Laberge Group, northwestern British Columbia: Canadian Journal of Earth Science, v. 34, p. 1030-1057.

Johnston, S.T., and Erdmer, P, 1995, Hot-side-up aureole in southwest Yukon and limits on terrane assembly of the northern Canadian Cordillera: Geology, v. 23, no. 5, p 419-422.

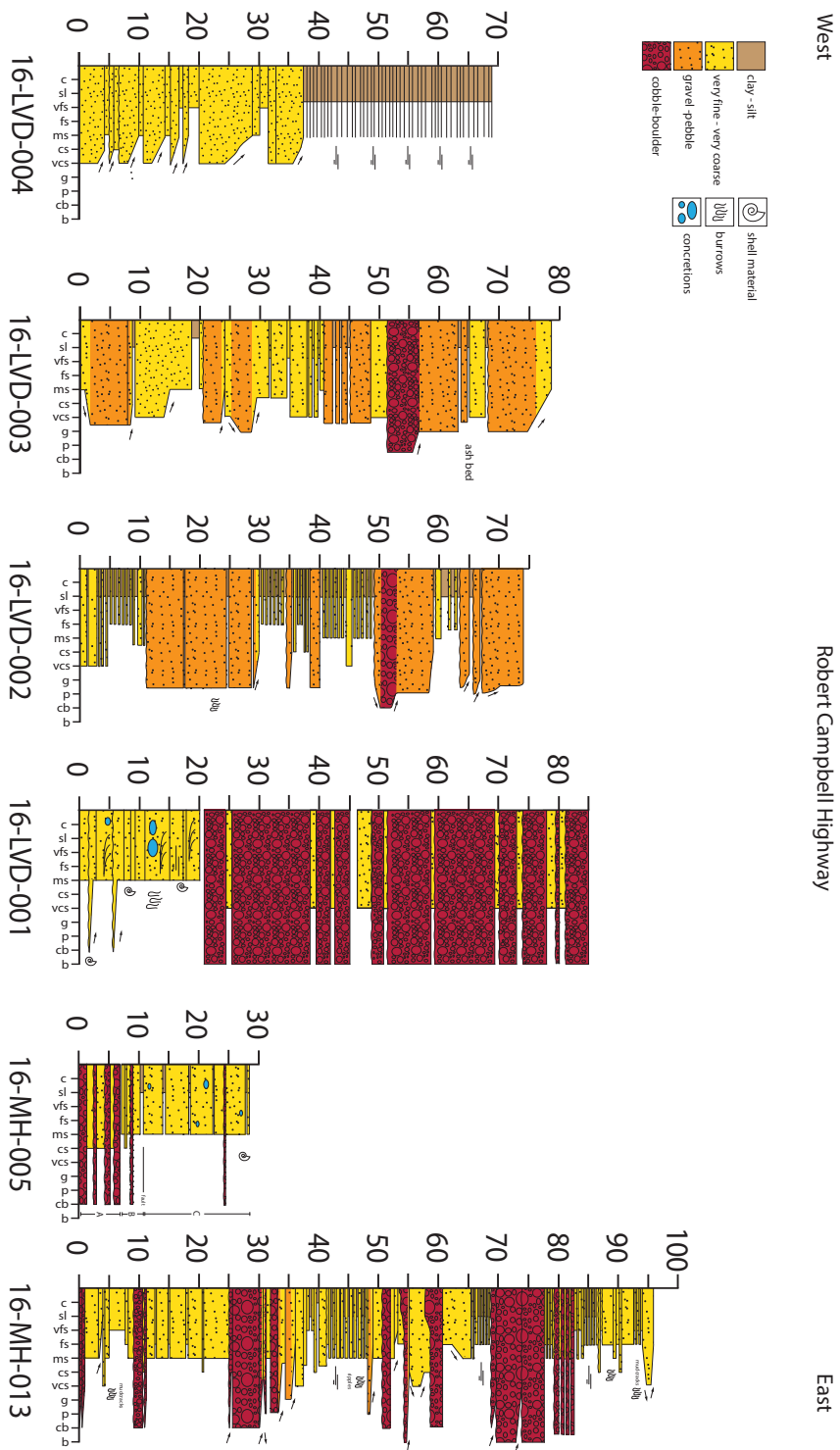
Liu, X-C., Wu, Y-B., Fisher, C.M., Hanchar, J.M., Beranek, L., Gao, S., and Wang, H., 2017, Tracing crustal evolution by U-Th-Pb, Sm-Nd, and Lu-Hf isotopes in detrital monazite and zircon from modern rivers: Geology, v. 45, p. 103-106, doi: 10.1130/G38720.1.

Pană, D.I., Poulton, T.P., and DuFrane, S.A., 2018, U-Pb detrital zircon dating supports Early Jurassic initiation of the Cordilleran foreland basin in southwestern Canada: Geological Society of American Bulletin, doi:10.1130/B31862.1.

Sack, P.J., Colpron, M., Crowley, J.L., Ryan, J.J., Allan, M.M., Beranek, L.P., Joyce, N., and Mortensen, J.K., 2019, Atlas of Late Triassic-Jurassic plutons in Yukon: Yukon Geological Survey Open File, in press.

Villeneuve, M.E., Ryan J.J., Gordey, S.P., and Piercy, S.J., 2003, Detailed thermal and provenance history of the Stewart River area (Yukon-Tanana terrane, western Yukon) through application of SHRIMP, $^{40}\text{Ar}/^{39}\text{Ar}$, and TIMS, *in* Geological Association of Canada-Mineral Association of Canada annual meeting. Vancouver, BC, Geological Association of Canada, Abstract 344.

Appendix A: Stratigraphic logs



Appendix B: Hand sample and thin section photographs

B.1 Hand samples



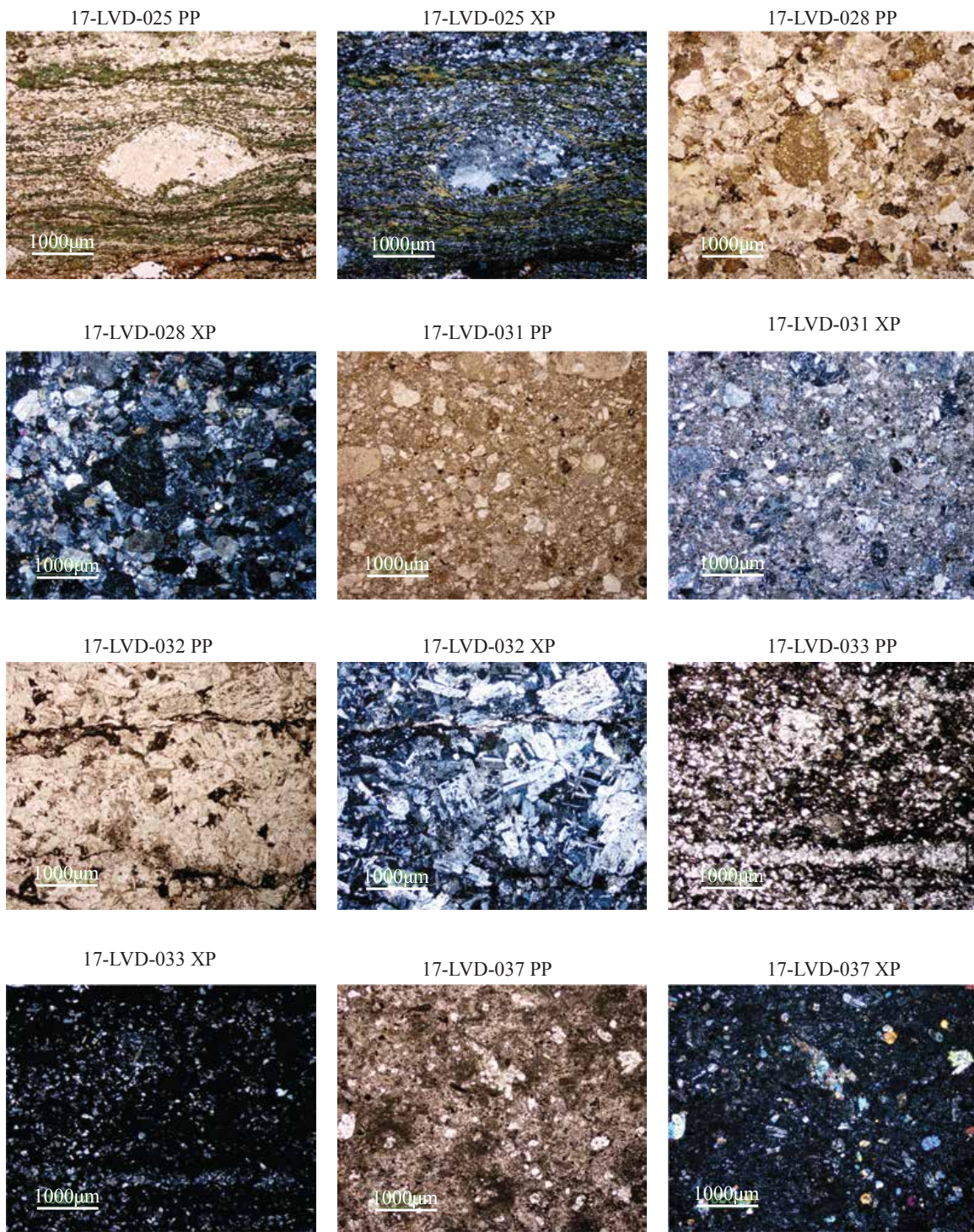


B.2 Thin sections









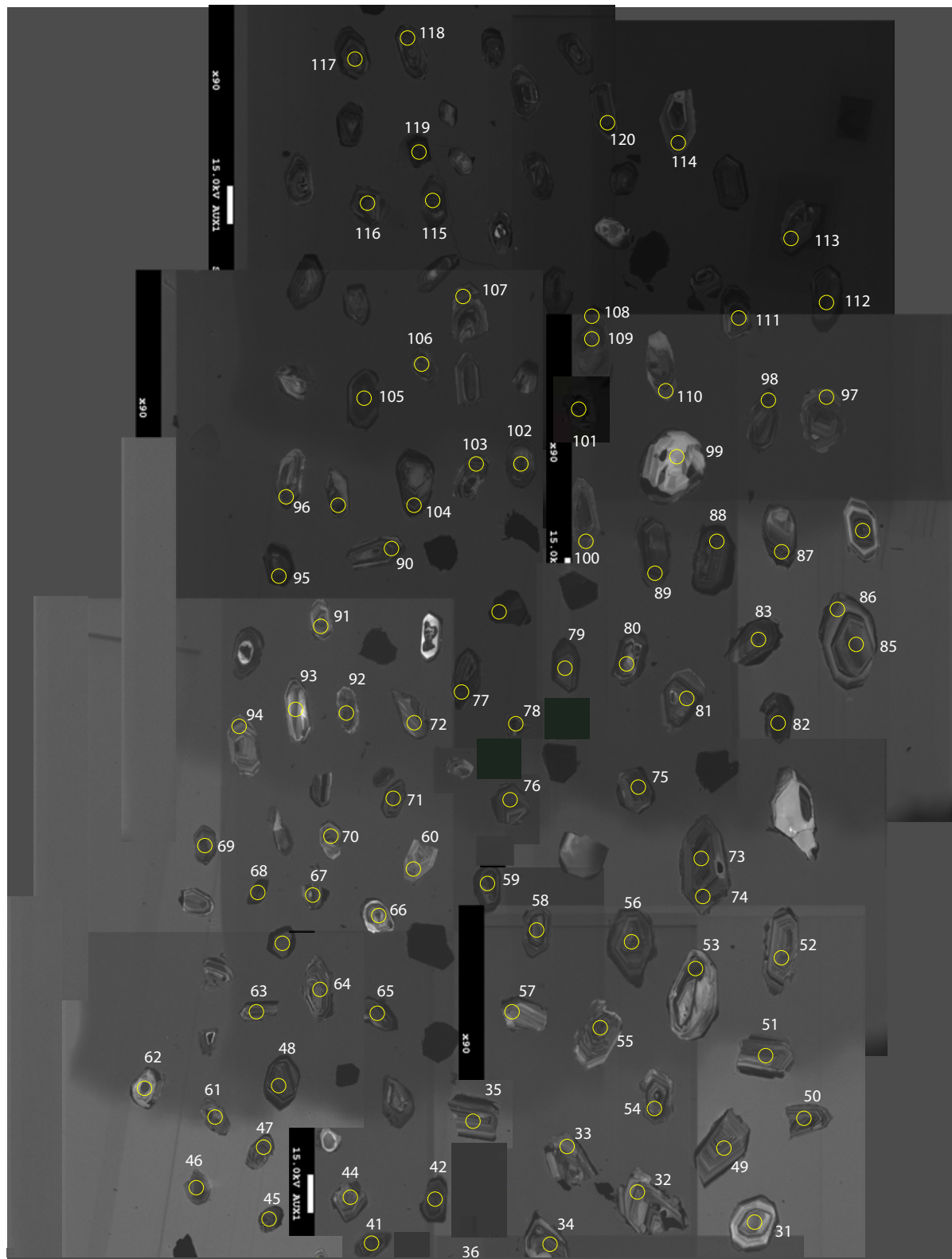
Appendix C: Grain maps

Two additional samples (16-LVD-007 and 17-LVD-026) were initially chosen for detrital zircon U-Pb-Hf analysis. Sample 16-LVD-007 collected from the North Klondike Highway, south of Carmacks, yielded a Cretaceous maximum depositional age and therefore is from a stratigraphic unit younger than the Laberge Group. Sample 17-LVD-026 is a cobble-sized amphibolite clast collected from a conglomerate unit near Fish Lake that was contaminated with detrital zircon crystals from the matrix. Therefore, the U-Pb and Hf isotope results of these samples are not included in the discussion and interpretations, but grain maps are reported in this appendix for reference.

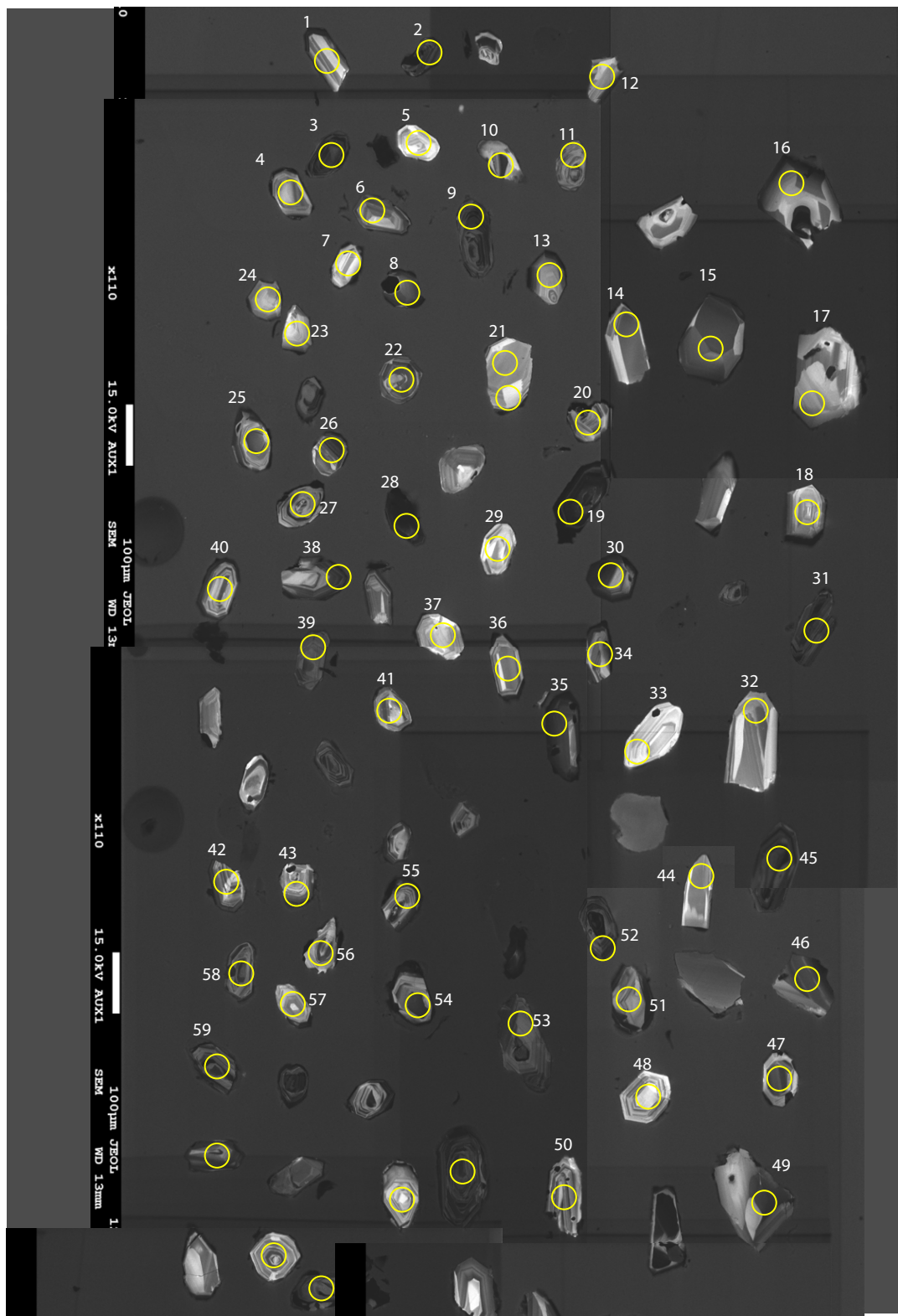
C.1 16-LVD-001B, Robert Campbell Highway



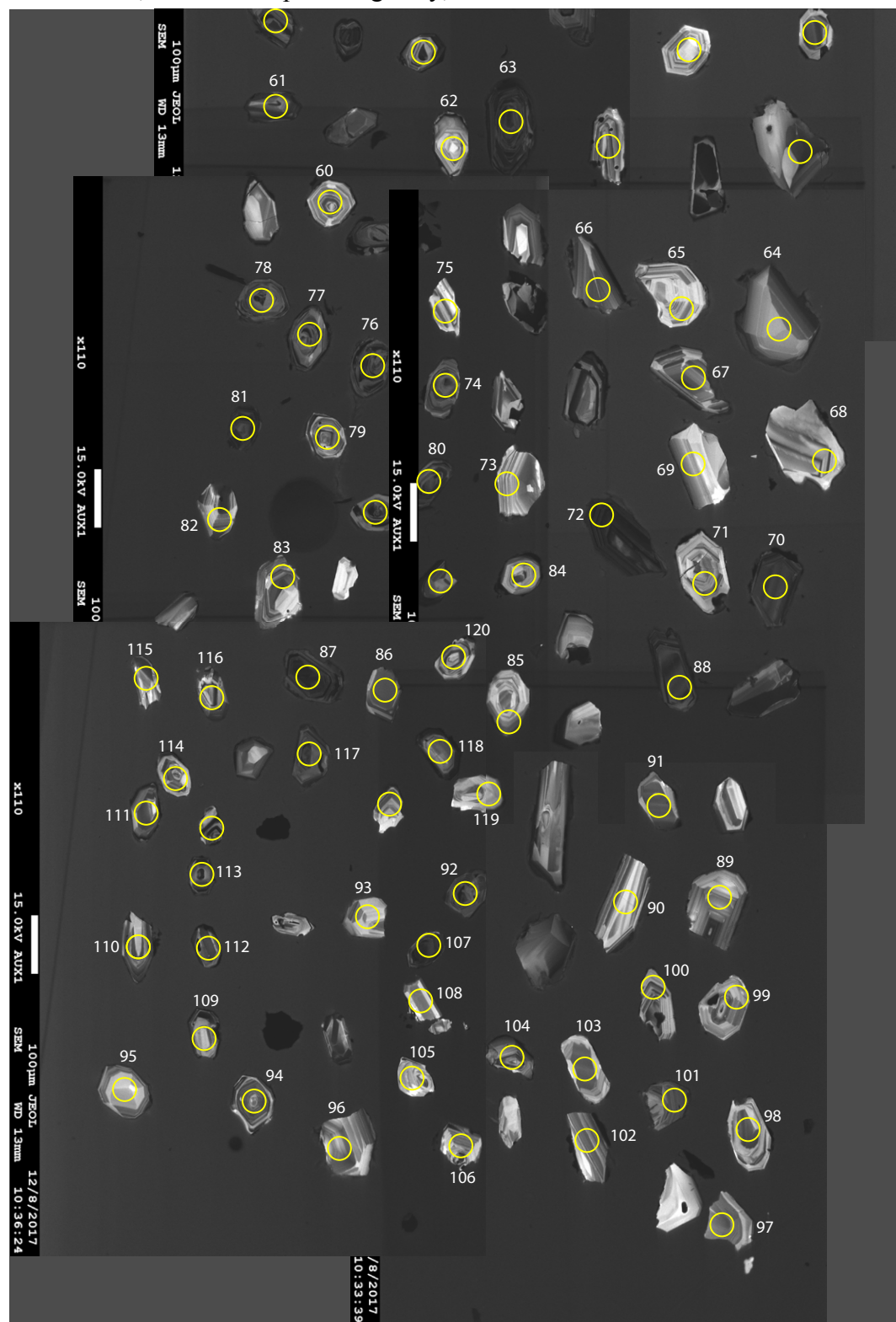
C.1 16-LVD-001B, Robert Campbell Highway, continued



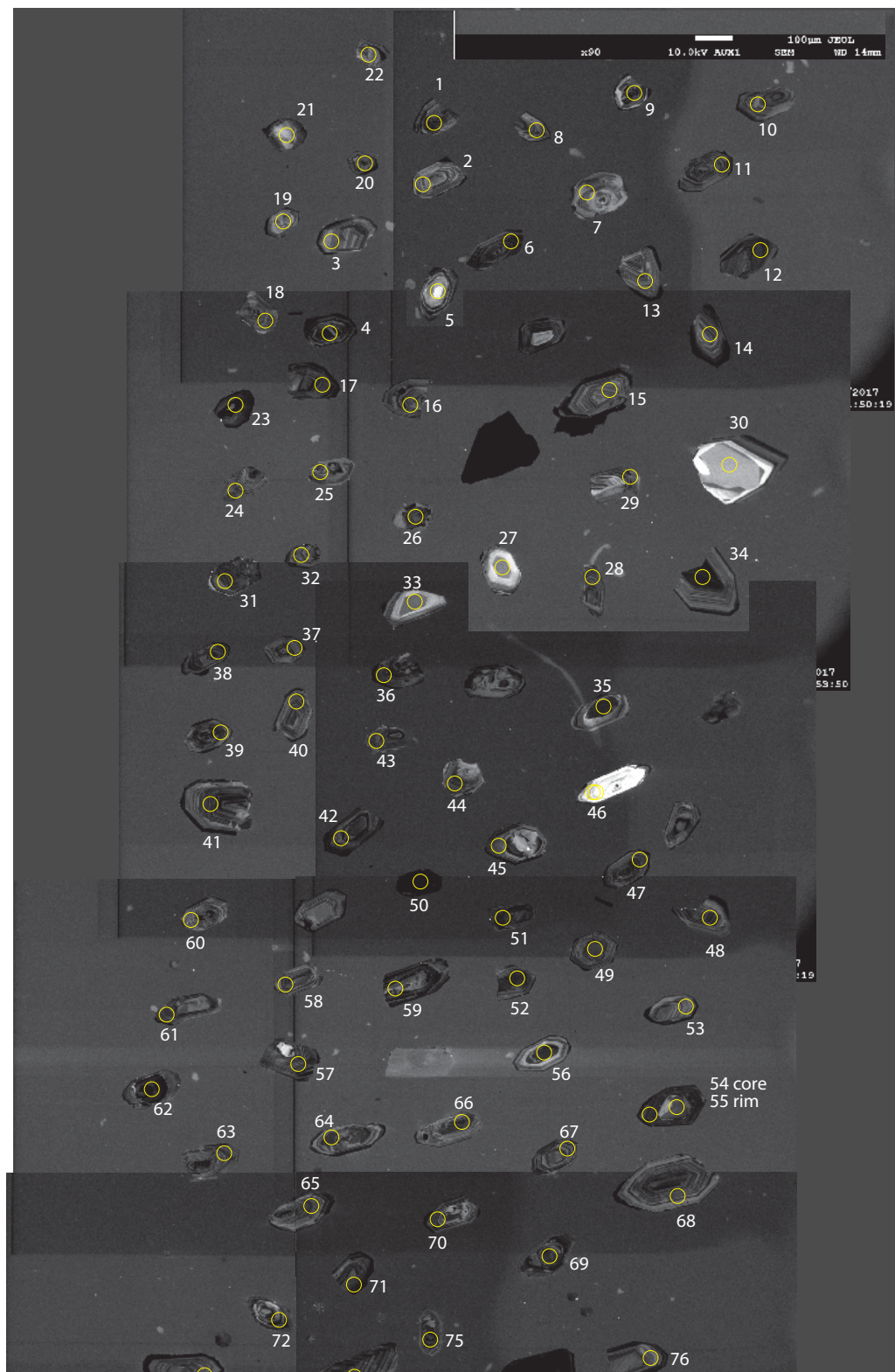
C.2 16-LVD-001C, Robert Campbell Highway



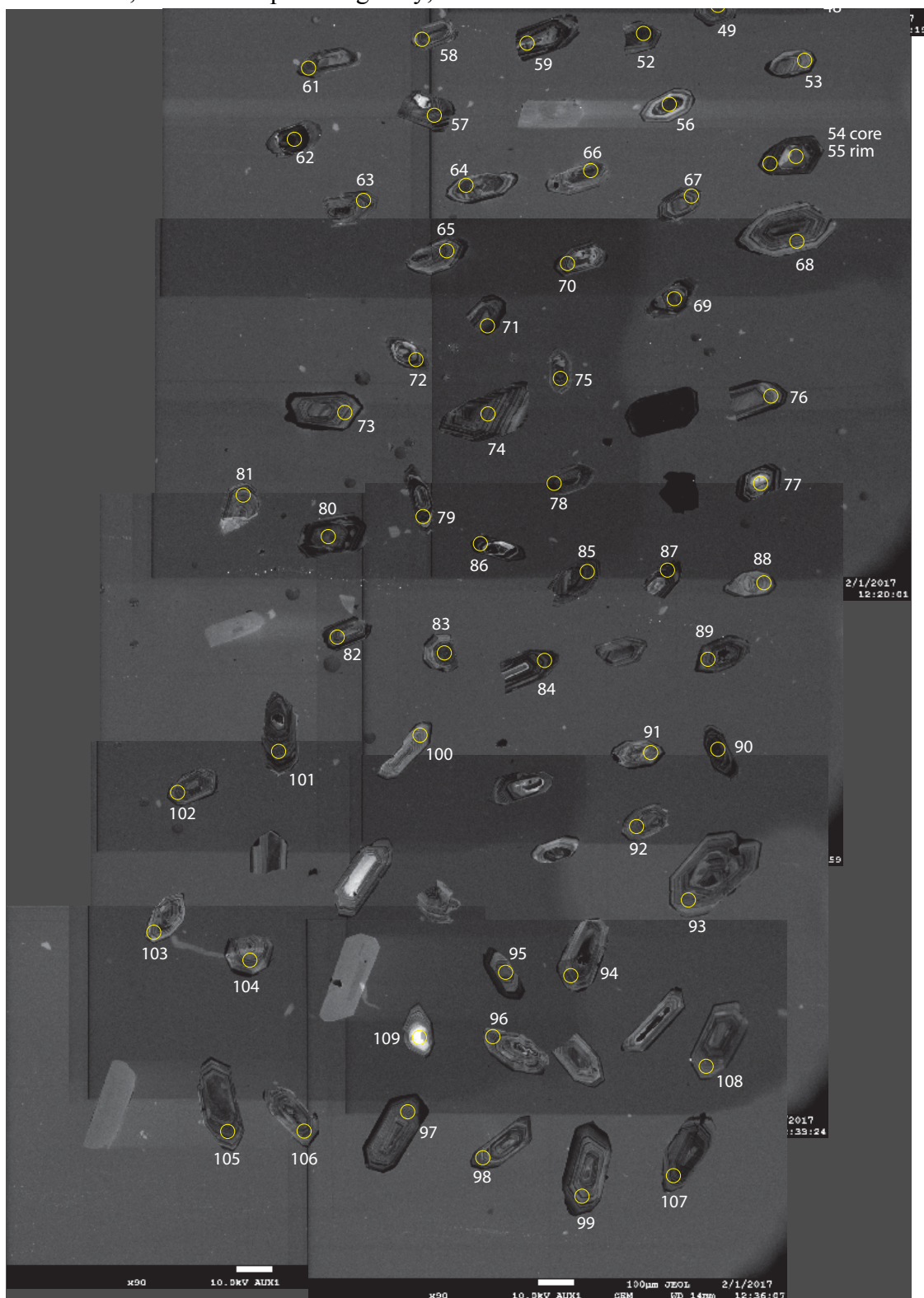
C.2 16-LVD-001C, Robert Campbell Highway, continued



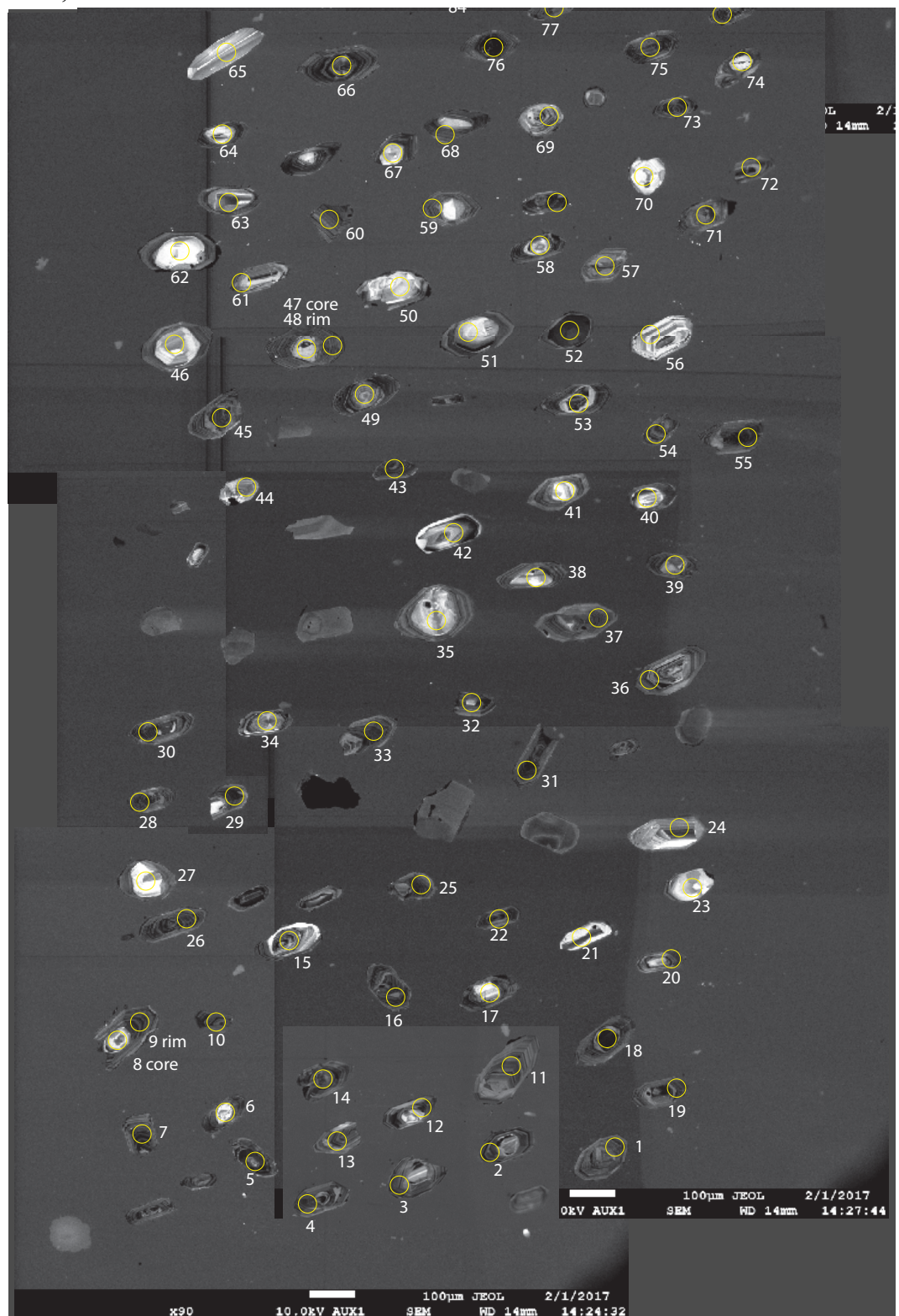
C.3 16-LVD-004, Robert Campbell Highway



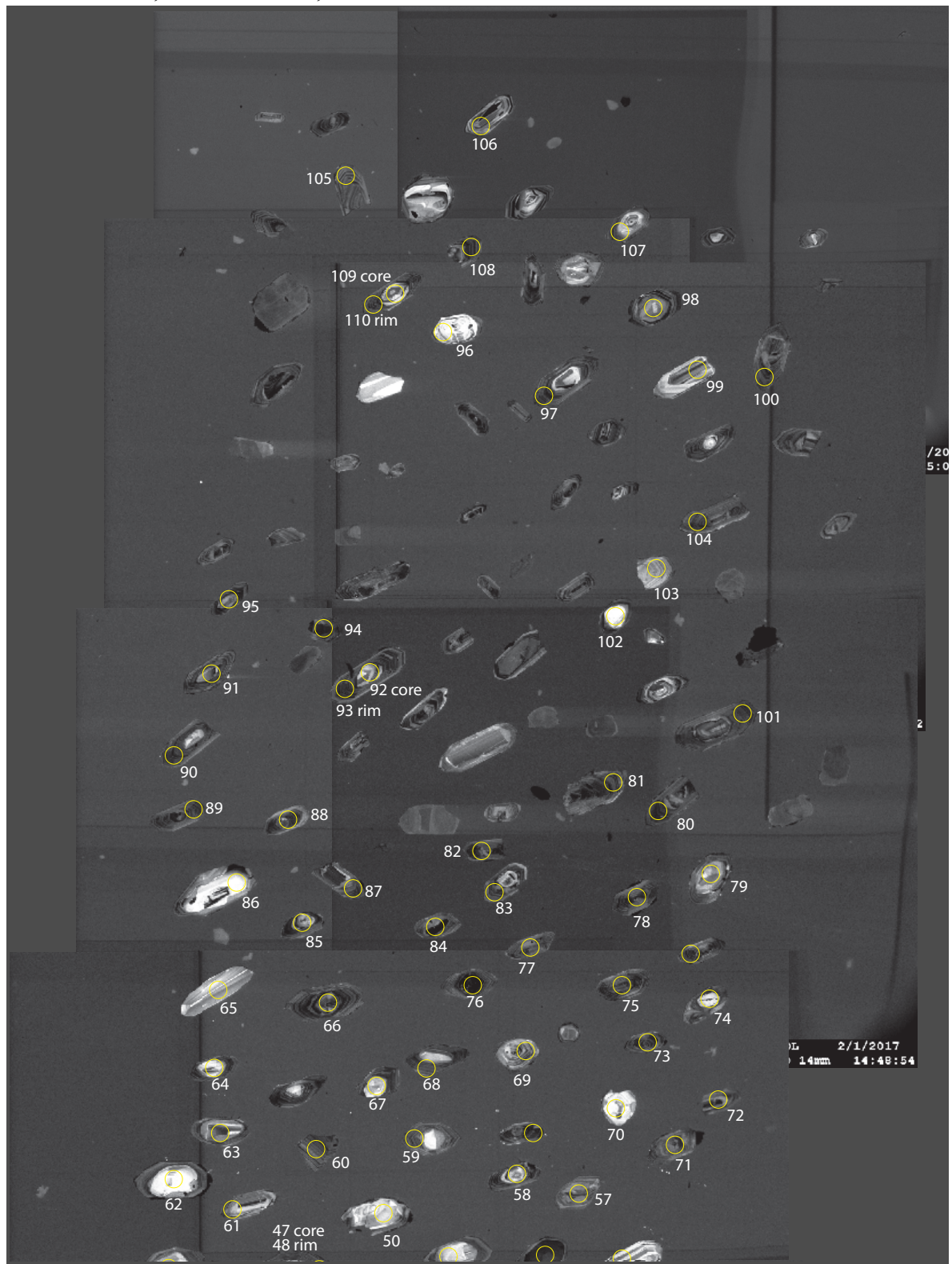
C.3 16-LVD-004, Robert Campbell Highway, continued



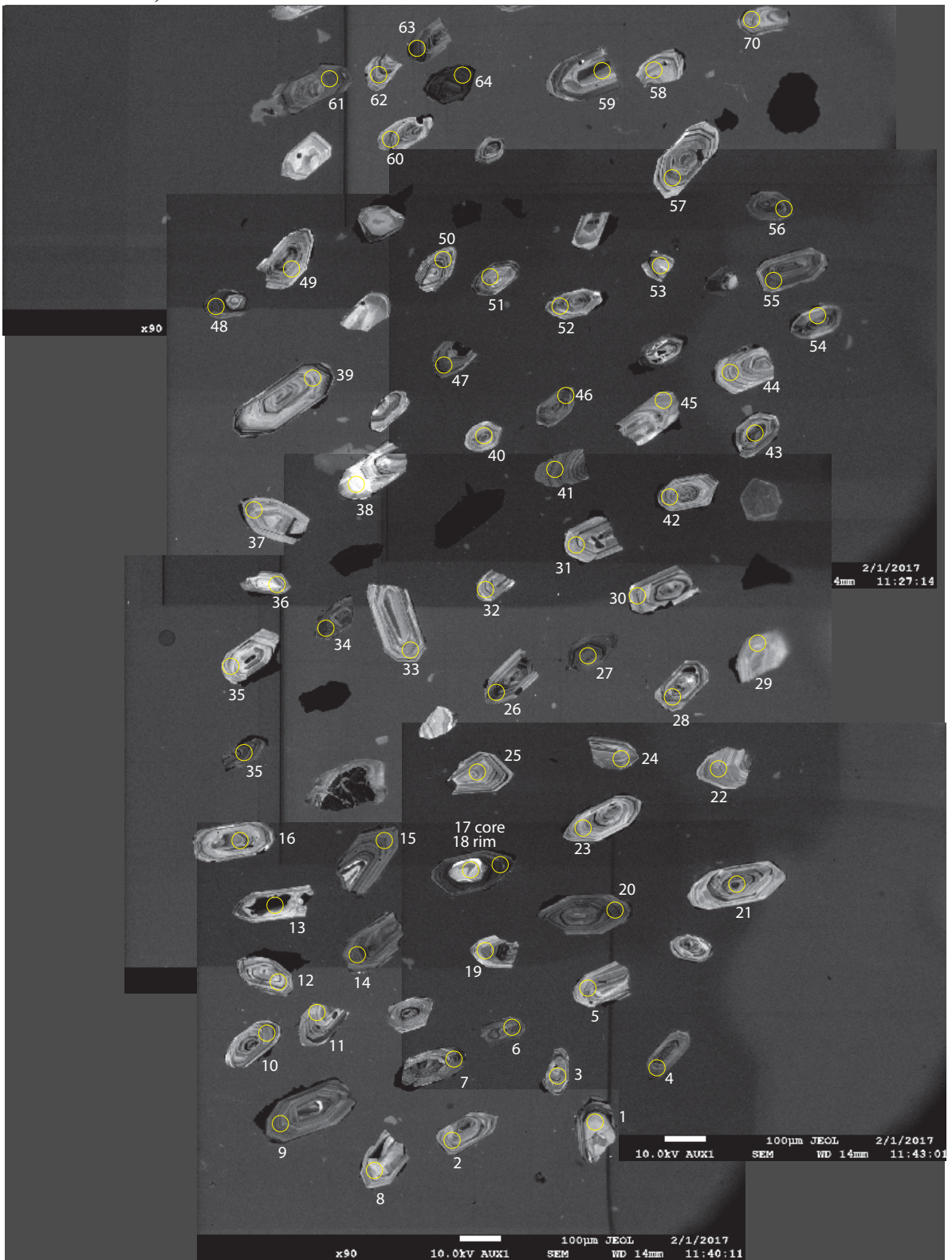
C.4 16-LVD-009, Mount Laurier



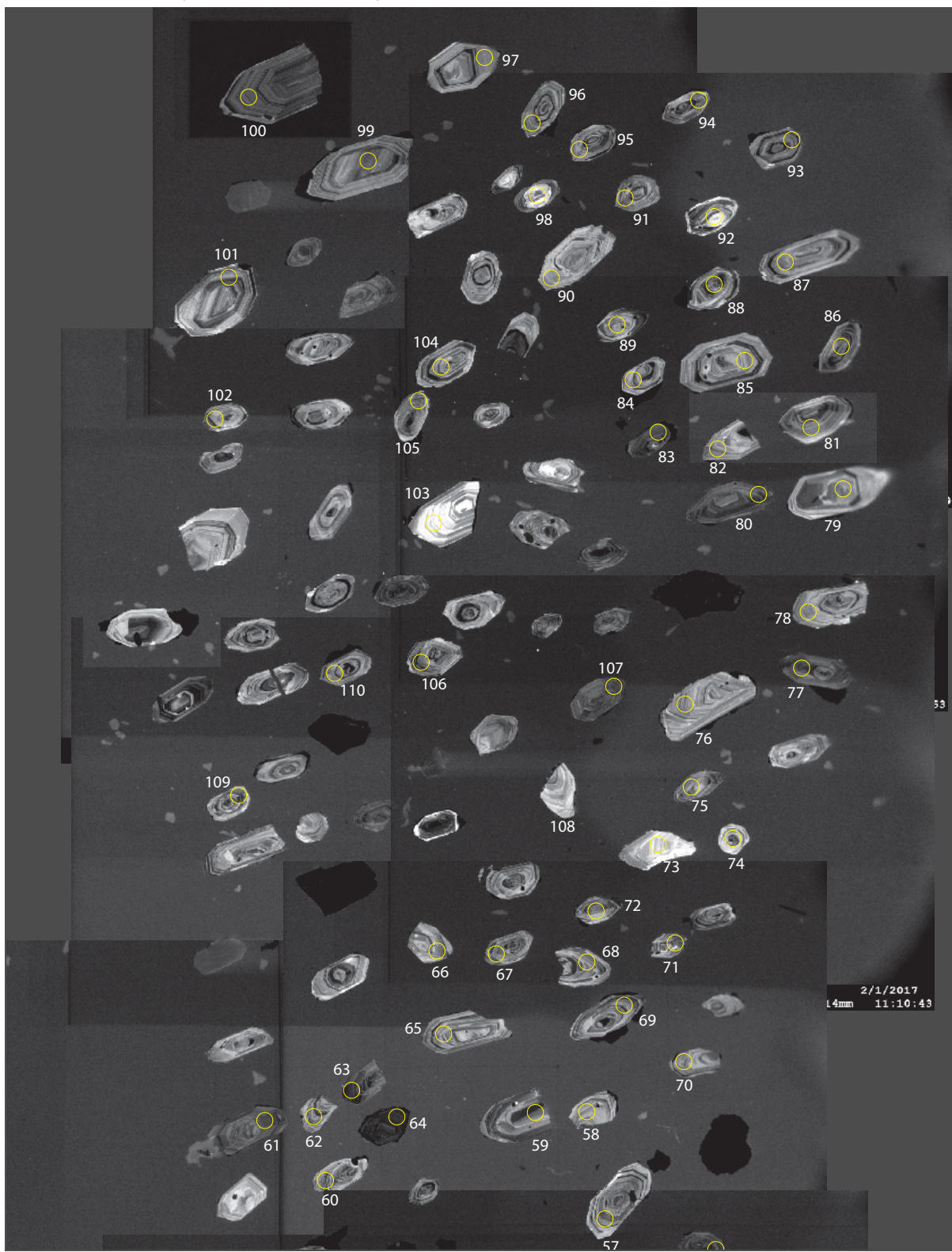
C.4 16-LVD-009, Mount Laurier, continued



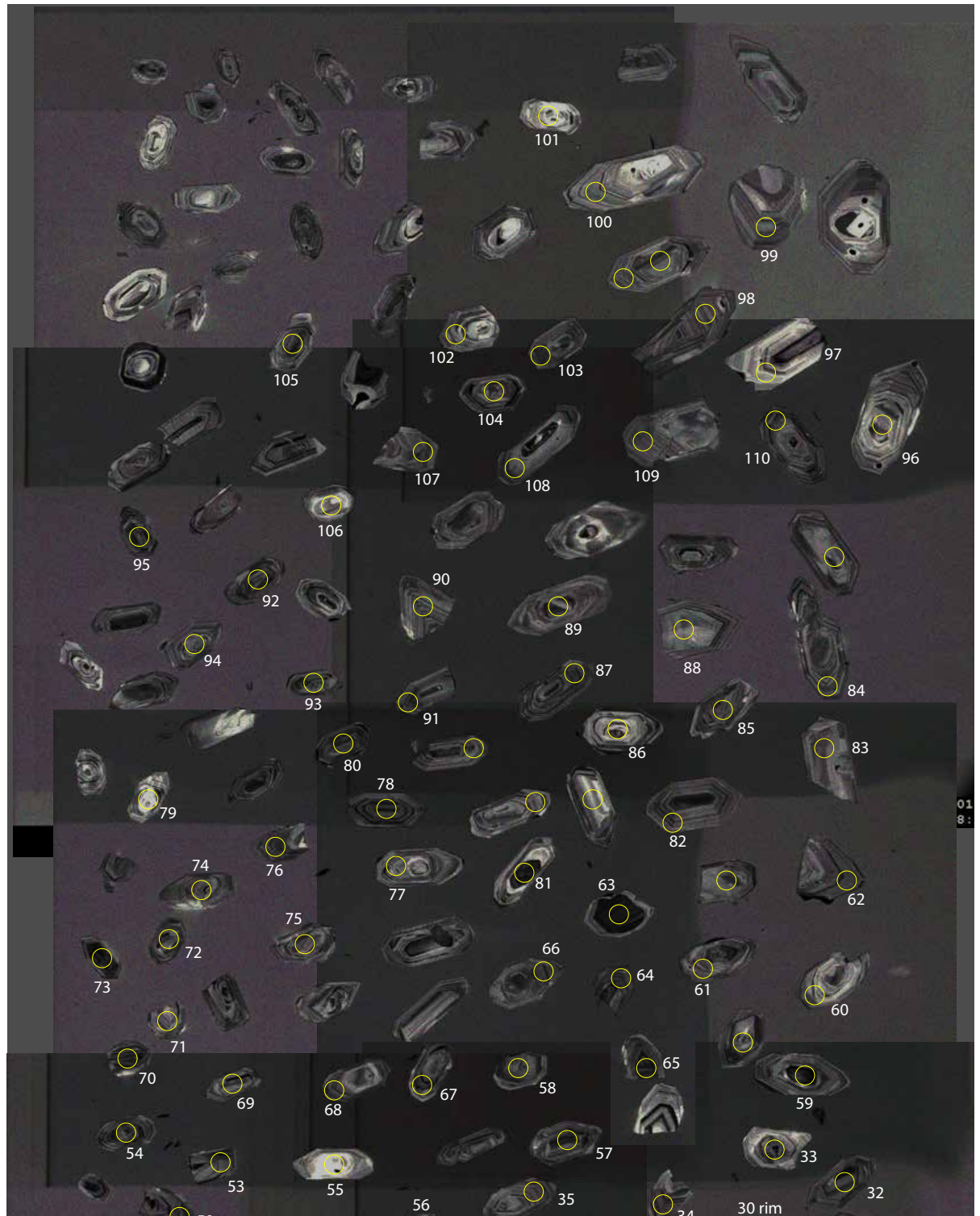
C.5 16-LVD-021, Ricthofen Island



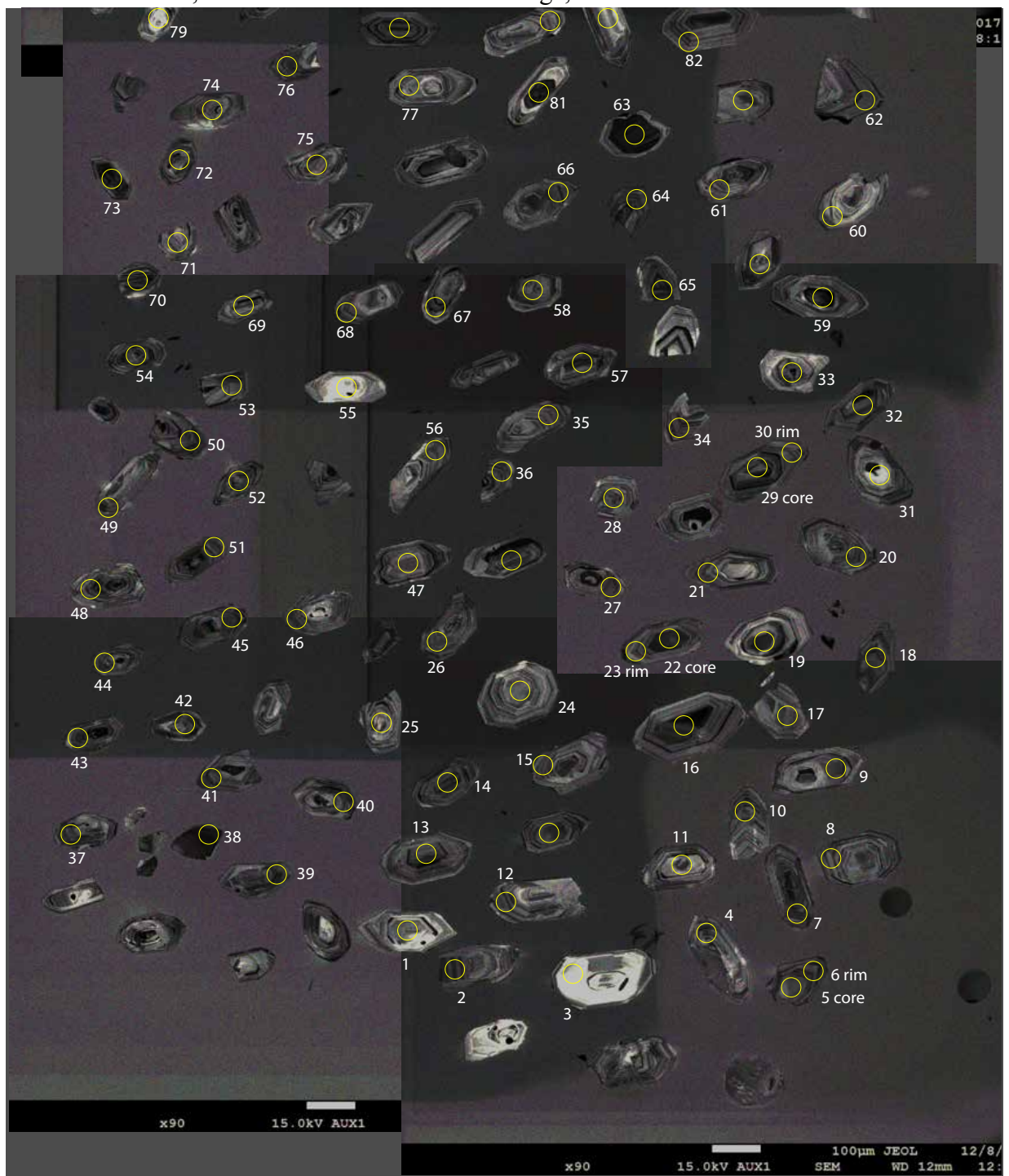
C.5 16-LVD-021, Richthofen Island, continued



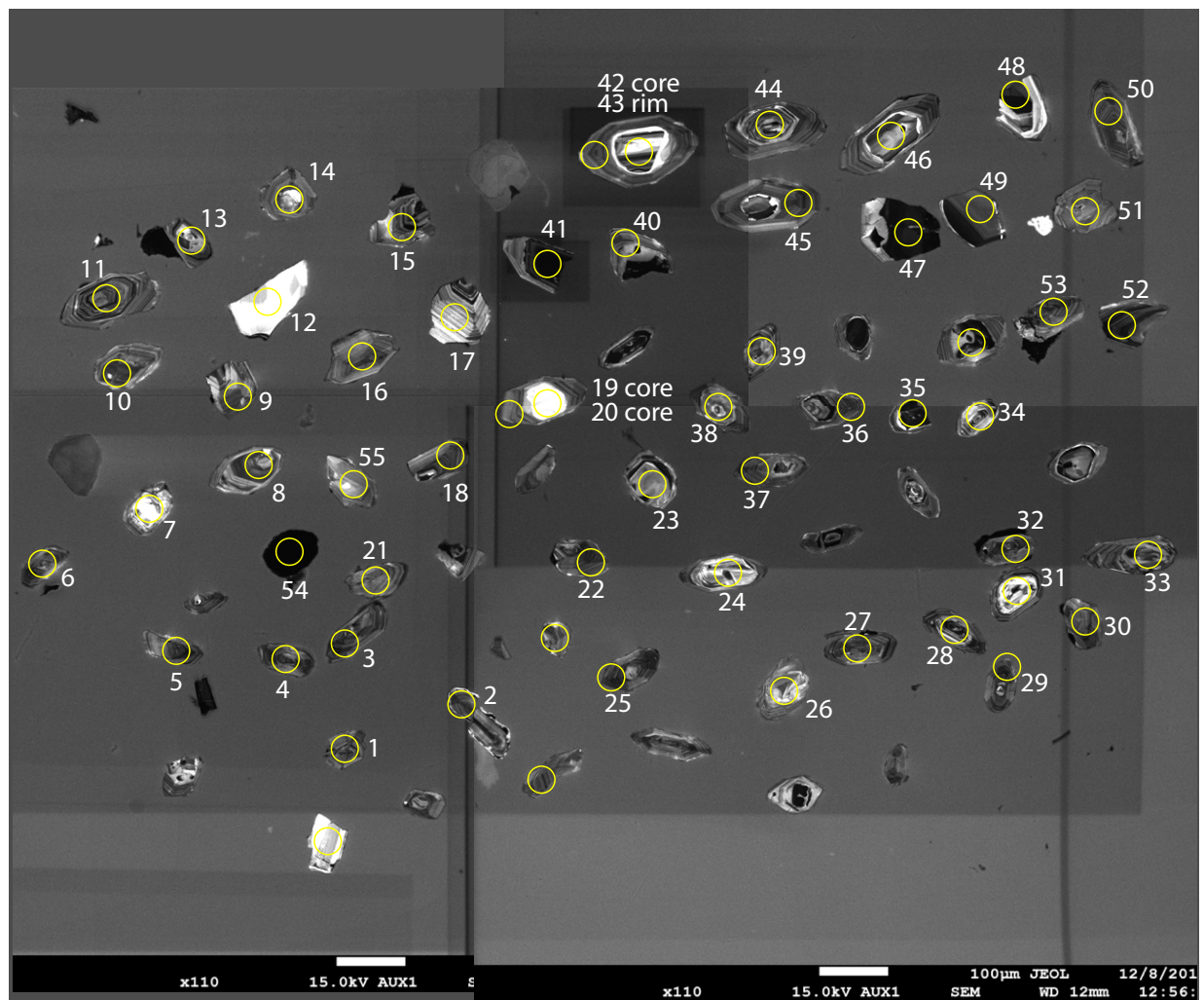
C.6 16-LVD-022, Eastern shoreline of Lake Laberge



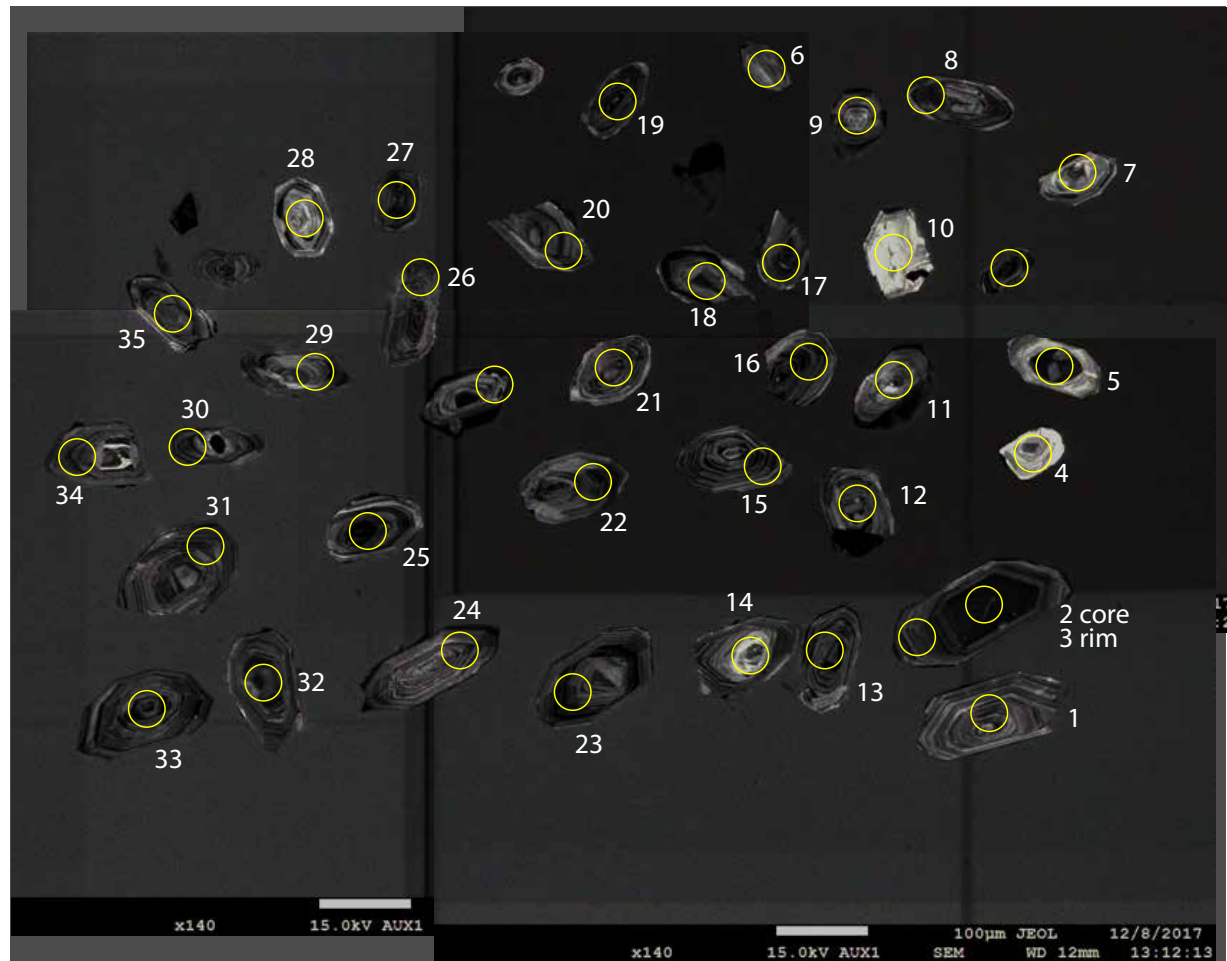
C.6 16-LVD-022, Eastern shoreline of Lake Laberge, continued



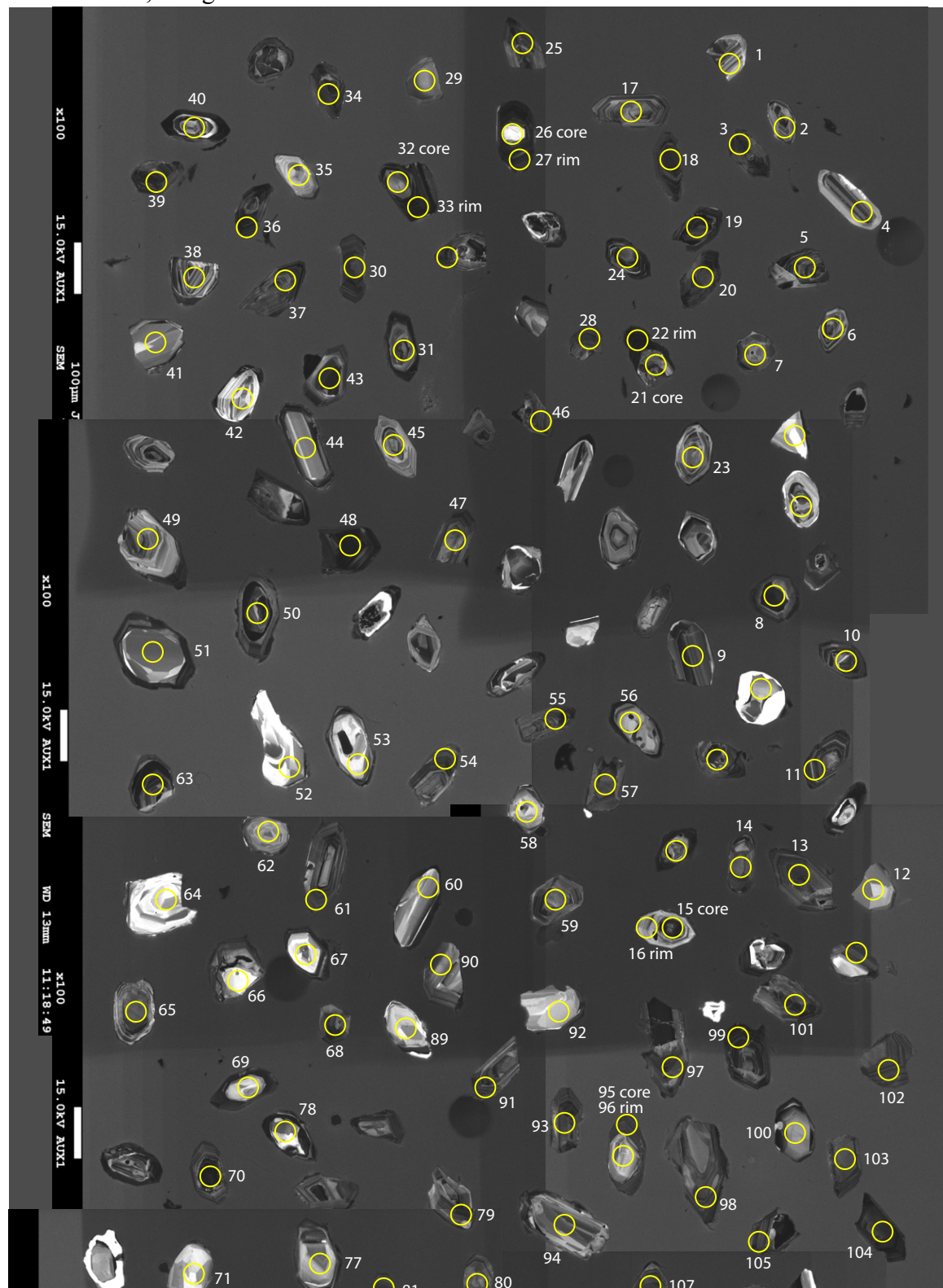
C.7 16-LVD-023, Eastern shoreline of Lake Laberge



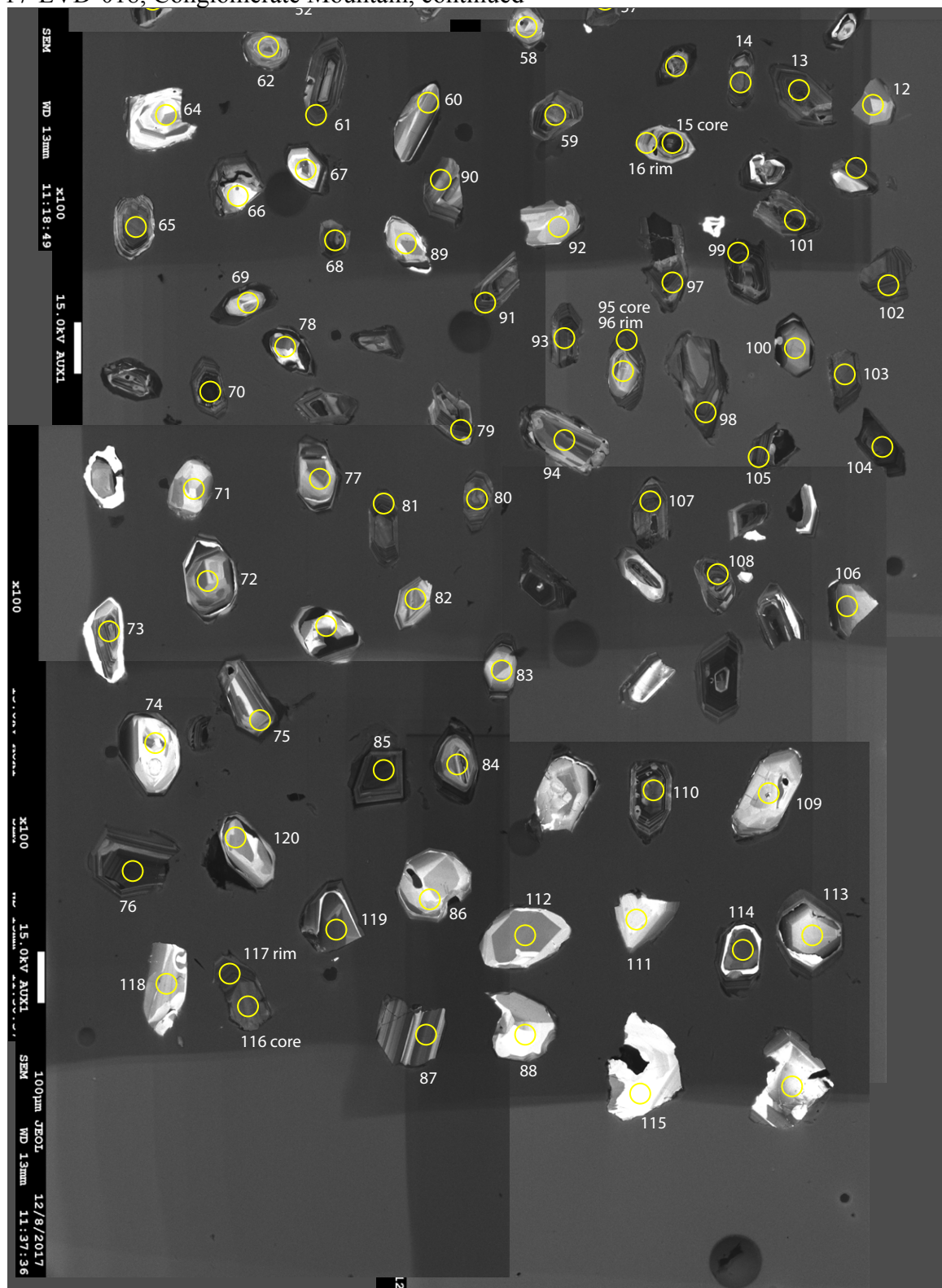
C.8 16-LVD-026, Fish Lake



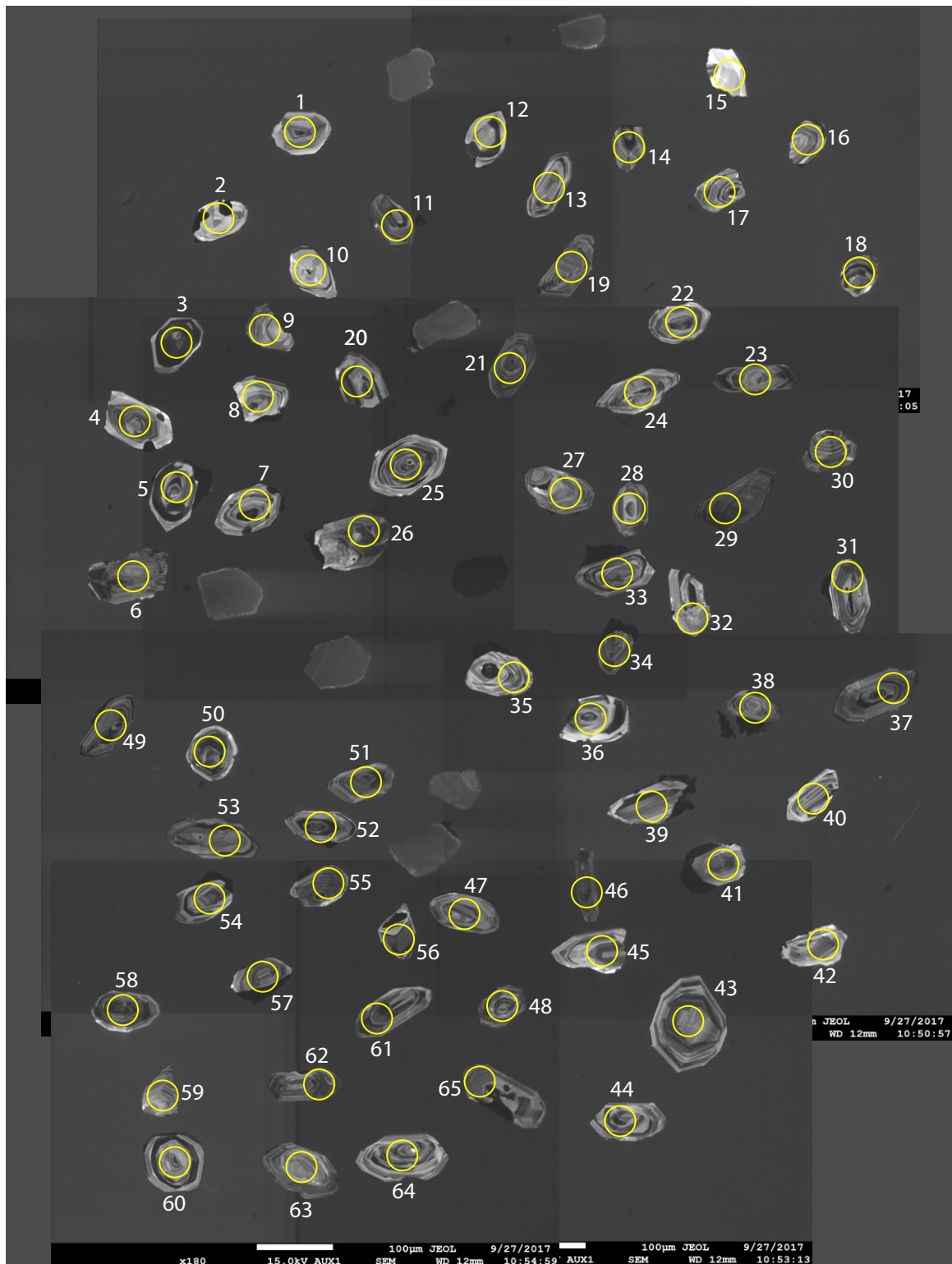
C.9 17-LVD-018, Conglomerate Mountain



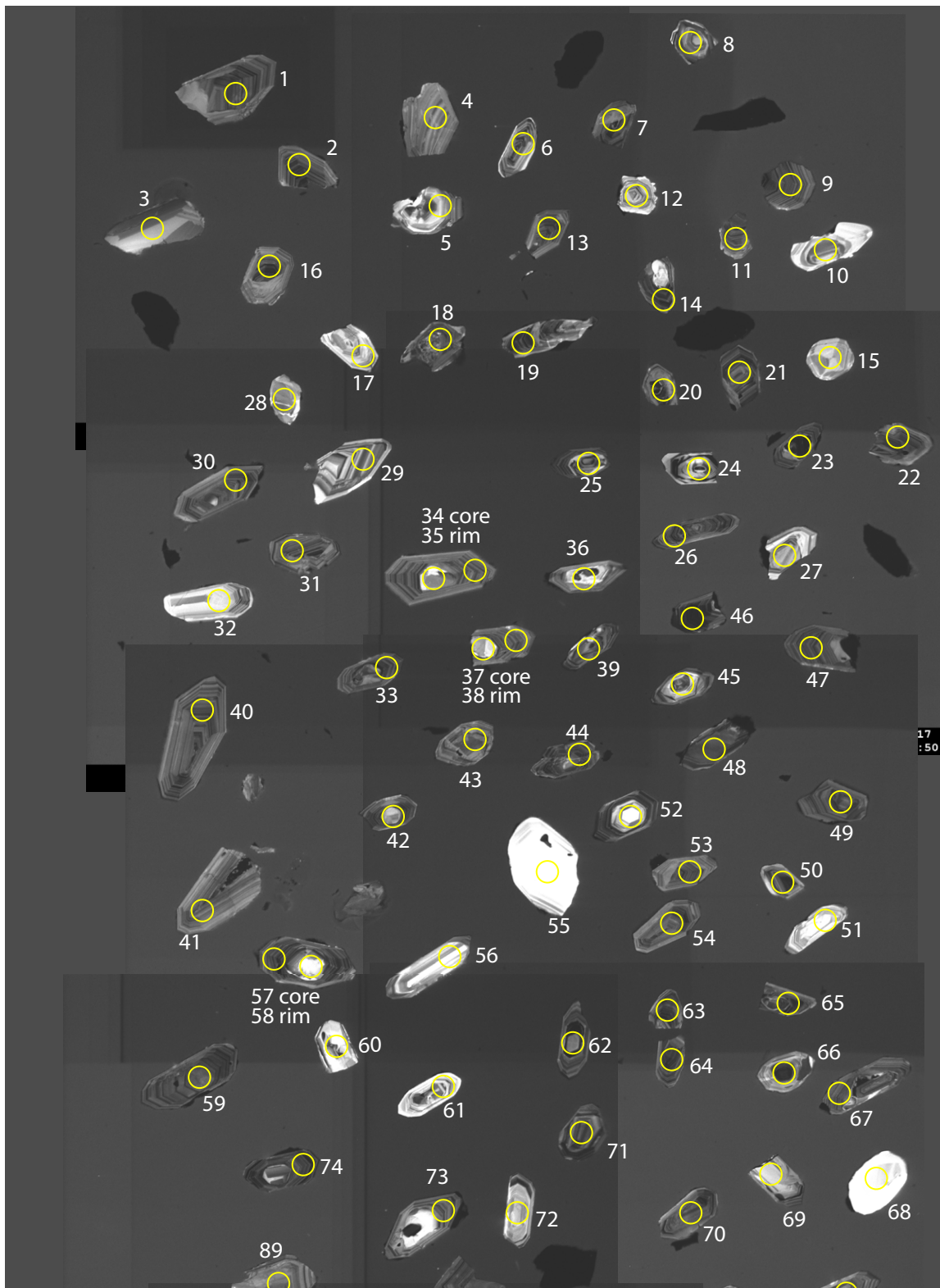
C.9 17-LVD-018, Conglomerate Mountain, continued



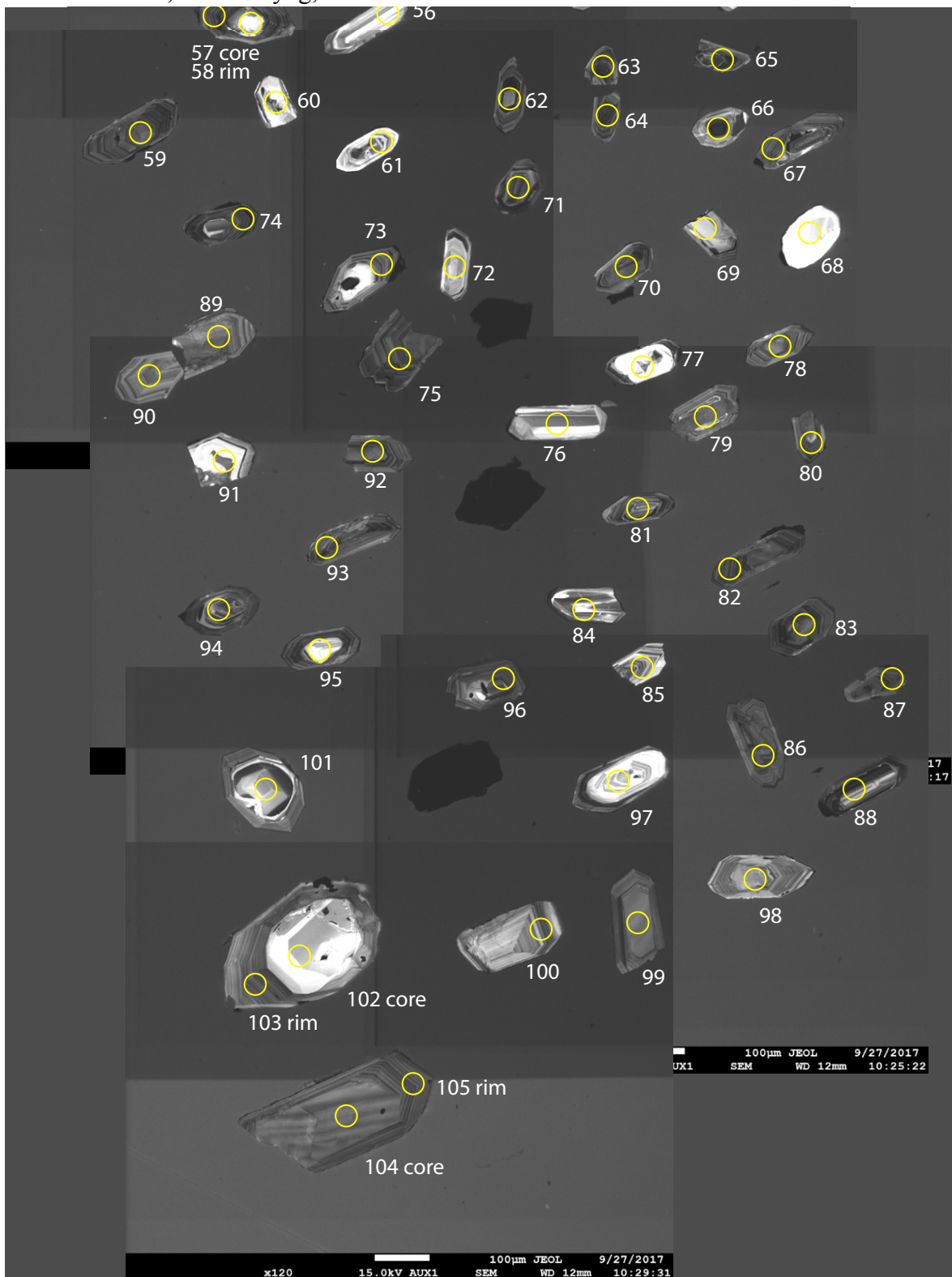
C.10 17-LVD-027, Takhini Subdivision



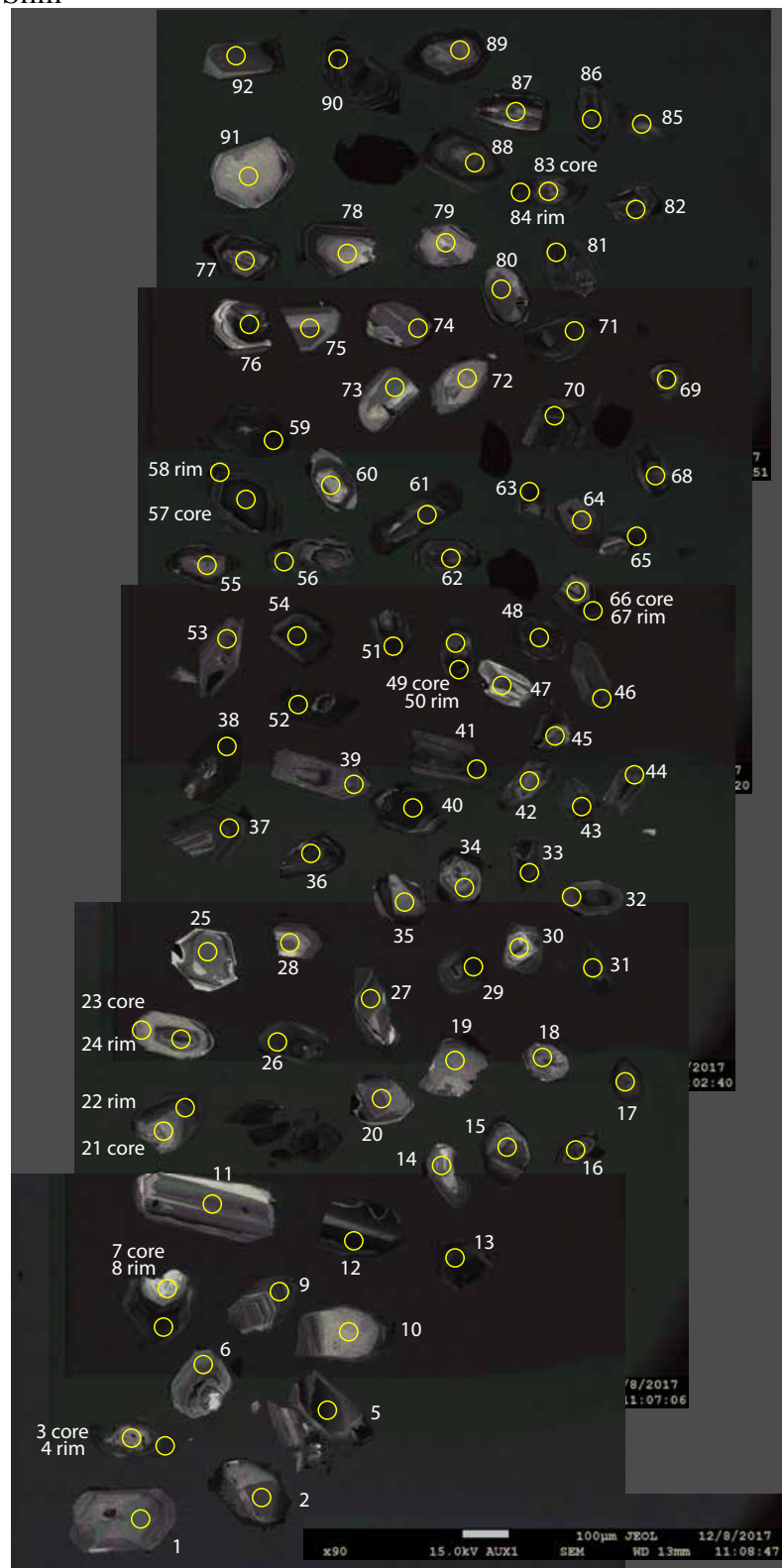
C.11 17-LVD-030, Mount Byng



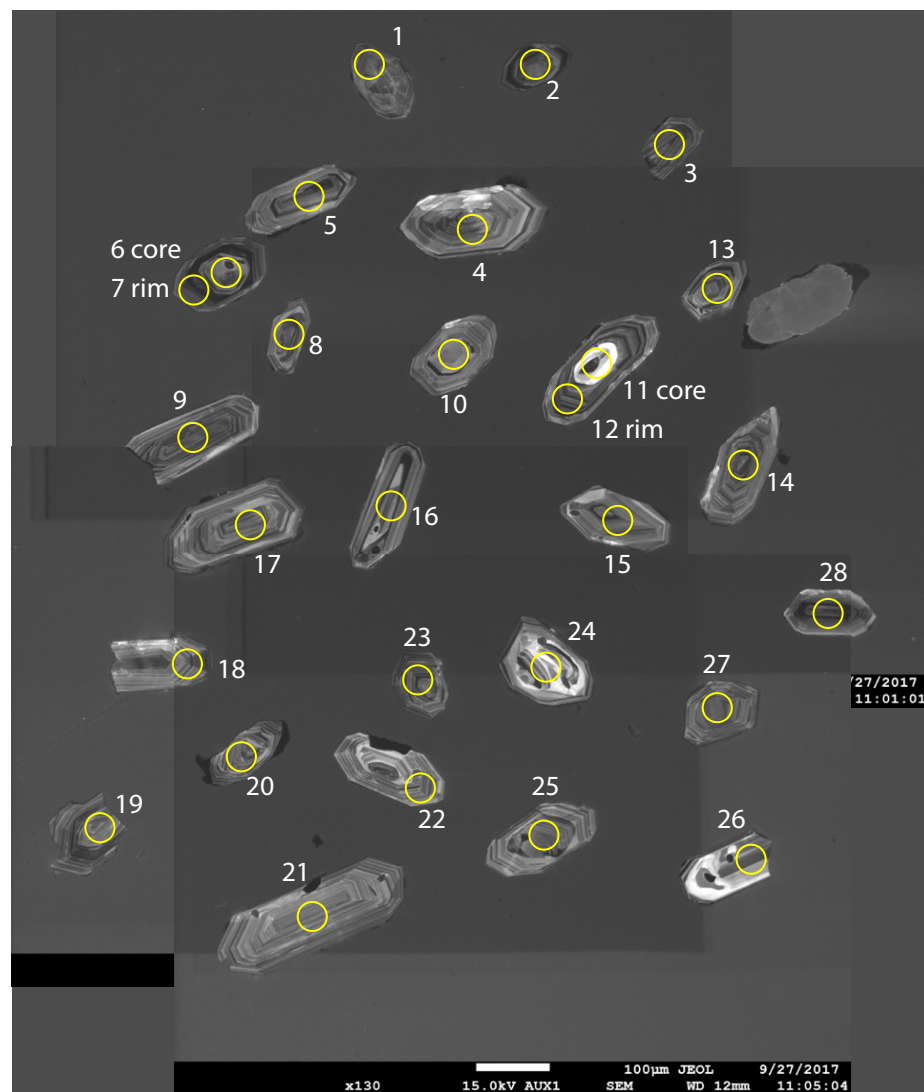
C.11 17-LVD-030, Mount Byng, continued



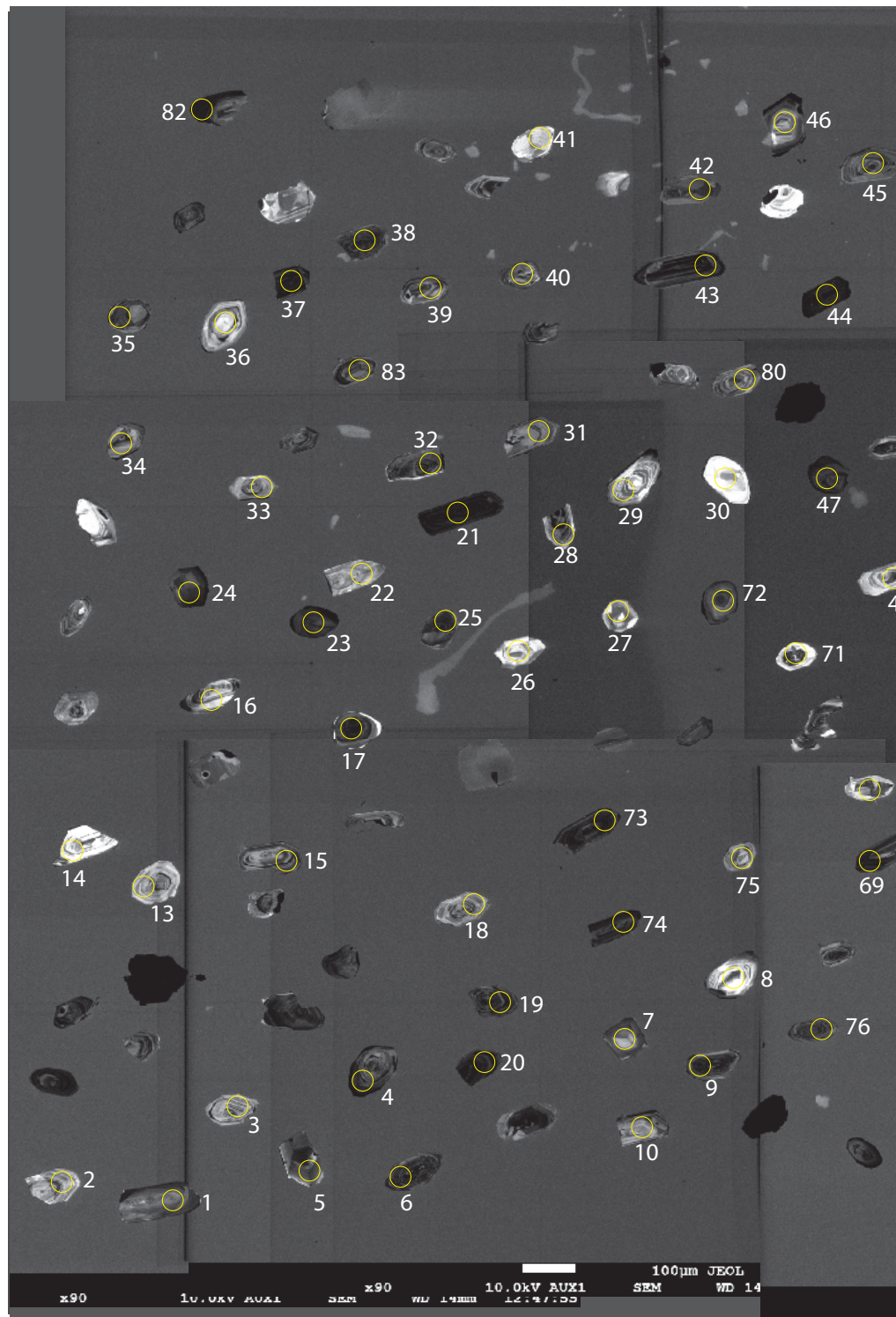
C.12 17-LVD-034, Mount Slim



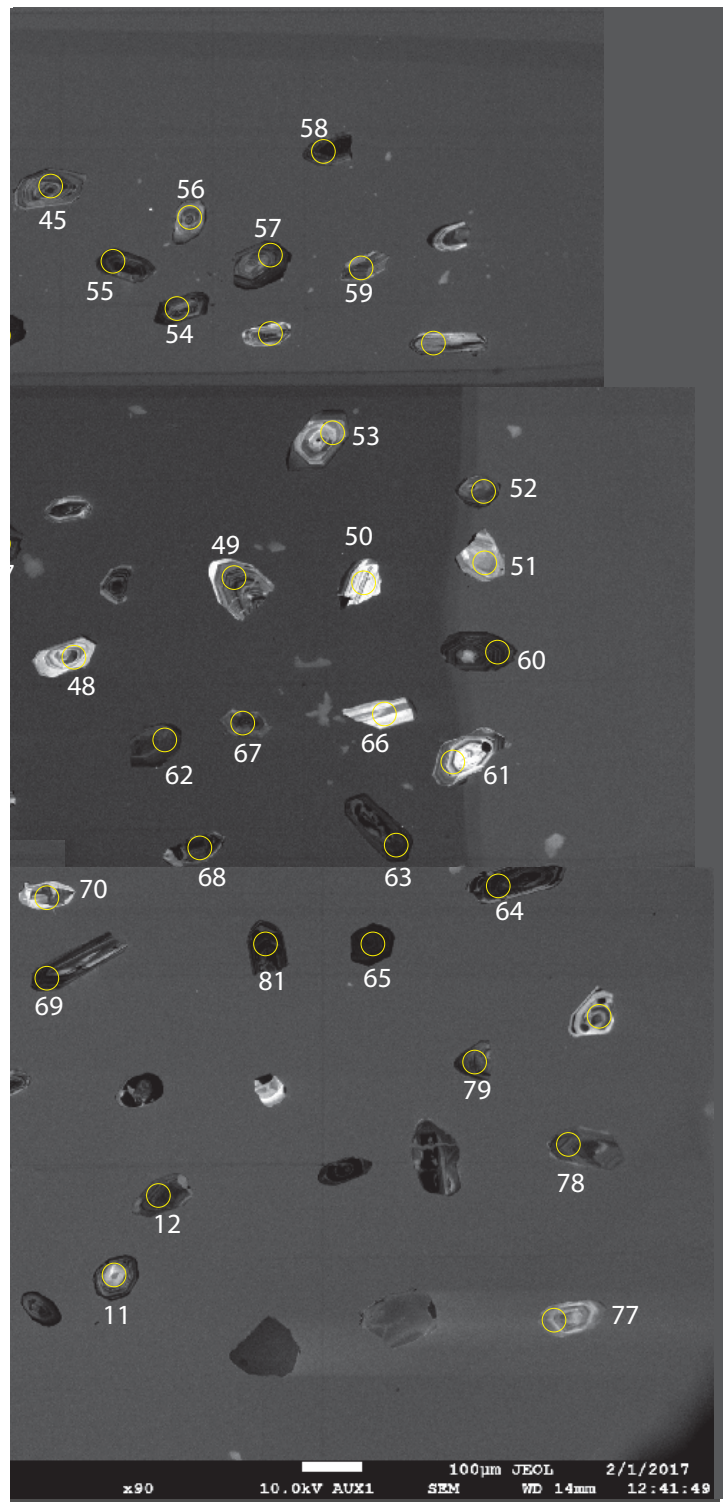
C.13 17-LVD-038, King Lake



C.14 16-LVD-007, Klondike Highway



C.13 16-LVD-007, Klondike Highway



Appendix D: Laser ablation split stream analytical data

Two additional samples (16-LVD-007 and 17-LVD-026) were initially chosen for detrital zircon U-Pb-Hf analysis. Sample 16-LVD-007 collected from the North Klondike Highway, south of Carmacks, yielded a Cretaceous maximum depositional age and therefore is from a stratigraphic unit younger than the Laberge Group. Sample 17-LVD-026 is a cobble-sized amphibolite clast collected from a conglomerate unit near Fish Lake that was contaminated with detrital zircon crystals from the matrix. Therefore, the U-Pb and Hf isotope results of these samples are not included in the discussion and interpretations, but reported in this appendix for reference.

D.1 U-Pb isotopic ratios

Tanglefoot formation

Whitehorse trough - Tanglefoot formation - Sample 16-LVD-001B, Robert Campbell Highway (Zone 08V 455577E 6877512N NAD 83)

Grain	Spot name	isotopic ratios										isotopic ages									
		U (ppm)	U/Th	$^{238}\text{U}/$		$^{207}\text{Pb}/$		^{207}Pb		^{206}Pb		^{207}Pb		\pm	^{207}Pb (Ma)	^{207}Pb		^{206}Pb		Best Age (Ma)	\pm
				^{206}Pb	2SE	^{206}Pb	2SE	^{235}U	2SE	^{238}U	2SE	ρho^*	^{206}Pb		^{235}U	(Ma)	^{238}U	(Ma)	^{206}Pb	^{238}U	
2	171214_119.FIN2	1192	1.3	30.9789	1.2476	0.0503	0.0021	0.2250	0.0093	0.0323	0.0007	0.24	209	97	206	8	205	4	205	4	n/a
3	171214_120.FIN2	896	1.1	31.5159	1.1919	0.0511	0.0018	0.2235	0.0082	0.0317	0.0006	0.32	245	81	204	7	201	3	201	3	n/a
4	171214_121.FIN2	496	2.0	31.1333	1.1631	0.0518	0.0021	0.2284	0.0094	0.0321	0.0006	0.34	277	93	208	8	204	3	204	3	n/a
5	171214_122.FIN2	1251	2.1	30.6843	1.1298	0.0502	0.0012	0.2262	0.0053	0.0326	0.0005	0.42	204	55	207	4	207	3	207	3	n/a
6	171214_123.FIN2	1184	3.0	31.1430	1.1639	0.0503	0.0010	0.2243	0.0046	0.0321	0.0004	0.26	209	46	205	4	204	2	204	2	n/a
7	171214_124.FIN2	1034	2.4	31.1721	1.1660	0.0506	0.0015	0.2234	0.0068	0.0321	0.0006	0.45	223	69	204	6	204	3	204	3	n/a
8	171214_125.FIN2	730	1.1	30.5344	1.3053	0.0507	0.0020	0.2280	0.0120	0.0328	0.0009	0.42	227	91	208	10	208	5	208	5	n/a
9	171214_126.FIN2	488	1.8	30.3951	1.2010	0.0506	0.0027	0.2290	0.0110	0.0329	0.0007	0.29	223	123	209	9	209	4	209	4	n/a
10	171214_127.FIN2	366	1.9	32.0308	1.2312	0.0505	0.0029	0.2180	0.0120	0.0312	0.0006	0.22	218	133	199	10	198	4	198	4	n/a
11	171214_128.FIN2	858	2.3	29.7619	1.1515	0.0504	0.0020	0.2350	0.0100	0.0336	0.0006	0.43	213	92	214	8	213	4	213	4	n/a
12	171214_129.FIN2	1383	2.2	31.7360	1.2086	0.0506	0.0011	0.2205	0.0048	0.0315	0.0004	0.25	223	50	202	4	200	3	200	3	n/a
14	171214_137.FIN2	670	1.5	32.0821	1.3380	0.0506	0.0021	0.2158	0.0098	0.0312	0.0007	0.51	223	96	198	8	198	4	198	4	n/a
15	171214_138.FIN2	754	1.2	33.0469	1.3105	0.0498	0.0025	0.2090	0.0110	0.0303	0.0006	0.37	186	117	193	9	192	4	192	4	n/a
17	171214_140.FIN2	767	0.7	33.9213	1.6109	0.0495	0.0027	0.2030	0.0140	0.0295	0.0010	0.63	172	127	187	12	187	6	187	6	n/a
18	171214_141.FIN2	1124	2.7	32.0308	1.2312	0.0501	0.0015	0.2167	0.0070	0.0312	0.0006	0.44	200	70	199	6	198	4	198	4	n/a
19	171214_142.FIN2	943	1.3	31.8979	1.3227	0.0507	0.0026	0.2200	0.0110	0.0314	0.0007	0.20	227	119	201	10	199	5	199	5	n/a
21	171214_144.FIN2	3467	1.3	34.2583	1.4084	0.0509	0.0015	0.2045	0.0063	0.0292	0.0006	0.39	236	68	189	5	186	4	186	4	n/a
22	171214_145.FIN2	827	1.4	32.0924	1.2359	0.0505	0.0015	0.2184	0.0072	0.0312	0.0006	0.48	218	69	200	6	198	4	198	4	n/a
23	171214_146.FIN2	942	1.4	34.2231	1.2883	0.0502	0.0015	0.2033	0.0063	0.0292	0.0004	0.32	204	69	188	5	186	3	186	3	n/a
24	171214_147.FIN2	849	1.3	33.2779	1.2182	0.0503	0.0012	0.2088	0.0056	0.0301	0.0004	0.41	209	55	192	5	191	3	191	3	n/a
25	171214_154.FIN2	965	2.7	31.6957	1.2055	0.0505	0.0014	0.2214	0.0066	0.0316	0.0005	0.33	218	64	203	6	200	3	200	3	n/a

Grain	Spot name	isotopic ratios										isotopic ages									
		U (ppm)	U/Th	$^{238}\text{U}/$		$^{207}\text{Pb}/$		^{207}Pb		^{206}Pb		rho*	^{206}Pb (Ma)	^{207}Pb (Ma)	^{207}Pb (Ma)	^{206}Pb (Ma)	^{238}U (Ma)	Best Age (Ma)	\pm		
				^{206}Pb	2SE	^{206}Pb	2SE	^{235}U	2SE	^{238}U	2SE										
26	171214_155.FIN2	594	1.8	30.8357	1.1410	0.0506	0.0016	0.2265	0.0071	0.0324	0.0005	0.24	223	73	207	6	206	3	206	3	n/a
27	171214_156.FIN2	770	1.7	32.5627	1.1664	0.0504	0.0012	0.2151	0.0053	0.0307	0.0004	0.30	213	55	197	5	195	2	195	2	n/a
28	171214_157.FIN2	1046	2.0	30.8261	1.2353	0.0508	0.0020	0.2254	0.0075	0.0324	0.0007	0.27	232	91	208	7	206	4	206	4	n/a
29	171214_158.FIN2	138	2.8	28.9855	1.5123	0.0515	0.0048	0.2440	0.0230	0.0345	0.0013	0.14	263	214	220	19	219	8	219	8	n/a
30	171214_159.FIN2	754	1.3	32.1440	1.2399	0.0504	0.0018	0.2180	0.0078	0.0311	0.0005	0.12	213	83	200	7	198	3	198	3	n/a
31	171214_160.FIN2	178	1.5	31.7460	1.7133	0.0520	0.0054	0.2260	0.0240	0.0315	0.0013	0.25	285	237	206	20	200	8	200	8	n/a
32	171214_161.FIN2	937	2.2	30.8737	1.2391	0.0507	0.0022	0.2250	0.0098	0.0324	0.0007	0.26	227	100	206	8	206	5	206	5	n/a
33	171214_162.FIN2	1033	1.5	33.1565	1.2093	0.0502	0.0014	0.2094	0.0059	0.0302	0.0004	0.30	204	65	193	5	192	3	192	3	n/a
34	171214_163.FIN2	925	1.7	32.2789	1.1461	0.0497	0.0015	0.2140	0.0066	0.0310	0.0004	0.19	181	70	197	6	197	3	197	3	n/a
35	171214_164.FIN2	521	2.0	33.5458	1.2379	0.0506	0.0021	0.2081	0.0078	0.0298	0.0005	0.06	223	96	191	7	189	3	189	3	n/a
36	171214_165.FIN2	592	1.6	32.6477	1.2790	0.0508	0.0026	0.2150	0.0110	0.0306	0.0007	0.27	232	118	197	9	195	4	195	4	n/a
37	171214_172.FIN2	1658	1.8	31.4465	1.4833	0.0509	0.0018	0.2212	0.0098	0.0318	0.0010	0.59	236	82	203	8	202	6	202	6	n/a
38	171214_173.FIN2	611	1.6	34.2466	1.7592	0.0511	0.0050	0.2040	0.0180	0.0292	0.0011	0.19	245	225	188	15	185	7	185	7	n/a
39	171214_174.FIN2	406	1.7	31.3087	1.1763	0.0507	0.0021	0.2246	0.0096	0.0319	0.0005	0.27	227	96	205	8	203	3	203	3	n/a
40	171214_175.FIN2	960	1.1	34.3407	1.4151	0.0514	0.0027	0.2040	0.0110	0.0291	0.0007	0.48	259	121	188	9	185	5	185	5	n/a
41	171214_176.FIN2	1049	2.1	31.7158	1.3077	0.0504	0.0017	0.2204	0.0077	0.0315	0.0007	0.34	213	78	202	6	200	4	200	4	n/a
42	171214_177.FIN2	937	2.1	32.4044	1.2601	0.0505	0.0015	0.2153	0.0066	0.0309	0.0005	0.30	218	69	198	6	196	3	196	3	n/a
43	171214_178.FIN2	938	1.6	33.2890	1.2190	0.0502	0.0010	0.2079	0.0045	0.0300	0.0003	0.45	204	46	192	4	191	2	191	2	n/a
44	171214_179.FIN2	1017	1.6	33.4784	1.3450	0.0494	0.0018	0.2047	0.0077	0.0299	0.0006	0.26	167	85	189	6	190	4	190	4	n/a
45	171214_180.FIN2	935	1.4	34.0832	1.5102	0.0515	0.0030	0.2090	0.0130	0.0293	0.0008	0.32	263	134	193	11	186	5	186	5	n/a
46	171214_181.FIN2	776	1.6	32.9707	1.1958	0.0507	0.0018	0.2139	0.0081	0.0303	0.0004	0.37	227	82	196	7	193	3	193	3	n/a
47	171214_182.FIN2	692	1.6	32.6371	1.2782	0.0507	0.0027	0.2150	0.0110	0.0306	0.0007	0.10	227	123	197	9	195	4	195	4	n/a
48	171214_183.FIN2	1810	2.8	32.5733	1.2732	0.0504	0.0015	0.2127	0.0062	0.0307	0.0006	0.13	213	69	196	5	195	4	195	4	n/a
49	171214_190.FIN2	671	2.1	32.0821	1.1322	0.0507	0.0013	0.2186	0.0057	0.0312	0.0003	0.25	227	59	200	5	198	2	198	2	n/a

Grain	Spot name	isotopic ratios										isotopic ages									
		U	U/Th	$^{238}\text{U}/$	$^{207}\text{Pb}/$		^{207}Pb		^{206}Pb			^{207}Pb	\pm	^{207}Pb	\pm	^{206}Pb	\pm	Best	\pm		
		(ppm)		^{206}Pb	2SE	^{206}Pb	2SE	^{235}U	2SE	^{238}U	2SE	rho*	^{206}Pb	(Ma)	^{235}U	(Ma)	^{238}U	(Ma)	Age	(Ma)	conc.
50	171214_191.FIN2	899	1.5	34.3525	1.2981	0.0505	0.0015	0.2026	0.0059	0.0291	0.0004	0.24	218	69	187	5	185	2	185	2	n/a
51	171214_192.FIN2	621	1.8	32.2893	1.3554	0.0504	0.0027	0.2160	0.0110	0.0310	0.0007	0.13	213	124	198	9	197	4	197	4	n/a
52	171214_193.FIN2	901	1.8	32.9489	1.1942	0.0507	0.0024	0.2132	0.0093	0.0304	0.0005	0.29	227	109	196	8	193	3	193	3	n/a
54	171214_195.FIN2	1029	1.3	31.0463	1.3494	0.0504	0.0024	0.2240	0.0100	0.0322	0.0009	0.17	213	110	205	9	204	6	204	6	n/a
55	171214_196.FIN2	1078	1.5	31.1818	1.2640	0.0504	0.0024	0.2228	0.0099	0.0321	0.0007	0.14	213	110	204	8	204	4	204	4	n/a
56	171214_197.FIN2	1169	2.3	32.0821	1.1322	0.0506	0.0012	0.2171	0.0051	0.0312	0.0004	0.28	223	55	199	4	198	3	198	3	n/a
57	171214_198.FIN2	797	1.8	33.2557	1.2165	0.0506	0.0016	0.2121	0.0072	0.0301	0.0005	0.22	223	73	195	6	191	3	191	3	n/a
58	171214_199.FIN2	1098	1.3	32.8515	1.2951	0.0504	0.0019	0.2106	0.0075	0.0304	0.0006	0.19	213	87	194	6	193	4	193	4	n/a
59	171214_200.FIN2	848	1.6	33.5571	1.3513	0.0515	0.0028	0.2120	0.0110	0.0298	0.0006	0.08	263	125	195	10	189	4	189	4	n/a
60	171214_201.FIN2	438	1.5	34.3997	1.4200	0.0509	0.0031	0.2040	0.0120	0.0291	0.0006	0.12	236	141	188	10	185	4	185	4	n/a
61	171214_208.FIN2	951	1.4	33.0907	1.3140	0.0503	0.0023	0.2099	0.0097	0.0302	0.0007	0.22	209	106	193	8	192	4	192	4	n/a
62	171214_209.FIN2	394	1.4	32.6691	1.2807	0.0513	0.0030	0.2170	0.0120	0.0306	0.0006	0.09	254	134	199	10	194	4	194	4	n/a
63	171214_210.FIN2	1421	1.0	32.8192	1.2925	0.0495	0.0021	0.2110	0.0100	0.0305	0.0005	0.26	172	99	194	9	194	3	194	3	n/a
64	171214_211.FIN2	705	1.3	34.0368	1.2744	0.0506	0.0017	0.2055	0.0066	0.0294	0.0004	0.13	223	78	190	6	187	2	187	2	n/a
66	171214_213.FIN2	803	2.4	17.7305	0.8488	0.0543	0.0033	0.4220	0.0290	0.0564	0.0019	0.31	384	137	356	20	353	11	353	11	n/a
69	171214_216.FIN2	1123	1.4	33.3333	1.5556	0.0503	0.0024	0.2080	0.0100	0.0300	0.0010	0.40	209	111	192	8	191	6	191	6	n/a
70	171214_217.FIN2	445	1.4	32.9056	1.4076	0.0513	0.0031	0.2150	0.0120	0.0304	0.0007	0.04	254	139	197	10	193	5	193	5	n/a
71	171214_218.FIN2	2470	1.3	30.2847	1.2840	0.0502	0.0016	0.2292	0.0075	0.0330	0.0008	0.43	204	74	209	6	209	5	209	5	n/a
72	171214_219.FIN2	1008	1.2	34.2114	1.4045	0.0498	0.0018	0.2017	0.0071	0.0292	0.0006	0.22	186	84	186	6	186	4	186	4	n/a
74	171215_011.FIN2	792	2.6	32.4886	0.9077	0.0505	0.0021	0.2130	0.0086	0.0308	0.0007	0.25	218	96	196	7	195	4	195	4	n/a
75	171215_012.FIN2	834	1.4	34.3053	0.9297	0.0501	0.0017	0.2020	0.0080	0.0292	0.0006	0.51	200	79	187	7	185	4	185	4	n/a
76	171215_013.FIN2	913	1.9	32.7547	0.7832	0.0503	0.0026	0.2109	0.0097	0.0305	0.0006	0.29	209	120	194	8	194	3	194	3	n/a
77	171215_014.FIN2	1365	1.5	32.9056	0.7146	0.0503	0.0012	0.2105	0.0050	0.0304	0.0005	0.36	209	55	194	4	193	3	193	3	n/a
78	171215_015.FIN2	923	1.0	34.1181	0.8381	0.0501	0.0017	0.2024	0.0073	0.0293	0.0006	0.39	200	79	187	6	186	4	186	4	n/a

Grain	Spot name	isotopic ratios												isotopic ages											
		U (ppm)	U/Th	$^{238}\text{U}/$		$^{207}\text{Pb}/$		^{207}Pb		^{206}Pb				^{207}Pb (Ma)	\pm	^{207}Pb (Ma)	\pm	^{206}Pb (Ma)	\pm	Best (Ma)	\pm				
				^{206}Pb	2SE	^{206}Pb	2SE	^{235}U	2SE	^{238}U	2SE	rho*	^{206}Pb		^{235}U	^{238}U	Age (Ma)	conc.							
79	171215_016.FIN2	592	1.7	30.7031	0.7730	0.0505	0.0019	0.2265	0.0078	0.0326	0.0006	0.13	218	87	207	6	207	4	207	4	n/a				
80	171215_017.FIN2	239	1.6	18.3824	0.5069	0.0530	0.0023	0.4010	0.0170	0.0544	0.0012	0.13	329	98	341	12	342	7	342	7	n/a				
82	171215_019.FIN2	490	1.8	31.9183	0.7437	0.0509	0.0021	0.2210	0.0092	0.0313	0.0005	0.25	236	95	202	8	199	3	199	3	n/a				
83	171215_020.FIN2	858	1.8	31.6056	0.6593	0.0504	0.0013	0.2207	0.0056	0.0316	0.0004	0.30	213	60	202	5	201	3	201	3	n/a				
84	171215_021.FIN2	1056	1.2	34.1880	0.7831	0.0499	0.0018	0.1993	0.0073	0.0293	0.0005	0.35	190	84	184	6	186	3	186	3	n/a				
85	171215_028.FIN2	694	1.2	31.6857	0.7731	0.0507	0.0017	0.2198	0.0080	0.0316	0.0006	0.40	227	77	201	7	200	4	200	4	n/a				
86	171215_029.FIN2	559	1.5	32.1958	0.7982	0.0503	0.0022	0.2182	0.0092	0.0311	0.0006	0.29	209	101	200	8	197	4	197	4	n/a				
87	171215_030.FIN2	526	1.8	30.9981	0.6822	0.0505	0.0016	0.2239	0.0076	0.0323	0.0005	0.25	218	73	205	6	205	3	205	3	n/a				
89	171215_032.FIN2	926	2.2	32.5098	0.7081	0.0507	0.0014	0.2169	0.0068	0.0308	0.0005	0.40	227	64	199	6	195	3	195	3	n/a				
90	171215_033.FIN2	829	3.1	31.5457	0.7961	0.0506	0.0021	0.2208	0.0094	0.0317	0.0006	0.25	223	96	202	8	201	4	201	4	n/a				
91	171215_034.FIN2	985	1.1	33.7952	1.0736	0.0504	0.0026	0.2050	0.0110	0.0296	0.0008	0.33	213	120	189	9	188	5	188	5	n/a				
92	171215_035.FIN2	1434	1.1	32.7654	1.0736	0.0507	0.0020	0.2120	0.0100	0.0305	0.0009	0.57	227	91	195	9	194	6	194	6	n/a				
93	171215_036.FIN2	421	1.0	34.4234	0.7228	0.0506	0.0019	0.2013	0.0073	0.0291	0.0004	0.20	223	87	186	6	185	3	185	3	n/a				
94	171215_037.FIN2	593	1.1	34.2466	0.7154	0.0503	0.0014	0.2024	0.0062	0.0292	0.0004	0.36	209	65	188	5	186	3	186	3	n/a				
95	171215_038.FIN2	988	1.8	31.1527	0.8928	0.0505	0.0017	0.2229	0.0088	0.0321	0.0008	0.59	218	78	204	7	204	5	204	5	n/a				
96	171215_039.FIN2	362	1.8	32.8731	0.8321	0.0509	0.0025	0.2150	0.0110	0.0304	0.0006	0.22	236	113	197	9	193	4	193	4	n/a				
97	171215_046.FIN2	1152	1.5	32.3625	0.8483	0.0509	0.0019	0.2139	0.0089	0.0309	0.0006	0.51	236	86	197	7	196	4	196	4	n/a				
98	171215_047.FIN2	907	2.4	31.1818	0.8848	0.0506	0.0028	0.2240	0.0140	0.0321	0.0008	0.43	223	128	205	11	203	5	203	5	n/a				
99	171215_048.FIN2	170	1.2	32.0924	0.8033	0.0514	0.0031	0.2240	0.0140	0.0312	0.0006	0.05	259	139	203	11	198	4	198	4	n/a				
100	171215_049.FIN2	679	1.8	33.5571	0.8333	0.0506	0.0023	0.2093	0.0099	0.0298	0.0006	0.29	223	105	193	8	189	4	189	4	n/a				
102	171215_051.FIN2	683	1.3	33.6361	0.7354	0.0504	0.0016	0.2069	0.0062	0.0297	0.0005	0.24	213	74	191	5	189	3	189	3	n/a				
103	171215_052.FIN2	792	1.5	34.1647	0.6536	0.0496	0.0010	0.2018	0.0047	0.0293	0.0003	0.39	176	47	186	4	186	2	186	2	n/a				
104	171215_053.FIN2	864	1.3	33.1455	1.0437	0.0504	0.0027	0.2097	0.0090	0.0302	0.0008	0.29	213	124	193	8	192	5	192	5	n/a				
105	171215_054.FIN2	822	2.3	33.3333	1.2222	0.0514	0.0034	0.2130	0.0130	0.0300	0.0010	0.12	259	152	196	11	191	6	191	6	n/a				

Grain	Spot name	isotopic ratios										isotopic ages									
		U (ppm)	U/Th	$^{238}\text{U}/$		$^{207}\text{Pb}/$		^{207}Pb		^{206}Pb				^{207}Pb (Ma)	\pm	^{207}Pb (Ma)	\pm	^{206}Pb (Ma)	\pm	Best (Ma)	\pm
				^{206}Pb	2SE	^{206}Pb	2SE	^{235}U	2SE	^{238}U	2SE	rho*	^{206}Pb	(Ma)	^{235}U	(Ma)	^{238}U	(Ma)	Age (Ma)	conc.	
106	171215_055.FIN2	1248	1.3	34.1764	0.9461	0.0503	0.0017	0.2003	0.0073	0.0293	0.0007	0.45	209	78	186	7	186	4	186	4	n/a
107	171215_056.FIN2	679	1.9	31.6356	0.6105	0.0507	0.0012	0.2216	0.0057	0.0316	0.0003	0.31	227	55	203	5	201	2	201	2	n/a
110	171215_065.FIN2	782	1.8	33.9559	0.7725	0.0504	0.0019	0.2075	0.0084	0.0295	0.0005	0.38	213	87	191	7	187	3	187	3	n/a
111	171215_066.FIN2	1262	1.2	31.1527	1.1646	0.0505	0.0026	0.2230	0.0130	0.0321	0.0010	0.48	218	119	204	11	204	7	204	7	n/a
112	171215_067.FIN2	1678	2.4	31.3676	0.7970	0.0512	0.0015	0.2242	0.0078	0.0319	0.0006	0.51	250	67	205	6	202	4	202	4	n/a
113	171215_068.FIN2	653	1.7	34.3053	0.7767	0.0502	0.0016	0.2044	0.0071	0.0292	0.0005	0.36	204	74	188	6	185	3	185	3	n/a
114	171215_069.FIN2	1181	1.6	33.7496	1.0024	0.0506	0.0018	0.2050	0.0078	0.0296	0.0007	0.46	223	82	189	7	188	5	188	5	n/a
115	171215_070.FIN2	699	1.5	34.0252	0.9493	0.0502	0.0027	0.2040	0.0120	0.0294	0.0007	0.51	204	125	188	10	187	4	187	4	n/a
117	171215_072.FIN2	625	1.6	33.8524	0.8939	0.0501	0.0020	0.2051	0.0087	0.0295	0.0006	0.30	200	93	189	7	188	4	188	4	n/a
118	171215_073.FIN2	1059	1.4	31.6356	0.7806	0.0509	0.0017	0.2205	0.0074	0.0316	0.0006	0.28	236	77	202	6	201	4	201	4	n/a
120	171215_075.FIN2	1098	1.7	32.6371	0.8415	0.0505	0.0014	0.2127	0.0075	0.0306	0.0006	0.57	218	64	196	6	195	4	195	4	n/a
Rejected Analysis																					
1	171214_118.FIN2	1152	1.3	32.4044	1.1551	0.0584	0.0016	0.2488	0.0070	0.0309	0.0004	0.40	545	60	225	6	196	3	196	3	n/a
13	171214_136.FIN2	646	1.6	31.0945	1.3536	0.0620	0.0027	0.2740	0.0130	0.0322	0.0009	0.33	674	93	246	10	204	6	204	6	n/a
16	171214_139.FIN2	1325	2.0	30.4507	1.2054	0.0542	0.0019	0.2461	0.0088	0.0328	0.0007	0.30	379	79	223	7	208	4	208	4	n/a
20	171214_143.FIN2	248	1.4	30.5624	1.2143	0.0576	0.0030	0.2590	0.0140	0.0327	0.0007	0.29	515	114	235	12	208	4	208	4	n/a
53	171214_194.FIN2	469	1.6	28.1770	1.1909	0.0677	0.0054	0.3340	0.0280	0.0355	0.0008	0.26	859	166	290	21	225	5	225	5	n/a
65	171214_212.FIN2	1448	1.6	35.5366	1.3891	0.0774	0.0023	0.3050	0.0110	0.0281	0.0004	0.47	1132	59	269	8	179	3	179	3	n/a
67	171214_214.FIN2	1649	1.6	32.4149	1.2609	0.0563	0.0025	0.2390	0.0100	0.0309	0.0006	0.28	464	98	217	9	196	4	196	4	n/a
68	171214_215.FIN2	1632	2.2	31.9591	1.4299	0.0610	0.0023	0.2600	0.0110	0.0313	0.0009	0.43	639	81	234	9	199	6	199	6	n/a
73	171215_010.FIN2	402	1.4	33.3222	0.8106	0.0547	0.0025	0.2280	0.0100	0.0300	0.0006	0.17	400	102	208	9	191	4	191	4	n/a
81	171215_018.FIN2	952	2.4	32.4992	0.9611	0.0503	0.0017	0.2126	0.0078	0.0308	0.0008	0.37	209	78	195	7	195	5	195	5	n/a
88	171215_031.FIN2	1766	1.5	32.5839	0.7963	0.0592	0.0016	0.2516	0.0067	0.0307	0.0006	0.31	574	59	228	5	195	4	195	4	n/a
101	171215_050.FIN2	1134	1.4	30.6654	0.7993	0.0562	0.0022	0.2538	0.0097	0.0326	0.0007	0.10	460	87	229	8	207	4	207	4	n/a

Grain	Spot name	isotopic ratios										isotopic ages									
		U	U/Th	$^{238}\text{U}/$		$^{207}\text{Pb}/$		^{207}Pb		^{206}Pb		^{207}Pb	\pm	^{207}Pb	\pm	^{206}Pb	\pm	Best	\pm		
		(ppm)		^{206}Pb	2SE	^{206}Pb	2SE	^{235}U	2SE	^{238}U	2SE	rho*	^{206}Pb	(Ma)	^{235}U	(Ma)	^{238}U	(Ma)	Age	(Ma)	conc.
108	171215_057.FIN2	2674	1.4	33.4113	0.8596	0.0824	0.0025	0.3382	0.0094	0.0299	0.0006	0.31	1255	59	296	7	190	4	190	4	n/a
109	171215_064.FIN2	1824	0.8	28.8101	0.7968	0.0797	0.0021	0.3830	0.0120	0.0347	0.0008	0.62	1190	52	329	9	220	5	220	5	n/a
116	171215_071.FIN2	489	1.3	32.8084	1.1840	0.0513	0.0035	0.2140	0.0140	0.0305	0.0010	0.18	254	157	196	12	194	6	194	6	n/a
119	171215_074.FIN2	2044	1.9	33.5345	0.8434	0.0624	0.0024	0.2580	0.0110	0.0298	0.0006	0.28	688	82	233	9	189	4	189	4	n/a

Grain	Spot name	isotopic ratios										isotopic ages							
		U	U/Th	$^{238}\text{U}/$	$^{207}\text{Pb}/$		^{207}Pb		^{206}Pb			^{207}Pb	\pm	^{207}Pb	\pm	^{206}Pb	\pm	Best	\pm
		(ppm)		^{206}Pb	2SE	^{206}Pb	2SE	^{235}U	2SE	^{238}U	2SE	rho*	^{206}Pb	(Ma)	^{235}U	(Ma)	^{238}U	(Ma)	Age

Whitehorse trough - Tanglefoot formation - Sample 16-LVD-001C, Robert Campbell Highway (Zone 08V 455577E 6877512N NAD 83)

Grain	Spot name	isotopic ratios										isotopic ages									
		U	U/Th	$^{238}\text{U}/$	$^{207}\text{Pb}/$		^{207}Pb		^{206}Pb			^{207}Pb	\pm	^{207}Pb	\pm	^{206}Pb	\pm	Best	\pm		
		(ppm)		^{206}Pb	2SE	^{206}Pb	2SE	^{235}U	2SE	^{238}U	2SE	rho	^{206}Pb	(Ma)	^{235}U	(Ma)	^{238}U	(Ma)	Age	(Ma)	conc.
1	171213_154.FIN2	171	2.1	27.7778	0.6944	0.0507	0.0028	0.2550	0.0140	0.0360	0.0006	0.04	227	128	229	11	228	3	228	3	n/a
3	171213_156.FIN2	751	1.5	32.3102	0.9082	0.0508	0.0031	0.2190	0.0130	0.0310	0.0006	0.13	232	141	200	11	197	4	197	4	n/a
4	171213_157.FIN2	284	2.4	28.2726	0.7993	0.0509	0.0045	0.2510	0.0240	0.0354	0.0008	0.43	236	204	227	19	224	5	224	5	n/a
5	171213_158.FIN2	69	2.9	28.5714	1.3061	0.0540	0.0110	0.2600	0.0570	0.0350	0.0014	0.11	371	459	227	45	222	9	222	9	n/a
7	171213_160.FIN2	104	2.7	28.2885	0.8803	0.0517	0.0041	0.2520	0.0200	0.0354	0.0008	0.04	272	182	225	16	224	5	224	5	n/a
9	171213_162.FIN2	1222	1.8	32.0102	0.8402	0.0494	0.0024	0.2140	0.0100	0.0312	0.0005	0.29	167	114	197	9	198	3	198	3	n/a
10	171213_163.FIN2	550	1.9	30.8642	1.1431	0.0511	0.0050	0.2290	0.0210	0.0324	0.0010	0.19	245	225	209	18	206	6	206	6	n/a
11	171213_164.FIN2	351	1.6	30.8642	1.4289	0.0516	0.0058	0.2300	0.0260	0.0324	0.0014	0.31	268	258	209	21	206	9	206	9	n/a
12	171213_165.FIN2	171	1.9	29.1545	1.0200	0.0511	0.0045	0.2430	0.0210	0.0343	0.0009	0.11	245	203	219	17	217	6	217	6	n/a
13	171213_172.FIN2	149	2.1	28.6780	0.9047	0.0514	0.0035	0.2470	0.0170	0.0349	0.0008	0.24	259	156	221	14	221	5	221	5	n/a
14	171213_173.FIN2	275	2.3	27.3000	0.7006	0.0509	0.0033	0.2580	0.0160	0.0366	0.0006	0.19	236	150	232	13	232	4	232	4	n/a
15	171213_174.FIN2	287	3.8	27.6472	0.7491	0.0511	0.0030	0.2540	0.0140	0.0362	0.0007	0.00	245	135	229	11	229	4	229	4	n/a
16	171213_175.FIN2	250	3.1	26.7594	0.6588	0.0515	0.0029	0.2660	0.0150	0.0374	0.0006	0.05	263	129	238	12	237	3	237	3	n/a
17	171213_176.FIN2	190	3.4	27.5406	0.7130	0.0517	0.0034	0.2600	0.0180	0.0363	0.0006	0.14	272	151	235	14	230	4	230	4	n/a
18	171213_177.FIN2	257	1.9	28.3286	0.9630	0.0519	0.0041	0.2540	0.0220	0.0353	0.0010	0.38	281	181	228	18	223	6	223	6	n/a
19	171213_178.FIN2	349	1.5	20.4248	0.4589	0.0527	0.0018	0.3550	0.0120	0.0490	0.0005	0.22	316	78	309	9	308	3	308	3	n/a
20	171213_179.FIN2	140	3.1	27.7778	0.9259	0.0515	0.0039	0.2550	0.0190	0.0360	0.0010	0.17	263	174	229	16	228	6	228	6	n/a
21	171213_180.FIN2	122	3.8	28.0899	1.1836	0.0527	0.0051	0.2580	0.0240	0.0356	0.0013	0.13	316	220	231	20	226	8	226	8	n/a

Grain	Spot name	isotopic ratios										isotopic ages									
		U	U/Th	$^{238}\text{U}/$		$^{207}\text{Pb}/$		^{207}Pb		^{206}Pb		rho*	^{207}Pb	\pm	^{207}Pb	\pm	^{206}Pb	\pm	Best	\pm	
				(ppm)	^{206}Pb	2SE	^{206}Pb	2SE	^{235}U	2SE	^{238}U	2SE									
22	171213_181.FIN2	367	2.2	27.3075	0.8203	0.0520	0.0034	0.2620	0.0160	0.0366	0.0009	0.03	285	150	236	13	232	6	232	6	n/a
23	171213_182.FIN2	167	2.8	28.9017	1.1694	0.0530	0.0052	0.2510	0.0230	0.0346	0.0012	0.01	329	223	226	18	219	7	219	7	n/a
24	171213_183.FIN2	112	3.6	28.5144	0.8131	0.0524	0.0036	0.2510	0.0170	0.0351	0.0007	0.08	303	157	225	13	222	5	222	5	n/a
26	171213_191.FIN2	235	2.3	28.3366	0.6424	0.0515	0.0018	0.2519	0.0092	0.0353	0.0004	0.29	263	80	227	7	224	2	224	2	n/a
27	171213_192.FIN2	224	2.3	27.5862	0.8371	0.0523	0.0052	0.2610	0.0250	0.0363	0.0008	0.19	299	227	234	21	230	5	230	5	n/a
28	171213_193.FIN2	1096	1.6	32.6264	0.8090	0.0504	0.0019	0.2129	0.0085	0.0307	0.0005	0.33	213	87	196	7	195	3	195	3	n/a
29	171213_194.FIN2	219	1.7	28.9855	1.3443	0.0530	0.0052	0.2520	0.0280	0.0345	0.0015	0.50	329	223	227	23	219	9	219	9	n/a
31	171213_196.FIN2	969	1.9	30.2389	0.9052	0.0525	0.0029	0.2390	0.0130	0.0331	0.0007	0.25	307	126	217	11	210	5	210	5	n/a
32	171213_197.FIN2	201	2.6	28.5714	1.3878	0.0529	0.0082	0.2560	0.0420	0.0350	0.0016	0.48	325	352	229	34	222	10	222	10	n/a
33	171213_198.FIN2	99	2.7	27.0270	0.9496	0.0522	0.0058	0.2640	0.0290	0.0370	0.0010	0.04	294	254	235	23	234	7	234	7	n/a
34	171213_199.FIN2	299	2.5	28.8268	0.8310	0.0521	0.0035	0.2430	0.0150	0.0347	0.0008	0.16	290	153	223	13	220	5	220	5	n/a
35	171213_200.FIN2	188	2.8	25.1256	0.8207	0.0522	0.0039	0.2840	0.0200	0.0398	0.0010	0.06	294	171	252	16	252	6	252	6	n/a
36	171213_201.FIN2	192	1.9	27.7547	0.6856	0.0525	0.0023	0.2580	0.0120	0.0360	0.0005	0.24	307	100	231	9	228	3	228	3	n/a
37	171213_208.FIN2	197	2.7	27.6932	0.7669	0.0523	0.0037	0.2590	0.0190	0.0361	0.0008	0.24	299	161	232	15	229	5	229	5	n/a
38	171213_209.FIN2	259	2.1	28.8517	0.9157	0.0514	0.0037	0.2440	0.0170	0.0347	0.0009	0.14	259	165	221	14	220	5	220	5	n/a
39	171213_210.FIN2	362	1.1	31.6456	0.7911	0.0516	0.0021	0.2218	0.0089	0.0316	0.0005	0.24	268	93	204	8	201	3	201	3	n/a
40	171213_211.FIN2	157	2.7	28.1770	0.9527	0.0524	0.0037	0.2480	0.0170	0.0355	0.0010	0.23	303	161	225	14	225	6	225	6	n/a
41	171213_212.FIN2	164	2.6	27.5482	1.2142	0.0529	0.0053	0.2570	0.0240	0.0363	0.0014	0.16	325	227	230	19	230	9	230	9	n/a
42	171213_213.FIN2	212	2.6	27.2035	0.7400	0.0522	0.0052	0.2640	0.0250	0.0368	0.0007	0.19	294	227	237	20	233	4	233	4	n/a
43	171213_214.FIN2	133	3.3	27.0270	0.8766	0.0520	0.0046	0.2610	0.0230	0.0370	0.0010	0.19	285	202	233	19	234	6	234	6	n/a
44	171213_215.FIN2	164	2.2	27.3448	0.6879	0.0525	0.0031	0.2590	0.0140	0.0366	0.0006	0.06	307	134	232	12	232	4	232	4	n/a
46	171213_217.FIN2	162	2.4	28.0112	1.2554	0.0521	0.0064	0.2530	0.0310	0.0357	0.0015	0.21	290	281	227	25	226	9	226	9	n/a
47	171213_218.FIN2	173	2.6	27.4499	0.6405	0.0522	0.0026	0.2580	0.0130	0.0364	0.0005	0.23	294	114	231	10	231	3	231	3	n/a
48	171213_219.FIN2	269	1.8	29.4464	0.7891	0.0498	0.0036	0.2300	0.0160	0.0340	0.0006	0.19	186	168	208	14	215	4	215	4	n/a

Grain	Spot name	isotopic ratios										isotopic ages									
		U (ppm)	U/Th	$^{238}\text{U}/$		$^{207}\text{Pb}/$		^{207}Pb		^{206}Pb		^{207}Pb (Ma)	\pm	^{207}Pb (Ma)	\pm	^{206}Pb (Ma)	\pm	Best (Ma)	\pm		
				^{206}Pb	2SE	^{206}Pb	2SE	^{235}U	2SE	^{238}U	2SE										
49	171214_010.FIN2	460	2.1	28.0978	1.1842	0.0506	0.0021	0.2540	0.0130	0.0356	0.0008	0.26	223	96	229	10	225	5	225	5	n/a
50	171214_011.FIN2	247	2.3	26.8025	1.0776	0.0519	0.0029	0.2690	0.0150	0.0373	0.0007	0.26	281	128	241	12	236	5	236	5	n/a
51	171214_012.FIN2	170	2.6	26.1097	1.1589	0.0536	0.0047	0.2720	0.0210	0.0383	0.0010	0.19	354	198	243	16	242	6	242	6	n/a
53	171214_014.FIN2	917	1.9	32.4781	1.2658	0.0504	0.0019	0.2151	0.0098	0.0308	0.0007	0.55	213	87	197	8	196	4	196	4	n/a
54	171214_015.FIN2	265	2.3	28.9939	1.0928	0.0518	0.0020	0.2480	0.0110	0.0345	0.0005	0.38	277	88	223	9	219	3	219	3	n/a
55	171214_016.FIN2	660	1.4	26.1438	1.0252	0.0514	0.0023	0.2700	0.0120	0.0383	0.0007	0.19	259	103	244	10	242	4	242	4	n/a
56	171214_017.FIN2	291	2.6	27.7393	1.0773	0.0518	0.0021	0.2531	0.0099	0.0361	0.0007	0.25	277	93	230	8	228	4	228	4	n/a
57	171214_018.FIN2	198	2.8	27.8552	1.7070	0.0526	0.0067	0.2570	0.0310	0.0359	0.0019	0.13	312	290	230	25	227	12	227	12	n/a
59	171214_020.FIN2	568	1.4	33.2447	1.4368	0.0506	0.0029	0.2120	0.0140	0.0301	0.0008	0.54	223	133	194	12	191	5	191	5	n/a
60	171214_021.FIN2	185	3.3	27.2480	1.4849	0.0523	0.0046	0.2620	0.0220	0.0367	0.0016	0.17	299	201	235	18	233	10	233	10	n/a
62	171214_029.FIN2	208	2.4	29.8508	1.1584	0.0515	0.0029	0.2380	0.0130	0.0335	0.0007	0.08	263	129	215	11	212	4	212	4	n/a
63	171214_030.FIN2	794	1.8	33.3445	1.2230	0.0502	0.0017	0.2080	0.0076	0.0300	0.0005	0.45	204	79	191	6	191	3	191	3	n/a
65	171214_032.FIN2	119	2.7	27.7008	1.1510	0.0519	0.0039	0.2560	0.0200	0.0361	0.0009	0.23	281	172	231	16	229	5	229	5	n/a
66	171214_033.FIN2	341	1.9	27.6091	1.1434	0.0515	0.0022	0.2530	0.0110	0.0362	0.0008	0.36	263	98	229	9	229	5	229	5	n/a
67	171214_034.FIN2	168	2.1	29.7619	1.4172	0.0508	0.0043	0.2410	0.0220	0.0336	0.0011	0.19	232	195	217	18	213	7	213	7	n/a
68	171214_035.FIN2	97	3.2	26.4550	1.2598	0.0537	0.0057	0.2760	0.0260	0.0378	0.0012	0.19	358	240	245	21	239	8	239	8	n/a
69	171214_036.FIN2	114	2.4	27.2554	1.1143	0.0520	0.0044	0.2650	0.0220	0.0367	0.0008	0.23	285	193	235	18	232	5	232	5	n/a
70	171214_037.FIN2	553	2.0	29.8418	1.3358	0.0496	0.0029	0.2360	0.0160	0.0335	0.0009	0.14	176	136	215	13	213	6	213	6	n/a
71	171214_038.FIN2	167	2.4	27.7778	1.2346	0.0518	0.0039	0.2580	0.0200	0.0360	0.0010	0.30	277	172	231	17	228	6	228	6	n/a
73	171214_046.FIN2	156	3.8	28.9519	1.2573	0.0520	0.0049	0.2490	0.0250	0.0345	0.0010	0.28	285	215	224	20	219	6	219	6	n/a
75	171214_048.FIN2	273	1.7	29.2740	1.1998	0.0515	0.0031	0.2440	0.0150	0.0342	0.0009	0.30	263	138	220	13	217	5	217	5	n/a
76	171214_049.FIN2	674	2.1	31.1236	1.2593	0.0501	0.0028	0.2240	0.0130	0.0321	0.0006	0.30	200	130	204	11	204	4	204	4	n/a
77	171214_050.FIN2	478	1.4	31.9387	1.2241	0.0498	0.0028	0.2170	0.0120	0.0313	0.0006	0.18	186	131	199	10	199	4	199	4	n/a
78	171214_051.FIN2	641	1.2	31.7360	1.2086	0.0508	0.0019	0.2186	0.0082	0.0315	0.0005	0.25	232	86	200	7	200	3	200	3	n/a

Grain	Spot name	isotopic ratios												isotopic ages									
		U	U/Th	$^{238}\text{U}/$		$^{207}\text{Pb}/$		^{207}Pb		^{206}Pb		rho*	^{207}Pb	\pm	^{207}Pb	\pm	^{206}Pb	\pm	Best	\pm			
				(ppm)	^{206}Pb	2SE	^{206}Pb	2SE	^{235}U	2SE	^{238}U	2SE		(Ma)	^{235}U	(Ma)	^{238}U	(Ma)	Age	(Ma)	conc.		
79	171214_052.FIN2	220	2.5	28.3046	1.1216	0.0516	0.0025	0.2510	0.0120	0.0353	0.0008	0.22	268	111	226	10	224	5	224	5	n/a		
81	171214_054.FIN2	1046	1.7	31.5060	1.2904	0.0509	0.0025	0.2220	0.0120	0.0317	0.0008	0.30	236	113	203	10	201	5	201	5	n/a		
82	171214_055.FIN2	398	2.3	28.7687	1.0759	0.0515	0.0018	0.2451	0.0082	0.0348	0.0005	0.19	263	80	222	7	220	3	220	3	n/a		
83	171214_056.FIN2	251	2.1	27.6167	1.0678	0.0518	0.0023	0.2590	0.0120	0.0362	0.0007	0.16	277	102	233	9	229	4	229	4	n/a		
84	171214_057.FIN2	375	2.5	26.9542	1.4531	0.0523	0.0034	0.2600	0.0170	0.0371	0.0016	0.38	299	148	234	14	235	10	235	10	n/a		
85	171214_064.FIN2	128	2.2	27.7547	1.0784	0.0522	0.0038	0.2580	0.0180	0.0360	0.0007	0.07	294	166	231	15	228	5	228	5	n/a		
86	171214_065.FIN2	280	2.3	27.5558	1.0631	0.0517	0.0023	0.2590	0.0110	0.0363	0.0006	0.06	272	102	232	9	230	4	230	4	n/a		
87	171214_066.FIN2	706	1.5	31.7662	1.1100	0.0504	0.0013	0.2203	0.0060	0.0315	0.0004	0.28	213	60	202	5	200	2	200	2	n/a		
88	171214_067.FIN2	760	2.0	30.9024	1.1459	0.0506	0.0014	0.2272	0.0068	0.0324	0.0004	0.33	223	64	208	6	205	3	205	3	n/a		
89	171214_068.FIN2	163	2.9	27.2480	1.0394	0.0521	0.0026	0.2640	0.0130	0.0367	0.0006	0.13	290	114	236	11	232	4	232	4	n/a		
90	171214_069.FIN2	198	1.7	28.2008	1.1134	0.0524	0.0038	0.2570	0.0190	0.0355	0.0008	0.19	303	165	230	15	225	5	225	5	n/a		
92	171214_071.FIN2	1008	1.2	29.7974	1.2430	0.0517	0.0019	0.2405	0.0098	0.0336	0.0008	0.51	272	84	219	8	213	5	213	5	n/a		
93	171214_072.FIN2	212	2.3	28.4091	1.4527	0.0523	0.0042	0.2560	0.0240	0.0352	0.0013	0.47	299	183	230	19	223	8	223	8	n/a		
94	171214_073.FIN2	327	2.3	28.1690	1.3489	0.0518	0.0031	0.2550	0.0170	0.0355	0.0013	0.30	277	137	230	14	225	8	225	8	n/a		
95	171214_074.FIN2	77	2.4	27.4725	1.1321	0.0538	0.0053	0.2650	0.0250	0.0364	0.0009	0.19	363	222	234	20	230	6	230	6	n/a		
96	171214_075.FIN2	87	4.0	26.9542	1.3804	0.0539	0.0061	0.2740	0.0290	0.0371	0.0014	0.04	367	255	243	23	235	9	235	9	n/a		
97	171214_082.FIN2	121	3.1	27.3224	1.4930	0.0526	0.0052	0.2660	0.0270	0.0366	0.0016	0.31	312	225	237	21	232	10	232	10	n/a		
98	171214_083.FIN2	239	2.3	28.0269	1.0212	0.0515	0.0022	0.2530	0.0100	0.0357	0.0005	0.10	263	98	229	9	226	3	226	3	n/a		
99	171214_084.FIN2	155	2.9	29.2654	1.1134	0.0518	0.0034	0.2440	0.0170	0.0342	0.0007	0.24	277	150	219	13	217	4	217	4	n/a		
100	171214_085.FIN2	377	2.1	27.4499	1.0549	0.0517	0.0038	0.2620	0.0190	0.0364	0.0007	0.05	272	168	235	15	231	5	231	5	n/a		
101	171214_086.FIN2	443	1.5	31.0366	1.1559	0.0506	0.0016	0.2243	0.0070	0.0322	0.0004	0.23	223	73	205	6	204	3	204	3	n/a		
102	171214_087.FIN2	149	2.2	26.4760	1.0515	0.0524	0.0029	0.2740	0.0150	0.0378	0.0008	0.24	303	126	244	12	239	5	239	5	n/a		
103	171214_088.FIN2	219	1.9	27.3973	1.2010	0.0516	0.0030	0.2570	0.0160	0.0365	0.0009	0.38	268	133	233	13	231	6	231	6	n/a		
104	171214_089.FIN2	261	2.3	27.2331	1.1125	0.0525	0.0041	0.2670	0.0210	0.0367	0.0009	0.09	307	178	238	16	232	6	232	6	n/a		

Grain	Spot name	isotopic ratios										isotopic ages									
		U	U/Th	$^{238}\text{U}/$		$^{207}\text{Pb}/$		^{207}Pb		^{206}Pb				^{207}Pb	\pm	^{207}Pb	\pm	^{206}Pb	\pm	Best	\pm
		(ppm)		^{206}Pb	2SE	^{206}Pb	2SE	^{235}U	2SE	^{238}U	2SE	rho*	^{206}Pb	(Ma)	^{235}U	(Ma)	^{238}U	(Ma)	Age	(Ma)	conc.
105	171214_090.FIN2	150	2.6	28.7274	1.2379	0.0526	0.0042	0.2510	0.0190	0.0348	0.0010	0.14	312	182	225	16	221	6	221	6	n/a
106	171214_091.FIN2	104	3.2	27.3598	1.1228	0.0522	0.0039	0.2650	0.0210	0.0366	0.0009	0.33	294	171	235	17	231	5	231	5	n/a
107	171214_092.FIN2	757	2.5	31.2110	1.2664	0.0511	0.0031	0.2270	0.0140	0.0320	0.0006	0.20	245	140	207	11	203	4	203	4	n/a
109	171214_100.FIN2	184	2.2	27.8862	1.0887	0.0510	0.0027	0.2530	0.0130	0.0359	0.0006	0.04	241	122	228	11	227	4	227	4	n/a
112	171214_103.FIN2	720	2.4	28.0662	1.1816	0.0580	0.0024	0.2860	0.0120	0.0356	0.0009	0.35	530	91	255	9	226	6	226	6	n/a
113	171214_104.FIN2	750	1.1	33.0033	1.6338	0.0512	0.0041	0.2120	0.0150	0.0303	0.0010	0.19	250	184	195	13	192	7	192	7	n/a
114	171214_105.FIN2	268	3.2	28.6533	1.3136	0.0521	0.0037	0.2530	0.0180	0.0349	0.0010	0.25	290	162	228	15	221	6	221	6	n/a
116	171214_107.FIN2	269	2.5	26.7380	1.4298	0.0525	0.0042	0.2670	0.0260	0.0374	0.0015	0.49	307	182	238	20	236	10	236	10	n/a
117	171214_108.FIN2	531	1.4	28.7853	1.1600	0.0518	0.0028	0.2500	0.0140	0.0347	0.0008	0.32	277	124	226	11	220	5	220	5	n/a
118	171214_109.FIN2	240	2.5	26.9324	1.0880	0.0525	0.0026	0.2650	0.0120	0.0371	0.0008	0.14	307	113	240	10	235	5	235	5	n/a
119	171214_110.FIN2	232	2.5	28.7109	1.0716	0.0524	0.0022	0.2510	0.0110	0.0348	0.0005	0.22	303	96	226	9	221	3	221	3	n/a
Rejected Analysis																					
2	171213_155.FIN2	1401	1.5	35.7782	0.9089	0.0558	0.0024	0.2154	0.0093	0.0280	0.0005	0.21	444	96	198	8	178	3	178	3	n/a
6	171213_159.FIN2	118	2.8	26.8384	0.8644	0.1152	0.0088	0.5930	0.0430	0.0373	0.0010	0.11	1883	138	468	28	236	6	236	6	n/a
8	171213_161.FIN2	551	2.2	29.9491	0.8342	0.0615	0.0031	0.2840	0.0140	0.0334	0.0007	0.27	657	108	253	11	212	4	212	4	n/a
25	171213_190.FIN2	325	2.1	28.3447	0.7874	0.0509	0.0026	0.2490	0.0130	0.0353	0.0007	0.12	236	118	225	10	224	4	224	4	n/a
30	171213_195.FIN2	331	2.1	27.7701	0.7712	0.0508	0.0025	0.2530	0.0120	0.0360	0.0008	0.17	232	114	228	9	228	5	228	5	n/a
45	171213_216.FIN2	696	1.8	29.8152	0.9778	0.0513	0.0033	0.2350	0.0160	0.0335	0.0009	0.31	254	148	214	13	213	6	213	6	n/a
52	171214_013.FIN2	2316	1.0	35.0754	1.4763	0.0700	0.0021	0.2724	0.0098	0.0285	0.0006	0.55	928	62	244	8	181	4	181	4	n/a
58	171214_019.FIN2	690	1.4	28.9436	1.1728	0.1287	0.0051	0.6120	0.0270	0.0346	0.0007	0.45	2080	70	483	17	219	4	219	4	n/a
61	171214_028.FIN2	541	2.3	29.4204	1.2983	0.0522	0.0025	0.2370	0.0120	0.0340	0.0010	0.45	294	109	216	10	215	6	215	6	n/a
64	171214_031.FIN2	114	3.2	27.4952	1.1340	0.0555	0.0034	0.2860	0.0190	0.0364	0.0008	0.33	432	136	251	15	230	5	230	5	n/a
72	171214_039.FIN2	496	2.9	27.6702	1.1485	0.0507	0.0045	0.2540	0.0230	0.0361	0.0009	0.12	227	205	229	18	229	6	229	6	n/a
74	171214_047.FIN2	967	1.2	32.4359	1.3677	0.0503	0.0018	0.2110	0.0068	0.0308	0.0007	0.26	209	83	194	6	196	4	196	4	n/a

Grain	Spot name	isotopic ratios										isotopic ages									
		U	U/Th	$^{238}\text{U}/$		$^{207}\text{Pb}/$		^{207}Pb		^{206}Pb				^{207}Pb	\pm	^{207}Pb	\pm	^{206}Pb	\pm	Best	\pm
		(ppm)		^{206}Pb	2SE	^{206}Pb	2SE	^{235}U	2SE	^{238}U	2SE	rho*	^{206}Pb	(Ma)	^{235}U	(Ma)	^{238}U	(Ma)	Age	(Ma)	conc.
80	171214_053.FIN2	725	1.5	31.4268	1.2839	0.0590	0.0028	0.2610	0.0130	0.0318	0.0008	0.37	567	103	235	11	202	5	202	5	n/a
91	171214_070.FIN2	926	1.4	30.2024	1.1858	0.0725	0.0027	0.3290	0.0140	0.0331	0.0006	0.29	1000	76	288	11	210	4	210	4	n/a
108	171214_093.FIN2	338	2.3	26.0417	1.2207	0.1062	0.0058	0.5560	0.0310	0.0384	0.0012	0.29	1735	100	446	20	243	7	243	7	n/a
110	171214_101.FIN2	506	2.3	28.1770	1.1909	0.0553	0.0029	0.2680	0.0130	0.0355	0.0008	0.03	424	121	241	10	225	5	225	5	n/a
111	171214_102.FIN2	157	2.9	26.8097	1.4375	0.0512	0.0065	0.2710	0.0360	0.0373	0.0015	0.04	250	292	240	28	236	10	236	10	n/a
115	171214_106.FIN2	191	2.3	29.5771	1.3122	0.0595	0.0043	0.2780	0.0200	0.0338	0.0010	0.19	585	157	247	16	214	6	214	6	n/a
120	171214_111.FIN2	301	2.9	27.1739	1.4030	0.0513	0.0041	0.2600	0.0220	0.0368	0.0014	0.47	254	184	234	18	233	9	233	9	n/a

Grain	Spot name	isotopic ratios										isotopic ages							
		U	U/Th	$^{238}\text{U}/$	$^{207}\text{Pb}/$		^{207}Pb		^{206}Pb			^{207}Pb	\pm	^{207}Pb	\pm	^{206}Pb	\pm	Best	\pm
		(ppm)		^{206}Pb	2SE	^{206}Pb	2SE	^{235}U	2SE	^{238}U	2SE	rho*	^{206}Pb	(Ma)	^{235}U	(Ma)	^{238}U	(Ma)	Age

Whitehorse trough - Tanglefoot formation - Sample 16-LVD-004, Robert Campbell Highway (Zone 08V 436493E 6888370N NAD 83)

Grain	Spot name	isotopic ratios										isotopic ages									
		U	U/Th	$^{238}\text{U}/$	$^{207}\text{Pb}/$		^{207}Pb		^{206}Pb			^{207}Pb	\pm	^{207}Pb	\pm	^{206}Pb	\pm	Best	\pm		
		(ppm)		^{206}Pb	2SE	^{206}Pb	2SE	^{235}U	2SE	^{238}U	2SE	rho	^{206}Pb	(Ma)	^{235}U	(Ma)	^{238}U	(Ma)	Age	(Ma)	conc.
1	170321_015.FIN2	635	1.9	32.4675	1.2650	0.0502	0.0018	0.2123	0.0077	0.0308	0.0005	0.30	204	83	195	7	196	3	196	3	n/a
2	170321_016.FIN2	280	1.8	34.6260	1.4388	0.0504	0.0032	0.2030	0.0130	0.0289	0.0006	0.31	213	147	187	11	184	4	184	4	n/a
3	170321_017.FIN2	977	1.4	34.6741	1.3225	0.0500	0.0014	0.1982	0.0056	0.0288	0.0005	0.32	195	65	183	5	183	3	183	3	n/a
4	170321_018.FIN2	633	2.1	32.6797	1.2816	0.0502	0.0021	0.2100	0.0089	0.0306	0.0005	0.37	204	97	195	8	194	3	194	3	n/a
5	170321_019.FIN2	348	2.1	34.1181	1.5133	0.0502	0.0034	0.2030	0.0130	0.0293	0.0008	0.23	204	157	188	11	186	5	186	5	n/a
6	170321_020.FIN2	636	3.2	31.2110	1.2664	0.0506	0.0023	0.2250	0.0110	0.0320	0.0007	0.37	223	105	206	9	203	4	203	4	n/a
7	170321_021.FIN2	347	1.6	31.9489	1.2249	0.0505	0.0033	0.2170	0.0150	0.0313	0.0006	0.26	218	151	199	12	199	4	199	4	n/a
8	170321_022.FIN2	410	1.9	33.0579	1.5300	0.0504	0.0039	0.2100	0.0150	0.0303	0.0009	0.23	213	179	193	12	192	6	192	6	n/a
10	170321_024.FIN2	740	1.6	34.4709	1.3071	0.0503	0.0018	0.1995	0.0070	0.0290	0.0005	0.17	209	83	185	6	184	3	184	3	n/a
11	170321_032.FIN2	336	1.6	31.6656	1.3035	0.0506	0.0021	0.2202	0.0097	0.0316	0.0007	0.25	223	96	202	8	200	4	200	4	n/a
12	170321_033.FIN2	450	1.4	30.8547	1.2376	0.0504	0.0017	0.2257	0.0077	0.0324	0.0006	0.25	213	78	207	6	206	4	206	4	n/a
13	170321_034.FIN2	215	1.7	32.8299	1.4011	0.0504	0.0030	0.2110	0.0120	0.0305	0.0008	0.19	213	138	194	10	193	5	193	5	n/a
14	170321_035.FIN2	135	2.0	31.2305	1.1704	0.0513	0.0025	0.2230	0.0100	0.0320	0.0005	0.04	254	112	204	9	203	3	203	3	n/a
16	170321_037.FIN2	426	1.9	31.7259	1.2078	0.0507	0.0026	0.2180	0.0120	0.0315	0.0006	0.34	227	119	200	10	200	3	200	3	n/a
17	170321_038.FIN2	507	2.4	31.3480	1.6706	0.0512	0.0025	0.2240	0.0130	0.0319	0.0012	0.56	250	112	205	11	202	8	202	8	n/a
18	170321_039.FIN2	408	1.7	33.9789	1.3855	0.0502	0.0021	0.2030	0.0100	0.0294	0.0006	0.57	204	97	187	9	187	3	187	3	n/a
19	170321_040.FIN2	259	1.9	33.4448	1.7897	0.0514	0.0054	0.2070	0.0210	0.0299	0.0011	0.02	259	241	190	17	190	7	190	7	n/a
20	170321_041.FIN2	387	1.6	33.0469	1.5289	0.0509	0.0033	0.2090	0.0140	0.0303	0.0010	0.34	236	150	192	12	192	6	192	6	n/a

Grain	Spot name	isotopic ratios										isotopic ages									
		U (ppm)	U/Th	$^{238}\text{U}/$		$^{207}\text{Pb}/$		^{207}Pb		^{206}Pb		rho*	^{206}Pb (Ma)	^{207}Pb (Ma)	^{207}Pb (Ma)	^{206}Pb (Ma)	^{238}U (Ma)	Age (Ma)	Best (Ma)	\pm	
				^{206}Pb	2SE	^{206}Pb	2SE	^{235}U	2SE	^{238}U	2SE										
21	170321_048.FIN2	218	1.5	13.7363	0.5849	0.0578	0.0042	0.5720	0.0430	0.0728	0.0017	0.34	522	159	458	28	453	10	453	10	n/a
22	170321_049.FIN2	251	3.2	30.0752	1.1759	0.0513	0.0025	0.2320	0.0110	0.0333	0.0006	0.23	254	112	211	9	211	3	211	3	n/a
24	170321_051.FIN2	418	1.7	34.3053	1.4122	0.0507	0.0019	0.2004	0.0074	0.0292	0.0007	0.30	227	87	185	6	185	4	185	4	n/a
25	170321_052.FIN2	360	1.6	34.8068	1.4538	0.0502	0.0030	0.1970	0.0110	0.0287	0.0007	0.05	204	139	182	9	183	5	183	5	n/a
26	170321_053.FIN2	388	2.0	33.8983	1.3789	0.0501	0.0021	0.2032	0.0090	0.0295	0.0006	0.27	200	97	188	8	187	4	187	4	n/a
27	170321_054.FIN2	92	1.3	31.0752	1.3519	0.0507	0.0046	0.2250	0.0210	0.0322	0.0009	0.31	227	210	204	18	204	5	204	5	n/a
28	170321_055.FIN2	521	1.9	34.6861	1.4438	0.0507	0.0029	0.2000	0.0110	0.0288	0.0006	0.03	227	132	185	9	183	4	183	4	n/a
29	170321_056.FIN2	162	1.8	18.8324	0.7802	0.0534	0.0022	0.3920	0.0170	0.0531	0.0011	0.35	346	93	335	13	334	7	334	7	n/a
30	170321_057.FIN2	91	9.8	29.9401	1.7032	0.0512	0.0059	0.2340	0.0280	0.0334	0.0015	0.25	250	265	212	23	212	9	212	9	n/a
31	170321_064.FIN2	769	2.3	18.4570	0.6813	0.0539	0.0013	0.4020	0.0110	0.0542	0.0007	0.39	367	54	342	8	340	4	340	4	n/a
32	170321_065.FIN2	307	1.8	33.3890	1.2263	0.0505	0.0019	0.2094	0.0083	0.0300	0.0004	0.44	218	87	193	7	190	3	190	3	n/a
33	170321_066.FIN2	123	1.7	34.0368	1.2744	0.0506	0.0022	0.2053	0.0087	0.0294	0.0004	0.09	223	101	188	7	187	2	187	2	n/a
34	170321_067.FIN2	679	1.6	35.1000	1.3552	0.0503	0.0015	0.1970	0.0062	0.0285	0.0005	0.40	209	69	182	5	181	3	181	3	n/a
35	170321_068.FIN2	361	1.7	17.6991	0.7831	0.0542	0.0031	0.4260	0.0280	0.0565	0.0014	0.58	379	129	360	20	354	9	354	9	n/a
36	170321_069.FIN2	856	1.5	33.4336	1.3414	0.0505	0.0019	0.2073	0.0078	0.0299	0.0006	0.35	218	87	191	7	190	4	190	4	n/a
37	170321_070.FIN2	597	1.5	33.7610	1.3678	0.0502	0.0022	0.2047	0.0086	0.0296	0.0005	0.13	204	102	189	7	188	3	188	3	n/a
38	170321_071.FIN2	872	1.4	35.6379	1.5241	0.0499	0.0023	0.1926	0.0091	0.0281	0.0007	0.27	190	107	179	8	178	4	178	4	n/a
39	170321_072.FIN2	941	1.5	33.4784	1.4570	0.0509	0.0031	0.2090	0.0130	0.0299	0.0007	0.29	236	141	192	11	190	4	190	4	n/a
40	170321_073.FIN2	339	1.7	34.3171	1.2954	0.0503	0.0015	0.2026	0.0059	0.0291	0.0004	0.17	209	69	187	5	185	2	185	2	n/a
41	170321_080.FIN2	761	1.8	34.6741	1.3225	0.0502	0.0012	0.1985	0.0048	0.0288	0.0003	0.25	204	55	184	4	183	2	183	2	n/a
42	170321_081.FIN2	352	2.5	32.0821	1.2351	0.0504	0.0026	0.2160	0.0110	0.0312	0.0006	0.18	213	120	198	9	198	4	198	4	n/a
43	170321_082.FIN2	878	1.6	34.9162	1.3411	0.0502	0.0015	0.1967	0.0063	0.0286	0.0004	0.40	204	69	182	5	182	2	182	2	n/a
44	170321_083.FIN2	361	2.6	34.0020	1.3874	0.0502	0.0024	0.2041	0.0098	0.0294	0.0005	0.16	204	111	188	8	187	3	187	3	n/a
45	170321_084.FIN2	236	1.4	34.5662	1.5533	0.0502	0.0035	0.2000	0.0140	0.0289	0.0008	0.08	204	162	185	12	184	5	184	5	n/a

Grain	Spot name	isotopic ratios												isotopic ages									
		U (ppm)	U/Th	$^{238}\text{U}/$		$^{207}\text{Pb}/$		^{207}Pb		^{206}Pb			rho*	^{207}Pb (Ma)	\pm	^{207}Pb (Ma)	\pm	^{206}Pb (Ma)	\pm	Best (Ma)	\pm		
				^{206}Pb	2SE	^{206}Pb	2SE	^{235}U	2SE	^{238}U	2SE	^{206}Pb											
47	170321_086.FIN2	445	1.9	33.8868	1.3780	0.0507	0.0020	0.2049	0.0081	0.0295	0.0005	0.23	227	91	189	7	188	3	188	3	n/a		
48	170321_087.FIN2	407	2.0	34.1414	1.3988	0.0505	0.0027	0.2030	0.0110	0.0293	0.0007	0.31	218	124	188	9	186	4	186	4	n/a		
49	170321_088.FIN2	651	1.6	35.0508	1.3514	0.0501	0.0015	0.1958	0.0053	0.0285	0.0004	0.07	200	70	181	5	181	3	181	3	n/a		
51	170321_096.FIN2	416	2.5	32.1234	1.3415	0.0508	0.0026	0.2150	0.0110	0.0311	0.0006	0.17	232	118	198	9	198	4	198	4	n/a		
52	170321_097.FIN2	294	1.5	31.5856	1.2969	0.0508	0.0025	0.2210	0.0110	0.0317	0.0006	0.10	232	114	202	9	201	4	201	4	n/a		
53	170321_098.FIN2	214	2.1	33.9559	1.2683	0.0506	0.0020	0.2033	0.0080	0.0295	0.0004	0.24	223	91	187	7	187	2	187	2	n/a		
54	170321_099.FIN2	413	1.3	19.0114	0.8674	0.0540	0.0028	0.3880	0.0220	0.0526	0.0015	0.45	371	117	332	16	331	9	331	9	n/a		
55	170321_100.FIN2	403	3.2	31.8269	1.2155	0.0505	0.0019	0.2195	0.0085	0.0314	0.0005	0.28	218	87	201	7	199	3	199	3	n/a		
57	170321_102.FIN2	417	4.8	33.9905	1.5020	0.0507	0.0034	0.2040	0.0130	0.0294	0.0008	0.23	227	155	188	11	187	5	187	5	n/a		
58	170321_103.FIN2	457	1.6	35.0877	1.7236	0.0496	0.0045	0.1960	0.0170	0.0285	0.0010	0.23	176	212	181	14	181	6	181	6	n/a		
59	170321_104.FIN2	367	2.1	18.7617	0.7744	0.0538	0.0024	0.4030	0.0190	0.0533	0.0011	0.06	363	101	343	14	335	7	335	7	n/a		
60	170321_112.FIN2	371	1.5	35.5492	1.5165	0.0500	0.0038	0.1970	0.0130	0.0281	0.0007	0.23	195	177	182	11	179	4	179	4	n/a		
61	170321_113.FIN2	431	2.0	35.5872	1.3931	0.0493	0.0018	0.1965	0.0070	0.0281	0.0003	0.16	162	85	182	6	179	2	179	2	n/a		
62	170321_114.FIN2	817	2.2	17.3400	0.6615	0.0539	0.0017	0.4380	0.0140	0.0577	0.0009	0.29	367	71	368	10	361	6	361	6	n/a		
63	170321_115.FIN2	517	1.9	32.6797	1.3884	0.0504	0.0032	0.2190	0.0150	0.0306	0.0006	0.27	213	147	200	13	194	4	194	4	n/a		
64	170321_116.FIN2	566	1.6	34.7464	1.4488	0.0487	0.0027	0.2010	0.0130	0.0288	0.0006	0.26	133	130	186	11	183	4	183	4	n/a		
65	170321_117.FIN2	398	2.1	34.9773	1.3458	0.0497	0.0033	0.2030	0.0130	0.0286	0.0005	0.10	181	155	187	11	182	3	182	3	n/a		
66	170321_118.FIN2	590	1.8	35.5240	1.3881	0.0489	0.0022	0.1937	0.0085	0.0282	0.0005	0.14	143	106	179	7	179	3	179	3	n/a		
67	170321_119.FIN2	885	1.4	35.2237	1.6129	0.0491	0.0020	0.1970	0.0100	0.0284	0.0009	0.56	153	95	182	9	181	6	181	6	n/a		
68	170321_120.FIN2	637	2.1	35.1000	1.3552	0.0497	0.0019	0.2019	0.0081	0.0285	0.0004	0.34	181	89	186	7	181	3	181	3	n/a		
69	170321_121.FIN2	890	2.4	18.6916	0.7686	0.0538	0.0028	0.4060	0.0220	0.0535	0.0012	0.34	363	117	346	16	336	7	336	7	n/a		
70	170321_128.FIN2	289	1.6	35.1865	1.3619	0.0494	0.0020	0.1974	0.0082	0.0284	0.0004	0.10	167	95	182	7	181	2	181	2	n/a		
71	170321_129.FIN2	388	2.7	34.4590	1.4249	0.0503	0.0045	0.2040	0.0180	0.0290	0.0007	0.19	209	207	188	16	184	4	184	4	n/a		
72	170321_130.FIN2	315	2.0	33.4448	1.4541	0.0504	0.0039	0.2100	0.0170	0.0299	0.0007	0.19	213	179	192	14	190	4	190	4	n/a		

Grain	Spot name	isotopic ratios										isotopic ages									
		U	U/Th	$^{238}\text{U}/$		$^{207}\text{Pb}/$		^{207}Pb		^{206}Pb		rho*	^{207}Pb	\pm	^{207}Pb	\pm	^{206}Pb	\pm	Best	\pm	
				(ppm)	^{206}Pb	2SE	^{206}Pb	2SE	^{235}U	2SE	^{238}U	2SE									
73	170321_131.FIN2	272	1.8	36.1795	1.4398	0.0504	0.0022	0.1946	0.0084	0.0276	0.0004	0.10	213	101	180	7	176	3	176	3	n/a
74	170321_132.FIN2	347	2.9	34.2349	1.4064	0.0501	0.0018	0.2042	0.0070	0.0292	0.0005	0.17	200	83	188	6	186	3	186	3	n/a
75	170321_133.FIN2	620	1.8	36.2188	1.3118	0.0495	0.0015	0.1896	0.0061	0.0276	0.0004	0.13	172	71	176	5	176	2	176	2	n/a
76	170321_134.FIN2	261	2.5	35.0140	1.3486	0.0503	0.0035	0.1970	0.0140	0.0286	0.0005	0.04	209	161	182	12	182	3	182	3	n/a
77	170321_135.FIN2	283	1.5	34.4709	1.6635	0.0533	0.0073	0.2140	0.0270	0.0290	0.0009	0.23	342	310	196	22	184	6	184	6	n/a
78	170321_136.FIN2	378	3.0	32.9056	1.2993	0.0503	0.0022	0.2109	0.0094	0.0304	0.0005	0.30	209	101	194	8	193	3	193	3	n/a
79	170321_137.FIN2	551	1.7	33.5571	1.3513	0.0524	0.0027	0.2120	0.0100	0.0298	0.0005	0.13	303	117	195	9	189	3	189	3	n/a
80	170321_144.FIN2	802	2.6	32.0513	1.3355	0.0508	0.0032	0.2160	0.0140	0.0312	0.0007	0.08	232	145	198	12	198	4	198	4	n/a
81	170321_145.FIN2	579	2.2	35.2485	1.3667	0.0510	0.0017	0.1951	0.0069	0.0284	0.0004	0.08	241	77	181	6	180	2	180	2	n/a
83	170321_147.FIN2	475	1.9	34.9773	1.4681	0.0508	0.0043	0.1970	0.0190	0.0286	0.0007	0.45	232	195	182	16	182	5	182	5	n/a
84	170321_148.FIN2	604	3.0	32.6264	1.2774	0.0506	0.0024	0.2103	0.0097	0.0307	0.0004	0.04	223	110	193	8	195	3	195	3	n/a
85	170321_149.FIN2	650	3.3	33.2890	1.3298	0.0511	0.0029	0.2080	0.0120	0.0300	0.0005	0.15	245	131	191	10	191	3	191	3	n/a
86	170321_150.FIN2	989	3.0	30.8642	1.7147	0.0503	0.0035	0.2190	0.0140	0.0324	0.0014	0.28	209	161	201	12	206	9	206	9	n/a
88	170321_152.FIN2	181	2.2	34.6500	1.5608	0.0510	0.0045	0.2000	0.0180	0.0289	0.0008	0.16	241	203	184	15	183	5	183	5	n/a
90	170321_160.FIN2	465	4.0	31.8269	1.3168	0.0508	0.0029	0.2180	0.0130	0.0314	0.0007	0.26	232	132	199	10	199	5	199	5	n/a
91	170321_161.FIN2	232	2.1	31.9591	1.3278	0.0513	0.0041	0.2160	0.0170	0.0313	0.0007	0.17	254	184	198	14	199	4	199	4	n/a
92	170321_162.FIN2	287	1.7	32.0924	1.2359	0.0505	0.0026	0.2170	0.0120	0.0312	0.0006	0.18	218	119	199	10	198	4	198	4	n/a
93	170321_163.FIN2	216	3.1	31.1818	1.4585	0.0508	0.0048	0.2240	0.0210	0.0321	0.0010	0.12	232	218	204	17	204	6	204	6	n/a
94	170321_164.FIN2	451	2.0	33.1455	1.2085	0.0506	0.0014	0.2084	0.0058	0.0302	0.0003	0.21	223	64	192	5	192	2	192	2	n/a
95	170321_165.FIN2	622	1.2	34.2114	1.5215	0.0499	0.0042	0.2020	0.0170	0.0292	0.0007	0.27	190	196	186	14	186	5	186	5	n/a
96	170321_166.FIN2	519	1.5	34.5304	1.4308	0.0505	0.0027	0.2000	0.0110	0.0290	0.0005	0.23	218	124	185	9	184	3	184	3	n/a
99	170321_169.FIN2	491	2.2	32.9056	1.2993	0.0501	0.0022	0.2070	0.0090	0.0304	0.0005	0.24	200	102	194	9	193	3	193	3	n/a
100	170324_039.FIN2	233	1.8	33.4336	1.2296	0.0509	0.0026	0.2090	0.0110	0.0299	0.0006	0.29	236	118	192	9	190	4	190	4	n/a
101	170324_040.FIN2	338	3.0	31.0656	1.0616	0.0506	0.0013	0.2254	0.0065	0.0322	0.0005	0.38	223	59	207	5	204	3	204	3	n/a

Grain	Spot name	isotopic ratios										isotopic ages									
		U	U/Th	$^{238}\text{U}/$	$^{207}\text{Pb}/$		^{207}Pb		^{206}Pb			^{207}Pb	\pm	^{207}Pb	\pm	^{206}Pb	\pm	Best	\pm		
		(ppm)		^{206}Pb	2SE	^{206}Pb	2SE	^{235}U	2SE	^{238}U	2SE	rho*	^{206}Pb	(Ma)	^{235}U	(Ma)	^{238}U	(Ma)	Age	(Ma)	conc.
102	170324_041.FIN2	426	1.5	32.1854	1.1395	0.0509	0.0011	0.2168	0.0052	0.0311	0.0005	0.45	236	50	199	4	197	3	197	3	n/a
103	170324_042.FIN2	335	1.3	32.8299	1.0778	0.0499	0.0015	0.2105	0.0067	0.0305	0.0004	0.25	190	70	194	6	193	3	193	3	n/a
104	170324_043.FIN2	316	2.4	30.9789	1.1516	0.0509	0.0017	0.2244	0.0073	0.0323	0.0007	0.31	236	77	205	6	205	5	205	5	n/a
105	170324_044.FIN2	509	2.9	30.4878	1.1154	0.0512	0.0012	0.2300	0.0062	0.0328	0.0006	0.49	250	54	210	5	208	4	208	4	n/a
106	170324_045.FIN2	386	1.7	31.8269	1.0129	0.0506	0.0011	0.2193	0.0055	0.0314	0.0004	0.43	223	50	201	5	199	2	199	2	n/a
107	170324_046.FIN2	451	2.9	31.2891	0.9790	0.0507	0.0010	0.2214	0.0045	0.0320	0.0003	0.38	227	46	203	4	203	2	203	2	n/a
108	170324_047.FIN2	333	1.7	32.3520	1.0467	0.0503	0.0012	0.2132	0.0052	0.0309	0.0004	0.41	209	55	196	5	196	3	196	3	n/a
109	170324_048.FIN2	57	1.2	33.3445	1.1119	0.0513	0.0030	0.2130	0.0120	0.0300	0.0005	0.02	254	134	194	10	191	3	191	3	n/a
Rejected Analysis																					
9	170321_023.FIN2	522	1.1	34.4471	1.4239	0.0858	0.0056	0.3450	0.0240	0.0290	0.0006	0.27	1334	126	299	18	184	4	184	4	n/a
15	170321_036.FIN2	422	1.4	33.6474	1.3586	0.0559	0.0022	0.2270	0.0084	0.0297	0.0006	0.20	448	87	207	7	189	4	189	4	n/a
23	170321_050.FIN2	862	4.5	35.3732	1.5015	0.0508	0.0015	0.1951	0.0076	0.0283	0.0006	0.59	232	68	181	7	180	4	180	4	n/a
46	170321_085.FIN2	54	0.9	73.5294	5.9472	0.0720	0.0140	0.1220	0.0180	0.0136	0.0010	0.23	986	396	125	24	87	6	87	6	n/a
50	170321_089.FIN2	2132	2.1	6.8213	0.3304	0.1090	0.0019	2.2040	0.0920	0.1466	0.0049	0.91	1783	32	1180	29	881	27	1783	32	49
56	170321_101.FIN2	1429	3.5	22.6757	1.1312	0.0541	0.0019	0.3250	0.0140	0.0441	0.0015	0.61	375	79	286	11	278	9	278	9	n/a
82	170321_146.FIN2	816	1.6	34.6741	1.3225	0.0605	0.0032	0.2340	0.0130	0.0288	0.0005	0.21	622	114	213	10	183	3	183	3	n/a
87	170321_151.FIN2	1047	2.5	30.4136	1.2950	0.0683	0.0032	0.2980	0.0130	0.0329	0.0008	0.31	878	97	265	10	209	5	209	5	n/a
89	170321_153.FIN2	875	4.3	34.3407	1.6510	0.0517	0.0042	0.2010	0.0160	0.0291	0.0009	0.10	272	186	186	13	185	6	185	6	n/a
97	170321_167.FIN2	522	2.2	33.6022	1.4678	0.0657	0.0045	0.2680	0.0180	0.0298	0.0008	0.16	797	144	240	15	189	5	189	5	n/a
98	170321_168.FIN2	670	1.6	34.4234	1.4220	0.0614	0.0031	0.2400	0.0120	0.0291	0.0006	0.46	653	108	218	10	185	4	185	4	n/a

Grain	Spot name	isotopic ratios										isotopic ages									
		U (ppm)	U/Th	$^{238}\text{U}/^{206}\text{Pb}$	2SE	$^{207}\text{Pb}/^{206}\text{Pb}$	2SE	^{207}Pb ^{235}U	2SE	^{206}Pb ^{238}U	2SE	rho*	^{207}Pb ^{206}Pb	\pm (Ma)	^{207}Pb ^{235}U	\pm (Ma)	^{206}Pb ^{238}U	\pm (Ma)	Best	\pm	

Whitehorse trough - Tanglefoot formation - Sample 17-LVD-018, Conglomerate Mountain (Zone 08V 453930E 6833117N NAD 83)

Grain	Spot name	isotopic ratios										isotopic ages									
		U (ppm)	U/Th	$^{238}\text{U}/^{206}\text{Pb}$	2SE	$^{207}\text{Pb}/^{206}\text{Pb}$	2SE	^{207}Pb ^{235}U	2SE	^{206}Pb ^{238}U	2SE	rho	^{207}Pb ^{206}Pb	\pm (Ma)	^{207}Pb ^{235}U	\pm (Ma)	^{206}Pb ^{238}U	\pm (Ma)	Age	(Ma)	conc.
2	171212b_146.FIN2	572	1.4	31.0559	0.9645	0.0517	0.0035	0.2270	0.0160	0.0322	0.0008	0.27	272	155	207	13	204	5	204	5	n/a
3	171212b_147.FIN2	430	2.9	33.1126	1.4254	0.0506	0.0034	0.2060	0.0130	0.0302	0.0012	0.14	223	155	190	11	192	7	192	7	n/a
4	171212b_148.FIN2	529	1.6	30.0842	0.8508	0.0509	0.0028	0.2300	0.0140	0.0332	0.0007	0.41	236	127	209	12	211	4	211	4	n/a
5	171212b_155.FIN2	979	1.5	19.8728	0.4739	0.0538	0.0013	0.3676	0.0091	0.0503	0.0008	0.05	363	54	318	7	317	5	317	5	n/a
6	171212b_156.FIN2	368	2.1	28.8517	0.9157	0.0517	0.0037	0.2430	0.0170	0.0347	0.0008	0.12	272	164	220	14	220	5	220	5	n/a
7	171212b_157.FIN2	278	2.2	19.3349	0.5234	0.0537	0.0024	0.3750	0.0160	0.0517	0.0010	0.19	358	101	322	12	325	6	325	6	n/a
8	171212b_158.FIN2	1455	1.2	17.7305	0.4716	0.0551	0.0016	0.4190	0.0130	0.0564	0.0011	0.35	416	65	355	9	354	7	354	7	n/a
9	171212b_159.FIN2	692	1.8	20.5381	0.5484	0.0547	0.0023	0.3620	0.0150	0.0487	0.0009	0.08	400	94	313	11	306	6	306	6	n/a
12	171212b_162.FIN2	341	1.6	21.9780	0.5796	0.0529	0.0024	0.3300	0.0140	0.0455	0.0008	0.09	325	103	289	11	287	5	287	5	n/a
13	171212b_163.FIN2	594	2.9	31.1333	0.7367	0.0514	0.0018	0.2237	0.0082	0.0321	0.0005	0.30	259	80	204	7	204	3	204	3	n/a
14	171212b_164.FIN2	546	2.6	35.2734	1.0203	0.0512	0.0031	0.1920	0.0110	0.0284	0.0006	0.15	250	139	180	10	180	4	180	4	n/a
15	171212b_165.FIN2	268	1.7	31.1430	1.0669	0.0524	0.0042	0.2270	0.0180	0.0321	0.0009	0.08	303	183	207	15	204	6	204	6	n/a
16	171212b_166.FIN2	339	2.1	29.7265	0.7069	0.0519	0.0021	0.2353	0.0099	0.0336	0.0005	0.21	281	93	213	8	213	3	213	3	n/a
17	171213_010.FIN2	401	2.3	30.6091	0.7214	0.0510	0.0018	0.2274	0.0077	0.0327	0.0004	0.18	241	81	208	6	207	3	207	3	n/a
18	171213_011.FIN2	1490	1.6	19.2271	0.4806	0.0534	0.0017	0.3780	0.0140	0.0520	0.0009	0.45	346	72	326	10	327	5	327	5	n/a
19	171213_012.FIN2	1276	1.8	19.1939	0.5158	0.0549	0.0015	0.3840	0.0120	0.0521	0.0010	0.35	408	61	329	9	327	6	327	6	n/a
20	171213_013.FIN2	587	2.6	30.9981	0.8264	0.0509	0.0022	0.2243	0.0084	0.0323	0.0006	0.19	236	100	205	7	205	4	205	4	n/a
21	171213_014.FIN2	647	1.5	20.2429	0.5737	0.0536	0.0025	0.3620	0.0180	0.0494	0.0011	0.42	354	105	313	13	311	6	311	6	n/a

Grain	Spot name	isotopic ratios								isotopic ages												
		U	U/Th	$^{238}\text{U}/$	$^{206}\text{Pb}/$	$^{207}\text{Pb}/$	^{235}U	^{206}Pb	^{207}Pb	^{238}U	^{206}Pb	\pm	^{207}Pb	\pm	^{206}Pb	\pm	Best	\pm				
		(ppm)		^{206}Pb	2SE	^{206}Pb	2SE	^{235}U	2SE	^{238}U	2SE	ρho^*	^{206}Pb	(Ma)	^{235}U	(Ma)	^{238}U	(Ma)	Age	(Ma)		conc.
22	171213_015.FIN2	1460	2.1	30.9693	0.7289	0.0506	0.0011	0.2235	0.0052	0.0323	0.0004	0.37	223	50	205	4	205	3	205	3	n/a	
24	171213_017.FIN2	932	1.9	19.1388	0.4762	0.0535	0.0014	0.3840	0.0110	0.0523	0.0007	0.44	350	59	329	8	328	5	328	5	n/a	
25	171213_018.FIN2	811	2.8	30.0391	0.7038	0.0506	0.0017	0.2317	0.0076	0.0333	0.0004	0.15	223	78	211	6	211	3	211	3	n/a	
27	171213_020.FIN2	1560	1.7	34.1647	1.2839	0.0511	0.0029	0.2040	0.0130	0.0293	0.0009	0.36	245	131	188	11	186	6	186	6	n/a	
28	171213_021.FIN2	456	2.5	29.1630	0.8165	0.0510	0.0035	0.2400	0.0180	0.0343	0.0007	0.35	241	158	218	14	217	4	217	4	n/a	
29	171213_028.FIN2	458	3.9	30.2115	1.1866	0.0519	0.0046	0.2340	0.0220	0.0331	0.0011	0.36	281	203	213	19	210	7	210	7	n/a	
30	171213_029.FIN2	477	3.1	30.2298	0.7859	0.0511	0.0022	0.2315	0.0099	0.0331	0.0006	0.21	245	99	211	8	210	4	210	4	n/a	
31	171213_030.FIN2	627	1.9	19.0803	0.4733	0.0535	0.0013	0.3853	0.0097	0.0524	0.0007	0.30	350	55	331	7	329	4	329	4	n/a	
32	171213_031.FIN2	361	3.2	28.6615	0.7968	0.0514	0.0027	0.2450	0.0130	0.0349	0.0007	0.17	259	121	222	11	221	4	221	4	n/a	
33	171213_032.FIN2	2006	1.7	31.0752	0.6760	0.0506	0.0009	0.2240	0.0038	0.0322	0.0003	0.27	224	39	205	3	204	2	204	2	n/a	
34	171213_033.FIN2	800	2.9	30.5998	0.7303	0.0507	0.0017	0.2289	0.0085	0.0327	0.0004	0.30	227	77	209	7	207	3	207	3	n/a	
35	171213_034.FIN2	335	2.0	28.6615	0.7722	0.0519	0.0025	0.2480	0.0120	0.0349	0.0006	0.25	281	110	224	10	221	4	221	4	n/a	
36	171213_035.FIN2	1314	3.0	31.0849	0.7634	0.0505	0.0021	0.2230	0.0087	0.0322	0.0005	0.10	218	96	204	7	204	3	204	3	n/a	
37	171213_036.FIN2	707	4.0	29.6560	0.7564	0.0508	0.0023	0.2360	0.0110	0.0337	0.0005	0.28	232	105	215	9	214	3	214	3	n/a	
38	171213_037.FIN2	490	5.9	19.0114	0.5060	0.0543	0.0025	0.3940	0.0180	0.0526	0.0010	0.24	384	103	336	13	331	6	331	6	n/a	
39	171213_038.FIN2	1688	1.8	29.7619	1.3287	0.0509	0.0030	0.2350	0.0120	0.0336	0.0013	0.17	236	136	214	10	213	8	213	8	n/a	
41	171213_046.FIN2	293	1.6	20.0763	0.4434	0.0537	0.0015	0.3670	0.0100	0.0498	0.0005	0.29	358	63	316	8	314	3	314	3	n/a	
42	171213_047.FIN2	572	1.9	20.1776	0.4886	0.0534	0.0021	0.3650	0.0140	0.0496	0.0007	0.10	346	89	315	10	312	4	312	4	n/a	
43	171213_048.FIN2	923	2.0	18.9000	0.4287	0.0535	0.0011	0.3900	0.0087	0.0529	0.0005	0.47	350	46	334	6	332	3	332	3	n/a	
44	171213_049.FIN2	216	1.5	19.6117	0.5000	0.0535	0.0019	0.3740	0.0140	0.0510	0.0008	0.38	350	80	321	10	321	5	321	5	n/a	
45	171213_050.FIN2	595	2.2	32.2061	0.8816	0.0499	0.0028	0.2130	0.0120	0.0311	0.0006	0.19	190	131	198	11	197	4	197	4	n/a	
47	171213_052.FIN2	465	3.2	30.4692	0.8170	0.0501	0.0027	0.2290	0.0130	0.0328	0.0006	0.27	200	125	208	11	208	4	208	4	n/a	
48	171213_053.FIN2	2348	2.0	33.8410	0.8360	0.0506	0.0021	0.2069	0.0081	0.0296	0.0004	0.10	223	96	191	7	188	3	188	3	n/a	
49	171213_054.FIN2	361	2.8	19.7394	0.5065	0.0536	0.0021	0.3760	0.0150	0.0507	0.0008	0.29	354	88	323	11	319	5	319	5	n/a	

Grain	Spot name	isotopic ratios										isotopic ages									
		U	U/Th	$^{238}\text{U}/$		$^{207}\text{Pb}/$		^{207}Pb		^{206}Pb		rho*	^{207}Pb	\pm	^{207}Pb	\pm	^{206}Pb	\pm	Best	\pm	
				(ppm)	^{206}Pb	2SE	^{206}Pb	2SE	^{235}U	2SE	^{238}U	2SE		(Ma)	^{235}U	(Ma)	^{238}U	(Ma)	Age	(Ma)	conc.
51	171213_056.FIN2	149	1.6	19.8413	0.5905	0.0537	0.0041	0.3720	0.0280	0.0504	0.0011	0.19	358	172	320	21	317	7	317	7	n/a
52	171213_057.FIN2	165	1.9	30.1114	0.8523	0.0508	0.0042	0.2330	0.0200	0.0332	0.0007	0.17	232	191	211	16	211	4	211	4	n/a
53	171213_064.FIN2	133	2.8	19.5695	0.6510	0.0542	0.0045	0.3840	0.0330	0.0511	0.0013	0.33	379	187	327	24	321	8	321	8	n/a
54	171213_065.FIN2	923	1.7	30.9502	0.9100	0.0502	0.0026	0.2240	0.0110	0.0323	0.0007	0.19	204	120	205	9	205	4	205	4	n/a
55	171213_066.FIN2	1121	2.4	31.7561	0.7563	0.0503	0.0016	0.2203	0.0079	0.0315	0.0004	0.37	209	74	202	7	200	3	200	3	n/a
56	171213_067.FIN2	184	3.1	19.2678	0.5569	0.0528	0.0029	0.3800	0.0210	0.0519	0.0011	0.14	320	125	328	17	326	7	326	7	n/a
57	171213_068.FIN2	716	2.7	30.2389	0.7864	0.0514	0.0025	0.2360	0.0120	0.0331	0.0006	0.30	259	112	215	10	210	4	210	4	n/a
58	171213_069.FIN2	257	1.9	30.1296	0.8987	0.0504	0.0036	0.2330	0.0170	0.0332	0.0007	0.27	213	165	211	14	211	5	211	5	n/a
59	171213_070.FIN2	375	2.2	30.9502	0.7951	0.0506	0.0025	0.2260	0.0100	0.0323	0.0005	0.19	223	114	206	8	205	3	205	3	n/a
60	171213_071.FIN2	241	1.9	29.9760	0.8896	0.0518	0.0051	0.2400	0.0240	0.0334	0.0007	0.13	277	225	217	19	212	5	212	5	n/a
61	171213_072.FIN2	1144	2.5	31.8066	0.7183	0.0505	0.0016	0.2207	0.0075	0.0314	0.0004	0.39	218	73	202	6	200	2	200	2	n/a
62	171213_073.FIN2	408	2.4	30.3675	0.7470	0.0507	0.0018	0.2290	0.0075	0.0329	0.0005	0.12	227	82	209	6	209	3	209	3	n/a
63	171213_074.FIN2	856	1.6	19.1865	0.4417	0.0527	0.0014	0.3820	0.0120	0.0521	0.0007	0.48	316	60	328	8	328	4	328	4	n/a
64	171213_075.FIN2	139	2.1	20.3252	0.5784	0.0530	0.0039	0.3600	0.0260	0.0492	0.0010	0.03	329	167	310	20	310	6	310	6	n/a
65	171213_082.FIN2	654	1.7	30.1568	0.7275	0.0508	0.0022	0.2332	0.0099	0.0332	0.0005	0.11	232	100	212	8	210	3	210	3	n/a
67	171213_084.FIN2	159	2.1	20.4583	0.5860	0.0543	0.0031	0.3710	0.0220	0.0489	0.0010	0.11	384	128	317	16	308	6	308	6	n/a
68	171213_085.FIN2	746	2.7	29.8329	0.8455	0.0515	0.0029	0.2360	0.0110	0.0335	0.0007	0.16	263	129	218	11	213	4	213	4	n/a
69	171213_086.FIN2	343	2.0	20.7728	0.4747	0.0527	0.0020	0.3530	0.0150	0.0481	0.0006	0.36	316	86	306	11	303	4	303	4	n/a
70	171213_087.FIN2	374	2.8	16.7785	0.4504	0.0540	0.0035	0.4460	0.0270	0.0596	0.0011	0.19	371	146	373	19	373	7	373	7	n/a
71	171213_088.FIN2	254	2.2	20.2511	0.4511	0.0535	0.0017	0.3660	0.0120	0.0494	0.0006	0.20	350	72	315	9	311	4	311	4	n/a
72	171213_089.FIN2	209	1.9	20.0200	0.5210	0.0534	0.0034	0.3710	0.0240	0.0500	0.0008	0.24	346	144	318	18	314	5	314	5	n/a
73	171213_090.FIN2	320	1.6	20.3874	0.4572	0.0532	0.0017	0.3610	0.0120	0.0491	0.0006	0.37	337	72	312	9	309	4	309	4	n/a
74	171213_091.FIN2	417	1.9	20.9380	0.4822	0.0530	0.0018	0.3530	0.0130	0.0478	0.0006	0.38	329	77	306	10	301	4	301	4	n/a
75	171213_092.FIN2	120	1.9	21.0526	0.5762	0.0536	0.0029	0.3520	0.0190	0.0475	0.0010	0.21	354	122	304	14	299	6	299	6	n/a

Grain	Spot name	isotopic ratios										isotopic ages									
		U	U/Th	$^{238}\text{U}/$		$^{207}\text{Pb}/$		^{207}Pb		^{206}Pb		rho*	^{207}Pb	\pm	^{207}Pb	\pm	^{206}Pb	\pm	Best	\pm	
				(ppm)	^{206}Pb	2SE	^{206}Pb	2SE	^{235}U	2SE	^{238}U	2SE									
76	171213_093.FIN2	523	2.2	19.5160	0.4570	0.0529	0.0019	0.3770	0.0140	0.0512	0.0007	0.22	325	82	324	10	322	4	322	4	n/a
77	171213_100.FIN2	188	2.3	20.3957	0.5408	0.0537	0.0034	0.3650	0.0220	0.0490	0.0009	0.19	358	143	315	17	309	6	309	6	n/a
78	171213_101.FIN2	429	2.7	21.1864	0.6284	0.0528	0.0030	0.3470	0.0210	0.0472	0.0010	0.33	320	129	301	16	297	6	297	6	n/a
79	171213_102.FIN2	463	2.5	31.1430	0.7759	0.0509	0.0023	0.2270	0.0098	0.0321	0.0005	0.19	236	104	207	8	204	3	204	3	n/a
80	171213_103.FIN2	347	2.7	29.8418	0.8015	0.0515	0.0034	0.2390	0.0150	0.0335	0.0006	0.05	263	152	217	12	213	4	213	4	n/a
81	171213_104.FIN2	1482	1.6	32.6052	0.7229	0.0502	0.0010	0.2145	0.0047	0.0307	0.0003	0.34	204	46	197	4	195	2	195	2	n/a
82	171213_105.FIN2	249	2.6	30.6373	0.7978	0.0509	0.0031	0.2300	0.0140	0.0326	0.0006	0.12	236	141	209	12	207	3	207	3	n/a
83	171213_106.FIN2	133	1.7	21.8818	0.7661	0.0534	0.0054	0.3370	0.0320	0.0457	0.0013	0.19	346	229	293	24	288	8	288	8	n/a
84	171213_107.FIN2	214	2.3	19.4666	0.5305	0.0533	0.0032	0.3800	0.0220	0.0514	0.0010	0.04	342	136	325	16	323	6	323	6	n/a
85	171213_108.FIN2	258	2.7	19.6967	0.5043	0.0536	0.0023	0.3790	0.0170	0.0508	0.0009	0.24	354	97	325	12	319	5	319	5	n/a
86	171213_109.FIN2	139	3.4	20.5465	0.5488	0.0545	0.0030	0.3630	0.0180	0.0487	0.0008	0.19	392	124	314	14	306	5	306	5	n/a
87	171213_110.FIN2	313	1.8	18.9861	0.4326	0.0525	0.0018	0.3840	0.0130	0.0527	0.0007	0.24	307	78	332	10	331	4	331	4	n/a
88	171213_111.FIN2	108	2.7	20.4499	0.5855	0.0529	0.0040	0.3590	0.0270	0.0489	0.0010	0.02	325	172	308	20	308	6	308	6	n/a
89	171213_118.FIN2	313	2.3	21.0084	0.7062	0.0525	0.0033	0.3480	0.0220	0.0476	0.0013	0.25	307	143	302	16	300	8	300	8	n/a
90	171213_119.FIN2	163	1.5	21.7391	0.8979	0.0521	0.0049	0.3310	0.0290	0.0460	0.0017	0.19	290	215	294	25	290	10	290	10	n/a
91	171213_120.FIN2	1306	2.1	31.4564	0.7124	0.0510	0.0014	0.2247	0.0063	0.0318	0.0004	0.38	241	63	206	5	202	2	202	2	n/a
92	171213_121.FIN2	176	2.4	20.8030	0.5626	0.0532	0.0026	0.3520	0.0160	0.0481	0.0009	0.21	337	111	307	13	303	6	303	6	n/a
93	171213_122.FIN2	1369	1.9	31.0945	0.7638	0.0500	0.0017	0.2239	0.0076	0.0322	0.0005	0.23	195	79	205	6	204	3	204	3	n/a
94	171213_123.FIN2	612	1.3	21.7155	0.6130	0.0532	0.0021	0.3380	0.0140	0.0461	0.0009	0.37	337	89	295	11	290	6	290	6	n/a
95	171213_124.FIN2	291	2.7	20.6186	0.5952	0.0525	0.0028	0.3540	0.0180	0.0485	0.0010	0.04	307	121	306	14	305	6	305	6	n/a
96	171213_125.FIN2	528	2.0	25.4972	0.6436	0.0511	0.0019	0.2787	0.0092	0.0392	0.0006	0.14	245	86	250	8	248	4	248	4	n/a
97	171213_126.FIN2	628	3.0	31.7158	0.7947	0.0506	0.0022	0.2218	0.0095	0.0315	0.0005	0.06	223	101	203	8	200	3	200	3	n/a
98	171213_127.FIN2	239	2.3	22.7790	0.9859	0.0518	0.0049	0.3170	0.0320	0.0439	0.0017	0.36	277	217	278	25	277	11	277	11	n/a
99	171213_128.FIN2	1472	1.9	20.1450	0.5276	0.0530	0.0019	0.3620	0.0130	0.0496	0.0008	0.56	329	81	314	10	312	5	312	5	n/a

Grain	Spot name	isotopic ratios										isotopic ages									
		U	U/Th	$^{238}\text{U}/$	$^{207}\text{Pb}/$		^{207}Pb		^{206}Pb		^{207}Pb	\pm	^{207}Pb	\pm	^{206}Pb	\pm	Best	\pm			
		(ppm)		^{206}Pb	2SE	^{206}Pb	2SE	^{235}U	2SE	^{238}U	2SE	rho*	^{206}Pb	(Ma)	^{235}U	(Ma)	^{238}U	(Ma)	Age	(Ma)	conc.
100	171213_129.FIN2	354	2.4	19.5695	0.5744	0.0530	0.0034	0.3800	0.0260	0.0511	0.0010	0.38	329	146	325	19	321	6	321	6	n/a
101	171213_136.FIN2	844	3.0	31.8167	0.7592	0.0510	0.0017	0.2228	0.0071	0.0314	0.0004	0.17	241	77	204	6	200	3	200	3	n/a
102	171213_137.FIN2	336	3.3	31.3185	0.8926	0.0499	0.0031	0.2190	0.0140	0.0319	0.0007	0.28	190	145	203	12	203	4	203	4	n/a
103	171213_138.FIN2	642	2.3	32.5733	0.8806	0.0513	0.0039	0.2200	0.0160	0.0307	0.0006	0.09	254	175	201	14	195	4	195	4	n/a
104	171213_139.FIN2	1888	1.4	32.1130	0.9900	0.0521	0.0034	0.2260	0.0140	0.0311	0.0007	0.19	290	149	207	11	198	5	198	5	n/a
105	171213_140.FIN2	1259	2.4	34.1530	0.8865	0.0510	0.0017	0.2068	0.0081	0.0293	0.0005	0.41	241	77	191	7	186	3	186	3	n/a
106	171213_141.FIN2	262	2.7	19.4628	0.4924	0.0530	0.0030	0.3780	0.0210	0.0514	0.0008	0.20	329	128	324	15	323	5	323	5	n/a
107	171213_142.FIN2	1259	2.3	34.1414	0.9092	0.0507	0.0019	0.2051	0.0078	0.0293	0.0005	0.30	227	87	189	7	186	3	186	3	n/a
108	171213_143.FIN2	1280	2.1	33.8639	0.8945	0.0505	0.0018	0.2069	0.0076	0.0295	0.0005	0.29	218	83	191	6	188	3	188	3	n/a
109	171213_144.FIN2	274	2.0	20.1410	0.4868	0.0530	0.0019	0.3680	0.0140	0.0497	0.0006	0.16	329	81	317	10	312	4	312	4	n/a
110	171213_145.FIN2	499	0.8	22.8311	0.7819	0.0528	0.0041	0.3230	0.0260	0.0438	0.0012	0.28	320	176	283	20	276	7	276	7	n/a
111	171213_146.FIN2	135	2.2	20.0642	0.4831	0.0528	0.0023	0.3660	0.0160	0.0498	0.0007	0.13	320	99	314	12	314	4	314	4	n/a
112	171213_147.FIN2	257	1.5	21.8103	0.5233	0.0534	0.0025	0.3380	0.0150	0.0459	0.0006	0.19	346	106	294	12	289	4	289	4	n/a
113	171215_082.FIN2	225	2.4	19.6464	0.6562	0.0539	0.0038	0.3740	0.0290	0.0509	0.0015	0.46	367	159	321	22	320	9	320	9	n/a
114	171215_083.FIN2	281	1.7	20.2020	0.4081	0.0536	0.0018	0.3650	0.0120	0.0495	0.0007	0.12	354	76	316	9	311	4	311	4	n/a
115	171215_084.FIN2	95	1.9	20.8768	0.6102	0.0544	0.0047	0.3590	0.0300	0.0479	0.0011	0.07	388	194	308	22	302	7	302	7	n/a
116	171215_085.FIN2	414	2.2	31.3676	0.7379	0.0521	0.0021	0.2281	0.0084	0.0319	0.0006	0.19	290	92	208	7	202	3	202	3	n/a
117	171215_086.FIN2	951	1.8	32.6264	0.7345	0.0504	0.0015	0.2130	0.0068	0.0307	0.0005	0.42	213	69	196	6	195	3	195	3	n/a
118	171215_087.FIN2	207	1.5	19.8020	0.7842	0.0545	0.0061	0.3760	0.0390	0.0505	0.0019	0.04	392	251	321	28	318	12	318	12	n/a
119	171215_088.FIN2	324	2.1	19.8098	0.5102	0.0537	0.0020	0.3720	0.0150	0.0505	0.0010	0.33	358	84	320	11	317	6	317	6	n/a
120	171215_089.FIN2	196	1.8	20.0803	0.5645	0.0539	0.0028	0.3650	0.0170	0.0498	0.0011	0.26	367	117	314	13	313	7	313	7	n/a
Rejected Analysis																					
1	171212b_145.FIN2	415	2.2	31.6456	1.0014	0.0576	0.0041	0.2460	0.0160	0.0316	0.0009	0.01	515	156	223	13	201	5	201	5	n/a
10	171212b_160.FIN2	618	2.6	19.8413	0.6299	0.0544	0.0031	0.3690	0.0220	0.0504	0.0012	0.27	388	128	318	17	317	8	317	8	n/a

Grain	Spot name	isotopic ratios										isotopic ages									
		U	U/Th	$^{238}\text{U}/$		$^{207}\text{Pb}/$		^{207}Pb		^{206}Pb		^{207}Pb	\pm	^{207}Pb	\pm	^{206}Pb	\pm	Best	\pm		
		(ppm)		^{206}Pb	2SE	^{206}Pb	2SE	^{235}U	2SE	^{238}U	2SE	rho*	^{206}Pb	(Ma)	^{235}U	(Ma)	^{238}U	(Ma)	Age	(Ma)	conc.
11	171212b_161.FIN2	410	1.9	30.5064	1.0237	0.0641	0.0039	0.2840	0.0190	0.0328	0.0009	0.45	745	129	253	15	208	5	208	5	n/a
23	171213_016.FIN2	447	2.6	28.3286	0.9630	0.0516	0.0039	0.2510	0.0180	0.0353	0.0010	0.02	268	173	227	14	224	6	224	6	n/a
26	171213_019.FIN2	214	2.7	22.4719	1.1615	0.0886	0.0083	0.5390	0.0560	0.0445	0.0021	0.48	1396	180	434	37	280	13	280	13	n/a
40	171213_039.FIN2	549	3.3	21.8103	0.6184	0.0521	0.0024	0.3340	0.0130	0.0459	0.0009	0.30	290	105	292	10	289	5	289	5	n/a
46	171213_051.FIN2	1301	2.3	33.7382	0.8537	0.0545	0.0029	0.2190	0.0130	0.0296	0.0005	0.45	392	119	201	11	188	3	188	3	n/a
50	171213_055.FIN2	1019	1.0	19.9720	0.4787	0.0555	0.0013	0.3837	0.0092	0.0501	0.0006	0.33	432	52	329	7	315	4	315	4	n/a
66	171213_083.FIN2	203	1.6	19.7239	0.5835	0.0535	0.0049	0.3750	0.0340	0.0507	0.0011	0.19	350	211	321	24	319	7	319	7	n/a

Grain	Spot name	isotopic ratios										isotopic ages									
		U	U/Th	$^{238}\text{U}/$	$^{207}\text{Pb}/$		^{207}Pb		^{206}Pb		^{207}Pb	\pm	^{207}Pb	\pm	^{206}Pb	\pm	Best	\pm			
		(ppm)		^{206}Pb	2SE	^{206}Pb	2SE	^{235}U	2SE	^{238}U	2SE	rho*	^{206}Pb	(Ma)	^{235}U	(Ma)	^{238}U	(Ma)	Age	(Ma)	

Richthofen formation

Whitehorse trough - Richthofen formation - Sample 16-LVD-009, Mount Laurier (Zone 08V 507457E 6765804N NAD 83)

Grain	Spot name	isotopic ratios										isotopic ages									
		U	U/Th	$^{238}\text{U}/$	$^{207}\text{Pb}/$		^{207}Pb		^{206}Pb		^{207}Pb	\pm	^{207}Pb	\pm	^{206}Pb	\pm	Best	\pm			
		(ppm)		^{206}Pb	2SE	^{206}Pb	2SE	^{235}U	2SE	^{238}U	2SE	rho	^{206}Pb	(Ma)	^{235}U	(Ma)	^{238}U	(Ma)	Age	(Ma)	
1	170322_170.FIN2	253	3.8	32.0205	0.8510	0.0506	0.0023	0.2180	0.0110	0.0312	0.0006	0.38	223	105	201	9	198	4	198	4	n/a
7	170322_176.FIN2	384	4.3	30.4878	1.0225	0.0505	0.0040	0.2290	0.0210	0.0328	0.0009	0.54	218	183	209	17	208	5	208	5	n/a
8	170322_177.FIN2	134	1.6	19.3424	0.5986	0.0543	0.0050	0.3870	0.0350	0.0517	0.0013	0.10	384	207	330	25	325	8	325	8	n/a
9	170322_178.FIN2	418	2.9	30.2389	0.7224	0.0510	0.0024	0.2320	0.0100	0.0331	0.0005	0.36	241	108	212	8	210	3	210	3	n/a
11	170322_186.FIN2	339	3.3	31.8167	0.7086	0.0502	0.0014	0.2169	0.0064	0.0314	0.0003	0.24	204	65	199	5	200	2	200	2	n/a
14	170322_189.FIN2	405	2.3	30.6279	1.0319	0.0506	0.0042	0.2290	0.0210	0.0327	0.0009	0.43	223	192	209	17	207	6	207	6	n/a
15	170322_190.FIN2	231	1.6	19.6078	0.8074	0.0543	0.0047	0.3830	0.0350	0.0510	0.0018	0.41	384	195	328	26	321	11	321	11	n/a
16	170322_191.FIN2	360	4.0	31.1721	0.7579	0.0511	0.0023	0.2270	0.0110	0.0321	0.0005	0.29	245	104	207	9	204	3	204	3	n/a
18	170322_193.FIN2	1049	1.6	19.2753	0.5201	0.0539	0.0013	0.3857	0.0095	0.0519	0.0010	0.45	367	54	331	7	326	6	326	6	n/a
22	170322_204.FIN2	572	2.5	31.9489	1.3270	0.0507	0.0035	0.2180	0.0150	0.0313	0.0011	0.29	227	160	200	13	198	7	198	7	n/a
23	170322_205.FIN2	59	2.1	18.3824	0.7772	0.0548	0.0070	0.3940	0.0470	0.0544	0.0020	0.29	404	286	344	40	341	12	341	12	n/a
24	170322_206.FIN2	304	1.1	20.2061	0.4899	0.0545	0.0020	0.3690	0.0130	0.0495	0.0007	0.28	392	82	320	11	311	4	311	4	n/a
25	170322_207.FIN2	815	3.5	33.1455	0.9997	0.0502	0.0021	0.2090	0.0100	0.0302	0.0007	0.48	204	97	193	9	192	4	192	4	n/a
26	170322_208.FIN2	268	3.8	30.1205	0.8437	0.0508	0.0029	0.2330	0.0130	0.0332	0.0007	0.19	232	132	212	11	211	4	211	4	n/a
27	170322_209.FIN2	146	2.0	19.7629	0.6640	0.0540	0.0047	0.3750	0.0300	0.0506	0.0014	0.36	371	196	322	22	318	8	318	8	n/a
31	170322_219.FIN2	378	4.0	32.8515	1.0253	0.0503	0.0034	0.2110	0.0140	0.0304	0.0008	0.21	209	157	194	12	193	5	193	5	n/a
32	170322_220.FIN2	377	3.5	30.8261	0.8932	0.0509	0.0025	0.2270	0.0110	0.0324	0.0007	0.11	236	113	207	9	206	4	206	4	n/a

Grain	Spot name	isotopic ratios												isotopic ages									
		U	U/Th	$^{238}\text{U}/$		$^{207}\text{Pb}/$		^{207}Pb		^{206}Pb				^{207}Pb	\pm	^{207}Pb	\pm	^{206}Pb	\pm	Best	\pm		
		(ppm)		^{206}Pb	2SE	^{206}Pb	2SE	^{235}U	2SE	^{238}U	2SE	rho*	^{206}Pb	(Ma)	^{235}U	(Ma)	^{238}U	(Ma)	Age	(Ma)	conc.		
33	170322_221.FIN2	559	3.1	31.6456	1.1016	0.0528	0.0041	0.2300	0.0180	0.0316	0.0009	0.16	320	176	210	15	201	6	201	6	n/a		
34	170322_222.FIN2	249	2.4	19.1571	0.5505	0.0538	0.0035	0.3870	0.0270	0.0522	0.0011	0.28	363	147	331	19	328	7	328	7	n/a		
35	170322_223.FIN2	100	3.6	19.5695	1.5702	0.0540	0.0100	0.3760	0.0700	0.0511	0.0040	0.14	371	417	322	49	321	25	321	25	n/a		
37	170323_010.FIN2	226	3.6	31.7158	1.1065	0.0506	0.0027	0.2170	0.0110	0.0315	0.0007	0.26	223	123	201	10	200	4	200	4	n/a		
40	170323_013.FIN2	155	1.8	18.6567	0.7658	0.0547	0.0055	0.4020	0.0380	0.0536	0.0017	0.36	400	225	340	28	337	10	337	10	n/a		
42	170323_015.FIN2	168	1.8	19.3050	0.7454	0.0551	0.0044	0.3810	0.0240	0.0518	0.0014	0.15	416	178	327	17	326	8	326	8	n/a		
43	170323_016.FIN2	654	3.1	33.4448	1.5660	0.0523	0.0030	0.2160	0.0140	0.0299	0.0012	0.56	299	131	198	12	190	7	190	7	n/a		
44	170323_017.FIN2	218	2.3	19.8413	0.8661	0.0535	0.0035	0.3700	0.0240	0.0504	0.0017	0.28	350	148	319	18	317	11	317	11	n/a		
45	170323_018.FIN2	565	3.6	28.0978	1.0263	0.0510	0.0020	0.2500	0.0110	0.0356	0.0009	0.40	241	90	226	9	225	5	225	5	n/a		
46	170323_025.FIN2	104	2.3	18.2482	0.7659	0.0544	0.0054	0.4080	0.0390	0.0548	0.0017	0.14	388	223	344	28	344	11	344	11	n/a		
48	170323_027.FIN2	380	2.5	30.6279	0.9193	0.0508	0.0016	0.2284	0.0076	0.0327	0.0004	0.39	232	73	208	6	207	3	207	3	n/a		
49	170323_028.FIN2	254	2.3	19.3424	0.6734	0.0537	0.0026	0.3820	0.0200	0.0517	0.0012	0.40	358	109	328	14	325	7	325	7	n/a		
50	170323_029.FIN2	95	2.6	19.0114	0.7952	0.0537	0.0038	0.3890	0.0300	0.0526	0.0017	0.44	358	160	331	22	330	11	330	11	n/a		
51	170323_030.FIN2	101	1.7	19.5313	0.8392	0.0539	0.0048	0.3770	0.0320	0.0512	0.0017	0.05	367	201	322	23	322	10	322	10	n/a		
52	170323_031.FIN2	372	2.6	17.9469	0.5798	0.0543	0.0014	0.4170	0.0130	0.0557	0.0010	0.50	384	58	353	9	350	6	350	6	n/a		
53	170323_032.FIN2	389	2.6	20.3998	0.6658	0.0524	0.0018	0.3550	0.0130	0.0490	0.0009	0.45	303	78	310	9.2	309	6	309	6	n/a		
54	170323_033.FIN2	429	2.9	32.3206	1.1491	0.0504	0.0031	0.2160	0.0130	0.0309	0.0008	0.14	213	142	198	10	196	5	196	5	n/a		
55	170323_034.FIN2	585	2.8	31.1333	0.9693	0.0504	0.0017	0.2232	0.0084	0.0321	0.0006	0.43	213	78	204	7	204	4	204	4	n/a		
56	170323_041.FIN2	280	1.2	18.7617	0.5984	0.0537	0.0020	0.3950	0.0150	0.0533	0.0010	0.26	358	84	337	11	335	6	335	6	n/a		
57	170323_042.FIN2	162	3.9	29.4464	0.9538	0.0505	0.0034	0.2380	0.0180	0.0340	0.0007	0.39	218	156	215	14	215	4	215	4	n/a		
60	170323_045.FIN2	374	4.4	31.2305	1.0729	0.0516	0.0023	0.2267	0.0099	0.0320	0.0006	0.11	268	102	207	8	203	4	203	4	n/a		
62	170323_047.FIN2	45	1.6	19.2308	0.7396	0.0546	0.0040	0.3870	0.0280	0.0520	0.0014	0.12	396	164	328	21	327	8	327	8	n/a		
65	170323_050.FIN2	100	1.2	19.0476	0.6893	0.0544	0.0034	0.3920	0.0250	0.0525	0.0012	0.14	388	140	334	18	330	8	330	8	n/a		
66	170323_057.FIN2	334	4.1	31.8979	1.0175	0.0522	0.0028	0.2220	0.0110	0.0314	0.0006	0.26	294	122	203	9	199	4	199	4	n/a		

Grain	Spot name	isotopic ratios										isotopic ages									
		U (ppm)	U/Th	$^{238}\text{U}/$		$^{207}\text{Pb}/$		^{207}Pb		^{206}Pb		rho*	^{206}Pb (Ma)	^{207}Pb (Ma)	^{207}Pb (Ma)	^{206}Pb (Ma)	^{238}U (Ma)	Best Age (Ma)	\pm	\pm	
				^{206}Pb	2SE	^{206}Pb	2SE	^{235}U	2SE	^{238}U	2SE										
68	170323_059.FIN2	295	4.7	29.8864	1.0718	0.0525	0.0026	0.2400	0.0110	0.0335	0.0009	0.08	307	113	218	9	212	5	212	5	n/a
69	170323_060.FIN2	282	1.7	18.7723	0.5991	0.0536	0.0019	0.3930	0.0140	0.0533	0.0009	0.19	354	80	335	10	335	6	335	6	n/a
70	170323_061.FIN2	96	1.9	18.7266	0.6663	0.0531	0.0031	0.3970	0.0270	0.0534	0.0013	0.46	333	132	336	20	335	8	335	8	n/a
71	170323_062.FIN2	263	3.0	30.6560	1.0338	0.0517	0.0028	0.2320	0.0130	0.0326	0.0007	0.37	272	124	211	11	207	4	207	4	n/a
73	170323_064.FIN2	766	2.2	31.4465	1.3844	0.0520	0.0032	0.2280	0.0160	0.0318	0.0011	0.50	285	141	209	13	202	7	202	7	n/a
75	170323_066.FIN2	284	3.6	30.0210	1.0815	0.0512	0.0031	0.2350	0.0150	0.0333	0.0008	0.28	250	139	213	12	211	5	211	5	n/a
78	170323_075.FIN2	553	3.6	31.7058	1.2063	0.0511	0.0025	0.2230	0.0110	0.0315	0.0008	0.23	245	113	204	9	200	5	200	5	n/a
79	170323_076.FIN2	169	1.7	19.6078	0.7305	0.0542	0.0037	0.3820	0.0280	0.0510	0.0013	0.28	379	154	326	20	321	8	321	8	n/a
80	170323_077.FIN2	1214	2.4	31.3480	1.3758	0.0500	0.0018	0.2210	0.0130	0.0319	0.0011	0.79	195	84	202	10	202	7	202	7	n/a
81	170323_078.FIN2	446	3.1	30.9215	0.9370	0.0510	0.0018	0.2273	0.0072	0.0323	0.0005	0.13	241	81	208	6	205	3	205	3	n/a
82	170323_079.FIN2	482	4.0	31.2500	1.3672	0.0516	0.0041	0.2280	0.0190	0.0320	0.0011	0.28	268	182	208	16	203	7	203	7	n/a
86	170323_089.FIN2	35	2.6	17.6056	0.5889	0.0557	0.0036	0.4340	0.0290	0.0568	0.0012	0.16	440	144	358	21	356	7	356	7	n/a
87	170323_090.FIN2	524	1.7	20.5761	0.6774	0.0528	0.0020	0.3550	0.0140	0.0486	0.0010	0.42	320	86	310	10	306	6	306	6	n/a
88	170323_091.FIN2	523	2.5	29.7619	1.2401	0.0508	0.0027	0.2350	0.0140	0.0336	0.0010	0.41	232	123	214	11	213	6	213	6	n/a
89	170323_092.FIN2	715	2.3	32.3939	1.2592	0.0505	0.0025	0.2160	0.0120	0.0309	0.0008	0.49	218	115	198	10	196	5	196	5	n/a
90	170323_093.FIN2	500	2.6	32.7332	1.0607	0.0501	0.0021	0.2110	0.0100	0.0306	0.0006	0.43	200	97	194	8	194	4	194	4	n/a
92	170323_095.FIN2	269	5.1	23.5073	0.7184	0.0533	0.0042	0.3130	0.0240	0.0425	0.0007	0.02	342	178	276	19	269	4	269	4	n/a
93	170323_096.FIN2	677	2.9	30.9215	0.9466	0.0505	0.0016	0.2262	0.0079	0.0323	0.0005	0.35	218	73	208	7	205	3	205	3	n/a
94	170323_097.FIN2	456	3.4	30.7314	0.9350	0.0507	0.0020	0.2282	0.0091	0.0325	0.0005	0.24	227	91	208	8	206	3	206	3	n/a
97	170323_106.FIN2	719	2.3	32.7011	1.1763	0.0502	0.0023	0.2120	0.0100	0.0306	0.0008	0.38	204	106	195	9	194	5	194	5	n/a
98	170323_107.FIN2	218	2.6	17.6367	0.6221	0.0544	0.0019	0.4220	0.0160	0.0567	0.0012	0.52	388	78	356	11	356	8	356	8	n/a
99	170323_108.FIN2	245	2.6	17.9212	0.7708	0.0548	0.0040	0.4200	0.0260	0.0558	0.0018	0.02	404	163	355	19	350	11	350	11	n/a
100	170323_109.FIN2	737	1.9	32.1647	1.2415	0.0521	0.0025	0.2240	0.0120	0.0311	0.0008	0.46	290	110	205	10	197	5	197	5	n/a
101	170324_071.FIN2	357	3.1	30.5810	1.0287	0.0508	0.0013	0.2290	0.0065	0.0327	0.0005	0.48	232	59	209	5	207	3	207	3	n/a

Grain	Spot name	isotopic ratios										isotopic ages									
		U	U/Th	$^{238}\text{U}/$	$^{207}\text{Pb}/$		^{207}Pb		^{206}Pb			^{207}Pb	\pm	^{207}Pb	\pm	^{206}Pb	\pm	Best	\pm		
		(ppm)		^{206}Pb	2SE	^{206}Pb	2SE	^{235}U	2SE	^{238}U	2SE	rho*	^{206}Pb	(Ma)	^{235}U	(Ma)	^{238}U	(Ma)	Age	(Ma)	conc.
103	170324_073.FIN2	117	2.0	17.6056	0.7749	0.0544	0.0042	0.4250	0.0370	0.0568	0.0017	0.46	388	173	358	26	356	11	356	11	n/a
104	170324_074.FIN2	310	5.2	31.7058	1.3068	0.0514	0.0026	0.2230	0.0120	0.0315	0.0008	0.36	259	116	204	10	200	5	200	5	n/a
105	170324_075.FIN2	325	4.1	32.4675	1.2650	0.0506	0.0038	0.2170	0.0190	0.0308	0.0007	0.61	223	174	199	16	196	5	196	5	n/a
106	170324_076.FIN2	366	1.1	19.1205	0.8774	0.0535	0.0027	0.3850	0.0170	0.0523	0.0018	0.14	350	114	330	13	329	11	329	11	n/a
107	170324_077.FIN2	150	1.8	18.4162	0.7461	0.0535	0.0020	0.4000	0.0160	0.0543	0.0014	0.41	350	85	341	11	341	9	341	9	n/a
108	170324_078.FIN2	683	2.1	28.3046	1.1216	0.0508	0.0016	0.2483	0.0090	0.0353	0.0008	0.57	232	73	225	7	224	5	224	5	n/a
109	170324_079.FIN2	233	3.0	30.2115	1.3691	0.0507	0.0034	0.2330	0.0160	0.0331	0.0010	0.43	227	155	212	13	210	7	210	7	n/a
110	170324_080.FIN2	513	2.6	32.0616	1.1307	0.0500	0.0018	0.2182	0.0085	0.0312	0.0006	0.21	195	84	200	7	198	4	198	4	n/a
Rejected Analysis																					
2	170322_171.FIN2	253	2.5	33.2226	1.0596	0.0844	0.0070	0.3360	0.0280	0.0301	0.0008	0.21	1302	161	293	22	191	5	191	5	n/a
3	170322_172.FIN2	184	3.6	31.5259	1.0933	0.0566	0.0057	0.2470	0.0230	0.0317	0.0010	0.36	476	223	223	18	201	6	201	6	n/a
4	170322_173.FIN2	533	1.6	24.1371	0.6409	0.0610	0.0023	0.3520	0.0170	0.0414	0.0008	0.67	639	81	305	13	262	5	262	5	n/a
5	170322_174.FIN2	568	2.1	20.2020	0.6122	0.0622	0.0029	0.4250	0.0220	0.0495	0.0011	0.40	681	100	359	16	311	7	311	7	n/a
6	170322_175.FIN2	315	2.8	32.3625	1.2568	0.0563	0.0052	0.2400	0.0230	0.0309	0.0011	0.16	464	205	218	18	197	7	197	7	n/a
10	170322_179.FIN2	678	3.0	33.0142	1.1989	0.0509	0.0032	0.2120	0.0140	0.0303	0.0009	0.40	236	145	195	12	192	6	192	6	n/a
12	170322_187.FIN2	245	2.3	25.1889	1.0152	0.0549	0.0042	0.2990	0.0230	0.0397	0.0014	0.20	408	171	265	17	251	9	251	9	n/a
13	170322_188.FIN2	468	3.3	31.7259	0.8656	0.0640	0.0032	0.2780	0.0150	0.0315	0.0006	0.28	742	106	248	12	200	4	200	4	n/a
17	170322_192.FIN2	149	1.9	19.8020	0.8627	0.0546	0.0061	0.3780	0.0400	0.0505	0.0020	0.36	396	251	324	29	317	12	317	12	n/a
19	170322_194.FIN2	199	4.1	29.5334	0.8112	0.0566	0.0032	0.2660	0.0170	0.0339	0.0007	0.50	476	125	238	14	215	4	215	4	n/a
20	170322_195.FIN2	482	18.5	35.4233	1.1293	0.0620	0.0038	0.2320	0.0130	0.0282	0.0007	0.35	674	131	212	11	179	5	179	5	n/a
21	170322_203.FIN2	250	1.5	20.9205	0.7440	0.0593	0.0045	0.3890	0.0280	0.0478	0.0015	0.11	578	165	332	21	301	9	301	9	n/a
28	170322_210.FIN2	212	3.4	30.5157	0.9033	0.0560	0.0041	0.2530	0.0180	0.0328	0.0007	0.09	452	163	227	15	208	5	208	5	n/a
29	170322_211.FIN2	319	3.5	32.1647	0.8794	0.0675	0.0049	0.2890	0.0210	0.0311	0.0006	0.12	853	151	257	16	197	4	197	4	n/a
30	170322_212.FIN2	454	1.6	19.5313	0.5722	0.0531	0.0024	0.3750	0.0180	0.0512	0.0012	0.36	333	102	323	13	322	7	322	7	n/a

Grain	Spot name	isotopic ratios										isotopic ages									
		U (ppm)	U/Th	$^{238}\text{U}/$		$^{207}\text{Pb}/$		^{207}Pb		^{206}Pb		^{207}Pb (Ma)	\pm	^{207}Pb (Ma)	\pm	^{206}Pb (Ma)	\pm	Best (Ma)	\pm		
				^{206}Pb	2SE	^{206}Pb	2SE	^{235}U	2SE	^{238}U	2SE										
36	170323_009.FIN2	127	3.5	25.5102	1.1063	0.0570	0.0055	0.3090	0.0310	0.0392	0.0014	0.32	492	213	272	24	248	9	248	9	n/a
38	170323_011.FIN2	127	3.1	28.2486	1.2768	0.0519	0.0053	0.2510	0.0240	0.0354	0.0013	0.14	281	234	226	19	224	8	224	8	n/a
39	170323_012.FIN2	172	3.0	29.4464	1.1272	0.0607	0.0050	0.2840	0.0260	0.0340	0.0010	0.50	629	177	253	21	215	6	215	6	n/a
41	170323_014.FIN2	204	2.8	32.0513	1.4382	0.0554	0.0047	0.2370	0.0190	0.0312	0.0012	0.07	428	189	215	15	198	7	198	7	n/a
47	170323_026.FIN2	184	3.6	7.4627	0.3063	0.0984	0.0034	1.8160	0.0770	0.1340	0.0042	0.62	1594	65	1049	28	811	24	811	24	51
58	170323_043.FIN2	349	3.1	20.7039	0.9859	0.0531	0.0048	0.3530	0.0330	0.0483	0.0019	0.17	333	205	306	24	304	12	304	12	n/a
59	170323_044.FIN2	130	4.0	26.0417	1.0851	0.0514	0.0044	0.2720	0.0240	0.0384	0.0012	0.26	259	197	243	19	243	7	243	7	n/a
61	170323_046.FIN2	319	1.9	20.5761	0.8891	0.0533	0.0032	0.3580	0.0230	0.0486	0.0017	0.40	342	136	310	17	306	10	306	10	n/a
63	170323_048.FIN2	219	1.3	21.2134	0.7200	0.0579	0.0026	0.3730	0.0160	0.0471	0.0010	0.33	526	98	321	12	297	6	297	6	n/a
64	170323_049.FIN2	234	2.7	25.7069	0.9913	0.0519	0.0047	0.2770	0.0230	0.0389	0.0010	0.36	281	207	247	19	246	7	246	7	n/a
67	170323_058.FIN2	138	2.5	18.7617	0.7392	0.0732	0.0044	0.5370	0.0320	0.0533	0.0015	0.26	1019	122	434	21	335	9	335	9	n/a
72	170323_063.FIN2	392	2.1	24.7525	1.1641	0.0519	0.0031	0.2890	0.0160	0.0404	0.0015	0.03	281	137	257	13	255	10	255	10	n/a
74	170323_065.FIN2	210	2.7	31.2500	1.3672	0.0571	0.0059	0.2510	0.0250	0.0320	0.0011	0.27	495	228	226	20	203	7	203	7	n/a
76	170323_073.FIN2	644	4.9	23.7530	0.9591	0.0788	0.0029	0.4570	0.0240	0.0421	0.0012	0.35	1167	73	381	17	266	8	266	8	n/a
77	170323_074.FIN2	294	4.0	31.1333	1.0662	0.0553	0.0030	0.2460	0.0160	0.0321	0.0007	0.50	424	121	223	13	204	4	204	4	n/a
83	170323_080.FIN2	250	3.8	31.5457	1.3932	0.0625	0.0050	0.2730	0.0230	0.0317	0.0011	0.38	691	171	244	19	201	7	201	7	n/a
84	170323_081.FIN2	1449	1.5	20.2020	0.6938	0.0568	0.0011	0.3880	0.0100	0.0495	0.0011	0.69	484	43	332	8	312	7	312	7	n/a
85	170323_082.FIN2	753	2.4	21.7391	1.2287	0.0631	0.0024	0.4010	0.0250	0.0460	0.0023	0.77	712	81	342	18	290	14	290	14	n/a
91	170323_094.FIN2	374	2.9	26.2467	1.0333	0.0518	0.0043	0.2740	0.0250	0.0381	0.0010	0.50	277	190	245	20	241	6	241	6	n/a
95	170323_098.FIN2	1072	3.0	25.3165	1.0255	0.0543	0.0019	0.2970	0.0130	0.0395	0.0011	0.66	384	79	264	10	250	7	250	7	n/a
96	170323_105.FIN2	88	1.5	19.4175	0.9426	0.0800	0.0100	0.5720	0.0810	0.0515	0.0021	0.46	1197	247	453	53	324	13	324	13	n/a
102	170324_072.FIN2	53	2.3	20.0000	1.0000	0.0610	0.0064	0.4230	0.0530	0.0500	0.0020	0.46	639	226	354	37	315	12	315	12	n/a

Grain	Spot name	isotopic ratios										isotopic ages									
		U	U/Th	$^{238}\text{U}/$	$^{207}\text{Pb}/$		^{207}Pb		^{206}Pb		^{207}Pb	\pm	^{207}Pb	\pm	^{206}Pb	\pm	Best	\pm			
		(ppm)		^{206}Pb	2SE	^{206}Pb	2SE	^{235}U	2SE	^{238}U	2SE	rho*	^{206}Pb	(Ma)	^{235}U	(Ma)	^{238}U	(Ma)	Age	(Ma)	

Whitehorse trough - Richthofen formation - Sample 16-LVD-021, Richthofen Island (Zone 08V 491272 6775151N NAD 83)

Grain	Spot name	isotopic ratios										isotopic ages									
		U	U/Th	$^{238}\text{U}/$	$^{207}\text{Pb}/$		^{207}Pb		^{206}Pb		^{207}Pb	\pm	^{207}Pb	\pm	^{206}Pb	\pm	Best	\pm			
		(ppm)		^{206}Pb	2SE	^{206}Pb	2SE	^{235}U	2SE	^{238}U	2SE	rho	^{206}Pb	(Ma)	^{235}U	(Ma)	^{238}U	(Ma)	Age	(Ma)	conc.
1	170322_009.FIN2	118	3.2	28.9436	0.7456	0.0521	0.0034	0.2460	0.0160	0.0346	0.0006	0.20	290	149	221	13	219	4	219	4	n/a
2	170322_010.FIN2	318	1.9	33.4672	1.3441	0.0513	0.0036	0.2120	0.0160	0.0299	0.0010	0.14	254	161	194	13	190	6	190	6	n/a
3	170322_011.FIN2	182	2.6	28.9855	1.0922	0.0512	0.0038	0.2450	0.0190	0.0345	0.0011	0.35	250	171	221	16	219	7	219	7	n/a
4	170322_012.FIN2	319	2.8	30.5157	0.7729	0.0500	0.0025	0.2300	0.0130	0.0328	0.0005	0.35	195	116	209	10	208	3	208	3	n/a
5	170322_013.FIN2	126	3.0	31.5358	0.8752	0.0516	0.0035	0.2260	0.0150	0.0317	0.0006	0.08	268	156	206	12	201	4	201	4	n/a
6	170322_014.FIN2	469	3.0	30.8261	1.0453	0.0526	0.0044	0.2340	0.0180	0.0324	0.0009	0.26	312	190	213	14	206	6	206	6	n/a
8	170322_016.FIN2	254	1.7	34.0716	0.8823	0.0499	0.0026	0.2020	0.0110	0.0294	0.0005	0.29	190	121	187	9	186	3	186	3	n/a
9	170322_017.FIN2	231	3.7	31.1333	0.8045	0.0502	0.0027	0.2240	0.0130	0.0321	0.0005	0.12	204	125	204	10	204	3	204	3	n/a
10	170322_018.FIN2	271	2.4	31.6156	0.9396	0.0519	0.0034	0.2230	0.0140	0.0316	0.0007	0.20	281	150	204	11	201	5	201	5	n/a
11	170322_025.FIN2	86	3.1	30.8833	1.1445	0.0515	0.0050	0.2280	0.0220	0.0324	0.0010	0.05	263	223	206	18	205	6	205	6	n/a
12	170322_026.FIN2	170	1.9	31.3972	0.7492	0.0510	0.0019	0.2253	0.0085	0.0319	0.0004	0.20	241	86	205	7	202	3	202	3	n/a
13	170322_027.FIN2	890	1.3	30.1750	0.8377	0.0510	0.0019	0.2338	0.0088	0.0331	0.0007	0.28	241	86	213	7	210	4	210	4	n/a
14	170322_028.FIN2	317	3.8	30.3306	0.6992	0.0506	0.0016	0.2302	0.0071	0.0330	0.0004	0.20	223	73	210	6	209	3	209	3	n/a
15	170322_029.FIN2	427	2.6	29.9670	0.8890	0.0504	0.0019	0.2300	0.0110	0.0334	0.0007	0.34	213	87	212	8	212	5	212	5	n/a
16	170322_030.FIN2	249	2.6	31.3972	0.8478	0.0516	0.0029	0.2270	0.0130	0.0319	0.0006	0.25	268	129	207	11	202	4	202	4	n/a
18	170322_032.FIN2	1027	4.5	32.2789	1.1461	0.0507	0.0033	0.2170	0.0150	0.0310	0.0009	0.39	227	150	199	13	197	6	197	6	n/a
19	170322_033.FIN2	235	3.1	29.2398	0.7695	0.0507	0.0022	0.2390	0.0100	0.0342	0.0006	0.16	227	100	217	9	217	4	217	4	n/a
20	170322_034.FIN2	467	2.5	29.7885	0.7986	0.0504	0.0025	0.2340	0.0120	0.0336	0.0006	0.51	213	115	216	9	213	4	213	4	n/a

Grain	Spot name	isotopic ratios												isotopic ages											
		U (ppm)	U/Th	$^{238}\text{U}/$		$^{207}\text{Pb}/$		^{207}Pb		^{206}Pb		rho*	^{207}Pb (Ma)	\pm	^{207}Pb (Ma)	\pm	^{206}Pb (Ma)	\pm	Best (Ma)	\pm					
				^{206}Pb	2SE	^{206}Pb	2SE	^{235}U	2SE	^{238}U	2SE														
21	170322_041.FIN2	500	1.7	31.8979	0.9361	0.0503	0.0024	0.2180	0.0110	0.0314	0.0007	0.42	209	111	200	10	199	4	199	4	n/a				
22	170322_042.FIN2	178	2.7	30.9789	1.0557	0.0504	0.0042	0.2240	0.0180	0.0323	0.0009	0.10	213	193	204	15	205	6	205	6	n/a				
23	170322_043.FIN2	305	1.9	31.4961	0.8234	0.0503	0.0025	0.2200	0.0110	0.0318	0.0006	0.16	209	115	202	9	202	3	202	3	n/a				
24	170322_044.FIN2	302	2.4	30.2572	1.0070	0.0504	0.0035	0.2310	0.0170	0.0331	0.0009	0.37	213	161	210	14	210	5	210	5	n/a				
25	170322_045.FIN2	147	2.6	29.8864	0.6967	0.0515	0.0022	0.2360	0.0100	0.0335	0.0004	0.06	263	98	215	8	212	3	212	3	n/a				
26	170322_046.FIN2	426	2.6	28.4657	0.7455	0.0517	0.0025	0.2510	0.0130	0.0351	0.0006	0.07	272	111	227	10	223	4	223	4	n/a				
27	170322_047.FIN2	251	3.7	29.4638	0.8334	0.0506	0.0030	0.2370	0.0140	0.0339	0.0007	0.22	223	137	215	12	215	4	215	4	n/a				
30	170322_050.FIN2	108	3.5	30.4044	0.8782	0.0505	0.0039	0.2310	0.0180	0.0329	0.0007	0.11	218	179	209	15	209	4	209	4	n/a				
31	170322_057.FIN2	107	2.0	30.6560	1.0338	0.0516	0.0042	0.2320	0.0200	0.0326	0.0009	0.26	268	187	210	16	207	6	207	6	n/a				
32	170322_058.FIN2	179	2.3	29.5072	0.7923	0.0509	0.0029	0.2380	0.0140	0.0339	0.0006	0.28	236	131	216	11	215	4	215	4	n/a				
33	170322_059.FIN2	231	1.7	30.2389	0.7407	0.0515	0.0023	0.2360	0.0110	0.0331	0.0005	0.17	263	103	215	9	210	3	210	3	n/a				
34	170322_060.FIN2	374	3.0	30.2480	0.7869	0.0509	0.0025	0.2320	0.0110	0.0331	0.0006	0.15	236	113	212	9	210	4	210	4	n/a				
35	170322_061.FIN2	130	1.7	30.5064	0.9306	0.0499	0.0035	0.2240	0.0150	0.0328	0.0008	0.04	190	163	204	13	208	5	208	5	n/a				
37	170322_063.FIN2	182	2.6	31.5358	0.7459	0.0514	0.0019	0.2240	0.0087	0.0317	0.0004	0.27	259	85	205	7	201	3	201	3	n/a				
39	170322_065.FIN2	304	1.9	32.6584	0.7679	0.0508	0.0020	0.2160	0.0087	0.0306	0.0004	0.14	232	91	198	7	194	3	194	3	n/a				
40	170322_066.FIN2	235	2.3	31.1333	0.9596	0.0516	0.0047	0.2280	0.0200	0.0321	0.0008	0.26	268	209	208	17	204	5	204	5	n/a				
41	170322_073.FIN2	378	3.8	30.3675	0.7101	0.0505	0.0019	0.2295	0.0086	0.0329	0.0004	0.20	218	87	209	7	209	3	209	3	n/a				
42	170322_074.FIN2	103	2.4	30.1024	0.8337	0.0515	0.0038	0.2330	0.0160	0.0332	0.0007	0.14	263	169	213	14	211	4	211	4	n/a				
44	170322_076.FIN2	165	2.4	30.9215	0.7649	0.0512	0.0024	0.2280	0.0110	0.0323	0.0005	0.21	250	108	207	9	205	3	205	3	n/a				
45	170322_077.FIN2	237	2.6	30.6466	0.8735	0.0512	0.0025	0.2310	0.0120	0.0326	0.0007	0.36	250	112	210	10	207	4	207	4	n/a				
46	170322_078.FIN2	351	2.8	30.1477	0.7544	0.0512	0.0023	0.2340	0.0110	0.0332	0.0005	0.18	250	103	213	9	210	3	210	3	n/a				
47	170322_079.FIN2	383	3.8	30.3122	1.0107	0.0518	0.0031	0.2360	0.0140	0.0330	0.0009	0.25	277	137	215	12	209	6	209	6	n/a				
48	170322_080.FIN2	818	3.4	31.0945	0.7155	0.0510	0.0014	0.2268	0.0065	0.0322	0.0004	0.36	241	63	207	5	204	3	204	3	n/a				
49	170322_081.FIN2	311	2.8	28.6697	0.8220	0.0503	0.0031	0.2420	0.0150	0.0349	0.0008	0.24	209	143	219	12	221	5	221	5	n/a				

Grain	Spot name	isotopic ratios										isotopic ages									
		U	U/Th	$^{238}\text{U}/$		$^{207}\text{Pb}/$		^{207}Pb		^{206}Pb		rho*	^{207}Pb	\pm	^{207}Pb	\pm	^{206}Pb	\pm	Best	\pm	
				(ppm)	^{206}Pb	2SE	^{206}Pb	2SE	^{235}U	2SE	^{238}U	2SE									
50	170322_082.FIN2	242	3.0	30.1024	0.9968	0.0511	0.0028	0.2340	0.0130	0.0332	0.0008	0.15	245	126	212	10	211	5	211	5	n/a
52	170322_090.FIN2	178	3.1	28.8018	0.7466	0.0520	0.0028	0.2490	0.0130	0.0347	0.0006	0.18	285	123	225	11	220	4	220	4	n/a
53	170322_091.FIN2	256	2.4	29.3255	1.1180	0.0511	0.0039	0.2410	0.0200	0.0341	0.0011	0.40	245	176	218	16	216	7	216	7	n/a
54	170322_092.FIN2	139	3.6	27.9720	0.7824	0.0521	0.0030	0.2560	0.0140	0.0358	0.0007	0.14	290	132	230	12	226	4	226	4	n/a
55	170322_093.FIN2	167	3.9	31.1624	0.8837	0.0529	0.0033	0.2220	0.0140	0.0321	0.0007	0.23	325	142	203	12	204	4	204	4	n/a
56	170322_094.FIN2	635	2.4	31.2695	0.8800	0.0503	0.0017	0.2220	0.0081	0.0320	0.0007	0.39	209	78	203	7	203	4	203	4	n/a
57	170322_095.FIN2	141	1.9	31.0656	0.8010	0.0520	0.0027	0.2300	0.0120	0.0322	0.0006	0.13	285	119	209	10	204	3	204	3	n/a
58	170322_096.FIN2	131	2.7	29.9401	1.3446	0.0517	0.0051	0.2360	0.0220	0.0334	0.0013	0.02	272	226	214	18	212	8	212	8	n/a
60	170322_098.FIN2	152	2.8	28.5225	0.8135	0.0512	0.0036	0.2440	0.0170	0.0351	0.0008	0.21	250	162	223	15	222	5	222	5	n/a
61	170322_105.FIN2	253	3.7	30.4229	0.7867	0.0508	0.0024	0.2300	0.0100	0.0329	0.0006	0.07	232	109	209	8	209	4	209	4	n/a
62	170322_106.FIN2	335	2.3	31.2013	0.7496	0.0512	0.0017	0.2253	0.0079	0.0321	0.0005	0.41	250	76	206	7	203	3	203	3	n/a
63	170322_107.FIN2	592	5.8	29.6384	0.8609	0.0505	0.0016	0.2357	0.0085	0.0337	0.0007	0.49	218	73	215	7	214	5	214	5	n/a
64	170322_108.FIN2	230	1.6	30.8261	0.7412	0.0503	0.0022	0.2260	0.0100	0.0324	0.0005	0.08	209	101	207	8	206	3	206	3	n/a
65	170322_109.FIN2	144	2.8	30.0752	0.7779	0.0510	0.0027	0.2310	0.0110	0.0333	0.0006	0.07	241	122	211	10	211	4	211	4	n/a
66	170322_110.FIN2	131	3.0	29.9401	0.7888	0.0514	0.0040	0.2370	0.0180	0.0334	0.0006	0.26	259	179	214	14	212	4	212	4	n/a
67	170322_111.FIN2	214	1.9	30.3859	0.8217	0.0508	0.0024	0.2300	0.0100	0.0329	0.0006	0.14	232	109	210	9	209	4	209	4	n/a
68	170322_112.FIN2	210	2.3	29.9312	0.8780	0.0507	0.0031	0.2330	0.0140	0.0334	0.0007	0.02	227	141	212	11	212	5	212	5	n/a
69	170322_113.FIN2	213	2.2	30.4600	0.7608	0.0509	0.0020	0.2308	0.0094	0.0328	0.0005	0.20	236	91	210	8	208	3	208	3	n/a
72	170322_122.FIN2	216	2.8	28.5633	0.7506	0.0512	0.0021	0.2470	0.0110	0.0350	0.0006	0.35	250	94	224	9	222	4	222	4	n/a
73	170322_123.FIN2	75	2.6	13.4409	0.3432	0.0572	0.0031	0.5890	0.0340	0.0744	0.0013	0.26	499	119	465	21	464	8	464	8	n/a
75	170322_125.FIN2	159	3.5	28.3286	0.7624	0.0513	0.0027	0.2490	0.0130	0.0353	0.0007	0.12	254	121	224	10	224	4	224	4	n/a
76	170322_126.FIN2	125	3.3	29.7265	0.7953	0.0510	0.0031	0.2360	0.0140	0.0336	0.0006	0.05	241	140	214	12	213	4	213	4	n/a
77	170322_127.FIN2	254	4.0	29.6209	0.7546	0.0506	0.0019	0.2357	0.0091	0.0338	0.0006	0.29	223	87	214	8	214	3	214	3	n/a
78	170322_128.FIN2	169	2.7	30.2115	1.0040	0.0514	0.0041	0.2350	0.0180	0.0331	0.0009	0.23	259	183	213	15	210	6	210	6	n/a

Grain	Spot name	isotopic ratios												isotopic ages								
		U	U/Th	$^{238}\text{U}/$	$^{207}\text{Pb}/$		^{207}Pb		^{206}Pb			^{207}Pb	\pm	^{207}Pb	\pm	^{206}Pb	\pm	Best	\pm			
		(ppm)		^{206}Pb	2SE	^{206}Pb	2SE	^{235}U	2SE	^{238}U	2SE	rho*	^{206}Pb	(Ma)	^{235}U	(Ma)	^{238}U	(Ma)	Age	(Ma)	conc.	
79	170322_129.FIN2	117	2.7	30.6749	1.2232	0.0530	0.0040	0.2270	0.0180	0.0326	0.0011	0.30	329	171	207	15	207	7	207	7	n/a	
80	170322_130.FIN2	230	2.9	29.5858	0.7003	0.0506	0.0018	0.2349	0.0086	0.0338	0.0005	0.23	223	82	214	7	214	3	214	3	n/a	
81	170322_138.FIN2	170	2.9	29.4724	0.8686	0.0516	0.0042	0.2410	0.0190	0.0339	0.0008	0.26	268	187	219	16	215	5	215	5	n/a	
82	170322_139.FIN2	123	3.1	30.2755	0.7608	0.0508	0.0023	0.2310	0.0110	0.0330	0.0005	0.17	232	105	210	9	210	3	210	3	n/a	
83	170322_140.FIN2	290	3.6	29.7354	0.8046	0.0509	0.0032	0.2370	0.0160	0.0336	0.0006	0.38	236	145	215	13	213	4	213	4	n/a	
84	170322_141.FIN2	145	2.9	29.3341	0.8605	0.0509	0.0036	0.2390	0.0170	0.0341	0.0008	0.22	236	163	216	14	216	5	216	5	n/a	
85	170322_142.FIN2	104	2.4	30.1114	0.8614	0.0514	0.0036	0.2360	0.0160	0.0332	0.0007	0.04	259	161	214	13	211	4	211	4	n/a	
87	170322_144.FIN2	148	1.9	31.0559	0.8487	0.0513	0.0028	0.2270	0.0130	0.0322	0.0006	0.16	254	126	207	11	204	4	204	4	n/a	
89	170322_146.FIN2	174	2.4	30.4321	0.7779	0.0513	0.0022	0.2330	0.0100	0.0329	0.0006	0.26	254	99	212	8	208	4	208	4	n/a	
90	170322_147.FIN2	182	2.2	29.9401	1.1653	0.0507	0.0043	0.2330	0.0200	0.0334	0.0011	0.22	227	196	211	16	212	7	212	7	n/a	
91	170322_154.FIN2	220	2.3	30.5064	0.9027	0.0514	0.0032	0.2320	0.0140	0.0328	0.0007	0.16	259	143	211	12	208	5	208	5	n/a	
92	170322_155.FIN2	172	2.4	18.2815	0.6684	0.0545	0.0037	0.4120	0.0310	0.0547	0.0016	0.30	392	152	349	22	343	10	343	10	n/a	
94	170322_157.FIN2	198	3.3	29.0782	0.7948	0.0523	0.0027	0.2480	0.0130	0.0344	0.0007	0.22	299	118	224	11	218	4	218	4	n/a	
95	170322_158.FIN2	108	2.7	27.9330	1.0924	0.0517	0.0050	0.2540	0.0240	0.0358	0.0012	0.03	272	222	228	19	227	7	227	7	n/a	
96	170322_159.FIN2	245	1.9	30.4136	0.8602	0.0502	0.0029	0.2330	0.0140	0.0329	0.0007	0.26	204	134	212	12	209	4	209	4	n/a	
99	170322_162.FIN2	240	2.8	27.3373	0.6651	0.0511	0.0021	0.2580	0.0100	0.0366	0.0005	0.20	245	95	232	8	232	3	232	3	n/a	
100	170322_163.FIN2	360	3.3	29.6121	0.7190	0.0508	0.0018	0.2364	0.0085	0.0338	0.0005	0.26	232	82	215	7	214	3	214	3	n/a	
101	170324_055.FIN2	219	2.5	29.0867	1.0152	0.0515	0.0021	0.2420	0.0100	0.0344	0.0006	0.27	263	94	219	8	218	4	218	4	n/a	
102	170324_056.FIN2	330	2.0	31.6156	1.2994	0.0506	0.0024	0.2170	0.0110	0.0316	0.0008	0.34	223	110	199	9	201	5	201	5	n/a	
103	170324_057.FIN2	117	3.5	18.4843	0.6833	0.0547	0.0028	0.3990	0.0200	0.0541	0.0011	0.32	400	115	339	14	340	7	340	7	n/a	
104	170324_058.FIN2	192	2.5	29.6912	1.0579	0.0518	0.0026	0.2360	0.0110	0.0337	0.0006	0.04	277	115	214	9	214	4	214	4	n/a	
105	170324_059.FIN2	267	2.3	29.7708	1.0636	0.0514	0.0029	0.2350	0.0140	0.0336	0.0006	0.32	259	130	214	12	213	4	213	4	n/a	
106	170324_060.FIN2	232	3.0	29.0192	1.0947	0.0518	0.0022	0.2410	0.0100	0.0345	0.0007	0.31	277	97	219	8	218	4	218	4	n/a	
107	170324_061.FIN2	290	1.9	29.5421	0.9600	0.0510	0.0014	0.2367	0.0065	0.0339	0.0005	0.25	241	63	215	5	215	3	215	3	n/a	

Grain	Spot name	isotopic ratios										isotopic ages									
		U	U/Th	$^{238}\text{U}/$	$^{207}\text{Pb}/$		^{207}Pb		^{206}Pb			^{207}Pb	\pm	^{207}Pb	\pm	^{206}Pb	\pm	Best	\pm		
		(ppm)		^{206}Pb	2SE	^{206}Pb	2SE	^{235}U	2SE	^{238}U	2SE	rho*	^{206}Pb	(Ma)	^{235}U	(Ma)	^{238}U	(Ma)	Age	(Ma)	conc.
108	170324_062.FIN2	179	2.8	30.9789	1.2476	0.0513	0.0027	0.2250	0.0120	0.0323	0.0008	0.23	254	121	205	10	205	5	205	5	n/a
109	170324_063.FIN2	382	1.6	32.2373	1.4549	0.0510	0.0034	0.2160	0.0170	0.0310	0.0010	0.58	241	154	198	14	197	6	197	6	n/a
110	170324_064.FIN2	269	2.0	29.3255	1.2900	0.0522	0.0053	0.2420	0.0230	0.0341	0.0010	0.26	294	232	219	19	216	7	216	7	n/a
Rejected Analysis																					
7	170322_015.FIN2	303	6.7	28.9268	0.7112	0.0553	0.0025	0.2640	0.0120	0.0346	0.0005	0.02	424	101	237	9	219	3	219	3	n/a
17	170322_031.FIN2	289	3.3	20.3666	0.8296	0.0534	0.0046	0.3620	0.0320	0.0491	0.0018	0.25	346	195	312	23	309	11	309	11	n/a
28	170322_048.FIN2	295	2.4	31.4564	0.8015	0.0521	0.0022	0.2277	0.0097	0.0318	0.0005	0.29	290	96	208	8	202	3	202	3	n/a
29	170322_049.FIN2	286	2.3	32.1647	0.9001	0.0514	0.0026	0.2210	0.0120	0.0311	0.0006	0.25	259	116	202	10	197	4	197	4	n/a
36	170322_062.FIN2	203	1.9	19.4175	0.8672	0.0539	0.0062	0.3810	0.0420	0.0515	0.0021	0.26	367	259	326	31	323	13	323	13	n/a
38	170322_064.FIN2	70	2.8	22.5225	0.7609	0.2020	0.0110	1.2440	0.0760	0.0444	0.0013	0.35	2842	89	813	34	280	8	280	8	n/a
43	170322_075.FIN2	471	2.0	31.6857	0.8233	0.0507	0.0019	0.2222	0.0088	0.0316	0.0006	0.26	227	87	203	7	200	3	200	3	n/a
51	170322_089.FIN2	313	1.4	28.7522	0.8019	0.0728	0.0047	0.3490	0.0230	0.0348	0.0007	0.20	1008	131	303	17	220	4	220	4	n/a
59	170322_097.FIN2	435	2.0	13.7741	0.4174	0.0561	0.0024	0.5630	0.0260	0.0726	0.0016	0.41	456	95	452	17	452	10	452	10	n/a
70	170322_114.FIN2	171	2.4	29.7885	0.8430	0.0567	0.0033	0.2620	0.0150	0.0336	0.0007	0.11	480	129	235	12	213	4	213	4	n/a
71	170322_121.FIN2	331	2.9	30.6373	1.0325	0.0711	0.0046	0.3190	0.0190	0.0326	0.0009	0.03	960	132	280	15	207	6	207	6	n/a
74	170322_124.FIN2	130	2.6	28.1136	0.6797	0.0515	0.0023	0.2520	0.0110	0.0356	0.0005	0.15	263	103	227	9	225	3	225	3	n/a
86	170322_143.FIN2	159	3.1	30.6749	1.1291	0.0542	0.0050	0.2320	0.0200	0.0326	0.0011	0.05	379	207	211	16	207	7	207	7	n/a
88	170322_145.FIN2	300	2.3	31.2500	1.1719	0.0500	0.0040	0.2200	0.0180	0.0320	0.0010	0.27	195	186	202	15	203	7	203	7	n/a
93	170322_156.FIN2	194	2.1	30.2755	0.9166	0.0517	0.0040	0.2360	0.0190	0.0330	0.0008	0.20	272	177	214	16	210	5	210	5	n/a
97	170322_160.FIN2	126	2.2	29.0107	0.8416	0.0515	0.0040	0.2430	0.0190	0.0345	0.0008	0.19	263	178	219	15	218	5	218	5	n/a
98	170322_161.FIN2	210	1.5	3.9841	0.2381	0.0921	0.0044	3.1900	0.2200	0.2510	0.0140	0.73	1469	91	1451	53	1444	72	1469	91	98

Grain	Spot name	isotopic ratios										isotopic ages							
		U	U/Th	$^{238}\text{U}/$	$^{207}\text{Pb}/$		^{207}Pb		^{206}Pb			^{207}Pb	\pm	^{207}Pb	\pm	^{206}Pb	\pm	Best	\pm
		(ppm)		^{206}Pb	2SE	^{206}Pb	2SE	^{235}U	2SE	^{238}U	2SE	rho*	^{206}Pb	(Ma)	^{235}U	(Ma)	^{238}U	(Ma)	Age

Whitehorse trough - Richthofen formation - Sample 16-LVD-022, Lake Laberge (Zone 08V 493602E 6778206N NAD 83)

Grain	Spot name	isotopic ratios										isotopic ages									
		U	U/Th	$^{238}\text{U}/$	$^{207}\text{Pb}/$		^{207}Pb		^{206}Pb			^{207}Pb	\pm	^{207}Pb	\pm	^{206}Pb	\pm	Best	\pm		
		(ppm)		^{206}Pb	2SE	^{206}Pb	2SE	^{235}U	2SE	^{238}U	2SE	rho	^{206}Pb	(Ma)	^{235}U	(Ma)	^{238}U	(Ma)	Age	(Ma)	conc.
1	170124_011.FIN2	82	1.9	30.9024	0.9550	0.0520	0.0028	0.2300	0.0130	0.0324	0.0006	0.27	285	123	210	11	205	4	205	4	n/a
2	170124_012.FIN2	151	1.7	30.7503	0.8321	0.0510	0.0013	0.2276	0.0059	0.0325	0.0004	0.18	241	59	208	5	206	2	206	2	n/a
4	170124_014.FIN2	219	2.5	31.8776	0.8536	0.0509	0.0013	0.2183	0.0054	0.0314	0.0003	0.16	236	59	200	5	199	2	199	2	n/a
5	170124_015.FIN2	391	1.9	31.1430	1.0669	0.0496	0.0013	0.2187	0.0068	0.0321	0.0007	0.59	176	61	201	6	204	5	204	5	n/a
6	170124_016.FIN2	270	2.3	31.4862	0.9914	0.0505	0.0019	0.2204	0.0082	0.0318	0.0007	0.16	218	87	202	7	202	4	202	4	n/a
7	170124_017.FIN2	259	2.3	32.6584	0.9492	0.0505	0.0013	0.2120	0.0055	0.0306	0.0005	0.25	218	60	195	5	194	3	194	3	n/a
8	170124_018.FIN2	161	2.3	30.0030	0.9002	0.0511	0.0019	0.2328	0.0084	0.0333	0.0006	0.23	245	86	212	7	211	4	211	4	n/a
9	170124_019.FIN2	124	3.4	31.8167	0.9414	0.0494	0.0019	0.2147	0.0092	0.0314	0.0005	0.36	167	90	197	8	200	3	200	3	n/a
10	170124_020.FIN2	181	2.7	29.9491	0.8969	0.0508	0.0025	0.2330	0.0120	0.0334	0.0006	0.21	232	114	212	10	212	4	212	4	n/a
11	170124_021.FIN2	168	1.8	30.9406	0.9095	0.0502	0.0016	0.2240	0.0080	0.0323	0.0005	0.36	204	74	206	7	205	3	205	3	n/a
12	170124_022.FIN2	141	2.2	32.2373	0.9561	0.0505	0.0018	0.2132	0.0089	0.0310	0.0005	0.37	218	83	197	7	197	3	197	3	n/a
13	170124_029.FIN2	158	2.1	31.0174	0.8755	0.0507	0.0015	0.2240	0.0066	0.0322	0.0004	0.26	227	68	205	6	205	3	205	3	n/a
14	170124_030.FIN2	260	1.9	30.5157	0.9312	0.0507	0.0018	0.2278	0.0083	0.0328	0.0007	0.34	227	82	208	7	208	4	208	4	n/a
15	170124_031.FIN2	152	2.6	29.8508	0.8465	0.0508	0.0016	0.2336	0.0075	0.0335	0.0005	0.24	232	73	213	6	212	3	212	3	n/a
16	170124_032.FIN2	67	1.2	18.8608	0.5692	0.0532	0.0021	0.3880	0.0160	0.0530	0.0009	0.21	337	89	333	11	333	5	333	5	n/a
17	170124_033.FIN2	125	3.4	30.3306	0.9107	0.0508	0.0022	0.2300	0.0100	0.0330	0.0006	0.30	232	100	210	9	209	4	209	4	n/a
19	170124_035.FIN2	119	1.3	18.5117	0.5826	0.0541	0.0018	0.4040	0.0170	0.0540	0.0010	0.51	375	75	344	12	339	6	339	6	n/a
20	170124_036.FIN2	176	2.2	30.3122	0.9188	0.0511	0.0018	0.2311	0.0086	0.0330	0.0006	0.30	245	81	211	7	209	4	209	4	n/a

Grain	Spot name	isotopic ratios										isotopic ages										Best	\pm	
		U	U/Th	$^{238}\text{U}/$		$^{207}\text{Pb}/$		^{207}Pb		^{206}Pb		rho*	^{206}Pb	(Ma)	^{207}Pb		\pm	^{207}Pb		\pm	^{206}Pb		\pm	
				(ppm)	^{206}Pb	2SE	^{206}Pb	2SE	^{235}U	2SE	^{238}U	2SE			^{235}U	(Ma)	^{238}U	(Ma)	Age	(Ma)	conc.			
23	170124_039.FIN2	178	2.1	31.5060	0.8636	0.0504	0.0014	0.2205	0.0062	0.0317	0.0004	0.25	213	64	202	5	201	2	201	2	n/a			
24	170124_040.FIN2	131	1.9	31.8066	0.9813	0.0505	0.0021	0.2180	0.0099	0.0314	0.0006	0.31	218	96	200	8	200	4	200	4	n/a			
25	170124_047.FIN2	93	2.5	30.8072	0.9491	0.0508	0.0027	0.2260	0.0120	0.0325	0.0006	0.14	232	123	206	10	206	4	206	4	n/a			
26	170124_048.FIN2	120	2.7	31.2402	0.8784	0.0510	0.0020	0.2249	0.0092	0.0320	0.0004	0.30	241	90	205	8	203	3	203	3	n/a			
27	170124_049.FIN2	312	2.3	31.7158	0.9958	0.0507	0.0019	0.2196	0.0075	0.0315	0.0006	0.13	227	87	201	6	200	4	200	4	n/a			
28	170124_050.FIN2	116	2.7	30.3767	0.8766	0.0506	0.0017	0.2285	0.0078	0.0329	0.0005	0.17	223	78	209	7	209	3	209	3	n/a			
29	170124_051.FIN2	175	2.3	30.7220	0.8683	0.0511	0.0020	0.2292	0.0092	0.0326	0.0004	0.24	245	90	209	8	207	3	207	3	n/a			
30	170124_052.FIN2	405	2.3	31.5358	0.9448	0.0510	0.0015	0.2217	0.0063	0.0317	0.0005	0.35	241	68	203	5	201	3	201	3	n/a			
31	170124_053.FIN2	151	2.6	30.6373	0.8354	0.0501	0.0012	0.2263	0.0059	0.0326	0.0004	0.24	200	56	207	5	207	2	207	2	n/a			
32	170124_054.FIN2	132	2.1	22.9885	0.7927	0.0522	0.0032	0.3110	0.0180	0.0435	0.0010	0.18	294	140	275	14	274	6	274	6	n/a			
34	170124_056.FIN2	135	2.1	31.0078	0.9615	0.0514	0.0023	0.2253	0.0092	0.0323	0.0007	0.02	259	103	206	8	205	4	205	4	n/a			
35	170124_057.FIN2	100	2.3	30.6560	0.9398	0.0512	0.0022	0.2290	0.0100	0.0326	0.0006	0.22	250	99	209	8	207	4	207	4	n/a			
36	170124_058.FIN2	254	1.6	31.2305	0.8876	0.0501	0.0014	0.2205	0.0059	0.0320	0.0005	0.26	200	65	203	5	203	3	203	3	n/a			
37	170124_065.FIN2	238	1.9	31.5956	0.8585	0.0503	0.0011	0.2195	0.0051	0.0317	0.0004	0.32	209	51	201	4	201	2	201	2	n/a			
38	170124_066.FIN2	555	3.5	31.4070	0.8582	0.0505	0.0009	0.2224	0.0043	0.0318	0.0004	0.34	217	43	204	4	202	2	202	2	n/a			
39	170124_067.FIN2	427	1.6	31.0752	0.9657	0.0504	0.0015	0.2236	0.0073	0.0322	0.0007	0.44	213	69	205	6	204	4	204	4	n/a			
40	170124_068.FIN2	236	2.2	30.0391	0.8392	0.0506	0.0013	0.2318	0.0065	0.0333	0.0004	0.35	223	59	211	5	211	3	211	3	n/a			
41	170124_069.FIN2	236	2.5	30.4785	0.8360	0.0505	0.0011	0.2282	0.0049	0.0328	0.0004	0.25	218	50	208	4	208	2	208	2	n/a			
42	170124_070.FIN2	314	2.2	31.1139	0.9294	0.0497	0.0015	0.2230	0.0073	0.0321	0.0005	0.26	181	70	204	6	204	3	204	3	n/a			
43	170124_071.FIN2	241	2.5	31.1527	1.0675	0.0506	0.0028	0.2240	0.0120	0.0321	0.0008	0.22	223	128	204	10	204	5	204	5	n/a			
44	170124_072.FIN2	241	1.8	30.9693	0.8440	0.0503	0.0013	0.2234	0.0057	0.0323	0.0004	0.21	209	60	205	5	205	2	205	2	n/a			
45	170124_073.FIN2	255	2.5	31.3972	1.0844	0.0509	0.0027	0.2240	0.0120	0.0319	0.0008	0.20	236	122	205	10	202	5	202	5	n/a			
46	170124_074.FIN2	161	2.4	31.8979	0.9157	0.0504	0.0018	0.2177	0.0079	0.0314	0.0005	0.15	213	83	199	7	199	3	199	3	n/a			
47	170124_075.FIN2	158	1.7	30.3398	1.0126	0.0509	0.0029	0.2310	0.0120	0.0330	0.0007	0.25	236	131	211	10	209	5	209	5	n/a			

Grain	Spot name	isotopic ratios												isotopic ages									
		U (ppm)	U/Th	$^{238}\text{U}/$		$^{207}\text{Pb}/$		^{207}Pb		^{206}Pb		rho*	^{206}Pb (Ma)	^{207}Pb (Ma)	^{207}Pb (Ma)	^{206}Pb (Ma)	^{238}U (Ma)	Best	\pm				
				^{206}Pb	2SE	^{206}Pb	2SE	^{235}U	2SE	^{238}U	2SE												
48	170124_076.FIN2	158	2.1	31.7058	0.9047	0.0506	0.0016	0.2209	0.0071	0.0315	0.0005	0.32	223	73	202	6	200	3	200	3	n/a		
49	170124_083.FIN2	304	2.4	29.8329	0.8722	0.0504	0.0016	0.2336	0.0074	0.0335	0.0005	0.26	213	74	213	6	213	3	213	3	n/a		
50	170124_084.FIN2	318	2.1	30.9119	0.8695	0.0501	0.0014	0.2255	0.0066	0.0324	0.0004	0.27	200	65	206	5	205	3	205	3	n/a		
51	170124_085.FIN2	535	2.5	30.9789	0.8349	0.0503	0.0010	0.2243	0.0045	0.0323	0.0003	0.35	207	44	205	4	205	2	205	2	n/a		
52	170124_086.FIN2	283	2.2	31.1236	1.0655	0.0505	0.0022	0.2237	0.0090	0.0321	0.0007	0.15	218	101	205	8	204	5	204	5	n/a		
53	170124_087.FIN2	262	2.2	32.8192	0.9694	0.0506	0.0018	0.2146	0.0074	0.0305	0.0005	0.24	223	82	197	6	194	3	194	3	n/a		
54	170124_088.FIN2	297	2.0	31.6556	0.9520	0.0505	0.0015	0.2206	0.0067	0.0316	0.0005	0.30	218	69	202	6	201	3	201	3	n/a		
55	170124_089.FIN2	128	1.3	31.2305	0.9461	0.0502	0.0023	0.2218	0.0099	0.0320	0.0006	0.16	204	106	204	8	203	4	203	4	n/a		
56	170124_090.FIN2	164	2.6	31.3873	0.8472	0.0507	0.0011	0.2231	0.0047	0.0319	0.0004	0.21	227	50	204	4	202	2	202	2	n/a		
57	170124_091.FIN2	582	3.5	31.1624	0.9031	0.0501	0.0011	0.2234	0.0058	0.0321	0.0005	0.53	200	51	205	5	204	3	204	3	n/a		
58	170124_092.FIN2	159	2.9	30.9119	0.8504	0.0506	0.0014	0.2273	0.0065	0.0324	0.0004	0.26	223	64	207	5	205	3	205	3	n/a		
59	170124_093.FIN2	119	2.9	31.5956	0.9583	0.0508	0.0022	0.2212	0.0096	0.0317	0.0006	0.24	232	100	202	8	201	4	201	4	n/a		
60	170124_100.FIN2	168	1.9	30.0300	0.8928	0.0505	0.0018	0.2324	0.0081	0.0333	0.0006	0.13	218	83	212	7	211	3	211	3	n/a		
63	170124_103.FIN2	417	3.7	30.7977	0.9485	0.0503	0.0015	0.2262	0.0071	0.0325	0.0006	0.45	209	69	207	6	206	4	206	4	n/a		
64	170124_104.FIN2	507	3.0	31.0656	0.8686	0.0501	0.0012	0.2234	0.0061	0.0322	0.0004	0.43	200	56	204	5	204	3	204	3	n/a		
65	170124_105.FIN2	178	2.9	30.6279	0.9381	0.0504	0.0023	0.2270	0.0100	0.0327	0.0007	0.17	213	106	207	8	207	4	207	4	n/a		
66	170124_106.FIN2	159	2.7	31.8471	0.9737	0.0502	0.0017	0.2185	0.0075	0.0314	0.0006	0.18	204	79	200	6	199	4	199	4	n/a		
68	170124_108.FIN2	107	3.0	30.7977	0.8821	0.0508	0.0018	0.2278	0.0080	0.0325	0.0005	0.23	232	82	208	7	206	3	206	3	n/a		
71	170124_111.FIN2	125	2.3	30.9885	0.8643	0.0509	0.0015	0.2268	0.0067	0.0323	0.0004	0.24	236	68	207	6	205	3	205	3	n/a		
72	170124_118.FIN2	132	2.1	30.2389	0.9144	0.0509	0.0028	0.2310	0.0120	0.0331	0.0006	0.11	236	127	211	10	210	4	210	4	n/a		
73	170124_119.FIN2	588	2.7	31.0849	0.8890	0.0508	0.0009	0.2248	0.0044	0.0322	0.0005	0.47	233	41	206	4	204	3	204	3	n/a		
75	170124_121.FIN2	186	1.9	30.8642	0.8478	0.0503	0.0012	0.2244	0.0056	0.0324	0.0004	0.27	209	55	206	5	206	2	206	2	n/a		
76	170124_122.FIN2	324	2.1	32.0205	0.8818	0.0502	0.0012	0.2157	0.0053	0.0312	0.0004	0.29	204	55	199	5	198	2	198	2	n/a		
77	170124_123.FIN2	160	1.9	30.9502	0.8717	0.0508	0.0014	0.2249	0.0064	0.0323	0.0004	0.27	232	64	205	5	205	3	205	3	n/a		

Grain	Spot name	isotopic ratios										isotopic ages									
		U	U/Th	$^{238}\text{U}/$	$^{207}\text{Pb}/$		^{207}Pb		^{206}Pb		^{207}Pb	\pm	^{207}Pb	\pm	^{206}Pb	\pm	Best	\pm			
		(ppm)		^{206}Pb	2SE	^{206}Pb	2SE	^{235}U	2SE	^{238}U	2SE	rho*	^{206}Pb	(Ma)	^{235}U	(Ma)	^{238}U	(Ma)	Age	(Ma)	conc.
78	170124_124.FIN2	237	1.8	31.2402	0.8491	0.0507	0.0011	0.2233	0.0049	0.0320	0.0004	0.29	227	50	204	4	203	2	203	2	n/a
79	170124_125.FIN2	151	1.9	30.4507	1.0200	0.0510	0.0025	0.2320	0.0130	0.0328	0.0007	0.46	241	113	211	11	208	5	208	5	n/a
80	170124_126.FIN2	298	1.7	30.1750	0.8559	0.0507	0.0018	0.2312	0.0077	0.0331	0.0005	0.10	227	82	211	6	210	3	210	3	n/a
82	170124_128.FIN2	345	2.9	30.5624	0.8780	0.0506	0.0012	0.2271	0.0055	0.0327	0.0005	0.34	223	55	208	5	208	3	208	3	n/a
83	170124_129.FIN2	328	1.9	29.5508	0.8471	0.0495	0.0014	0.2305	0.0068	0.0338	0.0005	0.38	172	66	210	6	215	3	215	3	n/a
84	170124_136.FIN2	159	2.4	30.7692	0.8331	0.0504	0.0012	0.2254	0.0056	0.0325	0.0003	0.32	213	55	206	5	206	2	206	2	n/a
85	170124_137.FIN2	172	2.7	31.1721	0.9717	0.0498	0.0015	0.2229	0.0083	0.0321	0.0006	0.51	186	70	204	7	204	4	204	4	n/a
86	170124_138.FIN2	202	1.8	31.0752	0.8498	0.0507	0.0013	0.2247	0.0058	0.0322	0.0004	0.28	227	59	205	5	204	2	204	2	n/a
88	170124_140.FIN2	107	2.1	30.4044	0.8874	0.0498	0.0020	0.2251	0.0094	0.0329	0.0005	0.28	186	94	206	8	209	3	209	3	n/a
89	170124_141.FIN2	164	1.9	30.9981	0.9609	0.0511	0.0028	0.2260	0.0130	0.0323	0.0006	0.27	245	126	207	10	205	4	205	4	n/a
90	170124_142.FIN2	78	3.0	29.2312	1.0254	0.0506	0.0030	0.2400	0.0140	0.0342	0.0009	0.12	223	137	217	12	217	5	217	5	n/a
91	170124_143.FIN2	230	2.7	29.5159	0.8538	0.0508	0.0014	0.2364	0.0067	0.0339	0.0005	0.31	232	64	215	6	215	3	215	3	n/a
92	170124_144.FIN2	167	2.1	30.5530	0.8681	0.0506	0.0016	0.2268	0.0075	0.0327	0.0005	0.39	223	73	208	6	208	3	208	3	n/a
93	170124_145.FIN2	232	2.3	30.3675	0.8392	0.0511	0.0012	0.2296	0.0052	0.0329	0.0004	0.18	245	54	210	4	209	3	209	3	n/a
94	170124_146.FIN2	144	2.0	30.5344	0.9323	0.0509	0.0020	0.2282	0.0085	0.0328	0.0006	0.13	236	91	208	7	208	4	208	4	n/a
95	170124_147.FIN2	234	2.0	30.7787	0.9284	0.0507	0.0015	0.2257	0.0066	0.0325	0.0006	0.27	227	68	206	6	206	4	206	4	n/a
96	170124_154.FIN2	85	2.4	30.7220	1.0382	0.0505	0.0023	0.2270	0.0110	0.0326	0.0008	0.27	218	105	207	9	206	5	206	5	n/a
97	170124_155.FIN2	93	2.5	30.1114	0.8251	0.0510	0.0016	0.2324	0.0074	0.0332	0.0004	0.15	241	72	211	6	211	2	211	2	n/a
98	170124_156.FIN2	140	2.7	30.8452	0.8848	0.0506	0.0017	0.2262	0.0076	0.0324	0.0005	0.16	223	78	207	6	206	3	206	3	n/a
99	170124_157.FIN2	149	2.6	30.0571	0.8763	0.0507	0.0016	0.2317	0.0080	0.0333	0.0005	0.35	227	73	211	7	211	3	211	3	n/a
100	170124_158.FIN2	166	2.2	30.8261	0.8267	0.0507	0.0012	0.2255	0.0052	0.0324	0.0003	0.15	227	55	206	4	206	2	206	2	n/a
101	170124_159.FIN2	122	1.9	30.5810	0.9352	0.0505	0.0023	0.2261	0.0099	0.0327	0.0006	0.10	218	105	207	9	207	4	207	4	n/a
102	170124_160.FIN2	130	2.8	30.2206	1.0046	0.0511	0.0027	0.2310	0.0120	0.0331	0.0008	0.12	245	122	210	10	210	5	210	5	n/a
103	170124_161.FIN2	233	2.0	31.9898	1.0233	0.0510	0.0022	0.2188	0.0098	0.0313	0.0006	0.28	241	99	200	8	198	4	198	4	n/a

Grain	Spot name	isotopic ratios												isotopic ages									
		U	U/Th	$^{238}\text{U}/$		$^{207}\text{Pb}/$		^{207}Pb		^{206}Pb				^{207}Pb	\pm	^{207}Pb	\pm	^{206}Pb	\pm	Best	\pm		
		(ppm)		^{206}Pb	2SE	^{206}Pb	2SE	^{235}U	2SE	^{238}U	2SE	rho*	^{206}Pb	(Ma)	^{235}U	(Ma)	^{238}U	(Ma)	Age	(Ma)			
104	170124_162.FIN2	143	2.2	30.4136	0.8787	0.0511	0.0016	0.2303	0.0076	0.0329	0.0005	0.30	245	72	210	6	209	3	209	3	n/a		
105	170124_163.FIN2	191	2.2	29.9760	0.8536	0.0510	0.0014	0.2326	0.0060	0.0334	0.0005	0.28	241	63	213	5	212	3	212	3	n/a		
106	170124_164.FIN2	140	2.0	30.9215	0.8796	0.0508	0.0017	0.2249	0.0077	0.0323	0.0005	0.25	232	77	206	7	205	3	205	3	n/a		
107	170124_165.FIN2	166	2.5	29.7265	0.9720	0.0512	0.0021	0.2360	0.0097	0.0336	0.0007	0.25	250	94	215	8	213	5	213	5	n/a		
108	170124_166.FIN2	129	2.7	30.5344	1.0256	0.0507	0.0023	0.2277	0.0099	0.0328	0.0007	0.19	227	105	208	8	208	5	208	5	n/a		
109	170124_167.FIN2	160	2.6	31.1333	0.8627	0.0509	0.0014	0.2244	0.0062	0.0321	0.0004	0.23	236	63	205	5	204	2	204	2	n/a		
110	170124_168.FIN2	296	1.7	31.4762	0.8818	0.0498	0.0011	0.2175	0.0051	0.0318	0.0004	0.44	186	51	200	4	202	3	202	3	n/a		
Rejected Analysis																							
3	170124_013.FIN2	72	2.3	31.2013	0.8762	0.0478	0.0019	0.2105	0.0082	0.0321	0.0004	0.11	89	94	193	7	203	3	203	3	n/a		
18	170124_034.FIN2	173	2.6	28.6780	0.9047	0.0509	0.0011	0.2416	0.0065	0.0349	0.0006	0.54	236	50	219	5	221	4	221	4	n/a		
21	170124_037.FIN2	139	2.1	22.2618	0.7434	0.0510	0.0011	0.3123	0.0091	0.0449	0.0009	0.61	241	50	274	7	283	6	283	6	n/a		
22	170124_038.FIN2	263	1.5	31.8573	0.8728	0.0517	0.0011	0.2228	0.0049	0.0314	0.0004	0.36	272	49	204	4	199	2	199	2	n/a		
33	170124_055.FIN2	209	2.1	30.6091	0.9369	0.0536	0.0015	0.2392	0.0069	0.0327	0.0006	0.40	354	63	218	6	207	4	207	4	n/a		
61	170124_101.FIN2	122	2.5	30.5717	0.8972	0.0463	0.0020	0.2110	0.0100	0.0327	0.0005	0.37	13	104	194	9	208	3	208	3	n/a		
62	170124_102.FIN2	190	2.2	28.8268	0.8061	0.0500	0.0014	0.2398	0.0067	0.0347	0.0005	0.25	195	65	218	6	220	3	220	3	n/a		
67	170124_107.FIN2	326	3.1	27.5103	0.8325	0.0525	0.0013	0.2636	0.0071	0.0364	0.0006	0.40	307	56	237	6	230	4	230	4	n/a		
69	170124_109.FIN2	161	1.9	31.4367	0.9191	0.0491	0.0020	0.2161	0.0092	0.0318	0.0005	0.33	153	95	198	8	202	3	202	3	n/a		
70	170124_110.FIN2	263	2.1	31.2598	0.9479	0.0495	0.0017	0.2191	0.0080	0.0320	0.0006	0.31	172	80	201	7	203	4	203	4	n/a		
74	170124_120.FIN2	130	2.5	30.3306	0.8647	0.0559	0.0019	0.2544	0.0095	0.0330	0.0005	0.40	448	76	229	8	209	3	209	3	n/a		
81	170124_127.FIN2	176	1.9	30.4785	0.8453	0.0489	0.0011	0.2207	0.0053	0.0328	0.0004	0.33	143	53	202	4	208	3	208	3	n/a		
87	170124_139.FIN2	196	2.5	30.4971	0.8836	0.0487	0.0017	0.2192	0.0078	0.0328	0.0005	0.30	133	82	201	7	208	3	208	3	n/a		

Grain	Spot name	isotopic ratios										isotopic ages									
		U	U/Th	$^{238}\text{U}/$	$^{207}\text{Pb}/$		^{207}Pb		^{206}Pb		^{207}Pb		^{207}Pb		^{206}Pb		^{206}Pb		Best	\pm	
		(ppm)		^{206}Pb	2SE	^{206}Pb	2SE	^{235}U	2SE	^{238}U	2SE	rho*	^{206}Pb	(Ma)	^{235}U	(Ma)	^{238}U	(Ma)	Age	(Ma)	conc.

Whitehorse trough - Richthofen formation - Sample 16-LVD-023, Lake Laberge (Zone 08V 495522E 6774110N NAD 83)

Grain	Spot name	isotopic ratios										isotopic ages									
		U	U/Th	$^{238}\text{U}/$	$^{207}\text{Pb}/$		^{207}Pb		^{206}Pb		^{207}Pb		^{207}Pb		^{206}Pb		^{206}Pb		Best	\pm	
		(ppm)		^{206}Pb	2SE	^{206}Pb	2SE	^{235}U	2SE	^{238}U	2SE	rho	^{206}Pb	(Ma)	^{235}U	(Ma)	^{238}U	(Ma)	Age	(Ma)	conc.
2	180129_011.FIN2	526	3.1	17.2652	1.1625	0.0549	0.0010	0.4254	0.0085	0.0579	0.0009	0.47	408	41	359	6	363	6	363	6	n/a
3	180129_012.FIN2	475	3.0	34.4471	2.2545	0.0521	0.0017	0.2029	0.0067	0.0290	0.0004	0.41	290	75	187	6	185	2	185	2	n/a
4	180129_013.FIN2	381	2.7	32.6264	2.2354	0.0530	0.0029	0.2160	0.0110	0.0307	0.0006	0.41	329	124	198	9	195	4	195	4	n/a
6	180129_015.FIN2	260	2.7	34.1297	2.5626	0.0519	0.0047	0.2010	0.0150	0.0293	0.0012	0.12	281	207	185	13	186	8	186	8	n/a
7	180129_016.FIN2	274	1.5	16.0514	1.1336	0.0562	0.0027	0.4700	0.0250	0.0623	0.0017	0.45	460	107	390	17	390	10	390	10	n/a
8	180129_017.FIN2	615	1.8	2.2153	0.1472	0.2004	0.0028	12.1600	0.2400	0.4514	0.0068	0.76	2829	23	2616	19	2401	30	2829	23	85
10	180129_019.FIN2	448	2.5	30.9119	2.1022	0.0524	0.0020	0.2263	0.0084	0.0324	0.0007	0.23	303	87	207	7	205	4	205	4	n/a
11	180129_020.FIN2	270	2.0	17.5902	1.1758	0.0559	0.0019	0.4230	0.0160	0.0569	0.0010	0.45	448	76	357	11	356	6	356	6	n/a
12	180129_021.FIN2	90	2.2	23.4577	1.5958	0.0544	0.0032	0.3090	0.0190	0.0426	0.0010	0.32	388	132	273	15	269	6	269	6	n/a
13	180129_022.FIN2	430	2.0	25.9740	1.8890	0.0535	0.0028	0.2770	0.0170	0.0385	0.0012	0.23	350	118	248	13	244	8	244	8	n/a
14	180129_029.FIN2	316	3.1	31.4169	2.0727	0.0504	0.0012	0.2199	0.0055	0.0318	0.0003	0.32	213	55	201	5	202	2	202	2	n/a
15	180129_030.FIN2	193	3.0	34.0020	2.3123	0.0513	0.0029	0.2070	0.0110	0.0294	0.0006	0.13	254	130	190	9	187	4	187	4	n/a
16	180129_031.FIN2	722	4.9	23.4192	1.6454	0.0539	0.0036	0.3180	0.0240	0.0427	0.0012	0.49	367	151	280	18	270	8	270	8	n/a
17	180129_032.FIN2	215	3.5	30.0120	2.0717	0.0509	0.0028	0.2350	0.0130	0.0333	0.0007	0.24	236	127	213	11	211	4	211	4	n/a
18	180129_033.FIN2	806	2.3	30.9598	2.2046	0.0508	0.0016	0.2250	0.0120	0.0323	0.0010	0.66	232	73	206	10	205	7	205	7	n/a
19	180129_034.FIN2	76	1.0	2.2222	0.1531	0.1705	0.0026	10.6600	0.2400	0.4500	0.0100	0.77	2563	26	2495	20	2395	45	2563	26	93
21	180129_036.FIN2	638	2.6	32.1958	2.2804	0.0508	0.0045	0.2190	0.0170	0.0311	0.0009	0.41	232	205	201	14	197	5	197	5	n/a
22	180129_037.FIN2	398	3.3	32.2269	2.2849	0.0505	0.0025	0.2190	0.0110	0.0310	0.0009	0.32	218	115	200	9	197	6	197	6	n/a

Grain	Spot name	isotopic ratios										isotopic ages									
		U	U/Th	$^{238}\text{U}/$	$^{207}\text{Pb}/$		^{207}Pb		^{206}Pb			^{207}Pb	\pm	^{207}Pb	\pm	^{206}Pb	\pm	Best	\pm		
		(ppm)		^{206}Pb	2SE	^{206}Pb	2SE	^{235}U	2SE	^{238}U	2SE	rho*	^{206}Pb	(Ma)	^{235}U	(Ma)	^{238}U	(Ma)	Age	(Ma)	conc.
23	180129_038.FIN2	334	59.3	26.3158	1.8698	0.0508	0.0023	0.2690	0.0130	0.0380	0.0010	0.55	232	105	241	10	240	6	240	6	n/a
24	180129_039.FIN2	274	1.5	3.7566	0.2681	0.0923	0.0025	3.4430	0.0920	0.2662	0.0071	0.46	1474	51	1513	21	1521	36	1474	51	103
25	180129_040.FIN2	506	2.5	33.5571	2.4774	0.0504	0.0034	0.2110	0.0150	0.0298	0.0010	0.30	213	156	194	12	190	6	190	6	n/a
Rejected Analysis																					
1	180125_059.FIN2	1	5.8	#####	11859.9200	-5.1000	6.6000	-0.0124	0.0018	0.0000	0.0000	0.01	#####	#####	-13	2	0	0	0	0	n/a
5	180129_014.FIN2	536	3.0	30.2115	2.5557	0.0586	0.0034	0.2630	0.0210	0.0331	0.0019	0.61	552	127	237	17	210	12	210	12	n/a
9	180129_018.FIN2	356	2.5	19.9601	1.3546	0.0551	0.0022	0.3680	0.0130	0.0501	0.0011	0.09	416	89	318	10	315	7	315	7	n/a
20	180129_035.FIN2	477	3.4	24.3309	2.0720	0.0687	0.0050	0.4000	0.0360	0.0411	0.0022	0.77	890	150	348	30	260	14	260	14	n/a
26	180129_047.FIN2	136	2.5	31.8471	2.3328	0.0581	0.0052	0.2610	0.0280	0.0314	0.0010	0.56	534	196	234	22	200	6	200	6	n/a
27	180129_048.FIN2	355	1.7	18.6220	1.3871	0.0530	0.0032	0.3950	0.0230	0.0537	0.0019	0.47	329	137	337	16	337	11	337	11	n/a
28	180129_049.FIN2	462	3.8	36.8460	2.5795	0.0547	0.0036	0.2110	0.0140	0.0271	0.0006	0.22	400	147	194	12	173	4	173	4	n/a
29	180129_050.FIN2	393	2.8	32.3625	2.5136	0.0490	0.0039	0.2160	0.0220	0.0309	0.0013	0.56	148	187	198	18	196	8	196	8	n/a
30	180129_051.FIN2	94	3.2	28.8184	2.2424	0.0502	0.0049	0.2440	0.0170	0.0347	0.0014	0.11	204	226	221	14	220	9	220	9	n/a
31	180129_052.FIN2	305	2.2	14.9254	1.0916	0.0632	0.0038	0.6020	0.0390	0.0670	0.0022	0.41	715	128	477	24	418	13	418	13	n/a
32	180129_053.FIN2	299	2.6	30.6749	2.4465	0.0557	0.0026	0.2550	0.0130	0.0326	0.0015	0.47	440	104	230	11	207	10	207	10	n/a
33	180129_054.FIN2	597	1.9	20.3666	1.4103	0.0540	0.0015	0.3780	0.0160	0.0491	0.0012	0.71	371	63	325	11	309	7	309	7	n/a
34	180129_055.FIN2	292	3.2	26.5252	2.3922	0.0514	0.0027	0.2750	0.0200	0.0377	0.0023	0.67	259	121	246	16	238	14	238	14	n/a
35	180129_056.FIN2	1011	1.4	17.0940	1.4318	0.0534	0.0017	0.4520	0.0240	0.0585	0.0030	0.83	346	72	378	17	366	19	366	19	n/a
36	180129_057.FIN2	291	2.5	30.3951	2.4020	0.0498	0.0025	0.2330	0.0150	0.0329	0.0014	0.56	186	117	211	12	208	9	208	9	n/a
37	180129_058.FIN2	358	3.2	34.8432	2.9137	0.0484	0.0030	0.2020	0.0180	0.0287	0.0016	0.40	119	146	186	15	182	10	182	10	n/a
38	180129_065.FIN2	449	2.4	25.9067	1.9464	0.0517	0.0029	0.2780	0.0180	0.0386	0.0015	0.51	272	129	248	14	244	9	244	9	n/a
39	180129_066.FIN2	271	2.3	25.7998	1.7972	0.0518	0.0022	0.2810	0.0130	0.0388	0.0009	0.33	277	97	251	10	245	6	245	6	n/a
40	180129_067.FIN2	362	2.5	33.8753	2.2951	0.0518	0.0027	0.2110	0.0110	0.0295	0.0005	0.36	277	119	194	10	188	3	188	3	n/a
41	180129_068.FIN2	1870	3.0	21.1060	1.4255	0.0531	0.0014	0.3444	0.0084	0.0474	0.0007	0.38	333	60	300	6	298	5	298	5	n/a

Grain	Spot name	isotopic ratios										isotopic ages									
		U (ppm)	U/Th	$^{238}\text{U}/$		$^{207}\text{Pb}/$		^{207}Pb		^{206}Pb				^{207}Pb (Ma)	\pm	^{207}Pb (Ma)	\pm	^{206}Pb (Ma)	\pm	Best	\pm
				^{206}Pb	2SE	^{206}Pb	2SE	^{235}U	2SE	^{238}U	2SE	rho*	^{206}Pb	^{235}U	^{238}U	Age	(Ma)	conc.			
42	180129_069.FIN2	391	2.4	3.8110	0.2614	0.0949	0.0013	3.4170	0.0650	0.2624	0.0052	0.73	1526	26	1506	15	1501	27	1526	26	98
43	180129_070.FIN2	409	2.9	30.5157	2.0487	0.0516	0.0015	0.2312	0.0077	0.0328	0.0006	0.44	268	67	211	6	208	4	208	4	n/a
44	180129_071.FIN2	463	1.4	22.3714	1.9519	0.0538	0.0040	0.3270	0.0280	0.0447	0.0026	0.54	363	168	287	21	282	16	282	16	n/a
45	180129_072.FIN2	477	3.2	30.6091	2.0612	0.0518	0.0016	0.2296	0.0076	0.0327	0.0005	0.42	277	71	209	6	207	3	207	3	n/a
46	180129_073.FIN2	329	2.2	14.3678	1.0735	0.0569	0.0024	0.5360	0.0230	0.0696	0.0025	0.37	488	93	435	15	434	15	434	15	n/a
47	180129_074.FIN2	750	2.8	20.0000	1.3600	0.0548	0.0015	0.3700	0.0120	0.0500	0.0011	0.68	404	61	319	9	315	7	315	7	n/a
48	180129_075.FIN2	209	4.0	33.3333	2.5556	0.0527	0.0034	0.2130	0.0160	0.0300	0.0013	0.49	316	147	195	14	190	8	190	8	n/a
49	180129_076.FIN2	466	2.8	11.6009	0.7940	0.0601	0.0013	0.6990	0.0200	0.0862	0.0020	0.65	607	47	537	12	533	12	533	12	n/a
50	180129_083.FIN2	976	2.8	36.4299	2.5216	0.0516	0.0028	0.1920	0.0120	0.0275	0.0007	0.57	268	124	178	10	175	4	175	4	n/a
51	180129_084.FIN2	503	1.7	20.5339	1.4757	0.0547	0.0023	0.3610	0.0150	0.0487	0.0015	0.43	400	94	312	11	307	9	307	9	n/a
52	180129_085.FIN2	849	2.1	18.3453	1.2116	0.0543	0.0012	0.4002	0.0098	0.0545	0.0009	0.50	384	50	341	7	342	5	342	5	n/a
53	180129_086.FIN2	364	2.9	33.0033	2.2874	0.0516	0.0021	0.2119	0.0089	0.0303	0.0008	0.26	268	93	196	8	192	5	192	5	n/a
54	180129_087.FIN2	22	-17.0	12.3457	2.7435	0.0640	0.0120	0.6800	0.1900	0.0810	0.0170	0.83	742	397	500	120	490	100	490	100	n/a
55	180129_088.FIN2	235	2.2	17.1233	1.1435	0.0535	0.0017	0.4310	0.0140	0.0584	0.0010	0.23	350	72	362	10	366	6	366	6	n/a

Grain	Spot name	isotopic ratios										isotopic ages									
		U	U/Th	$^{238}\text{U}/$	$^{207}\text{Pb}/$		^{207}Pb		^{206}Pb		^{207}Pb		^{207}Pb		^{206}Pb		^{206}Pb		Best	\pm	
		(ppm)		^{206}Pb	2SE	^{206}Pb	2SE	^{235}U	2SE	^{238}U	2SE	rho*	^{206}Pb	(Ma)	^{235}U	(Ma)	^{238}U	(Ma)	Age	(Ma)	conc.

Whitehorse trough - Richthofen formation - Sample 17-LVD-026, Metamorphic Clast Fish Lake (Zone 08V 485805E 6721676N NAD 83)

Grain	Spot name	isotopic ratios										isotopic ages									
		U	U/Th	$^{238}\text{U}/$	$^{207}\text{Pb}/$		^{207}Pb		^{206}Pb		^{207}Pb		^{207}Pb		^{206}Pb		^{206}Pb		Best	\pm	
		(ppm)		^{206}Pb	2SE	^{206}Pb	2SE	^{235}U	2SE	^{238}U	2SE	rho	^{206}Pb	(Ma)	^{235}U	(Ma)	^{238}U	(Ma)	Age	(Ma)	conc.
1	180125_012.FIN2	300	1.4	34.2231	0.3748	0.0500	0.0011	0.2021	0.0049	0.0292	0.0003	0.36	195	51	187	4	186	2	186	2	n/a
3	180125_014.FIN2	367	1.8	35.2858	0.4109	0.0497	0.0009	0.1942	0.0038	0.0283	0.0003	0.46	180	42	180	3	180	2	180	2	n/a
4	180125_015.FIN2	151	2.0	32.7011	0.8876	0.0529	0.0026	0.2240	0.0120	0.0306	0.0008	0.50	325	112	205	10	194	5	194	5	n/a
5	180125_016.FIN2	439	0.8	30.7409	0.5009	0.0502	0.0012	0.2264	0.0059	0.0325	0.0005	0.44	204	55	207	5	206	3	206	3	n/a
7	180125_018.FIN2	220	1.5	33.5008	0.9540	0.0508	0.0031	0.2100	0.0140	0.0299	0.0009	0.47	232	141	193	12	190	5	190	5	n/a
9	180125_020.FIN2	351	1.2	32.8947	1.4067	0.0510	0.0041	0.2140	0.0150	0.0304	0.0013	0.06	241	185	197	12	193	8	193	8	n/a
12	180125_023.FIN2	333	1.7	34.5304	0.3935	0.0500	0.0011	0.2008	0.0044	0.0290	0.0003	0.34	195	51	185	4	184	2	184	2	n/a
13	180125_030.FIN2	297	2.0	33.4336	0.5589	0.0502	0.0016	0.2075	0.0067	0.0299	0.0005	0.27	204	74	191	6	190	3	190	3	n/a
15	180125_032.FIN2	293	2.1	33.5683	0.4507	0.0498	0.0013	0.2058	0.0058	0.0298	0.0004	0.39	186	61	190	5	189	3	189	3	n/a
16	180125_033.FIN2	578	1.7	34.6621	0.7449	0.0502	0.0018	0.2003	0.0074	0.0289	0.0006	0.37	204	83	185	6	183	4	183	4	n/a
18	180125_035.FIN2	432	1.4	33.0142	0.6104	0.0502	0.0015	0.2103	0.0065	0.0303	0.0006	0.30	204	69	194	6	192	4	192	4	n/a
19	180125_036.FIN2	536	1.7	34.6500	0.6603	0.0501	0.0017	0.1999	0.0069	0.0289	0.0006	0.33	200	79	185	6	183	3	183	3	n/a
20	180125_037.FIN2	337	2.0	34.6500	0.5043	0.0501	0.0014	0.2002	0.0057	0.0289	0.0004	0.29	200	65	185	5	183	3	183	3	n/a
21	180125_038.FIN2	323	1.9	34.0484	0.7883	0.0505	0.0020	0.2053	0.0083	0.0294	0.0007	0.30	218	92	189	7	187	4	187	4	n/a
22	180125_039.FIN2	396	1.7	34.0600	0.4524	0.0501	0.0013	0.2022	0.0057	0.0294	0.0004	0.33	200	60	187	5	187	3	187	3	n/a
23	180125_040.FIN2	550	1.7	34.0368	0.4286	0.0502	0.0009	0.2036	0.0041	0.0294	0.0004	0.48	204	41	188	4	187	2	187	2	n/a
24	180125_041.FIN2	170	2.0	30.7598	0.5772	0.0501	0.0020	0.2261	0.0091	0.0325	0.0006	0.14	200	93	206	8	206	4	206	4	n/a
25	180125_048.FIN2	673	3.7	25.0125	0.6069	0.0517	0.0022	0.2870	0.0130	0.0400	0.0010	0.44	272	98	256	11	253	6	253	6	n/a

Grain	Spot name	isotopic ratios										isotopic ages									
		U	U/Th	$^{238}\text{U}/$	$^{207}\text{Pb}/$		^{207}Pb		^{206}Pb			^{207}Pb	\pm	^{207}Pb	\pm	^{206}Pb	\pm	Best	\pm		
		(ppm)		^{206}Pb	2SE	^{206}Pb	2SE	^{235}U	2SE	^{238}U	2SE	rho*	^{206}Pb	(Ma)	^{235}U	(Ma)	^{238}U	(Ma)	Age	(Ma)	conc.
27	180125_050.FIN2	398	3.0	31.7158	0.7947	0.0508	0.0024	0.2210	0.0120	0.0315	0.0008	0.46	232	109	202	10	200	5	200	5	n/a
28	180125_051.FIN2	220	1.3	33.6587	0.4872	0.0503	0.0015	0.2057	0.0063	0.0297	0.0004	0.31	209	69	190	5	189	3	189	3	n/a
Rejected Analysis																					
2	180125_013.FIN2	251	1.7	35.2361	0.4594	0.0549	0.0017	0.2150	0.0070	0.0284	0.0004	0.26	408	69	197	6	180	2	180	2	n/a
6	180125_017.FIN2	364	1.6	38.8350	1.2518	0.0698	0.0046	0.2470	0.0170	0.0258	0.0008	0.20	922	135	224	13	164	5	164	5	n/a
8	180125_019.FIN2	623	2.0	16.9779	0.6053	0.1170	0.0036	0.9460	0.0240	0.0589	0.0021	0.51	1911	55	676	13	369	12	369	12	n/a
10	180125_021.FIN2	156	1.1	35.2609	0.9201	0.0687	0.0051	0.2700	0.0200	0.0284	0.0007	0.19	890	153	241	16	180	5	180	5	n/a
11	180125_022.FIN2	289	1.2	36.6300	1.1807	0.0929	0.0076	0.3520	0.0310	0.0273	0.0009	0.38	1486	155	304	23	174	6	174	6	n/a
14	180125_031.FIN2	187	2.4	34.9406	0.8058	0.0507	0.0027	0.2000	0.0110	0.0286	0.0007	0.26	227	123	185	9	182	4	182	4	n/a
17	180125_034.FIN2	445	1.5	35.6761	0.5473	0.0578	0.0017	0.2241	0.0075	0.0280	0.0004	0.45	522	65	205	6	178	3	178	3	n/a
26	180125_049.FIN2	253	2.1	30.8452	0.8943	0.1116	0.0042	0.5010	0.0220	0.0324	0.0009	0.53	1826	68	412	15	206	6	206	6	n/a
29	180125_052.FIN2	253	2.4	30.6749	1.3173	0.1073	0.0075	0.4830	0.0340	0.0326	0.0014	0.29	1754	128	399	23	207	9	207	9	n/a
30	180125_053.FIN2	361	1.8	41.8761	1.0171	0.0517	0.0021	0.1661	0.0072	0.0239	0.0006	0.35	272	93	156	6	152	4	152	4	n/a
31	180125_054.FIN2	215	2.2	38.8954	0.9228	0.0508	0.0023	0.1806	0.0081	0.0257	0.0006	0.24	232	105	168	7	164	4	164	4	n/a
32	180125_055.FIN2	186	2.1	43.4783	0.9074	0.0496	0.0023	0.1578	0.0076	0.0230	0.0005	0.27	176	108	148	7	147	3	147	3	n/a
33	180125_056.FIN2	228	1.8	69.5894	2.0339	0.0503	0.0040	0.0993	0.0071	0.0144	0.0004	0.35	209	184	96	7	92	3	92	3	n/a
34	180125_057.FIN2	197	2.5	58.7890	1.4861	0.0496	0.0047	0.1170	0.0110	0.0170	0.0004	0.00	176	221	112	10	109	3	109	3	n/a
35	180125_058.FIN2	217	2.4	81.9672	6.7186	0.0511	0.0056	0.0845	0.0093	0.0122	0.0010	0.35	245	252	82	9	78	7	78	7	n/a

Grain	Spot name	isotopic ratios										isotopic ages									
		U	U/Th	$^{238}\text{U}/$	$^{207}\text{Pb}/$		^{207}Pb		^{206}Pb		^{207}Pb		^{207}Pb		^{206}Pb		^{206}Pb		Best	\pm	
		(ppm)		^{206}Pb	2SE	^{206}Pb	2SE	^{235}U	2SE	^{238}U	2SE	rho*	^{206}Pb	(Ma)	^{235}U	(Ma)	^{238}U	(Ma)	Age	(Ma)	conc.

Whitehorse trough - Richthofen formation - Sample 17-LVD-027, Takhini subdivision (Zone 08V 488086E 6748844N NAD 83)

Grain	Spot name	isotopic ratios										isotopic ages									
		U	U/Th	$^{238}\text{U}/$	$^{207}\text{Pb}/$		^{207}Pb		^{206}Pb		^{207}Pb		^{207}Pb		^{206}Pb		^{206}Pb		Best	\pm	
		(ppm)		^{206}Pb	2SE	^{206}Pb	2SE	^{235}U	2SE	^{238}U	2SE	rho	^{206}Pb	(Ma)	^{235}U	(Ma)	^{238}U	(Ma)	Age	(Ma)	conc.
1	171002_010.FIN2	357	1.9	33.2116	0.9817	0.0508	0.0043	0.2120	0.0170	0.0301	0.0006	0.21	232	195	194	14	191	4	191	4	n/a
2	171002_011.FIN2	182	2.2	32.8839	0.9948	0.0517	0.0032	0.2180	0.0140	0.0304	0.0007	0.21	272	142	200	12	193	4	193	4	n/a
3	171002_012.FIN2	572	2.4	31.9081	0.7941	0.0510	0.0018	0.2212	0.0081	0.0313	0.0004	0.19	241	81	203	7	199	3	199	3	n/a
4	171002_013.FIN2	433	2.0	30.6466	0.9392	0.0509	0.0039	0.2310	0.0200	0.0326	0.0007	0.42	236	177	211	16	207	5	207	5	n/a
5	171002_014.FIN2	522	1.7	32.4675	1.1596	0.0513	0.0033	0.2160	0.0130	0.0308	0.0009	0.08	254	148	198	11	196	5	196	5	n/a
6	171002_015.FIN2	468	4.3	29.3255	0.7310	0.0512	0.0025	0.2420	0.0110	0.0341	0.0004	0.04	250	112	220	9	216	3	216	3	n/a
7	171002_016.FIN2	333	1.9	31.2695	0.8213	0.0510	0.0024	0.2270	0.0110	0.0320	0.0005	0.20	241	108	207	9	203	3	203	3	n/a
8	171002_017.FIN2	195	3.5	30.8547	0.9520	0.0533	0.0037	0.2410	0.0190	0.0324	0.0008	0.59	342	157	219	16	206	5	206	5	n/a
9	171002_018.FIN2	284	1.9	32.6797	1.2816	0.0504	0.0053	0.2150	0.0260	0.0306	0.0010	0.54	213	244	197	21	194	6	194	6	n/a
10	171002_019.FIN2	280	2.3	33.4784	1.2329	0.0511	0.0046	0.2120	0.0210	0.0299	0.0009	0.44	245	207	195	18	190	6	190	6	n/a
11	171002_020.FIN2	572	2.2	34.4828	1.5458	0.0511	0.0056	0.2050	0.0210	0.0290	0.0012	0.10	245	252	189	18	185	8	185	8	n/a
13	171002_028.FIN2	291	2.4	32.7547	0.9227	0.0515	0.0034	0.2170	0.0140	0.0305	0.0006	0.06	263	152	199	11	194	4	194	4	n/a
14	171002_029.FIN2	363	2.3	33.4560	0.9850	0.0521	0.0042	0.2150	0.0190	0.0299	0.0006	0.40	290	184	197	15	190	4	190	4	n/a
15	171002_030.FIN2	173	2.3	32.5839	1.2741	0.0508	0.0086	0.2130	0.0350	0.0307	0.0010	0.21	232	391	195	29	195	6	195	6	n/a
16	171002_031.FIN2	189	2.4	34.6741	1.0941	0.0510	0.0056	0.2040	0.0210	0.0288	0.0007	0.21	241	253	188	18	183	4	183	4	n/a
17	171002_032.FIN2	438	1.8	30.7977	0.9485	0.0510	0.0031	0.2290	0.0140	0.0325	0.0007	0.17	241	140	209	11	206	5	206	5	n/a
18	171002_033.FIN2	538	1.5	31.2695	0.8800	0.0517	0.0035	0.2300	0.0150	0.0320	0.0006	0.31	272	155	209	12	203	4	203	4	n/a
19	171002_034.FIN2	288	6.5	33.0033	0.8714	0.0504	0.0024	0.2130	0.0110	0.0303	0.0005	0.05	213	110	195	9	192	3	192	3	n/a

Grain	Spot name	isotopic ratios										isotopic ages									
		U	U/Th	$^{238}\text{U}/$		$^{207}\text{Pb}/$		^{207}Pb		^{206}Pb				^{207}Pb	\pm	^{207}Pb	\pm	^{206}Pb	\pm	Best	\pm
		(ppm)		^{206}Pb	2SE	^{206}Pb	2SE	^{235}U	2SE	^{238}U	2SE	rho*	^{206}Pb	(Ma)	^{235}U	(Ma)	^{238}U	(Ma)	Age	(Ma)	conc.
20	171002_035.FIN2	467	2.0	31.6056	0.8990	0.0533	0.0025	0.2320	0.0100	0.0316	0.0006	0.16	342	106	212	9	201	4	201	4	n/a
23	171002_038.FIN2	236	3.6	32.2165	1.0379	0.0512	0.0040	0.2190	0.0170	0.0310	0.0008	0.27	250	180	200	14	197	5	197	5	n/a
24	171002_039.FIN2	274	2.4	32.1958	1.0366	0.0509	0.0024	0.2190	0.0120	0.0311	0.0008	0.48	236	109	200	10	197	5	197	5	n/a
25	171002_046.FIN2	345	2.8	29.8418	0.9796	0.0512	0.0032	0.2340	0.0120	0.0335	0.0009	0.13	250	144	213	10	213	5	213	5	n/a
26	171002_047.FIN2	426	2.9	29.7885	0.9761	0.0521	0.0030	0.2430	0.0140	0.0336	0.0008	0.33	290	132	221	12	213	5	213	5	n/a
27	171002_048.FIN2	314	3.0	32.3206	1.1491	0.0514	0.0037	0.2210	0.0170	0.0309	0.0009	0.37	259	165	202	14	196	6	196	6	n/a
28	171002_049.FIN2	426	1.9	31.1624	0.9614	0.0518	0.0037	0.2290	0.0170	0.0321	0.0007	0.24	277	164	209	14	204	4	204	4	n/a
29	171002_050.FIN2	548	4.5	29.6560	0.8179	0.0509	0.0023	0.2380	0.0120	0.0337	0.0006	0.39	236	104	216	10	214	4	214	4	n/a
30	171002_051.FIN2	402	2.7	32.5203	1.0576	0.0507	0.0027	0.2140	0.0120	0.0308	0.0008	0.34	227	123	197	10	195	5	195	5	n/a
31	171002_052.FIN2	328	2.4	20.0000	0.7200	0.0519	0.0030	0.3710	0.0310	0.0500	0.0014	0.39	281	132	319	22	315	9	315	9	n/a
33	171002_054.FIN2	398	2.0	30.0571	0.7860	0.0511	0.0025	0.2370	0.0120	0.0333	0.0005	0.28	245	113	215	10	211	3	211	3	n/a
34	171002_055.FIN2	668	3.1	32.6052	0.9674	0.0504	0.0033	0.2140	0.0130	0.0307	0.0006	0.21	213	152	196	11	195	4	195	4	n/a
36	171002_057.FIN2	227	2.5	30.7503	0.9456	0.0507	0.0032	0.2290	0.0140	0.0325	0.0008	0.20	227	146	208	12	206	5	206	5	n/a
37	171002_064.FIN2	528	2.2	30.1568	0.7639	0.0504	0.0017	0.2315	0.0080	0.0332	0.0004	0.12	213	78	211	7	210	3	210	3	n/a
39	171002_066.FIN2	296	1.8	32.5945	1.0412	0.0503	0.0033	0.2130	0.0140	0.0307	0.0007	0.17	209	152	196	12	195	5	195	5	n/a
41	171002_068.FIN2	300	2.3	33.3667	0.9909	0.0515	0.0053	0.2150	0.0230	0.0300	0.0006	0.40	263	236	197	19	190	4	190	4	n/a
42	171002_069.FIN2	357	2.4	31.4465	1.2856	0.0523	0.0042	0.2260	0.0150	0.0318	0.0012	0.21	299	183	207	12	202	7	202	7	n/a
43	171002_070.FIN2	298	1.8	32.1750	0.8075	0.0513	0.0028	0.2200	0.0110	0.0311	0.0004	0.03	254	126	201	10	197	3	197	3	n/a
44	171002_071.FIN2	355	2.2	32.9381	0.9873	0.0493	0.0028	0.2140	0.0160	0.0304	0.0006	0.33	162	133	197	13	193	4	193	4	n/a
45	171002_072.FIN2	260	2.2	32.8947	1.2985	0.0507	0.0056	0.2140	0.0230	0.0304	0.0010	0.10	227	255	196	19	193	6	193	6	n/a
47	171002_074.FIN2	436	2.3	33.2336	1.1045	0.0509	0.0037	0.2100	0.0140	0.0301	0.0008	0.21	236	168	194	11	191	5	191	5	n/a
50	171002_083.FIN2	838	1.5	32.0308	0.7900	0.0503	0.0013	0.2189	0.0054	0.0312	0.0004	0.07	209	60	201	4	198	2	198	2	n/a
51	171002_084.FIN2	579	3.0	31.6857	0.7931	0.0498	0.0018	0.2188	0.0080	0.0316	0.0004	0.25	186	84	201	7	200	3	200	3	n/a
53	171002_086.FIN2	990	2.3	35.0508	0.9828	0.0527	0.0022	0.1966	0.0074	0.0285	0.0005	0.21	316	95	182	6	181	3	181	3	n/a

Grain	Spot name	isotopic ratios										isotopic ages									
		U	U/Th	$^{238}\text{U}/$		$^{207}\text{Pb}/$		^{207}Pb		^{206}Pb		rho*	^{207}Pb	\pm	^{207}Pb	\pm	^{206}Pb	\pm	Best	\pm	
				(ppm)	^{206}Pb	2SE	^{206}Pb	2SE	^{235}U	2SE	^{238}U	2SE									
54	171002_087.FIN2	615	1.9	32.4044	0.9870	0.0516	0.0034	0.2210	0.0140	0.0309	0.0007	0.09	268	151	202	12	196	4	196	4	n/a
55	171002_088.FIN2	670	2.0	30.9406	0.8424	0.0511	0.0022	0.2274	0.0093	0.0323	0.0006	0.17	245	99	208	8	205	3	205	3	n/a
57	171002_090.FIN2	366	2.0	31.7460	1.3102	0.0511	0.0040	0.2210	0.0200	0.0315	0.0011	0.58	245	180	203	17	200	7	200	7	n/a
58	171002_091.FIN2	622	3.1	30.7031	1.0369	0.0509	0.0030	0.2270	0.0130	0.0326	0.0008	0.42	236	136	210	12	207	5	207	5	n/a
59	171002_092.FIN2	360	2.1	33.1895	1.2117	0.0498	0.0027	0.2080	0.0110	0.0301	0.0008	0.25	186	126	194	8	191	5	191	5	n/a
60	171002_093.FIN2	389	2.2	31.4762	0.9908	0.0518	0.0081	0.2280	0.0390	0.0318	0.0008	0.50	277	358	207	31	202	5	202	5	n/a
62	171002_101.FIN2	677	1.9	32.1854	0.8702	0.0508	0.0025	0.2180	0.0100	0.0311	0.0005	0.04	232	114	200	8	197	3	197	3	n/a
63	171002_102.FIN2	351	1.8	31.6656	0.8423	0.0509	0.0024	0.2210	0.0110	0.0316	0.0005	0.27	236	109	203	9	200	3	200	3	n/a
65	171002_104.FIN2	532	2.0	17.4825	0.4890	0.0545	0.0022	0.4310	0.0180	0.0572	0.0010	0.34	392	91	363	13	359	6	359	6	n/a
Rejected Analysis																					
12	171002_021.FIN2	442	1.7	33.1565	0.9125	0.0592	0.0032	0.2450	0.0120	0.0302	0.0005	0.21	574	118	222	9	192	3	192	3	n/a
21	171002_036.FIN2	444	2.0	30.6091	0.9369	0.0578	0.0029	0.2610	0.0130	0.0327	0.0008	0.30	522	110	235	11	207	5	207	5	n/a
22	171002_037.FIN2	405	1.9	34.2114	1.0066	0.0571	0.0037	0.2300	0.0150	0.0292	0.0006	0.20	495	143	210	13	186	4	186	4	n/a
32	171002_053.FIN2	279	2.3	29.4985	1.3923	0.0522	0.0049	0.2420	0.0250	0.0339	0.0014	0.41	294	214	219	20	215	9	215	9	n/a
35	171002_056.FIN2	355	2.6	35.1989	1.2390	0.0637	0.0038	0.2480	0.0160	0.0284	0.0008	0.52	732	126	225	13	181	5	181	5	n/a
38	171002_065.FIN2	380	2.5	32.1440	1.0022	0.0746	0.0041	0.3190	0.0170	0.0311	0.0007	0.23	1058	111	281	13	198	4	198	4	n/a
40	171002_067.FIN2	281	2.1	34.1414	1.1656	0.0667	0.0041	0.2710	0.0170	0.0293	0.0008	0.23	828	128	242	14	186	5	186	5	n/a
46	171002_073.FIN2	537	5.6	30.8642	1.1431	0.0531	0.0045	0.2350	0.0230	0.0324	0.0010	0.57	333	192	214	19	206	6	206	6	n/a
48	171002_075.FIN2	1444	0.7	37.8501	1.3753	0.0521	0.0020	0.1804	0.0085	0.0264	0.0008	0.45	290	88	168	7	168	5	168	5	n/a
49	171002_082.FIN2	549	3.5	29.2997	0.9443	0.0588	0.0026	0.2790	0.0140	0.0341	0.0009	0.49	560	96	250	11	216	5	216	5	n/a
52	171002_085.FIN2	833	1.9	33.8524	1.0314	0.0550	0.0024	0.2230	0.0100	0.0295	0.0007	0.29	412	98	204	9	188	4	188	4	n/a
56	171002_089.FIN2	554	3.7	33.4113	1.1052	0.0585	0.0032	0.2430	0.0160	0.0299	0.0008	0.54	549	119	220	13	190	5	190	5	n/a
61	171002_100.FIN2	855	2.7	31.3283	0.9324	0.0544	0.0043	0.2360	0.0170	0.0319	0.0007	0.21	388	177	215	14	203	4	203	4	n/a
64	171002_103.FIN2	501	1.8	33.1016	1.0957	0.0496	0.0031	0.2090	0.0120	0.0302	0.0008	0.13	176	146	192	10	192	5	192	5	n/a

Grain	Spot name	isotopic ratios											isotopic ages									
		U	U/Th	$^{238}\text{U}/$	$^{207}\text{Pb}/$		^{207}Pb		^{206}Pb		^{207}Pb		^{207}Pb		^{207}Pb		^{206}Pb		^{206}Pb		Best	\pm
		(ppm)		^{206}Pb	2SE	^{206}Pb	2SE	^{235}U	2SE	^{238}U	2SE	rho*	^{206}Pb	(Ma)	^{235}U	(Ma)	^{238}U	(Ma)	Age	(Ma)	conc.	

Whitehorse trough - Richthofen formation - Sample 17-LVD-030, Mount Byng (Zone 08V 539547E 6757952N NAD 83)

Grain	Spot name	isotopic ratios											isotopic ages									
		U	U/Th	$^{238}\text{U}/$	$^{207}\text{Pb}/$		^{207}Pb		^{206}Pb		^{207}Pb		^{207}Pb		^{207}Pb		^{206}Pb		Best		\pm	
		(ppm)		^{206}Pb	2SE	^{206}Pb	2SE	^{235}U	2SE	^{238}U	2SE	rho	^{206}Pb	(Ma)	^{235}U	(Ma)	^{238}U	(Ma)	Age	(Ma)	conc.	
1	171005b_018.FIN2	321	0.9	19.5313	0.6104	0.0533	0.0035	0.3750	0.0240	0.0512	0.0014	0.16	342	149	322	18	322	8	322	8	n/a	
2	171005b_019.FIN2	1182	1.8	31.4070	0.6609	0.0507	0.0014	0.2222	0.0061	0.0318	0.0004	0.18	227	64	203	5	202	3	202	3	n/a	
3	171005b_020.FIN2	408	1.2	24.5882	0.6046	0.0521	0.0022	0.2920	0.0130	0.0407	0.0007	0.26	290	96	260	10	257	4	257	4	n/a	
4	171005b_027.FIN2	586	2.9	32.8623	0.7883	0.0506	0.0022	0.2124	0.0093	0.0304	0.0005	0.20	223	101	195	8	193	3	193	3	n/a	
5	171005b_028.FIN2	184	3.0	30.3951	1.5706	0.0510	0.0066	0.2310	0.0290	0.0329	0.0016	0.07	241	298	209	24	209	10	209	10	n/a	
6	171005b_029.FIN2	580	1.6	31.0752	1.0622	0.0515	0.0031	0.2270	0.0130	0.0322	0.0009	0.14	263	138	208	10	204	6	204	6	n/a	
7	171005b_030.FIN2	1492	0.8	28.2486	0.6942	0.0514	0.0014	0.2508	0.0072	0.0354	0.0006	0.49	259	63	227	6	224	4	224	4	n/a	
8	171005b_031.FIN2	366	1.6	19.1939	0.4789	0.0525	0.0026	0.3830	0.0200	0.0521	0.0010	0.17	307	113	328	15	327	6	327	6	n/a	
9	171005b_032.FIN2	664	2.3	32.8084	0.8396	0.0500	0.0018	0.2092	0.0081	0.0305	0.0006	0.28	195	84	193	7	194	4	194	4	n/a	
10	171005b_033.FIN2	126	4.1	30.5810	1.1222	0.0512	0.0048	0.2290	0.0200	0.0327	0.0010	0.24	250	216	208	17	207	6	207	6	n/a	
11	171005b_034.FIN2	751	3.2	33.7382	1.0927	0.0511	0.0031	0.2090	0.0120	0.0296	0.0008	0.09	245	140	192	10	188	5	188	5	n/a	
12	171005b_035.FIN2	363	1.9	34.0252	0.8220	0.0509	0.0022	0.2070	0.0092	0.0294	0.0005	0.29	236	100	190	8	187	3	187	3	n/a	
13	171005b_036.FIN2	829	3.0	33.0033	0.6644	0.0505	0.0013	0.2112	0.0054	0.0303	0.0003	0.18	218	60	194	5	192	2	192	2	n/a	
14	171005b_037.FIN2	1294	1.9	34.4471	0.9730	0.0510	0.0023	0.2060	0.0099	0.0290	0.0007	0.36	241	104	190	8	185	4	185	4	n/a	
15	171005b_038.FIN2	248	1.1	19.8413	0.7086	0.0529	0.0033	0.3680	0.0240	0.0504	0.0016	0.25	325	142	317	17	317	10	317	10	n/a	
20	171005b_049.FIN2	593	2.7	32.0924	0.8445	0.0496	0.0019	0.2163	0.0097	0.0312	0.0006	0.42	176	89	199	8	198	4	198	4	n/a	
21	171005b_050.FIN2	548	3.5	31.8471	0.7201	0.0508	0.0020	0.2205	0.0085	0.0314	0.0005	0.10	232	91	202	7	199	3	199	3	n/a	
22	171005b_051.FIN2	1052	2.7	32.5203	0.8566	0.0499	0.0015	0.2133	0.0069	0.0308	0.0006	0.34	190	70	198	6	195	4	195	4	n/a	

Grain	Spot name	isotopic ratios										isotopic ages									
		U (ppm)	U/Th	$^{238}\text{U}/$		$^{207}\text{Pb}/$		^{207}Pb		^{206}Pb		rho*	^{207}Pb (Ma)	\pm	^{207}Pb (Ma)	\pm	^{206}Pb (Ma)	\pm	Best (Ma)	\pm	
				^{206}Pb	2SE	^{206}Pb	2SE	^{235}U	2SE	^{238}U	2SE										
24	171005b_053.FIN2	405	1.5	30.6749	1.1291	0.0506	0.0027	0.2310	0.0140	0.0326	0.0011	0.26	223	123	211	12	207	7	207	7	n/a
25	171005b_054.FIN2	600	1.9	18.9072	0.4647	0.0536	0.0017	0.3920	0.0140	0.0529	0.0009	0.44	354	72	335	10	332	5	332	5	n/a
26	171005b_055.FIN2	770	2.4	36.3108	0.7779	0.0501	0.0016	0.1900	0.0062	0.0275	0.0004	0.22	200	74	176	5	175	2	175	2	n/a
27	171005b_056.FIN2	454	1.6	33.6361	0.8938	0.0502	0.0024	0.2054	0.0092	0.0297	0.0006	0.13	204	111	189	8	189	4	189	4	n/a
29	171005b_064.FIN2	469	1.4	29.9133	0.6085	0.0506	0.0015	0.2353	0.0079	0.0334	0.0004	0.34	223	69	214	7	212	2	212	2	n/a
30	171005b_065.FIN2	991	3.2	32.4781	1.0232	0.0506	0.0022	0.2160	0.0100	0.0308	0.0008	0.47	223	101	198	9	196	5	196	5	n/a
31	171005b_066.FIN2	1304	1.7	33.9789	0.7851	0.0502	0.0018	0.2027	0.0077	0.0294	0.0005	0.34	204	83	187	7	187	3	187	3	n/a
33	171005b_068.FIN2	739	2.3	29.2141	0.7937	0.0509	0.0023	0.2410	0.0120	0.0342	0.0007	0.33	236	104	218	9	217	5	217	5	n/a
34	171005b_069.FIN2	150	1.2	20.2020	0.6938	0.0543	0.0060	0.3680	0.0410	0.0495	0.0015	0.11	384	248	316	31	311	9	311	9	n/a
35	171005b_070.FIN2	439	3.3	33.1675	0.6711	0.0506	0.0015	0.2098	0.0063	0.0302	0.0003	0.32	223	69	193	5	192	2	192	2	n/a
36	171005b_071.FIN2	609	1.1	28.3930	0.8868	0.0519	0.0028	0.2520	0.0140	0.0352	0.0009	0.36	281	123	228	12	223	6	223	6	n/a
38	171005b_073.FIN2	454	2.8	34.0136	1.3883	0.0513	0.0034	0.2070	0.0130	0.0294	0.0011	0.22	254	152	191	11	187	7	187	7	n/a
39	171005b_074.FIN2	841	1.3	24.4738	0.5990	0.0518	0.0016	0.2934	0.0094	0.0409	0.0008	0.34	277	71	261	7	258	5	258	5	n/a
40	171005b_081.FIN2	1012	2.2	32.6691	0.7791	0.0503	0.0015	0.2113	0.0073	0.0306	0.0005	0.52	209	69	194	6	194	3	194	3	n/a
41	171005b_082.FIN2	182	3.1	25.6739	0.6328	0.0523	0.0026	0.2790	0.0140	0.0390	0.0007	0.18	299	113	248	11	246	4	246	4	n/a
42	171005b_083.FIN2	609	2.4	30.7503	0.8321	0.0506	0.0035	0.2270	0.0160	0.0325	0.0007	0.16	223	160	207	13	206	4	206	4	n/a
43	171005b_084.FIN2	612	2.0	25.5102	0.8460	0.0516	0.0031	0.2800	0.0200	0.0392	0.0011	0.49	268	138	250	15	248	7	248	7	n/a
44	171005b_085.FIN2	1636	1.3	25.2589	0.6316	0.0524	0.0015	0.2850	0.0100	0.0396	0.0007	0.62	303	65	254	8	250	5	250	5	n/a
45	171005b_086.FIN2	453	1.9	15.7978	0.4742	0.0553	0.0026	0.4840	0.0250	0.0633	0.0015	0.40	424	105	400	17	396	9	396	9	n/a
46	171005b_087.FIN2	1675	1.8	32.2269	0.8101	0.0494	0.0015	0.2115	0.0070	0.0310	0.0006	0.42	167	71	195	6	197	4	197	4	n/a
47	171005b_088.FIN2	1025	2.5	34.0948	0.8253	0.0498	0.0023	0.2050	0.0110	0.0293	0.0005	0.18	186	108	189	9	187	4	187	4	n/a
48	171005b_089.FIN2	428	1.9	24.0385	0.8090	0.0523	0.0027	0.3000	0.0170	0.0416	0.0012	0.50	299	118	266	13	263	8	263	8	n/a
49	171005b_090.FIN2	619	3.3	32.3834	0.7865	0.0506	0.0018	0.2162	0.0078	0.0309	0.0005	0.28	223	82	198	7	196	3	196	3	n/a
50	171005b_091.FIN2	1190	1.5	32.9489	0.7274	0.0501	0.0012	0.2093	0.0059	0.0304	0.0004	0.45	200	56	193	5	193	3	193	3	n/a

Grain	Spot name	isotopic ratios										isotopic ages									
		U	U/Th	$^{238}\text{U}/$		$^{207}\text{Pb}/$		^{207}Pb		^{206}Pb		rho*	^{207}Pb	\pm	^{207}Pb	\pm	^{206}Pb	\pm	Best	\pm	
				(ppm)	^{206}Pb	2SE	^{206}Pb	2SE	^{235}U	2SE	^{238}U	2SE									
51	171005b_092.FIN2	135	2.8	34.5543	1.1462	0.0515	0.0046	0.2040	0.0180	0.0289	0.0008	0.20	263	205	187	15	184	5	184	5	n/a
52	171005b_099.FIN2	263	1.4	20.9820	0.5283	0.0539	0.0028	0.3540	0.0180	0.0477	0.0008	0.20	367	117	306	14	300	5	300	5	n/a
53	171005b_100.FIN2	646	2.3	34.3407	0.8963	0.0513	0.0023	0.2047	0.0087	0.0291	0.0006	0.19	254	103	189	7	185	4	185	4	n/a
54	171005b_101.FIN2	543	2.4	32.5415	0.7730	0.0506	0.0017	0.2141	0.0077	0.0307	0.0005	0.20	223	78	196	6	195	3	195	3	n/a
55	171005b_102.FIN2	163	2.3	30.9598	1.5336	0.0519	0.0052	0.2290	0.0230	0.0323	0.0015	0.30	281	229	208	19	205	10	205	10	n/a
56	171005b_103.FIN2	207	1.5	21.1417	0.8492	0.0524	0.0043	0.3430	0.0290	0.0473	0.0017	0.23	303	187	298	22	298	10	298	10	n/a
57	171005b_104.FIN2	350	2.5	22.6244	0.6654	0.0531	0.0034	0.3240	0.0200	0.0442	0.0010	0.07	333	145	284	15	279	6	279	6	n/a
58	171005b_105.FIN2	1300	1.9	34.5304	0.6677	0.0505	0.0009	0.2012	0.0041	0.0290	0.0003	0.49	216	42	186	4	184	2	184	2	n/a
59	171005b_106.FIN2	508	1.4	19.0840	0.4370	0.0539	0.0018	0.3890	0.0140	0.0524	0.0008	0.16	367	75	333	10	329	5	329	5	n/a
60	171005b_107.FIN2	666	1.4	19.0476	0.8345	0.0534	0.0031	0.3850	0.0300	0.0525	0.0021	0.61	346	131	330	22	330	13	330	13	n/a
61	171005b_108.FIN2	352	1.0	30.3030	1.3774	0.0515	0.0042	0.2360	0.0220	0.0330	0.0014	0.41	263	187	215	17	209	9	209	9	n/a
62	171005b_109.FIN2	1161	1.9	16.5563	0.4660	0.0543	0.0014	0.4540	0.0150	0.0604	0.0013	0.56	384	58	379	10	378	8	378	8	n/a
63	171005b_110.FIN2	1538	2.2	30.3951	1.1086	0.0510	0.0020	0.2310	0.0110	0.0329	0.0010	0.61	241	90	211	9	209	6	209	6	n/a
64	171005b_111.FIN2	749	3.2	32.0821	0.7514	0.0511	0.0019	0.2194	0.0079	0.0312	0.0005	0.17	245	86	201	7	198	3	198	3	n/a
65	171005b_118.FIN2	984	1.8	30.0752	0.8683	0.0509	0.0029	0.2340	0.0150	0.0333	0.0008	0.42	236	131	213	12	211	5	211	5	n/a
66	171005b_119.FIN2	813	1.7	14.8987	0.3330	0.0556	0.0012	0.5160	0.0130	0.0671	0.0009	0.34	436	48	422	8	419	6	419	6	n/a
68	171005b_121.FIN2	89	1.5	28.5714	1.4694	0.0518	0.0060	0.2510	0.0290	0.0350	0.0017	0.17	277	265	223	23	222	11	222	11	n/a
69	171005b_122.FIN2	344	1.2	18.7617	0.6336	0.0540	0.0030	0.3970	0.0250	0.0533	0.0015	0.47	371	125	338	18	335	9	335	9	n/a
70	171005b_123.FIN2	1246	2.0	33.1895	0.7270	0.0505	0.0017	0.2086	0.0075	0.0301	0.0004	0.41	218	78	192	6	191	3	191	3	n/a
71	171005b_124.FIN2	2600	0.6	19.8926	0.4749	0.0531	0.0014	0.3700	0.0120	0.0503	0.0008	0.54	333	60	319	9	316	5	316	5	n/a
72	171005b_125.FIN2	344	1.6	30.3030	1.1019	0.0512	0.0047	0.2330	0.0220	0.0330	0.0010	0.14	250	211	212	19	210	6	210	6	n/a
73	171005b_126.FIN2	738	2.0	27.2554	0.7057	0.0512	0.0021	0.2580	0.0110	0.0367	0.0007	0.29	250	94	233	9	232	4	232	4	n/a
74	171005b_127.FIN2	1818	2.7	30.5998	0.8427	0.0506	0.0022	0.2280	0.0110	0.0327	0.0007	0.50	223	101	208	9	207	4	207	4	n/a
75	171005b_128.FIN2	2292	0.9	20.0481	0.4421	0.0531	0.0013	0.3636	0.0097	0.0499	0.0007	0.39	333	56	314	7	314	4	314	4	n/a

Grain	Spot name	isotopic ratios										isotopic ages									
		U (ppm)	U/Th	$^{238}\text{U}/$		$^{207}\text{Pb}/$		^{207}Pb		^{206}Pb		^{207}Pb (Ma)	\pm	^{207}Pb (Ma)	\pm	^{206}Pb (Ma)	\pm	Best (Ma)	\pm		
				^{206}Pb	2SE	^{206}Pb	2SE	^{235}U	2SE	^{238}U	2SE										
76	171005b_129.FIN2	772	1.1	19.3424	0.6734	0.0539	0.0050	0.3830	0.0340	0.0517	0.0016	0.12	367	209	327	25	325	10	325	10	n/a
77	171006_010.FIN2	344	4.0	32.5733	1.3793	0.0524	0.0051	0.2220	0.0220	0.0307	0.0011	0.19	303	222	202	18	195	7	195	7	n/a
78	171006_011.FIN2	545	2.4	32.3520	0.8164	0.0509	0.0018	0.2181	0.0075	0.0309	0.0004	0.17	236	82	200	6	196	2	196	2	n/a
82	171006_015.FIN2	1375	2.0	34.8918	0.9496	0.0503	0.0018	0.1981	0.0063	0.0287	0.0005	0.24	209	83	183	5	182	3	182	3	n/a
83	171006_016.FIN2	742	2.9	31.9183	0.8660	0.0506	0.0019	0.2191	0.0089	0.0313	0.0005	0.46	223	87	201	7	199	3	199	3	n/a
84	171006_017.FIN2	465	1.0	20.9644	0.5714	0.0530	0.0026	0.3450	0.0150	0.0477	0.0008	0.24	329	111	300	11	300	5	300	5	n/a
85	171006_018.FIN2	453	2.0	33.0142	0.8611	0.0510	0.0018	0.2129	0.0076	0.0303	0.0004	0.21	241	81	195	6	192	3	192	3	n/a
86	171006_019.FIN2	821	2.3	31.5457	0.7862	0.0505	0.0013	0.2205	0.0056	0.0317	0.0003	0.22	218	60	202	5	201	2	201	2	n/a
88	171006_021.FIN2	1000	5.5	15.9236	0.4564	0.0549	0.0015	0.4750	0.0140	0.0628	0.0011	0.33	408	61	394	9	393	7	393	7	n/a
90	171006_029.FIN2	474	2.4	29.3858	0.8290	0.0512	0.0025	0.2370	0.0120	0.0340	0.0006	0.39	250	112	215	10	216	4	216	4	n/a
91	171006_030.FIN2	228	1.4	21.8245	0.5716	0.0531	0.0019	0.3320	0.0120	0.0458	0.0006	0.20	333	81	290	9	289	4	289	4	n/a
92	171006_031.FIN2	551	2.2	30.9502	0.8909	0.0509	0.0025	0.2250	0.0100	0.0323	0.0006	0.24	236	113	206	9	205	4	205	4	n/a
93	171006_032.FIN2	757	2.6	30.6185	0.7312	0.0507	0.0010	0.2288	0.0047	0.0327	0.0003	0.22	227	46	209	4	207	2	207	2	n/a
94	171006_033.FIN2	872	1.7	18.6567	0.4525	0.0536	0.0010	0.3971	0.0074	0.0536	0.0004	0.15	352	40	339	5	337	3	337	3	n/a
95	171006_034.FIN2	234	1.5	20.7039	1.0716	0.0538	0.0048	0.3530	0.0280	0.0483	0.0022	0.12	363	201	305	21	304	14	304	14	n/a
96	171006_035.FIN2	514	1.5	21.9974	0.5807	0.0524	0.0019	0.3330	0.0140	0.0455	0.0007	0.38	303	83	291	11	287	4	287	4	n/a
97	171006_036.FIN2	359	1.4	21.0084	0.8386	0.0531	0.0035	0.3470	0.0240	0.0476	0.0016	0.36	333	149	301	18	300	10	300	10	n/a
98	171006_037.FIN2	266	2.1	30.1205	1.0887	0.0513	0.0042	0.2340	0.0180	0.0332	0.0010	0.08	254	188	213	15	210	6	210	6	n/a
99	171006_038.FIN2	722	2.0	32.9815	0.8702	0.0507	0.0020	0.2113	0.0085	0.0303	0.0004	0.31	227	91	194	7	193	3	193	3	n/a
100	171006_039.FIN2	370	3.0	33.4448	0.8501	0.0506	0.0020	0.2080	0.0080	0.0299	0.0004	0.24	223	91	191	7	190	2	190	2	n/a
101	171006_046.FIN2	99	2.3	19.1571	0.6239	0.0542	0.0036	0.3880	0.0250	0.0522	0.0012	0.13	379	149	329	18	328	7	328	7	n/a
102	171006_047.FIN2	119	1.7	19.8926	0.5144	0.0540	0.0031	0.3730	0.0210	0.0503	0.0006	0.02	371	129	319	15	316	4	316	4	n/a
103	171006_048.FIN2	680	3.7	32.1543	0.7651	0.0503	0.0012	0.2159	0.0050	0.0311	0.0003	0.18	209	55	199	4	197	2	197	2	n/a
104	171006_049.FIN2	154	1.6	20.5339	0.7168	0.0533	0.0041	0.3550	0.0250	0.0487	0.0013	0.24	342	174	307	19	307	8	307	8	n/a

Grain	Spot name	isotopic ratios										isotopic ages									
		U	U/Th	$^{238}\text{U}/$	$^{207}\text{Pb}/$		^{207}Pb		^{206}Pb			^{207}Pb	\pm	^{207}Pb	\pm	^{206}Pb	\pm	Best	\pm		
		(ppm)		^{206}Pb	2SE	^{206}Pb	2SE	^{235}U	2SE	^{238}U	2SE	rho*	^{206}Pb	(Ma)	^{235}U	(Ma)	^{238}U	(Ma)	Age	(Ma)	conc.
105	171006_050.FIN2	780	4.2	32.0410	0.7905	0.0507	0.0013	0.2184	0.0056	0.0312	0.0003	0.10	227	59	200	5	198	2	198	2	n/a
Rejected Analysis																					
16	171005b_045.FIN2	399	2.7	34.3407	1.0731	0.0559	0.0033	0.2300	0.0160	0.0291	0.0008	0.25	448	131	209	13	185	5	185	5	n/a
17	171005b_046.FIN2	256	2.6	36.5230	1.0938	0.0544	0.0044	0.2080	0.0190	0.0274	0.0007	0.55	388	182	190	16	174	4	174	4	n/a
18	171005b_047.FIN2	852	2.1	25.5428	0.6002	0.0545	0.0020	0.2940	0.0110	0.0392	0.0006	0.32	392	82	262	9	248	4	248	4	n/a
19	171005b_048.FIN2	1141	2.2	33.2447	0.8068	0.0540	0.0021	0.2271	0.0093	0.0301	0.0005	0.37	371	88	208	8	191	3	191	3	n/a
23	171005b_052.FIN2	2140	4.2	24.1429	0.6412	0.0541	0.0019	0.3100	0.0120	0.0414	0.0008	0.38	375	79	274	9	262	5	262	5	n/a
28	171005b_063.FIN2	253	3.6	21.1417	0.6258	0.0607	0.0035	0.3970	0.0220	0.0473	0.0012	0.14	629	124	342	17	298	7	298	7	n/a
32	171005b_067.FIN2	234	1.9	30.3951	0.8038	0.0554	0.0032	0.2510	0.0140	0.0329	0.0007	0.09	428	129	227	11	209	4	209	4	n/a
37	171005b_072.FIN2	289	1.6	10.7527	0.4625	0.1216	0.0055	1.5800	0.1200	0.0930	0.0037	0.82	1980	81	952	45	573	22	573	22	29
67	171005b_120.FIN2	1870	2.2	26.5463	0.6836	0.0586	0.0015	0.3058	0.0088	0.0377	0.0007	0.53	552	56	271	7	238	5	238	5	n/a
79	171006_012.FIN2	364	1.2	21.2044	0.6295	0.0557	0.0024	0.3650	0.0160	0.0472	0.0010	0.22	440	96	315	12	297	6	297	6	n/a
80	171006_013.FIN2	485	2.0	21.9780	0.7729	0.0554	0.0036	0.3510	0.0240	0.0455	0.0012	0.24	428	145	305	18	287	7	287	7	n/a
81	171006_014.FIN2	438	1.9	24.3072	0.8272	0.0742	0.0045	0.4270	0.0290	0.0411	0.0010	0.49	1047	122	360	20	260	6	260	6	n/a
87	171006_020.FIN2	1515	3.6	27.4801	0.7552	0.0532	0.0013	0.2707	0.0080	0.0364	0.0006	0.43	337	55	243	6	230	4	230	4	n/a
89	171006_028.FIN2	3543	4.7	35.5745	0.9112	0.0533	0.0014	0.2061	0.0050	0.0281	0.0003	0.15	342	59	190	4	179	2	179	2	n/a

Grain	Spot name	isotopic ratios										isotopic ages								
		U	U/Th	$^{238}\text{U}/$	$^{207}\text{Pb}/$		^{207}Pb		^{206}Pb			^{207}Pb	\pm	^{207}Pb	\pm	^{206}Pb	\pm	Best	\pm	
		(ppm)		^{206}Pb	2SE	^{206}Pb	2SE	^{235}U	2SE	^{238}U	2SE	rho*	^{206}Pb	(Ma)	^{235}U	(Ma)	^{238}U	(Ma)	Age	(Ma)

Whitehorse trough - Richthofen formation - Sample 17-LVD-034, Mount Slim (Zone 08V 514475E 6751661N NAD 83)

Grain	Spot name	isotopic ratios										isotopic ages									
		U	U/Th	$^{238}\text{U}/$	$^{207}\text{Pb}/$		^{207}Pb		^{206}Pb			^{207}Pb	\pm	^{207}Pb	\pm	^{206}Pb	\pm	Best	\pm		
		(ppm)		^{206}Pb	2SE	^{206}Pb	2SE	^{235}U	2SE	^{238}U	2SE	rho	^{206}Pb	(Ma)	^{235}U	(Ma)	^{238}U	(Ma)	Age	(Ma)	conc
1	171212b_010.FIN2	169	1.3	29.7000	0.6704	0.0517	0.0021	0.2352	0.0095	0.0337	0.0004	0.26	272	93	214	8	214	3	214	3	n/a
2	171212b_011.FIN2	339	1.1	19.0767	0.4731	0.0553	0.0019	0.3890	0.0140	0.0524	0.0009	0.20	424	77	333	10	329	5	329	5	n/a
4	171212b_013.FIN2	739	3.0	29.8508	0.7930	0.0518	0.0023	0.2340	0.0110	0.0335	0.0006	0.35	277	102	213	9	212	4	212	4	n/a
5	171212b_014.FIN2	579	1.5	20.1532	0.4874	0.0538	0.0022	0.3650	0.0150	0.0496	0.0008	0.03	363	92	315	11	312	5	312	5	n/a
6	171212b_015.FIN2	432	2.4	30.9024	0.6971	0.0513	0.0016	0.2255	0.0070	0.0324	0.0004	0.22	254	72	206	6	205	3	205	3	n/a
7	171212b_016.FIN2	111	2.3	18.6916	0.5241	0.0558	0.0033	0.3970	0.0220	0.0535	0.0011	0.10	444	131	336	16	336	7	336	7	n/a
8	171212b_017.FIN2	1285	4.2	31.1430	0.7662	0.0509	0.0013	0.2237	0.0064	0.0321	0.0005	0.41	236	59	205	5	204	3	204	3	n/a
9	171212b_018.FIN2	817	8.1	28.0034	0.7685	0.0526	0.0022	0.2540	0.0120	0.0357	0.0007	0.35	312	95	230	10	226	4	226	4	n/a
10	171212b_019.FIN2	158	2.4	19.0840	0.6920	0.0544	0.0033	0.3940	0.0250	0.0524	0.0016	0.22	388	136	334	18	329	10	329	10	n/a
11	171212b_020.FIN2	176	1.1	18.8857	0.4637	0.0541	0.0021	0.3900	0.0150	0.0530	0.0008	0.20	375	87	333	11	333	5	333	5	n/a
12	171212b_021.FIN2	81	2.1	18.5874	0.7255	0.0547	0.0057	0.4020	0.0410	0.0538	0.0018	0.17	400	233	340	30	338	11	338	11	n/a
13	171212b_028.FIN2	2638	3.4	31.3676	0.6986	0.0508	0.0009	0.2238	0.0044	0.0319	0.0004	0.43	231	42	205	4	202	2	202	2	n/a
14	171212b_029.FIN2	137	1.5	18.3824	0.6758	0.0547	0.0039	0.4050	0.0270	0.0544	0.0017	0.19	400	160	342	19	341	10	341	10	n/a
15	171212b_030.FIN2	553	0.6	19.2345	0.4810	0.0536	0.0022	0.3840	0.0160	0.0520	0.0009	0.25	354	93	329	12	327	6	327	6	n/a
17	171212b_032.FIN2	832	1.4	30.2298	0.9138	0.0520	0.0024	0.2330	0.0140	0.0331	0.0008	0.23	285	106	212	12	210	5	210	5	n/a
18	171212b_033.FIN2	191	2.2	18.4502	0.6127	0.0543	0.0032	0.4090	0.0280	0.0542	0.0014	0.17	384	132	346	20	340	9	340	9	n/a
19	171212b_034.FIN2	234	1.1	18.9645	0.4675	0.0543	0.0024	0.3980	0.0170	0.0527	0.0008	0.05	384	99	338	12	331	5	331	5	n/a
20	171212b_035.FIN2	253	1.3	18.9215	0.4296	0.0542	0.0021	0.3970	0.0160	0.0529	0.0007	0.16	379	87	338	12	332	4	332	4	n/a

Grain	Spot name	isotopic ratios										isotopic ages									
		U	U/Th	$^{238}\text{U}/$		$^{207}\text{Pb}/$		^{207}Pb		^{206}Pb		rho*	^{206}Pb	\pm	^{207}Pb	\pm	^{206}Pb	\pm	Best	\pm	
				(ppm)	^{206}Pb	2SE	^{206}Pb	2SE	^{235}U	2SE	^{238}U	2SE									
21	171212b_036.FIN2	97	2.6	19.0840	0.6920	0.0533	0.0062	0.3820	0.0410	0.0524	0.0017	0.26	342	263	332	33	329	10	329	10	n/a
22	171212b_037.FIN2	246	2.8	18.2149	0.4645	0.0545	0.0022	0.4130	0.0160	0.0549	0.0010	0.03	392	91	350	11	345	6	345	6	n/a
23	171212b_038.FIN2	554	1.3	18.8679	0.6408	0.0532	0.0024	0.3890	0.0220	0.0530	0.0015	0.60	337	102	333	16	333	9	333	9	n/a
24	171212b_039.FIN2	448	1.6	18.9609	0.4314	0.0537	0.0013	0.3913	0.0096	0.0527	0.0006	0.20	358	55	335	7	331	4	331	4	n/a
25	171212b_046.FIN2	182	1.3	18.5529	0.6540	0.0534	0.0046	0.4020	0.0350	0.0539	0.0016	0.12	346	195	341	25	339	10	339	10	n/a
26	171212b_047.FIN2	912	2.0	17.9083	0.4169	0.0529	0.0012	0.4131	0.0097	0.0558	0.0007	0.37	325	52	351	7	350	4	350	4	n/a
27	171212b_048.FIN2	138	1.5	18.7617	0.5280	0.0535	0.0029	0.3960	0.0200	0.0533	0.0010	0.01	350	123	336	14	335	6	335	6	n/a
28	171212b_049.FIN2	122	1.8	19.8413	0.7480	0.0537	0.0048	0.3760	0.0310	0.0504	0.0017	0.26	358	202	322	23	317	10	317	10	n/a
29	171212b_050.FIN2	817	3.8	28.0978	0.6790	0.0511	0.0015	0.2521	0.0070	0.0356	0.0005	0.32	245	68	228	6	225	3	225	3	n/a
30	171212b_051.FIN2	344	1.1	20.9205	0.6565	0.0536	0.0030	0.3580	0.0200	0.0478	0.0012	0.28	354	126	309	15	301	8	301	8	n/a
31	171212b_052.FIN2	622	7.0	29.1715	0.9361	0.0511	0.0038	0.2440	0.0210	0.0343	0.0010	0.63	245	171	221	17	217	6	217	6	n/a
32	171212b_053.FIN2	813	3.9	27.9018	0.7318	0.0506	0.0026	0.2540	0.0110	0.0358	0.0007	0.26	223	119	230	9	227	4	227	4	n/a
33	171212b_054.FIN2	1428	3.8	32.2477	1.0399	0.0508	0.0022	0.2220	0.0110	0.0310	0.0008	0.30	232	100	203	9	197	5	197	5	n/a
34	171212b_055.FIN2	350	1.4	19.8020	0.7058	0.0537	0.0026	0.3720	0.0180	0.0505	0.0015	0.35	358	109	320	13	317	9	317	9	n/a
36	171212b_057.FIN2	410	0.9	19.4213	0.4903	0.0533	0.0021	0.3870	0.0170	0.0515	0.0009	0.36	342	89	331	12	324	5	324	5	n/a
37	171212b_064.FIN2	703	3.5	31.2013	0.8372	0.0508	0.0021	0.2290	0.0100	0.0321	0.0006	0.43	232	95	209	8	203	4	203	4	n/a
38	171212b_065.FIN2	659	2.5	25.9000	0.8050	0.0514	0.0029	0.2780	0.0160	0.0386	0.0010	0.17	259	130	249	12	244	6	244	6	n/a
39	171212b_066.FIN2	252	5.4	31.5358	0.7956	0.0510	0.0023	0.2270	0.0100	0.0317	0.0005	0.15	241	104	208	9	201	3	201	3	n/a
40	171212b_067.FIN2	1061	1.2	19.0440	0.5077	0.0531	0.0013	0.3930	0.0120	0.0525	0.0009	0.55	333	56	336	9	330	6	330	6	n/a
41	171212b_068.FIN2	448	6.7	31.5457	1.2937	0.0502	0.0030	0.2240	0.0150	0.0317	0.0012	0.38	204	139	205	12	201	8	201	8	n/a
43	171212b_070.FIN2	1838	2.9	31.9285	0.7442	0.0503	0.0013	0.2199	0.0054	0.0313	0.0004	0.32	209	60	202	5	199	3	199	3	n/a
44	171212b_071.FIN2	399	2.1	30.6749	1.1291	0.0506	0.0045	0.2310	0.0200	0.0326	0.0010	0.12	223	206	210	17	207	6	207	6	n/a
46	171212b_073.FIN2	636	1.4	31.1333	0.7560	0.0509	0.0017	0.2284	0.0078	0.0321	0.0005	0.22	236	77	208	6	204	3	204	3	n/a
48	171212b_075.FIN2	1063	1.0	19.1095	0.5112	0.0533	0.0015	0.3890	0.0110	0.0523	0.0009	0.36	342	64	333	8	329	6	329	6	n/a

Grain	Spot name	isotopic ratios											isotopic ages										
		U	U/Th	$^{238}\text{U}/$		$^{207}\text{Pb}/$		^{207}Pb		^{206}Pb		rho*	^{207}Pb	\pm	^{207}Pb	\pm	^{206}Pb	\pm	Best	\pm			
				(ppm)	^{206}Pb	2SE	^{206}Pb	2SE	^{235}U	2SE	^{238}U	2SE											
49	171212b_082.FIN2	769	1.3	18.4911	0.4787	0.0534	0.0014	0.4010	0.0110	0.0541	0.0010	0.44	346	59	342	8	339	6	339	6	n/a		
50	171212b_083.FIN2	1593	3.7	35.8423	1.7985	0.0511	0.0041	0.1990	0.0170	0.0279	0.0013	0.39	245	185	184	14	178	8	178	8	n/a		
51	171212b_084.FIN2	2477	2.9	34.1647	1.0505	0.0503	0.0018	0.2063	0.0086	0.0293	0.0007	0.46	209	83	190	7	186	5	186	5	n/a		
52	171212b_085.FIN2	2852	5.7	31.7360	1.2086	0.0507	0.0019	0.2228	0.0079	0.0315	0.0010	0.45	227	87	204	7	200	6	200	6	n/a		
54	171212b_087.FIN2	1997	4.2	32.5521	0.7629	0.0501	0.0013	0.2151	0.0052	0.0307	0.0004	0.22	200	60	198	4	195	3	195	3	n/a		
55	171212b_088.FIN2	583	1.4	20.7469	0.8609	0.0520	0.0033	0.3520	0.0230	0.0482	0.0018	0.37	285	145	305	17	303	11	303	11	n/a		
56	171212b_089.FIN2	515	3.6	24.0674	0.6372	0.0523	0.0026	0.3050	0.0170	0.0416	0.0007	0.39	299	113	270	13	262	5	262	5	n/a		
57	171212b_090.FIN2	253	1.7	20.0000	0.8000	0.0562	0.0057	0.3950	0.0410	0.0500	0.0018	0.23	460	225	336	30	315	11	315	11	n/a		
58	171212b_091.FIN2	1747	3.6	22.1730	0.7866	0.0523	0.0020	0.3290	0.0150	0.0451	0.0014	0.58	299	87	289	12	284	9	284	9	n/a		
59	171212b_092.FIN2	2800	3.0	30.5250	0.7454	0.0505	0.0011	0.2302	0.0053	0.0328	0.0005	0.38	218	50	210	4	208	3	208	3	n/a		
60	171212b_093.FIN2	317	1.5	19.8413	0.9842	0.0542	0.0032	0.3760	0.0230	0.0504	0.0023	0.37	379	133	322	17	317	14	317	14	n/a		
61	171212b_100.FIN2	436	1.0	18.9394	0.7174	0.0531	0.0029	0.3900	0.0240	0.0528	0.0017	0.50	333	124	333	17	332	11	332	11	n/a		
62	171212b_101.FIN2	1074	1.3	18.8324	0.6029	0.0536	0.0022	0.3950	0.0160	0.0531	0.0013	0.28	354	93	337	11	334	8	334	8	n/a		
63	171212b_102.FIN2	1405	3.5	32.8299	0.7868	0.0501	0.0016	0.2140	0.0073	0.0305	0.0005	0.24	200	74	197	6	193	3	193	3	n/a		
64	171212b_103.FIN2	448	1.3	19.3274	0.4856	0.0537	0.0020	0.3870	0.0150	0.0517	0.0009	0.41	358	84	331	11	325	6	325	6	n/a		
65	171212b_104.FIN2	1423	3.8	32.5521	0.9219	0.0506	0.0026	0.2190	0.0130	0.0307	0.0007	0.48	223	119	200	11	195	4	195	4	n/a		
66	171212b_105.FIN2	273	2.0	18.4843	0.6150	0.0540	0.0024	0.4020	0.0180	0.0541	0.0014	0.30	371	100	342	13	339	9	339	9	n/a		
67	171212b_106.FIN2	1201	3.8	34.4353	0.7826	0.0499	0.0010	0.2022	0.0047	0.0290	0.0004	0.45	190	47	187	4	185	2	185	2	n/a		
69	171212b_108.FIN2	279	1.7	19.5427	0.4965	0.0538	0.0021	0.3770	0.0130	0.0512	0.0008	0.09	363	88	325	10	322	5	322	5	n/a		
70	171212b_109.FIN2	895	5.1	32.5733	0.7215	0.0505	0.0013	0.2160	0.0054	0.0307	0.0004	0.23	218	60	198	5	195	2	195	2	n/a		
71	171212b_110.FIN2	1423	6.2	31.6056	0.8691	0.0504	0.0022	0.2205	0.0095	0.0316	0.0006	0.21	213	101	202	8	201	4	201	4	n/a		
72	171212b_111.FIN2	157	1.7	20.6186	0.6802	0.0546	0.0030	0.3640	0.0220	0.0485	0.0013	0.42	396	123	312	17	305	8	305	8	n/a		
73	171212b_118.FIN2	135	0.9	19.3461	0.4866	0.0551	0.0033	0.3950	0.0240	0.0517	0.0009	0.16	416	134	334	18	325	6	325	6	n/a		
75	171212b_120.FIN2	234	1.5	19.7239	0.7003	0.0538	0.0025	0.3800	0.0200	0.0507	0.0015	0.45	363	105	325	15	319	9	319	9	n/a		

Grain	Spot name	isotopic ratios											isotopic ages											
		U (ppm)	U/Th	$^{238}\text{U}/$		$^{207}\text{Pb}/$		^{207}Pb		^{206}Pb		rho*	^{207}Pb		\pm (Ma)	^{207}Pb		\pm (Ma)	^{206}Pb		\pm (Ma)	Best (Ma)	\pm (Ma)	
				^{206}Pb	2SE	^{206}Pb	2SE	^{235}U	2SE	^{238}U	2SE		^{206}Pb	^{235}U		^{238}U	^{206}Pb	^{235}U	^{238}U	^{206}Pb	^{235}U	^{238}U	^{206}Pb	^{235}U
76	171212b_121.FIN2	840	1.3	18.7266	0.5260	0.0542	0.0020	0.3970	0.0140	0.0534	0.0011	0.22	379	83	339	10	335	7	335	7	n/a			
77	171212b_122.FIN2	133	1.1	2.3923	0.1087	0.1429	0.0061	8.2400	0.4900	0.4180	0.0170	0.73	2263	74	2252	53	2249	78	2263	74	99			
79	171212b_124.FIN2	126	1.5	20.2347	0.5323	0.0546	0.0029	0.3690	0.0180	0.0494	0.0009	0.26	396	119	316	14	311	5	311	5	n/a			
80	171212b_125.FIN2	305	1.1	20.6058	0.4671	0.0535	0.0016	0.3600	0.0110	0.0485	0.0006	0.21	350	68	310	8	306	4	306	4	n/a			
81	171212b_126.FIN2	827	4.4	33.6814	0.7374	0.0505	0.0014	0.2064	0.0056	0.0297	0.0003	0.16	218	64	190	5	189	2	189	2	n/a			
82	171212b_127.FIN2	526	1.7	19.1828	0.4784	0.0533	0.0018	0.3860	0.0140	0.0521	0.0009	0.15	342	76	330	10	328	6	328	6	n/a			
83	171212b_128.FIN2	612	1.8	20.3666	0.6637	0.0531	0.0022	0.3590	0.0150	0.0491	0.0013	0.36	333	94	310	11	309	8	309	8	n/a			
84	171212b_129.FIN2	1357	3.5	32.3520	0.7327	0.0508	0.0014	0.2152	0.0061	0.0309	0.0004	0.34	232	64	198	5	196	2	196	2	n/a			
85	171212b_137.FIN2	644	9.4	31.2598	0.9576	0.0519	0.0031	0.2260	0.0140	0.0320	0.0008	0.39	281	137	207	11	203	5	203	5	n/a			
86	171212b_138.FIN2	661	1.6	31.7058	0.7037	0.0509	0.0015	0.2183	0.0063	0.0315	0.0004	0.27	236	68	201	5	200	2	200	2	n/a			
87	171212b_139.FIN2	317	2.0	19.5656	0.5359	0.0538	0.0021	0.3800	0.0160	0.0511	0.0010	0.41	363	88	325	12	321	6	321	6	n/a			
88	171212b_140.FIN2	359	1.5	20.8507	0.5217	0.0531	0.0018	0.3490	0.0120	0.0480	0.0008	0.19	333	77	303	9	302	5	302	5	n/a			
89	171212b_141.FIN2	341	1.4	19.0476	0.5442	0.0552	0.0027	0.3960	0.0200	0.0525	0.0011	0.30	420	109	337	15	330	7	330	7	n/a			
90	171212b_142.FIN2	2254	5.1	31.7460	0.7760	0.0505	0.0015	0.2193	0.0066	0.0315	0.0005	0.28	218	69	201	6	200	3	200	3	n/a			
91	171212b_143.FIN2	127	1.9	18.9753	0.6481	0.0559	0.0046	0.3940	0.0300	0.0527	0.0015	0.18	448	183	334	22	331	9	331	9	n/a			
92	171212b_144.FIN2	365	0.9	20.3542	0.4972	0.0536	0.0026	0.3570	0.0150	0.0491	0.0007	0.04	354	110	311	12	309	4	309	4	n/a			

Rejected Analysis

3	171212b_012.FIN2	203	1.3	18.6047	0.4154	0.0615	0.0024	0.4470	0.0180	0.0538	0.0007	0.07	657	84	372	12	337	4	337	4	n/a			
16	171212b_031.FIN2	509	1.8	31.0366	0.8669	0.0555	0.0028	0.2450	0.0110	0.0322	0.0007	0.27	432	112	222	9	204	4	204	4	n/a			
35	171212b_056.FIN2	168	2.2	19.6464	0.7334	0.0713	0.0063	0.5080	0.0470	0.0509	0.0016	0.35	966	180	411	31	320	10	320	10	n/a			
42	171212b_069.FIN2	247	1.8	30.4507	1.0200	0.0562	0.0044	0.2560	0.0180	0.0328	0.0009	0.26	460	174	230	14	208	6	208	6	n/a			
45	171212b_072.FIN2	469	1.6	7.0922	0.2314	0.1071	0.0026	2.1410	0.0870	0.1410	0.0037	0.70	1751	44	1157	28	850	21	850	21	49			
47	171212b_074.FIN2	430	1.1	20.3252	0.7849	0.0584	0.0032	0.4050	0.0270	0.0492	0.0017	0.54	545	120	344	19	309	10	309	10	n/a			
53	171212b_086.FIN2	399	3.9	21.6873	0.6114	0.0585	0.0026	0.3790	0.0170	0.0461	0.0009	0.26	549	97	325	13	291	6	291	6	n/a			

Grain	Spot name	isotopic ratios										isotopic ages									
		U	U/Th	$^{238}\text{U}/$	$^{207}\text{Pb}/$		^{207}Pb		^{206}Pb			^{207}Pb	\pm	^{207}Pb	\pm	^{206}Pb	\pm	Best	\pm		
		(ppm)		^{206}Pb	2SE	^{206}Pb	2SE	^{235}U	2SE	^{238}U	2SE	rho*	^{206}Pb	(Ma)	^{235}U	(Ma)	^{238}U	(Ma)	Age	(Ma)	conc.
68	171212b_107.FIN2	1194	1.5	17.0358	0.6675	0.0539	0.0022	0.4410	0.0240	0.0587	0.0020	0.59	367	92	371	17	368	12	368	12	n/a
74	171212b_119.FIN2	380	3.8	31.5756	1.1964	0.0584	0.0042	0.2560	0.0180	0.0317	0.0010	0.22	545	157	230	14	201	6	201	6	n/a
78	171212b_123.FIN2	223	1.8	20.4374	0.5012	0.0585	0.0025	0.3950	0.0170	0.0489	0.0008	0.18	549	93	336	12	308	5	308	5	n/a

Grain	Spot name	isotopic ratios								isotopic ages									
		U	U/Th	$^{238}\text{U}/$	$^{207}\text{Pb}/$	^{207}Pb	^{206}Pb	^{235}U	^{206}Pb	^{207}Pb	\pm	^{207}Pb	\pm	^{206}Pb	\pm	Best	\pm		
		(ppm)		^{206}Pb	2SE	^{206}Pb	2SE	^{235}U	2SE	^{238}U	2SE	rho*	^{206}Pb	(Ma)	^{235}U	(Ma)	^{238}U	(Ma)	Age

Whitehorse trough - Richthofen formation - Sample 17-LVD-038, King Lake (Zone 08V 474374E 6742564N NAD 83)

Grain	Spot name	isotopic ratios								isotopic ages											
		U	U/Th	$^{238}\text{U}/$	$^{207}\text{Pb}/$	^{207}Pb	^{206}Pb	^{235}U	^{206}Pb	^{207}Pb	\pm	^{207}Pb	\pm	^{206}Pb	\pm	Best	\pm				
		(ppm)		^{206}Pb	2SE	^{206}Pb	2SE	^{235}U	2SE	^{238}U	2SE	rho	^{206}Pb	(Ma)	^{235}U	(Ma)	^{238}U	(Ma)	Age	(Ma)	conc.
1	171002_105.FIN2	290	2.0	32.5203	1.1633	0.0506	0.0028	0.2150	0.0130	0.0308	0.0009	0.36	223	128	198	11	195	5	195	5	n/a
2	171002_106.FIN2	552	1.9	33.8524	0.9168	0.0503	0.0022	0.2080	0.0100	0.0295	0.0005	0.19	209	101	191	8	188	3	188	3	n/a
3	171002_107.FIN2	421	1.7	32.5415	1.1648	0.0506	0.0036	0.2150	0.0130	0.0307	0.0009	0.24	223	165	198	11	195	5	195	5	n/a
4	171002_108.FIN2	570	1.9	33.4336	0.9278	0.0498	0.0020	0.2072	0.0081	0.0299	0.0005	0.24	186	94	191	7	190	3	190	3	n/a
5	171002_109.FIN2	488	1.7	32.2477	0.9671	0.0505	0.0026	0.2170	0.0100	0.0310	0.0006	0.24	218	119	199	8	197	4	197	4	n/a
6	171002_110.FIN2	504	1.8	33.9674	0.8192	0.0506	0.0017	0.2035	0.0068	0.0294	0.0003	0.16	223	78	188	6	187	2	187	2	n/a
7	171002_111.FIN2	783	1.5	36.2057	1.0094	0.0499	0.0020	0.1921	0.0084	0.0276	0.0005	0.41	190	93	178	7	176	3	176	3	n/a
8	171002_122.FIN2	715	1.8	33.8983	1.1491	0.0501	0.0029	0.2040	0.0130	0.0295	0.0008	0.42	200	134	188	11	187	5	187	5	n/a
9	171002_123.FIN2	278	1.6	31.7460	1.4109	0.0505	0.0044	0.2170	0.0210	0.0315	0.0013	0.33	218	202	199	17	200	8	200	8	n/a
10	171002_124.FIN2	426	1.7	31.9693	0.8176	0.0501	0.0020	0.2170	0.0089	0.0313	0.0004	0.44	200	93	201	8	199	3	199	3	n/a
11	171002_125.FIN2	566	1.7	18.9394	0.6457	0.0534	0.0027	0.3920	0.0220	0.0528	0.0014	0.35	346	114	335	16	332	9	332	9	n/a
12	171002_126.FIN2	790	3.0	33.3667	0.8573	0.0500	0.0014	0.2075	0.0061	0.0300	0.0004	0.36	195	65	191	5	190	3	190	3	n/a
13	171002_127.FIN2	416	1.8	31.9898	0.8801	0.0505	0.0017	0.2207	0.0066	0.0313	0.0005	0.18	218	78	202	6	198	3	198	3	n/a
14	171002_128.FIN2	369	1.9	33.6135	0.7796	0.0507	0.0011	0.2064	0.0047	0.0298	0.0003	0.25	227	50	190	4	189	2	189	2	n/a
15	171002_129.FIN2	495	1.9	33.4113	0.8484	0.0508	0.0020	0.2084	0.0079	0.0299	0.0004	0.01	232	91	192	7	190	3	190	3	n/a
16	171002_130.FIN2	315	1.7	32.9598	1.1950	0.0500	0.0029	0.2110	0.0140	0.0303	0.0008	0.42	195	135	194	12	193	5	193	5	n/a
17	171002_131.FIN2	246	2.1	32.8731	0.8969	0.0507	0.0024	0.2105	0.0098	0.0304	0.0005	0.19	227	109	193	8	193	3	193	3	n/a
18	171002_132.FIN2	440	1.3	31.2402	0.8296	0.0507	0.0023	0.2230	0.0100	0.0320	0.0005	0.24	227	105	204	9	203	3	203	3	n/a

Grain	Spot name	isotopic ratios										isotopic ages									
		U	U/Th	$^{238}\text{U}/$		$^{207}\text{Pb}/$		^{207}Pb		^{206}Pb				^{207}Pb	\pm	^{207}Pb	\pm	^{206}Pb	\pm	Best	\pm
		(ppm)		^{206}Pb	2SE	^{206}Pb	2SE	^{235}U	2SE	^{238}U	2SE	rho*	^{206}Pb	(Ma)	^{235}U	(Ma)	^{238}U	(Ma)	Age	(Ma)	conc.
19	171002_133.FIN2	517	1.9	31.6756	0.7625	0.0497	0.0018	0.2192	0.0078	0.0316	0.0004	0.09	181	84	201	7	200	2	200	2	n/a
20	171005b_009.FIN2	605	1.6	36.2582	1.0649	0.0499	0.0024	0.1910	0.0100	0.0276	0.0007	0.39	190	112	177	9	175	4	175	4	n/a
21	171005b_010.FIN2	510	1.4	34.7222	0.7595	0.0504	0.0023	0.2006	0.0092	0.0288	0.0004	0.19	213	106	185	8	183	3	183	3	n/a
22	171005b_011.FIN2	915	1.2	36.9413	0.8188	0.0496	0.0014	0.1860	0.0054	0.0271	0.0004	0.33	176	66	173	5	172	2	172	2	n/a
23	171005b_012.FIN2	553	1.6	32.6158	1.0425	0.0502	0.0028	0.2120	0.0120	0.0307	0.0008	0.33	204	129	195	10	195	5	195	5	n/a
24	171005b_013.FIN2	584	1.4	33.0142	0.8502	0.0501	0.0026	0.2100	0.0100	0.0303	0.0006	0.13	200	121	193	9	192	4	192	4	n/a
25	171005b_014.FIN2	761	2.4	33.0251	0.9380	0.0504	0.0025	0.2110	0.0110	0.0303	0.0007	0.42	213	115	194	10	192	4	192	4	n/a
27	171005b_016.FIN2	836	1.5	35.0385	0.9576	0.0499	0.0024	0.1977	0.0098	0.0285	0.0006	0.25	190	112	183	8	181	4	181	4	n/a
28	171005b_017.FIN2	1741	1.2	36.7782	0.8927	0.0493	0.0021	0.1867	0.0085	0.0272	0.0005	0.39	162	100	174	7	173	3	173	3	n/a
Rejected Analysis																					
26	171005b_015.FIN2	367	1.1	34.9650	1.0758	0.0610	0.0036	0.2410	0.0140	0.0286	0.0007	0.17	639	127	219	12	182	5	182	5	n/a

Grain	Spot name	isotopic ratios										isotopic ages							
		U	U/Th	$^{238}\text{U}/$	$^{207}\text{Pb}/$		^{207}Pb		^{206}Pb			^{207}Pb	\pm	^{207}Pb	\pm	^{206}Pb	\pm	Best	\pm
		(ppm)		^{206}Pb	2SE	^{206}Pb	2SE	^{235}U	2SE	^{238}U	2SE	rho*	^{206}Pb	(Ma)	^{235}U	(Ma)	^{238}U	(Ma)	Age

Cretaceous

Sample 16-LVD-007, North Klondike Highway (Zone 08V 439338E 6865663N NAD 83)

Grain	Spot name	isotopic ratios										isotopic ages									
		U	U/Th	$^{238}\text{U}/$	$^{207}\text{Pb}/$		^{207}Pb		^{206}Pb			^{207}Pb	\pm	^{207}Pb	\pm	^{206}Pb	\pm	Best	\pm		
		(ppm)		^{206}Pb	2SE	^{206}Pb	2SE	^{235}U	2SE	^{238}U	2SE	rho	^{206}Pb	(Ma)	^{235}U	(Ma)	^{238}U	(Ma)	Age	(Ma)	
1	170323_110.FIN2	124	2.1	5.4025	0.1839	0.0752	0.0020	1.9210	0.0620	0.1851	0.0038	0.57	1074	53	1086	22	1094	21	1074	53	102
2	170323_111.FIN2	187	3.7	50.3778	2.1572	0.0529	0.0040	0.1440	0.0110	0.0199	0.0007	0.22	325	172	136	10	127	4	127	4	n/a
4	170323_113.FIN2	348	1.8	30.4692	1.0212	0.0518	0.0019	0.2329	0.0087	0.0328	0.0006	0.35	277	84	212	7	208	4	208	4	n/a
5	170323_114.FIN2	243	1.2	18.7970	0.7420	0.0530	0.0029	0.3890	0.0230	0.0532	0.0015	0.47	329	124	332	17	334	9	334	9	n/a
7	170323_122.FIN2	375	2.1	26.3852	0.9050	0.0511	0.0020	0.2670	0.0110	0.0379	0.0008	0.38	245	90	240	9	240	5	240	5	n/a
9	170323_124.FIN2	583	2.1	54.8546	2.1063	0.0500	0.0034	0.1257	0.0085	0.0182	0.0005	0.28	195	158	120	8	117	3	117	3	n/a
10	170323_125.FIN2	111	0.8	6.7204	0.2168	0.0717	0.0020	1.4640	0.0440	0.1488	0.0027	0.48	977	57	916	19	894	15	894	15	91
11	170323_126.FIN2	238	2.4	29.5159	0.9583	0.0526	0.0025	0.2430	0.0110	0.0339	0.0007	0.20	312	108	220	9	215	4	215	4	n/a
12	170323_127.FIN2	499	3.1	31.8066	0.9914	0.0511	0.0015	0.2205	0.0076	0.0314	0.0005	0.38	245	68	203	6	200	3	200	3	n/a
13	170323_128.FIN2	271	2.4	32.0513	1.0273	0.0513	0.0026	0.2220	0.0120	0.0312	0.0005	0.30	254	117	202	10	198	3	198	3	n/a
14	170323_129.FIN2	175	2.5	51.2558	1.7077	0.0480	0.0031	0.1288	0.0084	0.0195	0.0004	0.13	99	153	122	8	125	2	125	2	n/a
15	170323_130.FIN2	549	1.6	33.2116	1.0368	0.0501	0.0019	0.2092	0.0081	0.0301	0.0005	0.19	200	88	192	7	191	3	191	3	n/a
17	170323_138.FIN2	435	2.3	5.5710	0.2048	0.0756	0.0016	1.8740	0.0540	0.1795	0.0045	0.71	1084	42	1071	19	1064	25	1084	42	98
18	170323_139.FIN2	213	1.9	31.3087	1.0783	0.0518	0.0031	0.2280	0.0140	0.0319	0.0007	0.12	277	137	207	11	203	4	203	4	n/a
19	170323_140.FIN2	1273	1.3	51.7331	1.6593	0.0492	0.0013	0.1314	0.0041	0.0193	0.0003	0.55	157	62	125	4	123	2	123	2	n/a
20	170323_141.FIN2	790	3.9	36.6838	1.1304	0.0503	0.0012	0.1905	0.0050	0.0273	0.0004	0.39	209	55	177	4	173	3	173	3	n/a
22	170323_143.FIN2	124	2.2	29.6384	1.0541	0.0512	0.0037	0.2380	0.0180	0.0337	0.0008	0.30	250	166	215	15	214	5	214	5	n/a
23	170323_144.FIN2	362	1.3	5.6754	0.1900	0.0737	0.0019	1.8000	0.0620	0.1762	0.0036	0.71	1033	52	1043	22	1046	19	1033	52	101

Grain	Spot name	isotopic ratios												isotopic ages									
		U	U/Th	$^{238}\text{U}/$		$^{207}\text{Pb}/$		^{207}Pb		^{206}Pb			^{207}Pb	\pm	^{207}Pb	\pm	^{206}Pb	\pm	Best	\pm			
		(ppm)		^{206}Pb	2SE	^{206}Pb	2SE	^{235}U	2SE	^{238}U	2SE	rho*	^{206}Pb	(Ma)	^{235}U	(Ma)	^{238}U	(Ma)	Age	(Ma)	n/a		
24	170323_145.FIN2	316	2.0	37.1195	1.2676	0.0509	0.0026	0.1867	0.0088	0.0269	0.0006	0.22	236	118	173	8	171	4	171	4	n/a		
25	170323_146.FIN2	1037	3.3	54.2299	1.6469	0.0490	0.0013	0.1251	0.0037	0.0184	0.0003	0.40	148	62	120	3	118	2	118	2	n/a		
27	170323_154.FIN2	194	1.9	52.5210	1.7930	0.0483	0.0035	0.1280	0.0100	0.0190	0.0004	0.32	114	171	122	9	122	3	122	3	n/a		
28	170323_155.FIN2	538	2.6	33.7268	1.0579	0.0502	0.0018	0.2059	0.0080	0.0297	0.0005	0.43	204	83	190	7	188	3	188	3	n/a		
30	170323_157.FIN2	54	3.1	25.6410	0.9862	0.0509	0.0043	0.2710	0.0230	0.0390	0.0011	0.19	236	195	240	18	247	7	247	7	n/a		
32	170323_159.FIN2	596	2.4	31.0849	1.0629	0.0516	0.0022	0.2282	0.0091	0.0322	0.0007	0.58	268	98	211	9	204	5	204	5	n/a		
33	170323_160.FIN2	277	1.1	29.5858	1.0504	0.0529	0.0029	0.2490	0.0150	0.0338	0.0009	0.36	325	124	225	12	214	5	214	5	n/a		
34	170323_161.FIN2	240	1.6	34.1530	1.2831	0.0514	0.0038	0.2070	0.0150	0.0293	0.0008	0.10	259	170	190	12	186	5	186	5	n/a		
35	170323_162.FIN2	245	0.9	3.5211	0.1612	0.1226	0.0030	4.8200	0.2000	0.2840	0.0100	0.84	1994	43	1783	35	1612	52	1994	43	81		
36	170323_169.FIN2	69	3.0	27.2480	1.0394	0.0525	0.0050	0.2630	0.0220	0.0367	0.0010	0.39	307	217	235	18	232	6	232	6	n/a		
38	170323_171.FIN2	788	2.2	52.7983	1.7284	0.0490	0.0018	0.1281	0.0042	0.0189	0.0004	0.14	148	86	122	4	121	2	121	2	n/a		
39	170323_172.FIN2	849	1.5	54.7345	2.1271	0.0497	0.0025	0.1256	0.0069	0.0183	0.0005	0.45	181	117	120	6	117	3	117	3	n/a		
40	170323_173.FIN2	484	1.7	20.5761	0.7197	0.0532	0.0020	0.3590	0.0130	0.0486	0.0010	0.32	337	85	311	10	306	6	306	6	n/a		
41	170323_174.FIN2	134	2.1	19.5313	0.6866	0.0540	0.0030	0.3780	0.0200	0.0512	0.0011	0.17	371	125	323	15	322	7	322	7	n/a		
42	170323_175.FIN2	464	8.8	53.7346	1.7902	0.0494	0.0029	0.1268	0.0076	0.0186	0.0004	0.26	167	137	121	7	119	2	119	2	n/a		
46	170323_185.FIN2	202	2.4	30.9789	1.2476	0.0512	0.0040	0.2300	0.0200	0.0323	0.0009	0.50	250	180	209	17	205	6	205	6	n/a		
47	170323_186.FIN2	253	2.0	3.8139	0.1193	0.0926	0.0015	3.3590	0.0680	0.2622	0.0042	0.64	1480	31	1493	16	1501	21	1480	31	101		
49	170323_188.FIN2	367	2.7	30.7031	0.9333	0.0503	0.0014	0.2257	0.0063	0.0326	0.0005	0.31	209	65	206	5	207	3	207	3	n/a		
55	170323_194.FIN2	986	2.6	44.6229	1.5731	0.0502	0.0017	0.1553	0.0060	0.0224	0.0005	0.60	204	79	147	5	143	3	143	3	n/a		
61	170323_206.FIN2	136	2.7	50.8906	1.7093	0.0514	0.0039	0.1390	0.0100	0.0197	0.0004	0.16	259	174	131	9	125	3	125	3	n/a		
63	170323_208.FIN2	642	2.0	19.3424	0.7108	0.0541	0.0019	0.3880	0.0160	0.0517	0.0013	0.51	375	79	332	11	325	8	325	8	n/a		
64	170323_209.FIN2	1113	2.2	52.6039	1.6603	0.0491	0.0014	0.1295	0.0040	0.0190	0.0003	0.32	153	67	124	4	121	2	121	2	n/a		
65	170323_210.FIN2	811	2.0	17.3611	0.5425	0.0533	0.0012	0.4240	0.0110	0.0576	0.0010	0.53	342	51	359	8	361	6	361	6	n/a		
67	170324_010.FIN2	751	2.7	37.3972	1.5384	0.0522	0.0018	0.1922	0.0091	0.0267	0.0007	0.69	294	79	178	8	170	5	170	5	n/a		

Grain	Spot name	isotopic ratios										isotopic ages									
		U	U/Th	$^{238}\text{U}/$	$^{207}\text{Pb}/$		^{207}Pb		^{206}Pb		^{207}Pb	\pm	^{207}Pb	\pm	^{206}Pb	\pm	Best	\pm			
		(ppm)		^{206}Pb	2SE	^{206}Pb	2SE	^{235}U	2SE	^{238}U	2SE	rho*	^{206}Pb	(Ma)	^{235}U	(Ma)	^{238}U	(Ma)	Age	(Ma)	
68	170324_011.FIN2	619	1.9	17.5747	0.6486	0.0544	0.0016	0.4250	0.0130	0.0569	0.0012	0.47	388	66	359	10	357	7	357	7	n/a
69	170324_012.FIN2	1788	2.5	56.2430	2.3725	0.0497	0.0022	0.1211	0.0049	0.0178	0.0005	0.26	181	103	116	4	114	3	114	3	n/a
72	170324_015.FIN2	192	3.3	17.2117	0.6221	0.0548	0.0018	0.4360	0.0150	0.0581	0.0011	0.43	404	74	366	11	364	7	364	7	n/a
73	170324_016.FIN2	1124	2.5	53.9665	1.9513	0.0492	0.0015	0.1250	0.0043	0.0185	0.0004	0.45	157	71	120	4	118	2	118	2	n/a
78	170324_027.FIN2	1007	3.4	37.5657	1.3971	0.0511	0.0018	0.1862	0.0072	0.0266	0.0006	0.44	245	81	173	6	169	4	169	4	n/a
79	170324_028.FIN2	592	6.3	17.0707	0.6120	0.0550	0.0012	0.4420	0.0120	0.0586	0.0010	0.63	412	49	371	9	367	6	367	6	n/a
82	170324_031.FIN2	230	1.0	3.5855	0.1414	0.1081	0.0024	4.1300	0.1200	0.2789	0.0065	0.68	1768	41	1665	21	1585	33	1768	41	90
83	170324_032.FIN2	1010	1.6	56.6893	2.5388	0.0510	0.0025	0.1235	0.0075	0.0176	0.0006	0.51	241	113	118	7	113	4	113	4	n/a
Rejected Analysis																					
3	170323_112.FIN2	172	3.3	50.0751	1.8305	0.0537	0.0033	0.1472	0.0094	0.0200	0.0005	0.17	358	139	139	8	128	3	128	3	n/a
6	170323_121.FIN2	1330	3.5	40.6174	1.9797	0.0524	0.0014	0.1787	0.0090	0.0246	0.0010	0.87	303	61	166	8	157	6	157	6	n/a
8	170323_123.FIN2	221	3.5	54.5852	2.2347	0.0563	0.0046	0.1460	0.0130	0.0183	0.0006	0.18	464	181	138	11	117	4	117	4	n/a
16	170323_137.FIN2	168	2.2	29.4985	1.3923	0.0670	0.0043	0.3220	0.0280	0.0339	0.0013	0.48	838	134	282	21	215	8	215	8	n/a
21	170323_142.FIN2	3230	4.3	58.1058	2.4984	0.0612	0.0022	0.1456	0.0065	0.0172	0.0006	0.61	646	77	138	6	110	4	110	4	n/a
26	170323_153.FIN2	168	2.5	55.3710	2.1768	0.0571	0.0047	0.1400	0.0110	0.0181	0.0005	0.27	495	181	132	10	115	3	115	3	n/a
29	170323_156.FIN2	117	2.6	51.1509	2.2240	0.0561	0.0061	0.1520	0.0170	0.0196	0.0007	0.38	456	241	142	15	125	4	125	4	n/a
31	170323_158.FIN2	239	1.6	36.4564	1.1829	0.0523	0.0025	0.2010	0.0110	0.0274	0.0005	0.42	299	109	185	9	174	3	174	3	n/a
37	170323_170.FIN2	1353	2.4	4.0404	0.1796	0.2085	0.0024	7.2100	0.2200	0.2475	0.0084	0.95	2894	19	2135	27	1424	43	2894	43	49
43	170323_176.FIN2	879	0.8	47.2813	2.0790	0.0562	0.0037	0.1650	0.0150	0.0212	0.0007	0.72	460	146	155	13	135	5	135	5	n/a
44	170323_177.FIN2	957	2.8	24.3843	0.8324	0.0568	0.0020	0.3240	0.0120	0.0410	0.0009	0.31	484	78	285	9	259	5	259	5	n/a
45	170323_178.FIN2	395	2.2	31.4268	1.0864	0.0505	0.0018	0.2215	0.0089	0.0318	0.0007	0.48	218	83	203	7	202	5	202	5	n/a
48	170323_187.FIN2	314	1.4	31.1333	1.0662	0.0569	0.0026	0.2520	0.0110	0.0321	0.0007	0.22	488	101	227	9	204	4	204	4	n/a
50	170323_189.FIN2	174	3.0	52.1105	2.1724	0.0708	0.0080	0.1870	0.0210	0.0192	0.0006	0.39	952	231	173	18	123	4	123	4	n/a
51	170323_190.FIN2	128	2.7	32.0924	1.2359	0.0631	0.0058	0.2750	0.0280	0.0312	0.0009	0.37	712	195	245	22	198	5	198	5	n/a

Grain	Spot name	isotopic ratios												isotopic ages											
		U (ppm)	U/Th	$^{238}\text{U}/$		$^{207}\text{Pb}/$		^{207}Pb		^{206}Pb		rho*	^{206}Pb (Ma)	^{207}Pb (Ma)	^{207}Pb (Ma)	^{206}Pb (Ma)	Best	\pm	^{207}Pb (Ma)	^{207}Pb (Ma)	^{206}Pb (Ma)	Age	(Ma)	conc.	
				^{206}Pb	2SE	^{206}Pb	2SE	^{235}U	2SE	^{238}U	2SE														
52	170323_191.FIN2	1085	1.0	58.9623	2.0512	0.1236	0.0036	0.2896	0.0092	0.0170	0.0004	0.49	2009	52	258	7	108	2	108	2	n/a				
53	170323_192.FIN2	173	1.8	38.7147	1.3939	0.0599	0.0039	0.2130	0.0140	0.0258	0.0006	0.19	600	141	195	11	164	4	164	4	n/a				
54	170323_193.FIN2	481	2.3	32.4044	1.1551	0.0560	0.0020	0.2410	0.0100	0.0309	0.0007	0.49	452	79	219	8	196	4	196	4	n/a				
56	170323_201.FIN2	281	1.9	24.6853	0.7922	0.0609	0.0022	0.3370	0.0130	0.0405	0.0008	0.22	636	78	294	10	256	5	256	5	n/a				
57	170323_202.FIN2	248	1.8	30.2389	1.0058	0.0533	0.0019	0.2429	0.0088	0.0331	0.0006	0.24	342	81	221	7	210	4	210	4	n/a				
58	170323_203.FIN2	1240	3.1	42.1941	2.4925	0.0578	0.0027	0.1960	0.0190	0.0237	0.0013	0.96	522	102	180	16	151	8	151	8	n/a				
59	170323_204.FIN2	323	4.4	38.6100	1.4162	0.0604	0.0037	0.2170	0.0140	0.0259	0.0007	0.29	618	132	198	12	165	4	165	4	n/a				
60	170323_205.FIN2	1060	2.0	35.1370	1.3581	0.0697	0.0029	0.2760	0.0150	0.0285	0.0008	0.65	920	86	247	12	181	5	181	5	n/a				
62	170323_207.FIN2	104	0.8	2.8137	0.1029	0.1127	0.0030	5.5300	0.1700	0.3554	0.0087	0.57	1843	48	1902	27	1959	42	1843	42	106				
66	170324_009.FIN2	237	2.0	31.2500	1.6602	0.0595	0.0048	0.2620	0.0220	0.0320	0.0014	0.46	585	175	235	18	203	9	203	9	n/a				
70	170324_013.FIN2	351	0.9	28.4091	1.2106	0.0643	0.0041	0.3110	0.0200	0.0352	0.0011	0.52	752	135	274	16	223	7	223	7	n/a				
71	170324_014.FIN2	556	0.6	29.4118	1.4706	0.0565	0.0027	0.2640	0.0170	0.0340	0.0014	0.58	472	106	237	13	216	9	216	9	n/a				
74	170324_017.FIN2	445	2.4	18.1818	0.6612	0.0592	0.0020	0.4460	0.0160	0.0550	0.0011	0.37	574	73	373	11	345	7	345	7	n/a				
75	170324_018.FIN2	325	2.4	36.1795	1.4398	0.0619	0.0030	0.2340	0.0120	0.0276	0.0007	0.31	671	104	213	10	176	4	176	4	n/a				
76	170324_025.FIN2	505	1.7	33.3333	1.4444	0.0584	0.0037	0.2390	0.0170	0.0300	0.0009	0.31	545	138	217	13	191	6	191	6	n/a				
77	170324_026.FIN2	220	1.4	36.6300	1.6101	0.0554	0.0039	0.2070	0.0170	0.0273	0.0009	0.53	428	157	191	14	174	6	174	6	n/a				
80	170324_029.FIN2	492	2.1	32.1337	1.4456	0.0595	0.0039	0.2540	0.0180	0.0311	0.0010	0.43	585	142	229	15	198	6	198	6	n/a				
81	170324_030.FIN2	2839	1.3	61.6523	2.5467	0.0797	0.0023	0.1769	0.0065	0.0162	0.0005	0.62	1190	57	165	6	104	3	104	3	n/a				

* italicized rho values are the average rho values for the sample and replace negative rho values

D.2 Lu-Hf isotopic ratios

Tanglefoot formation

Whitehorse trough - Tanglefoot formation - Sample 16-LVD-001B, Robert Campbell Highway (Zone 08V 455577E 6877512N NAD 83)

Grain	Spot ID	corrected												MUN	$^{176}\text{Hf}/^{177}\text{Hf}$	EHf0	2SE	EHfi
		$^{176}\text{Hf}/^{177}\text{Hf}$	2SE	$^{176}\text{Lu}/^{177}\text{Hf}$	2SE	$^{176}\text{Yb}/^{177}\text{Hf}$	2SE	$^{178}\text{Hf}/^{177}\text{Hf}$	2SE	Total Hf Beam	LASS Age (Ma)							
2	16-LVD-001B_119	0.282575	0.000026	0.00096	0.00005	0.0243	0.0012	1.467178	0.000031	14.4	205	0.282571	-7.4	0.9	-3.0			
3	16-LVD-001B_120	0.282619	0.000026	0.00109	0.00006	0.0274	0.0017	1.467119	0.000043	11.5	201	0.282615	-5.9	0.9	-1.5			
4	16-LVD-001B_121	0.282743	0.000026	0.00130	0.00001	0.0327	0.0002	1.467159	0.000036	11.2	204	0.282738	-1.5	0.9	2.9			
5	16-LVD-001B_122	0.282716	0.000026	0.00144	0.00009	0.0318	0.0020	1.467143	0.000034	12.3	207	0.282710	-2.4	0.9	2.0			
6	16-LVD-001B_123	0.282680	0.000022	0.00116	0.00007	0.0243	0.0014	1.467170	0.000033	13.5	204	0.282676	-3.7	0.8	0.7			
7	16-LVD-001B_124	0.282714	0.000020	0.00108	0.00006	0.0233	0.0014	1.467176	0.000025	13.5	204	0.282710	-2.5	0.7	1.9			
8	16-LVD-001B_125	0.282746	0.000027	0.00149	0.00010	0.0391	0.0026	1.467151	0.000032	11.9	208	0.282740	-1.4	1.0	3.0			
9	16-LVD-001B_126	0.282556	0.000027	0.00081	0.00003	0.0192	0.0005	1.467177	0.000040	12.7	209	0.282553	-8.1	1.0	-3.6			
10	16-LVD-001B_127	0.282573	0.000022	0.00061	0.00005	0.0151	0.0012	1.467174	0.000032	12.0	198	0.282571	-7.5	0.8	-3.2			
11	16-LVD-001B_128	0.282704	0.000024	0.00096	0.00008	0.0219	0.0021	1.467177	0.000041	11.3	213	0.282700	-2.9	0.8	1.7			
12	16-LVD-001B_129	0.282708	0.000024	0.00127	0.00005	0.0277	0.0009	1.467237	0.000039	12.7	200	0.282703	-2.7	0.8	1.6			
14	16-LVD-001B_137	0.282720	0.000030	0.00080	0.00002	0.0189	0.0005	1.467180	0.000041	13.6	198	0.282717	-2.3	1.1	2.0			
15	16-LVD-001B_138	0.282758	0.000027	0.00154	0.00008	0.0386	0.0018	1.467202	0.000045	12.0	192	0.282752	-1.0	1.0	3.1			
17	16-LVD-001B_140	0.282809	0.000029	0.00265	0.00015	0.0673	0.0044	1.467174	0.000045	8.9	187	0.282800	0.8	1.0	4.7			
18	16-LVD-001B_141	0.282660	0.000019	0.00129	0.00003	0.0272	0.0006	1.467180	0.000031	13.1	198	0.282655	-4.4	0.7	-0.2			
19	16-LVD-001B_142	0.282584	0.000024	0.00117	0.00006	0.0285	0.0014	1.467218	0.000041	16.5	199	0.282580	-7.1	0.8	-2.8			
21	16-LVD-001B_144	0.282728	0.000019	0.00143	0.00013	0.0309	0.0027	1.467178	0.000036	15.5	186	0.282723	-2.0	0.7	1.9			
22	16-LVD-001B_145	0.282586	0.000023	0.00123	0.00006	0.0300	0.0016	1.467171	0.000034	14.7	198	0.282581	-7.0	0.8	-2.8			
23	16-LVD-001B_146	0.282561	0.000021	0.00107	0.00002	0.0256	0.0007	1.467193	0.000029	12.7	186	0.282557	-7.9	0.7	-3.9			
24	16-LVD-001B_147	0.282554	0.000018	0.00092	0.00007	0.0220	0.0015	1.467171	0.000036	12.1	191	0.282551	-8.2	0.6	-4.0			

Grain	Spot ID	corrected										MUN LASS Age (Ma)	$^{176}\text{Hf}/^{177}\text{Hf}$	EHf0	2SE	EHfi
		$^{176}\text{Hf}/^{177}\text{Hf}$	2SE	$^{176}\text{Lu}/^{177}\text{Hf}$	2SE	$^{176}\text{Yb}/^{177}\text{Hf}$	2SE	$^{178}\text{Hf}/^{177}\text{Hf}$	2SE	Total Hf Beam						
25	16-LVD-001B_154	0.282726	0.000020	0.00116	0.00003	0.0234	0.0008	1.467177	0.000040	13.4	200	0.282722	-2.1	0.7	2.2	
26	16-LVD-001B_155	0.282693	0.000027	0.00106	0.00003	0.0236	0.0005	1.467184	0.000031	11.8	206	0.282689	-3.3	1.0	1.2	
27	16-LVD-001B_156	0.282575	0.000021	0.00100	0.00001	0.0239	0.0003	1.467196	0.000027	12.5	195	0.282571	-7.4	0.7	-3.2	
28	16-LVD-001B_157	0.282702	0.000019	0.00092	0.00005	0.0203	0.0010	1.467204	0.000033	11.1	206	0.282698	-2.9	0.7	1.5	
29	16-LVD-001B_158	0.282914	0.000023	0.00036	0.00003	0.0091	0.0008	1.467177	0.000030	13.4	219	0.282913	4.6	0.8	9.4	
31	16-LVD-001B_160	0.282792	0.000017	0.00063	0.00001	0.0163	0.0004	1.467186	0.000039	10.9	200	0.282790	0.2	0.6	4.6	
32	16-LVD-001B_161	0.282690	0.000019	0.00090	0.00004	0.0194	0.0009	1.467193	0.000034	12.4	206	0.282687	-3.4	0.7	1.1	
33	16-LVD-001B_162	0.282577	0.000024	0.00106	0.00001	0.0253	0.0004	1.467167	0.000040	12.7	192	0.282573	-7.4	0.8	-3.2	
34	16-LVD-001B_163	0.282675	0.000022	0.00122	0.00003	0.0262	0.0007	1.467234	0.000039	12.1	197	0.282671	-3.9	0.8	0.3	
35	16-LVD-001B_164	0.282583	0.000027	0.00074	0.00001	0.0168	0.0003	1.467173	0.000034	13.1	189	0.282580	-7.1	1.0	-3.0	
36	16-LVD-001B_165	0.282696	0.000024	0.00118	0.00008	0.0275	0.0020	1.467160	0.000034	11.7	195	0.282692	-3.1	0.8	1.0	
37	16-LVD-001B_172	0.282710	0.000027	0.00158	0.00009	0.0350	0.0022	1.467243	0.000047	14.1	202	0.282704	-2.7	1.0	1.6	
38	16-LVD-001B_173	0.282569	0.000027	0.00119	0.00008	0.0291	0.0024	1.467208	0.000037	12.5	185	0.282565	-7.6	1.0	-3.7	
39	16-LVD-001B_174	0.282839	0.000025	0.00091	0.00005	0.0231	0.0014	1.467133	0.000034	11.3	203	0.282836	1.9	0.9	6.3	
40	16-LVD-001B_175	0.282636	0.000027	0.00117	0.00005	0.0287	0.0012	1.467225	0.000045	15.2	185	0.282632	-5.3	1.0	-1.3	
41	16-LVD-001B_176	0.282789	0.000031	0.00089	0.00008	0.0183	0.0016	1.467176	0.000033	14.8	200	0.282786	0.1	1.1	4.5	
42	16-LVD-001B_177	0.282701	0.000027	0.00147	0.00008	0.0320	0.0022	1.467180	0.000036	13.1	196	0.282696	-3.0	1.0	1.2	
43	16-LVD-001B_178	0.282544	0.000022	0.00097	0.00002	0.0229	0.0005	1.467159	0.000038	12.4	191	0.282541	-8.5	0.8	-4.4	
44	16-LVD-001B_179	0.282544	0.000022	0.00090	0.00003	0.0214	0.0005	1.467207	0.000036	12.4	190	0.282541	-8.5	0.8	-4.4	
45	16-LVD-001B_180	0.282565	0.000021	0.00101	0.00005	0.0242	0.0010	1.467178	0.000032	14.6	186	0.282561	-7.8	0.7	-3.8	
46	16-LVD-001B_181	0.282592	0.000025	0.00087	0.00004	0.0205	0.0010	1.467183	0.000040	12.7	193	0.282589	-6.8	0.9	-2.7	
47	16-LVD-001B_182	0.282691	0.000024	0.00090	0.00004	0.0201	0.0009	1.467185	0.000036	12.3	195	0.282688	-3.3	0.8	0.9	
49	16-LVD-001B_190	0.282684	0.000029	0.00103	0.00004	0.0218	0.0012	1.467221	0.000033	12.5	198	0.282680	-3.6	1.0	0.7	

Grain	Spot ID	corrected										MUN LASS Age (Ma)	$^{176}\text{Hf}/^{177}\text{Hf}$	EHf0	2SE	EHfi
		$^{176}\text{Hf}/^{177}\text{Hf}$	2SE	$^{176}\text{Lu}/^{177}\text{Hf}$	2SE	$^{176}\text{Yb}/^{177}\text{Hf}$	2SE	$^{178}\text{Hf}/^{177}\text{Hf}$	2SE	Total Hf Beam						
50	16-LVD-001B_191	0.282581	0.000024	0.00127	0.00001	0.0298	0.0005	1.467200	0.000038	12.2	185	0.282577	-7.2	0.8	-3.3	
51	16-LVD-001B_192	0.282690	0.000020	0.00080	0.00004	0.0185	0.0007	1.467173	0.000034	12.4	197	0.282687	-3.4	0.7	0.9	
52	16-LVD-001B_193	0.282561	0.000020	0.00100	0.00003	0.0233	0.0008	1.467184	0.000023	13.2	193	0.282557	-7.9	0.7	-3.8	
54	16-LVD-001B_195	0.282700	0.000028	0.00105	0.00004	0.0247	0.0008	1.467198	0.000030	12.8	204	0.282696	-3.0	1.0	1.4	
55	16-LVD-001B_196	0.282613	0.000027	0.00099	0.00004	0.0234	0.0009	1.467136	0.000040	12.5	204	0.282609	-6.1	1.0	-1.7	
56	16-LVD-001B_197	0.282713	0.000019	0.00082	0.00006	0.0166	0.0013	1.467157	0.000030	13.9	198	0.282710	-2.5	0.7	1.7	
57	16-LVD-001B_198	0.282576	0.000021	0.00077	0.00003	0.0180	0.0008	1.467191	0.000036	12.9	191	0.282573	-7.4	0.7	-3.2	
58	16-LVD-001B_199	0.282616	0.000029	0.00128	0.00004	0.0302	0.0011	1.467206	0.000048	10.1	193	0.282611	-6.0	1.0	-1.8	
59	16-LVD-001B_200	0.282537	0.000024	0.00123	0.00003	0.0295	0.0009	1.467147	0.000043	13.7	189	0.282533	-8.8	0.8	-4.7	
60	16-LVD-001B_201	0.282647	0.000027	0.00086	0.00002	0.0200	0.0004	1.467197	0.000030	12.3	185	0.282644	-4.9	1.0	-0.9	
61	16-LVD-001B_208	0.282566	0.000022	0.00094	0.00004	0.0227	0.0008	1.467170	0.000036	13.2	192	0.282563	-7.7	0.8	-3.6	
62	16-LVD-001B_209	0.282736	0.000025	0.00127	0.00004	0.0318	0.0011	1.467161	0.000039	11.4	194	0.282731	-1.7	0.9	2.4	
63	16-LVD-001B_210	0.282572	0.000037	0.00152	0.00010	0.0383	0.0029	1.467189	0.000046	14.4	194	0.282567	-7.5	1.3	-3.4	
64	16-LVD-001B_211	0.282543	0.000024	0.00094	0.00002	0.0219	0.0006	1.467172	0.000032	11.8	187	0.282540	-8.6	0.8	-4.5	
66	16-LVD-001B_213	0.282687	0.000032	0.00121	0.00014	0.0271	0.0033	1.467157	0.000047	12.2	353	0.282679	-3.5	1.1	4.1	
69	16-LVD-001B_216	0.282591	0.000027	0.00112	0.00003	0.0266	0.0008	1.467179	0.000042	14.3	191	0.282587	-6.9	1.0	-2.8	
70	16-LVD-001B_217	0.282593	0.000021	0.00114	0.00004	0.0271	0.0011	1.467180	0.000030	12.0	193	0.282589	-6.8	0.7	-2.6	
71	16-LVD-001B_218	0.282734	0.000025	0.00142	0.00002	0.0299	0.0008	1.467158	0.000039	14.9	209	0.282728	-1.8	0.9	2.7	
72	16-LVD-001B_219	0.282585	0.000016	0.00089	0.00003	0.0210	0.0008	1.467183	0.000038	12.3	186	0.282582	-7.1	0.6	-3.1	
74	16-LVD-001B_11	0.282552	0.000025	0.00113	0.00002	0.0276	0.0008	1.467196	0.000026	13.3	195	0.282548	-8.2	0.9	-4.0	
75	16-LVD-001B_12	0.282598	0.000029	0.00133	0.00006	0.0321	0.0014	1.467196	0.000042	11.8	185	0.282593	-6.6	1.0	-2.7	
76	16-LVD-001B_13	0.282666	0.000022	0.00060	0.00002	0.0133	0.0004	1.467175	0.000041	12.4	194	0.282664	-4.2	0.8	0.0	
77	16-LVD-001B_14	0.282773	0.000024	0.00126	0.00005	0.0283	0.0007	1.467185	0.000033	14.6	193	0.282768	-0.4	0.8	3.7	

Grain	Spot ID	corrected										MUN LASS Age (Ma)	$^{176}\text{Hf}/^{177}\text{Hf}$	EHf0	2SE	EHfi
		$^{176}\text{Hf}/^{177}\text{Hf}$	2SE	$^{176}\text{Lu}/^{177}\text{Hf}$	2SE	$^{176}\text{Yb}/^{177}\text{Hf}$	2SE	$^{178}\text{Hf}/^{177}\text{Hf}$	2SE	Total Hf Beam						
78	16-LVD-001B_15	0.282598	0.000030	0.00110	0.00006	0.0273	0.0016	1.467149	0.000042	14.2	186	0.282594	-6.6	1.1	-2.6	
79	16-LVD-001B_16	0.282715	0.000024	0.00128	0.00012	0.0310	0.0033	1.467167	0.000031	12.2	207	0.282710	-2.5	0.8	1.9	
80	16-LVD-001B_17	0.282469	0.000027	0.00084	0.00004	0.0227	0.0012	1.467146	0.000033	11.1	342	0.282464	-11.2	1.0	-3.8	
82	16-LVD-001B_19	0.282746	0.000023	0.00120	0.00005	0.0293	0.0012	1.467190	0.000026	11.8	199	0.282742	-1.4	0.8	2.9	
83	16-LVD-001B_20	0.282673	0.000025	0.00079	0.00004	0.0185	0.0008	1.467209	0.000035	12.3	201	0.282670	-4.0	0.9	0.4	
84	16-LVD-001B_21	0.282622	0.000022	0.00117	0.00004	0.0284	0.0010	1.467171	0.000030	12.7	186	0.282618	-5.8	0.8	-1.8	
87	16-LVD-001B_30	0.282729	0.000023	0.00082	0.00003	0.0203	0.0006	1.467149	0.000032	13.5	205	0.282726	-2.0	0.8	2.5	
89	16-LVD-001B_32	0.282726	0.000021	0.00116	0.00003	0.0239	0.0006	1.467176	0.000026	13.5	195	0.282722	-2.1	0.7	2.1	
90	16-LVD-001B_33	0.282683	0.000023	0.00048	0.00002	0.0108	0.0005	1.467172	0.000036	13.1	201	0.282681	-3.6	0.8	0.8	
91	16-LVD-001B_34	0.282701	0.000023	0.00117	0.00004	0.0279	0.0012	1.467188	0.000033	13.1	188	0.282697	-3.0	0.8	1.1	
92	16-LVD-001B_35	0.282552	0.000026	0.00111	0.00004	0.0271	0.0009	1.467167	0.000036	14.3	194	0.282548	-8.2	0.9	-4.1	
93	16-LVD-001B_36	0.282767	0.000040	0.00114	0.00008	0.0288	0.0024	1.467180	0.000041	13.3	185	0.282763	-0.6	1.4	3.3	
94	16-LVD-001B_37	0.282635	0.000021	0.00076	0.00002	0.0185	0.0006	1.467201	0.000031	13.3	186	0.282632	-5.3	0.7	-1.3	
95	16-LVD-001B_38	0.282664	0.000022	0.00108	0.00003	0.0245	0.0007	1.467177	0.000041	12.1	204	0.282660	-4.3	0.8	0.1	
96	16-LVD-001B_39	0.282717	0.000021	0.00089	0.00002	0.0219	0.0006	1.467160	0.000034	15.8	193	0.282714	-2.4	0.7	1.8	
97	16-LVD-001B_46	0.282571	0.000023	0.00091	0.00003	0.0222	0.0007	1.467164	0.000037	12.5	196	0.282568	-7.6	0.8	-3.3	
98	16-LVD-001B_47	0.282714	0.000017	0.00098	0.00007	0.0198	0.0014	1.467191	0.000026	14.2	203	0.282710	-2.5	0.6	1.9	
99	16-LVD-001B_48	0.282696	0.000023	0.00063	0.00001	0.0160	0.0003	1.467189	0.000039	12.0	198	0.282694	-3.1	0.8	1.2	
100	16-LVD-001B_49	0.282553	0.000025	0.00085	0.00002	0.0199	0.0005	1.467186	0.000027	13.4	189	0.282550	-8.2	0.9	-4.1	
102	16-LVD-001B_51	0.282578	0.000028	0.00120	0.00003	0.0290	0.0008	1.467200	0.000027	12.3	189	0.282574	-7.3	1.0	-3.3	
103	16-LVD-001B_52	0.282647	0.000023	0.00102	0.00005	0.0233	0.0012	1.467150	0.000035	13.2	186	0.282643	-4.9	0.8	-0.9	
104	16-LVD-001B_53	0.282579	0.000024	0.00088	0.00003	0.0207	0.0006	1.467153	0.000035	12.3	192	0.282576	-7.3	0.8	-3.1	
105	16-LVD-001B_54	0.282729	0.000027	0.00143	0.00007	0.0299	0.0018	1.467138	0.000028	13.4	191	0.282724	-2.0	1.0	2.1	

Grain	Spot ID	corrected										MUN LASS Age (Ma)	$^{176}\text{Hf}/^{177}\text{Hf}$	EHf0	2SE	EHfi
		$^{176}\text{Hf}/^{177}\text{Hf}$	2SE	$^{176}\text{Lu}/^{177}\text{Hf}$	2SE	$^{176}\text{Yb}/^{177}\text{Hf}$	2SE	$^{178}\text{Hf}/^{177}\text{Hf}$	2SE	Total Hf Beam						
106	16-LVD-001B_55	0.282595	0.000023	0.00115	0.00004	0.0272	0.0009	1.467181	0.000039	12.3	186	0.282591	-6.7	0.8	-2.7	
107	16-LVD-001B_56	0.282653	0.000021	0.00073	0.00004	0.0167	0.0007	1.467172	0.000033	12.9	201	0.282650	-4.7	0.7	-0.3	
110	16-LVD-001B_65	0.282582	0.000019	0.00107	0.00005	0.0256	0.0011	1.467160	0.000026	13.3	187	0.282578	-7.2	0.7	-3.2	
111	16-LVD-001B_66	0.282705	0.000031	0.00238	0.00010	0.0601	0.0027	1.467222	0.000034	10.6	204	0.282696	-2.8	1.1	1.4	
112	16-LVD-001B_67	0.282756	0.000019	0.00153	0.00002	0.0325	0.0005	1.467159	0.000030	13.4	202	0.282750	-1.0	0.7	3.3	
113	16-LVD-001B_68	0.282585	0.000024	0.00094	0.00006	0.0224	0.0014	1.467172	0.000029	12.7	185	0.282582	-7.1	0.8	-3.1	
114	16-LVD-001B_69	0.282626	0.000021	0.00076	0.00003	0.0169	0.0006	1.467198	0.000036	12.7	188	0.282623	-5.6	0.7	-1.5	
115	16-LVD-001B_70	0.282557	0.000022	0.00089	0.00004	0.0206	0.0008	1.467178	0.000032	13.1	187	0.282554	-8.1	0.8	-4.0	
117	16-LVD-001B_72	0.282570	0.000025	0.00108	0.00008	0.0256	0.0022	1.467190	0.000032	12.3	188	0.282566	-7.6	0.9	-3.6	
118	16-LVD-001B_73	0.282708	0.000025	0.00118	0.00002	0.0268	0.0005	1.467126	0.000031	12.1	201	0.282704	-2.7	0.9	1.6	
120	16-LVD-001B_75	0.282588	0.000022	0.00084	0.00003	0.0199	0.0007	1.467171	0.000035	12.7	195	0.282585	-7.0	0.8	-2.9	
Rejected Analysis																
1	16-LVD-001B_118	0.282586	0.000029	0.00104	0.00003	0.0269	0.0008	1.467164	0.000039	11.2	196	0.282582	-7.0	1.0	-2.8	
13	16-LVD-001B_136	0.282752	0.000028	0.00115	0.00006	0.0283	0.0017	1.467226	0.000041	11.2	204	0.282748	-1.2	1.0	3.2	
16	16-LVD-001B_139	0.282754	0.000026	0.00129	0.00004	0.0265	0.0012	1.467188	0.000042	15.9	208	0.282749	-1.1	0.9	3.4	
20	16-LVD-001B_143	0.282743	0.000032	0.00103	0.00005	0.0251	0.0012	1.467176	0.000036	9.5	208	0.282739	-1.5	1.1	3.0	
30	16-LVD-001B_159	0.282546	0.000034	0.00099	0.00002	0.0249	0.0006	1.467163	0.000049	14.7	198	0.282542	-8.5	1.2	-4.2	
48	16-LVD-001B_183	0.282674	0.000041	0.00151	0.00016	0.0333	0.0037	1.467172	0.000052	17.0	195	0.282668	-3.9	1.5	0.2	
53	16-LVD-001B_194	0.282720	0.000027	0.00076	0.00003	0.0183	0.0006	1.467203	0.000040	12.4	225	0.282717	-2.3	1.0	2.6	
65	16-LVD-001B_212	0.282723	0.000025	0.00154	0.00004	0.0368	0.0012	1.467183	0.000032	13.0	179	0.282718	-2.2	0.9	1.6	
67	16-LVD-001B_214	0.282616	0.000029	0.00168	0.00008	0.0417	0.0020	1.467161	0.000044	12.8	196	0.282610	-6.0	1.0	-1.8	
68	16-LVD-001B_215	0.282764	0.000025	0.00145	0.00012	0.0273	0.0017	1.467215	0.000049	15.7	199	0.282759	-0.7	0.9	3.5	
73	16-LVD-001B_10	0.282535	0.000018	0.00105	0.00013	0.0268	0.0035	1.467151	0.000040	17.0	191	0.282531	-8.8	0.6	-4.7	

Grain	Spot ID	<i>corrected</i>		2SE	176Lu/ 177Hf	2SE	176Yb/ 177Hf	2SE	178Hf/ 177Hf	2SE	Total Hf Beam	MUN LASS Age (Ma)	176Hf/ 177Hf	EHf0	2SE	EHfi
		176Hf/ 177Hf	2SE													
81	16-LVD-001B_18	0.282713	0.000024	0.00058	0.00006	0.0121	0.0012	1.467181	0.000037	14.6	195	0.282711	-2.5	0.8	1.7	
85	16-LVD-001B_28	0.282738	0.000024	0.00140	0.00006	0.0357	0.0013	1.467177	0.000040	11.9	200	0.282733	-1.7	0.8	2.6	
86	16-LVD-001B_29	0.282729	0.000024	0.00105	0.00005	0.0262	0.0013	1.467192	0.000026	12.6	197	0.282725	-2.0	0.8	2.3	
88	16-LVD-001B_31	0.282759	0.000025	0.00111	0.00007	0.0228	0.0015	1.467188	0.000034	13.1	195	0.282755	-0.9	0.9	3.3	
101	16-LVD-001B_50	0.282690	0.000029	0.00128	0.00006	0.0286	0.0014	1.467232	0.000037	12.7	207	0.282685	-3.4	1.0	1.1	
108	16-LVD-001B_57	0.282761	0.000025	0.00117	0.00003	0.0253	0.0008	1.467174	0.000036	16.6	190	0.282757	-0.8	0.9	3.2	
109	16-LVD-001B_64	0.282708	0.000052	0.00124	0.00009	0.0266	0.0026	1.467159	0.000049	19.1	220	0.282703	-2.7	1.8	2.0	
116	16-LVD-001B_71	0.282789	0.000025	0.00099	0.00009	0.0235	0.0022	1.467173	0.000033	11.2	194	0.282785	0.1	0.9	4.3	
119	16-LVD-001B_74	0.282784	0.000025	0.00136	0.00003	0.0277	0.0006	1.467191	0.000045	15.0	189	0.282779	0.0	0.9	4.1	

Whitehorse trough - Tanglefoot formation - Sample 16-LVD-001C, Robert Campbell Highway (Zone 08V 455577E 6877512N NAD 83)

Grain	Spot ID	<i>corrected</i>		2SE	176Lu/ 177Hf	2SE	176Yb/ 177Hf	2SE	178Hf/ 177Hf	2SE	Total Hf Beam	MUN LASS Age (Ma)	176Hf/ 177Hf	EHf0	2SE	EHfi
		176Hf/ 177Hf	2SE													
1	16-LVD-001C_154	0.282952	0.000027	0.00161	0.00007	0.0395	0.0017	1.467177	0.000040	12.6	228	0.282945	5.9	1.0	10.7	
3	16-LVD-001C_156	0.282692	0.000022	0.00114	0.00004	0.0266	0.0011	1.467209	0.000034	13.4	197	0.282688	-3.3	0.8	0.9	
4	16-LVD-001C_157	0.282947	0.000042	0.00152	0.00016	0.0405	0.0041	1.467149	0.000045	16.8	224	0.282941	5.7	1.5	10.5	
5	16-LVD-001C_158	0.282996	0.000038	0.00090	0.00004	0.0217	0.0010	1.467195	0.000037	12.7	222	0.282992	7.5	1.3	12.3	
7	16-LVD-001C_160	0.282961	0.000023	0.00101	0.00007	0.0257	0.0017	1.467148	0.000029	13.9	224	0.282957	6.2	0.8	11.1	
9	16-LVD-001C_162	0.282724	0.000027	0.00104	0.00007	0.0220	0.0013	1.467180	0.000034	13.5	198	0.282720	-2.2	1.0	2.1	
10	16-LVD-001C_163	0.282968	0.000023	0.00175	0.00014	0.0495	0.0040	1.467148	0.000033	14.6	206	0.282961	6.5	0.8	10.8	
11	16-LVD-001C_164	0.282772	0.000025	0.00108	0.00004	0.0273	0.0009	1.467130	0.000052	12.3	206	0.282768	-0.5	0.9	4.0	

Grain	Spot ID	corrected										MUN LASS Age (Ma)	$^{176}\text{Hf}/^{177}\text{Hf}$	EHf0	2SE	EHfi
		$^{176}\text{Hf}/^{177}\text{Hf}$	2SE	$^{176}\text{Lu}/^{177}\text{Hf}$	2SE	$^{176}\text{Yb}/^{177}\text{Hf}$	2SE	$^{178}\text{Hf}/^{177}\text{Hf}$	2SE	Total Hf Beam						
12	16-LVD-001C_165	0.282964	0.000023	0.00198	0.00010	0.0544	0.0027	1.467200	0.000027	11.6	217	0.282956	6.3	0.8	10.9	
13	16-LVD-001C_172	0.282947	0.000025	0.00133	0.00008	0.0373	0.0024	1.467173	0.000035	11.3	221	0.282941	5.7	0.9	10.4	
14	16-LVD-001C_173	0.282961	0.000029	0.00222	0.00009	0.0611	0.0025	1.467186	0.000043	11.9	232	0.282951	6.2	1.0	11.0	
15	16-LVD-001C_174	0.282963	0.000020	0.00154	0.00006	0.0403	0.0015	1.467215	0.000034	10.5	229	0.282956	6.3	0.7	11.2	
16	16-LVD-001C_175	0.282955	0.000018	0.00079	0.00001	0.0216	0.0002	1.467220	0.000037	13.7	237	0.282952	6.0	0.6	11.2	
17	16-LVD-001C_176	0.282948	0.000018	0.00073	0.00001	0.0201	0.0003	1.467217	0.000026	13.2	230	0.282945	5.8	0.6	10.8	
18	16-LVD-001C_177	0.282945	0.000021	0.00174	0.00010	0.0474	0.0030	1.467178	0.000040	10.4	223	0.282938	5.7	0.7	10.4	
19	16-LVD-001C_178	0.282669	0.000029	0.00189	0.00008	0.0481	0.0018	1.467153	0.000040	11.3	308	0.282658	-4.1	1.0	2.4	
20	16-LVD-001C_179	0.282958	0.000024	0.00142	0.00004	0.0350	0.0012	1.467178	0.000039	10.3	228	0.282952	6.1	0.8	11.0	
21	16-LVD-001C_180	0.282966	0.000023	0.00140	0.00002	0.0360	0.0005	1.467205	0.000040	10.5	226	0.282960	6.4	0.8	11.2	
22	16-LVD-001C_181	0.282987	0.000025	0.00205	0.00004	0.0556	0.0012	1.467165	0.000039	12.6	232	0.282978	7.1	0.9	12.0	
23	16-LVD-001C_182	0.282951	0.000030	0.00133	0.00004	0.0359	0.0011	1.467192	0.000042	12.0	219	0.282946	5.9	1.1	10.6	
24	16-LVD-001C_183	0.282951	0.000024	0.00101	0.00003	0.0268	0.0008	1.467140	0.000037	11.8	222	0.282947	5.9	0.8	10.7	
26	16-LVD-001C_191	0.282980	0.000022	0.00161	0.00004	0.0432	0.0012	1.467200	0.000031	11.8	224	0.282973	6.9	0.8	11.6	
27	16-LVD-001C_192	0.282965	0.000024	0.00138	0.00010	0.0357	0.0025	1.467180	0.000041	13.8	230	0.282959	6.4	0.8	11.3	
28	16-LVD-001C_193	0.282674	0.000024	0.00090	0.00003	0.0202	0.0005	1.467168	0.000030	12.5	195	0.282671	-3.9	0.8	0.3	
29	16-LVD-001C_194	0.282939	0.000031	0.00119	0.00007	0.0290	0.0017	1.467173	0.000041	13.1	219	0.282934	5.4	1.1	10.1	
31	16-LVD-001C_196	0.282789	0.000025	0.00147	0.00005	0.0337	0.0014	1.467181	0.000035	13.2	210	0.282783	0.1	0.9	4.6	
32	16-LVD-001C_197	0.282973	0.000025	0.00079	0.00008	0.0220	0.0023	1.467166	0.000027	10.9	222	0.282970	6.6	0.9	11.5	
33	16-LVD-001C_198	0.282952	0.000029	0.00122	0.00002	0.0296	0.0007	1.467200	0.000031	11.0	234	0.282947	5.9	1.0	10.9	
34	16-LVD-001C_199	0.282972	0.000020	0.00170	0.00008	0.0428	0.0020	1.467137	0.000038	11.8	220	0.282965	6.6	0.7	11.3	
35	16-LVD-001C_200	0.282945	0.000022	0.00150	0.00008	0.0404	0.0023	1.467203	0.000029	12.9	252	0.282938	5.7	0.8	11.0	
36	16-LVD-001C_201	0.282983	0.000030	0.00208	0.00008	0.0587	0.0023	1.467206	0.000032	10.4	228	0.282974	7.0	1.1	11.8	

Grain	Spot ID	corrected										MUN LASS Age (Ma)	$^{176}\text{Hf}/^{177}\text{Hf}$	EHf0	2SE	EHfi
		$^{176}\text{Hf}/^{177}\text{Hf}$	2SE	$^{176}\text{Lu}/^{177}\text{Hf}$	2SE	$^{176}\text{Yb}/^{177}\text{Hf}$	2SE	$^{178}\text{Hf}/^{177}\text{Hf}$	2SE	Total Hf Beam						
37	16-LVD-001C_208	0.282978	0.000025	0.00147	0.00008	0.0402	0.0020	1.467176	0.000033	14.1	229	0.282972	6.8	0.9	11.7	
38	16-LVD-001C_209	0.282961	0.000025	0.00153	0.00006	0.0372	0.0014	1.467175	0.000041	12.1	220	0.282955	6.2	0.9	10.9	
39	16-LVD-001C_210	0.282676	0.000019	0.00101	0.00007	0.0260	0.0017	1.467193	0.000039	12.7	201	0.282672	-3.9	0.7	0.5	
40	16-LVD-001C_211	0.282975	0.000027	0.00182	0.00025	0.0464	0.0067	1.467181	0.000030	11.8	225	0.282967	6.7	1.0	11.4	
41	16-LVD-001C_212	0.282933	0.000034	0.00136	0.00011	0.0380	0.0029	1.467203	0.000043	14.6	230	0.282927	5.2	1.2	10.1	
42	16-LVD-001C_213	0.282975	0.000035	0.00141	0.00004	0.0349	0.0012	1.467188	0.000036	13.2	233	0.282969	6.7	1.2	11.7	
43	16-LVD-001C_214	0.282941	0.000025	0.00113	0.00015	0.0260	0.0033	1.467221	0.000035	11.9	234	0.282936	5.5	0.9	10.6	
44	16-LVD-001C_215	0.282970	0.000027	0.00126	0.00013	0.0355	0.0040	1.467203	0.000032	12.9	232	0.282965	6.5	1.0	11.5	
46	16-LVD-001C_217	0.282950	0.000016	0.00130	0.00002	0.0366	0.0009	1.467191	0.000035	13.2	226	0.282944	5.8	0.6	10.7	
47	16-LVD-001C_218	0.282957	0.000025	0.00153	0.00003	0.0420	0.0009	1.467176	0.000040	11.2	231	0.282950	6.1	0.9	11.0	
48	16-LVD-001C_219	0.282955	0.000022	0.00139	0.00008	0.0340	0.0021	1.467178	0.000042	11.8	215	0.282949	6.0	0.8	10.6	
49	16-LVD-001C_10	0.282957	0.000026	0.00174	0.00005	0.0483	0.0012	1.467147	0.000035	12.0	225	0.282950	6.1	0.9	10.8	
50	16-LVD-001C_11	0.282968	0.000024	0.00158	0.00005	0.0423	0.0017	1.467157	0.000029	12.1	236	0.282961	6.5	0.8	11.5	
51	16-LVD-001C_12	0.282963	0.000025	0.00127	0.00009	0.0331	0.0023	1.467190	0.000035	11.5	242	0.282957	6.3	0.9	11.5	
53	16-LVD-001C_14	0.282808	0.000027	0.00110	0.00007	0.0268	0.0015	1.467219	0.000041	13.0	196	0.282804	0.8	1.0	5.0	
54	16-LVD-001C_15	0.282958	0.000031	0.00160	0.00011	0.0433	0.0030	1.467188	0.000036	12.8	219	0.282951	6.1	1.1	10.8	
55	16-LVD-001C_16	0.282974	0.000025	0.00214	0.00025	0.0574	0.0064	1.467195	0.000036	14.1	242	0.282964	6.7	0.9	11.7	
56	16-LVD-001C_17	0.282947	0.000026	0.00132	0.00003	0.0334	0.0010	1.467154	0.000044	11.3	228	0.282941	5.7	0.9	10.6	
57	16-LVD-001C_18	0.282979	0.000037	0.00127	0.00004	0.0315	0.0012	1.467201	0.000050	10.1	227	0.282974	6.9	1.3	11.7	
59	16-LVD-001C_20	0.282794	0.000024	0.00139	0.00003	0.0349	0.0010	1.467195	0.000036	11.8	191	0.282789	0.3	0.8	4.4	
60	16-LVD-001C_21	0.282976	0.000031	0.00118	0.00011	0.0320	0.0030	1.467196	0.000050	14.8	233	0.282971	6.8	1.1	11.7	
62	16-LVD-001C_29	0.282933	0.000023	0.00141	0.00011	0.0341	0.0028	1.467180	0.000043	9.9	212	0.282927	5.2	0.8	9.8	
63	16-LVD-001C_30	0.282678	0.000021	0.00100	0.00002	0.0231	0.0006	1.467191	0.000038	12.1	191	0.282674	-3.8	0.7	0.3	

Grain	Spot ID	<i>corrected</i>		2SE	176Lu/ 177Hf	2SE	176Yb/ 177Hf	2SE	178Hf/ 177Hf	2SE	Total Hf Beam	MUN LASS Age (Ma)	176Hf/ 177Hf	EHf0	2SE	EHfi
		176Hf/ 177Hf	2SE													
65	16-LVD-001C_32	0.282959	0.000028	0.00081	0.00005	0.0200	0.0013	1.467182	0.000031	10.6	229	0.282956	6.2	1.0	11.1	
66	16-LVD-001C_33	0.282976	0.000026	0.00244	0.00006	0.0727	0.0015	1.467150	0.000036	10.9	229	0.282966	6.8	0.9	11.5	
67	16-LVD-001C_34	0.282971	0.000026	0.00184	0.00004	0.0544	0.0014	1.467161	0.000042	11.3	213	0.282964	6.6	0.9	11.1	
68	16-LVD-001C_35	0.282966	0.000030	0.00086	0.00005	0.0241	0.0015	1.467182	0.000042	13.0	239	0.282962	6.4	1.1	11.6	
69	16-LVD-001C_36	0.282964	0.000023	0.00109	0.00001	0.0322	0.0004	1.467220	0.000038	12.1	232	0.282959	6.3	0.8	11.3	
70	16-LVD-001C_37	0.282733	0.000024	0.00135	0.00017	0.0353	0.0045	1.467201	0.000032	12.3	213	0.282728	-1.8	0.8	2.7	
71	16-LVD-001C_38	0.282979	0.000027	0.00105	0.00004	0.0295	0.0009	1.467197	0.000043	11.8	228	0.282975	6.9	1.0	11.8	
73	16-LVD-001C_46	0.282970	0.000024	0.00115	0.00002	0.0314	0.0008	1.467177	0.000043	11.5	219	0.282965	6.5	0.8	11.2	
75	16-LVD-001C_48	0.282955	0.000033	0.00135	0.00014	0.0349	0.0036	1.467188	0.000043	11.5	217	0.282950	6.0	1.2	10.6	
76	16-LVD-001C_49	0.282694	0.000031	0.00090	0.00004	0.0217	0.0012	1.467183	0.000042	14.3	204	0.282691	-3.2	1.1	1.2	
77	16-LVD-001C_50	0.282739	0.000029	0.00108	0.00010	0.0273	0.0026	1.467121	0.000057	14.3	199	0.282735	-1.6	1.0	2.7	
78	16-LVD-001C_51	0.282669	0.000030	0.00109	0.00009	0.0293	0.0024	1.467153	0.000046	15.2	200	0.282665	-4.1	1.1	0.2	
79	16-LVD-001C_52	0.282962	0.000023	0.00145	0.00005	0.0401	0.0018	1.467191	0.000035	13.9	224	0.282956	6.3	0.8	11.0	
81	16-LVD-001C_54	0.282531	0.000021	0.00091	0.00003	0.0223	0.0007	1.467207	0.000032	12.6	201	0.282528	-9.0	0.7	-4.6	
82	16-LVD-001C_55	0.282955	0.000026	0.00241	0.00018	0.0616	0.0045	1.467208	0.000037	11.7	220	0.282945	6.0	0.9	10.6	
83	16-LVD-001C_56	0.282963	0.000026	0.00215	0.00006	0.0624	0.0017	1.467228	0.000036	13.5	229	0.282954	6.3	0.9	11.1	
84	16-LVD-001C_57	0.282929	0.000025	0.00161	0.00013	0.0433	0.0036	1.467165	0.000030	12.3	235	0.282922	5.1	0.9	10.1	
85	16-LVD-001C_64	0.282973	0.000024	0.00142	0.00004	0.0410	0.0013	1.467215	0.000041	11.3	228	0.282967	6.6	0.8	11.5	
86	16-LVD-001C_65	0.282965	0.000035	0.00236	0.00010	0.0697	0.0030	1.467205	0.000035	10.7	230	0.282955	6.4	1.2	11.1	
87	16-LVD-001C_66	0.282728	0.000023	0.00134	0.00007	0.0334	0.0019	1.467155	0.000033	12.3	200	0.282723	-2.0	0.8	2.2	
88	16-LVD-001C_67	0.282705	0.000024	0.00082	0.00004	0.0193	0.0009	1.467187	0.000031	11.9	205	0.282702	-2.8	0.8	1.6	
89	16-LVD-001C_68	0.282985	0.000024	0.00092	0.00003	0.0266	0.0007	1.467177	0.000039	10.9	232	0.282981	7.1	0.8	12.1	
90	16-LVD-001C_69	0.282936	0.000032	0.00153	0.00018	0.0407	0.0053	1.467190	0.000036	10.1	225	0.282930	5.3	1.1	10.1	

Grain	Spot ID	corrected										MUN LASS Age (Ma)	$^{176}\text{Hf}/^{177}\text{Hf}$	EHf0	2SE	EHfi
		$^{176}\text{Hf}/^{177}\text{Hf}$	2SE	$^{176}\text{Lu}/^{177}\text{Hf}$	2SE	$^{176}\text{Yb}/^{177}\text{Hf}$	2SE	$^{178}\text{Hf}/^{177}\text{Hf}$	2SE	Total Hf Beam						
92	16-LVD-001C_71	0.282710	0.000020	0.00136	0.00006	0.0364	0.0016	1.467174	0.000035	11.1	213	0.282705	-2.7	0.7	1.9	
93	16-LVD-001C_72	0.282943	0.000027	0.00188	0.00010	0.0522	0.0025	1.467173	0.000048	11.7	223	0.282935	5.6	1.0	10.3	
94	16-LVD-001C_73	0.282966	0.000033	0.00205	0.00006	0.0593	0.0017	1.467215	0.000040	12.6	225	0.282957	6.4	1.2	11.1	
95	16-LVD-001C_74	0.282943	0.000027	0.00106	0.00011	0.0302	0.0033	1.467175	0.000036	11.1	230	0.282938	5.6	1.0	10.6	
96	16-LVD-001C_75	0.282946	0.000027	0.00086	0.00004	0.0242	0.0015	1.467178	0.000029	12.2	235	0.282942	5.7	1.0	10.8	
97	16-LVD-001C_82	0.282959	0.000024	0.00181	0.00006	0.0516	0.0023	1.467164	0.000034	10.3	232	0.282951	6.2	0.8	11.0	
98	16-LVD-001C_83	0.282979	0.000028	0.00161	0.00005	0.0448	0.0013	1.467193	0.000037	11.8	226	0.282972	6.9	1.0	11.6	
99	16-LVD-001C_84	0.282967	0.000030	0.00108	0.00003	0.0298	0.0010	1.467209	0.000036	13.2	217	0.282963	6.4	1.1	11.1	
100	16-LVD-001C_85	0.282964	0.000021	0.00166	0.00008	0.0425	0.0022	1.467179	0.000037	11.8	231	0.282957	6.3	0.7	11.2	
101	16-LVD-001C_86	0.282654	0.000024	0.00065	0.00001	0.0172	0.0003	1.467151	0.000029	12.2	204	0.282652	-4.6	0.8	-0.2	
102	16-LVD-001C_87	0.282964	0.000034	0.00140	0.00004	0.0410	0.0009	1.467183	0.000033	13.6	239	0.282958	6.3	1.2	11.4	
103	16-LVD-001C_88	0.282973	0.000026	0.00175	0.00011	0.0499	0.0032	1.467157	0.000041	11.5	231	0.282965	6.6	0.9	11.5	
104	16-LVD-001C_89	0.282970	0.000033	0.00152	0.00011	0.0439	0.0030	1.467159	0.000036	12.3	232	0.282963	6.5	1.2	11.5	
105	16-LVD-001C_90	0.282989	0.000036	0.00090	0.00004	0.0252	0.0012	1.467183	0.000045	15.3	221	0.282985	7.2	1.3	12.0	
106	16-LVD-001C_91	0.282956	0.000025	0.00096	0.00005	0.0254	0.0014	1.467150	0.000037	12.4	231	0.282952	6.0	0.9	11.1	
107	16-LVD-001C_92	0.282790	0.000032	0.00116	0.00010	0.0260	0.0021	1.467147	0.000057	14.5	203	0.282786	0.2	1.1	4.5	
109	16-LVD-001C_100	0.282955	0.000024	0.00135	0.00005	0.0376	0.0013	1.467221	0.000034	11.5	227	0.282949	6.0	0.8	10.9	
112	16-LVD-001C_103	0.282994	0.000038	0.00224	0.00024	0.0608	0.0081	1.467212	0.000058	14.3	226	0.282985	7.4	1.3	12.1	
113	16-LVD-001C_104	0.282754	0.000024	0.00126	0.00005	0.0333	0.0016	1.467171	0.000031	13.1	192	0.282749	-1.1	0.8	3.0	
114	16-LVD-001C_105	0.282964	0.000039	0.00152	0.00005	0.0418	0.0018	1.467181	0.000039	14.0	221	0.282958	6.3	1.4	11.0	
117	16-LVD-001C_108	0.282658	0.000028	0.00100	0.00003	0.0264	0.0005	1.467141	0.000037	12.9	220	0.282654	-4.5	1.0	0.3	
119	16-LVD-001C_110	0.282935	0.000027	0.00132	0.00004	0.0346	0.0011	1.467164	0.000036	11.5	221	0.282930	5.3	1.0	10.0	

Rejected Analysis

Grain	Spot ID	<i>corrected</i>		2SE	176Lu/ 177Hf	2SE	176Yb/ 177Hf	2SE	178Hf/ 177Hf	2SE	Total Hf Beam	MUN LASS Age (Ma)	176Hf/ 177Hf	EHf0	2SE	EHfi
		176Hf/ 177Hf	2SE													
2	16-LVD-001C_155	0.282793	0.000024	0.00136	0.00008	0.0312	0.0018	1.467174	0.000041	15.2	178	0.282788	0.3	0.8	4.1	
6	16-LVD-001C_159	0.282980	0.000033	0.00123	0.00003	0.0328	0.0009	1.467194	0.000042	12.1	236	0.282975	6.9	1.2	12.0	
8	16-LVD-001C_161	0.282992	0.000022	0.00173	0.00008	0.0464	0.0024	1.467133	0.000048	14.0	212	0.282985	7.3	0.8	11.8	
25	16-LVD-001C_190	0.282973	0.000030	0.00131	0.00012	0.0325	0.0030	1.467209	0.000050	14.0	224	0.282968	6.6	1.1	11.4	
30	16-LVD-001C_195	0.282955	0.000019	0.00103	0.00010	0.0278	0.0029	1.467195	0.000038	11.2	228	0.282951	6.0	0.7	10.9	
45	16-LVD-001C_216	0.282713	0.000021	0.00091	0.00004	0.0215	0.0011	1.467206	0.000032	12.2	213	0.282709	-2.5	0.7	2.1	
52	16-LVD-001C_13	0.282691	0.000033	0.00142	0.00013	0.0380	0.0040	1.467203	0.000043	16.5	181	0.282686	-3.3	1.2	0.5	
58	16-LVD-001C_19	0.282778	0.000023	0.00119	0.00005	0.0298	0.0012	1.467176	0.000034	12.6	219	0.282773	-0.2	0.8	4.5	
61	16-LVD-001C_28	0.282971	0.000037	0.00171	0.00015	0.0457	0.0043	1.467226	0.000039	16.7	215	0.282964	6.6	1.3	11.1	
64	16-LVD-001C_31	0.282953	0.000027	0.00056	0.00002	0.0162	0.0005	1.467152	0.000024	12.0	230	0.282951	5.9	1.0	11.0	
72	16-LVD-001C_39	0.282859	0.000026	0.00113	0.00010	0.0274	0.0028	1.467191	0.000029	16.3	229	0.282854	2.6	0.9	7.5	
74	16-LVD-001C_47	0.282673	0.000031	0.00120	0.00011	0.0297	0.0027	1.467208	0.000040	12.2	196	0.282669	-4.0	1.1	0.2	
80	16-LVD-001C_53	0.282747	0.000029	0.00137	0.00007	0.0362	0.0020	1.467163	0.000046	13.9	202	0.282742	-1.3	1.0	3.0	
91	16-LVD-001C_70	0.282946	0.000023	0.00154	0.00013	0.0448	0.0041	1.467145	0.000035	12.2	210	0.282940	5.7	0.8	10.2	
108	16-LVD-001C_93	0.282961	0.000034	0.00198	0.00009	0.0582	0.0022	1.467177	0.000052	14.3	243	0.282952	6.2	1.2	11.3	
110	16-LVD-001C_101	0.282983	0.000038	0.00213	0.00005	0.0560	0.0016	1.467233	0.000039	12.2	225	0.282974	7.0	1.3	11.7	
111	16-LVD-001C_102	0.282953	0.000028	0.00159	0.00007	0.0445	0.0021	1.467155	0.000042	12.2	236	0.282946	5.9	1.0	11.0	
115	16-LVD-001C_106	0.282906	0.000026	0.00133	0.00003	0.0377	0.0008	1.467190	0.000037	14.4	214	0.282901	4.3	0.9	8.9	
116	16-LVD-001C_107	0.282969	0.000032	0.00154	0.00018	0.0394	0.0050	1.467192	0.000043	12.1	236	0.282962	6.5	1.1	11.5	
118	16-LVD-001C_109	0.282946	0.000034	0.00142	0.00018	0.0378	0.0051	1.467194	0.000041	13.6	235	0.282940	5.7	1.2	10.7	
120	16-LVD-001C_111	0.282976	0.000048	0.00151	0.00009	0.0412	0.0024	1.467193	0.000037	14.3	233	0.282969	6.8	1.7	11.7	

Grain	Spot ID	<i>corrected</i>		2SE	176Lu/ 177Hf	2SE	176Yb/ 177Hf	2SE	178Hf/ 177Hf	2SE	Total Hf Beam	MUN LASS Age (Ma)	176Hf/ 177Hf ⁱ	EHf0	2SE	EHfi
		176Hf/ 177Hf														

Whitehorse trough - Tanglefoot formation - Sample 16-LVD-004, Robert Campbell Highway (Zone 08V 436493E 6888370N NAD 83)

Grain	Spot ID	<i>corrected</i>		2SE	176Lu/ 177Hf	2SE	176Yb/ 177Hf	2SE	178Hf/ 177Hf	2SE	Total Hf Beam	MUN LASS Age (Ma)	176Hf/ 177Hf ⁱ	EHf0	2SE	EHfi
		176Hf/ 177Hf														
1	16-LVD-004_15	0.282603	0.000033	0.00102	0.00005	0.0240	0.0014	1.467213	0.000036	11.8	196	0.282599	-6.4	1.2	-2.2	
2	16-LVD-004_16	0.282694	0.000033	0.00109	0.00007	0.0268	0.0017	1.467199	0.000033	12.5	184	0.282690	-3.2	1.2	0.7	
3	16-LVD-004_17	0.282611	0.000030	0.00076	0.00003	0.0188	0.0008	1.467196	0.000047	13.1	183	0.282608	-6.2	1.1	-2.2	
4	16-LVD-004_18	0.282696	0.000042	0.00152	0.00012	0.0379	0.0033	1.467206	0.000051	15.7	194	0.282690	-3.1	1.5	1.0	
6	16-LVD-004_20	0.282768	0.000031	0.00109	0.00002	0.0229	0.0007	1.467191	0.000039	15.7	203	0.282764	-0.6	1.1	3.8	
7	16-LVD-004_21	0.282593	0.000026	0.00086	0.00003	0.0208	0.0009	1.467189	0.000039	11.4	199	0.282590	-6.8	0.9	-2.5	
8	16-LVD-004_22	0.282677	0.000029	0.00110	0.00005	0.0268	0.0011	1.467223	0.000047	13.2	192	0.282673	-3.8	1.0	0.3	
10	16-LVD-004_24	0.282604	0.000032	0.00100	0.00002	0.0238	0.0004	1.467174	0.000030	10.7	184	0.282601	-6.4	1.1	-2.4	
11	16-LVD-004_32	0.282580	0.000029	0.00115	0.00002	0.0288	0.0005	1.467232	0.000038	12.9	200	0.282576	-7.2	1.0	-2.9	
12	16-LVD-004_33	0.282597	0.000030	0.00125	0.00005	0.0300	0.0012	1.467174	0.000032	11.1	206	0.282592	-6.6	1.1	-2.2	
13	16-LVD-004_34	0.282635	0.000023	0.00070	0.00002	0.0169	0.0006	1.467160	0.000036	11.4	193	0.282632	-5.3	0.8	-1.1	
14	16-LVD-004_35	0.282676	0.000031	0.00059	0.00003	0.0148	0.0008	1.467241	0.000032	10.4	203	0.282674	-3.9	1.1	0.6	
16	16-LVD-004_37	0.282564	0.000032	0.00111	0.00001	0.0260	0.0005	1.467200	0.000037	10.9	200	0.282560	-7.8	1.1	-3.5	
17	16-LVD-004_38	0.282622	0.000025	0.00143	0.00006	0.0355	0.0013	1.467200	0.000037	11.6	202	0.282617	-5.8	0.9	-1.5	
18	16-LVD-004_39	0.282549	0.000023	0.00074	0.00007	0.0175	0.0018	1.467194	0.000038	12.1	187	0.282546	-8.3	0.8	-4.3	
19	16-LVD-004_40	0.282638	0.000044	0.00065	0.00005	0.0156	0.0010	1.467248	0.000054	14.6	190	0.282636	-5.2	1.6	-1.1	
20	16-LVD-004_41	0.282575	0.000037	0.00090	0.00005	0.0211	0.0014	1.467161	0.000046	15.4	192	0.282572	-7.4	1.3	-3.3	
21	16-LVD-004_48	0.282343	0.000043	0.00046	0.00006	0.0126	0.0015	1.467196	0.000035	8.8	453	0.282339	-15.6	1.5	-5.7	
22	16-LVD-004_49	0.282839	0.000031	0.00041	0.00004	0.0084	0.0010	1.467186	0.000058	13.8	211	0.282837	1.9	1.1	6.5	

Grain	Spot ID	corrected										MUN LASS Age (Ma)	$^{176}\text{Hf}/^{177}\text{Hf}$	EHf0	2SE	EHfi
		$^{176}\text{Hf}/^{177}\text{Hf}$	2SE	$^{176}\text{Lu}/^{177}\text{Hf}$	2SE	$^{176}\text{Yb}/^{177}\text{Hf}$	2SE	$^{178}\text{Hf}/^{177}\text{Hf}$	2SE	Total Hf Beam						
24	16-LVD-004_51	0.282575	0.000019	0.00073	0.00002	0.0170	0.0005	1.467235	0.000038	11.2	185	0.282572	-7.4	0.7	-3.4	
25	16-LVD-004_52	0.282575	0.000039	0.00125	0.00006	0.0305	0.0014	1.467204	0.000043	14.8	183	0.282571	-7.4	1.4	-3.5	
26	16-LVD-004_53	0.282599	0.000026	0.00111	0.00006	0.0263	0.0014	1.467228	0.000036	12.6	187	0.282595	-6.6	0.9	-2.6	
27	16-LVD-004_54	0.282705	0.000028	0.00065	0.00005	0.0168	0.0015	1.467239	0.000042	10.0	204	0.282703	-2.8	1.0	1.6	
28	16-LVD-004_55	0.282621	0.000029	0.00113	0.00013	0.0282	0.0036	1.467175	0.000044	11.0	183	0.282617	-5.8	1.0	-1.9	
29	16-LVD-004_56	0.282692	0.000027	0.00052	0.00001	0.0117	0.0003	1.467204	0.000034	11.8	334	0.282689	-3.3	1.0	4.0	
30	16-LVD-004_57	0.282903	0.000031	0.00035	0.00005	0.0084	0.0015	1.467181	0.000036	11.3	212	0.282902	4.2	1.1	8.8	
31	16-LVD-004_64	0.282340	0.000020	0.00076	0.00002	0.0198	0.0006	1.467198	0.000038	11.9	340	0.282335	-15.7	0.7	-8.3	
32	16-LVD-004_65	0.282624	0.000023	0.00106	0.00003	0.0243	0.0006	1.467210	0.000041	11.1	190	0.282620	-5.7	0.8	-1.6	
33	16-LVD-004_66	0.282704	0.000023	0.00106	0.00007	0.0269	0.0019	1.467231	0.000035	9.7	187	0.282700	-2.9	0.8	1.2	
34	16-LVD-004_67	0.282573	0.000022	0.00103	0.00007	0.0254	0.0021	1.467200	0.000034	12.8	181	0.282570	-7.5	0.8	-3.6	
35	16-LVD-004_68	0.282338	0.000027	0.00132	0.00008	0.0360	0.0021	1.467191	0.000040	12.0	354	0.282329	-15.8	1.0	-8.2	
36	16-LVD-004_69	0.282621	0.000017	0.00078	0.00004	0.0182	0.0009	1.467225	0.000032	11.4	190	0.282618	-5.8	0.6	-1.7	
37	16-LVD-004_70	0.282598	0.000019	0.00115	0.00007	0.0264	0.0018	1.467175	0.000031	12.4	188	0.282594	-6.6	0.7	-2.6	
38	16-LVD-004_71	0.282662	0.000023	0.00135	0.00005	0.0319	0.0013	1.467218	0.000046	14.9	178	0.282658	-4.3	0.8	-0.5	
39	16-LVD-004_72	0.282706	0.000028	0.00111	0.00009	0.0259	0.0025	1.467200	0.000043	12.6	190	0.282702	-2.8	1.0	1.3	
40	16-LVD-004_73	0.282572	0.000024	0.00101	0.00006	0.0235	0.0015	1.467204	0.000039	11.3	185	0.282569	-7.5	0.8	-3.5	
41	16-LVD-004_80	0.282622	0.000022	0.00068	0.00004	0.0154	0.0006	1.467206	0.000034	11.2	183	0.282620	-5.8	0.8	-1.8	
42	16-LVD-004_81	0.282584	0.000021	0.00116	0.00010	0.0272	0.0025	1.467200	0.000044	11.0	198	0.282580	-7.1	0.7	-2.9	
43	16-LVD-004_82	0.282572	0.000028	0.00090	0.00003	0.0212	0.0008	1.467190	0.000037	15.4	182	0.282569	-7.5	1.0	-3.6	
44	16-LVD-004_83	0.282597	0.000032	0.00083	0.00005	0.0190	0.0010	1.467217	0.000036	12.0	187	0.282594	-6.6	1.1	-2.6	
45	16-LVD-004_84	0.282605	0.000021	0.00077	0.00003	0.0189	0.0008	1.467198	0.000044	10.7	184	0.282602	-6.4	0.7	-2.4	
47	16-LVD-004_86	0.282582	0.000027	0.00116	0.00004	0.0272	0.0011	1.467226	0.000037	12.3	188	0.282578	-7.2	1.0	-3.2	

Grain	Spot ID	corrected										MUN LASS Age (Ma)	$^{176}\text{Hf}/^{177}\text{Hf}$	EHf0	2SE	EHfi
		$^{176}\text{Hf}/^{177}\text{Hf}$	2SE	$^{176}\text{Lu}/^{177}\text{Hf}$	2SE	$^{176}\text{Yb}/^{177}\text{Hf}$	2SE	$^{178}\text{Hf}/^{177}\text{Hf}$	2SE	Total Hf Beam						
48	16-LVD-004_87	0.282642	0.000029	0.00068	0.00003	0.0154	0.0005	1.467175	0.000035	11.5	186	0.282640	-5.1	1.0	-1.0	
49	16-LVD-004_88	0.282607	0.000020	0.00121	0.00006	0.0281	0.0014	1.467240	0.000045	10.7	181	0.282603	-6.3	0.7	-2.4	
51	16-LVD-004_96	0.282769	0.000024	0.00094	0.00005	0.0191	0.0011	1.467208	0.000045	15.8	198	0.282766	-0.6	0.8	3.7	
52	16-LVD-004_97	0.282580	0.000021	0.00117	0.00002	0.0270	0.0004	1.467236	0.000041	10.9	201	0.282576	-7.2	0.7	-2.9	
53	16-LVD-004_98	0.282690	0.000022	0.00081	0.00006	0.0179	0.0013	1.467196	0.000032	12.1	187	0.282687	-3.4	0.8	0.7	
54	16-LVD-004_99	0.282832	0.000032	0.00160	0.00013	0.0427	0.0037	1.467200	0.000039	9.3	331	0.282822	1.7	1.1	8.7	
55	16-LVD-004_100	0.282799	0.000027	0.00100	0.00002	0.0230	0.0005	1.467185	0.000031	12.0	199	0.282795	0.5	1.0	4.8	
57	16-LVD-004_102	0.282782	0.000026	0.00123	0.00006	0.0282	0.0013	1.467181	0.000044	13.8	187	0.282778	-0.1	0.9	3.9	
58	16-LVD-004_103	0.282605	0.000028	0.00110	0.00007	0.0253	0.0019	1.467223	0.000037	10.9	181	0.282601	-6.4	1.0	-2.5	
59	16-LVD-004_104	0.282336	0.000031	0.00108	0.00008	0.0277	0.0022	1.467195	0.000044	10.9	335	0.282329	-15.9	1.1	-8.7	
60	16-LVD-004_112	0.282651	0.000021	0.00089	0.00004	0.0206	0.0008	1.467213	0.000035	13.1	179	0.282648	-4.7	0.7	-0.9	
61	16-LVD-004_113	0.282584	0.000024	0.00082	0.00002	0.0184	0.0004	1.467226	0.000036	11.9	179	0.282581	-7.1	0.8	-3.2	
62	16-LVD-004_114	0.282377	0.000021	0.00123	0.00004	0.0312	0.0011	1.467210	0.000031	11.6	361	0.282369	-14.4	0.7	-6.7	
63	16-LVD-004_115	0.282549	0.000025	0.00097	0.00005	0.0217	0.0012	1.467194	0.000034	11.2	194	0.282545	-8.3	0.9	-4.2	
64	16-LVD-004_116	0.282639	0.000025	0.00113	0.00007	0.0267	0.0016	1.467217	0.000038	11.0	183	0.282635	-5.2	0.9	-1.2	
65	16-LVD-004_117	0.282574	0.000021	0.00083	0.00004	0.0193	0.0009	1.467186	0.000040	11.3	182	0.282571	-7.5	0.7	-3.5	
66	16-LVD-004_118	0.282573	0.000025	0.00103	0.00004	0.0238	0.0011	1.467182	0.000035	10.5	179	0.282570	-7.5	0.9	-3.6	
67	16-LVD-004_119	0.282587	0.000024	0.00145	0.00005	0.0342	0.0013	1.467170	0.000035	10.6	181	0.282582	-7.0	0.8	-3.2	
68	16-LVD-004_120	0.282560	0.000035	0.00133	0.00011	0.0313	0.0024	1.467207	0.000043	13.7	181	0.282555	-8.0	1.2	-4.1	
70	16-LVD-004_128	0.282558	0.000030	0.00145	0.00009	0.0331	0.0022	1.467174	0.000042	9.3	181	0.282553	-8.0	1.1	-4.2	
71	16-LVD-004_129	0.282606	0.000024	0.00122	0.00003	0.0286	0.0008	1.467177	0.000029	11.4	184	0.282602	-6.3	0.8	-2.4	
73	16-LVD-004_131	0.282587	0.000024	0.00059	0.00002	0.0135	0.0004	1.467203	0.000038	11.7	176	0.282585	-7.0	0.8	-3.2	
74	16-LVD-004_132	0.282788	0.000016	0.00106	0.00004	0.0202	0.0011	1.467222	0.000039	12.4	186	0.282784	0.1	0.6	4.1	

Grain	Spot ID	corrected										MUN LASS Age (Ma)	$^{176}\text{Hf}/^{177}\text{Hf}$	EHf0	2SE	EHfi
		$^{176}\text{Hf}/^{177}\text{Hf}$	2SE	$^{176}\text{Lu}/^{177}\text{Hf}$	2SE	$^{176}\text{Yb}/^{177}\text{Hf}$	2SE	$^{178}\text{Hf}/^{177}\text{Hf}$	2SE	Total Hf Beam						
75	16-LVD-004_133	0.282597	0.000029	0.00139	0.00003	0.0333	0.0007	1.467240	0.000046	12.1	176	0.282592	-6.6	1.0	-2.9	
76	16-LVD-004_134	0.282566	0.000030	0.00104	0.00007	0.0236	0.0017	1.467173	0.000041	10.3	182	0.282562	-7.7	1.1	-3.8	
77	16-LVD-004_135	0.282686	0.000022	0.00084	0.00005	0.0204	0.0012	1.467154	0.000046	11.3	184	0.282683	-3.5	0.8	0.5	
78	16-LVD-004_136	0.282752	0.000021	0.00128	0.00006	0.0261	0.0014	1.467213	0.000034	11.8	193	0.282747	-1.2	0.7	3.0	
79	16-LVD-004_137	0.282713	0.000024	0.00103	0.00007	0.0234	0.0016	1.467206	0.000035	12.0	189	0.282709	-2.5	0.8	1.5	
80	16-LVD-004_144	0.282736	0.000028	0.00157	0.00008	0.0325	0.0020	1.467145	0.000033	12.9	198	0.282730	-1.7	1.0	2.5	
81	16-LVD-004_145	0.282584	0.000019	0.00083	0.00003	0.0188	0.0006	1.467233	0.000035	13.0	180	0.282581	-7.1	0.7	-3.2	
83	16-LVD-004_147	0.282599	0.000019	0.00076	0.00004	0.0172	0.0010	1.467228	0.000040	11.7	182	0.282596	-6.6	0.7	-2.6	
84	16-LVD-004_148	0.282777	0.000026	0.00129	0.00008	0.0262	0.0016	1.467217	0.000032	12.3	195	0.282772	-0.3	0.9	3.9	
85	16-LVD-004_149	0.282772	0.000020	0.00117	0.00004	0.0234	0.0009	1.467194	0.000035	12.9	191	0.282768	-0.5	0.7	3.6	
88	16-LVD-004_152	0.282632	0.000027	0.00069	0.00004	0.0156	0.0008	1.467207	0.000045	12.0	183	0.282630	-5.4	1.0	-1.4	
90	16-LVD-004_160	0.282702	0.000020	0.00133	0.00011	0.0272	0.0024	1.467181	0.000030	12.1	199	0.282697	-2.9	0.7	1.3	
91	16-LVD-004_161	0.282679	0.000025	0.00075	0.00004	0.0169	0.0010	1.467200	0.000043	11.5	199	0.282676	-3.7	0.9	0.6	
92	16-LVD-004_162	0.282627	0.000022	0.00098	0.00006	0.0224	0.0014	1.467208	0.000031	11.4	198	0.282623	-5.6	0.8	-1.3	
93	16-LVD-004_163	0.282711	0.000024	0.00082	0.00004	0.0163	0.0009	1.467198	0.000028	13.2	204	0.282708	-2.6	0.8	1.8	
94	16-LVD-004_164	0.282551	0.000018	0.00092	0.00003	0.0214	0.0005	1.467201	0.000038	14.3	192	0.282548	-8.3	0.6	-4.1	
95	16-LVD-004_165	0.282638	0.000027	0.00149	0.00008	0.0354	0.0021	1.467204	0.000025	14.4	186	0.282633	-5.2	1.0	-1.3	
96	16-LVD-004_166	0.282588	0.000018	0.00098	0.00002	0.0227	0.0006	1.467183	0.000036	13.6	184	0.282585	-7.0	0.6	-3.0	
99	16-LVD-004_169	0.282588	0.000022	0.00085	0.00002	0.0200	0.0006	1.467208	0.000037	13.0	193	0.282585	-7.0	0.8	-2.8	
100	16-LVD-004_39	0.282657	0.000021	0.00079	0.00003	0.0178	0.0007	1.467220	0.000038	12.8	190	0.282654	-4.5	0.7	-0.4	
101	16-LVD-004_40	0.282748	0.000017	0.00075	0.00007	0.0145	0.0014	1.467225	0.000028	15.6	204	0.282745	-1.3	0.6	3.1	
102	16-LVD-004_41	0.282587	0.000022	0.00132	0.00007	0.0304	0.0017	1.467214	0.000034	13.6	197	0.282582	-7.0	0.8	-2.8	
103	16-LVD-004_42	0.282660	0.000024	0.00119	0.00002	0.0277	0.0006	1.467190	0.000033	14.0	193	0.282656	-4.4	0.8	-0.3	

Grain	Spot ID	corrected									Total Hf Beam	MUN LASS Age (Ma)	176Hf/177Hf	EHf0	2SE	EHfi
		176Hf/177Hf	2SE	176Lu/177Hf	2SE	176Yb/177Hf	2SE	178Hf/177Hf	2SE							
104	16-LVD-004_43	0.282547	0.000020	0.00095	0.00002	0.0214	0.0004	1.467197	0.000031	13.6	205	0.282543	-8.4	0.7	-4.0	
105	16-LVD-004_44	0.282748	0.000021	0.00082	0.00002	0.0168	0.0004	1.467217	0.000030	17.6	208	0.282745	-1.3	0.7	3.2	
106	16-LVD-004_45	0.282557	0.000018	0.00103	0.00005	0.0237	0.0012	1.467218	0.000027	14.2	199	0.282553	-8.1	0.6	-3.8	
107	16-LVD-004_46	0.282750	0.000018	0.00152	0.00003	0.0304	0.0006	1.467177	0.000033	14.4	203	0.282744	-1.2	0.6	3.1	
108	16-LVD-004_47	0.282561	0.000020	0.00077	0.00004	0.0171	0.0008	1.467226	0.000032	14.5	196	0.282558	-7.9	0.7	-3.7	
109	16-LVD-004_48	0.282786	0.000018	0.00071	0.00002	0.0177	0.0005	1.467180	0.000041	13.8	191	0.282783	0.0	0.6	4.2	
Rejected Analysis																
5	16-LVD-004_19	0.282837	0.000048	0.00072	0.00003	0.0168	0.0010	1.467216	0.000054	16.6	186	0.282835	1.8	1.7	5.9	
9	16-LVD-004_23	0.282696	0.000033	0.00141	0.00008	0.0342	0.0027	1.467184	0.000035	9.6	184	0.282691	-3.1	1.2	0.8	
15	16-LVD-004_36	0.282590	0.000026	0.00110	0.00007	0.0264	0.0018	1.467222	0.000042	11.2	189	0.282586	-6.9	0.9	-2.8	
23	16-LVD-004_50	0.282788	0.000030	0.00143	0.00007	0.0318	0.0014	1.467224	0.000031	13.5	180	0.282783	0.1	1.1	3.9	
46	16-LVD-004_85	0.282339	0.000033	0.00082	0.00003	0.0218	0.0007	1.467181	0.000048	13.6	87	0.282338	-15.8	1.2	-13.9	
50	16-LVD-004_89	0.282146	0.000045	0.00268	0.00037	0.0830	0.0140	1.467215	0.000048	13.7	881	0.282102	-22.6	1.6	-4.5	
56	16-LVD-004_101	0.282371	0.000029	0.00150	0.00007	0.0392	0.0017	1.467189	0.000048	14.9	278	0.282363	-14.6	1.0	-8.7	
69	16-LVD-004_121	0.282347	0.000042	0.00078	0.00014	0.0202	0.0038	1.467194	0.000036	10.9	336	0.282342	-15.5	1.5	-8.2	
72	16-LVD-004_130	0.282917	0.000028	0.00155	0.00011	0.0372	0.0028	1.467248	0.000066	12.9	190	0.282911	4.7	1.0	8.7	
82	16-LVD-004_146	0.282593	0.000021	0.00110	0.00002	0.0257	0.0006	1.467227	0.000041	12.7	183	0.282589	-6.8	0.7	-2.9	
86	16-LVD-004_150	0.282626	0.000039	0.00153	0.00008	0.0315	0.0022	1.467187	0.000040	14.0	206	0.282620	-5.6	1.4	-1.3	
89	16-LVD-004_153	0.282728	0.000058	0.00111	0.00010	0.0264	0.0021	1.467198	0.000040	16.4	185	0.282724	-2.0	2.1	2.0	
97	16-LVD-004_167	0.282566	0.000022	0.00093	0.00006	0.0220	0.0014	1.467215	0.000039	13.9	189	0.282563	-7.7	0.8	-3.7	
98	16-LVD-004_168	0.282573	0.000023	0.00116	0.00006	0.0280	0.0014	1.467188	0.000033	13.2	185	0.282569	-7.5	0.8	-3.5	

Whitehorse trough - Tanglefoot formation - Sample 17-LVD-018, Conglomerate Mountain (Zone 08V 453930E 6833117N NAD 83)

Grain	Spot ID	<i>corrected</i>		2SE	176Lu/ ¹⁷⁷ Hf	2SE	176Yb/ ¹⁷⁷ Hf	2SE	178Hf/ ¹⁷⁷ Hf	2SE	Total Hf Beam	MUN LASS Age (Ma)	¹⁷⁶ Hf/ ¹⁷⁷ Hfi	EHf0	2SE	EHfi	
		¹⁷⁶ Hf/ ¹⁷⁷ Hf															
<i>corrected</i>																	
Grain	Spot ID	¹⁷⁶ Hf/ ¹⁷⁷ Hf	2SE	176Lu/ ¹⁷⁷ Hf	2SE	176Yb/ ¹⁷⁷ Hf	2SE	178Hf/ ¹⁷⁷ Hf	2SE	Total Hf Beam	MUN LASS Age (Ma)	¹⁷⁶ Hf/ ¹⁷⁷ Hfi	EHf0	2SE	EHfi		
				177Hf		177Hf		177Hf				177Hfi					
2	17-LVD-018_146	0.282957	0.000029	0.00130	0.00004	0.0318	0.0011	1.467152	0.000026	9.9	204	0.282952	6.1	1.0	10.5		
3	17-LVD-018_147	0.282824	0.000034	0.00144	0.00003	0.0310	0.0006	1.467148	0.000035	12.4	192	0.282819	1.4	1.2	5.5		
4	17-LVD-018_148	0.282973	0.000018	0.00088	0.00014	0.0225	0.0036	1.467188	0.000043	12.1	211	0.282970	6.6	0.6	11.2		
5	17-LVD-018_155	0.282911	0.000024	0.00152	0.00018	0.0323	0.0041	1.467209	0.000036	13.3	317	0.282902	4.5	0.8	11.2		
6	17-LVD-018_156	0.282931	0.000028	0.00116	0.00002	0.0273	0.0004	1.467195	0.000036	12.6	220	0.282926	5.2	1.0	9.9		
7	17-LVD-018_157	0.282903	0.000026	0.00053	0.00002	0.0110	0.0004	1.467211	0.000033	11.5	325	0.282900	4.2	0.9	11.3		
8	17-LVD-018_158	0.282846	0.000029	0.00216	0.00009	0.0561	0.0027	1.467193	0.000046	11.6	354	0.282832	2.2	1.0	9.5		
9	17-LVD-018_159	0.282889	0.000024	0.00167	0.00007	0.0377	0.0016	1.467177	0.000028	13.6	306	0.282879	3.7	0.8	10.2		
12	17-LVD-018_162	0.282878	0.000024	0.00076	0.00004	0.0200	0.0012	1.467198	0.000031	11.9	287	0.282874	3.3	0.8	9.5		
13	17-LVD-018_163	0.282747	0.000027	0.00151	0.00003	0.0311	0.0005	1.467181	0.000027	13.0	204	0.282741	-1.3	1.0	3.0		
14	17-LVD-018_164	0.282800	0.000015	0.00096	0.00003	0.0196	0.0006	1.467175	0.000039	15.9	180	0.282797	0.5	0.5	4.4		
15	17-LVD-018_165	0.282938	0.000029	0.00127	0.00007	0.0318	0.0018	1.467219	0.000035	10.4	204	0.282933	5.4	1.0	9.8		
16	17-LVD-018_166	0.282907	0.000022	0.00082	0.00005	0.0201	0.0012	1.467200	0.000046	11.0	213	0.282904	4.3	0.8	8.9		
17	17-LVD-018_10	0.282938	0.000026	0.00103	0.00004	0.0247	0.0012	1.467192	0.000041	14.8	207	0.282934	5.4	0.9	9.9		
18	17-LVD-018_11	0.282957	0.000035	0.00381	0.00039	0.1070	0.0120	1.467175	0.000035	13.3	327	0.282934	6.1	1.2	12.5		
19	17-LVD-018_12	0.282892	0.000038	0.00287	0.00015	0.0773	0.0038	1.467167	0.000049	13.4	327	0.282874	3.8	1.3	10.5		
20	17-LVD-018_13	0.282760	0.000034	0.00128	0.00004	0.0278	0.0008	1.467176	0.000037	14.3	205	0.282755	-0.9	1.2	3.5		
21	17-LVD-018_14	0.282823	0.000025	0.00158	0.00019	0.0387	0.0045	1.467210	0.000040	12.7	311	0.282814	1.3	0.9	7.9		
22	17-LVD-018_15	0.282745	0.000027	0.00190	0.00010	0.0434	0.0019	1.467194	0.000038	12.7	205	0.282738	-1.4	1.0	2.9		
24	17-LVD-018_17	0.282881	0.000020	0.00119	0.00008	0.0274	0.0020	1.467197	0.000031	14.1	328	0.282874	3.4	0.7	10.4		

Grain	Spot ID	corrected										MUN LASS Age (Ma)	$^{176}\text{Hf}/^{177}\text{Hf}$	EHf0	2SE	EHfi
		$^{176}\text{Hf}/^{177}\text{Hf}$	2SE	$^{176}\text{Lu}/^{177}\text{Hf}$	2SE	$^{176}\text{Yb}/^{177}\text{Hf}$	2SE	$^{178}\text{Hf}/^{177}\text{Hf}$	2SE	Total Hf Beam						
25	17-LVD-018_18	0.282809	0.000023	0.00125	0.00003	0.0270	0.0006	1.467149	0.000045	13.1	211	0.282804	0.8	0.8	5.4	
27	17-LVD-018_20	0.282742	0.000046	0.00172	0.00009	0.0389	0.0020	1.467188	0.000053	14.9	186	0.282736	-1.5	1.6	2.4	
28	17-LVD-018_21	0.282802	0.000018	0.00066	0.00004	0.0144	0.0009	1.467176	0.000029	12.4	217	0.282799	0.6	0.6	5.3	
30	17-LVD-018_29	0.282741	0.000022	0.00104	0.00007	0.0227	0.0014	1.467185	0.000032	11.2	210	0.282737	-1.6	0.8	3.0	
31	17-LVD-018_30	0.282862	0.000027	0.00087	0.00006	0.0193	0.0015	1.467183	0.000031	12.1	329	0.282857	2.7	1.0	9.9	
32	17-LVD-018_31	0.282932	0.000023	0.00045	0.00002	0.0094	0.0005	1.467196	0.000033	11.1	221	0.282930	5.2	0.8	10.0	
33	17-LVD-018_32	0.282687	0.000028	0.00143	0.00007	0.0338	0.0017	1.467138	0.000041	13.9	204	0.282682	-3.5	1.0	0.9	
34	17-LVD-018_33	0.282825	0.000026	0.00141	0.00005	0.0309	0.0010	1.467188	0.000045	12.7	207	0.282820	1.4	0.9	5.8	
35	17-LVD-018_34	0.282973	0.000026	0.00072	0.00002	0.0182	0.0003	1.467161	0.000046	13.6	221	0.282970	6.6	0.9	11.5	
36	17-LVD-018_35	0.282812	0.000034	0.00146	0.00008	0.0326	0.0018	1.467186	0.000044	15.5	204	0.282806	1.0	1.2	5.3	
37	17-LVD-018_36	0.282886	0.000022	0.00119	0.00005	0.0277	0.0014	1.467194	0.000048	15.2	214	0.282881	3.6	0.8	8.2	
38	17-LVD-018_37	0.282911	0.000027	0.00144	0.00025	0.0331	0.0061	1.467179	0.000034	14.6	331	0.282902	4.5	1.0	11.5	
39	17-LVD-018_38	0.282839	0.000038	0.00122	0.00013	0.0273	0.0026	1.467202	0.000044	12.7	213	0.282834	1.9	1.3	6.5	
41	17-LVD-018_46	0.282912	0.000025	0.00129	0.00007	0.0354	0.0020	1.467195	0.000032	11.8	314	0.282904	4.5	0.9	11.2	
42	17-LVD-018_47	0.282950	0.000027	0.00187	0.00018	0.0429	0.0044	1.467177	0.000047	10.4	312	0.282939	5.8	1.0	12.4	
43	17-LVD-018_48	0.282858	0.000024	0.00106	0.00004	0.0276	0.0010	1.467161	0.000033	12.8	332	0.282851	2.6	0.8	9.8	
44	17-LVD-018_49	0.282916	0.000028	0.00107	0.00003	0.0290	0.0008	1.467200	0.000042	13.6	321	0.282910	4.6	1.0	11.5	
45	17-LVD-018_50	0.282947	0.000021	0.00098	0.00010	0.0237	0.0025	1.467118	0.000027	13.7	197	0.282943	5.7	0.7	10.0	
47	17-LVD-018_52	0.282799	0.000025	0.00126	0.00004	0.0270	0.0012	1.467197	0.000033	12.6	208	0.282794	0.5	0.9	4.9	
48	17-LVD-018_53	0.282710	0.000021	0.00127	0.00007	0.0292	0.0012	1.467195	0.000033	11.7	188	0.282706	-2.7	0.7	1.4	
49	17-LVD-018_54	0.282898	0.000023	0.00086	0.00005	0.0193	0.0012	1.467185	0.000040	11.7	319	0.282893	4.0	0.8	10.9	
51	17-LVD-018_56	0.282882	0.000026	0.00115	0.00001	0.0314	0.0004	1.467195	0.000032	12.3	317	0.282875	3.4	0.9	10.2	
52	17-LVD-018_57	0.282957	0.000026	0.00050	0.00003	0.0128	0.0007	1.467213	0.000042	11.8	211	0.282955	6.1	0.9	10.7	

Grain	Spot ID	corrected										MUN LASS Age (Ma)	$^{176}\text{Hf}/^{177}\text{Hf}$	EHf0	2SE	EHfi
		$^{176}\text{Hf}/^{177}\text{Hf}$	2SE	$^{176}\text{Lu}/^{177}\text{Hf}$	2SE	$^{176}\text{Yb}/^{177}\text{Hf}$	2SE	$^{178}\text{Hf}/^{177}\text{Hf}$	2SE	Total Hf Beam						
53	17-LVD-018_64	0.282878	0.000024	0.00046	0.00003	0.0107	0.0008	1.467193	0.000045	11.2	321	0.282875	3.3	0.8	10.3	
54	17-LVD-018_65	0.282973	0.000026	0.00128	0.00003	0.0306	0.0007	1.467249	0.000044	11.9	205	0.282968	6.6	0.9	11.0	
55	17-LVD-018_66	0.282810	0.000036	0.00127	0.00005	0.0268	0.0009	1.467194	0.000041	13.3	200	0.282805	0.9	1.3	5.2	
56	17-LVD-018_67	0.282819	0.000025	0.00057	0.00002	0.0115	0.0005	1.467209	0.000040	10.8	326	0.282816	1.2	0.9	8.3	
57	17-LVD-018_68	0.282783	0.000021	0.00107	0.00006	0.0224	0.0013	1.467241	0.000030	14.0	210	0.282779	-0.1	0.7	4.4	
58	17-LVD-018_69	0.282948	0.000023	0.00076	0.00005	0.0187	0.0015	1.467195	0.000032	13.9	211	0.282945	5.8	0.8	10.3	
59	17-LVD-018_70	0.282939	0.000025	0.00107	0.00002	0.0250	0.0006	1.467184	0.000034	13.6	205	0.282935	5.4	0.9	9.9	
60	17-LVD-018_71	0.282938	0.000032	0.00103	0.00011	0.0243	0.0030	1.467189	0.000050	11.0	212	0.282934	5.4	1.1	10.0	
61	17-LVD-018_72	0.282793	0.000024	0.00118	0.00007	0.0258	0.0013	1.467165	0.000037	12.1	200	0.282789	0.3	0.8	4.6	
62	17-LVD-018_73	0.282976	0.000024	0.00083	0.00003	0.0186	0.0007	1.467189	0.000033	11.3	209	0.282973	6.8	0.8	11.3	
63	17-LVD-018_74	0.282954	0.000030	0.00247	0.00007	0.0545	0.0017	1.467188	0.000036	10.9	328	0.282939	6.0	1.1	12.7	
64	17-LVD-018_75	0.282887	0.000025	0.00065	0.00002	0.0148	0.0003	1.467185	0.000039	10.8	310	0.282883	3.6	0.9	10.4	
65	17-LVD-018_82	0.282969	0.000020	0.00114	0.00006	0.0272	0.0013	1.467186	0.000042	13.5	210	0.282965	6.5	0.7	11.0	
67	17-LVD-018_84	0.282882	0.000024	0.00108	0.00002	0.0274	0.0006	1.467179	0.000037	10.6	308	0.282876	3.4	0.8	10.1	
68	17-LVD-018_85	0.282818	0.000037	0.00128	0.00002	0.0273	0.0005	1.467167	0.000054	14.4	213	0.282813	1.2	1.3	5.7	
69	17-LVD-018_86	0.282897	0.000022	0.00121	0.00013	0.0296	0.0035	1.467206	0.000035	12.3	303	0.282890	4.0	0.8	10.5	
70	17-LVD-018_87	0.282723	0.000021	0.00152	0.00013	0.0369	0.0035	1.467142	0.000036	11.5	373	0.282712	-2.2	0.7	5.7	
71	17-LVD-018_88	0.282894	0.000020	0.00118	0.00003	0.0256	0.0007	1.467172	0.000052	9.0	311	0.282887	3.9	0.7	10.5	
72	17-LVD-018_89	0.282914	0.000020	0.00058	0.00000	0.0153	0.0001	1.467179	0.000034	12.2	314	0.282911	4.6	0.7	11.4	
73	17-LVD-018_90	0.282890	0.000023	0.00109	0.00002	0.0257	0.0006	1.467171	0.000033	10.9	309	0.282884	3.7	0.8	10.4	
74	17-LVD-018_91	0.282912	0.000026	0.00073	0.00004	0.0176	0.0015	1.467155	0.000038	11.5	301	0.282908	4.5	0.9	11.0	
75	17-LVD-018_92	0.282883	0.000023	0.00085	0.00002	0.0216	0.0006	1.467151	0.000034	11.9	299	0.282878	3.5	0.8	10.0	
76	17-LVD-018_93	0.282890	0.000021	0.00075	0.00004	0.0148	0.0008	1.467200	0.000034	10.0	322	0.282885	3.7	0.7	10.7	

Grain	Spot ID	corrected										MUN LASS Age (Ma)	$^{176}\text{Hf}/^{177}\text{Hf}$	EHf0	2SE	EHfi
		$^{176}\text{Hf}/^{177}\text{Hf}$	2SE	$^{176}\text{Lu}/^{177}\text{Hf}$	2SE	$^{176}\text{Yb}/^{177}\text{Hf}$	2SE	$^{178}\text{Hf}/^{177}\text{Hf}$	2SE	Total Hf Beam						
77	17-LVD-018_100	0.282896	0.000023	0.00040	0.00003	0.0083	0.0005	1.467191	0.000036	11.9	309	0.282894	3.9	0.8	10.7	
78	17-LVD-018_101	0.282915	0.000034	0.00264	0.00015	0.0649	0.0037	1.467219	0.000045	9.6	297	0.282900	4.6	1.2	10.7	
79	17-LVD-018_102	0.282978	0.000027	0.00142	0.00005	0.0330	0.0010	1.467206	0.000040	10.4	204	0.282973	6.8	1.0	11.2	
80	17-LVD-018_103	0.282788	0.000016	0.00080	0.00008	0.0172	0.0016	1.467196	0.000033	13.8	213	0.282785	0.1	0.6	4.7	
81	17-LVD-018_104	0.282803	0.000030	0.00116	0.00006	0.0246	0.0011	1.467171	0.000031	13.8	195	0.282799	0.6	1.1	4.8	
82	17-LVD-018_105	0.282951	0.000031	0.00078	0.00001	0.0189	0.0004	1.467160	0.000037	11.5	207	0.282948	5.9	1.1	10.4	
83	17-LVD-018_106	0.282925	0.000022	0.00092	0.00001	0.0241	0.0003	1.467202	0.000027	11.9	288	0.282920	5.0	0.8	11.2	
84	17-LVD-018_107	0.282899	0.000028	0.00103	0.00007	0.0225	0.0016	1.467194	0.000028	10.4	323	0.282893	4.0	1.0	11.0	
85	17-LVD-018_108	0.282898	0.000022	0.00051	0.00004	0.0114	0.0009	1.467166	0.000034	13.7	319	0.282895	4.0	0.8	11.0	
86	17-LVD-018_109	0.282907	0.000020	0.00031	0.00000	0.0064	0.0000	1.467167	0.000037	11.7	306	0.282905	4.3	0.7	11.1	
87	17-LVD-018_110	0.282865	0.000022	0.00199	0.00003	0.0461	0.0009	1.467223	0.000032	10.6	331	0.282853	2.8	0.8	9.8	
88	17-LVD-018_111	0.282855	0.000027	0.00113	0.00005	0.0267	0.0013	1.467162	0.000036	9.7	308	0.282848	2.5	1.0	9.1	
89	17-LVD-018_118	0.282910	0.000035	0.00119	0.00006	0.0269	0.0016	1.467167	0.000040	10.7	300	0.282903	4.4	1.2	10.9	
90	17-LVD-018_119	0.282892	0.000031	0.00078	0.00004	0.0216	0.0012	1.467194	0.000035	13.3	290	0.282888	3.8	1.1	10.1	
91	17-LVD-018_120	0.282789	0.000023	0.00118	0.00004	0.0249	0.0006	1.467209	0.000032	12.7	202	0.282785	0.1	0.8	4.5	
92	17-LVD-018_121	0.282895	0.000020	0.00061	0.00001	0.0156	0.0005	1.467173	0.000027	13.1	303	0.282892	3.9	0.7	10.5	
93	17-LVD-018_122	0.282802	0.000022	0.00145	0.00003	0.0308	0.0007	1.467163	0.000038	12.1	204	0.282796	0.6	0.8	4.9	
94	17-LVD-018_123	0.282885	0.000034	0.00094	0.00006	0.0238	0.0021	1.467184	0.000036	11.5	290	0.282880	3.5	1.2	9.8	
95	17-LVD-018_124	0.282948	0.000029	0.00221	0.00016	0.0515	0.0041	1.467180	0.000041	9.7	305	0.282935	5.8	1.0	12.1	
96	17-LVD-018_125	0.282832	0.000026	0.00155	0.00010	0.0353	0.0027	1.467148	0.000036	13.3	248	0.282825	1.7	0.9	6.9	
97	17-LVD-018_126	0.282777	0.000022	0.00111	0.00005	0.0239	0.0010	1.467170	0.000041	12.2	200	0.282773	-0.3	0.8	4.0	
98	17-LVD-018_127	0.282836	0.000029	0.00116	0.00009	0.0273	0.0025	1.467219	0.000035	11.4	277	0.282830	1.8	1.0	7.8	
99	17-LVD-018_128	0.282874	0.000027	0.00102	0.00003	0.0226	0.0007	1.467123	0.000034	13.4	312	0.282868	3.1	1.0	9.9	

Grain	Spot ID	<i>corrected</i>		2SE	176Lu/ 177Hf	2SE	176Yb/ 177Hf	2SE	178Hf/ 177Hf	2SE	Total Hf Beam	MUN LASS Age (Ma)	176Hf/ 177Hf	EHf0	2SE	EHf1
		176Hf/ 177Hf	2SE													
100	17-LVD-018_129	0.282889	0.000023	0.00107	0.00008	0.0235	0.0020	1.467203	0.000031	11.4	321	0.282883	3.7	0.8	10.6	
101	17-LVD-018_136	0.282782	0.000027	0.00110	0.00002	0.0229	0.0005	1.467163	0.000029	14.0	200	0.282778	-0.1	1.0	4.2	
102	17-LVD-018_137	0.282773	0.000029	0.00118	0.00004	0.0247	0.0009	1.467187	0.000038	11.4	203	0.282769	-0.4	1.0	3.9	
103	17-LVD-018_138	0.282808	0.000021	0.00112	0.00003	0.0234	0.0008	1.467191	0.000033	12.4	195	0.282804	0.8	0.7	5.0	
104	17-LVD-018_139	0.282739	0.000025	0.00153	0.00006	0.0352	0.0013	1.467211	0.000043	12.9	198	0.282733	-1.6	0.9	2.6	
105	17-LVD-018_140	0.282794	0.000025	0.00127	0.00009	0.0368	0.0037	1.467201	0.000034	15.0	186	0.282790	0.3	0.9	4.3	
106	17-LVD-018_141	0.282894	0.000026	0.00057	0.00002	0.0126	0.0004	1.467169	0.000031	13.1	323	0.282891	3.9	0.9	10.9	
107	17-LVD-018_142	0.282776	0.000021	0.00125	0.00006	0.0265	0.0011	1.467184	0.000034	12.1	186	0.282772	-0.3	0.7	3.7	
108	17-LVD-018_143	0.282796	0.000019	0.00103	0.00002	0.0214	0.0005	1.467158	0.000043	15.8	188	0.282792	0.4	0.7	4.4	
109	17-LVD-018_144	0.282882	0.000021	0.00105	0.00009	0.0253	0.0024	1.467162	0.000032	9.9	312	0.282876	3.4	0.7	10.2	
110	17-LVD-018_145	0.282937	0.000028	0.00173	0.00017	0.0441	0.0050	1.467190	0.000048	10.2	276	0.282928	5.4	1.0	11.2	
111	17-LVD-018_146	0.282919	0.000026	0.00096	0.00004	0.0242	0.0008	1.467196	0.000037	10.4	314	0.282913	4.7	0.9	11.5	
112	17-LVD-018_147	0.282924	0.000025	0.00155	0.00005	0.0408	0.0013	1.467175	0.000041	11.8	289	0.282916	4.9	0.9	11.1	
113	17-LVD-018_82	0.282926	0.000026	0.00142	0.00018	0.0291	0.0035	1.467153	0.000037	9.1	320	0.282917	5.0	0.9	11.8	
114	17-LVD-018_83	0.282901	0.000019	0.00075	0.00001	0.0162	0.0002	1.467207	0.000038	12.2	311	0.282897	4.1	0.7	10.9	
115	17-LVD-018_84	0.282884	0.000024	0.00073	0.00005	0.0189	0.0012	1.467172	0.000036	11.0	302	0.282880	3.5	0.8	10.1	
116	17-LVD-018_85	0.282791	0.000021	0.00097	0.00002	0.0198	0.0004	1.467177	0.000036	12.4	202	0.282787	0.2	0.7	4.6	
117	17-LVD-018_86	0.282762	0.000026	0.00101	0.00008	0.0211	0.0015	1.467172	0.000031	12.8	195	0.282758	-0.8	0.9	3.4	
118	17-LVD-018_87	0.282911	0.000025	0.00128	0.00007	0.0336	0.0016	1.467199	0.000033	10.3	318	0.282903	4.5	0.9	11.3	
119	17-LVD-018_88	0.282915	0.000021	0.00061	0.00002	0.0156	0.0006	1.467178	0.000032	13.3	317	0.282911	4.6	0.7	11.5	
120	17-LVD-018_89	0.282881	0.000027	0.00124	0.00003	0.0319	0.0009	1.467211	0.000036	10.6	313	0.282874	3.4	1.0	10.1	
Rejected Analysis																
1	17-LVD-018_145	0.282984	0.000057	0.00138	0.00011	0.0333	0.0028	1.467200	0.000073	9.2	201	0.282979	7.0	2.0	11.3	

Grain	Spot ID	<i>corrected</i>									Total Hf Beam	MUN LASS Age (Ma)	176Hf/ 177Hfi	EHf0	2SE	EHfi
		176Hf/ 177Hf	2SE	176Lu/ 177Hf	2SE	176Yb/ 177Hf	2SE	178Hf/ 177Hf	2SE							
10	17-LVD-018_160	0.282821	0.000034	0.00112	0.00003	0.0254	0.0005	1.467154	0.000032	15.6	317	0.282814	1.3	1.2	8.1	
11	17-LVD-018_161	0.282793	0.000027	0.00099	0.00007	0.0216	0.0013	1.467166	0.000050	14.0	208	0.282789	0.3	1.0	4.8	
23	17-LVD-018_16	0.282946	0.000033	0.00112	0.00007	0.0268	0.0018	1.467130	0.000046	14.0	224	0.282941	5.7	1.2	10.5	
26	17-LVD-018_19	0.282825	0.000028	0.00068	0.00018	0.0164	0.0040	1.467191	0.000043	13.9	280	0.282821	1.4	1.0	7.5	
29	17-LVD-018_28	0.282937	0.000054	0.00167	0.00037	0.0369	0.0083	1.467165	0.000060	12.6	210	0.282930	5.4	1.9	9.8	
40	17-LVD-018_39	0.282914	0.000023	0.00177	0.00009	0.0427	0.0022	1.467197	0.000045	13.5	289	0.282904	4.6	0.8	10.7	
46	17-LVD-018_51	0.282754	0.000026	0.00096	0.00002	0.0211	0.0005	1.467181	0.000036	13.0	188	0.282751	-1.1	0.9	3.0	
50	17-LVD-018_55	0.282940	0.000046	0.00507	0.00029	0.1334	0.0073	1.467127	0.000049	9.3	315	0.282910	5.5	1.6	11.4	
66	17-LVD-018_83	0.282914	0.000027	0.00075	0.00003	0.0199	0.0008	1.467177	0.000045	11.5	319	0.282910	4.6	1.0	11.5	

Richthofen formation

Whitehorse trough - Richthofen formation - Sample 16-LVD-009, Mount Laurier (Zone 08V 507457E 6765804N NAD 83)

Grain	Spot ID	<i>corrected</i>									Total Hf Beam	MUN LASS Age (Ma)	176Hf/ 177Hfi	EHf0	2SE	EHfi
		176Hf/ 177Hf	2SE	176Lu/ 177Hf	2SE	176Yb/ 177Hf	2SE	178Hf/ 177Hf	2SE							
1	16-LVD-009_170	0.282759	0.000020	0.00061	0.00005	0.0122	0.0010	1.467215	0.000033	13.5	198	0.282757	-0.9	0.7	3.4	
7	16-LVD-009_176	0.282784	0.000029	0.00083	0.00009	0.0161	0.0020	1.467200	0.000050	18.3	208	0.282781	0.0	1.0	4.5	
8	16-LVD-009_177	0.282834	0.000030	0.00143	0.00005	0.0348	0.0015	1.467195	0.000045	15.2	325	0.282825	1.7	1.1	8.7	
9	16-LVD-009_178	0.282791	0.000021	0.00087	0.00006	0.0171	0.0011	1.467243	0.000040	15.9	210	0.282788	0.2	0.7	4.8	
11	16-LVD-009_186	0.282777	0.000024	0.00070	0.00003	0.0135	0.0005	1.467221	0.000040	12.9	200	0.282774	-0.3	0.8	4.1	
14	16-LVD-009_189	0.282786	0.000021	0.00090	0.00005	0.0179	0.0009	1.467186	0.000041	16.9	207	0.282783	0.0	0.7	4.5	
15	16-LVD-009_190	0.282773	0.000024	0.00173	0.00002	0.0406	0.0006	1.467209	0.000047	17.6	321	0.282763	-0.4	0.8	6.4	

Grain	Spot ID	corrected										MUN LASS Age (Ma)	$^{176}\text{Hf}/^{177}\text{Hf}$	EHf0	2SE	EHfi
		$^{176}\text{Hf}/^{177}\text{Hf}$	2SE	$^{176}\text{Lu}/^{177}\text{Hf}$	2SE	$^{176}\text{Yb}/^{177}\text{Hf}$	2SE	$^{178}\text{Hf}/^{177}\text{Hf}$	2SE	Total Hf Beam						
16	16-LVD-009_191	0.282779	0.000019	0.00101	0.00007	0.0199	0.0015	1.467208	0.000038	18.4	204	0.282775	-0.2	0.7	4.2	
23	16-LVD-009_205	0.282843	0.000021	0.00155	0.00010	0.0349	0.0024	1.467180	0.000041	13	341	0.282833	2.1	0.7	9.3	
24	16-LVD-009_206	0.282806	0.000029	0.00194	0.00051	0.0500	0.0140	1.467177	0.000046	16.3	311	0.282795	0.7	1.0	7.3	
25	16-LVD-009_207	0.282786	0.000029	0.00119	0.00004	0.0239	0.0010	1.467206	0.000031	13.7	192	0.282782	0.0	1.0	4.1	
27	16-LVD-009_209	0.282834	0.000033	0.00157	0.00007	0.0358	0.0017	1.467212	0.000039	14.2	318	0.282825	1.7	1.2	8.5	
31	16-LVD-009_219	0.282820	0.000031	0.00123	0.00018	0.0245	0.0039	1.467228	0.000050	19.2	193	0.282816	1.2	1.1	5.4	
33	16-LVD-009_221	0.282769	0.000025	0.00096	0.00004	0.0190	0.0007	1.467213	0.000040	14.6	201	0.282765	-0.6	0.9	3.8	
34	16-LVD-009_222	0.282690	0.000033	0.00158	0.00006	0.0341	0.0015	1.467197	0.000042	15.8	328	0.282680	-3.4	1.2	3.6	
35	16-LVD-009_223	0.282798	0.000027	0.00093	0.00006	0.0212	0.0018	1.467197	0.000028	13	321	0.282792	0.5	1.0	7.4	
37	16-LVD-009_10	0.282781	0.000022	0.00095	0.00005	0.0187	0.0010	1.467222	0.000040	13.9	200	0.282777	-0.1	0.8	4.2	
42	16-LVD-009_15	0.282788	0.000020	0.00110	0.00003	0.0233	0.0006	1.467221	0.000052	14.8	326	0.282781	0.1	0.7	7.1	
44	16-LVD-009_17	0.282702	0.000029	0.00182	0.00011	0.0400	0.0024	1.467231	0.000053	15.7	317	0.282691	-2.9	1.0	3.7	
45	16-LVD-009_18	0.282757	0.000028	0.00107	0.00003	0.0223	0.0006	1.467263	0.000039	15.8	225	0.282752	-1.0	1.0	3.9	
46	16-LVD-009_25	0.282830	0.000025	0.00115	0.00016	0.0256	0.0037	1.467233	0.000034	12.3	344	0.282823	1.6	0.9	9.0	
48	16-LVD-009_27	0.282801	0.000024	0.00068	0.00007	0.0136	0.0014	1.467213	0.000042	12.7	207	0.282798	0.6	0.8	5.1	
49	16-LVD-009_28	0.282713	0.000026	0.00156	0.00005	0.0344	0.0011	1.467242	0.000042	13.5	325	0.282704	-2.5	0.9	4.3	
50	16-LVD-009_29	0.282708	0.000022	0.00085	0.00010	0.0178	0.0021	1.467260	0.000040	13.2	330	0.282703	-2.7	0.8	4.4	
51	16-LVD-009_30	0.282724	0.000025	0.00065	0.00004	0.0161	0.0010	1.467235	0.000039	12.8	322	0.282720	-2.2	0.9	4.9	
52	16-LVD-009_31	0.282636	0.000021	0.00103	0.00003	0.0201	0.0006	1.467226	0.000032	14.4	350	0.282629	-5.3	0.7	2.3	
53	16-LVD-009_32	0.282866	0.000018	0.00063	0.00010	0.0142	0.0025	1.467233	0.000032	19.1	309	0.282862	2.9	0.6	9.6	
55	16-LVD-009_34	0.282783	0.000025	0.00102	0.00002	0.0203	0.0006	1.467213	0.000037	14.6	204	0.282779	-0.1	0.9	4.3	
56	16-LVD-009_41	0.282738	0.000021	0.00143	0.00005	0.0367	0.0012	1.467217	0.000038	11.1	335	0.282729	-1.7	0.7	5.5	
57	16-LVD-009_42	0.282786	0.000024	0.00031	0.00002	0.0062	0.0004	1.467252	0.000042	16.8	215	0.282785	0.0	0.8	4.8	

Grain	Spot ID	corrected										MUN LASS Age (Ma)	$^{176}\text{Hf}/^{177}\text{Hf}$	EHf0	2SE	EHfi
		$^{176}\text{Hf}/^{177}\text{Hf}$	2SE	$^{176}\text{Lu}/^{177}\text{Hf}$	2SE	$^{176}\text{Yb}/^{177}\text{Hf}$	2SE	$^{178}\text{Hf}/^{177}\text{Hf}$	2SE	Total Hf Beam						
60	16-LVD-009_45	0.282745	0.000023	0.00049	0.00001	0.0096	0.0001	1.467235	0.000046	16.5	203	0.282743	-1.4	0.8	3.0	
62	16-LVD-009_47	0.282720	0.000026	0.00093	0.00003	0.0237	0.0007	1.467248	0.000043	11.15	327	0.282714	-2.3	0.9	4.8	
65	16-LVD-009_50	0.282669	0.000032	0.00162	0.00012	0.0441	0.0032	1.467195	0.000030	14.3	330	0.282659	-4.1	1.1	2.9	
66	16-LVD-009_57	0.282795	0.000028	0.00132	0.00011	0.0288	0.0031	1.467268	0.000039	14.4	199	0.282790	0.4	1.0	4.6	
68	16-LVD-009_59	0.282759	0.000019	0.00095	0.00004	0.0188	0.0006	1.467220	0.000037	13.2	212	0.282755	-0.9	0.7	3.7	
69	16-LVD-009_60	0.282890	0.000033	0.00191	0.00008	0.0446	0.0017	1.467200	0.000039	16.2	335	0.282878	3.7	1.2	10.7	
70	16-LVD-009_61	0.282873	0.000024	0.00122	0.00002	0.0298	0.0006	1.467227	0.000042	14.8	335	0.282865	3.1	0.8	10.3	
71	16-LVD-009_62	0.282822	0.000029	0.00067	0.00006	0.0134	0.0012	1.467272	0.000036	18	207	0.282819	1.3	1.0	5.8	
75	16-LVD-009_66	0.282779	0.000024	0.00088	0.00001	0.0174	0.0002	1.467263	0.000054	15.3	211	0.282776	-0.2	0.8	4.4	
78	16-LVD-009_75	0.282776	0.000034	0.00085	0.00002	0.0170	0.0005	1.467252	0.000062	17.9	200	0.282773	-0.3	1.2	4.0	
79	16-LVD-009_76	0.282792	0.000025	0.00081	0.00017	0.0203	0.0050	1.467226	0.000023	18.26	321	0.282787	0.2	0.9	7.2	
80	16-LVD-009_77	0.282793	0.000030	0.00137	0.00006	0.0297	0.0013	1.467225	0.000040	17.2	202	0.282788	0.3	1.1	4.6	
81	16-LVD-009_78	0.282786	0.000023	0.00078	0.00004	0.0159	0.0008	1.467225	0.000039	15.2	205	0.282783	0.0	0.8	4.5	
86	16-LVD-009_89	0.282825	0.000026	0.00050	0.00002	0.0105	0.0004	1.467242	0.000038	10.81	356	0.282822	1.4	0.9	9.2	
87	16-LVD-009_90	0.282728	0.000029	0.00256	0.00034	0.0700	0.0100	1.467207	0.000039	16.3	306	0.282713	-2.0	1.0	4.3	
89	16-LVD-009_92	0.282819	0.000019	0.00097	0.00003	0.0199	0.0006	1.467199	0.000058	18.1	196	0.282815	1.2	0.7	5.4	
90	16-LVD-009_93	0.282804	0.000032	0.00079	0.00003	0.0161	0.0005	1.467237	0.000044	15.3	194	0.282801	0.7	1.1	4.9	
92	16-LVD-009_95	0.282772	0.000025	0.00074	0.00004	0.0153	0.0009	1.467253	0.000037	14.8	269	0.282768	-0.5	0.9	5.4	
93	16-LVD-009_96	0.282779	0.000022	0.00092	0.00004	0.0187	0.0007	1.467217	0.000043	15.1	205	0.282775	-0.2	0.8	4.2	
94	16-LVD-009_97	0.282815	0.000038	0.00126	0.00009	0.0282	0.0028	1.467224	0.000033	16.4	206	0.282810	1.1	1.3	5.5	
97	16-LVD-009_106	0.282780	0.000025	0.00070	0.00005	0.0146	0.0011	1.467205	0.000029	17.7	194	0.282777	-0.2	0.9	4.1	
98	16-LVD-009_107	0.282725	0.000033	0.00134	0.00008	0.0310	0.0020	1.467262	0.000045	16.46	356	0.282716	-2.1	1.2	5.5	
99	16-LVD-009_108	0.282728	0.000034	0.00083	0.00003	0.0196	0.0010	1.467218	0.000027	21	350	0.282723	-2.0	1.2	5.6	

Grain	Spot ID	corrected										MUN LASS Age (Ma)	176Hf/ 177Hf	EHf0	2SE	EHfi
		176Hf/ 177Hf	2SE	176Lu/ 177Hf	2SE	176Yb/ 177Hf	2SE	178Hf/ 177Hf	2SE	Total Hf Beam						
100	16-LVD-009_109	0.282796	0.000039	0.00086	0.00002	0.0186	0.0003	1.467201	0.000052	17.6	197	0.282793	0.4	1.4	4.7	
101	16-LVD-009_71	0.282799	0.000024	0.00084	0.00007	0.0172	0.0013	1.467211	0.000031	14.1	207	0.282796	0.5	0.8	5.0	
103	16-LVD-009_73	0.282833	0.000030	0.00090	0.00002	0.0221	0.0008	1.467238	0.000037	17	356	0.282827	1.7	1.1	9.4	
104	16-LVD-009_74	0.282782	0.000025	0.00077	0.00001	0.0150	0.0003	1.467261	0.000041	18.3	200	0.282779	-0.1	0.9	4.2	
106	16-LVD-009_76	0.282740	0.000019	0.00190	0.00027	0.0469	0.0074	1.467225	0.000050	17.9	329	0.282728	-1.6	0.7	5.3	
107	16-LVD-009_77	0.282852	0.000027	0.00113	0.00009	0.0279	0.0027	1.467187	0.000040	16.6	341	0.282845	2.4	1.0	9.7	
108	16-LVD-009_78	0.282813	0.000023	0.00117	0.00011	0.0255	0.0024	1.467227	0.000049	15.5	224	0.282808	1.0	0.8	5.8	
109	16-LVD-009_79	0.282836	0.000028	0.00149	0.00019	0.0337	0.0050	1.467211	0.000045	16.24	210	0.282830	1.8	1.0	6.3	
110	16-LVD-009_80	0.282835	0.000026	0.00117	0.00006	0.0240	0.0011	1.467239	0.000046	16.2	198	0.282831	1.8	0.9	6.0	
Rejected Analysis																
2	16-LVD-009_171 don't use, too short	0.282813	0.000044	0.00184	0.00025	0.0441	0.0073	1.467207	0.000053	20.7	191	0.282806	1.0	1.6	5.0	
3	16-LVD-009_172 don't use too short	0.282727	0.000029	0.00056	0.00002	0.0120	0.0008	1.467231	0.000029	20	201	0.282725	-2.1	1.0	2.3	
4	16-LVD-009_173 don't use, too short	0.282813	0.000027	0.00108	0.00006	0.0243	0.0016	1.467178	0.000047	19.3	262	0.282808	1.0	1.0	6.6	
5	16-LVD-009_174 don't use, too short	0.282786	0.000036	0.00182	0.00010	0.0404	0.0025	1.467186	0.000035	20.4	311	0.282775	0.0	1.3	6.6	
6	16-LVD-009_175 don't use, too short	0.282854	0.000056	0.00196	0.00038	0.0422	0.0088	1.467241	0.000059	18.9	197	0.282847	2.4	2.0	6.6	
10	16-LVD-009_179 don't use, too short	0.282758	0.000045	0.00115	0.00006	0.0230	0.0016	1.467224	0.000046	23.2	192	0.282754	-1.0	1.6	3.2	
12	16-LVD-009_187 too short, don't use	0.282819	0.000045	0.00134	0.00003	0.0283	0.0015	1.467216	0.000062	18.3	251	0.282813	1.2	1.6	6.6	
13	16-LVD-009_188	0.282810	0.000026	0.00102	0.00004	0.0200	0.0008	1.467235	0.000041	16.2	200	0.282806	0.9	0.9	5.2	
17	16-LVD-009_192	0.282803	0.000036	0.00061	0.00002	0.0149	0.0007	1.467212	0.000033	21.5	317	0.282799	0.6	1.3	7.6	
18	16-LVD-009_193	0.282891	0.000034	0.00305	0.00046	0.0680	0.0110	1.467148	0.000057	12.2	326	0.282872	3.7	1.2	10.4	

Grain	Spot ID	<i>corrected</i>		2SE	176Lu/ 177Hf	2SE	176Yb/ 177Hf	2SE	178Hf/ 177Hf	2SE	Total Hf Beam	MUN LASS Age (Ma)	176Hf/ 177Hf	EHf0	2SE	EHfi
		176Hf/ 177Hf	2SE													
19	16-LVD-009_194	0.282812	0.000030	0.00085	0.00006	0.0172	0.0015	1.467225	0.000029	18.1	215	0.282809	1.0	1.1	5.6	
20	16-LVD-009_195	0.282714	0.000027	0.00043	0.00017	0.0107	0.0049	1.467214	0.000038	27.7	179	0.282713	-2.5	1.0	1.4	
21	16-LVD-009_203	0.282855	0.000027	0.00168	0.00034	0.0386	0.0087	1.467235	0.000027	19.89	301	0.282846	2.5	1.0	8.8	
22	16-LVD-009_204	0.282780	0.000040	0.00138	0.00007	0.0280	0.0016	1.467231	0.000089	22.8	198	0.282775	-0.2	1.4	4.1	
26	16-LVD-009_208	0.282791	0.000034	0.00102	0.00017	0.0208	0.0043	1.467226	0.000039	19.1	211	0.282787	0.2	1.2	4.8	
28	16-LVD-009_210	0.282798	0.000028	0.00093	0.00005	0.0184	0.0010	1.467197	0.000034	19.5	208	0.282794	0.5	1.0	5.0	
29	16-LVD-009_211	0.282828	0.000033	0.00103	0.00005	0.0212	0.0011	1.467191	0.000056	16.6	197	0.282824	1.5	1.2	5.8	
30	16-LVD-009_212	0.282904	0.000035	0.00189	0.00011	0.0440	0.0032	1.467221	0.000047	18.5	322	0.282893	4.2	1.2	11.0	
36	16-LVD-009_220	0.282821	0.000030	0.00093	0.00002	0.0180	0.0005	1.467229	0.000039	20.4	206	0.282817	1.3	1.1	5.7	
36	16-LVD-009_9	0.282877	0.000026	0.00168	0.00014	0.0381	0.0035	1.467254	0.000037	14.3	248	0.282869	3.3	0.9	8.5	
38	16-LVD-009_11	0.282776	0.000022	0.00037	0.00008	0.0073	0.0015	1.467311	0.000028	14	224	0.282774	-0.3	0.8	4.6	
39	16-LVD-009_12	0.282855	0.000027	0.00129	0.00002	0.0320	0.0011	1.467219	0.000041	17	215	0.282850	2.5	1.0	7.1	
40	16-LVD-009_13	0.282695	0.000034	0.00074	0.00006	0.0174	0.0018	1.467211	0.000031	18.3	337	0.282690	-3.2	1.2	4.2	
41	16-LVD-009_14	0.282855	0.000018	0.00069	0.00007	0.0142	0.0013	1.467234	0.000042	15.3	198	0.282852	2.5	0.6	6.8	
43	16-LVD-009_16	0.282833	0.000069	0.00127	0.00007	0.0260	0.0015	1.467248	0.000061	20.3	190	0.282828	1.7	2.4	5.8	
47	16-LVD-009_26	0.282042	0.000027	0.00087	0.00002	0.0221	0.0005	1.467173	0.000041	15.8	811	0.282029	-26.3	1.0	-8.6	
54	16-LVD-009_33	0.282777	0.000054	0.00100	0.00008	0.0199	0.0018	1.467187	0.000083	22.2	196	0.282773	-0.3	1.9	4.0	
58	16-LVD-009_43	0.282841	0.000043	0.00123	0.00005	0.0271	0.0018	1.467285	0.000042	15.7	304	0.282834	2.0	1.5	8.5	
59	16-LVD-009_44	0.282798	0.000024	0.00055	0.00006	0.0110	0.0011	1.467193	0.000048	16.3	243	0.282796	0.5	0.8	5.8	
61	16-LVD-009_46	0.282748	0.000040	0.00161	0.00022	0.0396	0.0061	1.467240	0.000042	18.8	306	0.282739	-1.3	1.4	5.2	
63	16-LVD-009_48	0.282827	0.000036	0.00194	0.00013	0.0515	0.0037	1.467229	0.000054	14.2	297	0.282816	1.5	1.3	7.7	
64	16-LVD-009_49	0.282876	0.000028	0.00124	0.00005	0.0289	0.0018	1.467227	0.000061	17.2	246	0.282870	3.2	1.0	8.5	
67	16-LVD-009_58	0.282848	0.000030	0.00149	0.00002	0.0337	0.0006	1.467267	0.000053	13.2	335	0.282839	2.2	1.1	9.4	

Grain	Spot ID	<i>corrected</i>		2SE	176Lu/ 177Hf	2SE	176Yb/ 177Hf	2SE	178Hf/ 177Hf	2SE	Total Hf Beam	MUN LASS Age (Ma)	176Hf/ 177Hf	EHf0	2SE	EHfi
		176Hf/ 177Hf	2SE													
72	16-LVD-009_63	0.282808	0.000033	0.00122	0.00019	0.0276	0.0053	1.467172	0.000060	17.4	255	0.282802	0.8	1.2	6.3	
73	16-LVD-009_64	0.282802	0.000065	0.00120	0.00010	0.0254	0.0020	1.467222	0.000043	19	202	0.282797	0.6	2.3	4.9	
74	16-LVD-009_65	0.282871	0.000028	0.00095	0.00006	0.0212	0.0022	1.467225	0.000041	16.6	203	0.282867	3.0	1.0	7.4	
76	16-LVD-009_73	0.282927	0.000034	0.00289	0.00032	0.0658	0.0072	1.467231	0.000040	16.2	266	0.282913	5.0	1.2	10.4	
77	16-LVD-009_74	0.282819	0.000024	0.00070	0.00001	0.0137	0.0002	1.467289	0.000063	19.2	204	0.282816	1.2	0.8	5.6	
82	16-LVD-009_79	0.282792	0.000044	0.00117	0.00002	0.0236	0.0006	1.467234	0.000063	19.8	203	0.282788	0.2	1.6	4.6	
83	16-LVD-009_80	0.282855	0.000031	0.00097	0.00005	0.0251	0.0017	1.467240	0.000046	14.3	201	0.282851	2.5	1.1	6.8	
84	16-LVD-009_81	0.282811	0.000026	0.00165	0.00011	0.0361	0.0029	1.467165	0.000034	17.5	312	0.282801	0.9	0.9	7.5	
85	16-LVD-009_82	0.282829	0.000034	0.00146	0.00011	0.0316	0.0026	1.467226	0.000031	19.4	290	0.282821	1.6	1.2	7.7	
88	16-LVD-009_91	0.282806	0.000030	0.00121	0.00003	0.0276	0.0011	1.467258	0.000049	18.8	213	0.282801	0.7	1.1	5.3	
91	16-LVD-009_94	0.282805	0.000026	0.00086	0.00003	0.0177	0.0005	1.467251	0.000057	15.7	241	0.282801	0.7	0.9	5.9	
95	16-LVD-009_98	0.282711	0.000057	0.00171	0.00005	0.0366	0.0005	1.467162	0.000067	22.4	250	0.282703	-2.6	2.0	2.7	
96	16-LVD-009_105	0.282865	0.000032	0.00084	0.00008	0.0217	0.0024	1.467252	0.000049	15.8	324	0.282860	2.8	1.1	9.9	
102	16-LVD-009_72	0.282841	0.000023	0.00046	0.00004	0.0106	0.0010	1.467228	0.000049	18.8	315	0.282838	2.0	0.8	8.9	
105	16-LVD-009_75	0.282798	0.000057	0.00068	0.00003	0.0137	0.0006	1.467240	0.000110	23.4	196	0.282795	0.5	2.0	4.7	

Whitehorse trough - Richthofen formation - Sample 16-LVD-021, Richthofen Island (Zone 08V 491272 6775151N NAD 83)

Grain	Spot ID	<i>corrected</i>		2SE	176Lu/ 177Hf	2SE	176Yb/ 177Hf	2SE	178Hf/ 177Hf	2SE	Total Hf Beam	MUN LASS Age (Ma)	176Hf/ 177Hf	EHf0	2SE	EHfi
		176Hf/ 177Hf	2SE													
1	16-LVD-021_009	0.282927	0.000029	0.00057	0.00001	0.0137	0.0003	1.467185	0.000035	13.9	219	0.282925	5.0	1.0	9.8	
2	16-LVD-021_010	0.282855	0.000025	0.00109	0.00003	0.0229	0.0006	1.467193	0.000036	13.6	190	0.282851	2.5	0.9	6.6	

Grain	Spot ID	<i>corrected</i>													
		$^{176}\text{Hf}/^{177}\text{Hf}$	2SE	$^{176}\text{Lu}/^{177}\text{Hf}$	2SE	$^{176}\text{Yb}/^{177}\text{Hf}$	2SE	$^{178}\text{Hf}/^{177}\text{Hf}$	2SE	Total Hf Beam	MUN LASS Age (Ma)	$^{176}\text{Hf}/^{177}\text{Hf}$	EHf0	2SE	EHfi
3	16-LVD-021_011	0.282840	0.000029	0.00098	0.00005	0.0206	0.0012	1.467242	0.000030	15.2	219	0.282836	1.9	1.0	6.7
4	16-LVD-021_012	0.282808	0.000020	0.00092	0.00006	0.0196	0.0012	1.467223	0.000045	16.2	208	0.282804	0.8	0.7	5.3
5	16-LVD-021_013	0.282858	0.000027	0.00082	0.00004	0.0189	0.0009	1.467190	0.000044	14.5	201	0.282855	2.6	1.0	6.9
6	16-LVD-021_014	0.282834	0.000026	0.00092	0.00004	0.0194	0.0008	1.467278	0.000039	16.6	206	0.282830	1.7	0.9	6.2
8	16-LVD-021_016	0.282862	0.000023	0.00087	0.00003	0.0199	0.0007	1.467204	0.000029	15.6	186	0.282859	2.7	0.8	6.8
9	16-LVD-021_017	0.282831	0.000020	0.00056	0.00002	0.0114	0.0003	1.467201	0.000028	13.3	204	0.282829	1.6	0.7	6.1
10	16-LVD-021_018	0.282861	0.000027	0.00083	0.00001	0.0194	0.0001	1.467222	0.000047	15.2	201	0.282858	2.7	1.0	7.0
11	16-LVD-021_25	0.282809	0.000024	0.00092	0.00011	0.0214	0.0026	1.467186	0.000036	13.25	205	0.282805	0.8	0.8	5.3
12	16-LVD-021_26	0.282860	0.000019	0.00101	0.00008	0.0245	0.0021	1.467265	0.000037	11.9	202	0.282856	2.7	0.7	7.0
13	16-LVD-021_27	0.283060	0.000045	0.00343	0.00065	0.0860	0.0160	1.467242	0.000054	11.51	210	0.283047	9.7	1.6	13.9
14	16-LVD-021_28	0.282841	0.000024	0.00080	0.00005	0.0165	0.0011	1.467191	0.000032	14.5	209	0.282838	2.0	0.8	6.5
15	16-LVD-021_29	0.282829	0.000022	0.00072	0.00004	0.0155	0.0009	1.467230	0.000035	14.2	212	0.282826	1.6	0.8	6.2
16	16-LVD-021_30	0.282863	0.000025	0.00154	0.00005	0.0364	0.0012	1.467234	0.000048	11.5	202	0.282857	2.8	0.9	7.0
18	16-LVD-021_32	0.282794	0.000027	0.00091	0.00007	0.0210	0.0016	1.467223	0.000045	17	197	0.282791	0.3	1.0	4.6
19	16-LVD-021_33	0.282953	0.000029	0.00135	0.00005	0.0310	0.0014	1.467243	0.000048	15.3	217	0.282948	5.9	1.0	10.6
20	16-LVD-021_34	0.282801	0.000020	0.00079	0.00006	0.0171	0.0013	1.467200	0.000036	16	213	0.282798	0.6	0.7	5.2
21	16-LVD-021_41	0.282855	0.000030	0.00131	0.00010	0.0298	0.0022	1.467239	0.000033	15.9	199	0.282850	2.5	1.1	6.7
22	16-LVD-021_42	0.282853	0.000023	0.00052	0.00001	0.0115	0.0004	1.467238	0.000035	13.2	205	0.282851	2.4	0.8	6.9
23	16-LVD-021_43	0.282858	0.000030	0.00104	0.00002	0.0239	0.0007	1.467198	0.000035	14.7	202	0.282854	2.6	1.1	6.9
24	16-LVD-021_44	0.282960	0.000024	0.00120	0.00009	0.0276	0.0025	1.467237	0.000041	15	210	0.282955	6.2	0.8	10.7
25	16-LVD-021_45	0.282807	0.000021	0.00063	0.00001	0.0150	0.0004	1.467221	0.000030	13.4	212	0.282804	0.8	0.7	5.4
26	16-LVD-021_46	0.282955	0.000016	0.00136	0.00012	0.0322	0.0033	1.467207	0.000032	13.7	223	0.282949	6.0	0.6	10.8
27	16-LVD-021_47	0.282815	0.000023	0.00077	0.00002	0.0164	0.0005	1.467185	0.000048	17.4	215	0.282812	1.1	0.8	5.7

Grain	Spot ID	corrected										MUN LASS Age (Ma)	$^{176}\text{Hf}/^{177}\text{Hf}$	EHf0	2SE	EHfi
		$^{176}\text{Hf}/^{177}\text{Hf}$	2SE	$^{176}\text{Lu}/^{177}\text{Hf}$	2SE	$^{176}\text{Yb}/^{177}\text{Hf}$	2SE	$^{178}\text{Hf}/^{177}\text{Hf}$	2SE	Total Hf Beam						
30	16-LVD-021_50	0.282862	0.000023	0.00097	0.00005	0.0219	0.0009	1.467224	0.000042	12.9	209	0.282858	2.7	0.8	7.2	
31	16-LVD-021_57	0.282831	0.000027	0.00075	0.00005	0.0183	0.0013	1.467209	0.000026	14.3	207	0.282828	1.6	1.0	6.1	
32	16-LVD-021_58	0.282851	0.000023	0.00103	0.00004	0.0244	0.0010	1.467240	0.000040	13.7	215	0.282847	2.3	0.8	7.0	
33	16-LVD-021_59	0.282811	0.000030	0.00103	0.00008	0.0254	0.0021	1.467212	0.000036	12.7	210	0.282807	0.9	1.1	5.4	
34	16-LVD-021_60	0.282847	0.000020	0.00096	0.00005	0.0202	0.0010	1.467212	0.000042	16.9	210	0.282843	2.2	0.7	6.7	
35	16-LVD-021_61	0.282811	0.000023	0.00152	0.00009	0.0376	0.0022	1.467217	0.000039	11.99	208	0.282805	0.9	0.8	5.3	
37	16-LVD-021_63	0.282880	0.000026	0.00097	0.00006	0.0222	0.0014	1.467227	0.000029	13	201	0.282876	3.4	0.9	7.7	
39	16-LVD-021_65	0.282813	0.000023	0.00105	0.00008	0.0225	0.0015	1.467223	0.000033	12.4	194	0.282809	1.0	0.8	5.2	
40	16-LVD-021_66	0.282862	0.000031	0.00104	0.00007	0.0231	0.0019	1.467204	0.000044	15.3	204	0.282858	2.7	1.1	7.1	
41	16-LVD-021_73	0.282810	0.000023	0.00081	0.00001	0.0165	0.0002	1.467242	0.000042	16.1	209	0.282807	0.9	0.8	5.4	
42	16-LVD-021_74	0.282864	0.000024	0.00118	0.00008	0.0285	0.0021	1.467240	0.000031	12.6	211	0.282859	2.8	0.8	7.3	
44	16-LVD-021_76	0.282850	0.000020	0.00078	0.00002	0.0175	0.0004	1.467200	0.000036	12.8	205	0.282847	2.3	0.7	6.8	
45	16-LVD-021_77	0.282836	0.000025	0.00072	0.00002	0.0169	0.0004	1.467258	0.000030	12.6	207	0.282833	1.8	0.9	6.3	
46	16-LVD-021_78	0.282827	0.000029	0.00109	0.00004	0.0235	0.0011	1.467212	0.000039	16.7	210	0.282823	1.5	1.0	6.0	
47	16-LVD-021_79	0.282819	0.000026	0.00102	0.00008	0.0214	0.0016	1.467212	0.000036	14.9	209	0.282815	1.2	0.9	5.7	
48	16-LVD-021_80	0.282747	0.000027	0.00075	0.00003	0.0166	0.0006	1.467269	0.000037	17.9	204	0.282744	-1.3	1.0	3.1	
49	16-LVD-021_81	0.282929	0.000025	0.00099	0.00008	0.0232	0.0021	1.467180	0.000042	16.4	221	0.282925	5.1	0.9	9.9	
50	16-LVD-021_82	0.282827	0.000038	0.00120	0.00006	0.0274	0.0017	1.467163	0.000045	17.2	211	0.282822	1.5	1.3	6.0	
52	16-LVD-021_90	0.282955	0.000027	0.00105	0.00007	0.0251	0.0019	1.467221	0.000064	16.8	220	0.282951	6.0	1.0	10.8	
53	16-LVD-021_91	0.282864	0.000033	0.00101	0.00009	0.0240	0.0022	1.467236	0.000048	15.6	216	0.282860	2.8	1.2	7.5	
54	16-LVD-021_92	0.282950	0.000035	0.00097	0.00010	0.0219	0.0024	1.467219	0.000047	18.5	226	0.282946	5.8	1.2	10.7	
55	16-LVD-021_93	0.282834	0.000024	0.00101	0.00010	0.0222	0.0024	1.467226	0.000032	13.7	204	0.282830	1.7	0.8	6.1	
56	16-LVD-021_94	0.282825	0.000029	0.00099	0.00002	0.0214	0.0005	1.467193	0.000024	17.2	203	0.282821	1.4	1.0	5.8	

Grain	Spot ID	corrected										MUN LASS Age (Ma)	$^{176}\text{Hf}/^{177}\text{Hf}$	EHf0	2SE	EHfi
		$^{176}\text{Hf}/^{177}\text{Hf}$	2SE	$^{176}\text{Lu}/^{177}\text{Hf}$	2SE	$^{176}\text{Yb}/^{177}\text{Hf}$	2SE	$^{178}\text{Hf}/^{177}\text{Hf}$	2SE	Total Hf Beam						
57	16-LVD-021_95	0.282837	0.000027	0.00138	0.00007	0.0329	0.0017	1.467247	0.000036	12.4	204	0.282832	1.8	1.0	6.2	
58	16-LVD-021_96	0.282857	0.000027	0.00093	0.00002	0.0217	0.0003	1.467211	0.000038	13.5	212	0.282853	2.5	1.0	7.1	
60	16-LVD-021_98	0.282837	0.000022	0.00110	0.00003	0.0260	0.0008	1.467232	0.000038	12.6	222	0.282832	1.8	0.8	6.6	
61	16-LVD-021_105	0.282793	0.000020	0.00044	0.00001	0.0087	0.0003	1.467206	0.000033	14.7	209	0.282791	0.3	0.7	4.9	
62	16-LVD-021_106	0.282875	0.000028	0.00109	0.00002	0.0256	0.0006	1.467198	0.000037	12.5	203	0.282871	3.2	1.0	7.6	
63	16-LVD-021_107	0.282862	0.000024	0.00101	0.00009	0.0222	0.0018	1.467227	0.000033	14.4	214	0.282858	2.7	0.8	7.3	
64	16-LVD-021_108	0.282917	0.000029	0.00153	0.00004	0.0353	0.0011	1.467228	0.000042	11.9	206	0.282911	4.7	1.0	9.0	
65	16-LVD-021_109	0.282845	0.000024	0.00070	0.00006	0.0162	0.0013	1.467211	0.000038	12.4	211	0.282842	2.1	0.8	6.7	
66	16-LVD-021_110	0.282860	0.000025	0.00073	0.00001	0.0172	0.0003	1.467206	0.000038	15	212	0.282857	2.7	0.9	7.3	
67	16-LVD-021_111	0.282863	0.000032	0.00134	0.00007	0.0332	0.0017	1.467229	0.000046	16.5	209	0.282858	2.8	1.1	7.2	
68	16-LVD-021_112	0.282837	0.000020	0.00082	0.00003	0.0193	0.0004	1.467229	0.000039	12.9	212	0.282834	1.8	0.7	6.4	
69	16-LVD-021_113	0.282874	0.000030	0.00112	0.00007	0.0256	0.0022	1.467229	0.000039	14	208	0.282870	3.1	1.1	7.6	
72	16-LVD-021_122	0.282942	0.000031	0.00102	0.00006	0.0250	0.0014	1.467203	0.000037	13.5	222	0.282938	5.6	1.1	10.3	
73	16-LVD-021_123	0.282730	0.000022	0.00063	0.00001	0.0167	0.0003	1.467235	0.000037	14.1	464	0.282725	-1.9	0.8	8.2	
75	16-LVD-021_125	0.282907	0.000034	0.00070	0.00007	0.0162	0.0016	1.467223	0.000048	18.5	224	0.282904	4.3	1.2	9.2	
76	16-LVD-021_126	0.282834	0.000021	0.00053	0.00001	0.0122	0.0001	1.467202	0.000033	12.4	213	0.282832	1.7	0.7	6.4	
77	16-LVD-021_127	0.282779	0.000031	0.00086	0.00005	0.0183	0.0011	1.467173	0.000039	14.1	214	0.282776	-0.2	1.1	4.4	
78	16-LVD-021_128	0.282837	0.000027	0.00065	0.00001	0.0154	0.0001	1.467248	0.000031	14.2	210	0.282834	1.8	1.0	6.4	
79	16-LVD-021_129	0.282853	0.000025	0.00089	0.00009	0.0213	0.0024	1.467223	0.000038	13.2	207	0.282850	2.4	0.9	6.9	
80	16-LVD-021_130	0.282809	0.000020	0.00079	0.00004	0.0172	0.0007	1.467194	0.000030	14.1	214	0.282806	0.8	0.7	5.5	
81	16-LVD-021_138	0.282938	0.000022	0.00105	0.00007	0.0253	0.0017	1.467197	0.000038	13.3	215	0.282934	5.4	0.8	10.0	
82	16-LVD-021_139	0.282859	0.000023	0.00083	0.00004	0.0194	0.0005	1.467252	0.000042	13.5	210	0.282856	2.6	0.8	7.2	
83	16-LVD-021_140	0.282844	0.000043	0.00084	0.00004	0.0182	0.0010	1.467237	0.000041	18.2	213	0.282841	2.1	1.5	6.7	

Grain	Spot ID	corrected										MUN LASS Age (Ma)	176Hf/ 177Hf	EHf0	2SE	EHfi
		176Hf/ 177Hf	2SE	176Lu/ 177Hf	2SE	176Yb/ 177Hf	2SE	178Hf/ 177Hf	2SE	Total Hf Beam						
84	16-LVD-021_141	0.282872	0.000031	0.00103	0.00004	0.0227	0.0014	1.467221	0.000041	17.7	216	0.282868	3.1	1.1	7.7	
85	16-LVD-021_142	0.282824	0.000027	0.00116	0.00007	0.0278	0.0017	1.467219	0.000026	12.8	211	0.282819	1.4	1.0	5.9	
87	16-LVD-021_144	0.282826	0.000028	0.00120	0.00009	0.0295	0.0024	1.467199	0.000029	12.8	204	0.282821	1.4	1.0	5.8	
89	16-LVD-021_146	0.282855	0.000024	0.00099	0.00005	0.0236	0.0012	1.467228	0.000050	14.4	208	0.282851	2.5	0.8	7.0	
90	16-LVD-021_147	0.282849	0.000024	0.00090	0.00003	0.0214	0.0007	1.467225	0.000026	12.5	212	0.282845	2.3	0.8	6.8	
91	16-LVD-021_154	0.282859	0.000028	0.00137	0.00009	0.0323	0.0027	1.467206	0.000031	16.8	208	0.282854	2.6	1.0	7.1	
92	16-LVD-021_155	0.282937	0.000039	0.00104	0.00002	0.0236	0.0005	1.467221	0.000051	15.9	343	0.282930	5.4	1.4	12.8	
94	16-LVD-021_157	0.282942	0.000036	0.00122	0.00009	0.0298	0.0028	1.467271	0.000051	16.3	218	0.282937	5.6	1.3	10.2	
95	16-LVD-021_158	0.282816	0.000030	0.00112	0.00011	0.0266	0.0034	1.467233	0.000032	13.6	227	0.282811	1.1	1.1	6.0	
96	16-LVD-021_159	0.282864	0.000038	0.00133	0.00006	0.0324	0.0017	1.467220	0.000046	15.5	209	0.282859	2.8	1.3	7.2	
99	16-LVD-021_162	0.282975	0.000030	0.00126	0.00001	0.0264	0.0005	1.467184	0.000028	13.5	232	0.282970	6.7	1.1	11.7	
100	16-LVD-021_163	0.282792	0.000025	0.00081	0.00005	0.0184	0.0011	1.467206	0.000042	14.8	214	0.282789	0.2	0.9	4.9	
101	16-LVD-021_55	0.282978	0.000030	0.00146	0.00018	0.0315	0.0032	1.467234	0.000037	12.3	218	0.282972	6.8	1.1	11.5	
102	16-LVD-021_56	0.282848	0.000037	0.00121	0.00002	0.0303	0.0005	1.467215	0.000047	15.2	201	0.282843	2.2	1.3	6.5	
103	16-LVD-021_57	0.282914	0.000034	0.00126	0.00006	0.0297	0.0015	1.467229	0.000038	11.04	340	0.282906	4.6	1.2	11.8	
104	16-LVD-021_58	0.282839	0.000038	0.00104	0.00005	0.0251	0.0010	1.467195	0.000045	13.2	214	0.282835	1.9	1.3	6.5	
105	16-LVD-021_59	0.282859	0.000040	0.00096	0.00002	0.0226	0.0006	1.467280	0.000041	14.3	213	0.282855	2.6	1.4	7.2	
106	16-LVD-021_60	0.282933	0.000035	0.00094	0.00012	0.0220	0.0026	1.467229	0.000027	16.1	218	0.282929	5.2	1.2	10.0	
107	16-LVD-021_61	0.282774	0.000030	0.00087	0.00002	0.0213	0.0005	1.467212	0.000035	14.5	215	0.282770	-0.4	1.1	4.3	
108	16-LVD-021_62	0.282830	0.000025	0.00064	0.00003	0.0156	0.0008	1.467232	0.000036	16	205	0.282828	1.6	0.9	6.1	
110	16-LVD-021_64	0.282854	0.000031	0.00142	0.00004	0.0371	0.0013	1.467230	0.000042	16.4	216	0.282848	2.4	1.1	7.0	
Rejected Analysis																
7	16-LVD-021_015	0.282886	0.000023	0.00096	0.00004	0.0204	0.0009	1.467226	0.000036	18.5	219	0.282882	3.6	0.8	8.3	

Grain	Spot ID	<i>corrected</i>										MUN LASS Age (Ma)	176Hf/ 177Hf	EHf0	2SE	EHfi
		176Hf/ 177Hf	2SE	176Lu/ 177Hf	2SE	176Yb/ 177Hf	2SE	178Hf/ 177Hf	2SE	Total Hf Beam						
17	16-LVD-021_31	0.282894	0.000027	0.00100	0.00012	0.0210	0.0027	1.467207	0.000033	11.33	309	0.282888	3.9	1.0	10.5	
28	16-LVD-021_48	0.282852	0.000030	0.00104	0.00003	0.0247	0.0012	1.467226	0.000046	16.7	202	0.282848	2.4	1.1	6.7	
29	16-LVD-021_49	0.282828	0.000043	0.00074	0.00003	0.0178	0.0008	1.467170	0.000043	18.8	197	0.282825	1.5	1.5	5.8	
36	16-LVD-021_62	0.282828	0.000024	0.00128	0.00006	0.0318	0.0016	1.467232	0.000044	13.7	323	0.282820	1.5	0.8	8.4	
38	16-LVD-021_64	0.282854	0.000024	0.00048	0.00002	0.0114	0.0005	1.467235	0.000034	9.91	280	0.282851	2.4	0.8	8.6	
43	16-LVD-021_75	0.282876	0.000042	0.00158	0.00016	0.0403	0.0043	1.467223	0.000030	15.3	200	0.282870	3.2	1.5	7.5	
51	16-LVD-021_89	0.282791	0.000042	0.00102	0.00006	0.0251	0.0014	1.467228	0.000046	17.06	220	0.282787	0.2	1.5	5.0	
59	16-LVD-021_97	0.282824	0.000025	0.00171	0.00009	0.0434	0.0030	1.467225	0.000031	14.2	452	0.282810	1.4	0.9	10.9	
70	16-LVD-021_114	0.282861	0.000024	0.00097	0.00006	0.0248	0.0017	1.467236	0.000030	13.8	213	0.282857	2.7	0.8	7.3	
71	16-LVD-021_121	0.282879	0.000049	0.00134	0.00007	0.0303	0.0024	1.467182	0.000041	18.1	207	0.282874	3.3	1.7	7.7	
74	16-LVD-021_124	0.282975	0.000027	0.00092	0.00002	0.0222	0.0004	1.467271	0.000031	10.9	225	0.282971	6.7	1.0	11.6	
86	16-LVD-021_143	0.282929	0.000025	0.00130	0.00010	0.0324	0.0028	1.467234	0.000037	14.9	207	0.282924	5.1	0.9	9.5	
88	16-LVD-021_145	0.282836	0.000029	0.00172	0.00016	0.0410	0.0044	1.467243	0.000045	13.2	203	0.282829	1.8	1.0	6.1	
93	16-LVD-021_156	0.282850	0.000039	0.00169	0.00008	0.0430	0.0023	1.467183	0.000045	13.6	210	0.282843	2.3	1.4	6.7	
97	16-LVD-021_160	0.282929	0.000031	0.00048	0.00002	0.0106	0.0004	1.467210	0.000044	9.8	218	0.282927	5.1	1.1	9.9	
98	16-LVD-021_161	0.282057	0.000028	0.00111	0.00002	0.0326	0.0007	1.467238	0.000060	17.3	1444	0.282027	-25.7	1.0	5.7	
109	16-LVD-021_63	0.282928	0.000063	0.00135	0.00011	0.0339	0.0031	1.467290	0.000094	20.39	197	0.282923	5.1	2.2	9.3	

Whitehorse trough - Richthofen formation - Sample 16-LVD-022, Lake Laberge (Zone 08V 493602E 6778206N NAD 83)

Grain	Spot ID	<i>corrected</i>										MUN LASS Age (Ma)	176Hf/ 177Hf	EHf0	2SE	EHfi
		176Hf/ 177Hf	2SE	176Lu/ 177Hf	2SE	176Yb/ 177Hf	2SE	178Hf/ 177Hf	2SE	Total Hf Beam						

Grain	Spot ID	corrected										MUN LASS Age (Ma)	$^{176}\text{Hf}/^{177}\text{Hf}$	EHf0	2SE	EHfi
		$^{176}\text{Hf}/^{177}\text{Hf}$	2SE	$^{176}\text{Lu}/^{177}\text{Hf}$	2SE	$^{176}\text{Yb}/^{177}\text{Hf}$	2SE	$^{178}\text{Hf}/^{177}\text{Hf}$	2SE	Total Hf Beam						
1	16-LVD-022_11	0.282789	0.000026	0.00105	0.00004	0.0266	0.0011	1.467175	0.000032	11.6	205	0.282785	0.1	0.9	4.6	
2	16-LVD-022_12	0.282754	0.000025	0.00129	0.00004	0.0321	0.0011	1.467194	0.000033	11.2	206	0.282749	-1.1	0.9	3.3	
4	16-LVD-022_14	0.282747	0.000019	0.00067	0.00003	0.0150	0.0007	1.467177	0.000034	13.78	199	0.282745	-1.3	0.7	3.0	
5	16-LVD-022_15	0.282740	0.000027	0.00109	0.00009	0.0270	0.0022	1.467176	0.000032	12	204	0.282736	-1.6	1.0	2.8	
6	16-LVD-022_16	0.282786	0.000019	0.00079	0.00005	0.0176	0.0011	1.467205	0.000031	13.3	202	0.282783	0.0	0.7	4.4	
7	16-LVD-022_17	0.282766	0.000020	0.00086	0.00003	0.0197	0.0007	1.467215	0.000041	14.9	194	0.282763	-0.7	0.7	3.5	
8	16-LVD-022_18	0.282767	0.000020	0.00060	0.00002	0.0141	0.0005	1.467205	0.000039	13.4	211	0.282765	-0.6	0.7	4.0	
9	16-LVD-022_19	0.282765	0.000019	0.00044	0.00001	0.0096	0.0003	1.467146	0.000037	12.5	200	0.282763	-0.7	0.7	3.7	
10	16-LVD-022_20	0.282759	0.000019	0.00060	0.00005	0.0136	0.0011	1.467198	0.000037	17.2	212	0.282757	-0.9	0.7	3.7	
12	16-LVD-022_22	0.282768	0.000021	0.00057	0.00003	0.0136	0.0007	1.467194	0.000036	15.4	197	0.282766	-0.6	0.7	3.7	
13	16-LVD-022_29	0.282807	0.000022	0.00047	0.00005	0.0105	0.0012	1.467192	0.000032	12.7	205	0.282805	0.8	0.8	5.3	
14	16-LVD-022_30	0.282653	0.000027	0.00102	0.00004	0.0237	0.0010	1.467181	0.000036	11.6	208	0.282649	-4.7	1.0	-0.2	
15	16-LVD-022_31	0.282776	0.000019	0.00053	0.00002	0.0121	0.0004	1.467144	0.000031	12.6	212	0.282774	-0.3	0.7	4.3	
16	16-LVD-022_32	0.282759	0.000023	0.00094	0.00009	0.0237	0.0021	1.467191	0.000029	12.8	333	0.282753	-0.9	0.8	6.3	
17	16-LVD-022_33	0.282772	0.000020	0.00042	0.00003	0.0085	0.0007	1.467208	0.000030	15.3	209	0.282770	-0.5	0.7	4.1	
19	16-LVD-022_35	0.282735	0.000023	0.00152	0.00006	0.0403	0.0018	1.467165	0.000025	11.42	339	0.282725	-1.8	0.8	5.4	
20	16-LVD-022_36	0.282773	0.000020	0.00059	0.00002	0.0130	0.0005	1.467185	0.000035	13	209	0.282771	-0.4	0.7	4.1	
23	16-LVD-022_39	0.282770	0.000018	0.00096	0.00003	0.0225	0.0006	1.467149	0.000033	12.5	201	0.282766	-0.5	0.6	3.8	
24	16-LVD-022_40	0.282778	0.000022	0.00101	0.00005	0.0254	0.0016	1.467194	0.000035	13.7	200	0.282774	-0.2	0.8	4.1	
25	16-LVD-022_47	0.282801	0.000025	0.00105	0.00008	0.0263	0.0023	1.467158	0.000041	11.7	206	0.282797	0.6	0.9	5.0	
26	16-LVD-022_48	0.282746	0.000025	0.00091	0.00004	0.0215	0.0007	1.467156	0.000028	12.7	203	0.282743	-1.4	0.9	3.0	
27	16-LVD-022_49	0.282779	0.000020	0.00084	0.00005	0.0197	0.0010	1.467199	0.000040	16.2	200	0.282776	-0.2	0.7	4.1	
28	16-LVD-022_50	0.282774	0.000019	0.00074	0.00003	0.0176	0.0008	1.467201	0.000038	12.7	209	0.282771	-0.4	0.7	4.2	

Grain	Spot ID	corrected										MUN LASS Age (Ma)	$^{176}\text{Hf}/^{177}\text{Hf}$	EHf0	2SE	EHfi
		$^{176}\text{Hf}/^{177}\text{Hf}$	2SE	$^{176}\text{Lu}/^{177}\text{Hf}$	2SE	$^{176}\text{Yb}/^{177}\text{Hf}$	2SE	$^{178}\text{Hf}/^{177}\text{Hf}$	2SE	Total Hf Beam						
29	16-LVD-022_51	0.282761	0.000021	0.00119	0.00012	0.0274	0.0028	1.467196	0.000028	12	207	0.282756	-0.8	0.7	3.6	
30	16-LVD-022_52	0.282763	0.000021	0.00074	0.00002	0.0162	0.0003	1.467158	0.000036	13.8	201	0.282760	-0.8	0.7	3.6	
31	16-LVD-022_53	0.282756	0.000019	0.00054	0.00001	0.0122	0.0004	1.467205	0.000040	13.7	207	0.282754	-1.0	0.7	3.5	
32	16-LVD-022_54	0.282791	0.000020	0.00123	0.00004	0.0292	0.0009	1.467168	0.000037	12.2	274	0.282785	0.2	0.7	6.1	
34	16-LVD-022_56	0.282768	0.000020	0.00069	0.00002	0.0164	0.0006	1.467224	0.000035	13.2	205	0.282765	-0.6	0.7	3.9	
35	16-LVD-022_57	0.282791	0.000023	0.00078	0.00003	0.0186	0.0008	1.467146	0.000038	13.5	207	0.282788	0.2	0.8	4.7	
36	16-LVD-022_58	0.282799	0.000024	0.00093	0.00003	0.0224	0.0006	1.467178	0.000038	12.2	203	0.282795	0.5	0.8	4.9	
37	16-LVD-022_65	0.282751	0.000024	0.00102	0.00001	0.0238	0.0004	1.467188	0.000033	12	201	0.282747	-1.2	0.8	3.1	
38	16-LVD-022_66	0.282807	0.000023	0.00153	0.00007	0.0308	0.0015	1.467190	0.000027	11.9	202	0.282801	0.8	0.8	5.1	
39	16-LVD-022_67	0.282764	0.000022	0.00085	0.00003	0.0197	0.0007	1.467194	0.000040	13	204	0.282761	-0.7	0.8	3.7	
40	16-LVD-022_68	0.282736	0.000023	0.00076	0.00004	0.0176	0.0007	1.467184	0.000043	14.2	211	0.282733	-1.7	0.8	2.9	
41	16-LVD-022_69	0.282801	0.000021	0.00095	0.00007	0.0211	0.0014	1.467204	0.000030	12.5	208	0.282797	0.6	0.7	5.1	
42	16-LVD-022_70	0.282788	0.000027	0.00110	0.00007	0.0258	0.0015	1.467195	0.000042	13.6	204	0.282784	0.1	1.0	4.5	
43	16-LVD-022_71	0.282774	0.000030	0.00106	0.00005	0.0245	0.0008	1.467217	0.000041	16.8	204	0.282770	-0.4	1.1	4.0	
44	16-LVD-022_72	0.282748	0.000024	0.00105	0.00002	0.0247	0.0006	1.467195	0.000035	13.2	205	0.282744	-1.3	0.8	3.1	
45	16-LVD-022_73	0.282759	0.000025	0.00080	0.00004	0.0185	0.0008	1.467173	0.000044	15.3	202	0.282756	-0.9	0.9	3.5	
46	16-LVD-022_74	0.282758	0.000023	0.00078	0.00004	0.0178	0.0008	1.467187	0.000040	12.09	199	0.282755	-1.0	0.8	3.4	
47	16-LVD-022_75	0.282768	0.000021	0.00075	0.00003	0.0188	0.0007	1.467200	0.000026	12.15	209	0.282765	-0.6	0.7	3.9	
48	16-LVD-022_76	0.282790	0.000024	0.00105	0.00003	0.0246	0.0006	1.467210	0.000033	13.2	200	0.282786	0.2	0.8	4.5	
49	16-LVD-022_83	0.282770	0.000027	0.00118	0.00003	0.0275	0.0008	1.467157	0.000035	13.3	213	0.282765	-0.5	1.0	4.0	
50	16-LVD-022_84	0.282757	0.000024	0.00092	0.00007	0.0216	0.0013	1.467196	0.000023	16.1	205	0.282753	-1.0	0.8	3.4	
51	16-LVD-022_85	0.282771	0.000023	0.00122	0.00003	0.0279	0.0008	1.467174	0.000034	13.3	205	0.282766	-0.5	0.8	3.9	
52	16-LVD-022_86	0.282789	0.000024	0.00111	0.00005	0.0262	0.0010	1.467199	0.000047	15.9	204	0.282785	0.1	0.8	4.5	

Grain	Spot ID	corrected										MUN LASS Age (Ma)	$^{176}\text{Hf}/^{177}\text{Hf}$	EHf0	2SE	EHfi
		$^{176}\text{Hf}/^{177}\text{Hf}$	2SE	$^{176}\text{Lu}/^{177}\text{Hf}$	2SE	$^{176}\text{Yb}/^{177}\text{Hf}$	2SE	$^{178}\text{Hf}/^{177}\text{Hf}$	2SE	Total Hf Beam						
53	16-LVD-022_87	0.282763	0.000021	0.00087	0.00003	0.0210	0.0006	1.467161	0.000036	15.2	194	0.282760	-0.8	0.7	3.4	
54	16-LVD-022_88	0.282785	0.000026	0.00107	0.00007	0.0258	0.0013	1.467178	0.000028	17.4	201	0.282781	0.0	0.9	4.3	
55	16-LVD-022_89	0.282758	0.000025	0.00092	0.00012	0.0244	0.0033	1.467152	0.000032	12.74	203	0.282755	-1.0	0.9	3.4	
56	16-LVD-022_90	0.282752	0.000020	0.00065	0.00001	0.0151	0.0006	1.467157	0.000029	12.77	202	0.282750	-1.2	0.7	3.2	
57	16-LVD-022_91	0.282776	0.000027	0.00154	0.00010	0.0334	0.0021	1.467169	0.000037	12.8	204	0.282770	-0.3	1.0	4.0	
58	16-LVD-022_92	0.282758	0.000020	0.00060	0.00004	0.0126	0.0005	1.467165	0.000038	13.8	205	0.282756	-1.0	0.7	3.5	
59	16-LVD-022_93	0.282773	0.000020	0.00052	0.00003	0.0124	0.0007	1.467170	0.000036	13.8	201	0.282771	-0.4	0.7	4.0	
60	16-LVD-022_100	0.282772	0.000024	0.00095	0.00009	0.0242	0.0021	1.467187	0.000035	11.82	211	0.282768	-0.5	0.8	4.1	
63	16-LVD-022_103	0.282800	0.000025	0.00136	0.00009	0.0311	0.0021	1.467169	0.000038	11.6	206	0.282795	0.5	0.9	4.9	
64	16-LVD-022_104	0.282783	0.000022	0.00101	0.00008	0.0219	0.0019	1.467173	0.000035	12.8	204	0.282779	-0.1	0.8	4.3	
65	16-LVD-022_105	0.282801	0.000024	0.00078	0.00009	0.0176	0.0022	1.467200	0.000043	14.3	207	0.282798	0.6	0.8	5.1	
66	16-LVD-022_106	0.282763	0.000022	0.00083	0.00005	0.0199	0.0011	1.467155	0.000041	13.1	199	0.282760	-0.8	0.8	3.5	
68	16-LVD-022_108	0.282776	0.000017	0.00051	0.00002	0.0117	0.0004	1.467178	0.000033	14.7	206	0.282774	-0.3	0.6	4.2	
71	16-LVD-022_111	0.282761	0.000025	0.00081	0.00003	0.0194	0.0007	1.467185	0.000034	12.4	205	0.282758	-0.8	0.9	3.6	
72	16-LVD-022_118	0.282778	0.000027	0.00157	0.00007	0.0360	0.0017	1.467200	0.000044	13	210	0.282772	-0.2	1.0	4.2	
73	16-LVD-022_119	0.282778	0.000020	0.00187	0.00014	0.0412	0.0032	1.467195	0.000035	14.4	204	0.282771	-0.2	0.7	4.0	
75	16-LVD-022_121	0.282758	0.000035	0.00109	0.00005	0.0267	0.0012	1.467184	0.000036	12.66	206	0.282754	-1.0	1.2	3.5	
76	16-LVD-022_122	0.282773	0.000019	0.00099	0.00004	0.0238	0.0009	1.467196	0.000035	13.2	198	0.282769	-0.4	0.7	3.9	
77	16-LVD-022_123	0.282740	0.000026	0.00106	0.00005	0.0264	0.0012	1.467179	0.000027	12.22	205	0.282736	-1.6	0.9	2.8	
78	16-LVD-022_124	0.282781	0.000024	0.00123	0.00004	0.0299	0.0011	1.467212	0.000028	13.1	203	0.282776	-0.1	0.8	4.2	
79	16-LVD-022_125	0.282769	0.000026	0.00096	0.00010	0.0254	0.0023	1.467178	0.000052	16.7	208	0.282765	-0.6	0.9	3.9	
80	16-LVD-022_126	0.282793	0.000021	0.00143	0.00008	0.0355	0.0021	1.467182	0.000033	12.22	210	0.282787	0.3	0.7	4.8	
82	16-LVD-022_128	0.282784	0.000023	0.00124	0.00011	0.0270	0.0023	1.467221	0.000026	12.9	208	0.282779	0.0	0.8	4.4	

Grain	Spot ID	corrected										MUN LASS Age (Ma)	$^{176}\text{Hf}/^{177}\text{Hf}$	EHf0	2SE	EHfi
		$^{176}\text{Hf}/^{177}\text{Hf}$	2SE	$^{176}\text{Lu}/^{177}\text{Hf}$	2SE	$^{176}\text{Yb}/^{177}\text{Hf}$	2SE	$^{178}\text{Hf}/^{177}\text{Hf}$	2SE	Total Hf Beam						
83	16-LVD-022_129	0.282752	0.000021	0.00146	0.00020	0.0387	0.0057	1.467213	0.000033	12.58	215	0.282746	-1.2	0.7	3.4	
84	16-LVD-022_136	0.282768	0.000021	0.00066	0.00001	0.0166	0.0003	1.467164	0.000040	12.09	206	0.282765	-0.6	0.7	3.9	
86	16-LVD-022_138	0.282770	0.000020	0.00120	0.00010	0.0301	0.0025	1.467199	0.000033	13.44	204	0.282765	-0.5	0.7	3.8	
88	16-LVD-022_140	0.282777	0.000021	0.00069	0.00002	0.0179	0.0005	1.467182	0.000032	12.03	209	0.282774	-0.3	0.7	4.3	
89	16-LVD-022_141	0.282755	0.000021	0.00061	0.00002	0.0148	0.0004	1.467221	0.000032	12.32	205	0.282753	-1.1	0.7	3.4	
90	16-LVD-022_142	0.282754	0.000026	0.00073	0.00003	0.0179	0.0008	1.467200	0.000036	12.06	217	0.282751	-1.1	0.9	3.6	
91	16-LVD-022_143	0.282756	0.000021	0.00070	0.00003	0.0168	0.0009	1.467188	0.000042	12.98	215	0.282753	-1.0	0.7	3.7	
92	16-LVD-022_144	0.282778	0.000023	0.00128	0.00005	0.0324	0.0015	1.467209	0.000032	12.4	208	0.282773	-0.2	0.8	4.2	
93	16-LVD-022_145	0.282748	0.000026	0.00126	0.00006	0.0314	0.0014	1.467197	0.000038	14.21	209	0.282743	-1.3	0.9	3.2	
94	16-LVD-022_146	0.282772	0.000026	0.00096	0.00005	0.0244	0.0011	1.467186	0.000034	13.1	208	0.282768	-0.5	0.9	4.0	
95	16-LVD-022_147	0.282761	0.000028	0.00121	0.00004	0.0298	0.0009	1.467189	0.000038	15.2	206	0.282756	-0.8	1.0	3.6	
96	16-LVD-022_154	0.282766	0.000023	0.00062	0.00001	0.0162	0.0003	1.467204	0.000036	11.93	206	0.282764	-0.7	0.8	3.8	
97	16-LVD-022_155	0.282767	0.000030	0.00073	0.00002	0.0191	0.0005	1.467177	0.000034	12.8	211	0.282764	-0.6	1.1	3.9	
98	16-LVD-022_156	0.282776	0.000021	0.00055	0.00001	0.0131	0.0003	1.467201	0.000038	13.25	206	0.282774	-0.3	0.7	4.2	
99	16-LVD-022_157	0.282756	0.000024	0.00052	0.00002	0.0130	0.0003	1.467185	0.000034	12.9	211	0.282754	-1.0	0.8	3.6	
100	16-LVD-022_158	0.282779	0.000022	0.00076	0.00002	0.0197	0.0005	1.467184	0.000033	12.1	206	0.282776	-0.2	0.8	4.3	
101	16-LVD-022_159	0.282775	0.000023	0.00105	0.00005	0.0285	0.0016	1.467168	0.000036	12.05	207	0.282771	-0.4	0.8	4.1	
102	16-LVD-022_160	0.282767	0.000020	0.00073	0.00004	0.0174	0.0009	1.467177	0.000038	12.83	210	0.282764	-0.6	0.7	3.9	
103	16-LVD-022_161	0.282759	0.000023	0.00084	0.00006	0.0209	0.0014	1.467197	0.000037	12.09	198	0.282756	-0.9	0.8	3.4	
104	16-LVD-022_162	0.282806	0.000027	0.00110	0.00010	0.0284	0.0029	1.467163	0.000035	12.23	209	0.282802	0.7	1.0	5.2	
105	16-LVD-022_163	0.282783	0.000018	0.00160	0.00020	0.0393	0.0049	1.467186	0.000032	12	212	0.282777	-0.1	0.6	4.4	
106	16-LVD-022_164	0.282775	0.000028	0.00090	0.00006	0.0237	0.0019	1.467215	0.000035	12.4	205	0.282772	-0.4	1.0	4.1	
107	16-LVD-022_165	0.282775	0.000022	0.00074	0.00003	0.0174	0.0005	1.467224	0.000026	13.8	213	0.282772	-0.4	0.8	4.3	

Grain	Spot ID	<i>corrected</i>		2SE	176Lu/ 177Hf	2SE	176Yb/ 177Hf	2SE	178Hf/ 177Hf	2SE	Total Hf Beam	MUN LASS Age (Ma)	176Hf/ 177Hf	EHf0	2SE	EHfi
		176Hf/ 177Hf	2SE													
108	16-LVD-022_166	0.282767	0.000023	0.00055	0.00002	0.0133	0.0004	1.467146	0.000037	14.5	208	0.282765	-0.6	0.8	3.9	
109	16-LVD-022_167	0.282778	0.000018	0.00060	0.00003	0.0142	0.0007	1.467209	0.000036	12.9	204	0.282776	-0.2	0.6	4.2	
110	16-LVD-022_168	0.282755	0.000024	0.00088	0.00004	0.0216	0.0007	1.467160	0.000038	12.9	202	0.282752	-1.1	0.8	3.3	
Rejected Analysis																
3	16-LVD-022_13	0.282760	0.000018	0.00056	0.00002	0.0140	0.0006	1.467185	0.000035	11.66	203	0.282758	-0.9	0.6	3.6	
11	16-LVD-022_21	0.282767	0.000027	0.00115	0.00004	0.0291	0.0012	1.467205	0.000038	14.6	205	0.282763	-0.6	1.0	3.8	
18	16-LVD-022_34	0.282769	0.000021	0.00054	0.00002	0.0123	0.0006	1.467267	0.000038	14.4	221	0.282767	-0.6	0.7	4.3	
21	16-LVD-022_37	0.282773	0.000022	0.00074	0.00004	0.0177	0.0010	1.467185	0.000029	12.7	283	0.282769	-0.4	0.8	5.7	
22	16-LVD-022_38	0.282755	0.000023	0.00141	0.00013	0.0361	0.0034	1.467177	0.000036	12	199	0.282750	-1.1	0.8	3.2	
33	16-LVD-022_55	0.282754	0.000029	0.00103	0.00005	0.0260	0.0017	1.467191	0.000045	12.9	207	0.282750	-1.1	1.0	3.4	
61	16-LVD-022_101	0.282739	0.000029	0.00111	0.00002	0.0266	0.0006	1.467206	0.000035	11.66	208	0.282735	-1.6	1.0	2.8	
62	16-LVD-022_102	0.282762	0.000018	0.00093	0.00007	0.0221	0.0017	1.467180	0.000036	12.78	220	0.282758	-0.8	0.6	3.9	
67	16-LVD-022_107	0.282954	0.000040	0.00123	0.00004	0.0288	0.0013	1.467204	0.000034	18	230	0.282949	6.0	1.4	10.9	
69	16-LVD-022_109	0.282760	0.000026	0.00129	0.00012	0.0327	0.0033	1.467191	0.000034	14.7	202	0.282755	-0.9	0.9	3.4	
70	16-LVD-022_110	0.282761	0.000019	0.00080	0.00005	0.0183	0.0012	1.467155	0.000042	15.4	203	0.282758	-0.8	0.7	3.6	
74	16-LVD-022_120	0.282767	0.000020	0.00088	0.00004	0.0214	0.0011	1.467167	0.000033	13.4	209	0.282764	-0.6	0.7	3.9	
81	16-LVD-022_127	0.282782	0.000028	0.00111	0.00006	0.0261	0.0017	1.467185	0.000026	13.2	208	0.282778	-0.1	1.0	4.4	
85	16-LVD-022_137	0.282768	0.000040	0.00068	0.00002	0.0175	0.0007	1.467262	0.000038	17.1	204	0.282765	-0.6	1.4	3.8	
87	16-LVD-022_139	0.282805	0.000018	0.00107	0.00004	0.0252	0.0009	1.467196	0.000037	12.23	208	0.282801	0.7	0.6	5.2	

Whitehorse trough - Richthofen formation - Sample 16-LVD-023, Lake Laberge (Zone 08V 495522E 6774110N NAD 83)

Grain	Spot ID	corrected													
		176Hf/ 177Hf	2SE	176Lu/ 177Hf	2SE	176Yb/ 177Hf	2SE	178Hf/ 177Hf	2SE	Total Hf Beam	MUN LASS Age (Ma)	176Hf/ 177Hf	EHf0	2SE	EHf
2	16-LVD-023_11	0.282600	0.000018	0.00147	0.00001	0.0342	0.0003	1.467194	0.000055	15.5	363	0.282590	-6.5	0.6	1.2
3	16-LVD-023_12	0.282747	0.000025	0.00110	0.00003	0.0222	0.0006	1.467190	0.000043	13.8	185	0.282743	-1.3	0.9	2.6
4	16-LVD-023_13	0.282711	0.000035	0.00100	0.00003	0.0201	0.0007	1.467182	0.000034	16.8	195	0.282707	-2.6	1.2	1.6
11	16-LVD-023_20	0.282401	0.000026	0.00083	0.00003	0.0180	0.0006	1.467171	0.000036	12.5	356	0.282395	-13.6	0.9	-5.8
12	16-LVD-023_21	0.282944	0.000026	0.00059	0.00001	0.0138	0.0004	1.467171	0.000037	12.3	269	0.282941	5.6	0.9	11.5
13	16-LVD-023_22	0.282848	0.000022	0.00131	0.00004	0.0283	0.0012	1.467162	0.000033	11.5	244	0.282842	2.2	0.8	7.4
14	16-LVD-023_29	0.282701	0.000025	0.00086	0.00004	0.0175	0.0007	1.467180	0.000034	11.8	202	0.282698	-3.0	0.9	1.4
15	16-LVD-023_30	0.282696	0.000029	0.00067	0.00004	0.0138	0.0008	1.467161	0.000044	10.2	187	0.282694	-3.1	1.0	0.9
16	16-LVD-023_31	0.282676	0.000022	0.00111	0.00008	0.0241	0.0020	1.467191	0.000036	14.3	270	0.282670	-3.9	0.8	1.9
17	16-LVD-023_32	0.282957	0.000020	0.00107	0.00004	0.0217	0.0007	1.467154	0.000030	12.51	211	0.282953	6.1	0.7	10.6
19	16-LVD-023_34	0.281190	0.000021	0.00056	0.00001	0.0147	0.0002	1.467223	0.000046	13.5	2563	0.281163	-56.4	0.7	0.9
21	16-LVD-023_36	0.282702	0.000025	0.00104	0.00003	0.0216	0.0006	1.467172	0.000041	16.1	197	0.282698	-2.9	0.9	1.3
22	16-LVD-023_37	0.282703	0.000034	0.00100	0.00002	0.0203	0.0005	1.467173	0.000040	13.3	197	0.282699	-2.9	1.2	1.3
23	16-LVD-023_38	0.282895	0.000022	0.00050	0.00015	0.0090	0.0025	1.467173	0.000042	15.2	240	0.282893	3.9	0.8	9.2
Rejected Analysis															
1	16-LVD-023_59	0.282743	0.000038	0.00103	0.00001	0.0242	0.0006	1.467178	0.000043	18	0	0.282743	-1.5	1.3	-1.5
5	16-LVD-023_14	0.282677	0.000050	0.00098	0.00001	0.0198	0.0003	1.467166	0.000082	20.96	210	0.282673	-3.8	1.8	0.7
6	16-LVD-023_15	0.282608	0.000091	0.00106	0.00004	0.0216	0.0008	1.467151	0.000094	19.86	186	0.282604	-6.3	3.2	-2.3
7	16-LVD-023_16	0.282991	0.000046	0.00402	0.00019	0.1113	0.0054	1.467182	0.000047	13.1	390	0.282962	7.3	1.6	14.9
8	16-LVD-023_17	0.281043	0.000034	0.00121	0.00004	0.0293	0.0011	1.467165	0.000046	15.9	2829	0.280977	-61.6	1.2	0.5
9	16-LVD-023_18	0.282683	0.000020	0.00085	0.00007	0.0199	0.0016	1.467168	0.000045	10.5	315	0.282678	-3.6	0.7	3.2

Grain	Spot ID	<i>corrected</i>		2SE		176Lu/ 177Hf		2SE		176Yb/ 177Hf		2SE		178Hf/ 177Hf		2SE		Total Hf Beam	MUN LASS Age (Ma)	176Hf/ 177Hf		EHf0	2SE	EHfi		
		176Hf/ 177Hf																								
10	16-LVD-023_19	0.282731	0.000047	0.00104	0.00002	0.0217	0.0005	1.467228	0.000049	18.2	205	0.282727	-1.9	1.7	2.5											
18	16-LVD-023_33	0.282692	0.000032	0.00119	0.00007	0.0245	0.0013	1.467137	0.000050	16.8	205	0.282687	-3.3	1.1	1.1											
20	16-LVD-023_35	0.281900	0.000180	0.00049	0.00003	0.0111	0.0005	1.467140	0.000034	13.9	260	0.281898	-31.3	6.4	-25.6											
24	16-LVD-023_39	0.282026	0.000036	0.00160	0.00006	0.0438	0.0016	1.467143	0.000058	18.9	1474	0.281981	-26.8	1.3	4.8											
25	16-LVD-023_40	0.282688	0.000022	0.00090	0.00002	0.0181	0.0002	1.467161	0.000078	20.3	190	0.282685	-3.4	0.8	0.7											
26	16-LVD-023_47	0.282755	0.000036	0.00054	0.00003	0.0119	0.0003	1.467124	0.000047	18.4	200	0.282753	-1.1	1.3	3.3											
27	16-LVD-023_48	0.282725	0.000041	0.00111	0.00004	0.0245	0.0010	1.467233	0.000046	18.5	337	0.282718	-2.1	1.5	5.1											
28	16-LVD-023_49	0.282555	0.000082	0.00154	0.00010	0.0357	0.0031	1.467159	0.000017	20.3	173	0.282550	-8.1	2.9	-4.5											
29	16-LVD-023_50	0.282750	0.000048	0.00122	0.00001	0.0249	0.0002	1.467169	0.000057	17.1	196	0.282746	-1.2	1.7	3.0											
30	16-LVD-023_51	0.282748	0.000025	0.00098	0.00005	0.0198	0.0010	1.467186	0.000038	14.7	220	0.282744	-1.3	0.9	3.4											
31	16-LVD-023_52	0.282890	0.000020	0.00099	0.00006	0.0212	0.0019	1.467178	0.000046	19.5	418	0.282882	3.7	0.7	12.8											
32	16-LVD-023_53	0.282686	0.000051	0.00102	0.00008	0.0211	0.0016	1.467229	0.000064	20.6	207	0.282682	-3.5	1.8	1.0											
33	16-LVD-023_54	0.282614	0.000029	0.00201	0.00018	0.0447	0.0035	1.467141	0.000060	18.2	309	0.282602	-6.0	1.0	0.4											
34	16-LVD-023_55	0.282971	0.000042	0.00112	0.00003	0.0206	0.0006	1.467171	0.000068	15.5	238	0.282966	6.6	1.5	11.7											
35	16-LVD-023_56	0.282778	0.000032	0.00222	0.00004	0.0533	0.0009	1.467181	0.000055	17.8	366	0.282763	-0.2	1.1	7.4											
36	16-LVD-023_57	0.282753	0.000031	0.00076	0.00006	0.0158	0.0017	1.467193	0.000024	17.5	208	0.282750	-1.1	1.1	3.4											
37	16-LVD-023_58	0.282670	0.000029	0.00119	0.00005	0.0242	0.0010	1.467171	0.000084	20.4	182	0.282666	-4.1	1.0	-0.2											
38	16-LVD-023_65	0.282702	0.000029	0.00109	0.00004	0.0248	0.0005	1.467166	0.000029	17.9	244	0.282697	-2.9	1.0	2.3											
39	16-LVD-023_66	0.282710	0.000031	0.00088	0.00004	0.0175	0.0008	1.467216	0.000052	14	245	0.282706	-2.7	1.1	2.7											
40	16-LVD-023_67	0.282696	0.000027	0.00094	0.00005	0.0191	0.0011	1.467168	0.000033	16.1	188	0.282693	-3.1	1.0	0.9											
41	16-LVD-023_68	0.282571	0.000039	0.00291	0.00013	0.0778	0.0038	1.467150	0.000037	20.5	298	0.282555	-7.6	1.4	-1.5											
42	16-LVD-023_69	0.282054	0.000032	0.00091	0.00014	0.0248	0.0040	1.467131	0.000039	17.4	1526	0.282028	-25.9	1.1	7.6											
43	16-LVD-023_70	0.282702	0.000031	0.00089	0.00010	0.0182	0.0020	1.467148	0.000033	12.1	208	0.282699	-2.9	1.1	1.6											

Grain	Spot ID	<i>corrected</i>		2SE	176Lu/ 177Hf	2SE	176Yb/ 177Hf	2SE	178Hf/ 177Hf	2SE	Total Hf Beam	MUN LASS Age (Ma)	176Hf/ 177Hf	EHf0	2SE	EHfi
		176Hf/ 177Hf	2SE													
44	16-LVD-023_71	0.282906	0.000025	0.00118	0.00007	0.0266	0.0018	1.467174	0.000034	11.68	282	0.282900	4.3	0.9	10.3	
45	16-LVD-023_72	0.282712	0.000024	0.00097	0.00005	0.0200	0.0010	1.467184	0.000039	11.9	207	0.282708	-2.6	0.8	1.9	
46	16-LVD-023_73	0.282576	0.000028	0.00117	0.00006	0.0286	0.0014	1.467181	0.000038	11.25	434	0.282567	-7.4	1.0	1.9	
47	16-LVD-023_74	0.282739	0.000026	0.00099	0.00007	0.0229	0.0019	1.467177	0.000037	10.53	315	0.282733	-1.6	0.9	5.2	
48	16-LVD-023_75	0.282917	0.000042	0.00073	0.00005	0.0146	0.0012	1.467196	0.000057	8.7	190	0.282914	4.7	1.5	8.8	
49	16-LVD-023_76	0.282724	0.000018	0.00194	0.00002	0.0476	0.0004	1.467140	0.000030	16.3	533	0.282705	-2.2	0.6	9.1	
50	16-LVD-023_83	0.282716	0.000023	0.00106	0.00004	0.0218	0.0008	1.467178	0.000043	16	175	0.282713	-2.4	0.8	1.3	
51	16-LVD-023_84	0.282821	0.000046	0.00253	0.00056	0.0700	0.0160	1.467158	0.000028	14	307	0.282806	1.3	1.6	7.6	
52	16-LVD-023_85	0.282611	0.000038	0.00197	0.00009	0.0475	0.0018	1.467175	0.000049	15.3	342	0.282598	-6.2	1.3	1.0	
53	16-LVD-023_86	0.282758	0.000034	0.00095	0.00003	0.0200	0.0007	1.467181	0.000044	14.9	192	0.282755	-1.0	1.2	3.2	
55	16-LVD-023_88	0.282733	0.000019	0.00075	0.00004	0.0175	0.0009	1.467190	0.000038	12.9	366	0.282728	-1.8	0.7	6.1	

*grain 54 not included b/c not zircon

Whitehorse trough - Richthofen formation - Sample 17-LVD-026, Metamorphic Clast Fish Lake (Zone 08V 485805E 6721676N NAD 83)

Grain	Spot ID	<i>corrected</i>		2SE	176Lu/ 177Hf	2SE	176Yb/ 177Hf	2SE	178Hf/ 177Hf	2SE	Total Hf Beam	MUN LASS Age (Ma)	176Hf/ 177Hf	EHf0	2SE	EHfi
		176Hf/ 177Hf	2SE													
1	17-LVD-026_12	0.282657	0.000021	0.00123	0.00006	0.0292	0.0017	1.467192	0.000030	12.96	186	0.282653	-4.5	0.7	-0.6	
3	17-LVD-026_14	0.282328	0.000017	0.00060	0.00001	0.0149	0.0003	1.467206	0.000031	14.1	180	0.282326	-16.2	0.6	-12.2	
4	17-LVD-026_15	0.282789	0.000034	0.00046	0.00003	0.0116	0.0009	1.467194	0.000039	16.1	194	0.282787	0.1	1.2	4.4	
5	17-LVD-026_16	0.282774	0.000029	0.00154	0.00016	0.0407	0.0048	1.467145	0.000056	11.97	206	0.282768	-0.4	1.0	4.0	
7	17-LVD-026_18	0.282336	0.000026	0.00097	0.00003	0.0249	0.0007	1.467180	0.000033	13.11	190	0.282333	-15.9	0.9	-11.8	
9	17-LVD-026_20	0.282448	0.000028	0.00080	0.00002	0.0199	0.0009	1.467179	0.000044	16.2	193	0.282445	-11.9	1.0	-7.7	

Grain	Spot ID	corrected										MUN LASS Age (Ma)	$^{176}\text{Hf}/^{177}\text{Hf}$	EHf0	2SE	EHfi
		$^{176}\text{Hf}/^{177}\text{Hf}$	2SE	$^{176}\text{Lu}/^{177}\text{Hf}$	2SE	$^{176}\text{Yb}/^{177}\text{Hf}$	2SE	$^{178}\text{Hf}/^{177}\text{Hf}$	2SE	Total Hf Beam						
13	17-LVD-026_30	0.282590	0.000027	0.00114	0.00010	0.0285	0.0027	1.467162	0.000040	14.9	190	0.282586	-6.9	1.0	-2.8	
15	17-LVD-026_32	0.282586	0.000030	0.00104	0.00012	0.0248	0.0032	1.467212	0.000036	15.1	189	0.282582	-7.0	1.1	-3.0	
16	17-LVD-026_33	0.282598	0.000036	0.00146	0.00005	0.0358	0.0016	1.467230	0.000040	17.6	183	0.282593	-6.6	1.3	-2.7	
18	17-LVD-026_35	0.282596	0.000027	0.00111	0.00009	0.0266	0.0028	1.467199	0.000024	14.8	192	0.282592	-6.7	1.0	-2.5	
20	17-LVD-026_37	0.282578	0.000024	0.00096	0.00003	0.0227	0.0009	1.467185	0.000039	12.8	183	0.282575	-7.3	0.8	-3.4	
21	17-LVD-026_38	0.282564	0.000025	0.00108	0.00002	0.0269	0.0004	1.467143	0.000032	15.5	187	0.282560	-7.8	0.9	-3.8	
22	17-LVD-026_39	0.282572	0.000020	0.00089	0.00004	0.0209	0.0010	1.467167	0.000040	18.5	187	0.282569	-7.5	0.7	-3.5	
23	17-LVD-026_40	0.282552	0.000027	0.00129	0.00013	0.0315	0.0030	1.467233	0.000037	14.9	187	0.282547	-8.2	1.0	-4.3	
24	17-LVD-026_41	0.282864	0.000020	0.00130	0.00003	0.0301	0.0009	1.467191	0.000035	13.5	206	0.282859	2.8	0.7	7.2	
25	17-LVD-026_48	0.282595	0.000023	0.00116	0.00005	0.0278	0.0014	1.467210	0.000029	16.6	253	0.282590	-6.7	0.8	-1.3	
27	17-LVD-026_50	0.282836	0.000023	0.00126	0.00005	0.0252	0.0010	1.467211	0.000063	15.1	200	0.282831	1.8	0.8	6.1	
28	17-LVD-026_51	0.282552	0.000033	0.00093	0.00006	0.0240	0.0014	1.467211	0.000044	14.25	189	0.282549	-8.2	1.2	-4.2	
Rejected Analysis																
2	17-LVD-026_13	0.282771	0.000025	0.00156	0.00008	0.0371	0.0022	1.467193	0.000054	11.62	180	0.282766	-0.5	0.9	3.3	
6	17-LVD-026_17	0.282700	0.000140	0.00117	0.00013	0.0285	0.0027	1.467250	0.000120	19.6	164	0.282696	-3.0	5.0	0.5	
8	17-LVD-026_19	0.282203	0.000040	0.00077	0.00003	0.0199	0.0005	1.467191	0.000049	21.9	369	0.282198	-20.6	1.4	-12.6	
10	17-LVD-026_21	0.282520	0.000040	0.00050	0.00007	0.0141	0.0017	1.467239	0.000058	20	180	0.282518	-9.4	1.4	-5.4	
11	17-LVD-026_22	0.282519	0.000031	0.00116	0.00014	0.0298	0.0038	1.467215	0.000048	11.77	174	0.282515	-9.4	1.1	-5.7	
12	17-LVD-026_23	0.282697	0.000022	0.00155	0.00005	0.0383	0.0012	1.467183	0.000033	15.9	184	0.282692	-3.1	0.8	0.8	
14	17-LVD-026_31	0.282336	0.000024	0.00072	0.00005	0.0182	0.0012	1.467174	0.000035	12.09	182	0.282334	-15.9	0.9	-11.9	
17	17-LVD-026_34	0.282420	0.000022	0.00105	0.00005	0.0261	0.0013	1.467213	0.000041	15.1	178	0.282416	-12.9	0.8	-9.1	
19	17-LVD-026_36	0.282550	0.000031	0.00129	0.00007	0.0328	0.0021	1.467132	0.000052	19.7	183	0.282546	-8.3	1.1	-4.4	
26	17-LVD-026_49	0.282612	0.000031	0.00077	0.00001	0.0188	0.0002	1.467147	0.000078	17.1	206	0.282609	-6.1	1.1	-1.7	

Grain	Spot ID	<i>corrected</i>		2SE	176Lu/ 177Hf	2SE	176Yb/ 177Hf	2SE	178Hf/ 177Hf	2SE	Total Hf Beam	MUN LASS Age (Ma)	176Hf/ 177Hf	EHf0	2SE	EHfi
		176Hf/ 177Hf	2SE													
29	17-LVD-026_52	0.282719	0.000035	0.00090	0.00003	0.0217	0.0007	1.467193	0.000049	18.9	207	0.282716	-2.3	1.2	2.1	
30	17-LVD-026_53	0.282547	0.000048	0.00100	0.00005	0.0241	0.0011	1.467135	0.000093	13.6	152	0.282544	-8.4	1.7	-5.1	
31	17-LVD-026_54	0.282530	0.000022	0.00050	0.00001	0.0121	0.0003	1.467150	0.000034	16.2	164	0.282528	-9.0	0.8	-5.4	
32	17-LVD-026_55	0.282549	0.000021	0.00112	0.00006	0.0275	0.0017	1.467158	0.000036	13.06	147	0.282546	-8.3	0.7	-5.2	
33	17-LVD-026_56	0.282565	0.000028	0.00113	0.00005	0.0276	0.0013	1.467176	0.000035	14	92	0.282563	-7.8	1.0	-5.8	
34	17-LVD-026_57	0.282555	0.000029	0.00099	0.00006	0.0238	0.0013	1.467178	0.000051	15.7	109	0.282553	-8.1	1.0	-5.8	
35	17-LVD-026_58	0.282514	0.000027	0.00097	0.00007	0.0233	0.0018	1.467196	0.000041	16.9	78	0.282513	-9.6	1.0	-7.9	

Whitehorse trough - Richthofen formation - Sample 17-LVD-027, Takhini subdivision (Zone 08V 488086E 6748844N NAD 83)

Grain	Spot ID	<i>corrected</i>		2SE	176Lu/ 177Hf	2SE	176Yb/ 177Hf	2SE	178Hf/ 177Hf	2SE	Total Hf Beam	MUN LASS Age (Ma)	176Hf/ 177Hf	EHf0	2SE	EHfi
		176Hf/ 177Hf	2SE													
1	17-LVD-027_10	0.282946	0.000030	0.00082	0.00006	0.0207	0.0013	1.467179	0.000047	18.6	191	0.282943	5.7	1.1	9.8	
2	17-LVD-027_11	0.282871	0.000032	0.00101	0.00002	0.0249	0.0005	1.467188	0.000027	18.0	193	0.282867	3.0	1.1	7.2	
3	17-LVD-027_12	0.282926	0.000037	0.00162	0.00017	0.0394	0.0041	1.467193	0.000023	17.3	199	0.282920	5.0	1.3	9.2	
4	17-LVD-027_13	0.282886	0.000024	0.00165	0.00008	0.0401	0.0020	1.467202	0.000050	17.1	207	0.282880	3.6	0.8	8.0	
5	17-LVD-027_14	0.282870	0.000022	0.00199	0.00031	0.0488	0.0083	1.467190	0.000045	16.6	196	0.282863	3.0	0.8	7.1	
6	17-LVD-027_15	0.282938	0.000026	0.00133	0.00006	0.0304	0.0017	1.467245	0.000042	19.5	216	0.282933	5.4	0.9	10.0	
7	17-LVD-027_16	0.282931	0.000038	0.00148	0.00007	0.0374	0.0017	1.467175	0.000045	17.1	203	0.282925	5.2	1.3	9.5	
8	17-LVD-027_17	0.283002	0.000043	0.00099	0.00013	0.0226	0.0031	1.467226	0.000037	13.1	206	0.282998	7.7	1.5	12.1	
9	17-LVD-027_18	0.282907	0.000030	0.00088	0.00002	0.0192	0.0005	1.467194	0.000033	15.3	194	0.282904	4.3	1.1	8.5	
10	17-LVD-027_19	0.282891	0.000028	0.00119	0.00008	0.0287	0.0020	1.467173	0.000053	19.8	190	0.282887	3.7	1.0	7.8	

Grain	Spot ID	corrected										MUN LASS Age (Ma)	$^{176}\text{Hf}/^{177}\text{Hf}$	EHf0	2SE	EHfi
		$^{176}\text{Hf}/^{177}\text{Hf}$	2SE	$^{176}\text{Lu}/^{177}\text{Hf}$	2SE	$^{176}\text{Yb}/^{177}\text{Hf}$	2SE	$^{178}\text{Hf}/^{177}\text{Hf}$	2SE	Total Hf Beam						
11	17-LVD-027_20	0.282910	0.000041	0.00126	0.00005	0.0299	0.0019	1.467198	0.000063	20.0	185	0.282906	4.4	1.4	8.4	
16	17-LVD-027_31	0.282825	0.000042	0.00126	0.00004	0.0292	0.0009	1.467206	0.000075	14.7	183	0.282821	1.4	1.5	5.3	
17	17-LVD-027_32	0.282906	0.000028	0.00143	0.00003	0.0360	0.0007	1.467205	0.000045	13.7	206	0.282900	4.3	1.0	8.7	
18	17-LVD-027_33	0.282855	0.000030	0.00120	0.00002	0.0292	0.0006	1.467168	0.000047	15.6	203	0.282850	2.5	1.1	6.8	
19	17-LVD-027_34	0.282851	0.000025	0.00125	0.00003	0.0277	0.0007	1.467173	0.000034	17.5	192	0.282846	2.3	0.9	6.5	
20	17-LVD-027_35	0.282940	0.000035	0.00108	0.00011	0.0268	0.0027	1.467253	0.000047	12.9	201	0.282936	5.5	1.2	9.8	
24	17-LVD-027_39	0.282982	0.000036	0.00108	0.00005	0.0253	0.0012	1.467164	0.000073	15.3	197	0.282978	7.0	1.3	11.2	
25	17-LVD-027_46	0.282831	0.000025	0.00120	0.00006	0.0280	0.0015	1.467201	0.000037	15.2	213	0.282826	1.6	0.9	6.2	
26	17-LVD-027_47	0.282798	0.000038	0.00098	0.00003	0.0219	0.0008	1.467204	0.000060	16.3	213	0.282794	0.5	1.3	5.1	
29	17-LVD-027_50	0.282794	0.000028	0.00109	0.00003	0.0254	0.0007	1.467132	0.000044	17.9	214	0.282790	0.3	1.0	4.9	
30	17-LVD-027_51	0.282863	0.000024	0.00138	0.00006	0.0271	0.0011	1.467167	0.000035	14.9	195	0.282858	2.8	0.8	6.9	
33	17-LVD-027_54	0.282894	0.000038	0.00135	0.00008	0.0324	0.0024	1.467199	0.000049	16.9	211	0.282889	3.9	1.3	8.4	
34	17-LVD-027_55	0.282828	0.000040	0.00111	0.00004	0.0260	0.0009	1.467171	0.000047	14.3	195	0.282824	1.5	1.4	5.7	
36	17-LVD-027_57	0.282869	0.000023	0.00088	0.00004	0.0194	0.0010	1.467204	0.000034	14.5	206	0.282866	3.0	0.8	7.4	
37	17-LVD-027_64	0.282886	0.000030	0.00118	0.00010	0.0231	0.0023	1.467209	0.000051	17.5	210	0.282881	3.6	1.1	8.1	
39	17-LVD-027_66	0.282909	0.000017	0.00131	0.00004	0.0334	0.0012	1.467201	0.000041	13.3	195	0.282904	4.4	0.6	8.5	
41	17-LVD-027_68	0.282913	0.000034	0.00166	0.00010	0.0414	0.0025	1.467200	0.000048	12.4	190	0.282907	4.5	1.2	8.6	
43	17-LVD-027_70	0.282908	0.000027	0.00112	0.00013	0.0244	0.0031	1.467155	0.000049	15.2	197	0.282904	4.3	1.0	8.6	
44	17-LVD-027_71	0.282903	0.000034	0.00134	0.00009	0.0329	0.0025	1.467138	0.000038	15.6	193	0.282898	4.2	1.2	8.3	
45	17-LVD-027_72	0.282908	0.000029	0.00114	0.00007	0.0292	0.0017	1.467195	0.000058	14.3	193	0.282904	4.3	1.0	8.5	
47	17-LVD-027_74	0.282878	0.000032	0.00094	0.00006	0.0205	0.0010	1.467179	0.000042	19.0	191	0.282875	3.3	1.1	7.4	
50	17-LVD-027_83	0.282854	0.000047	0.00249	0.00012	0.0617	0.0032	1.467193	0.000049	17.4	198	0.282845	2.4	1.7	6.5	
51	17-LVD-027_84	0.282832	0.000026	0.00116	0.00004	0.0274	0.0010	1.467219	0.000055	17.3	200	0.282828	1.7	0.9	6.0	

Grain	Spot ID	corrected										MUN LASS Age (Ma)	$^{176}\text{Hf}/^{177}\text{Hf}$	EHf0	2SE	EHfi
		$^{176}\text{Hf}/^{177}\text{Hf}$	2SE	$^{176}\text{Lu}/^{177}\text{Hf}$	2SE	$^{176}\text{Yb}/^{177}\text{Hf}$	2SE	$^{178}\text{Hf}/^{177}\text{Hf}$	2SE	Total Hf Beam						
58	17-LVD-027_91	0.282852	0.000034	0.00111	0.00002	0.0253	0.0004	1.467206	0.000055	16.3	207	0.282848	2.4	1.2	6.8	
59	17-LVD-027_92	0.282874	0.000026	0.00083	0.00004	0.0200	0.0011	1.467190	0.000034	16.8	191	0.282871	3.1	0.9	7.3	
60	17-LVD-027_93	0.282862	0.000038	0.00101	0.00005	0.0239	0.0011	1.467221	0.000039	17.4	202	0.282858	2.7	1.3	7.1	
63	17-LVD-027_102	0.282875	0.000025	0.00114	0.00005	0.0251	0.0009	1.467190	0.000052	16.7	200	0.282871	3.2	0.9	7.5	
65	17-LVD-027_104	0.282324	0.000027	0.00083	0.00002	0.0219	0.0007	1.467192	0.000037	16.9	359	0.282318	-16.3	1.0	-8.5	
Rejected Analysis																
	17-LVD-027_21	0.282840	0.000039	0.00138	0.00002	0.0339	0.0008	1.467187	0.000068	19.8	192	0.282835	1.9	1.4	6.0	
13	17-LVD-027_28	0.282978	0.000035	0.00125	0.00006	0.0295	0.0017	1.467148	0.000034	17.3	194	0.282973	6.8	1.2	11.0	
14	17-LVD-027_29	0.282873	0.000060	0.00117	0.00010	0.0261	0.0031	1.467117	0.000034	17.9	190	0.282869	3.1	2.1	7.2	
15	17-LVD-027_30	0.282902	0.000054	0.00061	0.00001	0.0150	0.0001	1.467196	0.000076	20.9	195	0.282900	4.1	1.9	8.4	
21	17-LVD-027_36	0.282792	0.000026	0.00108	0.00009	0.0259	0.0021	1.467235	0.000054	15.9	207	0.282788	0.2	0.9	4.7	
22	17-LVD-027_37	0.282931	0.000050	0.00139	0.00003	0.0356	0.0008	1.467235	0.000068	16.9	186	0.282926	5.2	1.8	9.1	
23	17-LVD-027_38	0.282973	0.000030	0.00102	0.00004	0.0244	0.0009	1.467177	0.000064	16.2	197	0.282969	6.6	1.1	10.9	
27	17-LVD-027_48	0.282891	0.000021	0.00057	0.00001	0.0111	0.0002	1.467091	0.000043	18.9	196	0.282889	3.7	0.7	8.0	
28	17-LVD-027_49	0.282863	0.000042	0.00131	0.00006	0.0318	0.0015	1.467212	0.000031	17.4	204	0.282858	2.8	1.5	7.1	
31	17-LVD-027_52	0.282923	0.000042	0.00133	0.00008	0.0317	0.0018	1.467192	0.000064	16.6	315	0.282915	4.9	1.5	11.6	
32	17-LVD-027_53	0.282860	0.000070	0.00084	0.00003	0.0212	0.0009	1.467257	0.000042	15.6	215	0.282857	2.7	2.5	7.3	
35	17-LVD-027_56	0.282873	0.000046	0.00094	0.00003	0.0232	0.0009	1.467220	0.000042	18.2	181	0.282870	3.1	1.6	7.0	
38	17-LVD-027_65	0.282931	0.000057	0.00096	0.00009	0.0192	0.0017	1.467170	0.000040	15.6	198	0.282927	5.2	2.0	9.4	
40	17-LVD-027_67	0.282881	0.000041	0.00182	0.00012	0.0463	0.0032	1.467154	0.000055	12.9	186	0.282875	3.4	1.4	7.3	
42	17-LVD-027_69	0.282869	0.000038	0.00121	0.00004	0.0305	0.0008	1.467231	0.000076	16.6	202	0.282864	3.0	1.3	7.3	
46	17-LVD-027_73	0.282780	0.000110	0.00099	0.00003	0.0244	0.0009	1.467260	0.000200	16.7	206	0.282776	-0.2	3.9	4.3	
48	17-LVD-027_75	0.282837	0.000054	0.00170	0.00009	0.0390	0.0024	1.467171	0.000047	18.8	168	0.282832	1.8	1.9	5.4	

Grain	Spot ID	<i>corrected</i>		2SE	176Lu/ 177Hf	2SE	176Yb/ 177Hf	2SE	178Hf/ 177Hf	2SE	Total Hf Beam	MUN LASS Age (Ma)	176Hf/ 177Hf	EHf0	2SE	EHfi
		176Hf/ 177Hf	2SE													
49	17-LVD-027_82	0.282912	0.000048	0.00160	0.00007	0.0378	0.0019	1.467191	0.000046	15.7	216	0.282906	4.5	1.7	9.1	
52	17-LVD-027_85	0.282809	0.000050	0.00103	0.00014	0.0242	0.0034	1.467246	0.000052	17.5	188	0.282805	0.8	1.8	4.9	
53	17-LVD-027_86	0.282852	0.000052	0.00166	0.00014	0.0345	0.0029	1.467138	0.000042	22.6	181	0.282846	2.4	1.8	6.2	
54	17-LVD-027_87	0.282893	0.000044	0.00169	0.00003	0.0417	0.0008	1.467174	0.000060	20.8	196	0.282887	3.8	1.6	8.0	
55	17-LVD-027_88	0.282807	0.000044	0.00100	0.00006	0.0238	0.0017	1.467156	0.000060	20.9	205	0.282803	0.8	1.6	5.2	
56	17-LVD-027_89	0.282765	0.000053	0.00152	0.00010	0.0321	0.0019	1.467206	0.000065	16.8	190	0.282760	-0.7	1.9	3.3	
57	17-LVD-027_90	0.282818	0.000095	0.00099	0.00003	0.0235	0.0006	1.467120	0.000120	12.7	200	0.282814	1.2	3.4	5.5	
61	17-LVD-027_100	0.282984	0.000052	0.00139	0.00017	0.0328	0.0043	1.467187	0.000094	19.7	203	0.282979	7.0	1.8	11.4	
62	17-LVD-027_101	0.282784	0.000058	0.00113	0.00006	0.0240	0.0012	1.467173	0.000097	18.7	197	0.282780	0.0	2.1	4.2	
64	17-LVD-027_103	0.282868	0.000033	0.00144	0.00013	0.0350	0.0030	1.467210	0.000036	14.8	192	0.282863	2.9	1.2	7.0	

Whitehorse trough - Richthofen formation - Sample 17-LVD-030, Mount Byng (Zone 08V 539547E 6757952N NAD 83)

Grain	Spot ID	<i>corrected</i>		2SE	176Lu/ 177Hf	2SE	176Yb/ 177Hf	2SE	178Hf/ 177Hf	2SE	Total Hf Beam	MUN LASS Age (Ma)	176Hf/ 177Hf	EHf0	2SE	EHfi
		176Hf/ 177Hf	2SE													
2	17-LVD-030_019	0.282770	0.000020	0.00067	0.00002	0.0137	0.0004	1.467140	0.000029	14.2	202	0.282767	-0.5	0.7	3.9	
3	17-LVD-030_020	0.282896	0.000018	0.00102	0.00003	0.0265	0.0006	1.467192	0.000038	13.5	257	0.282891	3.9	0.6	9.5	
4	17-LVD-030_027	0.282779	0.000019	0.00056	0.00004	0.0113	0.0009	1.467163	0.000028	15.0	193	0.282777	-0.2	0.7	4.0	
5	17-LVD-030_028	0.282998	0.000032	0.00147	0.00012	0.0284	0.0029	1.467122	0.000041	14.3	209	0.282992	7.5	1.1	12.0	
6	17-LVD-030_029	0.282967	0.000038	0.00202	0.00011	0.0428	0.0026	1.467162	0.000039	15.2	204	0.282959	6.4	1.3	10.7	
7	17-LVD-030_030	0.282738	0.000023	0.00150	0.00013	0.0339	0.0025	1.467174	0.000040	13.8	224	0.282732	-1.7	0.8	3.1	
8	17-LVD-030_031	0.282727	0.000039	0.00140	0.00006	0.0316	0.0015	1.467175	0.000043	15.9	327	0.282718	-2.1	1.4	4.9	

Grain	Spot ID	corrected										MUN LASS Age (Ma)	176Hf/ 177Hf	EHf0	2SE	EHfi
		176Hf/ 177Hf	2SE	176Lu/ 177Hf	2SE	176Yb/ 177Hf	2SE	178Hf/ 177Hf	2SE	Total Hf Beam						
9	17-LVD-030_032	0.282779	0.000024	0.00055	0.00003	0.0112	0.0006	1.467193	0.000024	14.8	194	0.282777	-0.2	0.8	4.0	
10	17-LVD-030_033	0.282970	0.000034	0.00101	0.00008	0.0239	0.0021	1.467209	0.000039	14.9	207	0.282966	6.5	1.2	11.0	
12	17-LVD-030_035	0.282915	0.000031	0.00128	0.00002	0.0279	0.0005	1.467202	0.000035	13.0	187	0.282911	4.6	1.1	8.6	
13	17-LVD-030_036	0.282777	0.000023	0.00084	0.00004	0.0175	0.0007	1.467171	0.000028	15.2	192	0.282774	-0.3	0.8	3.9	
14	17-LVD-030_037	0.282800	0.000032	0.00092	0.00002	0.0203	0.0004	1.467208	0.000053	19.5	185	0.282797	0.5	1.1	4.5	
15	17-LVD-030_038	0.282744	0.000034	0.00094	0.00003	0.0253	0.0009	1.467200	0.000041	15.9	317	0.282738	-1.4	1.2	5.4	
20	17-LVD-030_049	0.282818	0.000031	0.00116	0.00011	0.0258	0.0028	1.467165	0.000043	15.2	198	0.282814	1.2	1.1	5.4	
21	17-LVD-030_050	0.282745	0.000029	0.00087	0.00006	0.0181	0.0011	1.467154	0.000025	18.5	199	0.282742	-1.4	1.0	2.9	
22	17-LVD-030_051	0.282755	0.000029	0.00071	0.00002	0.0147	0.0003	1.467243	0.000050	17.9	195	0.282752	-1.1	1.0	3.2	
24	17-LVD-030_053	0.282965	0.000046	0.00144	0.00021	0.0307	0.0043	1.467138	0.000051	14.8	207	0.282959	6.4	1.6	10.8	
25	17-LVD-030_054	0.282705	0.000032	0.00130	0.00008	0.0308	0.0021	1.467203	0.000039	15.1	332	0.282697	-2.8	1.1	4.3	
26	17-LVD-030_055	0.282771	0.000022	0.00095	0.00004	0.0198	0.0009	1.467195	0.000044	16.3	175	0.282768	-0.5	0.8	3.3	
27	17-LVD-030_056	0.282933	0.000022	0.00137	0.00010	0.0288	0.0020	1.467218	0.000029	12.7	189	0.282928	5.2	0.8	9.3	
29	17-LVD-030_064	0.282920	0.000018	0.00119	0.00008	0.0286	0.0020	1.467155	0.000029	14.9	212	0.282915	4.8	0.6	9.3	
30	17-LVD-030_065	0.282729	0.000023	0.00070	0.00005	0.0144	0.0009	1.467161	0.000028	15.4	196	0.282726	-2.0	0.8	2.3	
31	17-LVD-030_066	0.282773	0.000018	0.00076	0.00005	0.0166	0.0013	1.467154	0.000032	14.7	187	0.282770	-0.4	0.6	3.6	
33	17-LVD-030_068	0.282783	0.000016	0.00078	0.00004	0.0182	0.0006	1.467177	0.000041	16.1	217	0.282780	-0.1	0.6	4.6	
34	17-LVD-030_069	0.282867	0.000022	0.00093	0.00002	0.0252	0.0006	1.467191	0.000029	14.0	311	0.282862	2.9	0.8	9.6	
35	17-LVD-030_070	0.282743	0.000023	0.00034	0.00001	0.0072	0.0004	1.467129	0.000028	15.5	192	0.282742	-1.5	0.8	2.7	
36	17-LVD-030_071	0.282937	0.000030	0.00129	0.00004	0.0288	0.0009	1.467173	0.000033	15.4	223	0.282932	5.4	1.1	10.1	
38	17-LVD-030_073	0.282840	0.000033	0.00063	0.00003	0.0134	0.0006	1.467203	0.000040	17.2	187	0.282838	1.9	1.2	6.0	
39	17-LVD-030_074	0.282722	0.000025	0.00121	0.00006	0.0311	0.0019	1.467202	0.000042	16.5	258	0.282716	-2.2	0.9	3.3	
40	17-LVD-030_081	0.282758	0.000018	0.00074	0.00005	0.0158	0.0012	1.467215	0.000030	15.4	194	0.282755	-1.0	0.6	3.3	

Grain	Spot ID	corrected										MUN LASS Age (Ma)	$^{176}\text{Hf}/^{177}\text{Hf}$	EHf0	2SE	EHfi
		$^{176}\text{Hf}/^{177}\text{Hf}$	2SE	$^{176}\text{Lu}/^{177}\text{Hf}$	2SE	$^{176}\text{Yb}/^{177}\text{Hf}$	2SE	$^{178}\text{Hf}/^{177}\text{Hf}$	2SE	Total Hf Beam						
41	17-LVD-030_082	0.282751	0.000017	0.00043	0.00004	0.0104	0.0010	1.467174	0.000024	15.7	246	0.282749	-1.2	0.6	4.2	
42	17-LVD-030_083	0.282807	0.000032	0.00090	0.00007	0.0201	0.0014	1.467164	0.000043	18.5	206	0.282804	0.8	1.1	5.2	
43	17-LVD-030_084	0.282721	0.000026	0.00070	0.00006	0.0152	0.0013	1.467163	0.000041	21.2	248	0.282718	-2.3	0.9	3.1	
44	17-LVD-030_085	0.282847	0.000022	0.00102	0.00003	0.0250	0.0008	1.467159	0.000037	19.1	250	0.282842	2.2	0.8	7.6	
45	17-LVD-030_086	0.282812	0.000032	0.00115	0.00006	0.0270	0.0015	1.467208	0.000033	18.6	396	0.282803	1.0	1.1	9.5	
46	17-LVD-030_087	0.282794	0.000027	0.00135	0.00011	0.0313	0.0024	1.467208	0.000035	16.3	197	0.282789	0.3	1.0	4.5	
47	17-LVD-030_088	0.282787	0.000020	0.00081	0.00005	0.0170	0.0010	1.467178	0.000031	16.6	187	0.282784	0.1	0.7	4.1	
48	17-LVD-030_089	0.282784	0.000028	0.00145	0.00008	0.0335	0.0024	1.467179	0.000038	17.8	263	0.282777	0.0	1.0	5.6	
50	17-LVD-030_091	0.282963	0.000034	0.00291	0.00025	0.0711	0.0064	1.467185	0.000034	10.6	193	0.282953	6.3	1.2	10.2	
51	17-LVD-030_092	0.282920	0.000024	0.00058	0.00001	0.0136	0.0003	1.467193	0.000047	15.1	184	0.282918	4.8	0.8	8.8	
52	17-LVD-030_099	0.282858	0.000024	0.00117	0.00007	0.0296	0.0019	1.467182	0.000030	13.4	300	0.282851	2.6	0.8	9.0	
53	17-LVD-030_100	0.282791	0.000021	0.00089	0.00003	0.0190	0.0005	1.467211	0.000039	15.7	185	0.282788	0.2	0.7	4.2	
54	17-LVD-030_101	0.282782	0.000020	0.00091	0.00002	0.0191	0.0003	1.467149	0.000029	15.3	195	0.282779	-0.1	0.7	4.1	
55	17-LVD-030_102	0.282930	0.000024	0.00122	0.00015	0.0309	0.0038	1.467191	0.000035	12.0	205	0.282925	5.1	0.8	9.5	
56	17-LVD-030_103	0.282822	0.000034	0.00121	0.00004	0.0308	0.0011	1.467153	0.000053	15.6	298	0.282815	1.3	1.2	7.7	
57	17-LVD-030_104	0.282806	0.000020	0.00088	0.00004	0.0191	0.0011	1.467176	0.000031	14.7	279	0.282801	0.7	0.7	6.8	
58	17-LVD-030_105	0.282760	0.000019	0.00075	0.00003	0.0162	0.0006	1.467203	0.000036	13.8	184	0.282757	-0.9	0.7	3.1	
59	17-LVD-030_106	0.282712	0.000027	0.00200	0.00010	0.0492	0.0028	1.467183	0.000035	12.6	329	0.282700	-2.6	1.0	4.3	
60	17-LVD-030_107	0.282818	0.000023	0.00142	0.00013	0.0380	0.0036	1.467204	0.000043	14.3	330	0.282809	1.2	0.8	8.2	
61	17-LVD-030_108	0.282911	0.000041	0.00101	0.00008	0.0229	0.0020	1.467223	0.000052	13.4	209	0.282907	4.5	1.4	9.0	
64	17-LVD-030_111	0.282784	0.000029	0.00111	0.00005	0.0237	0.0012	1.467234	0.000049	16.9	198	0.282780	0.0	1.0	4.2	
65	17-LVD-030_118	0.282758	0.000029	0.00105	0.00009	0.0228	0.0021	1.467221	0.000059	15.7	211	0.282754	-1.0	1.0	3.6	
66	17-LVD-030_119	0.282358	0.000024	0.00093	0.00007	0.0276	0.0017	1.467191	0.000041	16.0	419	0.282351	-15.1	0.8	-6.0	

Grain	Spot ID	corrected										MUN LASS Age (Ma)	$^{176}\text{Hf}/^{177}\text{Hf}$	EHf0	2SE	EHfi
		$^{176}\text{Hf}/^{177}\text{Hf}$	2SE	$^{176}\text{Lu}/^{177}\text{Hf}$	2SE	$^{176}\text{Yb}/^{177}\text{Hf}$	2SE	$^{178}\text{Hf}/^{177}\text{Hf}$	2SE	Total Hf Beam						
68	17-LVD-030_121	0.282954	0.000022	0.00092	0.00004	0.0223	0.0008	1.467171	0.000037	10.9	222	0.282950	6.0	0.8	10.8	
69	17-LVD-030_122	0.282726	0.000023	0.00150	0.00011	0.0405	0.0031	1.467182	0.000037	13.9	335	0.282717	-2.1	0.8	5.0	
70	17-LVD-030_123	0.282759	0.000025	0.00107	0.00006	0.0230	0.0014	1.467195	0.000051	15.4	191	0.282755	-0.9	0.9	3.2	
71	17-LVD-030_124	0.282796	0.000030	0.00150	0.00019	0.0384	0.0050	1.467180	0.000034	15.4	316	0.282787	0.4	1.1	7.1	
72	17-LVD-030_125	0.282887	0.000029	0.00146	0.00006	0.0325	0.0014	1.467142	0.000045	12.0	210	0.282881	3.6	1.0	8.1	
73	17-LVD-030_126	0.282827	0.000030	0.00063	0.00005	0.0133	0.0008	1.467212	0.000033	14.8	232	0.282824	1.5	1.1	6.6	
74	17-LVD-030_127	0.282771	0.000032	0.00094	0.00009	0.0204	0.0019	1.467187	0.000046	15.2	207	0.282767	-0.5	1.1	4.0	
75	17-LVD-030_128	0.282795	0.000024	0.00120	0.00005	0.0282	0.0014	1.467153	0.000027	14.0	314	0.282788	0.4	0.8	7.1	
76	17-LVD-030_129	0.282706	0.000033	0.00172	0.00017	0.0472	0.0053	1.467193	0.000045	12.4	325	0.282696	-2.8	1.2	4.1	
77	17-LVD-030_010	0.282970	0.000020	0.00085	0.00006	0.0212	0.0018	1.467210	0.000029	18.4	195	0.282967	6.5	0.7	10.8	
78	17-LVD-030_011	0.282970	0.000027	0.00149	0.00007	0.0314	0.0018	1.467185	0.000039	15.1	196	0.282965	6.5	1.0	10.7	
82	17-LVD-030_015	0.282785	0.000029	0.00140	0.00002	0.0330	0.0003	1.467219	0.000035	16.0	182	0.282780	0.0	1.0	3.9	
83	17-LVD-030_016	0.282751	0.000021	0.00068	0.00006	0.0143	0.0013	1.467196	0.000033	14.5	199	0.282748	-1.2	0.7	3.1	
84	17-LVD-030_017	0.282853	0.000026	0.00233	0.00020	0.0654	0.0059	1.467184	0.000034	11.5	300	0.282840	2.4	0.9	8.6	
85	17-LVD-030_018	0.282904	0.000029	0.00154	0.00007	0.0360	0.0014	1.467216	0.000030	13.1	192	0.282898	4.2	1.0	8.3	
86	17-LVD-030_019	0.282751	0.000019	0.00102	0.00004	0.0223	0.0008	1.467181	0.000030	13.3	201	0.282747	-1.2	0.7	3.1	
88	17-LVD-030_021	0.282333	0.000029	0.00148	0.00008	0.0458	0.0024	1.467163	0.000043	13.4	393	0.282322	-16.0	1.0	-7.6	
90	17-LVD-030_029	0.282776	0.000022	0.00047	0.00004	0.0102	0.0007	1.467173	0.000028	14.8	216	0.282774	-0.3	0.8	4.4	
91	17-LVD-030_030	0.282953	0.000031	0.00310	0.00045	0.0960	0.0150	1.467165	0.000036	11.2	289	0.282936	5.9	1.1	11.8	
92	17-LVD-030_031	0.282801	0.000019	0.00123	0.00005	0.0289	0.0016	1.467191	0.000028	14.2	205	0.282796	0.6	0.7	5.0	
93	17-LVD-030_032	0.282771	0.000017	0.00093	0.00003	0.0203	0.0007	1.467175	0.000034	14.2	207	0.282767	-0.5	0.6	4.0	
94	17-LVD-030_033	0.282783	0.000023	0.00205	0.00010	0.0566	0.0025	1.467188	0.000040	14.4	337	0.282770	-0.1	0.8	7.0	
95	17-LVD-030_034	0.282805	0.000022	0.00078	0.00004	0.0200	0.0017	1.467161	0.000030	15.3	304	0.282801	0.7	0.8	7.3	

Grain	Spot ID	<i>corrected</i>		2SE	176Lu/ 177Hf	2SE	176Yb/ 177Hf	2SE	178Hf/ 177Hf	2SE	Total Hf Beam	MUN LASS Age (Ma)	176Hf/ 177Hf	EHf0	2SE	EHf1
		176Hf/ 177Hf	2SE													
96	17-LVD-030_035	0.282756	0.000022	0.00119	0.00004	0.0338	0.0013	1.467177	0.000030	13.3	287	0.282750	-1.0	0.8	5.1	
97	17-LVD-030_036	0.282825	0.000025	0.00128	0.00014	0.0323	0.0037	1.467155	0.000032	12.6	300	0.282818	1.4	0.9	7.8	
98	17-LVD-030_037	0.282917	0.000025	0.00168	0.00010	0.0387	0.0029	1.467206	0.000038	12.1	210	0.282910	4.7	0.9	9.1	
99	17-LVD-030_038	0.282793	0.000018	0.00135	0.00019	0.0348	0.0055	1.467169	0.000030	14.2	193	0.282788	0.3	0.6	4.4	
100	17-LVD-030_039	0.282918	0.000021	0.00167	0.00005	0.0356	0.0010	1.467176	0.000030	12.2	190	0.282912	4.7	0.7	8.7	
101	17-LVD-030_046	0.282848	0.000018	0.00065	0.00002	0.0154	0.0004	1.467192	0.000030	13.2	328	0.282844	2.2	0.6	9.4	
102	17-LVD-030_047	0.282686	0.000025	0.00083	0.00006	0.0230	0.0015	1.467203	0.000032	12.5	316	0.282681	-3.5	0.9	3.4	
103	17-LVD-030_048	0.282745	0.000020	0.00042	0.00001	0.0092	0.0002	1.467224	0.000028	15.6	197	0.282743	-1.4	0.7	2.9	
104	17-LVD-030_049	0.282835	0.000031	0.00085	0.00005	0.0216	0.0014	1.467178	0.000030	14.4	307	0.282830	1.8	1.1	8.4	
105	17-LVD-030_050	0.282713	0.000020	0.00086	0.00003	0.0190	0.0006	1.467170	0.000031	15.9	198	0.282710	-2.5	0.7	1.7	
Rejected Analysis																
1	17-LVD-030_018	0.282817	0.000023	0.00099	0.00007	0.0224	0.0018	1.467190	0.000028	14.6	322	0.282811	1.1	0.8	8.1	
11	17-LVD-030_034	0.282853	0.000066	0.00076	0.00006	0.0158	0.0013	1.467201	0.000080	18.7	188	0.282850	2.4	2.3	6.5	
16	17-LVD-030_045	0.282796	0.000032	0.00070	0.00009	0.0147	0.0018	1.467138	0.000060	16.6	185	0.282794	0.4	1.1	4.4	
17	17-LVD-030_046	0.282947	0.000034	0.00072	0.00008	0.0142	0.0015	1.467176	0.000046	11.7	174	0.282945	5.7	1.2	9.5	
18	17-LVD-030_047	0.282852	0.000038	0.00251	0.00050	0.0600	0.0120	1.467173	0.000049	12.6	248	0.282840	2.4	1.3	7.5	
19	17-LVD-030_048	0.282790	0.000035	0.00095	0.00004	0.0203	0.0007	1.467183	0.000045	17.4	191	0.282787	0.2	1.2	4.3	
23	17-LVD-030_052	0.282667	0.000033	0.00359	0.00030	0.0964	0.0079	1.467173	0.000038	25.2	262	0.282649	-4.2	1.2	1.0	
28	17-LVD-030_063	0.282857	0.000030	0.00027	0.00001	0.0063	0.0003	1.467185	0.000048	17.2	298	0.282855	2.5	1.1	9.1	
32	17-LVD-030_067	0.282914	0.000021	0.00082	0.00003	0.0175	0.0006	1.467161	0.000042	11.1	209	0.282911	4.6	0.7	9.1	
37	17-LVD-030_072	0.281633	0.000042	0.00102	0.00006	0.0270	0.0015	1.467151	0.000047	18.2	573	0.281622	-40.7	1.5	-28.4	
49	17-LVD-030_090	0.282781	0.000027	0.00070	0.00003	0.0148	0.0007	1.467169	0.000038	17.8	196	0.282778	-0.1	1.0	4.1	
62	17-LVD-030_109	0.282674	0.000038	0.00176	0.00007	0.0448	0.0024	1.467119	0.000043	18.1	378	0.282662	-3.9	1.3	4.1	

Grain	Spot ID	<i>corrected</i>		2SE	176Lu/ 177Hf	2SE	176Yb/ 177Hf	2SE	178Hf/ 177Hf	2SE	Total Hf Beam	MUN LASS Age (Ma)	176Hf/ 177Hf	EHf0	2SE	EHfi
		176Hf/ 177Hf	2SE													
63	17-LVD-030_110	0.282760	0.000120	0.00102	0.00003	0.0224	0.0002	1.467193	0.000036	18.8	209	0.282756	-0.9	4.2	3.6	
67	17-LVD-030_120	0.282786	0.000021	0.00126	0.00005	0.0297	0.0016	1.467182	0.000033	14.8	238	0.282780	0.0	0.7	5.1	
79	17-LVD-030_012	0.282838	0.000033	0.00144	0.00009	0.0360	0.0028	1.467203	0.000041	12.5	297	0.282830	1.9	1.2	8.2	
80	17-LVD-030_013	0.282817	0.000025	0.00079	0.00003	0.0193	0.0006	1.467196	0.000043	18.8	287	0.282813	1.1	0.9	7.4	
81	17-LVD-030_014	0.282842	0.000025	0.00094	0.00011	0.0223	0.0028	1.467185	0.000031	16.7	260	0.282837	2.0	0.9	7.6	
87	17-LVD-030_020	0.282746	0.000024	0.00100	0.00004	0.0216	0.0008	1.467174	0.000027	15.8	230	0.282742	-1.4	0.8	3.6	
89	17-LVD-030_028	0.282773	0.000016	0.00082	0.00004	0.0200	0.0007	1.467179	0.000024	18.9	179	0.282770	-0.4	0.6	3.5	

Whitehorse trough - Richthofen formation - Sample 17-LVD-034, Mount Slim (Zone 08V 514475E 6751661N NAD 83)

Grain	Spot ID	<i>corrected</i>		2SE	176Lu/ 177Hf	2SE	176Yb/ 177Hf	2SE	178Hf/ 177Hf	2SE	Total Hf Beam	MUN LASS Age (Ma)	176Hf/ 177Hf	EHf0	2SE	EHfi
		176Hf/ 177Hf	2SE													
1	17-LVD-034_10	0.282932	0.000028	0.00093	0.00005	0.0197	0.0009	1.467137	0.000037	7.7	214	0.282928	5.2	1.0	9.8	
2	17-LVD-034_11	0.282521	0.000024	0.00093	0.00008	0.0259	0.0022	1.467147	0.000031	11.4	329	0.282515	-9.3	0.8	-2.2	
4	17-LVD-034_13	0.282778	0.000018	0.00074	0.00002	0.0175	0.0005	1.467155	0.000031	13.8	212	0.282775	-0.2	0.6	4.4	
5	17-LVD-034_14	0.282745	0.000024	0.00046	0.00006	0.0125	0.0017	1.467179	0.000031	12.7	312	0.282742	-1.4	0.8	5.4	
6	17-LVD-034_15	0.282921	0.000025	0.00134	0.00004	0.0285	0.0008	1.467183	0.000037	11.2	205	0.282916	4.8	0.9	9.2	
7	17-LVD-034_16	0.282856	0.000026	0.00073	0.00006	0.0175	0.0013	1.467182	0.000045	10.6	336	0.282851	2.5	0.9	9.8	
8	17-LVD-034_17	0.282795	0.000016	0.00044	0.00002	0.0104	0.0006	1.467215	0.000038	13.1	204	0.282793	0.4	0.6	4.8	
9	17-LVD-034_18	0.282946	0.000021	0.00165	0.00010	0.0346	0.0019	1.467182	0.000033	11.6	226	0.282939	5.7	0.7	10.5	
10	17-LVD-034_19	0.282806	0.000021	0.00041	0.00001	0.0108	0.0002	1.467150	0.000034	13.4	329	0.282803	0.7	0.7	8.0	
11	17-LVD-034_20	0.282627	0.000026	0.00113	0.00005	0.0317	0.0015	1.467192	0.000031	11.2	333	0.282620	-5.6	0.9	1.6	

Grain	Spot ID	corrected										MUN LASS Age (Ma)	$^{176}\text{Hf}/^{177}\text{Hf}$	EHf0	2SE	EHfi
		$^{176}\text{Hf}/^{177}\text{Hf}$	2SE	$^{176}\text{Lu}/^{177}\text{Hf}$	2SE	$^{176}\text{Yb}/^{177}\text{Hf}$	2SE	$^{178}\text{Hf}/^{177}\text{Hf}$	2SE	Total Hf Beam						
12	17-LVD-034_21	0.282787	0.000024	0.00058	0.00002	0.0147	0.0004	1.467162	0.000035	12.7	338	0.282783	0.1	0.8	7.5	
13	17-LVD-034_28	0.282784	0.000023	0.00099	0.00003	0.0247	0.0009	1.467167	0.000030	12.7	202	0.282780	0.0	0.8	4.3	
14	17-LVD-034_29	0.282822	0.000023	0.00106	0.00002	0.0284	0.0006	1.467221	0.000030	11.6	341	0.282815	1.3	0.8	8.7	
15	17-LVD-034_30	0.282772	0.000031	0.00293	0.00019	0.0806	0.0052	1.467166	0.000033	9.5	327	0.282754	-0.5	1.1	6.2	
17	17-LVD-034_32	0.282957	0.000022	0.00121	0.00005	0.0264	0.0014	1.467162	0.000042	13.6	210	0.282952	6.1	0.8	10.6	
18	17-LVD-034_33	0.282650	0.000027	0.00067	0.00003	0.0144	0.0007	1.467217	0.000042	10.8	340	0.282646	-4.8	1.0	2.7	
19	17-LVD-034_34	0.282550	0.000020	0.00089	0.00005	0.0253	0.0014	1.467188	0.000035	12.4	331	0.282544	-8.3	0.7	-1.1	
20	17-LVD-034_35	0.282814	0.000021	0.00104	0.00002	0.0265	0.0003	1.467128	0.000029	13.7	332	0.282808	1.0	0.7	8.2	
21	17-LVD-034_36	0.282775	0.000025	0.00063	0.00003	0.0158	0.0008	1.467180	0.000034	11.9	329	0.282771	-0.4	0.9	6.8	
22	17-LVD-034_37	0.282775	0.000025	0.00042	0.00003	0.0082	0.0005	1.467196	0.000039	10.9	345	0.282772	-0.4	0.9	7.2	
23	17-LVD-034_38	0.282891	0.000026	0.00143	0.00011	0.0328	0.0026	1.467183	0.000037	11.4	333	0.282882	3.7	0.9	10.8	
24	17-LVD-034_39	0.282866	0.000022	0.00109	0.00004	0.0246	0.0009	1.467162	0.000029	11.9	331	0.282859	2.9	0.8	10.0	
25	17-LVD-034_46	0.282793	0.000022	0.00175	0.00006	0.0462	0.0016	1.467187	0.000035	10.4	339	0.282782	0.3	0.8	7.4	
26	17-LVD-034_47	0.282749	0.000025	0.00198	0.00011	0.0489	0.0028	1.467224	0.000030	13.1	350	0.282736	-1.3	0.9	6.1	
27	17-LVD-034_48	0.282867	0.000027	0.00109	0.00006	0.0293	0.0017	1.467176	0.000032	12.7	335	0.282860	2.9	1.0	10.1	
28	17-LVD-034_49	0.282677	0.000025	0.00078	0.00001	0.0195	0.0002	1.467181	0.000040	10.9	317	0.282672	-3.8	0.9	3.1	
29	17-LVD-034_50	0.282791	0.000024	0.00080	0.00007	0.0187	0.0016	1.467199	0.000036	12.3	225	0.282788	0.2	0.8	5.1	
30	17-LVD-034_51	0.282857	0.000037	0.00161	0.00008	0.0451	0.0020	1.467222	0.000037	16.1	301	0.282848	2.5	1.3	8.9	
31	17-LVD-034_52	0.282809	0.000027	0.00092	0.00001	0.0221	0.0004	1.467137	0.000050	16.6	217	0.282805	0.8	1.0	5.5	
32	17-LVD-034_53	0.282898	0.000036	0.00072	0.00009	0.0161	0.0019	1.467188	0.000062	12.6	227	0.282895	4.0	1.3	8.9	
33	17-LVD-034_54	0.282818	0.000019	0.00106	0.00003	0.0249	0.0007	1.467225	0.000036	12.4	197	0.282814	1.2	0.7	5.4	
34	17-LVD-034_55	0.282881	0.000021	0.00114	0.00003	0.0272	0.0006	1.467209	0.000046	11.4	317	0.282874	3.4	0.7	10.2	
36	17-LVD-034_57	0.282747	0.000031	0.00174	0.00007	0.0470	0.0021	1.467158	0.000034	12.1	324	0.282736	-1.3	1.1	5.5	

Grain	Spot ID	corrected										MUN LASS Age (Ma)	$^{176}\text{Hf}/^{177}\text{Hf}$	EHf0	2SE	EHfi
		$^{176}\text{Hf}/^{177}\text{Hf}$	2SE	$^{176}\text{Lu}/^{177}\text{Hf}$	2SE	$^{176}\text{Yb}/^{177}\text{Hf}$	2SE	$^{178}\text{Hf}/^{177}\text{Hf}$	2SE	Total Hf Beam						
37	17-LVD-034_64	0.282797	0.000021	0.00062	0.00003	0.0138	0.0007	1.467202	0.000029	14.3	203	0.282795	0.4	0.7	4.9	
38	17-LVD-034_65	0.282698	0.000024	0.00079	0.00007	0.0184	0.0014	1.467178	0.000032	13.0	244	0.282694	-3.1	0.8	2.2	
39	17-LVD-034_66	0.282576	0.000023	0.00056	0.00004	0.0113	0.0008	1.467189	0.000032	13.1	201	0.282574	-7.4	0.8	-3.0	
40	17-LVD-034_67	0.282797	0.000029	0.00235	0.00012	0.0583	0.0028	1.467159	0.000043	11.7	330	0.282782	0.4	1.0	7.3	
41	17-LVD-034_68	0.282784	0.000019	0.00102	0.00003	0.0223	0.0007	1.467154	0.000034	13.4	201	0.282780	0.0	0.7	4.3	
43	17-LVD-034_70	0.282791	0.000028	0.00099	0.00004	0.0224	0.0008	1.467141	0.000037	13.6	199	0.282787	0.2	1.0	4.5	
44	17-LVD-034_71	0.282931	0.000026	0.00084	0.00010	0.0188	0.0019	1.467160	0.000040	12.3	207	0.282928	5.2	0.9	9.6	
46	17-LVD-034_73	0.282637	0.000029	0.00078	0.00005	0.0168	0.0011	1.467174	0.000033	12.7	204	0.282634	-5.2	1.0	-0.8	
48	17-LVD-034_75	0.282795	0.000027	0.00280	0.00013	0.0756	0.0037	1.467147	0.000038	13.3	329	0.282778	0.4	1.0	7.1	
49	17-LVD-034_82	0.282764	0.000031	0.00198	0.00005	0.0489	0.0012	1.467180	0.000045	10.1	339	0.282751	-0.7	1.1	6.4	
50	17-LVD-034_83	0.282823	0.000036	0.00131	0.00010	0.0310	0.0022	1.467190	0.000043	12.2	178	0.282819	1.3	1.3	5.1	
51	17-LVD-034_84	0.282819	0.000019	0.00075	0.00002	0.0182	0.0003	1.467151	0.000040	14.2	186	0.282816	1.2	0.7	5.2	
52	17-LVD-034_85	0.282673	0.000020	0.00127	0.00009	0.0284	0.0019	1.467199	0.000040	13.8	200	0.282668	-4.0	0.7	0.3	
54	17-LVD-034_87	0.282788	0.000025	0.00063	0.00004	0.0145	0.0009	1.467186	0.000031	13.3	195	0.282786	0.1	0.9	4.4	
55	17-LVD-034_88	0.282717	0.000022	0.00078	0.00002	0.0207	0.0007	1.467189	0.000043	11.2	303	0.282713	-2.4	0.8	4.2	
56	17-LVD-034_89	0.282765	0.000023	0.00081	0.00003	0.0178	0.0006	1.467204	0.000031	13.3	262	0.282761	-0.7	0.8	5.0	
57	17-LVD-034_90	0.282635	0.000020	0.00068	0.00001	0.0141	0.0002	1.467125	0.000025	11.6	315	0.282631	-5.3	0.7	1.6	
58	17-LVD-034_91	0.282712	0.000023	0.00049	0.00001	0.0106	0.0002	1.467153	0.000031	15.6	284	0.282709	-2.6	0.8	3.7	
59	17-LVD-034_92	0.282706	0.000025	0.00120	0.00003	0.0270	0.0007	1.467204	0.000040	11.8	208	0.282701	-2.8	0.9	1.7	
60	17-LVD-034_93	0.282891	0.000027	0.00087	0.00009	0.0222	0.0024	1.467217	0.000046	11.0	317	0.282886	3.7	1.0	10.6	
61	17-LVD-034_100	0.282737	0.000029	0.00156	0.00010	0.0398	0.0024	1.467225	0.000038	11.2	332	0.282727	-1.7	1.0	5.4	
62	17-LVD-034_101	0.282733	0.000029	0.00182	0.00005	0.0475	0.0012	1.467183	0.000035	12.1	334	0.282722	-1.8	1.0	5.2	
63	17-LVD-034_102	0.282793	0.000020	0.00073	0.00002	0.0178	0.0003	1.467160	0.000043	15.4	193	0.282790	0.3	0.7	4.5	

Grain	Spot ID	corrected										MUN LASS Age (Ma)	$^{176}\text{Hf}/^{177}\text{Hf}$	EHf0	2SE	EHfi
		$^{176}\text{Hf}/^{177}\text{Hf}$	2SE	$^{176}\text{Lu}/^{177}\text{Hf}$	2SE	$^{176}\text{Yb}/^{177}\text{Hf}$	2SE	$^{178}\text{Hf}/^{177}\text{Hf}$	2SE	Total Hf Beam						
64	17-LVD-034_103	0.282729	0.000019	0.00091	0.00002	0.0230	0.0002	1.467157	0.000025	13.5	325	0.282723	-2.0	0.7	5.1	
65	17-LVD-034_104	0.282831	0.000029	0.00101	0.00008	0.0228	0.0017	1.467146	0.000050	14.2	195	0.282827	1.6	1.0	5.8	
66	17-LVD-034_105	0.282856	0.000021	0.00149	0.00010	0.0364	0.0025	1.467216	0.000035	10.5	339	0.282847	2.5	0.7	9.7	
67	17-LVD-034_106	0.282826	0.000022	0.00083	0.00006	0.0189	0.0013	1.467167	0.000041	12.5	185	0.282823	1.4	0.8	5.5	
69	17-LVD-034_108	0.282902	0.000029	0.00176	0.00027	0.0406	0.0062	1.467189	0.000038	10.5	322	0.282891	4.1	1.0	10.9	
70	17-LVD-034_109	0.282793	0.000017	0.00056	0.00002	0.0127	0.0003	1.467155	0.000030	13.3	195	0.282791	0.3	0.6	4.5	
71	17-LVD-034_110	0.282806	0.000023	0.00133	0.00008	0.0306	0.0018	1.467192	0.000038	14.3	201	0.282801	0.7	0.8	5.0	
72	17-LVD-034_111	0.282639	0.000022	0.00064	0.00002	0.0164	0.0003	1.467220	0.000033	12.0	305	0.282635	-5.2	0.8	1.5	
73	17-LVD-034_118	0.282705	0.000022	0.00092	0.00008	0.0246	0.0021	1.467192	0.000039	12.1	325	0.282699	-2.8	0.8	4.2	
75	17-LVD-034_120	0.282718	0.000020	0.00076	0.00002	0.0196	0.0006	1.467198	0.000034	11.1	319	0.282713	-2.4	0.7	4.6	
76	17-LVD-034_121	0.282810	0.000029	0.00212	0.00008	0.0475	0.0019	1.467201	0.000036	8.8	335	0.282797	0.9	1.0	7.9	
77	17-LVD-034_122	0.281053	0.000023	0.00032	0.00003	0.0093	0.0009	1.467201	0.000031	12.3	2263	0.281039	-61.2	0.8	-10.8	
79	17-LVD-034_124	0.282619	0.000018	0.00093	0.00001	0.0237	0.0003	1.467182	0.000047	10.6	311	0.282614	-5.9	0.6	0.9	
80	17-LVD-034_125	0.282525	0.000022	0.00134	0.00008	0.0366	0.0021	1.467182	0.000038	11.4	306	0.282517	-9.2	0.8	-2.7	
81	17-LVD-034_126	0.282773	0.000027	0.00065	0.00002	0.0145	0.0004	1.467157	0.000034	13.3	189	0.282771	-0.4	1.0	3.7	
82	17-LVD-034_127	0.282773	0.000028	0.00223	0.00004	0.0530	0.0011	1.467162	0.000038	11.1	328	0.282759	-0.4	1.0	6.4	
83	17-LVD-034_128	0.282750	0.000028	0.00136	0.00006	0.0310	0.0015	1.467188	0.000028	11.2	309	0.282742	-1.2	1.0	5.4	
84	17-LVD-034_129	0.282798	0.000018	0.00092	0.00006	0.0214	0.0013	1.467187	0.000034	11.8	196	0.282795	0.5	0.6	4.7	
85	17-LVD-034_137	0.282804	0.000016	0.00063	0.00003	0.0141	0.0005	1.467204	0.000038	13.8	203	0.282802	0.7	0.6	5.1	
86	17-LVD-034_138	0.282914	0.000021	0.00100	0.00003	0.0215	0.0008	1.467152	0.000030	13.9	200	0.282910	4.6	0.7	8.9	
87	17-LVD-034_139	0.282821	0.000029	0.00111	0.00015	0.0266	0.0038	1.467208	0.000043	12.4	321	0.282814	1.3	1.0	8.2	
88	17-LVD-034_140	0.282765	0.000021	0.00113	0.00006	0.0252	0.0014	1.467152	0.000035	11.1	302	0.282759	-0.7	0.7	5.8	
89	17-LVD-034_141	0.282729	0.000019	0.00079	0.00000	0.0201	0.0002	1.467184	0.000033	11.6	330	0.282724	-2.0	0.7	5.2	

Grain	Spot ID	<i>corrected</i>										MUN LASS Age (Ma)	176Hf/ 177Hf	EHf0	2SE	EHfi
		176Hf/ 177Hf	2SE	176Lu/ 177Hf	2SE	176Yb/ 177Hf	2SE	178Hf/ 177Hf	2SE	Total Hf Beam						
90	17-LVD-034_142	0.282817	0.000024	0.00081	0.00002	0.0185	0.0004	1.467155	0.000040	11.6	200	0.282814	1.1	0.8	5.5	
91	17-LVD-034_143	0.282626	0.000027	0.00102	0.00005	0.0218	0.0009	1.467174	0.000039	9.5	331	0.282620	-5.6	1.0	1.5	
92	17-LVD-034_144	0.282850	0.000027	0.00158	0.00019	0.0427	0.0051	1.467170	0.000038	12.0	309	0.282841	2.3	1.0	8.9	
Rejected Analysis																
3	17-LVD-034_12	0.282734	0.000028	0.00130	0.00008	0.0332	0.0022	1.467212	0.000035	10.9	337	0.282726	-1.8	1.0	5.4	
16	17-LVD-034_31	0.282939	0.000033	0.00171	0.00010	0.0380	0.0020	1.467186	0.000053	11.8	204	0.282932	5.4	1.2	9.8	
35	17-LVD-034_56	0.282782	0.000017	0.00058	0.00001	0.0152	0.0002	1.467177	0.000037	12.6	320	0.282779	-0.1	0.6	6.9	
42	17-LVD-034_69	0.282977	0.000034	0.00125	0.00013	0.0288	0.0037	1.467257	0.000055	11.5	208	0.282972	6.8	1.2	11.3	
45	17-LVD-034_72	0.282362	0.000039	0.00147	0.00005	0.0391	0.0012	1.467191	0.000057	9.8	850	0.282339	-15.0	1.4	3.2	
47	17-LVD-034_74	0.282810	0.000025	0.00106	0.00010	0.0272	0.0029	1.467219	0.000040	11.2	309	0.282804	0.9	0.9	7.5	
53	17-LVD-034_86	0.282904	0.000025	0.00048	0.00006	0.0113	0.0016	1.467185	0.000038	13.3	291	0.282901	4.2	0.9	10.6	
68	17-LVD-034_107	0.282828	0.000033	0.00182	0.00028	0.0451	0.0080	1.467192	0.000042	13.4	368	0.282815	1.5	1.2	9.3	
74	17-LVD-034_119	0.282733	0.000038	0.00130	0.00008	0.0327	0.0017	1.467179	0.000036	12.3	201	0.282728	-1.8	1.3	2.5	
78	17-LVD-034_123	0.282704	0.000029	0.00128	0.00012	0.0313	0.0027	1.467192	0.000043	10.3	308	0.282697	-2.9	1.0	3.7	

Whitehorse trough - Richthofen formation - Sample 17-LVD-038, King Lake (Zone 08V 474374E 6742564N NAD 83)

Grain	Spot ID	<i>corrected</i>										MUN LASS Age (Ma)	176Hf/ 177Hf	EHf0	2SE	EHfi
		176Hf/ 177Hf	2SE	176Lu/ 177Hf	2SE	176Yb/ 177Hf	2SE	178Hf/ 177Hf	2SE	Total Hf Beam						
1	17-LVD-038_105	0.282588	0.000023	0.00083	0.00002	0.0192	0.0004	1.467220	0.000037	14.4	195	0.282585	-7.0	0.8	-2.7	
2	17-LVD-038_106	0.282557	0.000020	0.00115	0.00005	0.0270	0.0013	1.467218	0.000033	17.2	188	0.282553	-8.1	0.7	-4.0	
4	17-LVD-038_108	0.282586	0.000020	0.00104	0.00005	0.0243	0.0013	1.467199	0.000031	13.9	190	0.282582	-7.0	0.7	-2.9	

Grain	Spot ID	corrected										MUN LASS Age (Ma)	$^{176}\text{Hf}/^{177}\text{Hf}$	EHf0	2SE	EHfi
		$^{176}\text{Hf}/^{177}\text{Hf}$	2SE	$^{176}\text{Lu}/^{177}\text{Hf}$	2SE	$^{176}\text{Yb}/^{177}\text{Hf}$	2SE	$^{178}\text{Hf}/^{177}\text{Hf}$	2SE	Total Hf Beam						
5	17-LVD-038_109	0.282594	0.000031	0.00121	0.00006	0.0289	0.0014	1.467174	0.000041	16.8	197	0.282590	-6.8	1.1	-2.5	
6	17-LVD-038_110	0.282587	0.000032	0.00193	0.00014	0.0445	0.0033	1.467200	0.000032	11.3	187	0.282580	-7.0	1.1	-3.1	
7	17-LVD-038_111	0.282585	0.000021	0.00143	0.00009	0.0352	0.0023	1.467198	0.000031	13.3	176	0.282580	-7.1	0.7	-3.3	
8	17-LVD-038_122	0.282546	0.000021	0.00112	0.00004	0.0270	0.0011	1.467154	0.000046	17.0	187	0.282542	-8.5	0.7	-4.4	
10	17-LVD-038_124	0.282558	0.000024	0.00102	0.00004	0.0247	0.0011	1.467169	0.000037	15.6	199	0.282554	-8.0	0.8	-3.7	
12	17-LVD-038_126	0.282556	0.000022	0.00119	0.00011	0.0274	0.0026	1.467168	0.000032	19.6	190	0.282552	-8.1	0.8	-4.0	
13	17-LVD-038_127	0.282566	0.000022	0.00121	0.00005	0.0292	0.0012	1.467190	0.000029	14.2	198	0.282561	-7.7	0.8	-3.5	
14	17-LVD-038_128	0.282580	0.000018	0.00105	0.00004	0.0249	0.0011	1.467178	0.000030	14.1	189	0.282576	-7.2	0.6	-3.2	
15	17-LVD-038_129	0.282714	0.000026	0.00117	0.00004	0.0239	0.0009	1.467180	0.000029	14.4	190	0.282710	-2.5	0.9	1.6	
16	17-LVD-038_130	0.282591	0.000030	0.00171	0.00018	0.0421	0.0046	1.467143	0.000033	14.8	193	0.282585	-6.9	1.1	-2.8	
17	17-LVD-038_131	0.282578	0.000014	0.00115	0.00003	0.0278	0.0010	1.467199	0.000027	14.1	193	0.282574	-7.3	0.5	-3.2	
18	17-LVD-038_132	0.282548	0.000015	0.00079	0.00001	0.0191	0.0003	1.467226	0.000030	16.2	203	0.282545	-8.4	0.5	-4.0	
19	17-LVD-038_133	0.282572	0.000018	0.00107	0.00006	0.0256	0.0015	1.467167	0.000039	14.5	200	0.282568	-7.5	0.6	-3.2	
20	17-LVD-038_009	0.282566	0.000031	0.00103	0.00003	0.0244	0.0008	1.467219	0.000044	17.3	175	0.282563	-7.7	1.1	-4.0	
21	17-LVD-038_010	0.282560	0.000027	0.00100	0.00002	0.0238	0.0004	1.467157	0.000032	13.0	183	0.282557	-8.0	1.0	-4.0	
22	17-LVD-038_011	0.282610	0.000023	0.00094	0.00005	0.0221	0.0013	1.467132	0.000034	13.1	172	0.282607	-6.2	0.8	-2.5	
23	17-LVD-038_012	0.282552	0.000023	0.00120	0.00008	0.0290	0.0020	1.467145	0.000038	16.5	195	0.282548	-8.2	0.8	-4.1	
24	17-LVD-038_013	0.282802	0.000031	0.00160	0.00006	0.0380	0.0016	1.467139	0.000037	11.8	192	0.282796	0.6	1.1	4.7	
25	17-LVD-038_014	0.282810	0.000022	0.00124	0.00003	0.0237	0.0005	1.467166	0.000041	13.3	192	0.282806	0.9	0.8	5.0	
27	17-LVD-038_016	0.282572	0.000024	0.00123	0.00005	0.0295	0.0014	1.467188	0.000030	13.1	181	0.282568	-7.5	0.8	-3.7	
28	17-LVD-038_017	0.282604	0.000036	0.00128	0.00012	0.0306	0.0030	1.467201	0.000067	18.8	173	0.282600	-6.4	1.3	-2.7	
Rejected Analysis																
3	17-LVD-038_107	0.282655	0.000034	0.00139	0.00011	0.0334	0.0033	1.467210	0.000039	14.9	195	0.282650	-4.6	1.2	-0.4	

Grain	Spot ID	<i>corrected</i>									Total Hf Beam	MUN LASS Age (Ma)	176Hf/177Hf	EHf0	2SE	EHfi
		176Hf/177Hf	2SE	176Lu/177Hf	2SE	176Yb/177Hf	2SE	178Hf/177Hf	2SE							
9	17-LVD-038_123	0.282585	0.000026	0.00169	0.00037	0.0414	0.0095	1.467170	0.000031	13.2	200	0.282579	-7.1	0.9	-2.9	
11	17-LVD-038_125	0.282507	0.000021	0.00114	0.00012	0.0271	0.0033	1.467189	0.000026	16.7	332	0.282500	-9.8	0.7	-2.7	
26	17-LVD-038_015	0.282516	0.000028	0.00103	0.00022	0.0265	0.0058	1.467160	0.000032	13.6	182	0.282512	-9.5	1.0	-5.6	

Cretaceous

Sample 16-LVD-007, North Klondike Highway (Zone 08V 439338E 6865663N NAD 83)

Grain	Spot ID	<i>corrected</i>									Total Hf Beam	MUN LASS Age (Ma)	176Hf/177Hf	EHf0	2SE	EHfi
		176Hf/177Hf	2SE	176Lu/ 177Hf	2SE	176Yb/ 177Hf	2SE	178Hf/177Hf	2SE							
1	16-LVD-007_110	0.282180	0.000035	0.00044	0.00001	0.0132	0.0004	1.467207	0.000024	18.2	1074	0.282171	-21.4	1.2	2.4	
2	16-LVD-007_111	0.283004	0.000029	0.00103	0.00004	0.0238	0.0011	1.467198	0.000042	14.8	127	0.283002	7.7	1.0	10.5	
4	16-LVD-007_113	0.282444	0.000023	0.00104	0.00005	0.0259	0.0009	1.467233	0.000038	13.8	208	0.282440	-12.1	0.8	-7.6	
5	16-LVD-007_114	0.283079	0.000038	0.00389	0.00024	0.1199	0.0073	1.467243	0.000051	15.1	334	0.283055	10.4	1.3	17.0	
7	16-LVD-007_122	0.282996	0.000032	0.00144	0.00008	0.0425	0.0024	1.467223	0.000041	19.4	240	0.282990	7.5	1.1	12.6	
10	16-LVD-007_125	0.282107	0.000022	0.00090	0.00013	0.0255	0.0036	1.467213	0.000041	14.2	894	0.282092	-24.0	0.8	-4.5	
11	16-LVD-007_126	0.282970	0.000020	0.00106	0.00006	0.0259	0.0010	1.467211	0.000047	17.1	215	0.282966	6.5	0.7	11.2	
12	16-LVD-007_127	0.282485	0.000026	0.00133	0.00005	0.0327	0.0016	1.467247	0.000046	14.9	200	0.282480	-10.6	0.9	-6.4	
13	16-LVD-007_128	0.282930	0.000026	0.00102	0.00006	0.0238	0.0014	1.467207	0.000046	14.4	198	0.282926	5.1	0.9	9.4	
14	16-LVD-007_129	0.283063	0.000028	0.00178	0.00016	0.0425	0.0042	1.467217	0.000047	14.7	125	0.283059	9.8	1.0	12.5	
15	16-LVD-007_130	0.282867	0.000029	0.00138	0.00005	0.0342	0.0012	1.467255	0.000034	14.2	191	0.282862	2.9	1.0	7.0	
19	16-LVD-007_140	0.282934	0.000029	0.00141	0.00008	0.0357	0.0018	1.467237	0.000041	14.8	123	0.282931	5.3	1.0	7.9	
20	16-LVD-007_141	0.282900	0.000028	0.00167	0.00004	0.0428	0.0007	1.467245	0.000034	15.5	173	0.282895	4.1	1.0	7.7	
22	16-LVD-007_143	0.282613	0.000031	0.00100	0.00006	0.0208	0.0013	1.467197	0.000036	12.2	214	0.282609	-6.1	1.1	-1.5	

Grain	Spot ID	corrected										MUN LASS Age (Ma)	$^{176}\text{Hf}/^{177}\text{Hf}$	EHf0	2SE	EHfi
		$^{176}\text{Hf}/^{177}\text{Hf}$	2SE	$^{176}\text{Lu}/^{177}\text{Hf}$	2SE	$^{176}\text{Yb}/^{177}\text{Hf}$	2SE	$^{178}\text{Hf}/^{177}\text{Hf}$	2SE	Total Hf Beam						
23	16-LVD-007_144	0.282053	0.000033	0.00077	0.00000	0.0220	0.0002	1.467251	0.000050	17.8	1033	0.282038	-25.9	1.2	-3.3	
24	16-LVD-007_145	0.282595	0.000028	0.00094	0.00003	0.0256	0.0011	1.467227	0.000031	12.2	171	0.282592	-6.7	1.0	-3.0	
25	16-LVD-007_146	0.282527	0.000031	0.00090	0.00006	0.0253	0.0016	1.467199	0.000045	18.5	118	0.282525	-9.1	1.1	-6.6	
27	16-LVD-007_154	0.283127	0.000044	0.00176	0.00011	0.0446	0.0031	1.467247	0.000054	13.8	122	0.283123	12.1	1.6	14.7	
28	16-LVD-007_155	0.282994	0.000021	0.00190	0.00005	0.0462	0.0016	1.467199	0.000041	16.4	188	0.282987	7.4	0.7	11.3	
30	16-LVD-007_157	0.282970	0.000028	0.00109	0.00013	0.0273	0.0038	1.467208	0.000037	14.1	247	0.282965	6.5	1.0	11.9	
32	16-LVD-007_159	0.282758	0.000028	0.00141	0.00003	0.0309	0.0005	1.467181	0.000037	19	204	0.282753	-1.0	1.0	3.4	
33	16-LVD-007_160	0.282792	0.000031	0.00099	0.00005	0.0248	0.0014	1.467244	0.000056	15.8	214	0.282788	0.2	1.1	4.9	
34	16-LVD-007_161	0.282751	0.000031	0.00109	0.00007	0.0278	0.0017	1.467184	0.000046	16.5	186	0.282747	-1.2	1.1	2.8	
35	16-LVD-007_162	0.281418	0.000023	0.00079	0.00004	0.0232	0.0013	1.467273	0.000044	14.6	1994	0.281388	-48.3	0.8	-4.3	
36	16-LVD-007_169	0.282913	0.000024	0.00050	0.00003	0.0116	0.0008	1.467247	0.000044	14.6	232	0.282911	4.5	0.8	9.6	
38	16-LVD-007_171	0.282578	0.000035	0.00116	0.00004	0.0315	0.0014	1.467246	0.000036	18.4	121	0.282575	-7.3	1.2	-4.7	
40	16-LVD-007_173	0.282436	0.000037	0.00098	0.00008	0.0256	0.0022	1.467186	0.000052	19.1	306	0.282430	-12.3	1.3	-5.7	
41	16-LVD-007_174	0.282648	0.000029	0.00162	0.00003	0.0434	0.0012	1.467244	0.000041	12.6	322	0.282638	-4.8	1.0	2.0	
42	16-LVD-007_175	0.282964	0.000019	0.00197	0.00005	0.0409	0.0009	1.467226	0.000034	16.2	119	0.282960	6.3	0.7	8.8	
47	16-LVD-007_186	0.281997	0.000024	0.00084	0.00005	0.0230	0.0013	1.467219	0.000045	14	1480	0.281973	-27.9	0.9	4.6	
49	16-LVD-007_188	0.282814	0.000020	0.00149	0.00011	0.0344	0.0022	1.467204	0.000037	14.2	207	0.282808	1.0	0.7	5.4	
61	16-LVD-007_206	0.283027	0.000024	0.00072	0.00003	0.0158	0.0007	1.467207	0.000037	14.4	125	0.283025	8.6	0.8	11.3	
63	16-LVD-007_208	0.282611	0.000028	0.00041	0.00007	0.0111	0.0026	1.467198	0.000037	22.7	325	0.282609	-6.2	1.0	1.0	
64	16-LVD-007_209	0.282684	0.000033	0.00166	0.00016	0.0459	0.0046	1.467256	0.000038	17.7	121	0.282680	-3.6	1.2	-1.0	
65	16-LVD-007_210	0.282270	0.000024	0.00047	0.00001	0.0132	0.0002	1.467249	0.000036	13.2	361	0.282267	-18.2	0.9	-10.3	
67	16-LVD-007_10	0.282944	0.000023	0.00148	0.00008	0.0381	0.0022	1.467219	0.000042	17.4	171	0.282939	5.6	0.8	9.3	
68	16-LVD-007_11	0.282224	0.000031	0.00124	0.00004	0.0340	0.0010	1.467216	0.000043	18.2	357	0.282216	-19.8	1.1	-12.2	

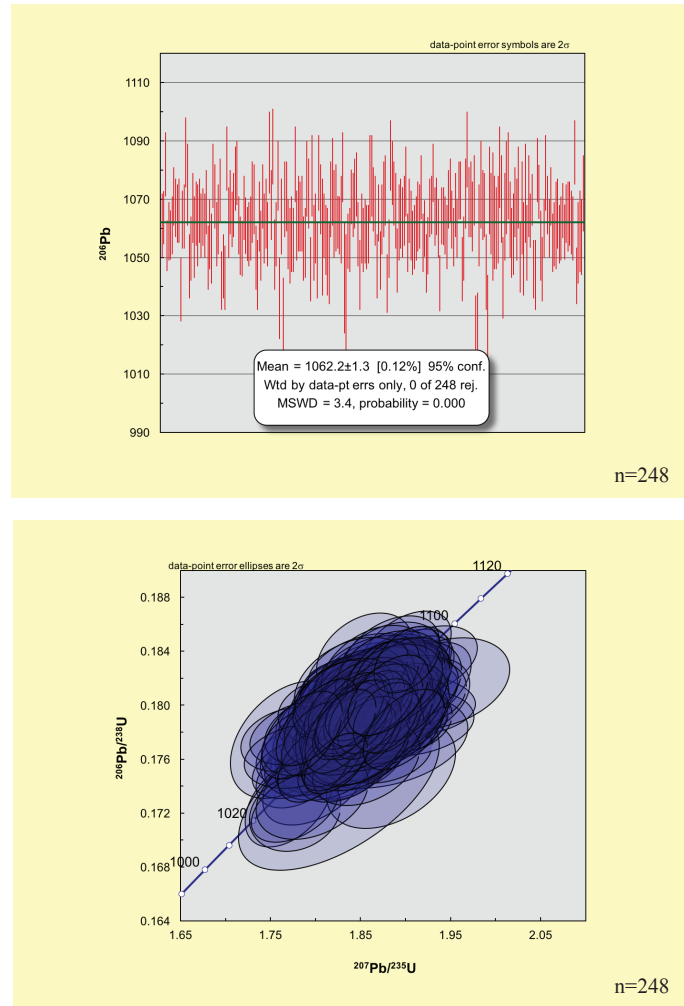
Grain	Spot ID	<i>corrected</i>		2SE	176Lu/ 177Hf	2SE	176Yb/ 177Hf	2SE	178Hf/ 177Hf	2SE	Total Hf Beam	MUN LASS Age (Ma)	176Hf/ 177Hf	EHf0	2SE	EHfi
		176Hf/ 177Hf	2SE													
72	16-LVD-007_15	0.282533	0.000030	0.00028	0.00004	0.0068	0.0011	1.467209	0.000045	16.2	350	0.282531	-8.9	1.1	-1.2	
78	16-LVD-007_27	0.282592	0.000028	0.00248	0.00009	0.0583	0.0020	1.467243	0.000048	17.6	169	0.282584	-6.8	1.0	-3.3	
79	16-LVD-007_28	0.282218	0.000027	0.00029	0.00006	0.0097	0.0020	1.467175	0.000032	20.8	367	0.282216	-20.1	1.0	-12.0	
Rejected Analysis																
3	16-LVD-007_112	0.282985	0.000032	0.00075	0.00006	0.0179	0.0014	1.467231	0.000039	17.3	128	0.282983	7.1	1.1	9.8	
6	16-LVD-007_121	0.282266	0.000059	0.00076	0.00008	0.0216	0.0020	1.467201	0.000059	25.7	157	0.282264	-18.4	2.1	-15.0	
8	16-LVD-007_123	0.283031	0.000033	0.00166	0.00039	0.0400	0.0100	1.467229	0.000043	22.8	117	0.283027	8.7	1.2	11.2	
9	16-LVD-007_124	0.282566	0.000041	0.00125	0.00008	0.0347	0.0029	1.467189	0.000050	21.1	117	0.282563	-7.7	1.5	-5.3	
16	16-LVD-007_137	0.282983	0.000051	0.00196	0.00006	0.0469	0.0014	1.467185	0.000034	15.1	215	0.282975	7.0	1.8	11.5	
17	16-LVD-007_138	0.282228	0.000032	0.00124	0.00004	0.0385	0.0014	1.467187	0.000027	21.1	1084	0.282203	-19.7	1.1	3.7	
18	16-LVD-007_139	0.282767	0.000019	0.00115	0.00011	0.0275	0.0030	1.467201	0.000053	17.3	203	0.282763	-0.6	0.7	3.7	
21	16-LVD-007_142	0.282605	0.000062	0.00326	0.00033	0.0960	0.0110	1.467237	0.000044	23.4	110	0.282598	-6.4	2.2	-4.2	
26	16-LVD-007_153	0.283049	0.000041	0.00128	0.00005	0.0299	0.0009	1.467262	0.000083	16.4	115	0.283046	9.3	1.4	11.8	
29	16-LVD-007_156	0.283091	0.000034	0.00129	0.00009	0.0303	0.0022	1.467220	0.000038	13.3	125	0.283088	10.8	1.2	13.5	
31	16-LVD-007_158	0.282825	0.000026	0.00067	0.00001	0.0169	0.0003	1.467235	0.000053	17	174	0.282823	1.4	0.9	5.2	
37	16-LVD-007_170	0.280996	0.000035	0.00280	0.00016	0.0891	0.0047	1.467176	0.000052	15.63	2894	0.280841	-63.3	1.2	-2.8	
39	16-LVD-007_172	0.282621	0.000036	0.00120	0.00007	0.0327	0.0020	1.467245	0.000062	17.3	117	0.282618	-5.8	1.3	-3.3	
43	16-LVD-007_176	0.282887	0.000038	0.00209	0.00028	0.0547	0.0079	1.467263	0.000046	13	135	0.282882	3.6	1.3	6.4	
44	16-LVD-007_177	0.282619	0.000036	0.00149	0.00012	0.0354	0.0032	1.467241	0.000043	18.1	259	0.282612	-5.9	1.3	-0.4	
45	16-LVD-007_178	0.282629	0.000020	0.00159	0.00011	0.0373	0.0029	1.467192	0.000031	13.2	202	0.282623	-5.5	0.7	-1.2	
46	16-LVD-007_185	0.282912	0.000017	0.00088	0.00007	0.0202	0.0015	1.467251	0.000053	17.6	205	0.282909	4.5	0.6	8.9	
48	16-LVD-007_187	0.282803	0.000035	0.00142	0.00013	0.0358	0.0034	1.467271	0.000036	9.9	204	0.282798	0.6	1.2	5.0	
50	16-LVD-007_189	0.283046	0.000030	0.00080	0.00004	0.0180	0.0008	1.467281	0.000055	13.2	123	0.283044	9.2	1.1	11.9	

Grain	Spot ID	<i>corrected</i>		2SE	176Lu/ 177Hf	2SE	176Yb/ 177Hf	2SE	178Hf/ 177Hf	2SE	Total Hf Beam	MUN LASS Age (Ma)	176Hf/ 177Hf	EHf0	2SE	EHfi
		176Hf/ 177Hf	2SE													
51	16-LVD-007_190	0.282780	0.000019	0.00051	0.00001	0.0119	0.0004	1.467296	0.000047	14.5	198	0.282778	-0.2	0.7	4.2	
52	16-LVD-007_191	0.282882	0.000031	0.00136	0.00004	0.0383	0.0012	1.467218	0.000050	18.38	108	0.282879	3.4	1.1	5.7	
53	16-LVD-007_192	0.282545	0.000025	0.00090	0.00004	0.0238	0.0010	1.467262	0.000045	9.96	164	0.282542	-8.5	0.9	-4.9	
54	16-LVD-007_193	0.282777	0.000036	0.00179	0.00009	0.0393	0.0021	1.467154	0.000068	15.87	196	0.282770	-0.3	1.3	3.8	
55	16-LVD-007_194	0.282835	0.000040	0.00100	0.00004	0.0248	0.0010	1.467213	0.000073	17.9	143	0.282832	1.8	1.4	4.8	
56	16-LVD-007_201	0.282902	0.000030	0.00081	0.00003	0.0184	0.0010	1.467254	0.000035	17.4	256	0.282898	4.1	1.1	9.7	
57	16-LVD-007_202	0.282450	0.000027	0.00084	0.00004	0.0205	0.0009	1.467231	0.000037	14.2	210	0.282447	-11.8	1.0	-7.3	
58	16-LVD-007_203	0.282480	0.000110	0.00136	0.00018	0.0371	0.0056	1.467204	0.000043	19.9	151	0.282476	-10.8	3.9	-7.6	
59	16-LVD-007_204	0.282915	0.000022	0.00112	0.00006	0.0257	0.0017	1.467206	0.000086	15.3	165	0.282912	4.6	0.8	8.1	
60	16-LVD-007_205	0.282920	0.000120	0.00204	0.00028	0.0560	0.0120	1.467214	0.000087	18.7	181	0.282913	4.8	4.2	8.6	
62	16-LVD-007_207	0.281545	0.000026	0.00084	0.00003	0.0230	0.0008	1.467226	0.000038	14.7	1848	0.281516	-43.8	0.9	-3.2	
66	16-LVD-007_9	0.282778	0.000039	0.00087	0.00004	0.0223	0.0013	1.467269	0.000099	24.31	203	0.282775	-0.2	1.4	4.1	
69	16-LVD-007_12	0.282518	0.000024	0.00152	0.00004	0.0434	0.0008	1.467240	0.000120	22.6	114	0.282515	-9.4	0.8	-7.0	
70	16-LVD-007_13	0.282435	0.000075	0.00202	0.00006	0.0561	0.0019	1.467193	0.000081	20.01	223	0.282427	-12.4	2.7	-7.7	
71	16-LVD-007_14	0.282995	0.000056	0.00531	0.00010	0.1451	0.0022	1.467270	0.000110	16.57	216	0.282974	7.4	2.0	11.5	
73	16-LVD-007_16	0.282560	0.000032	0.00121	0.00006	0.0327	0.0021	1.467201	0.000066	18	118	0.282557	-8.0	1.1	-5.4	
74	16-LVD-007_17	0.282550	0.000030	0.00086	0.00003	0.0210	0.0008	1.467213	0.000048	17.7	345	0.282544	-8.3	1.1	-0.8	
75	16-LVD-007_18	0.283057	0.000071	0.00121	0.00004	0.0274	0.0012	1.467258	0.000088	21	176	0.283053	9.6	2.5	13.4	
76	16-LVD-007_25	0.282600	0.000190	0.00119	0.00006	0.0303	0.0015	1.467280	0.000120	21.6	191	0.282596	-6.5	6.7	-2.5	
77	16-LVD-007_26	0.282714	0.000033	0.00109	0.00007	0.0262	0.0026	1.467213	0.000063	16.1	174	0.282710	-2.5	1.2	1.2	
80	16-LVD-007_29	0.282799	0.000050	0.00134	0.00003	0.0313	0.0006	1.467163	0.000066	22.9	198	0.282794	0.5	1.8	4.7	
81	16-LVD-007_30	0.282660	0.000033	0.00183	0.00008	0.0511	0.0021	1.467232	0.000044	20	104	0.282656	-4.4	1.2	-2.2	
82	16-LVD-007_31	0.281840	0.000031	0.00073	0.00014	0.0202	0.0040	1.467242	0.000067	15.1	1768	0.281816	-33.4	1.1	5.6	

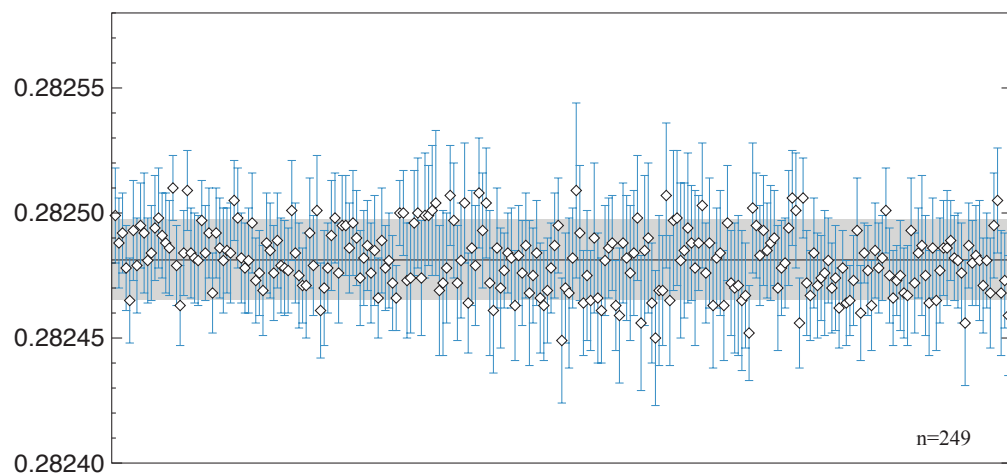
Grain	Spot ID	<i>corrected</i>		2SE	176Lu/ 177Hf	2SE	176Yb/ 177Hf	2SE	178Hf/ 177Hf	2SE	Total Hf Beam	MUN LASS Age (Ma)	176Hf/ 177Hf	EHf0	2SE	EHfi
		176Hf/ 177Hf	2SE													
83	16-LVD-007_32	0.282643	0.000043	0.00125	0.00013	0.0318	0.0033	1.467292	0.000051	19.7	113	0.282640	-5.0	1.5	-2.6	

D.3 U-Pb and Hf standards

Primary U-Pb standard 91500



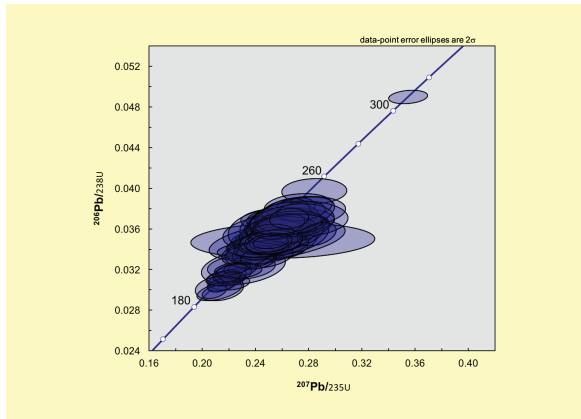
Primary Lu-Hf standard Plesovice



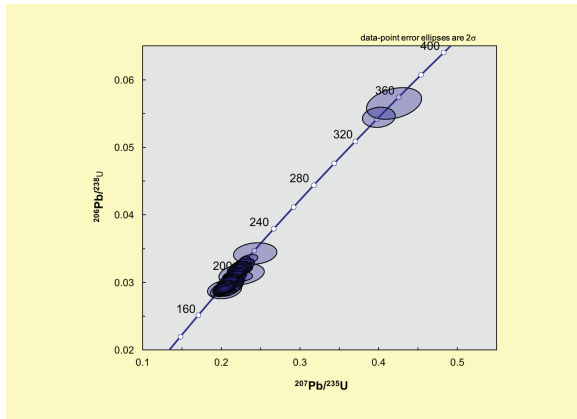
Appendix E: Isoplot diagrams

E.1 Concordia plots

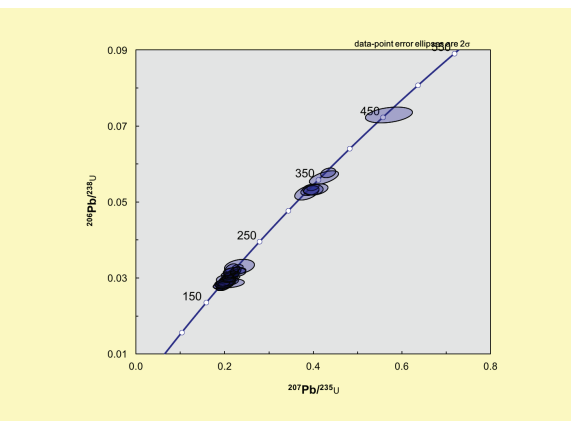
16-LVD-001C, Robert Campbell Highway



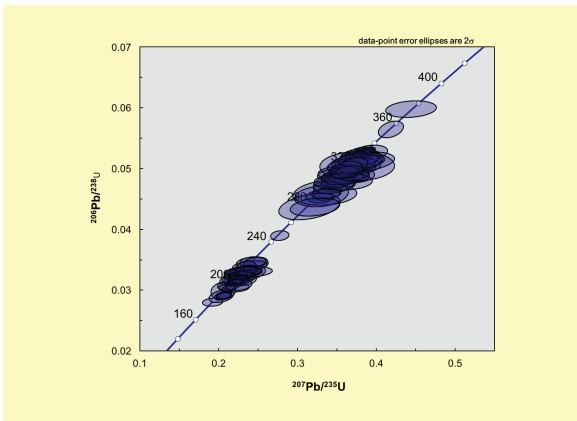
16-LVD-001B, Robert Campbell Highway



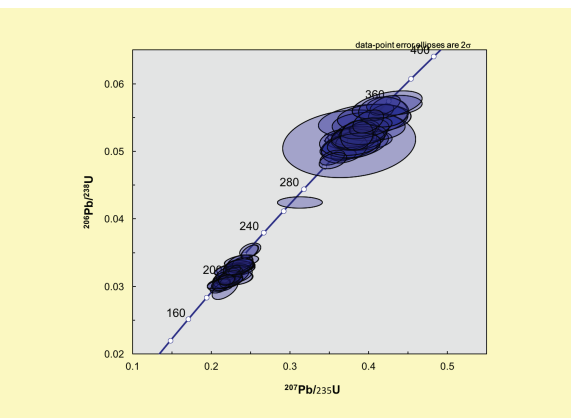
16-LVD-004, Robert Campbell Highway



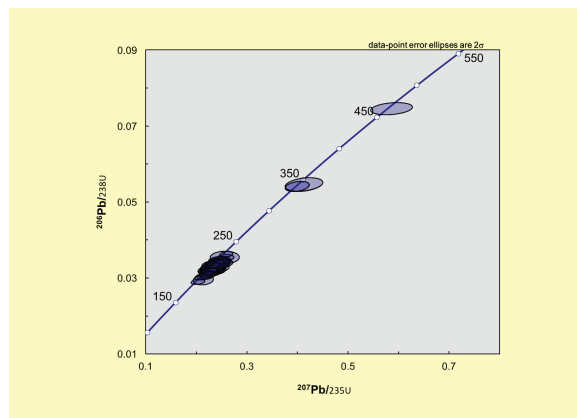
17-LVD-018, Conglomerate Mountain



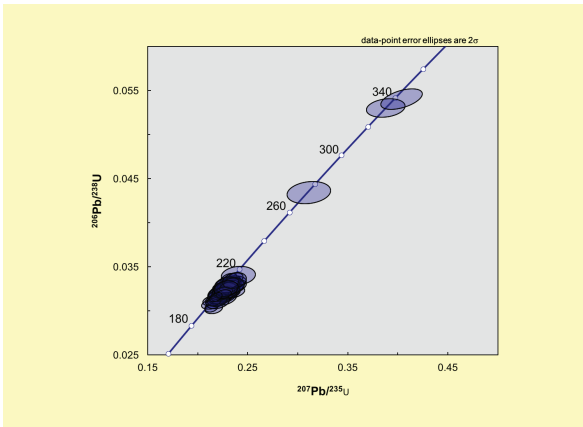
16-LVD-009, Mount Laurier



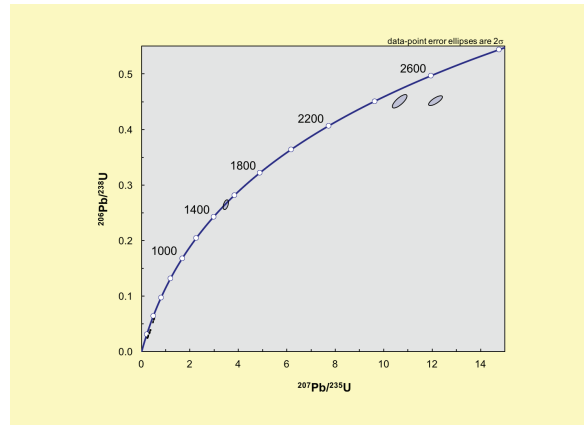
16-LVD-021, Richthofen Island



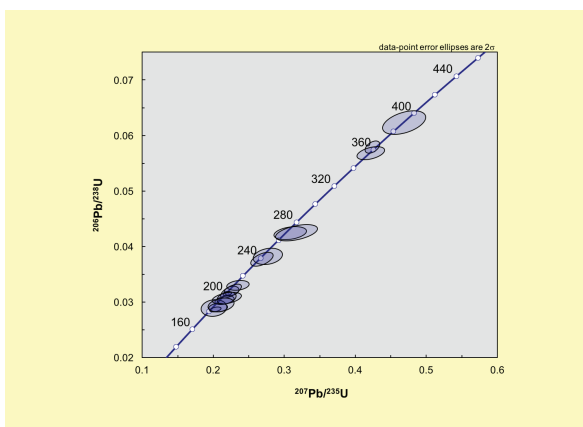
16-LVD-022, Lake Laberge



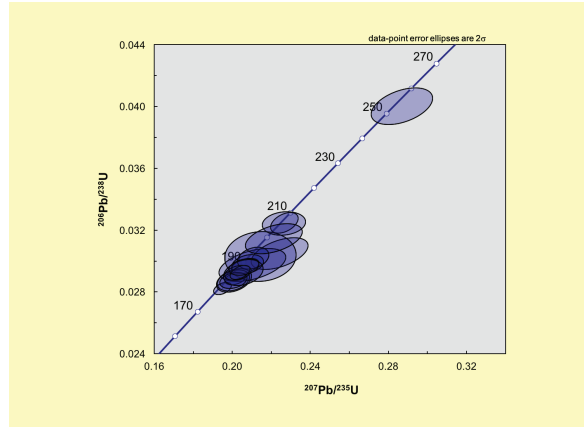
16-LVD-023, Lake Laberge (1/2)



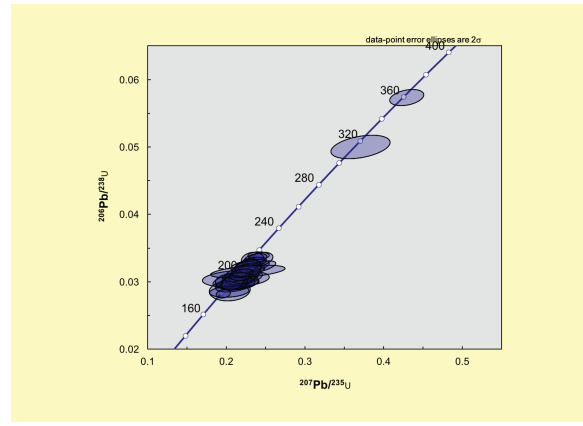
16-LVD-023, Lake Laberge (2/2)



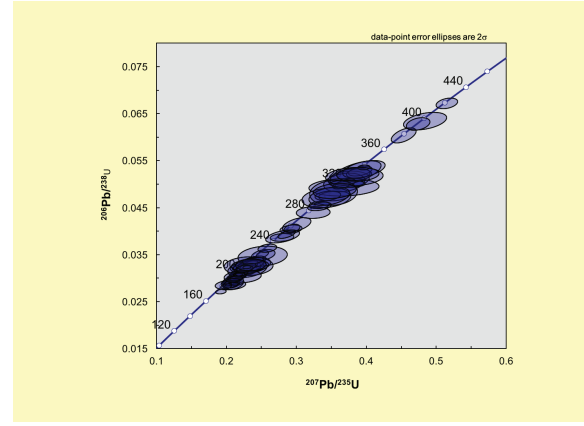
17-LVD-026, Metamorphic clast, Fish Lake



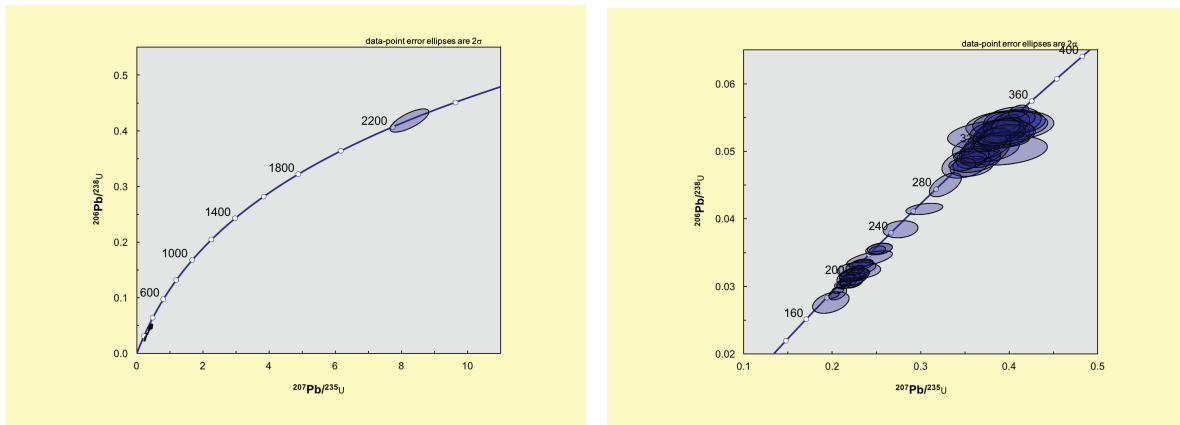
17-LVD-027, Takhini Subdivision



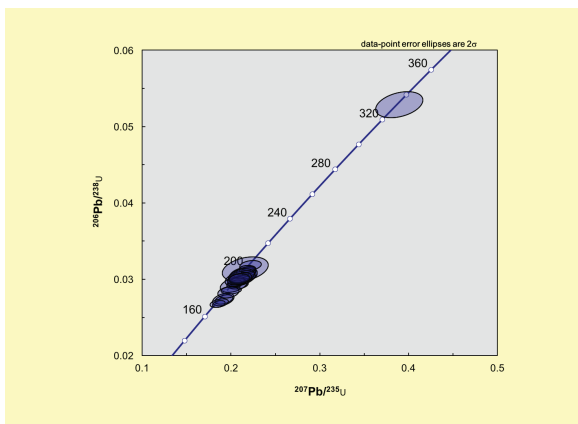
17-LVD-030, Mount Byng



17-LVD-034, Mount Slim

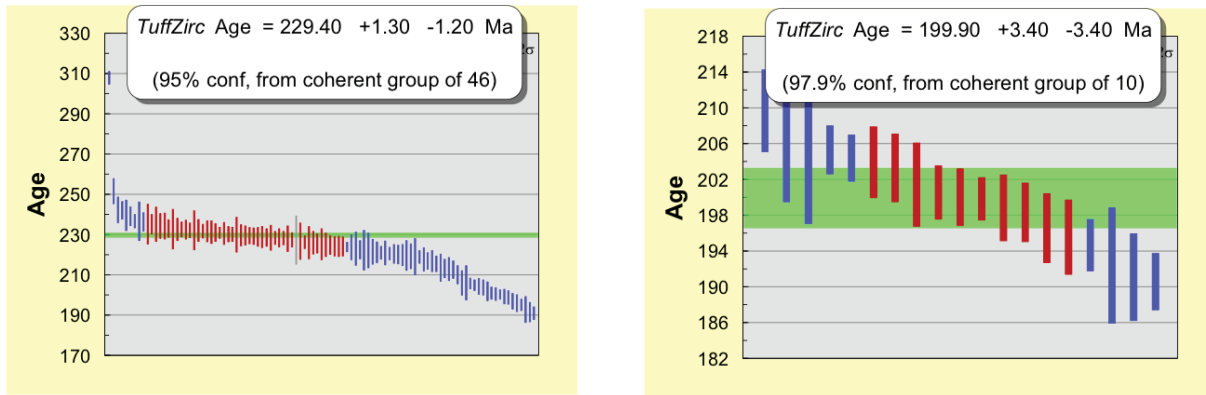


17-LVD-038, King Lake

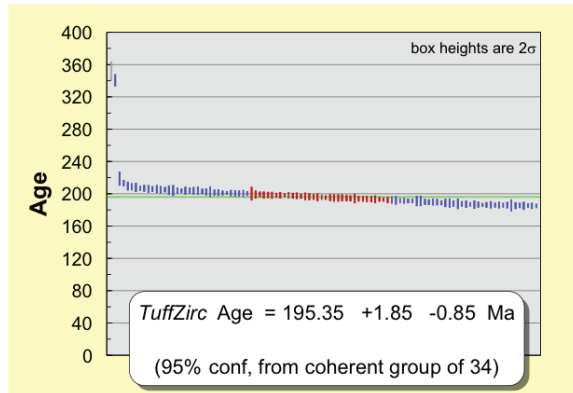


E.2 TuffZirc plots

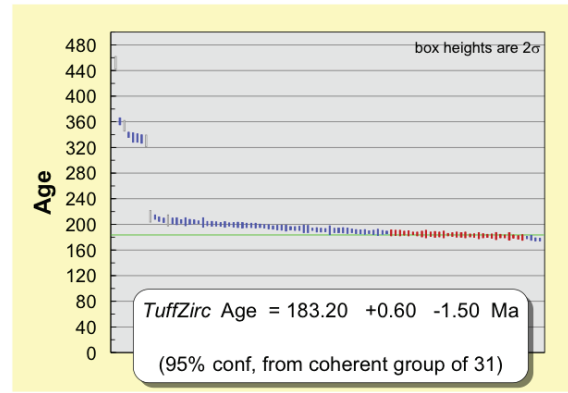
16-LVD-001C, Robert Campbell Highway



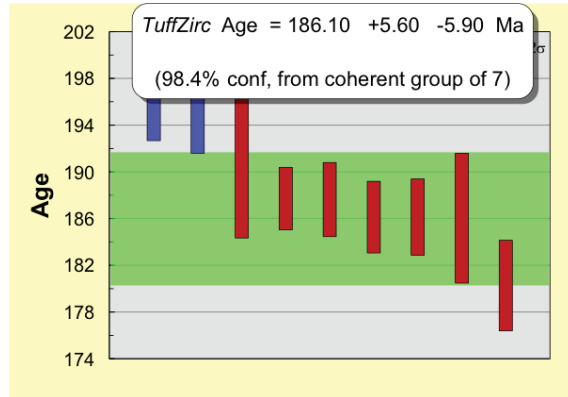
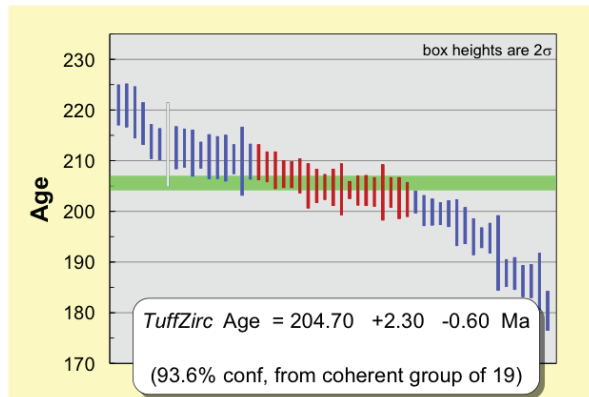
16-LVD-001B, Robert Campbell Highway



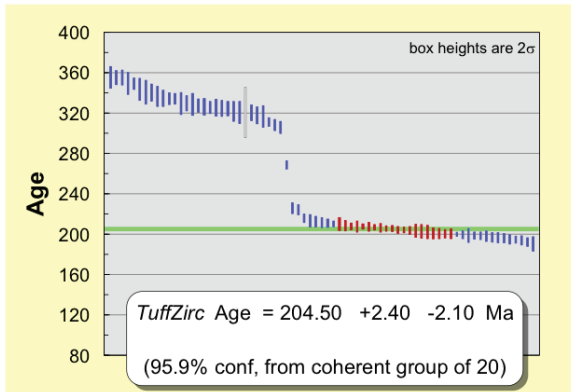
16-LVD-004, Robert Campbell Highway



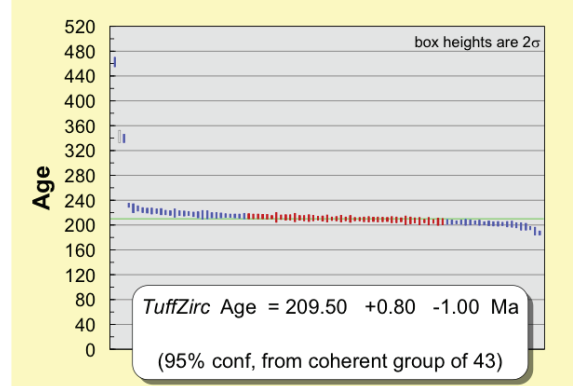
17-LVD-018, Conglomerate Mountain



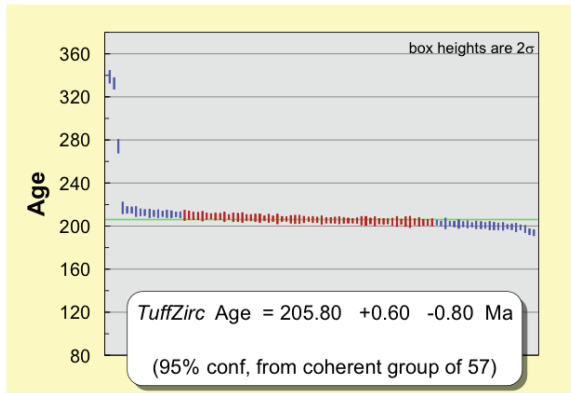
16-LVD-009, Mount Laurier



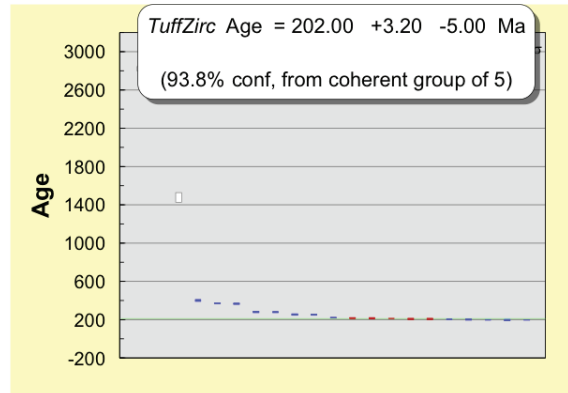
16-LVD-021, Richthofen Island



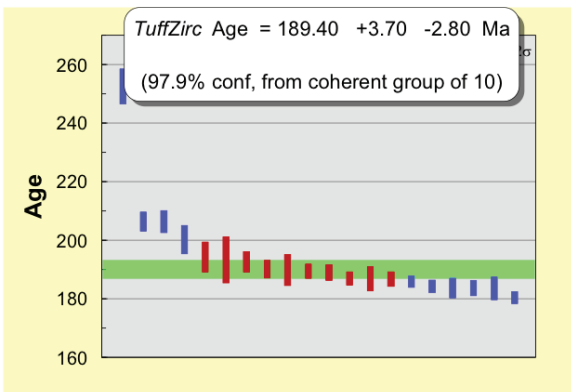
16-LVD-022, Lake Laberge



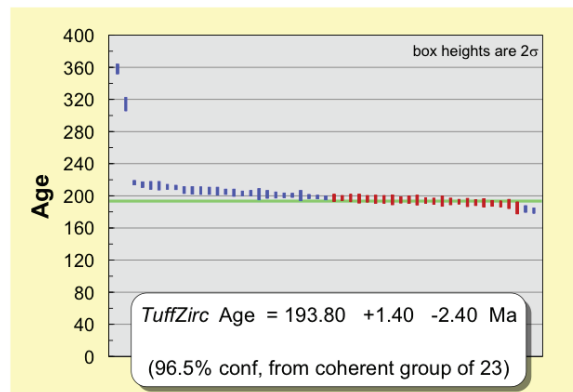
16-LVD-023, Lake Laberge



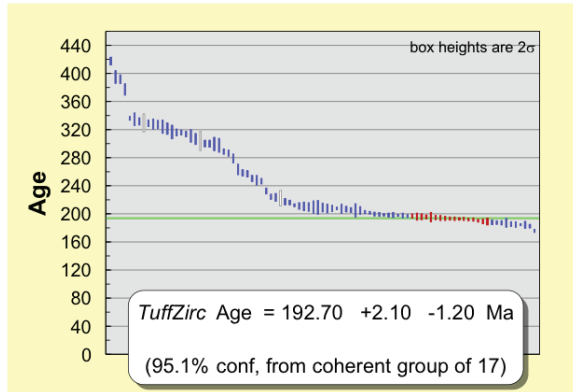
17-LVD-026, Metamorphic clast, Fish Lake



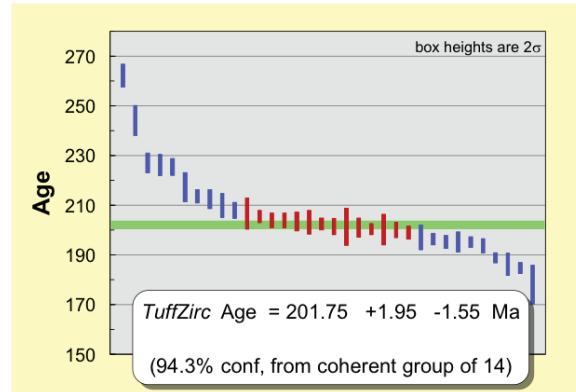
17-LVD-027, Takhini Subdivision



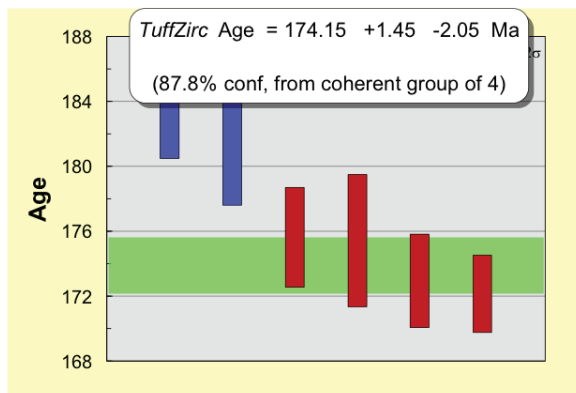
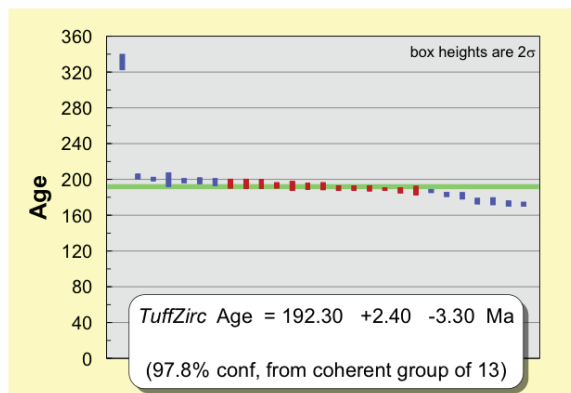
17-LVD-030, Mount Byng



17-LVD-034, Mount Slim

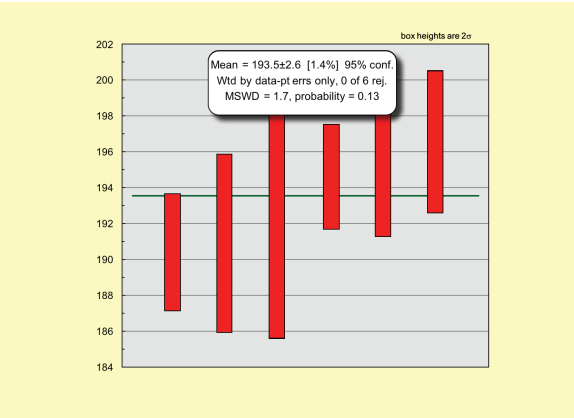


17-LVD-038, King Lake

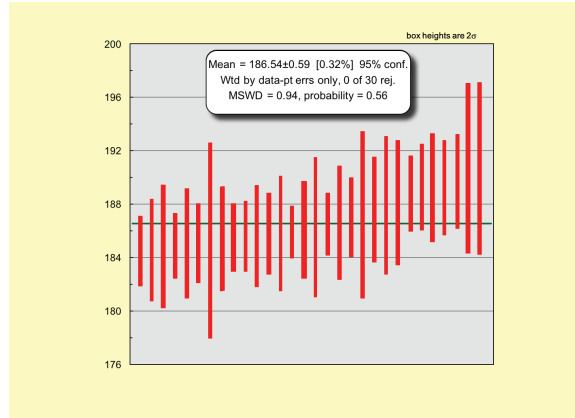


E.3 Weighted mean plots

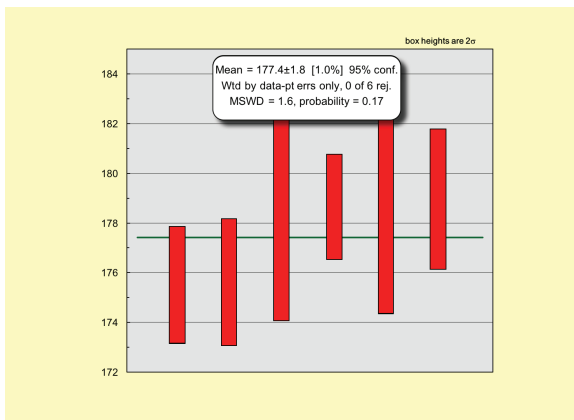
16-LVD-001C, Robert Campbell Highway



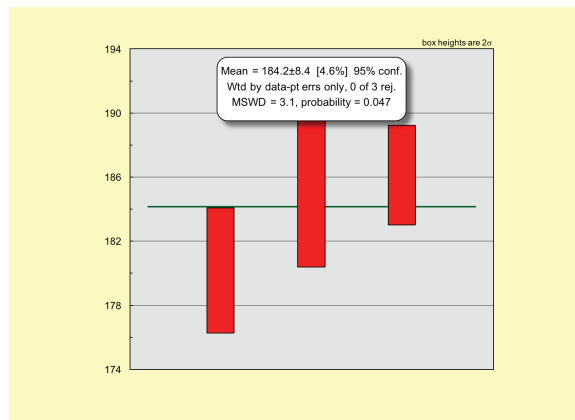
16-LVD-001B, Robert Campbell Highway



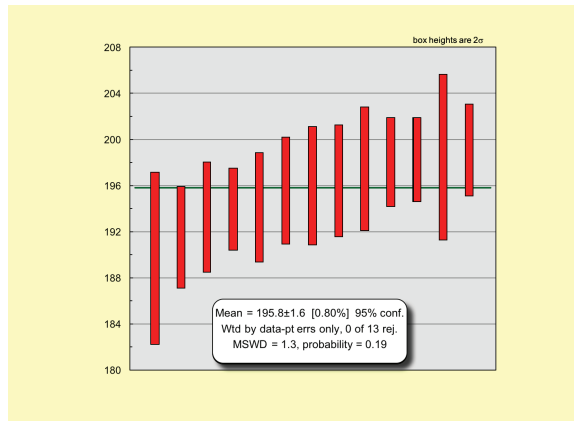
16-LVD-004, Robert Campbell Highway



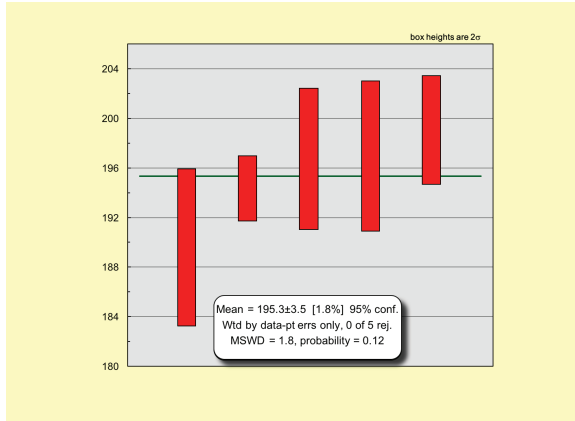
17-LVD-018, Conglomerate Mountain



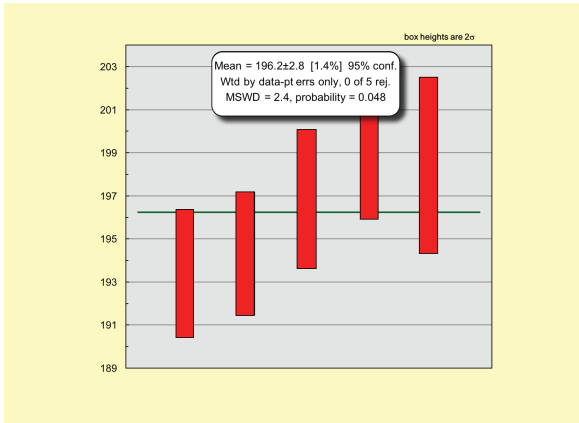
16-LVD-009, Mount Laurier



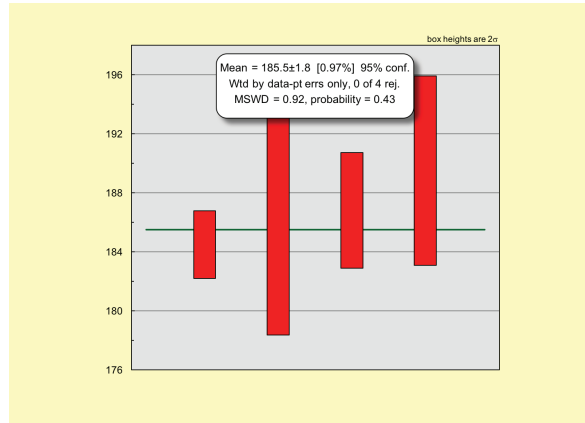
16-LVD-021, Richthofen Island



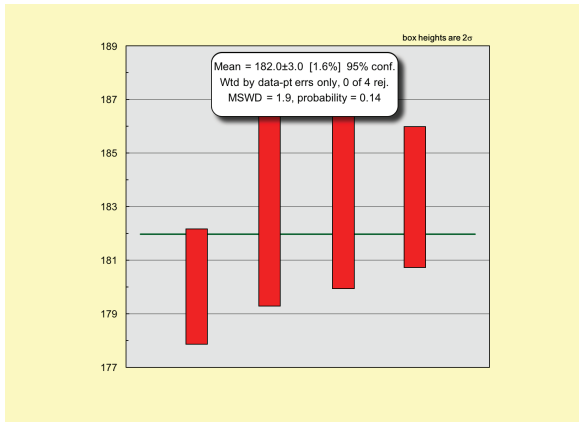
16-LVD-022, Lake Laberge



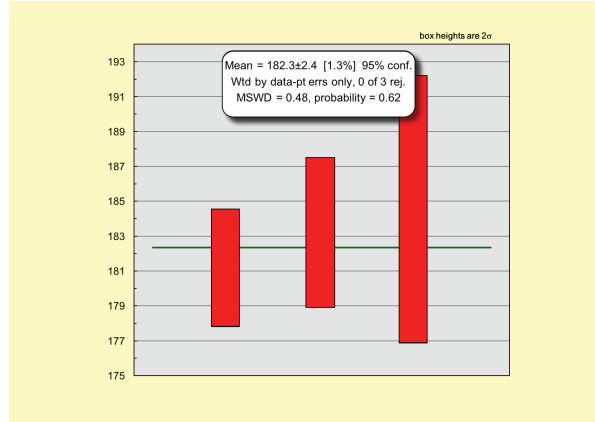
16-LVD-023, Lake Laberge



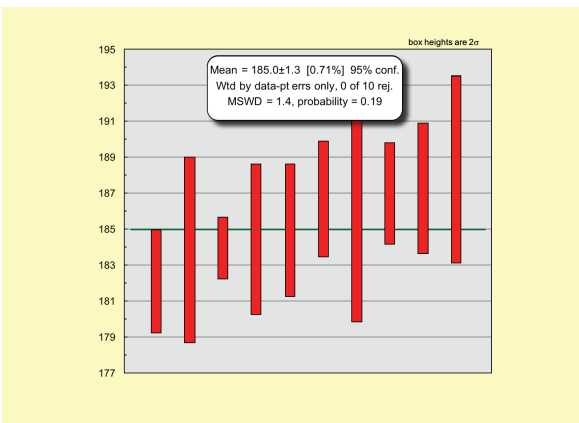
17-LVD-026, Metmorphc clast, Fish Lake



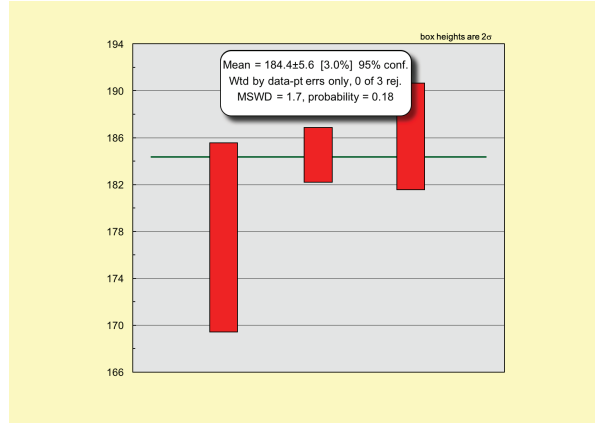
17-LVD-027, Takhini Subdivision



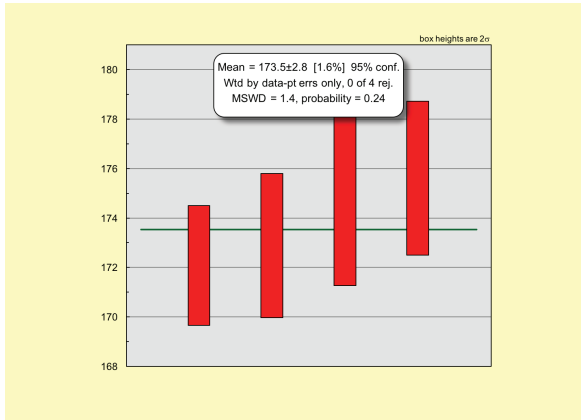
17-LVD-030, Mount Byng



17-LVD-034, Mount Slim

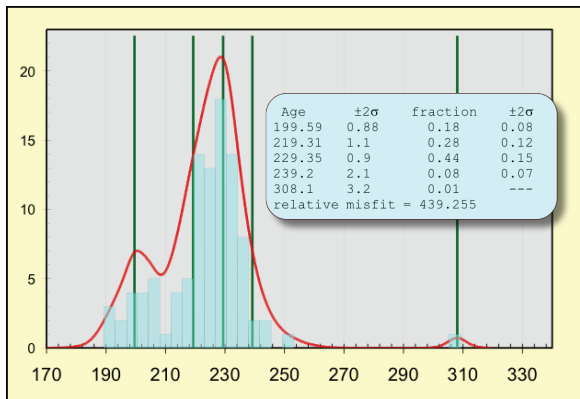


17-LVD-038, King Lake

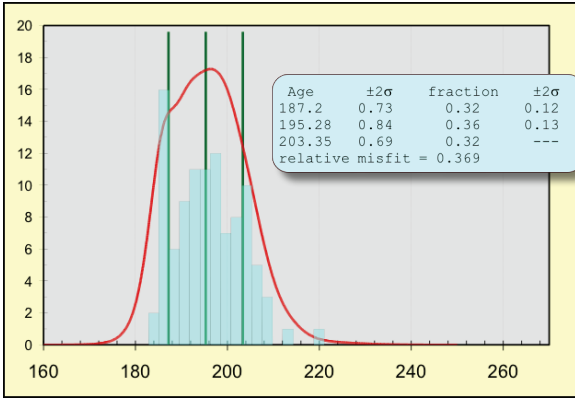


E.4 Unmix plots

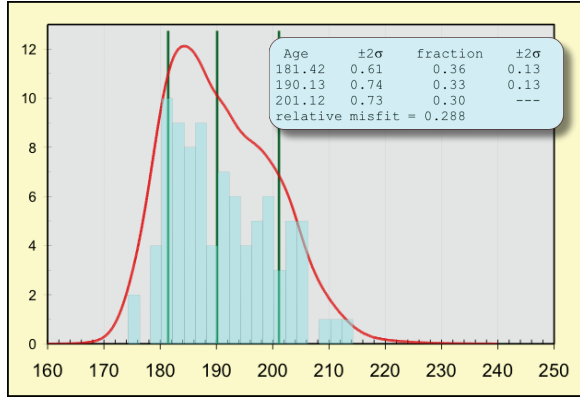
16-LVD-001C, Robert Campbell Highway



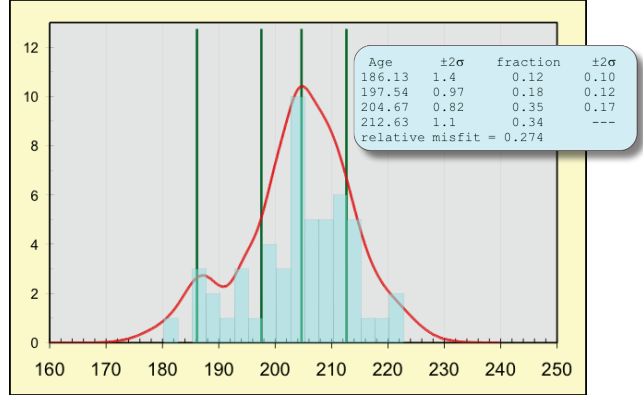
16-LVD-001B, Robert Campbell Highway



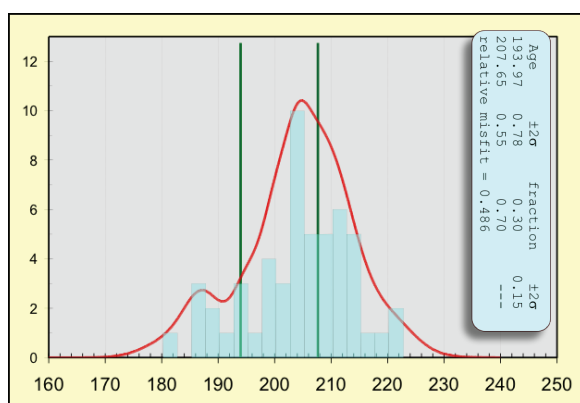
16-LVD-004, Robert Campbell Highway



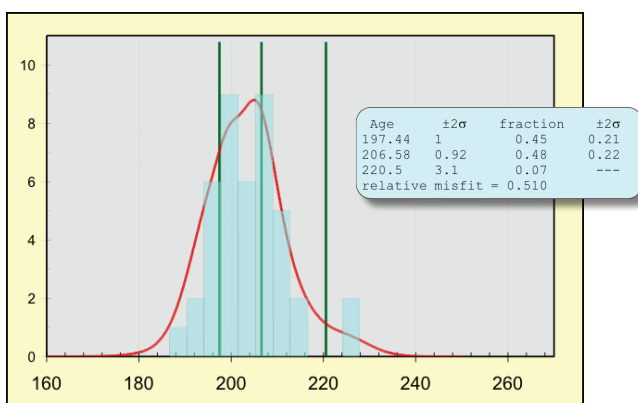
17-LVD-018, Conglomerate Mountain



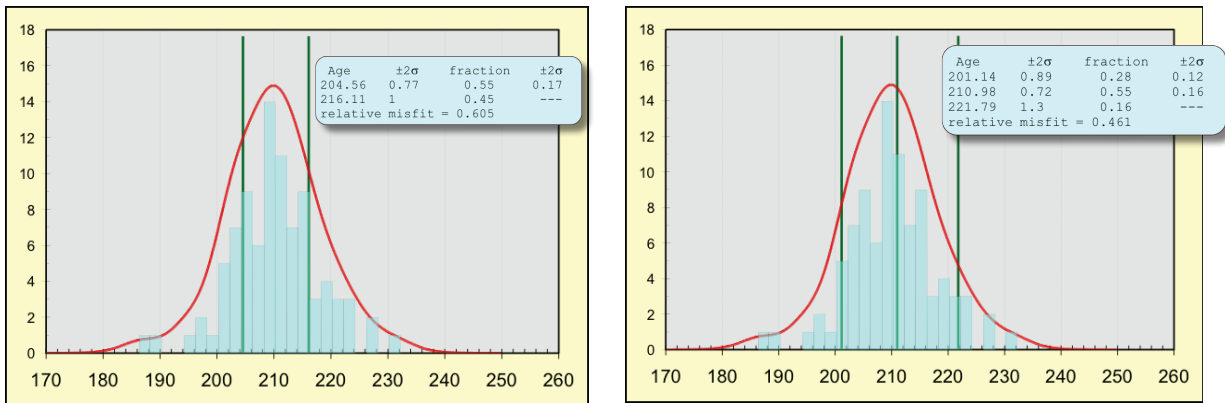
17-LVD-018, Conglomerate Mountain



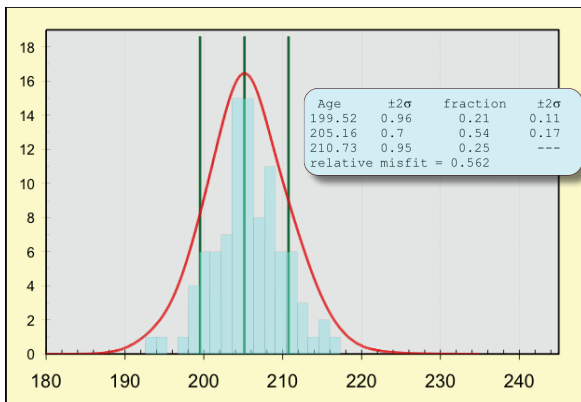
16-LVD-009, Mount Laurier



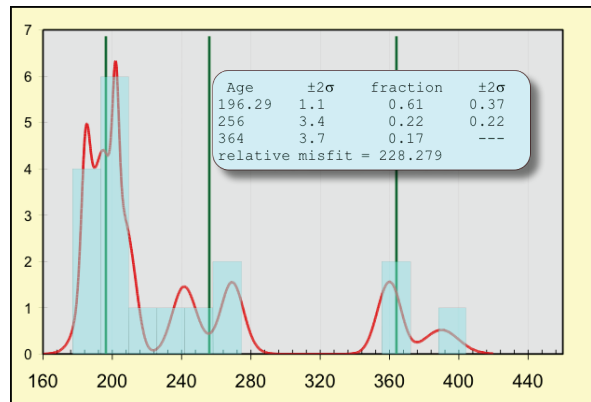
16-LVD-021, Richthofen Island



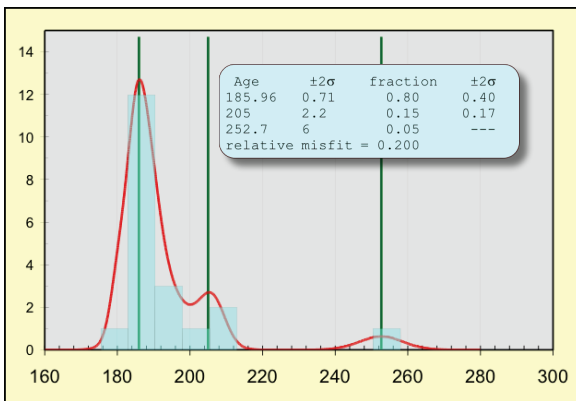
16-LVD-022, Lake Laberge



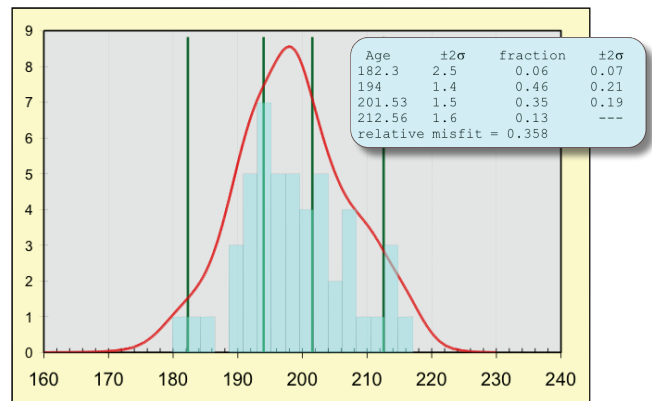
16-LVD-023, Lake Laberge



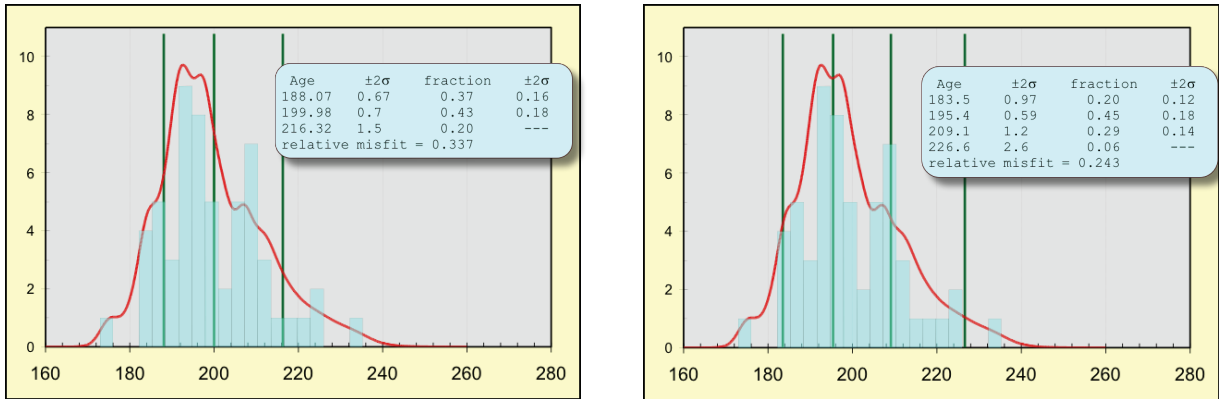
17-LVD-026, Metamorphic clast, Fish Lake



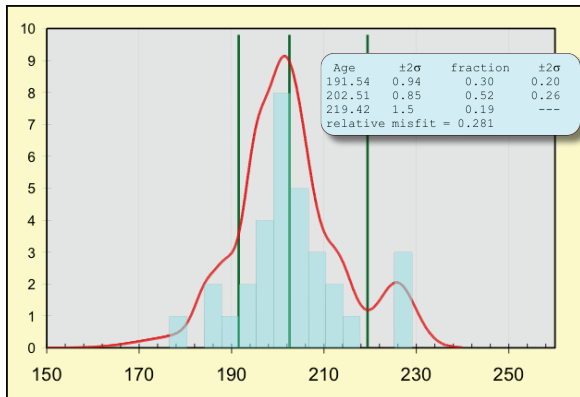
17-LVD-027, Takhini Subdivision



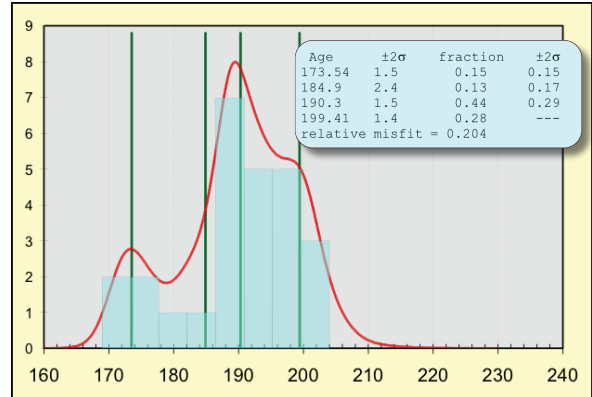
17-LVD-030, Mount Byng



17-LVD-034, Mount Slim



17-LVD-038, King Lake



Appendix F: Yukon Exploration and Geology publications

F.1 van Drecht et al. (2017)

Jurassic stratigraphy and tectonic evolution of the Whitehorse trough, central Yukon: Project outline and preliminary field results

L.H. van Drecht, L.P. Beranek*

Department of Earth Sciences, Memorial University of Newfoundland

M. Hutchison

Yukon Geological Survey

van Drecht, L.H., Beranek, L.P. and Hutchison, M., 2017. Jurassic stratigraphy and tectonic evolution of the Whitehorse trough, central Yukon: Project outline and preliminary field results. In: Yukon Exploration and Geology 2016, K.E. MacFarlane and L.H. Weston (eds.), Yukon Geological Survey, p. 207-223.

ABSTRACT

Lower to Middle Jurassic strata of the Laberge Group define the Whitehorse trough and preserve syntectonic sedimentation in central Yukon during the exhumation of adjacent terranes. A two-year project was initiated in summer 2016 to investigate Laberge Group stratigraphy and test the relationships between the timing of exhumation, sedimentation, and terrane accretion in the northern Canadian Cordillera. Field studies along the Robert Campbell and North Klondike highways near Carmacks targeted marginal marine, tidal and fluvial-dominated strata of the Tanglefoot formation that were likely deposited in semi-arid environments. Studied outcrops of fan-delta conglomerate and turbiditic strata of the Richthofen formation along the eastern shoreline of Lake Laberge and on Mount Laurier are consistent with the south-directed deepening of the Whitehorse trough. Field observations will be integrated with detrital zircon (U-Pb and Hf isotope) studies to constrain the provenance of the Laberge Group and reconstruct source-to-sink pathways in the Whitehorse trough.

* lberanek@mun.ca

INTRODUCTION

The Intermontane terranes of the Canadian Cordillera (e.g., Slide Mountain, Yukon-Tanana, Stikinia) accreted to the western margin of Laurentia during the late Paleozoic to mid-Mesozoic (e.g., Nelson *et al.*, 2013). The early growth of the northern Canadian Cordillera is in part recorded by the Whitehorse trough, a sedimentary basin that developed on top of the Intermontane terranes during Early to Middle Jurassic closure of the Cache Creek Ocean and accretion of Stikinia (Nelson *et al.*, 2013; Colpron *et al.*, 2015). The Whitehorse trough (Fig. 1) is a regionally significant depocentre that extends over 600 km from the Carmacks region of central Yukon to the Dease Lake region of northern British Columbia. Synorogenic strata of the Laberge Group filled the Whitehorse trough in central Yukon (e.g., Tempelman-Kluit, 1984; Lowey *et al.*, 2009) and were most likely sourced from exhumed basement units of the Yukon-Tanana, Stikinia and Quesnellia terranes (e.g., Dickie and Hein, 1995; Hart *et al.*, 1995; Colpron *et al.*, 2015). The northern apex of the Whitehorse trough near Carmacks consists of marginal marine to fluvial strata of the Tanglefoot formation, whereas the middle parts of the trough near Lake Laberge contain turbiditic strata of the Richthofen formation (Tempelman-Kluit, 1984; Lowey, 2004; Lowey *et al.*, 2009). Mass-flow fan-delta conglomerate is present in both formations (Tempelman-Kluit, 1984; Lowey, 2004). North-to-south, longitudinal changes in sedimentary facies imply a deepening of the Whitehorse trough to the south (Lowey, 2004; Lowey *et al.*, 2009).

Despite recent advances in understanding the sedimentology and depositional setting of Laberge Group strata (e.g., Lowey *et al.*, 2009; Bordet, 2016; Colpron *et al.*, 2016), comparatively few investigations have addressed the stratigraphic responses of Jurassic unroofing or tested relationships between the timing of exhumation, sedimentation and terrane accretion (e.g., Hart *et al.*, 1995; Colpron *et al.*, 2015). For example, Colpron *et al.* (2015) used detrital zircon U-Pb ages to suggest that basal Laberge Group strata young from northeast (Rhaetian-Hettangian) to southwest (Pleinsbachian-Toarcian) across the Whitehorse trough in central Yukon. The westward younging of basal Laberge Group strata may indicate that subsidence followed uplift of the western shoulder of the Whitehorse trough (Colpron *et al.*, 2015). The cause of subsidence is uncertain, but in some regions

may be connected to tectonic loading and west-directed emplacement of the Cache Creek terrane on top of Stikinia (e.g., Mihalynuk *et al.*, 1994, 2004). A two-year project was initiated in summer 2016 to test these hypotheses and constrain the field geology and detrital zircon (U-Pb and Hf isotope) provenance signatures of Laberge Group strata. The short-term objectives of the project, which in part are presented in this report, are to define the physical stratigraphy, depositional setting and basal contact relationships of Laberge Group strata along the Robert Campbell and North Klondike highways, the eastern shoreline of Lake Laberge, and near Mount Laurier. The long-term objectives of the project are to constrain the source-to-sink pathways and paleodrainage systems of the Whitehorse trough in central Yukon and link the timing and nature of Laberge Group sedimentation to the Jurassic exhumation of the Intermontane terranes.

TECTONIC SETTING

The western edge of Laurentia was an accretionary margin that underwent several collisional events during the late Paleozoic to Mesozoic. In Late Triassic-Jurassic time, arc sequences of the Yukon-Tanana, Stikinia and Quesnellia terranes evolved along a tectonically complex margin. The most popular model for the Late Triassic-Jurassic margin involves the collision of the Kutcho arc, counterclockwise bending of the Intermontane terranes, and subsequent entrapment of oceanic rock units assigned to the Cache Creek terrane (Mihalynuk *et al.*, 1994; Logan and Mihalynuk, 2014; Colpron *et al.*, 2015). During the Late Triassic to Early Jurassic, pluton emplacement accompanied counterclockwise bending and rapid exhumation of the Yukon-Tanana, Stikinia and Quesnellia terranes in central Yukon (e.g., Johnston *et al.*, 1996). Lower to Middle Jurassic strata of the Laberge Group were shed into the Whitehorse trough during regional tectonism and likely sourced from these exhumed basement rocks. Unconformable contact relationships between the Laberge Group and underlying rock units of the Lewes River Group (Fig. 2; Mesozoic Stikinia) suggest that block faulting pre-dated Early to Middle Jurassic sedimentation in central Yukon (Hart *et al.*, 1995; Colpron *et al.*, 2007, 2015).

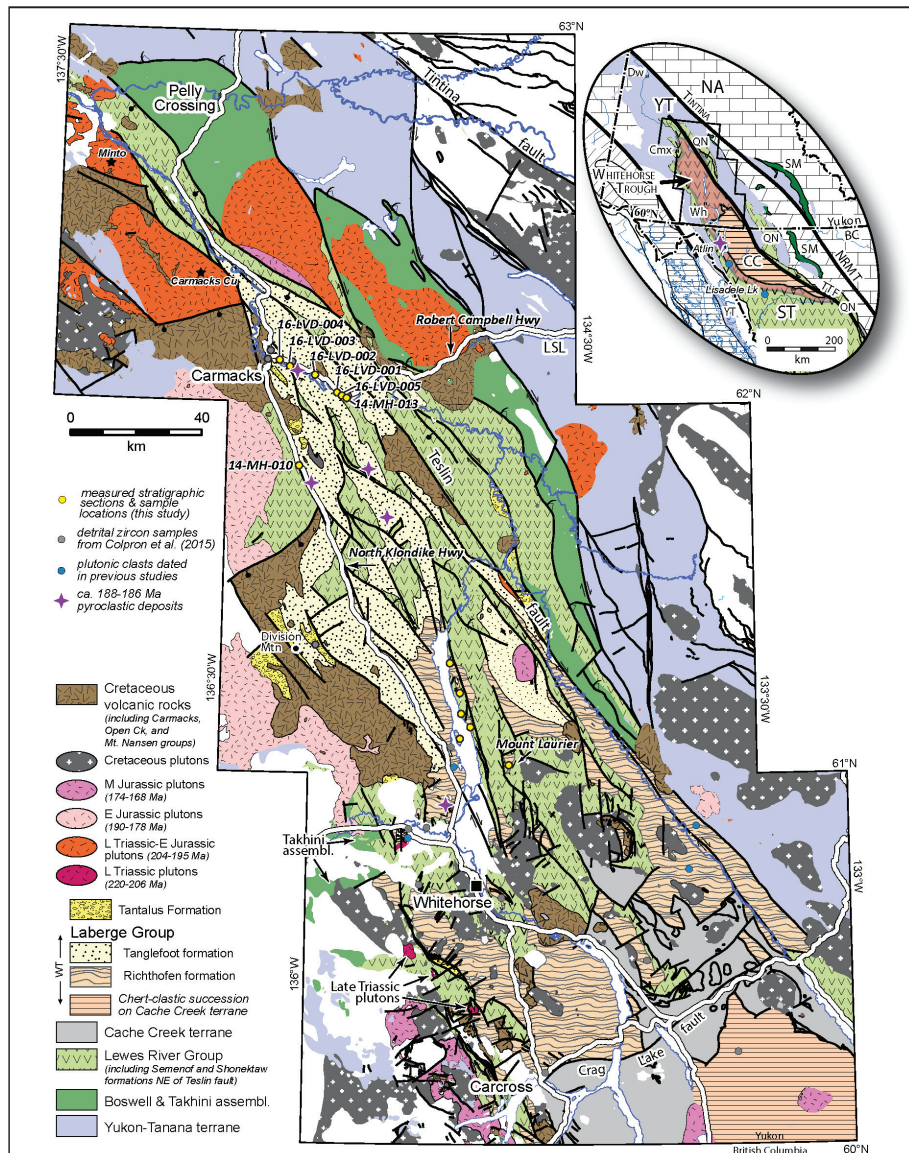


Figure 1. Regional geology of the Whitehorse trough area modified from Colpron et al. (2015). Locations of 2016 field sites are shown by yellow dots. Field locations on the Robert Campbell Highway represent measured stratigraphic sections. Locations on Lake Laberge and Mount Laurier indicate sampling locations. Grey and blue dots denote detrital zircon sample locations of Colpron et al. (2015) and previously dated plutonic clasts. The inset map shows Intermontane terranes and their present geometry. Abbreviations: CC = Cache Creek terrane; CMx = Carmacks; Dw = Dawson; LSL = Little Salmon Lake; NA = rocks of ancestral North America; NRMT = Northern Rocky Mountain Trench fault; QN = Quesnellia; SM = Slide Mountain terrane; ST = Stikinia; TTF = Teslin-Thibert fault; Wh = Whitehorse; and YT = Yukon-Tanana terrane.

STRATIGRAPHIC FRAMEWORK

LEWES RIVER GROUP

The Lewes River Group of Stikinia is a 3000 m-thick assemblage of basalt and andesite, flow breccia, crystal tuff, conglomerate, greywacke, limestone and shale (Fig. 2; Tempelman-Kluit, 1984; Dickie and Hein, 1995; Hart, 1997). The Povoas formation (Carnian) represents the main volcanic unit of the Lewes River Group and is characterized by lava flows, volcanic breccia, tuff and agglomerate (Tempelman-Kluit, 1984, 2009). The Aksala formation represents a volcanic lull following Carnian magmatism and consists of the Casca (Carnian-Norian), Hancock (Norian-Rhaetian) and Mandanna (Rhaetian) members (Fig. 3; Tempelman-Kluit, 2009). The Casca member comprises lithic sandstone, argillite and conglomerate, the Hancock member is a reefal limestone and the Mandanna member is a maroon lithic sandstone, mudstone and conglomeratic sequence that locally interfingers with the Hancock member (Tempelman-Kluit, 1984; Dickie and Hein, 1995).

LABERGE GROUP

The Whitehorse trough contains ~3000 m of siliciclastic strata assigned to the Laberge Group (Dickie and Hein, 1995). In central Yukon, the Laberge Group is divided into the Tanglefoot formation, Richthofen formation and Nordenskiöld dacite (Tempelman-Kluit, 1984). Field mapping and seismic surveys indicate that southwest-verging fold and thrust faults structurally characterize the Whitehorse trough (Colpron *et al.*, 2007; White *et al.*, 2012). Upper Jurassic to Lower Cretaceous fluviodeltaic rocks of the Tantalus Formation unconformably overlie the Laberge Group (Hart and Radloff, 1990; Dickie and Hein, 1995).

Tanglefoot formation

The Tanglefoot formation (Fig. 2) is restricted to the northern half of the Whitehorse trough and characterized by interbedded Sinemurian-Bajocian sandstone and mudstone, matrix-supported conglomerate, pebbly sandstone, coal and abundant terrestrial plant and marginal marine fossils (Lowey, 2004). Previously, all mappable conglomerate in the Whitehorse trough was included in a ‘Conglomerate formation’ (Tempelman-Kluit, 1984). However, conglomerate is present in both of Tanglefoot and Richthofen formations (Lowey, 2004).

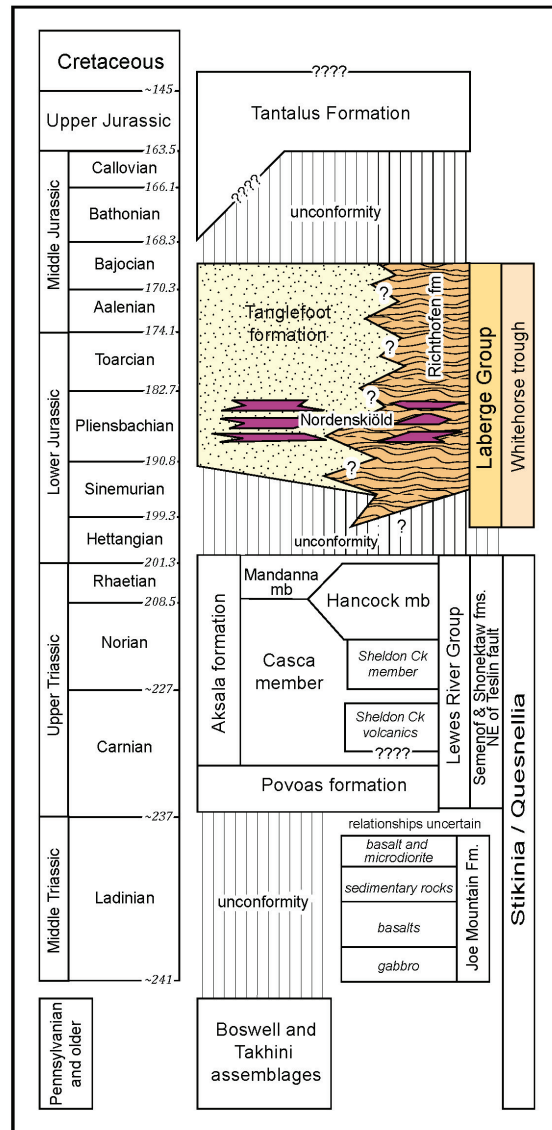


Figure 2. Schematic stratigraphy of Stikinia, Quesnellia and the Whitehorse trough as compiled by Colpron *et al.* (2015).

Richthofen formation

The Richthofen formation consists of Sinemurian-Bajocian graded siltstone to very fine grained sandstone and mudstone couplets or thin-bedded turbidite (Lowey, 2004) that are associated with mass-flow conglomerate. Pebby sandstone, massive sandstone, volcanioclastic rocks and minor limestone are also present in the Richthofen formation (Lowey *et al.*, 2009). The type area is located along the west shore of Lake Laberge where the Richthofen formation crops out along the beach beside the Lake Laberge campground boat launch (Tempelman-Kluit, 1984; Lowey, 2004).

Nordenskiöld dacite

The Nordenskiöld dacite consists of epiclastic and primary dacitic tuff and flows (Tempelman-Kluit, 1984) that have been identified at three stratigraphic levels in the Tanglefoot and Richthofen formations (Colpron *et al.*, 2007). Zircon U-Pb ages of 188.1 ± 0.4 Ma, 187.2 ± 0.4 Ma, and 186.5 ± 0.3 Ma indicate that the Nordenskiöld dacite

preserves several eruptive events during the Early Jurassic (Colpron and Friedman, 2008).

2016 FIELD STUDIES

The Whitehorse trough was studied in four areas during summer 2016. Stratigraphic sections of the Laberge Group were measured or described at seven locations along the Robert Campbell and North Klondike highways (Fig. 1). Laberge Group rocks were regionally mapped along the east shore of Lake Laberge and at Mount Laurier because of the lack of continuous sections in these areas.

ROBERT CAMPBELL HIGHWAY

The Tanglefoot formation is well exposed along the Robert Campbell Highway east of Carmacks (Fig. 1). Six stratigraphic sections were measured between Carmacks and Frenchman Road and range from 12 to 96 m thick (Fig. 3).

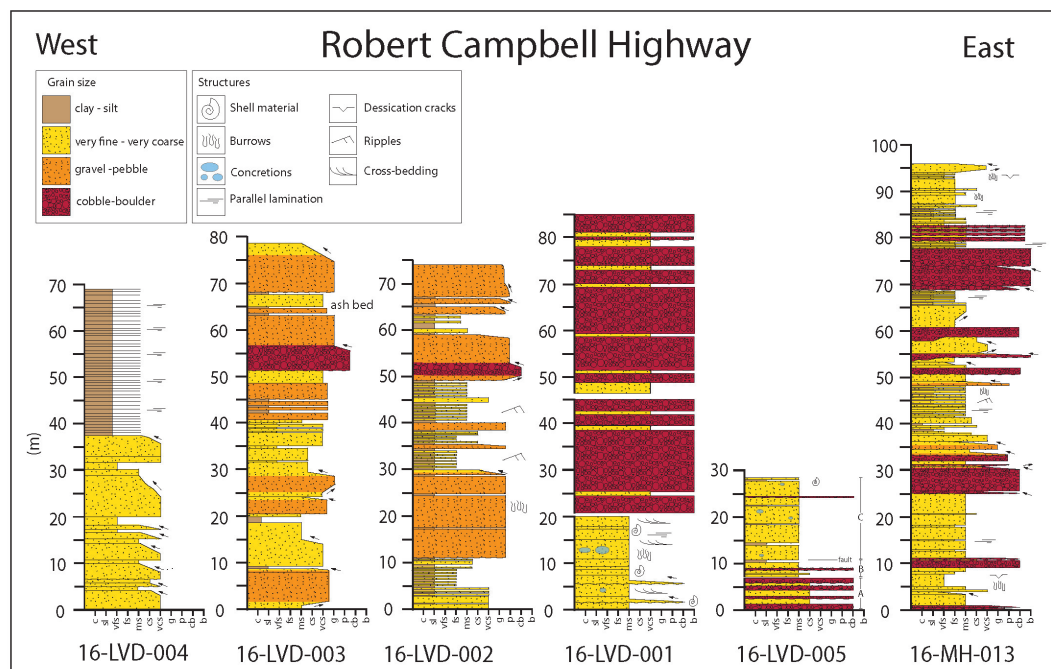


Figure 3. Measured stratigraphic sections from the Robert Campbell Highway. Sections young from east to west. Arrows indicate fining upward or coarsening upward. Grain size abbreviations: c=clay, sl=silt, vfs=very fine grained, fs=fine-grained, ms=medium-grained, cs=coarse-grained, vcs=very coarse grained, g=granule, p=pebble, cb=cobble, and b=boulder.

LOCALITY 1: 14-MH-013 (EAGLES NEST BLUFF)

Ninety-six metres of Tanglefoot formation crop out on the north side of the Robert Campbell Highway, 25 km east of Carmacks (base of section: zone 08V 456959E 6877113N NAD83; Figs. 3 and 4a). Immediately west of this section, a prominent bluff of Hancock member limestone is exposed. This section comprises maroon and grey, medium-grained sandstone with mud drapes and mudstone/siltstone interbeds that alternate with pebble to boulder conglomerate. Shallow cross-bedding, ripples, burrows, desiccation cracks (Fig. 4b), rain-drop impressions and reduction halos characterize the medium-grained sandstone. These beds have blocky weathering patterns and generally fine-upwards, with the exception of few beds

that coarsen up. Conglomeratic beds are composed of subrounded to rounded, poorly sorted, matrix-supported, polymictic clasts (Fig. 4c) and are typically associated with coarsening upward beds. The matrix is composed of poorly-sorted, medium to coarse-grained sandstone and the clasts consist of plutonic rocks, volcanic rocks, limestone and mudstone. The bases of the conglomerate beds are erosional and typically have the largest clasts at the bottom and fine upwards into very coarse sandstone that incorporates floating pebbles. Some conglomerate units cut channel scours (Fig. 4d) into the beds below. Overturned beds dip steeply (75°) to the west and young to the east. Detrital zircon U-Pb data are consistent with Hettangian to Sinemurian depositional ages at this locality (Cronon et al., 2015).

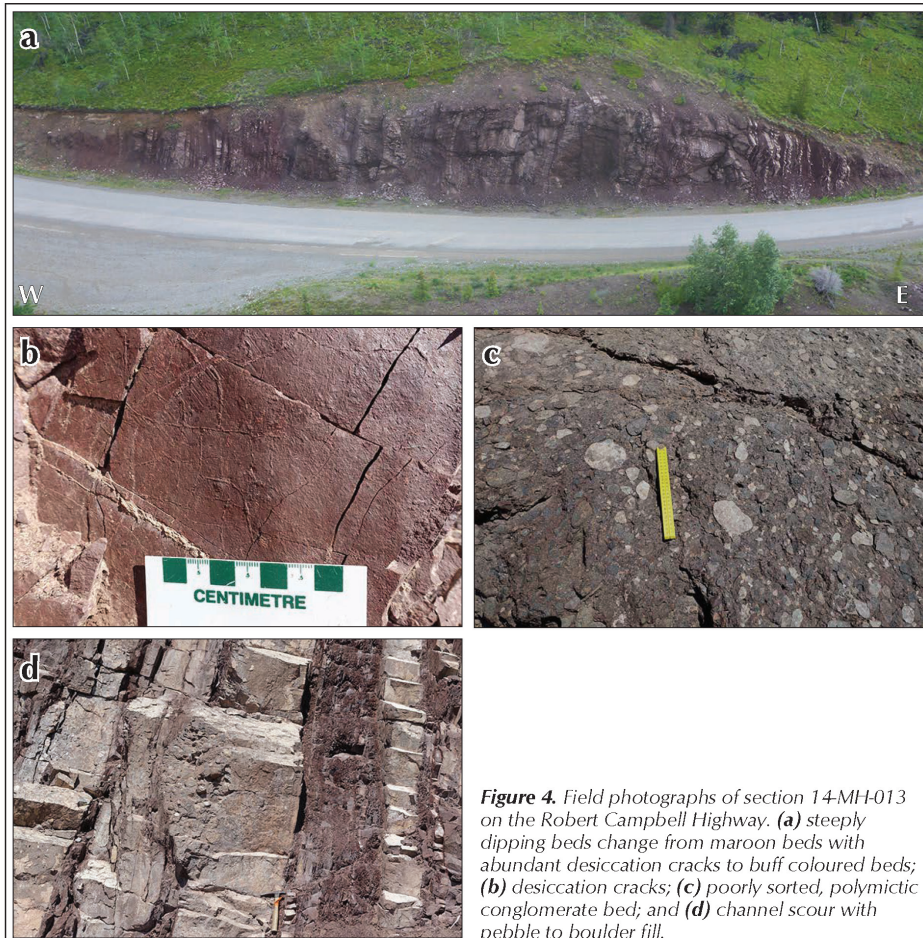


Figure 4. Field photographs of section 14-MH-013 on the Robert Campbell Highway. (a) steeply dipping beds change from maroon beds with abundant desiccation cracks to buff coloured beds; (b) desiccation cracks; (c) poorly sorted, polymictic conglomerate bed; and (d) channel scour with pebble to boulder fill.

LOCALITY 2: 16-LVD-005

Section 16-LVD-005 is ~0.6 km to the west of Eagles Nest Bluff (Fig. 1). Thirty-six metres of west-dipping rocks were measured in three parts (A, B, C) due to the discontinuity of beds and truncation by faults (base of section: zone 08V 456074E 6877576N NAD83). Fracturing and weathered surfaces made it difficult to observe small-scale sedimentary structures. The stratigraphic younging direction of this section was challenging to determine and therefore units are referred to in cardinal directions.

The eastern most unit (A) comprises seven metres of pebble to boulder, subrounded to rounded, poorly sorted, matrix-supported conglomerate and coarse-grained sandstone with floating pebbles. Plutonic, volcanic, limestone and mudstone clasts are present in the conglomerate. Unit B (11.5 m thick) is dominated by medium to coarse-grained sandstone, with minor conglomerate beds and mudstone/siltstone towards the top of the section. Unit C (western most) comprises 17.5 m of laminated, blue-grey to green, medium-grained, well-sorted sandstone. Large concretions (9-15 cm diameter) are present throughout this unit (Fig. 5a), and a gastropod cast was collected near the top of the section at 17 m (Fig. 5b). Cross-beds are rarely preserved throughout the section, which may be due to the weathered and fractured surface making identification difficult.

LOCALITY 3: 16-LVD-001 (COLUMBIA DISASTER)

A westward-dipping and westward-younging section was measured along the north bank of the Yukon River to the west of Eagles Nest Bluff. The section is 80 m-thick and is divided into two distinct units (base of section: zone 08V 455577E 6877512N NAD83). The lower 20 m consists of green-buff, medium-grained, well-sorted sandstone. The upper section contains thick beds of pebble to boulder conglomerate interbedded with coarse to very coarse grained sandstone. Sixty metres of the upper section were measured along the river, but an approximate 120+ m of stratigraphy is present (Fig. 6a).

Low-angle cross-beds, concretions (up to 50 cm; Fig. 6b), abundant shell material and burrows characterize the lower sandstone unit. Erosional surfaces followed by a pebble lag are present throughout this unit and typically include shell material. At 1.6 m from the base of this section a 5 cm gastropod shell (Fig. 6c) was incorporated in a pebble lag. This macrofossil is intact and has matrix within its whorls indicating that it is not *in situ*, but has probably been transported a short distance. Multiple bivalve-rich beds are present and range in thickness from 3-10 cm (Fig. 6d). The upper 15 m of the stratigraphy is covered by overburden. Conglomeratic beds can be observed cropping out below this unit when river levels are low.

Above the overburden, the upper unit consists of thickly bedded, poorly-sorted conglomerate that ranges in thickness from 0.5 to 5 m. Interbeds of coarse to very coarse grained sandstone range from 30 cm to 2 m thick and typically have floating pebbles or boulders (Fig. 6e).



Figure 5. Field photographs of section 16-LVD-005 on the Robert Campbell Highway. (a) concretion in medium-grained, well-sorted sandstone; and (b) cast of gastropod macrofossil at 17 m.

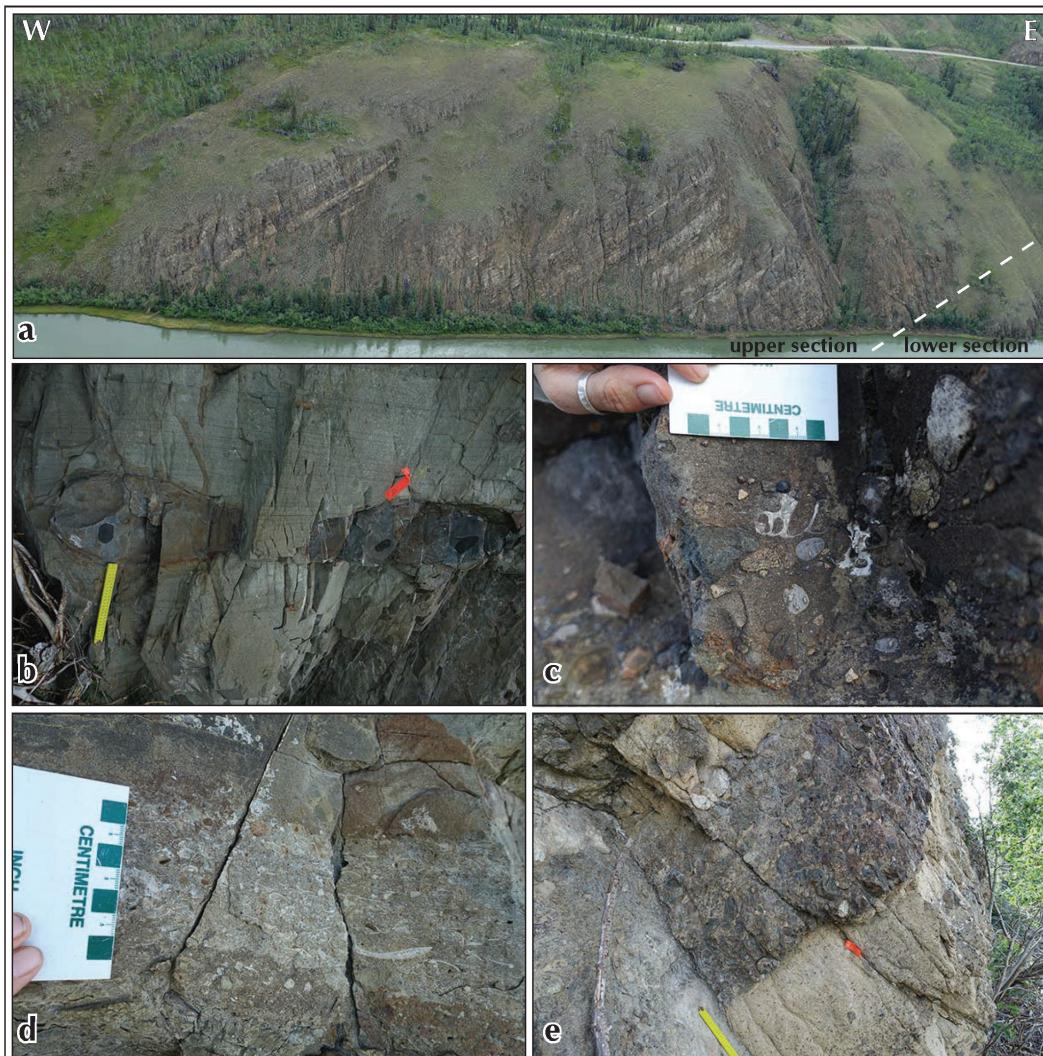


Figure 6. Field photographs of section 16-LVD-001 on the Robert Campbell Highway. (a) Overall view of the section along the Yukon River. Dark beds represent conglomeratic beds and buff coloured beds represent medium to coarse-grained beds. The lower unit is located on the far right and strata young to the left (west); (b) two aligned concretions in medium-grained, well sorted sandstone; (c) gastropod shell at 1.6 m; (d) macrofossil rich bed; and (e) pebble to boulder, poorly sorted, polymictic conglomerate and medium to coarse-grained sandstone.

LOCALITY 4: 16-LVD-002 OR (14-MH-016):

This 74 m-thick section comprises massive, very thickly bedded, very coarse to gravel sandstone, pebble to cobble conglomerate and interbedded fine to medium-grained sandstone and mudstone/siltstone that dip to the west (base of section: zone 08V 441784E 6885870N NAD83). Buff coloured, very coarse grained sandstone is massive and very thickly bedded (1-10 m) and incorporates angular mud rip-up clasts and floating pebbles (Fig. 7a). These beds typically have erosional bases with pebble lags. An example of burrowing (Fig. 7b) is found in the lower half of this section and interpreted as *Psilonichnus* (Colpron et al., 2016). Poorly sorted pebble to cobble conglomerate beds fine-upwards and are associated with very coarse grained beds.

Three units (6-8 m) of interbedded, fine to medium-grained sandstone and brown-black mudstone/siltstone punctuate massive sandstone units (Fig. 3). Planar lamination, rootlets, rare charcoal, waver-rippled bed tops and flame

structures (Fig. 7c) characterize these rocks. Mottled beds of rusty orange, medium-grained sandstone and clay beds occur throughout these units. Compressional deformation is displayed in interbedded fine to medium-grained sandstone and mudstone/siltstone (Fig. 7d).

LOCALITY 5: 16-LVD-003

Section 16-LVD-003 is 77 m-thick and exposed along a road cut ~10 km east of Carmacks (base of section: zone 08V 441317E 6886180N NAD83). The stratigraphic section was measured on the north side of the road because of better outcrop quality. This section is dominated by thickly bedded (0.5 to 8 m), buff coloured, very coarse and granular, poorly sorted, massive sandstone interbedded with medium-grained sandstone and mudstone. Medium-grained sandstone beds are characterized by parallel laminations and mud rip-up clasts (1 mm to 2 cm). Medium to thickly bedded medium-grained sandstone beds are interbedded with mottled black mudstone and poorly lithified white sandstone.

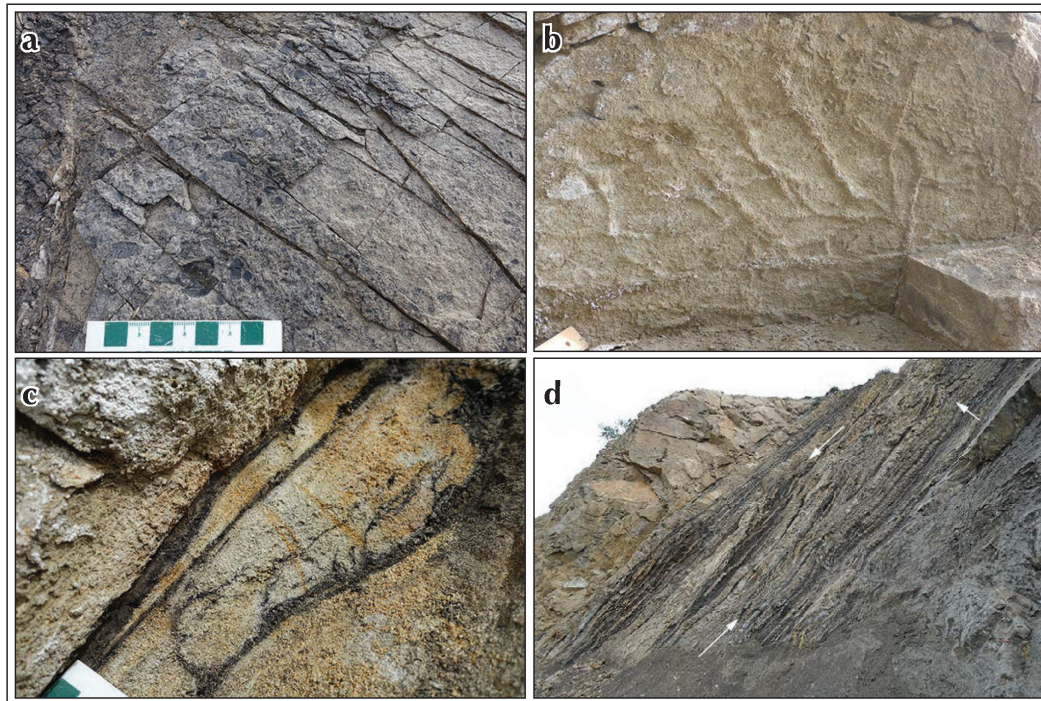


Figure 7. Field photographs of section 16-LVD-002 on the Robert Campbell Highway. (a) Surface of a rip-up mud clast-rich bed; (b) burrows interpreted to be *Psilonichnus*; (c) flame structures; and (d) compressional structures indicated by arrows.

One 3 m-thick bed of pebble to cobble, matrix-supported conglomerate is present with an erosive base that grades into granular sandstone. A Pliensbachian ash bed occurs at 65 m (Colpron *et al.*, 2015) on the south side of the road.

LOCALITY 6: 16-LVD-004 (CARMACKS AIRPORT)

This section crops out near the Carmacks airport and is the westernmost section measured on the Robert Campbell Highway. The stratigraphy has a total thickness of 67 m and is divided into two west-dipping conformable units (Fig. 8a; base of section: zone 08V 436493E 6888370N NAD83). The lower unit is dominated by buff coloured, very coarse-grained sandstone (Fig. 8b) interbedded with medium to thickly bedded (1-5 cm) silt to medium-grained sandstone. Finer grained interbeds have parallel lamination, faint cross-bedding, possible wave ripples, flame structures (Fig. 8c), and mud rip-up clasts. Very coarse grained beds are typically massive with localized wave ripples and erosional bases that fine-

upwards to medium to coarse-grained sandstone. A shift to medium-grained sandstone interbedded with very fine grained sandstone occurs at 38 m (Fig. 8d). This upper unit has an overall dark brown-blue appearance with thin (1 cm) white fine to medium-grained sandstone beds and mud rip-up clasts. The medium-grained sandstone beds are typically 0.5 to 2 cm thick, but 20 to 30 cm-thick beds are also present. Fine-grained sandstone beds are 0.3 to 1 cm thick.

NORTH KLONDIKE HIGHWAY

A 12-m thick section (14-MH-10) was measured on the east side of the North Klondike Highway, 20 km south of Carmacks (Fig. 9; base of section: zone 08V 457323E 6865678N NAD83). It is characterized by dark grey-brown, thinly bedded, fine to medium-grained sandstone and mudstone/siltstone and a sharp transition to white-buff, very coarse grained sandstone at 5 m (Fig. 10a).

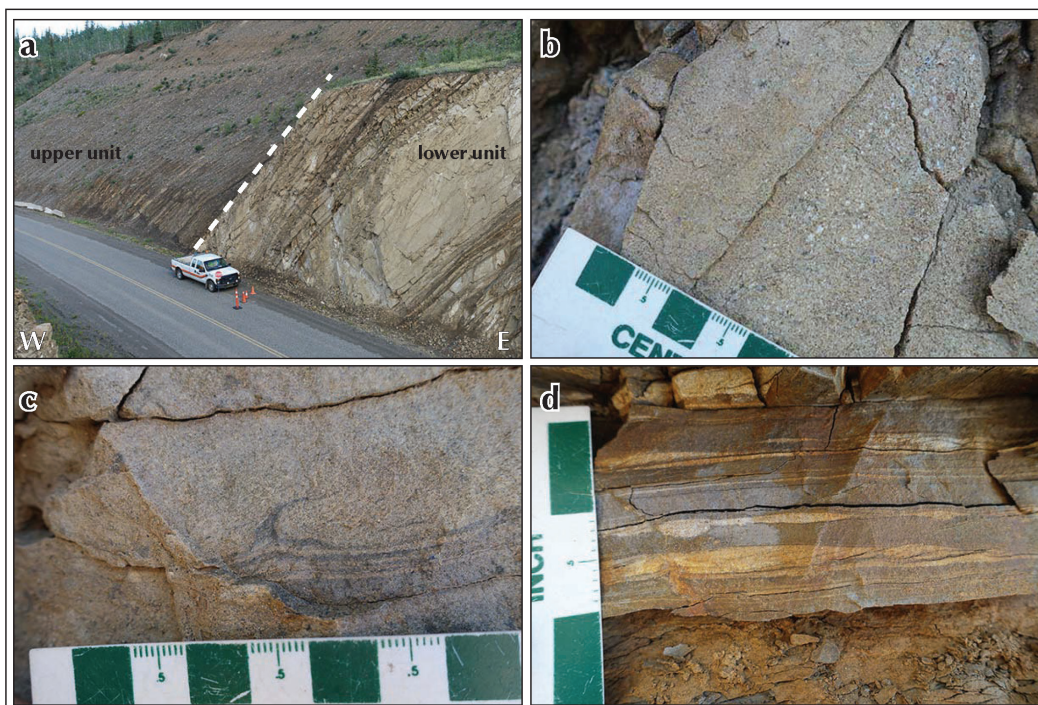


Figure 8. Field photographs of section 16-LVD-004 on the Robert Campbell Highway. (a) Overall view of the section which has two units; (b) parallel laminations in the lower half of the section; (c) flame structure in the lower half of the section; and (d) thinly bedded, wavy sandstone.

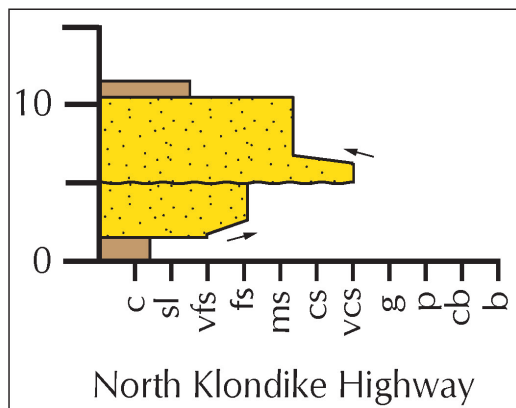


Figure 9. Measured stratigraphic section 14-MH-010 from the North Klondike Highway just south of Carmacks. This section is potentially a key to tie the Robert Campbell sections to Division Mountain stratigraphy. See figure 3 for legend and grain size abbreviations.

A flame structure (Fig. 10b) along this contact shows that strata are right way up and young northward. Coarsening upward trends are seen at the bed and section scale. Fine to medium-grained sandstone is internally massive, but some beds show cross-bedding and wave ripples (Fig. 10c). Sedimentary structures are not easily seen in the weathered mudstone beds, but their thickness and frequency decreases up section. Very coarse grained sandstone units (Fig. 10d) have abundant cross-bedding, wavy lamination and large plant fragment represented by coaly stringers. Abundant mica is present in both fine and coarse-grained sandstone.

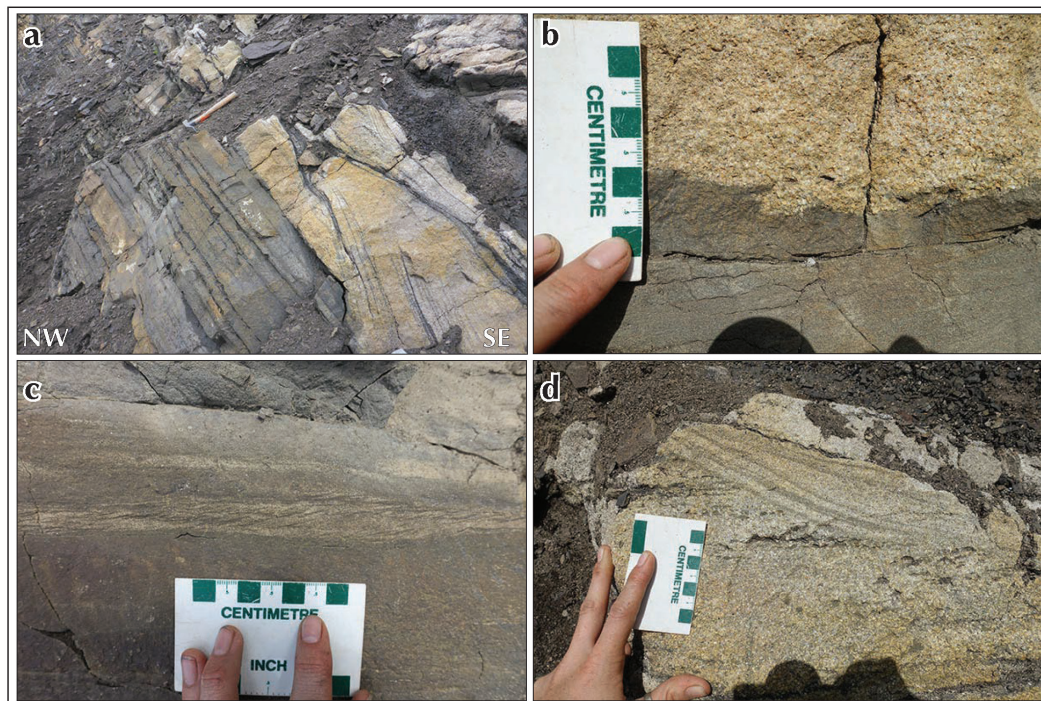


Figure 10. Field photographs of section 14-MH-010 on the North Klondike Highway. (a) Contact between dark brown fine-grained sandstone to buff coloured coarse-grained sandstone; (b) flame structure at the contact indicated stratigraphic up direction; (c) dark brown fine-grained sandstone with cross-bedding; and (d) buff coloured coarse-grained sandstone.

LAKE LABERGE

The Lewes River Group and basal Laberge rocks (Richthofen formation) crop out along the east side of Lake Laberge and are included in a multi-year regional mapping project initiated by the Yukon Geological Survey in 2015 (Bordet, 2016). The contact between the resistant Hancock member limestone, which forms prominent north to south-trending ridges, and Richthofen formation rocks was targeted during 2016 field investigations. The similar lithologies of the upper stratigraphic level of the Lewes River Group and overlying Richthofen formation make differentiation of these strata difficult. Due to these similarities, contact relationships with Hancock member limestone are also difficult to constrain. Where Laberge Group is positively identified, it unconformably overlies the Lewes River Group.

Small-scale sedimentary structures were difficult to distinguish in vegetated, inland areas because of the recessive nature of Richthofen formation mudstone/siltstone and fine-grained sandstone. Rocks that crop out along the shoreline of Lake Laberge therefore provide the best type of exposures to document such features. Interbedded mudstone and fine-grained sandstone of the Richthofen formation are continuous along ~11 km of the Lake Laberge shoreline by the mouth of Laurier Creek. Small-scale faulting affects some shoreline exposures (Fig. 11a). Some thin-bedded units have burrowed beds (Fig. 11b), flame structures, cm-scale concretions (Fig. 11c), soft-sediment deformation and are intermittently slightly calcareous. Massive, medium-grained sandstone beds have rare burrows, floating pebbles and are interbedded with mudstone and fine-grained sandstone. Soft sediment deformation, mudstone rip-up clasts (Fig. 11d), and limestone clasts (Fig. 11e) are also abundant south of Laurier Creek. Richthofen formation rocks in proximity to limestone are either pale green-blue, fine to medium-grained sandstone and have aligned concretions or interbedded fine-grained sandstone and mudstone that incorporates subangular to subrounded limestone clasts (3 cm to 1 m). Rare monomictic limestone conglomerate of the Lewes River Group is also present throughout the field area (Fig. 11f).

The eastern shoreline of Richthofen Island exposes west dipping, thin-bedded mudstone/siltstone and fine-grained sandstone, fine to medium-grained sandstone with floating pebbles and matrix-supported pebble to boulder conglomerate with sedimentary, plutonic and volcanic clasts. Brown-black mudstone and buff fine-

grained sandstone are rhythmically bedded and display synsedimentary deformation. Buff coloured, fine to medium-grained sandstone is massive and incorporates floating pebbles to cobbles, which include mudstone and limestone clasts. An unusually large limestone clast measuring ~20 by 20 m was observed on Richthofen Island.

MOUNT LAURIER

Mount Laurier is located northeast of Whitehorse between Lake Laberge and Teslin Mountain. This area is underlain by west-dipping Hancock member limestone and overlying strata of the basal Laberge Group (Bordet, 2016; Figs. 12 and 13a). Mount Laurier was visited in 2016 as part of this project to study Laberge Group strata in greater detail. Laminated, thinly bedded, dark brown-black mudstone and blue-grey, very fine to fine-grained sandstone were observed to unconformably overlie the massive limestone. Brown, matrix-supported pebble to boulder polymictic conglomerate (Fig. 13b) overlies finer grained units and makes up the ridge of Mount Laurier (Figs. 5 and 13c). Poorly-sorted, subrounded to rounded, sedimentary clasts (mudstone, limestone and rare chert), and intrusive and volcanic clasts constitute the conglomerate. The clasts range in size from 2 to 15 cm with rare larger clasts (20 to 60 cm). Buff coloured fine to medium-grained sandstone beds and lenses occur throughout the conglomerate (Fig. 12) and have cross-beds, climbing ripples and soft sediment deformation (Fig. 13d,e).

PRELIMINARY CONCLUSIONS

New stratigraphic observations and field mapping in 2016 helped to constrain the depositional history of the northern Whitehorse trough. Maroon coloured Tanglefoot formation rock units at the lower Robert Campbell Highway section (14-MH-013) are consistent with a semi-arid climate (desiccation cracks and oxidization) that was punctuated with intervening fan-delta conglomeratic sedimentation and may indicate a marginal marine to fluvial environment. Section 16-LVD-005, west of Eagles Nest Bluff, likely preserves a shift to shallow-marine sedimentation with the occurrences of cross-beds, concretions and rare fossils. Farther west, at locality 16-LVD-001, strata also are consistent with a shallow marine environment, but at this locality, abundant shell material is present and suggests proximity to the Hancock reef. This depositional setting is then disrupted

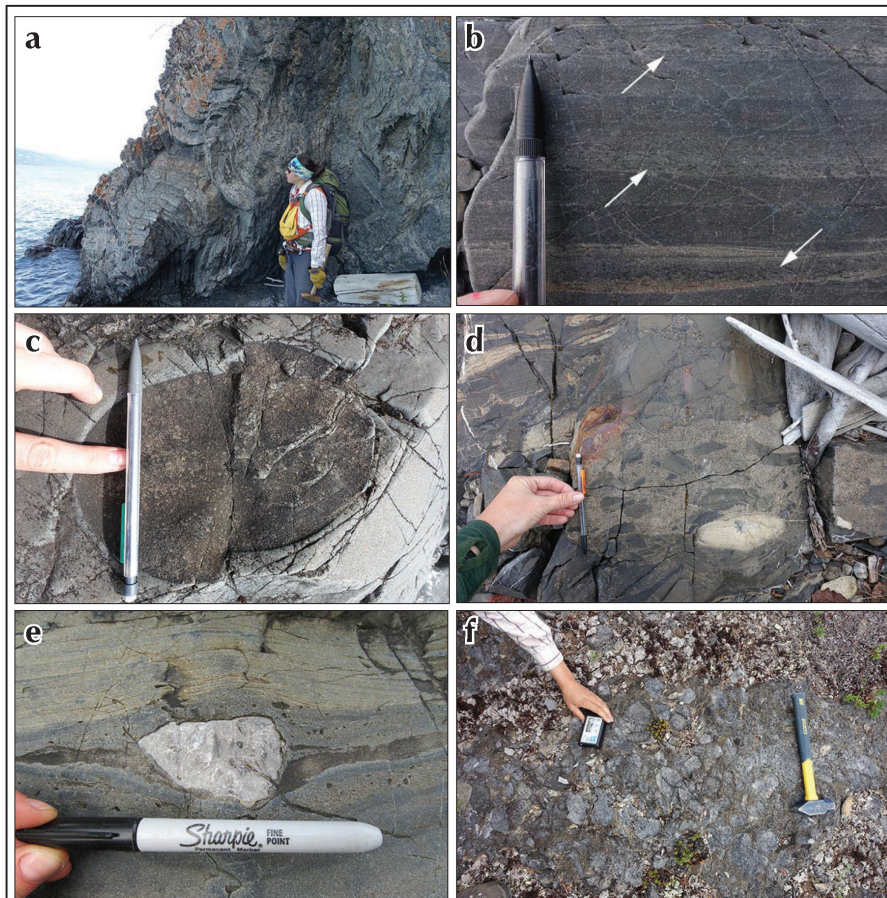


Figure 11. Field photographs of Laberge Group strata, Lake Laberge. **(a)** Folding in fine-grained thinly bedded sandstone and mudstone interpreted to be Richthofen formation; **(b)** thinly bedded burrowed beds on the shoreline of Lake Laberge; **(c)** faulted concretion in interpreted Richthofen formation strata; **(d)** angular mudstone rip-up clasts in a medium to coarse-grained matrix; **(e)** small limestone clast within Richthofen formation strata; and **(f)** monomictic limestone conglomerate of Lewes River Group.

by the emplacement of thick beds of pebble to boulder conglomerate that could be fan-delta deposits. At section 16-LVD-002, *Psilonichnus* burrows and wave-rippled beds suggest a shift to an estuarine or tidal delta depositional environment. Section 16-LVD-003 and the lower half of section 16-LVD-004 appear to be a continuation of this depositional environment, with coarse sedimentation dominating. A decrease in energy of the depositional system occurs at 37 m in section 16-LVD-004 and is

comparable to the packages of thinly interbedded sandstone and mudstone in section 16-LVD-002. On the North Klondike Highway, the coarsening upward, wave-rippled bed tops and coal fragments of section 14-MH-010 are consistent with a tidal delta or estuarine depositional environment. This section may represent an important tie between the Robert Campbell Highway sections and coal deposits at Division Mountain ~80 km south of Carmacks. The sharp boundary in this section is also

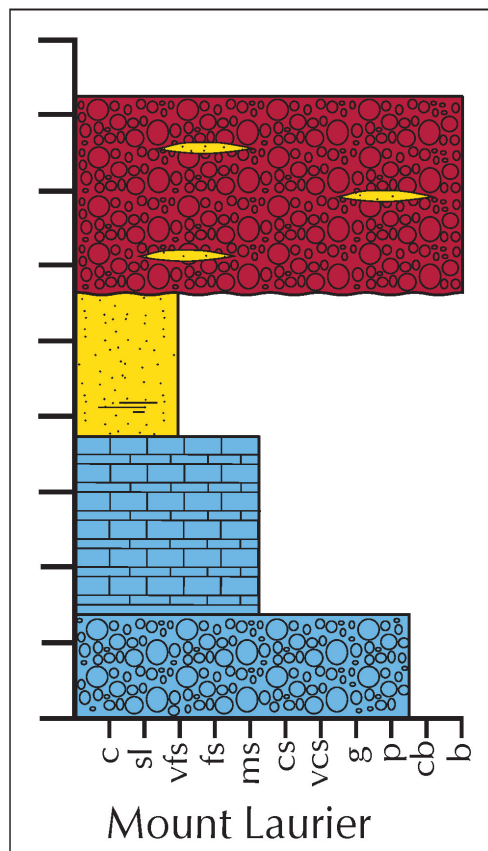


Figure 12. Schematic stratigraphic section of Mount Laurier stratigraphy. See figure 3 for legend and grain size abbreviations. Blue = limestone, yellow = fine to very coarse grained sandstone, and red = pebble to boulder conglomerate.

observed at Division Mountain and is associated with the change from coal-barren to coal-bearing strata (Colpron et al., 2016). During summer 2016, Tanglefoot formation strata were only observed along the Robert Campbell and North Klondike highways, which is consistent with the observation that these rocks are restricted to the northern Whitehorse trough (e.g., Lowey, 2004).

On the east side of Lake Laberge, finely bedded sandstone and mudstone packages are preliminarily interpreted to be Richthofen formation as they resemble rock units at the type section near the Lake Laberge campground. At Mount Laurier, thinly bedded sandstone and mudstone of the Richthofen formation are overlain by conglomerate that may represent submarine fan deposits. Sedimentary successions at both locations are indicative of turbiditic facies and likely indicate a deepening of the depositional environment from the Robert Campbell Highway in the north to Lake Laberge in the south. Limestone clasts included in Richthofen formation strata are probably eroded from Hancock member reef facies. In these areas, there are stratigraphic, and potentially structural, contacts between Lewes River and Laberge group strata that will be the focus of future field and laboratory investigations. For example, uncertain contact relationships will be informed by detrital zircon U-Pb studies that seek to discriminate upper Lewes River Group strata from basal Laberge Group strata.

ACKNOWLEDGEMENTS

This project is supported by the Yukon Geological Survey. Helicopter support was provided by Heli Dynamics. We are grateful to Sarah Ellis and Daphnee Tuzlak for providing field assistance. Esther Bordet provided constructive and helpful comments that improved this manuscript.



Figure 13. Field photographs of Laberge Group strata, Mount Laurier. (a) Laberge Group overlying Hancock member limestone at Mount Laurier; (b) subrounded to rounded, poorly-sorted, polymictic conglomerate; (c) Mount Laurier ridge dominated by Laberge Group conglomerate; (d) truncated soft sediment deformation in fine to medium-grained sandstone; and (e) climbing ripples in fine to medium-grained sandstone.

REFERENCES

- Bordet, E., 2016. Bedrock geology map of the Teslin Mountain and East Lake Laberge areas, parts of NTS 105E/2, 3 and 6. Yukon Geological Survey, Open File 2016-38, scale 1:50 000.
- Colpron, M., Gordey, S.P., Lowey, G.W., White, D. and Piercy, S.J., 2007. Geology of the northern Whitehorse trough, Yukon (NTS 105E/12, 13, and parts of 11 and 14; 105L/4 and parts of 3 and 5; parts of 115H/9 and 16; 115L/1 and part of 8). Yukon Geological Survey, Open File 2007-6, scale 1:150 000.
- Colpron, M. and Friedman R.M., 2008. U-Pb zircon ages for the Nordenskiöld formation (Laberge Group) and Cretaceous intrusive rocks, Whitehorse trough, Yukon. In: Yukon Exploration and Geology 2007, D.S. Emond, L.R. Blackburn, R.P. Hill and L.H. Weston (eds.), Yukon Geological Survey, p. 139-151.
- Colpron, M., Crowley, J.L., Gehrels, G., Long, D.G.F., Murphy, D.C., Beranek, L. and Bickerton, L., 2015. Birth of the northern Cordilleran orogen, as recorded by detrital zircons in Jurassic synorogenic strata and regional exhumation in Yukon. *Lithosphere*, vol. 7, p. 541-562.
- Colpron, M., Israel, S. and Hutchison, M., 2016. Tectonics of the Intermontane and Insular terranes, and development of Mesozoic synorogenic basins in southern Yukon: Carmacks to Kluane Lake. GAC®-MAC 2016 Whitehorse, Field Trip Guide Book, 108 p.
- Dickie, J.R. and Hein, R.J., 1995. Conglomeratic fan deltas and submarine fans of the Jurassic Laberge Group, Whitehorse Trough, Yukon Territory, Canada: fore-arc sedimentation and unroofing of a volcanic arc complex. *Sedimentary Geology*, vol. 98, p. 263-292.
- Hart C.J.R., 1997. A Transect across Northern Stikinia: Geology of the Northern Whitehorse Map Area, Southern Yukon Territory (105D/13-16). Exploration and Geological Services Division, Yukon Region, Indian and Northern Affairs Canada, Bulletin 8, 112 p.
- Hart, C.J.R. and Radloff, J.K., 1990. Geology of Whitehorse, Alligator lake, Fenwick Creek, Carcross and Part of Robinson Map Areas (105D/11, 6, 3, 2 & 7). Yukon Geological Survey, Open File 1990-4(G), scale 1:50 000.
- Hart, C.J.R., Dickie, J.R., Ghosh, D.K. and Armstrong, R.L., 1995. Provenance constraints for Whitehorse Trough conglomerate: U-Pb zircon dates and initial Sr ratios of granitic clasts in Jurassic Laberge Group, Yukon Territory. In: *Jurassic Magmatism and Tectonics of the North American Cordillera*, D.M. Miller and C. Busby (eds.), Geological Society of America Special Paper 299, p. 47-63.
- Johnston, S.T., Mortensen, J.K. and Erdmer, P., 1996. Igneous and metagneous age constraints for the Aishihik metamorphic suite, southwest Yukon. *Canadian Journal of Earth Sciences*, vol. 33, p. 1543-1555.
- Logan, J.M. and Mihalynuk, M.G., 2014. Tectonic controls on early Mesozoic paired alkaline porphyry deposit belts (Cu-Au±Ag-Pt-Pd-Mo) within the Canadian Cordillera. *Economic Geology*, vol. 109, p. 827-858.
- Lowey, G.W., 2004. Preliminary lithostratigraphy of the Laberge Group (Jurassic), south-central Yukon: Implications concerning the petroleum potential of the Whitehorse trough, In: Yukon Exploration and Geology 2003, D.S. Emond and L.L. Lewis (eds.), Yukon Geological Survey, p. 129-142.
- Lowey, G.W., Long, D.G.F., Fowler, M.G., Sweet, A.R. and Orchard, M.J., 2009. Petroleum source rock potential of Whitehorse trough: A frontier basin in south-central Yukon. *Bulletin of Canadian Petroleum Geology*, vol. 57, p. 350-386.
- Mihalynuk, M.G., Nelson, J.A. and Diakow, L.J., 1994. Cache Creek terrane entrapment: Oroclinal paradox within the Canadian Cordillera. *Tectonics*, vol. 13, p. 575-595.
- Mihalynuk, M.G., Erdmer, P., Ghent, E.D., Cordey, F., Archibald, D.A., Friedman, R.M. and Johannson, G.G., 2004. Coherent French Range blueschist: Subduction to exhumation in <2.5 m.y.? *Geological Society of America Bulletin*, vol. 116, p. 910-922.
- Nelson, J.L., Colpron, M. and Israel, S. 2013. The Cordillera of British Columbia, Yukon, and Alaska: Tectonics and Metallogeny. In: *Tectonics, Metallogeny and Discovery: The North American Cordillera and Similar Accretionary Settings*, M. Colpron, T. Bissig, B.G. Rush and J.F.H. Thompson (eds.), Society of Economic Geologists Special Publication 17, p. 53-103.

- Tempelman-Kluit, D.J., 1984. Geology, Laberge (105E) and Carmacks (115I), Yukon Territory. Geological Survey of Canada, Open File 1101, scale 1:250 000.
- Tempelman-Kluit, D.J., 2009. Geology of Carmacks and Laberge map areas, central Yukon: Incomplete draft manuscript on stratigraphy, structure and its early interpretation (ca. 1986). Geological Survey of Canada, Open File 5982, 399 p.
- White, D., Colpron, M. and Buffett, G., 2012. Seismic and geological constraints on the structure of the northern Whitehorse trough, Yukon, Canada. *Bulletin of Canadian Petroleum Geology*, vol. 60, p. 239-255.

New investigations of basal Laberge Group stratigraphy, Whitehorse trough, central Yukon

L.H. van Drecht and L.P. Beranek

Department of Earth Sciences, Memorial University of Newfoundland

van Drecht, L.H. and Beranek, L.P., 2018. New investigations of basal Laberge Group stratigraphy, Whitehorse trough, central Yukon. In: Yukon Exploration and Geology 2017, K.E. MacFarlane (ed.), Yukon Geological Survey, p. 151-163.

ABSTRACT

The tectonic evolution of the Whitehorse trough in central Yukon is largely preserved by the Early to Middle Jurassic Laberge Group, an ~3000-m thick succession of synorogenic clastic strata that unconformably overlies arc and arc marginal rocks of the Lewes River Group. A two-year project was initiated to test a Sinemurian to Toarcian transgression of basal Laberge Group strata westward across the Whitehorse trough and examine the regional relationships between the timing of Jurassic exhumation, sedimentation, and terrane accretion in the northern Canadian Cordillera. Field studies in 2017 targeted basal Laberge Group strata at seven locations in central Yukon. At each field locality, basal Laberge Group strata are known or inferred to unconformably overlie the Povoas formation and multiple units of the Aksala formation. Pre-Early Jurassic unconformities may indicate variable basin topography due to the complex internal stratigraphy of the Lewes River Group, or that regional exhumation and erosion affected the Whitehorse trough prior to Laberge Group sedimentation.

* lberanek@mun.ca

INTRODUCTION

The early growth of the northern Canadian Cordillera is marked by the late Paleozoic to mid-Mesozoic accretion of the Intermontane terranes to the western Laurentian margin, crustal thickening in the Cordilleran hinterland, and initial subsidence in the Alberta foreland basin (e.g., Cant and Stockmal, 1989; Colpron *et al.*, 2007, 2015; Nelson *et al.*, 2013). This early growth is in part recorded by the Whitehorse trough, a sedimentary basin that developed on top of the Intermontane terranes in a transitional forearc to wedge-top setting during the Early to Middle Jurassic closure of the Cache Creek Ocean (Nelson *et al.*, 2013; Colpron *et al.*, 2015). The Whitehorse trough is regionally extensive and spans more than 600 km from the Carmacks region of central Yukon (Fig. 1) to the Dease Lake region of northern British Columbia. The northern apex of the trough near Carmacks is characterized by proximal, marginal marine to fluvial strata of the Tanglefoot formation, whereas the central part of the trough near Whitehorse consists of distal, deep-marine mass-flow deposits of the Richthofen formation, suggesting a deepening of the basin towards the south (e.g., Dickie and Hein, 1995; Tempelman-Kluit, 1984; Lowey, 2004; Lowey *et al.*, 2009). Laberge Group strata unconformably overlie several Upper Triassic units of the Lewes River Group (Stikinia; Cairnes, 1910; Tempelman-Kluit, 1984; Dickie and Hein, 1995; Lowey, 2004, 2008; Colpron *et al.*, 2007), which likely reflects the lateral discontinuity of Carnian-Rhaetian rock units in central Yukon (Bordet, 2016a,b, 2017) and/or exhumation of the Intermontane terranes (e.g., Knight *et al.*, 2013; Joyce *et al.*, 2015; Colpron *et al.*, 2015), creating topography within the Whitehorse trough prior to Early Jurassic sedimentation.

Previous studies of the Whitehorse trough have mostly focused on the sedimentology and depositional setting of the Laberge Group (e.g., Hart and Radloff, 1990; Dickie and Hein, 1995; Lowey *et al.*, 2008; Bordet, 2016a), but relatively few studies (Hart *et al.*, 1995) have examined the stratigraphic responses of Jurassic exhumation and erosion or tested relationships between the timing of exhumation, sedimentation and terrane accretion. Recently, Colpron *et al.* (2015) investigated these relationships and hypothesized a westward younging of basal Laberge Group strata across the Whitehorse trough, which may indicate that subsidence followed exhumation

and uplift of its western shoulder. A two-year project was initiated in summer 2016 to test the hypotheses of Colpron *et al.* (2015) and constrain the field geology and detrital zircon (U-Pb and Hf isotope) signatures of Laberge Group strata in central Yukon. The objectives of the 2016 field season, summarized by van Drecht *et al.* (2017), focused on the physical stratigraphy and depositional setting of Laberge Group rock units at four localities. The objectives of the 2017 field season, presented in this report, were to identify the contact relationships between basal Laberge Group and underlying Lewes River Group strata in the Mandanna Lake, Conglomerate Mountain, Fish Lake, Takhini subdivision, King Lake, Mount Byng and Mount Slim areas to test the westerly transgression of basal strata hypothesized by Colpron *et al.* (2015). Forthcoming detrital zircon U-Pb and Hf isotope studies will use these stratigraphic constraints to more fully define the provenance and paleodrainage history of Laberge Group rock units and provide new insights on the evolution of the Intermontane terranes.

TECTONIC SETTING

The Intermontane terranes (Yukon-Tanana, Stikinia and Quesnellia) were in proximity to western Laurentia by the Early Triassic (Beranek and Mortensen, 2011) and later imbricated following the Late Triassic-Early Jurassic closure of the Cache Creek Ocean (Mihalynuk *et al.*, 1994). The most widely accepted model to explain the imbrication and subsequent geometry of the Intermontane terranes involves the counterclockwise bending and subsequent entrapment of oceanic rock units assigned to the Cache Creek terrane (Mihalynuk *et al.*, 1994; Logan and Mihalynuk, 2014; Colpron *et al.*, 2015). Late Triassic to Early Jurassic crustal thickening and pluton emplacement in central Yukon was accompanied by rapid exhumation of the Yukon-Tanana, Stikinia and Quesnellia terranes (e.g., Johnston *et al.*, 1996). Lower to Middle Jurassic synorogenic strata of the Laberge Group were likely sourced from exhumed plutons and basement rocks assigned to Stikinia.

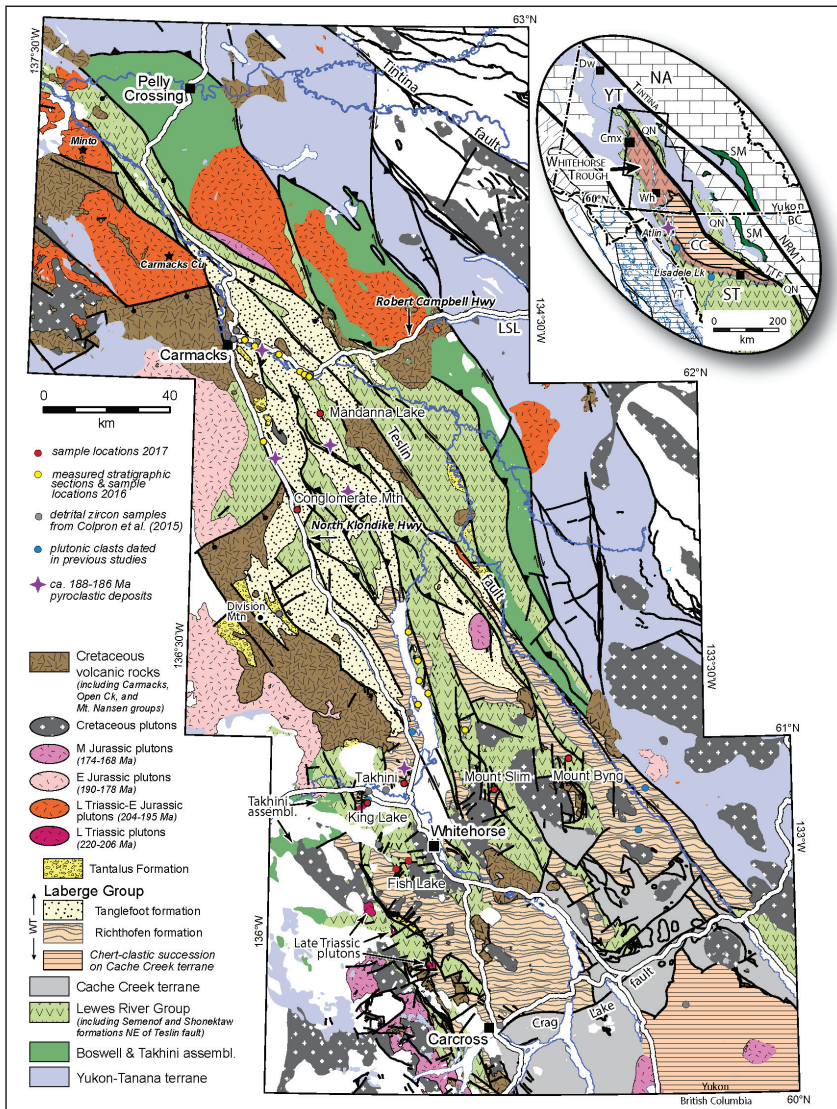


Figure 1. Regional geology of the Whitehorse trough area modified from Colpron (2015). Locations of 2016 field sites are shown by yellow dots and 2017 field sites are shown by red dots. Field locations on the Robert Campbell Highway represent measured stratigraphic sections. Locations at Mandanna Lake, Conglomerate Mountain, Takhini, King Lake, Fish Lake, Mount Byng, and Mount Slim indicate sampling locations. Grey and blue dots denote detrital zircon sample locations of (Colpron et al. 2015) and previously dated plutonic clasts (Hart et al., 1995). The inset shows the location of the Whitehorse trough relative to the Intermontane terranes of the northern Canadian Cordillera. Abbreviations: CC-Cache Creek terrane; CMx-Carmacks; Dw-Dawson; LSL-Little Salmon Lake; NA-rocks of ancestral North America; NRMT-Northern Rocky Mountain Trench Fault; QN-Quesnellia; SM-Slide Mountain terrane; ST-Stikinia; TTF-Teslin-Thibert fault; Wh-Whitehorse; YT-Yukon-Tanana terrane.

STRATIGRAPHIC FRAMEWORK

LEWES RIVER GROUP

The stratigraphy of the Lewes River Group is complex due to lateral facies changes from west to east across central Yukon (Wheeler, 1961; Bordet 2016a, 2017). The Povoas formation is the lowermost unit of the Lewes River Group and consists of Carnian basalt and andesite, volcanic breccia, tuff and agglomerate (Fig. 2; Tempelman-Kluit, 1984, 2009). The overlying Carnian-Rhaetian Aksala formation records a break in regional magmatism and is characterized by micritic limestone, fossiliferous limestone, calcareous mudstone-sandstone, lithic sandstone, argillite and calcareous conglomerate (Tozer, 1958; Tempelman-Kluit, 1984; Bordet, 2016a, 2017). Tozer (1958) divided these Upper Triassic rocks into seven limestone units that are regionally interbedded with, or laterally equivalent to Norian-Rhaetian clastic strata, whereas Tempelman-Kluit (1984) divided these rocks into the Casca (lithic sandstone, argillite and conglomerate), Hancock (limestone), and Mandanna members (maroon weathering lithic sandstone, mudstone and conglomerate). Recent mapping by Bordet (2016a,b, 2017) broadly supports the interpretations of Tozer (1958) and argues for the presence of several Norian and younger carbonate units within the Lewes River Group, which implies that not all Upper Triassic carbonate strata are equivalent to the Rhaetian Hancock member. In this paper, the Casca and Hancock members of Tempelman-Kluit (1984) are referred to as green lithic sandstone and limestone of the Aksala formation, respectively, to more accurately reflect the revised stratigraphy of Bordet (2016b, 2017). The Mandanna member nomenclature is used as per Templeman-Kluit (1984) because it does not crop out in the updated map area of Bordet (2016b) and accurately represents the upper Aksala formation.

LABERGE GROUP

The Lower to Middle Jurassic Laberge Group is a 3000 m-thick sedimentary succession that was first described in central Yukon along the shoreline of Lake Laberge (Dawson, 1887). The Laberge Group is divided into the Sinemurian-Bajocian Tanglefoot and Richthofen formations and Pliensbachian Nordenskiöld dacite (Fig 2; Tempelman-Kluit, 1984; Dickie and Hein, 1995; Lowey, 2004). Post-Bajocian fluvio-deltaic rocks of the Tantalus Formation unconformably overlie the Laberge Group in central Yukon (Fig. 2; Hart and Radloff, 1990; Dickie and Hein, 1995; Colpron et al., 2015).

The Tanglefoot formation (Fig. 2) consists of interbedded sandstone and mudstone, mass-flow conglomerate, pebbly sandstone, and coal with abundant terrestrial plant and marginal marine fossils. The Tanglefoot formation is restricted to the northern apex of the Whitehorse trough and was deposited in a proximal marginal marine to fluvial setting (Lowey, 2004; Hutchison, 2017). The type area for this formation is located at Tanglefoot Mountain, north of Lake Laberge (Lowey, 2004) and good exposures are also present along the Robert Campbell Highway (Fig. 1; van Drecht et al., 2017).

The Richthofen formation (Fig. 2) consists of graded siltstone, very fine grained sandstone with mudstone couplets, mass-flow conglomerate, pebbly sandstone, massive sandstone, volcanioclastic rocks and minor limestone (Lowey, 2004; Lowey et al., 2009). Richthofen formation strata are restricted to the central part of the trough and were deposited in a distal mass-flow setting.

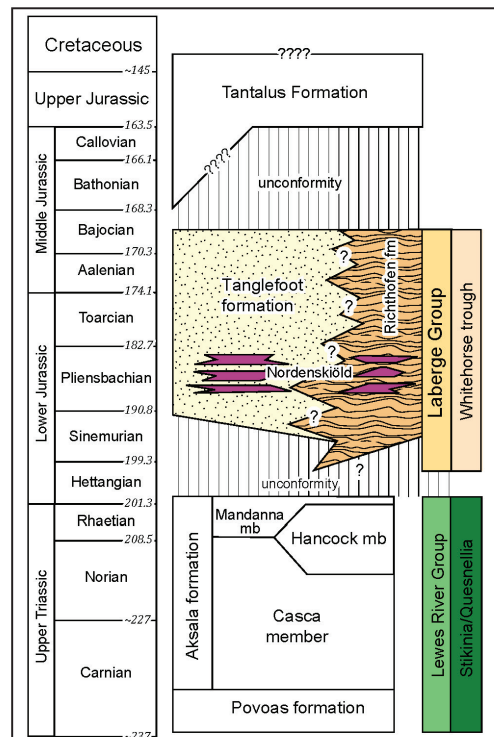


Figure 2. Schematic stratigraphy of Stikinia, Quesnellia and the Whitehorse trough complied by Colpron et al. (2015).

The type area is located at the Lake Laberge campground along the western shoreline of Lake Laberge (Tempelman-Kluit, 1984; Lowey, 2004). Good exposures of the Richthofen formation can also be seen along the eastern shoreline of Lake Laberge and flanks of Mount Laurier.

Well-rounded, cobble to boulder, clast to matrix-supported, mass-flow conglomerate units occur throughout the Richthofen and Tanglefoot formations (Hart *et al.*, 1995). Sinemurian conglomerate units comprise volcanic and sedimentary (predominantly limestone) clasts, whereas Pliensbachian and younger strata contain a larger proportion of plutonic rock clasts that imply the unroofing of a nearby arc complex (Dickie and Hein, 1995; Hart *et al.*, 1995; Shirmohammad *et al.*, 2011). In northern British Columbia, Pliensbachian and younger strata of the Whitehorse trough also include metamorphic clasts, which have not been observed in Yukon prior to this field season (Dickie and Hein, 1995; Shirmohammad *et al.*, 2011). Laberge Group conglomerate units were likely deposited as debris flows, sheet floods and bar deposits (Dickie and Hein, 1988). Paleocurrent indicators (flute casts, wavy stratification, bar-swash lamination) suggest that sediment transport was from west to east, transverse to the north-to-south deepening direction of the Whitehorse trough as indicated by longitudinal facies changes (Dickie and Hein, 1988, 1995; Hart *et al.*, 1995; Lowey, 2004, Lowey *et al.*, 2008).

The Nordenskiöld dacite consists of epiclastic and primary dacitic tuffs and flows (Tempelman-Kluit, 1984) that have been mapped at three stratigraphic levels in the Laberge Group and represent volcanic episodes at 188.1 ± 0.4 Ma, 187.2 ± 0.4 Ma and 186.5 ± 0.3 Ma (Colpron *et al.*, 2007). Zircon U-Pb ages of the Nordenskiöld dacite indicate active volcanism during deposition of the Laberge Group (Colpron and Friedman, 2008).

CONTACT RELATIONSHIPS

Numerous workers, including Cairnes (1910), Cockfield and Bell (1926), Bostock and Lees (1938), Wheeler (1961), Tempelman-Kluit (1984), and Hart and Radloff (1990), have described the contact relationship between the Lewes River and Laberge groups in central Yukon. The contact has been described as a conformity (Bostock and Lees, 1938; Tempelman-Kluit, 1984; Hart and Radloff, 1990), an unconformity (Lowey, 2008), a disconformity (Hart and Radloff, 1990), an angular unconformity (Cockfield and Bell, 1926; Wheeler, 1961; Lowey, 2008), or as changing from a disconformity on the western margin of the basin to

a conformity in the central region (Wheeler, 1961). Lowey (2008) proposed that the contact is an unconformity that spans the entire Whitehorse trough, typically marked by basal conglomerate in the Richthofen and Tanglefoot formations.

2017 FIELD STUDIES

The 2017 field season focused on describing the contact relationships between the Lewes River and Laberge groups at Mandanna Lake, Conglomerate Mountain, Fish Lake, Takhini subdivision, King Lake, Mount Byng and Mount Slim (Fig. 1). In the northern apex of the trough, the Tanglefoot formation overlies massive limestone and maroon weathering sandstone of the upper Aksala formation at Mandanna Lake and Conglomerate Mountain. In the central part of the trough the Richthofen formation overlies massive limestone and green sandstone of the Aksala formation and gabbro of the Povoas formation at Fish Lake, King Lake, Mount Byng and Mount Slim.

TANGLEFOOT FORMATION

Mandanna Lake

The Laberge Group overlies limestone of the Aksala formation to the southwest of Mandanna Lake (Fig. 1; zone 08V, 459834 E, 6857184 N, NAD83), ~30 km southeast of Carmacks (Colpron *et al.*, 2007). Basal Laberge Group strata at this locality consist of massive, brown, cobble to pebble, clast to matrix-supported, polymictic conglomerate of the Tanglefoot formation. Conglomerate clasts are dominantly felsic plutonic and volcanic rocks with lesser amounts of sedimentary rocks. Clasts are subrounded to rounded, poorly sorted and range in size from 2 to 20 cm (Fig. 3a). Dark blue-grey, massive, medium to coarse-grained, poorly sorted sandstone underlies the ~3 m-thick conglomerate unit and dips to the northeast (Fig. 3b). This outcrop represents probable basal Laberge Group as limestone crops out west of this locality, but the contact is covered and not directly observed. The contact is inferred to be unconformable.

Conglomerate Mountain

Tanglefoot formation conglomerate overlies maroon weathering sandstone of the upper Aksala formation at Conglomerate Mountain, ~110 km north of Whitehorse along the North Klondike Highway (Fig. 1; zone 08V, 453930 E, 6833117 N, NAD83). At this locality, maroon weathering, medium to coarse-grained, poorly sorted,

massive to burrowed sandstone of the Mandanna member dips towards the southeast (Fig. 5a,b). A thick unit of massive, brown, matrix to clast-supported, polymictic cobble to boulder conglomerate of the Tanglefoot formation overlies the Mandanna member (Fig. 4a). The overlying conglomerate is composed of subrounded to rounded, poorly sorted, volcanic and plutonic clasts with

minor sedimentary clasts that range in size from 0.3 to 127 cm (Fig. 5c). Felsic plutonic rocks make up the greatest fraction of the boulder-sized clasts, whereas volcanic and sedimentary clasts make up finer clast sizes. The matrix is buff coloured, medium to coarse-grained, poorly sorted sandstone (Fig. 5d). The contact at Conglomerate Mountain is covered but interpreted to be unconformable.

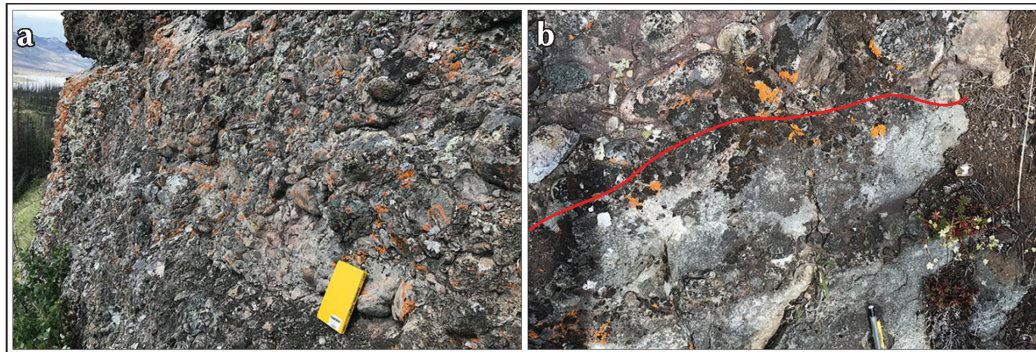


Figure 3. Field photographs of the Tanglefoot formation at Mandanna Lake. (a) Poorly sorted cobble to boulder conglomerate; and (b) annotated photo of the contact between conglomerate (top) and medium to coarse-grained sandstone (bottom).

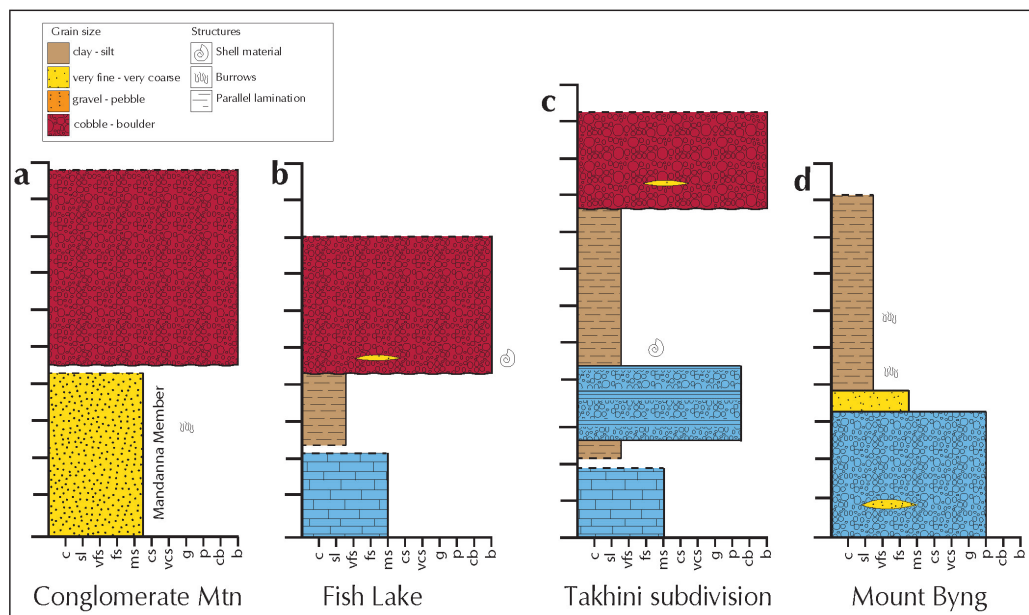


Figure 4. Schematic stratigraphy at (a) Conglomerate Mountain, (b) Fish Lake, (c) Takhini subdivision, and (d) Mount Byng. Grain size abbreviations: c = clay, sl = silt, vfs = very fine grained, fs = fine-grained, ms = medium-grained, cs = coarse-grained, vcs = very coarse grained, g = granule, p = pebble, cb = cobble, b = boulder.

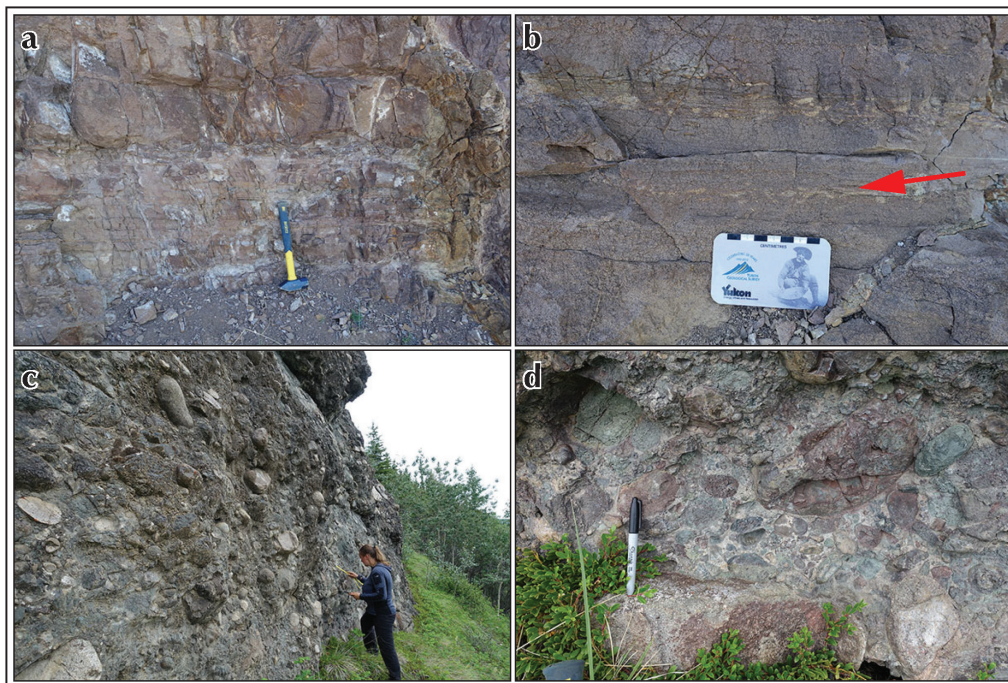


Figure 5. Field photographs of the Tanglefoot formation at Conglomerate Mountain. (a) Medium to coarse-grained, poorly sorted, massive Mandanna formation sandstone; (b) example of burrows in the Mandanna formation; (c) outcrop scale photo of Laberge Group polymictic pebble to boulder conglomerate; and (d) fresh surface of Laberge Group polymictic pebble to boulder conglomerate.

RICHTHOSEN FORMATION

Fish Lake

Basal Laberge Group strata crop out in the Fish Lake area ~16 km southwest of Whitehorse and are inferred to overlie the Mandanna member sandstone and Aksala formation limestone (Fig. 1; zone 08V, 485805 E, 6721676 N, NAD 83). At this locality, the contact is covered and not directly observed; basal strata are inferred by the proximity to limestone. The ridge west of Fish Lake comprises massive, brown, matrix-supported, pebble to cobble, poorly sorted, polymictic conglomerate that overlies dark blue, very fine to fine-grained sandstone of the Richthofen formation (Fig. 4b). Conglomerate units at this locality consist of subrounded to rounded clasts of felsic plutonic, volcanic and metamorphic rocks that range in size from 1 to 8 cm (Fig. 6a). Plutonic and volcanic clasts are the most abundant; three foliated mafic rock clasts were also

observed (Fig. 6b,c). A recrystallized ammonite (Fig. 6d) from a dark blue, medium-grained sandstone lens near the contact with the Lewes River Group was collected for biostratigraphic analysis. Fine-grained maroon clasts are also present in the sandstone lens, which likely indicates proximity to the Mandanna member, although it does not crop out at this locality. Along the southern end of the ridge, very fine grained, dark blue Richthofen formation sandstone with buff coloured laminae underlies the conglomerate and is locally intruded by rhyolite dikes. Basal Laberge Group strata also crop out along the eastern side of Fish Lake (Fig. 1; zone 08V, 488343 E, 6724611 N, NAD 83). This locality is characterized by pebble to cobble, subrounded to rounded, poorly sorted, polymictic (felsic plutonic and volcanic) conglomerate with fine to medium-grained sandstone lenses, comparable to strata immediately west. The contact at Fish Lake is interpreted to be unconformable.

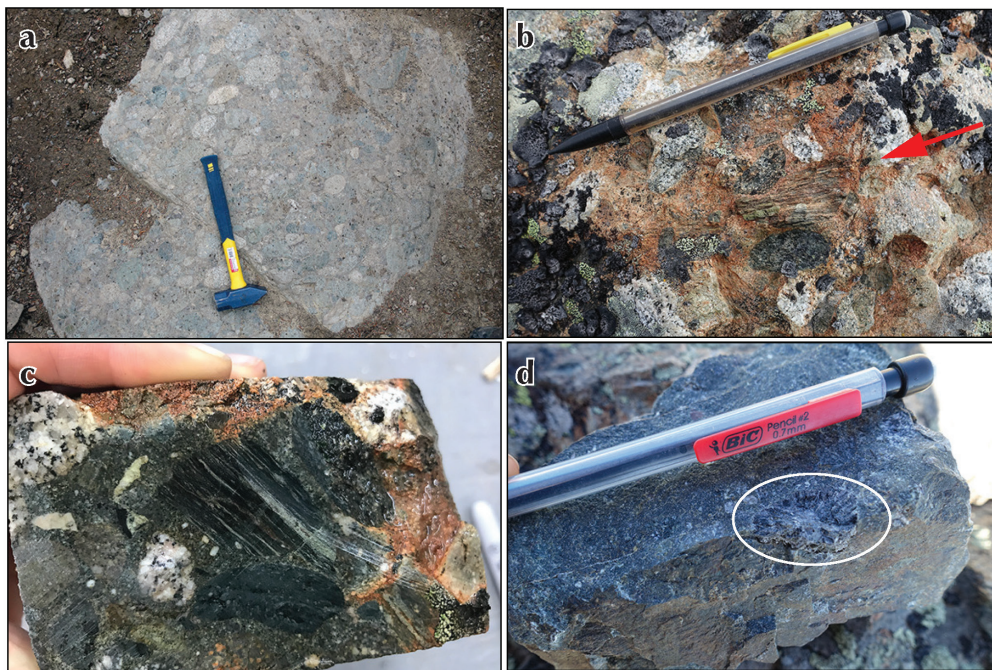


Figure 6. Field photographs of the Richthofen formation at Fish Lake. **(a)** Laberge Group polymictic pebble to cobble conglomerate; **(b)** foliated mafic clast in the conglomerate annotated by red arrow; **(c)** fresh surface of the same clast from **b**; and **(d)** ammonite fossil in dark blue medium-grained sandstone lens.

Takhini subdivision

Basal Laberge Group strata overlie limestone of the Askala formation in the Takhini subdivision area (Figs. 1 and 4c; zone 08V, 488086 E, 6748844 N, NAD 83). The base of this section consists of monomictic limestone conglomerate and laminated limestone (Fig. 7a). Conglomeratic beds range from 14 to 28 cm thick, whereas laminated beds range from 7 to 10 cm thick. Conglomerate clasts are white to dark blue in a dark blue carbonate matrix (Fig. 7a). The limestone unit is overlain by dark blue, very fine to fine-grained, mudstone/sandstone couplets and pebble to cobble, rounded to subrounded, poorly sorted conglomerate of the Richthofen formation (Fig. 7b) that is intruded by fine-grained intermediate dikes. Ammonite and gastropod fossils occur in very fine to fine-grained sandstone beds directly overlying limestone beds. The contact at Takhini subdivision is interpreted as unconformable.

King Lake

Basal Laberge Group strata crop out near King Lake ~20 km northwest of Whitehorse (Fig. 1). At this locality, crystal (quartz, feldspar) lithic tuff of the Nordenskiöld dacite nonconformably overlies Late Triassic gabbro of the Povoas formation (zone 08V, 474374 E, 6742564 N, NAD 83; Fig. 8a,b). Poorly sorted, polymictic pebble to cobble conglomerate of the Richthofen formation (Fig. 8c) overlies the tuff and is the dominant lithology that makes up the prominent ridges around King Lake. Subrounded to rounded clasts range from 1 to 8 cm. Conglomerate units at this locality are very weathered and typically not well exposed, but the clasts appear to be volcanic and felsic plutonic rocks.



Figure 7. Field photographs of the Richthofen formation at Takhini subdivision. (a) Monomicitic limestone conglomerate and laminated limestone; and (b) contact between dark blue very fine to fine-grained sandstone and mudstone couplets and pebble to boulder conglomerate.



Figure 8. Field photographs of the Richthofen formation at King Lake. (a) Contact between Nordenskiöld dacite crystal lithic tuff and Povoas formation gabbro; (b) fresh surface of crystal lithic tuff; and (c) Laberge Group polymictic pebble to cobble conglomerate.

Mount Byng

Northeast of Mount Byng, the Richthofen formation overlies limestone that is currently mapped as undifferentiated Aksala formation (Fig. 4d; zone 08V, 539547 E, 6757952 N, NAD 83; Hart and Radloff, 1990). The base of this section consists of light grey-blue, pebble to cobble, poorly sorted, clast to matrix-supported, limestone conglomerate (Fig. 9a). Subrounded to rounded limestone clasts that range in size from 1 to 7 cm are the most abundant components in the conglomerate. Subrounded to rounded, pebble-sized, dark grey volcanic porphyry clasts are less abundant. The limestone unit is overlain by dark grey-blue, very fine to fine-grained Richthofen formation sandstone with buff coloured laminations. Richthofen formation strata at this location are comparable to those in other areas of the Whitehorse trough and typically characterized by fining-up mudstone and sandstone couplets (Fig. 9b) with rare burrows. Couplets range in thickness from 0.5 to 3 cm, with very fine grained material making up darker coloured beds and the fine-grained sand characterizing buff coloured beds. Contacts between beds are often wavy and buff coloured beds locally pinch and swell (Fig. 9c). The contact between the Laberge Group and Lewes River Group at Mount Byng is interpreted to be unconformable.

Mount Slim

Basal Laberge Group strata crop out at two localities southeast of Mount Slim, located ~20 km northeast of Whitehorse. In this area, the Richthofen formation overlies volcaniclastic sandstone and limestone of the Aksala formation. At the first locality, dark grey mudstone and buff coloured sandstone couplets of the Richthofen formation overlie green, fine to medium-grained sandstone mapped as the Casca member (Fig. 1; zone 08V, 517754 E, 6746129 N, NAD 83; Hart and Radloff, 1990; Fig 10a). Nearby dikes give the weathered surface of Richthofen formation strata a rusty, red-brown colour. At the second locality, the Richthofen formation unconformably overlies grey-blue limestone of the Aksala formation (zone 08V, 514475 E, 6751661 N, NAD 83). Dark grey, 0.2 to 2 cm unlined burrows are abundant at this locality and typically occur in buff-coloured beds (Fig. 10b,c). Smaller burrows are parallel to bedding whereas larger burrows are vertical (Fig. 10b,c). Burrowed mudstone and sandstone couplets at this location resemble Richthofen formation strata described along the eastern shore of Lake Laberge during the 2016 field season (van Drecht *et al.*, 2017). The contacts between the Laberge Group and Lewes River Group in the Mount Slim area are interpreted to be unconformable.

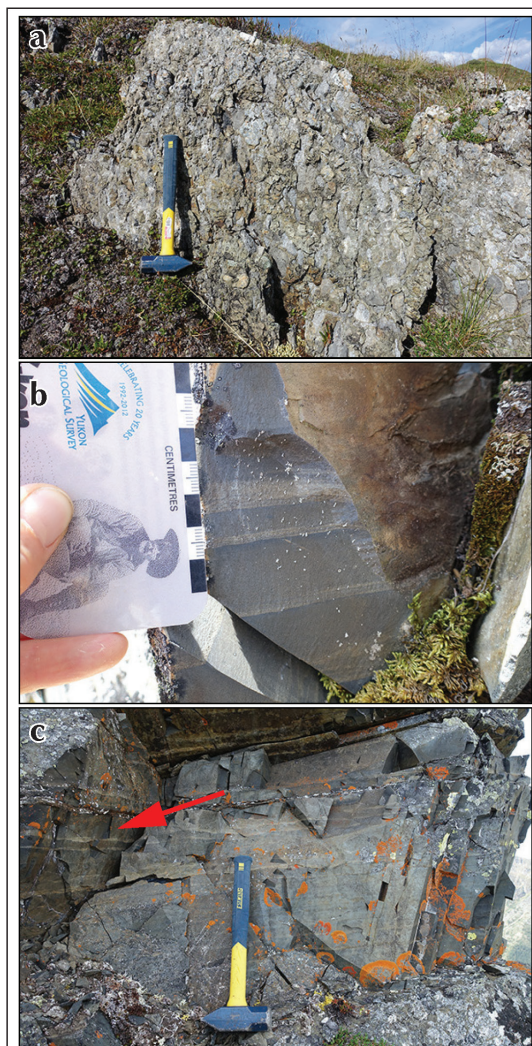


Figure 9. Field photographs of the Richthofen formation at Mount Byng. (a) Pebble to cobble limestone conglomerate; (b) Richthofen formation mudstone and sandstone couplets; and (c) example of wavy contacts between mudstone and sandstone couplets.

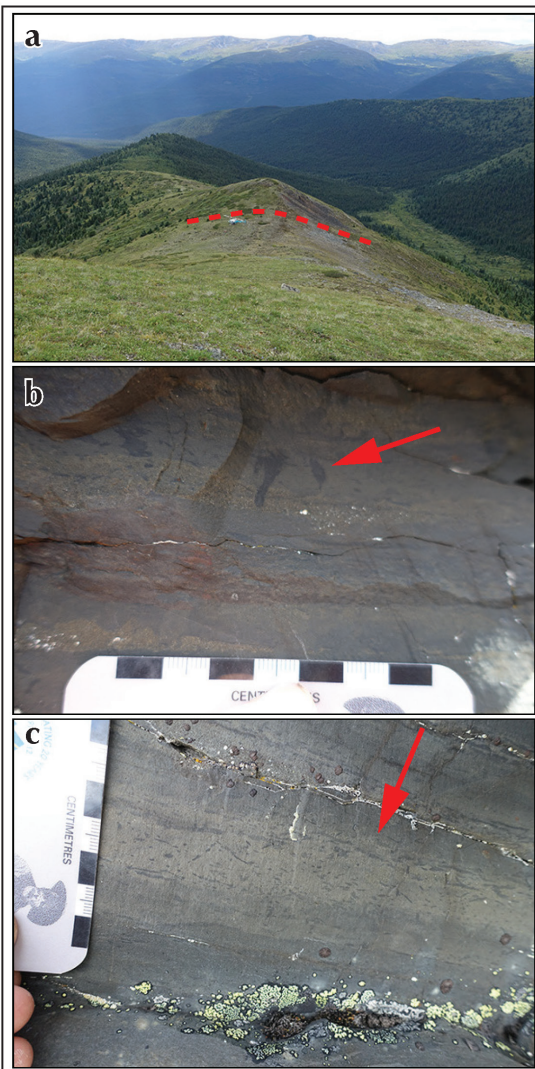


Figure 10. Field photographs of the Richthofen formation at Mount Slim. (a) Rusty, red weathering Richthofen formation (near helicopter; above red line) overlying sandstone of the Askala formation (foreground; below red line); (b) vertical burrows in Richthofen formation mudstone and sandstone couplets; and (c) horizontal burrows in Richthofen formation mudstone and sandstone couplets.

CONCLUSIONS

The Laberge Group-Lewes River Group contact observed at various locations during summer 2017 is apparently unconformable, which is consistent with a period of latest Triassic-earliest Jurassic erosion and/or nondeposition across the Whitehorse trough (e.g., Lowey, 2008). The Laberge Group overlies multiple Carnian to Rhaetian units of the Lewes River Group, likely due to a combination of the complex internal stratigraphy and/or exhumation of the Whitehorse trough shoulders, creating topography prior to Early Jurassic sedimentation in central Yukon. The Lewes River Group is interpreted as a volcanic arc complex that formed a topographic high and was fringed by reef buildups and shallow lagoons (Bordet, 2017). The complex paleotopography created by the Late Triassic volcanic arc was further enhanced by the widespread exhumation and erosion, suggested by the unconformable relationships with the overlying Laberge Group. Variable paleotopography within the Lewes River Group in the latest Triassic-earliest Jurassic likely influenced paleodrainage pathways during Early to Middle Jurassic Laberge Group deposition.

In the northern apex of the trough, basal Tanglefoot formation rocks overlie the Norian-Rhaetian carbonate sequences of the Aksala formation at Mandanna Lake and Rhaetian Mandanna member at Conglomerate Mountain. In the central region of the trough, basal Richthofen formation rocks overlie carbonate sequences of the Aksala formation at Takhini subdivision and Fish Lake as well as clastic rocks of the Aksala formation at Mount Slim and the Carnian Povoas formation at King Lake. This suggests that latest Triassic-earliest Jurassic exhumation and erosion of the Lewes River Group may have been greater on the western flank of the trough to expose mafic volcanic rocks of the Povoas formation, prior to Laberge Group sedimentation. The contact between the Povoas formation gabbro and basal Laberge Group strata at King Lake may also suggest that exhumation was followed by rapid subsidence, allowing basal Laberge Group strata to transgress west.

Proximal Tanglefoot formation strata at Mandanna Lake and Conglomerate Mountain are consistent with deposition in a submarine mass-flow fan setting. Distal strata of the Richthofen formation described at Fish Lake, Takhini subdivision, King Lake, Mount Byng and Mount Slim are indicative of turbiditic facies and consistent with deposition in a distal submarine fan setting. Although rare, the foliated mafic rock clasts at Fish Lake suggest that

these Laberge Group units may represent Pliensbachian or younger conglomeratic beds, as metamorphic rock fragments are only observed in such strata in northern British Columbia (Shirmohammad *et al.*, 2011). This may indicate a potentially younger depositional age for basal strata at this locality, relative to basal strata in the western region of the trough. It is uncertain whether limestone conglomerate at the Takhini subdivision and Mount Byng field localities belong to the uppermost Lewes River Group or basal Laberge Group.

Stratigraphic constraints and detrital zircon U-Pb and Hf isotope studies of samples collected during the 2016 and 2017 field seasons will be used to test the Sinemurian to Toarcian transgression of basal Laberge Group strata westward across the Whitehorse trough. Isotopic studies will also be used to more fully define the depositional age, provenance and paleodrainage history of Laberge Group rock units and provide new insights on the evolution of the Intermontane terranes in the northern Canadian Cordillera.

ACKNOWLEDGEMENTS

Field logistics for this project were supported by the Yukon Geological Survey. We are grateful to Maurice Colpron for helpful field discussions and Pia Blake and Alexina Boileau for field assistance. TRK provided excellent helicopter support. Esther Bordet provided valuable discussions and constructive comments that improved this manuscript. Karen MacFarlane provided helpful editorial comments.

REFERENCES

- Beranek, L.P. and Mortensen, J.K., 2011. The timing and provenance record of the Late Permian Klondike orogeny in northwestern Canada and arc-continent collision along western North America. *Tectonics*, vol. 30, TC5017, doi: 10.1029/2010TC002849.
- Bordet, E., 2016a. Preliminary results on the Middle Triassic-Middle Jurassic stratigraphy and structure of the Teslin Mountain area, southern Yukon. *In: Yukon Exploration and Geology 2015*, K.E. MacFarlane and M.G. Nordling (eds.), Yukon Geological Survey, p. 43-61.
- Bordet, E., 2016b. Bedrock geology map of the Teslin Mountain and East Lake Laberge areas, parts of NTS 105E/2, 3 and 6. Yukon Geological Survey, Open File 2016-38, scale 1:50 000.
- Bordet, E., 2017. Updates on the Middle Triassic-Middle Jurassic stratigraphy and structure of the Teslin Mountain and east Lake Laberge areas, south-central Yukon. *In: Yukon Exploration and Geology 2016*, K.E. MacFarlane and L.H. Weston (eds.), Yukon Geological Survey, p. 1-24.
- Bostock, H.S. and Lees, E.J., 1938. Laberge map-area, Yukon. Geological Survey of Canada, Memoir 217, 32 p.
- Cairnes, D.D., 1910. Preliminary memoir on the Lewes and Nordenškiöld rivers coal district, Yukon Territory. Geological Survey of Canada, Memoir 5, 70 p.
- Cant, D.J. and Stockmal, G.S., 1989. The Alberta foreland basin: Relationships between stratigraphy and Cordilleran terrane-accretion events. *Canadian Journal of Earth Sciences*, vol. 26, p. 1964-1975.
- Cockfield, W.E. and Bell, A.H., 1926. Whitehorse District, Yukon. Geological Survey of Canada, Memoir 150, 63 p.
- Colpron, M., Gordey, S.P., Lowey, G.W., White, D. and Piercy, S.J., 2007. Geology of the northern Whitehorse trough, Yukon (NTS 105E/12, 13, and parts of 11 and 14; 105L/4 and parts of 3 and 5; parts of 115H/9 and 16; 115I/1 and part of 8) (1:150 000 scale). Yukon Geological Survey, Open File 2007-6.
- Colpron, M. and Friedman R.M., 2008. U-Pb zircon ages for the Nordenškiöld formation (Laberge Group) and Cretaceous intrusive rocks, Whitehorse trough, Yukon. *In: Yukon Exploration and Geology 2007*, D.S. Emond, L.R. Blackburn, R.P. Hill and L.H. Weston (eds.), Yukon Geological Survey, p. 139-151.
- Colpron, M., Crowley, J.L., Gehrels, G., Long, D.G.F., Murphy, D.C., Beranek, L. and Bickerton, L., 2015. Birth of the northern Cordilleran orogeny, as recorded by detrital zircons in Jurassic synorogenic strata and regional exhumation in Yukon. *Lithosphere*, vol. 7, p. 541-562.
- Colpron, M., Israel, S. and Hutchison, M., 2016. Tectonics of the Intermontane and Insular terranes, and development of Mesozoic synorogenic basins in southern Yukon: Carmacks to Kluane Lake. GAC®-MAC 2016 Whitehorse Field Trip Guidebook, June 4-6.
- Dawson, G.M., 1887. Report on exploration in the Yukon District, N.W.T., and adjacent northern portion of British Columbia. Geological Survey of Canada, Annual Report, vol. 3, part B, 277 p.

- Dickie, J.R. and Hein, R.J., 1988. Facies and depositional setting of Laberge conglomerates (Jurassic), Whitehorse Trough, Yukon. In: Yukon Geology Volume 2, J.G. Abbott (ed.), Exploration and Geological Services Division, Indian and Northern Affairs Canada, p. 26-32.
- Dickie, J.R. and Hein, R.J., 1995. Conglomeratic fan deltas and submarine fans of the Jurassic Laberge Group, Whitehorse Trough, Yukon Territory, Canada: fore-arc sedimentation and unroofing of a volcanic arc complex. *Sedimentary Geology*, vol. 98, p. 263-292.
- Hart, C.J.R. and Radloff, J.K., 1990. Geology of Whitehorse, Alligator lake, Fenwick Creek, Carcross and Part of Robinson Map Areas (105D/11, 6, 3, 2 & 7). Yukon Geological Survey, Open File 1990-4(G), scale 1:50 000.
- Hart, C.J.R., Dickie, J.R., Ghosh, D.K. and Armstrong, R.L., 1995. Provenance constraints for Whitehorse Trough conglomerate: U-Pb zircon dates and initial Sr ratios of granitic clasts in Jurassic Laberge Group, Yukon Territory. In: *Jurassic Magmatism and Tectonics of the North American Cordillera*, D.M. Miller and C. Busby (eds.), Geological Society of America Special Paper 299, p. 47-63.
- Hutchison, M.P. 2017. Whitehorse trough: Past, present and future petroleum research – with a focus on reservoir characterization of the northern Laberge Group. Yukon Geological Survey, Open File 2017-2, 48 p.
- Johnston, S.T., Mortensen, J.K. and Erdmer, P., 1996. Igneous and metagneous age constraints for the Aishihik metamorphic suite, southwest Yukon. *Canadian Journal of Earth Sciences*, vol. 33, p. 1543-1555.
- Joyce, N., Ryan, J.J., Colpron, M., Murphy, D.C. and Hart, C.J.R., 2015. Compilation of 40Ar/39Ar ages for southern Yukon. Geological Survey of Canada, Open File 7924.
- Knight, E., Schneider, D.A. and Ryan, J.J., 2013. Thermochronology of the Yukon-Tanana terrane, west-central Yukon: Evidence for Jurassic extension and exhumation in the northern Canadian Cordillera. *The Journal of Geology*, vol. 121, p. 371-400.
- Logan, J.M. and Mihalynuk, M.G., 2014. Tectonic controls on early Mesozoic paired alkaline porphyry deposit belts ($\text{Cu-Au} \pm \text{Ag-Pt-Pd-Mo}$) within the Canadian Cordillera. *Economic Geology*, vol. 109, p. 827-858.
- Lowey, G.W., 2004. Preliminary lithostratigraphy of the Laberge Group (Jurassic), south-central Yukon: Implications concerning the petroleum potential of the Whitehorse trough. In: Yukon Exploration and Geology 2003, D.S. Emond and L.L. Lewis (eds.), Yukon Geological Survey, p. 129-142.
- Lowey, G.W., 2008. Summary of the stratigraphy, sedimentology and hydrocarbon potential of the Laberge Group (Lower-Middle Jurassic), Whitehorse trough, Yukon. In: Yukon Exploration and Geology 2007, D.S. Emond, L.R. Blackburn, R.P. Hill and L.H. Weston (eds.), Yukon Geological Survey, p. 179-197.
- Lowey, G.W., Long, D.G.F., Fowler, M.G., Sweet, A.R. and Orchard, M.J., 2009. Petroleum source rock potential of Whitehorse trough: A frontier basin in south-central Yukon. *Bulletin of Canadian Petroleum Geology*, vol. 57, p. 350-386.
- Mihalynuk, M.G., Nelson, J.A. and Diakow, L.J., 1994. Cache Creek terrane entrapment: Oroclinal paradox within the Canadian Cordillera. *Tectonics*, vol. 13, p. 575-595.
- Nelson, J.L., Colpron, M. and Israel, S. 2013. The Cordillera of British Columbia, Yukon, and Alaska: Tectonics and Metallogeny (Chapter 3). In: *Tectonics, Metallogeny and discovery: The North American Cordillera and similar accretionary settings*, M. Colpron, T. Bissig, B.G. Rusk and J.F.H. Thompson (eds.), Society of Economic Geologists, Special Publication Number 17, p. 53-109.
- Shirmohammad, F., Smith, P.L., Anderson, R.G. and McNicoll, V.J. 2011. The Jurassic succession at Lisadale Lake (Tulsequah map area, British Columbia, Canada) and its bearing on the tectonic evolution of the Stikine terrane. *Volumina Jurassica*, vol. 9, p. 43-60.
- Tempelman-Kluit, D.J., 1984. Geology, Laberge (105E) and Carmacks (115I), Yukon Territory. Geologic Survey of Canada, Open File 1101, 10 p.
- Tozer, E., 1958. Stratigraphy of the Lewes River Group (Triassic), central Laberge area, Yukon Territory. Geological Survey of Canada, Bulletin 43, 28 p.
- van Drecht, L.H., Beranek, L.P. and Hutchison, M., 2017. Jurassic stratigraphy and tectonic evolution of the Whitehorse trough, central Yukon: Project outline and preliminary field results. In: Yukon Exploration and Geology 2016, K.E. MacFarlane and L.H. Weston (eds.), Yukon Geological Survey, p. 207-223.
- Wheeler, J.O., 1961. Whitehorse map-area, Yukon Territory. Geological Survey of Canada, Memoir 312, 156 p.